To the Graduate Council:

I am submitting herewith a dissertation written by Steven Michael Claggett entitled "Developing a New Dispersion Model for Predicting Air Pollution Levels in the Cavity Region of a Building Wake and Complex Terrain". I have examined the final copy of this dissertation for form and content and recommend that it be accepted in partial fulfillment of the requirements for the degree of Doctor of Philosophy, with a major in Civil Engineering.

Terry L. Miller, Major Professor

We have read this dissertation
and recommend its acceptance:

Wayne T. Davis

James T. Arnett

Lawrence T. Miller

Accepted for the Council:

Associate Vice Chancellor
and the Dean of The Graduate School

DEVELOPING A NEW DISPERSION MODEL FOR PREDICTING AIR POLLUTION LEVELS IN THE CAVITY REGION OF A BUILDING WAKE AND COMPLEX TERRAIN

A Dissertation

Presented for the

Doctor of Philosophy

Degree

The University of Tennessee, Knoxville

Steven Michael Claggett

May 1996

Copyright © 1996, by Steven Michael Claggett

All rights reserved

To Amy, Bryan, and Mom

The best of what I have become -
That part of me is you

ACKNOWLEDGMENTS

Completing this dissertation was a difficult and lonely task. I would not have succeeded if it were not for the encouragement and support of my family, friends, and doctoral committee. They often had more faith in my abilities than I did.

I thank Dr. James Smoot and Dr. Lawrence Miller for their participation on my committee. My research has benefited from their instruction. I appreciate Dr. Arijit Pakrasi's participation on my committee and his contributions to my research. His enthusiasm is inspiring. I am grateful for my long association with Dr. Wayne Davis who 20 years ago served as my major professor for my Master's degree. I thank him for his guidance in my research and his continued support in my graduate studies. The most difficult part of this dissertation to formulate are the words that properly communicate my gratitude to Dr. Terry Miller. He is my major professor, my mentor, my friend. I owe him a debt that can never be repaid.

I thank three close and dear friends, Dr. Parham Cain, Dr. Cynthia McIlvaine, and Dr. Rebecca Mirsky, who preceded me through the program. They made it look easy. Thanks for blazing a trail wide enough for me to follow. A special thanks to Janet

Morgan who'll be writing her dissertation one day. And I thank Sara and Neil McIlvaine for their kindness and devotion.

I acknowledge my family for their perseverance through these years. Your sacrifice will not be forgotten. I dedicate this dissertation to you: my daughter, Amy; my son, Bryan; and my mother, Eleanor.

ABSTRACT

There are several deficiencies in the capabilities of the United States Environmental Protection Agency's (EPA) guideline air dispersion models that limit their effectiveness in predicting concentrations for conditions that can have the greatest effect on plume dispersion. A new model was developed based on the EPA's Industrial Source Complex Short-Term (ISCST2) model. The new model is called ISCST2C to denote its capabilities of predicting refined concentrations in the cavity region of a building wake and on complex terrain according to the EPA's intermediate terrain policy.

Three cavity algorithms are contained in the model: the Hosker formulation (from the EPA's screening dispersion model called SCREEN2); the Schulman-Scire formulation; and a Gaussian formulation that was developed as part of this research. The Gaussian formulation is consistent with existing EPA guidance for predicting concentrations due to plume downwash. The complex terrain algorithms are based on the EPA's rural complex terrain dispersion model called COMPLEX I and the EPA's urban complex terrain dispersion model called SHORTZ.

The sensitivity of the ISCST2C model predictions to changes in input parameter values was analyzed by preparing curves of the normalized concentration ($\chi u/Q$) along the plume centerline versus downwind distance. At the end of the cavity and beginning of the near-wake, there are large discontinuities between the concentration predictions of the Hosker and Schulman-Scire cavity algorithms and the ISCST2 near-wake algorithm. There is continuity between the concentration predictions of the Gaussian cavity algorithm and the ISCST2 near-wake algorithm for plume heights no more than 1.2 times the building height.

The three cavity algorithms of the ISCST2C model were tested by comparing predicted concentrations against measured concentrations from a field experiment. Tracer gas was released from a variety of heights for a broad set of meteorological conditions. Concentration measurements were made along an arc traversing the width of the cavity. The resulting crosswind concentration profiles tend to support the hypothesis of the Gaussian formulation that horizontal plume dispersion within the cavity generally follow a Gaussian distribution. The Gaussian cavity algorithm generally predicts measured concentrations in the cavity more accurately and more precisely than either the Hosker or Schulman-Scire algorithms.

TABLE OF CONTENTS

Chapter	Title	Page
1.	Introduction	1
	1.1 Overview	1
	1.2 Problem Statement	2
	1.3 Objectives Statement	4
	1.4 Organization	5
2.	Literature Review	7
	2.1 Introduction	7
	2.2 Air Dispersion Modeling Basics	8
	2.2.1 Atmospheric Turbulence and Plume Diffusion	9
	Fanning Plume	11
	Fumigating Plume	11
	Looping Plume	12
	Coning Plume	13
	Lofting Plume	13
	2.2.2 Atmospheric Stability Classification Schemes	14
	2.2.3 A Simple Geometric Plume Model	15
	2.2.4 The Gaussian Distribution	18
	2.2.5 The Gaussian Plume Equation	20
	2.2.6 Simplified Forms of the Gaussian Plume Equation	22
	2.2.7 Dispersion Coefficients	23
	2.2.8 Transport Wind Speed	25
	2.2.9 Plume Trapping	26
	2.2.10 $\chi u/Q$ Curves	28
	2.2.11 Fumigation	30
	2.2.12 Area, Volume, Line, and Instantaneous Sources	34
	Area Source Dispersion	34
	Volume Source Dispersion	35

Chapter Title Page

2.2.12 Area, Volume, Line, and Instantaneous Sources (continued)
Line Source Dispersion 37
Instantaneous Source Dispersion 39
2.3 Plume Rise 41
2.3.1 Briggs' Plume Rise Formulas 42
Buoyancy and Momentum Flux 44
Gradual Rise of a Bent-Over Plume 47
Gradual Buoyant Plume Rise 51
Gradual Momentum Plume Rise 52
Final Buoyant Plume Rise 55
Final Momentum Plume Rise 56
2.3.2 Road Map for Final Plume Rise 57
2.3.3 Stack-Tip Downwash 58
2.3.4 Buoyancy-Induced Dispersion 59
2.4 Building Wake Effects 61
2.4.1 GEP Stack Height 62
2.4.2 Cavity Region 64
Hosker Formulation 65
Schulman-Scire Formulation 68
2.4.3 Near-Wake and Far-Wake Regions 74
Huber-Snyder Formulation 75
Schulman-Scire Formulation 79
2.4.4 Road Map for Enhanced Dispersion Due to Building Wake Effects 85
2.5 Complex Terrain 86
2.5.1 EPA Recommendations 87
2.5.2 Valley Model 90
2.5.3 COMPLEX I Model 92
2.5.4 SHORTZ Model 97

3. Development of the ISCST2C Model 103
3.1 Overview 103
3.2 Model Conception 103
3.3 Model Formulation and Construction 105
3.3.1 Governing Equations 106
Hosker Formulation 106
Schulman-Scire Formulation 109
Gaussian Cavity Formulation 113
COMPLEX I Model 117

Chapter Title Page

3.3.1 Governing Equations (continued)
SHORTZ Model 121
3.3.2 Solution Scheme 123
Refined Cavity Concentrations 123
Complex Terrain 125
3.3.3 Computer Code 126
3.3.4 Setup and Execution of the ISCST2C Model 127
Input Data File Setup 127
Modifications Made to the CO Pathway 128
Modifications Made to the SO Pathway 131
Modifications Made to the ME Pathway 134
Model Execution 136
3.4 Model Testing 138
3.4.1 Comparison of ISCST2 and ISCST2C Predictions 138
3.4.2 Comparison of SCREEN2 Cavity and ISCST2C Cavity Predictions 139
3.4.3 Comparison of SCREEN2C Cavity and ISCST2C Cavity Predictions 139
3.4.4 Comparison of COMPLEX I and ISCST2C Predictions 140
3.4.5 Comparison of SHORTZ and ISCST2C Predictions 141

4. Application of the ISCST2C Model 142
4.1 Introduction 142
4.2 Review of Building Wake Measurement Studies 143
4.3 Data Collection and Compilation 145
4.3.1 Source Parameters 145
4.3.2 Meteorology 147
4.3.3 Receptor Locations 149
4.3.4 Measured Concentrations 150
4.4 Model Runs 152
4.5 Summarizing Model Results 152
4.6 Sensitivity Analysis 153
4.7 Measured Versus Predicted Concentrations 154
4.7.1 Crosswind Concentration Distributions 154
4.7.2 Testing Model Performance 155
4.7.3 Performance Measures 156
4.7.4 Presentation of Results 157
4.8 Interpreting Results 162

Chapter Title Page

5. Discussion of Results 163
5.1 Introduction 163
5.2 Sensitivity Analysis 164
5.2.1 Cavity, Near-Wake, and Far-Wake Algorithms 164
5.2.2 Complex Terrain Algorithms 167
5.3 Crosswind Concentration Distributions 167
5.4 Measured Versus Predicted Concentrations 169
5.4.1 Criteria Used to Interpret Results 169
5.4.2 Performance of the Hosker Cavity Algorithm 171
5.4.3 Performance of the Schulman-Scire Cavity Algorithm 173
5.4.4 Performance of the Gaussian Cavity Algorithm 174
5.4.5 Predicting Plume Centerline Concentrations 176
5.4.6 Performance Comparison of the Cavity Algorithms 178
5.4.7 Performance Comparison With the ISCST2 Wake Algorithms 181

6. Conclusions 183
6.1 Introduction 183
6.2 Research Findings 183
6.3 Recent Release of the ISCST3 Model 188
6.4 Recommendations for Further Research 190

List of References 192

APPENDICES 207

APPENDIX A Tables 208

APPENDIX B Figures 276

APPENDIX C Quick Reference of Pathways/Keywords/Parameters 429

APPENDIX D Full Reference of Pathways/Keywords/Parameters 435

VITA 458

LIST OF TABLES

Table	Title	Page
1.1	Regulatory Gaussian Plume Models	209
2.1	Cramer's Classifications of Atmospheric Stability	210
2.2	Key to Pasquill's Atmospheric Stability Categories	211
2.3	Turner's Key to Pasquill's Stability Categories	212
2.4	Steps in Determining Turner's Net Radiation Index	213
2.5	Insolation Class Number	214
2.6	Relationships of the Vertical Temperature Gradient and the Standard Deviation of the Horizontal Wind Direction Fluctuations to Pasquill's Stability Categories	215
2.7	Plume Spreading Angles	216
2.8	Areas of the Normal Curve	217
2.9	Parameters Used to Calculate Pasquill-Gifford Rural σ_y	218
2.10	Parameters Used to Calculate Pasquill-Gifford Rural σ_z	219
2.11	Variation of Calculated Concentration with Sampling Time	221
2.12	Briggs' Formulas to Calculate McElroy-Pooler Urban Dispersion Coefficients	222
2.13	Wind Profile Exponents	223
2.14	Road Map for Calculating Concentrations Due to Plume Trapping	224
2.15	Comparison of Plume Rise Formulas	225
2.16	Comparison of Predicted Plume Rise with Observations for Neutral Conditions	227
2.17	Road Map for Calculating Final Plume Rise	228
2.18	Road Map to Account for Plume Downwash within the Near-Wake Region of a Building (for 3 L $\leq$ x < 10 L)	229
2.19	Default Values of σ_A and σ_E as a Function of Pasquill Stability Category	230
2.20	Default Values of the Wind Profile Exponents Built Into the SHORTZ Model	231

Table	Title	Page
3.1	ISCST2C Model Subroutines that Support the Cavity and Complex Terrain Concentration Predictions	232
3.2	ISCST2C Model Default Values for Hourly Turbulent Intensities	238
3.3	Default Card Image Format Available as an Option to Access an ASCII Meteorological Data File	239
3.4	Comparison of ISCST2C Model and ISCST2 Model Predictions, 3-Hour Average Concentrations	240
3.5	Comparison of ISCST2C Model and ISCST2 Model Predictions, 24-Hour Average Concentrations	241
3.6	Comparison of ISCST2C Model and SCREEN2 Model Cavity Algorithm Predictions	242
3.7	Comparison of ISCST2C Model and SCREEN2C Model Cavity Algorithm Predictions	243
3.8	Comparison of ISCST2C Model and COMPLEX I Model Predictions	244
3.9	Comparison of ISCST2C Model and SHORTZ Model Predictions	246
4.1	Field Experiments Conducted in Building Wakes	247
4.2	Release Characteristics of the EOCR Tracer Gas Experiment	248
4.3	Direction-Specific Building Dimensions of the EOCR Building for Ground-Level Releases on the Northeast Face	249
4.4	Direction-Specific Building Dimensions of the EOCR Building for Ground-Level Releases on the Northwest Face	250
4.5	Direction-Specific Building Dimensions of the EOCR Building for Ground-Level Releases on the Southwest Face	251
4.6	Direction-Specific Building Dimensions of the EOCR Building for Roof-Level Releases	252
4.7	Direction-Specific Building Dimensions of the EOCR Building for Stack-Level Releases	253
4.8	Initial Estimate of Stability Category as a Function of the Standard Deviation of the Horizontal Wind Direction	254
4.9	Wind Speed Adjustment for Determining the Pasquill Stability Category from the Standard Deviation of the Horizontal Wind Direction	255
4.10	Meteorological Conditions During the EOCR Tracer Gas Release Experiment, Ground-Level Releases	256
4.11	Meteorological Conditions During the EOCR Tracer Gas Release Experiment, Roof-Level Releases	257
4.12	Meteorological Conditions During the EOCR Tracer Gas Release Experiment, Stack-Level Releases	258

Table Title Page

4.13 Sampling Locations Within the Cavity Region of the EOCR Building During the Ground-Level Tracer Gas Releases 259
4.14 Sampling Locations Within the Near-Wake Region of the EOCR Building During the Ground-Level Tracer Gas Releases 260
4.15 Sampling Locations Within the Far-Wake Region of the EOCR Building During the Ground-Level Tracer Gas Releases 261
4.16 Sampling Locations Within the Cavity Region of the EOCR Building During the Roof-Level Tracer Gas Releases 262
4.17 Sampling Locations Within the Near-Wake Region of the EOCR Building During the Roof-Level Tracer Gas Releases 263
4.18 Sampling Locations Within the Far-Wake Region of the EOCR Building During the Roof-Level Tracer Gas Releases 264
4.19 Sampling Locations Within the Cavity Region of the EOCR Building During the Stack-Level Tracer Gas Releases 265
4.20 Sampling Locations Within the Near-Wake Region of the EOCR Building During the Stack-Level Tracer Gas Releases 266
4.21 Sampling Locations Within the Far-Wake Region of the EOCR Building During the Stack-Level Tracer Gas Releases 267
4.22 Statistical Data Summary of Measured Versus Predicted Concentrations, Hosker Cavity Algorithm 268
4.23 Statistical Data Summary of Measured Versus Predicted Concentrations, Schulman-Scire Cavity Algorithm 269
4.24 Statistical Data Summary of Measured Versus Predicted Concentrations, Gaussian Cavity Algorithm 270
4.25 Statistical Data Summary of Measured Versus Predicted Concentrations, Hosker Cavity Algorithm, Plume Centerline Locations Within the Cavity 271
4.26 Statistical Data Summary of Measured Versus Predicted Concentrations, Schulman-Scire Cavity Algorithm, Plume Centerline Locations Within the Cavity 272
4.27 Statistical Data Summary of Measured Versus Predicted Concentrations, Gaussian Cavity Algorithm, Plume Centerline Locations Within the Cavity 273
4.28 Statistical Data Summary of Measured Versus Predicted Concentrations, ISCST2 Wake Algorithm, Plume Centerline Locations Within the Near-Wake 274
4.29 Statistical Data Summary of Measured Versus Predicted Concentrations, ISCST2 Wake Algorithm, Plume Centerline Locations Within the Far-Wake 275

LIST OF FIGURES

Figure	Title	Page
2.1	Various Types of Smoke Plume Patterns Observed in the Atmosphere (Slade, 1968)	277
2.2	Unstable, Neutral, and Stable Atmospheres Based on Temperature Change with Height	278
2.3	Illustration of Dispersion for a Simple Geometric Plume	279
2.4	Trigonometric Relationships of a Simple Geometric Plume	280
2.5	Typical Wind Speed and Wind Direction Traces (Kao, 1984)	281
2.6	Gaussian Distribution	282
2.7	Normalized Gaussian Distribution	283
2.8	Area Under the Gaussian Distribution Curve	284
2.9	Illustration of Plume Dispersion from an Elevated Point Source	285
2.10	Illustration of Plume Reflection Using an Image Plume	286
2.11	Rural and Urban Horizontal Dispersion Coefficients (σ_y) as a Function of Stability Category	287
2.12	Rural and Urban Vertical Dispersion Coefficients (σ_z) as a Function of Stability Category	288
2.13	Typical Variation of Wind Speed with Height (Smith, 1963)	289
2.14	Variation of Wind Speed with Surface Roughness (Davenport, 1963)	290
2.15	Multiple Image Sources for Plume Reflection	291
2.16	$\chi u/Q$ with Distance for Various Plume Heights (H in m) and Limits to Vertical Mixing (H_m in m), A Stability, Rural Dispersion Coefficients	292
2.17	$\chi u/Q$ with Distance for Various Plume Heights (H in m) and Limits to Vertical Mixing (H_m in m), B Stability, Rural Dispersion Coefficients	293
2.18	$\chi u/Q$ with Distance for Various Plume Heights (H in m) and Limits to Vertical Mixing (H_m in m), C Stability, Rural Dispersion Coefficients	294
2.19	$\chi u/Q$ with Distance for Various Plume Heights (H in m) and Limits to Vertical Mixing (H_m in m), D Stability, Rural Dispersion Coefficients	295

Figure Title Page

2.20 $\chi u/Q$ with Distance for Various Plume Heights (H in m) and Limits to Vertical Mixing (H_m in m), E Stability, Rural Dispersion Coefficients 296
2.21 $\chi u/Q$ with Distance for Various Plume Heights (H in m) and Limits to Vertical Mixing (H_m in m), F Stability, Rural Dispersion Coefficients.....297
2.22 $\chi u/Q$ with Distance for Various Plume Heights (H in m) and Limits to Vertical Mixing (H_m in m), A/B Stability, Urban Dispersion Coefficients 298
2.23 $\chi u/Q$ with Distance for Various Plume Heights (H in m) and Limits to Vertical Mixing (H_m in m), C Stability, Urban Dispersion Coefficients 299
2.24 $\chi u/Q$ with Distance for Various Plume Heights (H in m) and Limits to Vertical Mixing (H_m in m), D Stability, Urban Dispersion Coefficients.....300
2.25 $\chi u/Q$ with Distance for Various Plume Heights (H in m) and Limits to Vertical Mixing (H_m in m), E/F Stability, Urban Dispersion Coefficients 301
2.26 Isopleths of $\chi u/Q$ (m^{-2}) for a Ground-Level Source, A Stability, Rural Dispersion Coefficients.....302
2.27 Isopleths of $\chi u/Q$ (m^{-2}) for a Ground-Level Source, B Stability, Rural Dispersion Coefficients.....303
2.28 Isopleths of $\chi u/Q$ (m^{-2}) for a Ground-Level Source, C Stability, Rural Dispersion Coefficients.....304
2.29 Isopleths of $\chi u/Q$ (m^{-2}) for a Ground-Level Source, D Stability, Rural Dispersion Coefficients.....305
2.30 Isopleths of $\chi u/Q$ (m^{-2}) for a Ground-Level Source, E Stability, Rural Dispersion Coefficients.....306
2.31 Isopleths of $\chi u/Q$ (m^{-2}) for a Ground-Level Source, F Stability, Rural Dispersion Coefficients.....307
2.32 Isopleths of $\chi u/Q$ (m^{-2}) for a Ground-Level Source, A/B Stability, Urban Dispersion Coefficients.....308
2.33 Isopleths of $\chi u/Q$ (m^{-2}) for a Ground-Level Source, C Stability, Urban Dispersion Coefficients.....309
2.34 Isopleths of $\chi u/Q$ (m^{-2}) for a Ground-Level Source, D Stability, Urban Dispersion Coefficients.....310
2.35 Isopleths of $\chi u/Q$ (m^{-2}) for a Ground-Level Source, E/F Stability, Urban Dispersion Coefficients.....311
2.36 Distance to Maximum Concentration Versus Maximum $\chi u/Q$ as a Function of Stability and Plume Height (m), Rural Dispersion Coefficients.....312
2.37 Distance to Maximum Concentration Versus Maximum $\chi u/Q$ as a Function of Stability and Plume Height (m), Urban Dispersion Coefficients.....313

Figure Title Page

2.38 Cross-Section of a Fumigating Plume 314
2.39 Profile of a Fumigating Plume 315
2.40 Illustration of Plume Dispersion from an Area Source 316
2.41 Illustration of Plume Dispersion from a Volume Source (Top View) 317
2.42 Illustration of Plume Dispersion from a Volume Source (Side View) 318
2.43 Illustration of Plume Dispersion from a Finite Line Source 319
2.44 Illustration of Puff Dispersion from an Instantaneous Source 320
2.45 Plume Rise Versus Wind Speed in Near-Neutral Conditions (Briggs, 1969) 321
2.46 Plume Rise Times Wind Speed Versus Downwind Distance in Near-Neutral Conditions (Briggs, 1969) 323
2.47 Rise of Buoyant Plumes in Stable Air in Cross-Wind at the TVA Paradise and Gallatin Plants (Briggs, 1969) 324
2.48 Cavity, Near-Wake, and Far-Wake Regions of a Building Wake 325
2.49 GEP Areas of Influence 326
2.50 Maximum Wake Cavity Height Behind Block-Type Obstacles in Near-Uniform Flow (Hosker, 1984) 327
2.51 Empirical Expression for Wake Cavity Length Compared to Data on Rectangular Prisms in Nearly Uniform Flow ($h_L/h_b \leq 2$) (Hosker, 1984) 328
2.52 Empirical Expression for Wake Cavity Length Compared to Data on Rectangular Prisms in Nearly Uniform Flow ($h_L/h_b > 2$) (Hosker, 1984) 329
2.53 Illustration of Stretched-String Distance (ASHRAE, 1993) 330
2.54 Vertical Width of the Plume in the Wake Region 331
2.55 Horizontal Width of the Plume in the Wake Region 332
2.56 Linear Decay Factor Used in the Schulman-Scire Wake Algorithm 333
2.57 Initial Shape of a Plume Emitted Close to the Roof of a Building (Schulman and Scire, 1980) 334
2.58 Simple, Intermediate, and Complex Terrain Regimes 335
2.59 Plume Interception of Elevated Terrain in the Valley Model (EPA, 1977b) 336
2.60 Use of Terrain Adjustment Factors to Alter Plume Height in the COMPLEX I Model 337
2.61 Horizontal Plume Widths of the COMPLEX I Model Compared with Pasquill-Gifford σ_y Values 338
2.62 Default Rural Horizontal Dispersion Coefficients (σ_y) Used in the SHORTZ Model 339

Figure Title Page

2.63 Default Rural Vertical Dispersion Coefficients (σ_z) Used in the SHORTZ Model 340
2.64 Default Urban Horizontal Dispersion Coefficients (σ_y) Used in the SHORTZ Model 341
2.65 Default Urban Vertical Dispersion Coefficients (σ_z) Used in the SHORTZ Model 342

3.1 Stretched-String Distance as Defined in the Schulman-Scire Cavity Algorithm 343
3.2 Vertical Width of the Plume in the Cavity Region (Roof-Level Release) 344
3.3 Horizontal Width of the Plume in the Cavity Region 345

4.1 EOCR Building Plot Plan 346
4.2 Sampling Grid Used During the EOCR Tracer Gas Release Experiment 347
4.3 Crosswind Concentration Distributions Within the Cavity Region of the EOCR Building During the Ground-Level Tracer Gas Releases 348
4.4 Crosswind Concentration Distributions Within the Cavity Region of the EOCR Building During the Roof-Level Tracer Gas Releases 350
4.5 Crosswind Concentration Distributions Within the Cavity Region of the EOCR Building During the Stack-Level Tracer Gas Releases 352
4.6 Control Data File for an ISCST2C Model Run, EOCR Tests, Roof-Level Release, Cavity Region Receptors 354
4.7 $\chi u/Q$ with Distance for Various Plume Heights (m) and Representative Building Configurations, Hosker Cavity Algorithm 356
4.8 $\chi u/Q$ with Distance for Various Plume Heights (m) and Representative Building Configurations, Schulman-Scire Cavity Algorithm 357
4.9 $\chi u/Q$ with Distance for Various Plume Heights (m) and Representative Building Configurations, Gaussian Cavity Algorithm 358
4.10 $\chi u/Q$ with Distance for Various Plume Heights Above Terrain Height ($H - H_T$, in m), A Stability, COMPLEX I Algorithm 359
4.11 $\chi u/Q$ with Distance for Various Plume Heights Above Terrain Height ($H - H_T$, in m), B Stability, COMPLEX I Algorithm 360
4.12 $\chi u/Q$ with Distance for Various Plume Heights Above Terrain Height ($H - H_T$, in m), C Stability, COMPLEX I Algorithm 361
4.13 $\chi u/Q$ with Distance for Various Plume Heights Above Terrain Height ($H - H_T$, in m), D Stability, COMPLEX I Algorithm 362
4.14 $\chi u/Q$ with Distance for Various Plume Heights Above Terrain Height ($H - H_T$, in m), E Stability, COMPLEX I Algorithm 363

Figure Title Page

4.15 $\chi u/Q$ with Distance for Various Plume Heights Above Terrain Height ($H - H_T$, in m), F Stability, COMPLEX I Algorithm 364
4.16 $\chi u/Q$ with Distance for Various Plume Heights Above Terrain Height ($H - H_T$, in m), A Stability, SHORTZ Algorithm 365
4.17 $\chi u/Q$ with Distance for Various Plume Heights Above Terrain Height ($H - H_T$, in m), B Stability, SHORTZ Algorithm....366
4.18 $\chi u/Q$ with Distance for Various Plume Heights Above Terrain Height ($H - H_T$, in m), C Stability, SHORTZ Algorithm....367
4.19 $\chi u/Q$ with Distance for Various Plume Heights Above Terrain Height ($H - H_T$, in m), D Stability, SHORTZ Algorithm 368
4.20 Crosswind Concentration Distributions Within the Cavity Region of the EOCR Building During Tracer Gas Release Test #3....369
4.21 Crosswind Concentration Distributions Within the Cavity Region of the EOCR Building During Tracer Gas Release Test #4....370
4.22 Crosswind Concentration Distributions Within the Cavity Region of the EOCR Building During Tracer Gas Release Test #5....371
4.23 Crosswind Concentration Distributions Within the Cavity Region of the EOCR Building During Tracer Gas Release Test #6....372
4.24 Crosswind Concentration Distributions Within the Cavity Region of the EOCR Building During Tracer Gas Release Test #7....373
4.25 Crosswind Concentration Distributions Within the Cavity Region of the EOCR Building During Tracer Gas Release Test #8....374
4.26 Crosswind Concentration Distributions Within the Cavity Region of the EOCR Building During Tracer Gas Release Test #11....375
4.27 Crosswind Concentration Distributions Within the Cavity Region of the EOCR Building During Tracer Gas Release Test #12....376
4.28 Crosswind Concentration Distributions Within the Cavity Region of the EOCR Building During Tracer Gas Release Test #13....377
4.29 Crosswind Concentration Distributions Within the Cavity Region of the EOCR Building During Tracer Gas Release Test #14....378
4.30 Crosswind Concentration Distributions Within the Cavity Region of the EOCR Building During Tracer Gas Release Test #15....379
4.31 Crosswind Concentration Distributions Within the Cavity Region of the EOCR Building During Tracer Gas Release Test #16....380
4.32 Crosswind Concentration Distributions Within the Cavity Region of the EOCR Building During Tracer Gas Release Test #17....381
4.33 Crosswind Concentration Distributions Within the Cavity Region of the EOCR Building During Tracer Gas Release Test #18....382

Figure Title Page

4.34 Crosswind Concentration Distributions Within the Cavity Region of the EOCR Building During Tracer Gas Release Test #19 383
4.35 Crosswind Concentration Distributions Within the Cavity Region of the EOCR Building During Tracer Gas Release Test #20 384
4.36 Crosswind Concentration Distributions Within the Cavity Region of the EOCR Building During Tracer Gas Release Test #21 385
4.37 Crosswind Concentration Distributions Within the Cavity Region of the EOCR Building During Tracer Gas Release Test #22 386
4.38 Crosswind Concentration Distributions Within the Cavity Region of the EOCR Building During Tracer Gas Release Test #23 387
4.39 Crosswind Concentration Distributions Within the Cavity Region of the EOCR Building During Tracer Gas Release Test #24 388
4.40 Observed σ_y Values During the EOCR Tracer Gas Release Experiment 389
4.41 Scatter Diagrams of Measured Versus Predicted Concentrations Within the Cavity Region of the EOCR Building, All Data 390
4.42 Scatter Diagrams of Measured Versus Predicted Concentrations Within the Cavity Region of the EOCR Building, Ground-Level Release 391
4.43 Scatter Diagrams of Measured Versus Predicted Concentrations Within the Cavity Region of the EOCR Building, Roof-Level Release 392
4.44 Scatter Diagrams of Measured Versus Predicted Concentrations Within the Cavity Region of the EOCR Building, Stack-Level Release 393
4.45 Scatter Diagrams of Measured Versus Predicted Concentrations Within the Cavity Region of the EOCR Building, Unstable Atmosphere 394
4.46 Scatter Diagrams of Measured Versus Predicted Concentrations Within the Cavity Region of the EOCR Building, Neutral Atmosphere 395
4.47 Scatter Diagrams of Measured Versus Predicted Concentrations Within the Cavity Region of the EOCR Building, Stable Atmosphere 396
4.48 Scatter Diagrams of Measured Versus Predicted Concentrations Within the Cavity Region of the EOCR Building, $u_h \leq 1.0$ m/s 397
4.49 Scatter Diagrams of Measured Versus Predicted Concentrations Within the Cavity Region of the EOCR Building, 1.0 m/s $\leq u_h < 3.0$ m/s 398
4.50 Scatter Diagrams of Measured Versus Predicted Concentrations Within the Cavity Region of the EOCR Building, 3.0 m/s $\leq u_h < 5.0$ m/s 399
4.51 Scatter Diagrams of Measured Versus Predicted Concentrations Within the Cavity Region of the EOCR Building, 5.0 m/s $< u_h$ 400
4.52 Scatter Diagrams of Measured Versus Predicted Concentrations Within the Cavity Region of the EOCR Building, Plume Centerline Locations 401
4.53 Scatter Diagrams of Measured Versus Predicted Concentrations Within the Cavity Region of the EOCR Building, Crosswind Locations 402

Figure Title Page

4.54 Cumulative Frequency Distributions of Measured and Predicted Concentrations Within the Cavity, All Data 403
4.55 Cumulative Frequency Distributions of Measured and Predicted Concentrations Within the Cavity, Ground-Level Release 404
4.56 Cumulative Frequency Distributions of Measured and Predicted Concentrations Within the Cavity, Roof-Level Release 405
4.57 Cumulative Frequency Distributions of Measured and Predicted Concentrations Within the Cavity, Stack-Level Release 406
4.58 Cumulative Frequency Distributions of Measured and Predicted Concentrations Within the Cavity, Unstable Atmosphere 407
4.59 Cumulative Frequency Distributions of Measured and Predicted Concentrations Within the Cavity, Neutral Atmosphere 408
4.60 Cumulative Frequency Distributions of Measured and Predicted Concentrations Within the Cavity, Stable Atmosphere 409
4.61 Cumulative Frequency Distributions of Measured and Predicted Concentrations Within the Cavity, $u_h \leq 1.0$ m/s 410
4.62 Cumulative Frequency Distributions of Measured and Predicted Concentrations Within the Cavity, 1.0 m/s $\leq u_h <$ 3.0 m/s 411
4.63 Cumulative Frequency Distributions of Measured and Predicted Concentrations Within the Cavity, 3.0 m/s $\leq u_h <$ 5.0 m/s 412
4.64 Cumulative Frequency Distributions of Measured and Predicted Concentrations Within the Cavity, 5.0 m/s $< u_h$ 413
4.65 Cumulative Frequency Distributions of Measured and Predicted Concentrations Within the Cavity, Plume Centerline Locations 414
4.66 Cumulative Frequency Distributions of Measured and Predicted Concentrations Within the Cavity, Crosswind Locations 415
4.67 Scatter Diagrams of Measured Versus Predicted Concentrations at Plume Centerline Locations in the Cavity, Near-Wake, and Far-Wake Regions 416
4.68 Cumulative Frequency Distributions of Measured and Predicted Concentrations Along Plume Centerline in the Cavity, Near-Wake, and Far-Wake 417
4.69 Concentration Profiles, Ground-Level Release, (Measurements denoted by symbols ° and $^{\Delta}$; Predictions denoted by lines —— and – –) 418
4.70 Concentration Profiles, Roof-Level Release, (Measurements denoted by symbols ° and $^{\Delta}$; Predictions denoted by lines —— and – –) 419
4.71 Concentration Profiles, Stack-Level Release, (Measurements denoted by symbols ° and $^{\Delta}$; Predictions denoted by lines —— and – –) 420

Figure Title Page

5.1 Statistical Summary Diagram, Hosker Cavity Algorithm....421
5.2 Statistical Summary Diagram, Schulman-Scire Cavity Algorithm....422
5.3 Statistical Summary Diagram, Gaussian Cavity Algorithm....423
5.4 Statistical Summary Diagram, Hosker Cavity Algorithm, Plume Centerline Locations Within the Cavity....424
5.5 Statistical Summary Diagram, Schulman-Scire Cavity Algorithm, Plume Centerline Locations Within the Cavity....425
5.6 Statistical Summary Diagram, Gaussian Cavity Algorithm, Plume Centerline Locations Within the Cavity....426
5.7 Statistical Summary Diagram, ISCST2 Wake Algorithm, Plume Centerline Locations Within the Near-Wake....427
5.8 Statistical Summary Diagram, ISCST2 Wake Algorithm, Plume Centerline Locations Within the Far-Wake....428

NOMENCLATURE

Abbreviations

ASHRAE	American Society of Heating, Refrigerating, and Air-Conditioning Engineers
12B2	dibromodifluoromethane
BLP	Buoyant Line Plume
BPIP	Building Profile Input Program
BPIPC	Building Profile Input Program - Cavity
COMPLEX I	screening rural complex terrain dispersion model
CRSTER	refined single source dispersion model
CTDM	Complex Terrain Model Development
CTDMPLUS	refined complex terrain dispersion model developed from the Complex Terrain Model Development project
CTSCREEN	screening version of the CTDMPLUS dispersion model
DOS	Disk Operating System
Dsbh	Direction-Specific Building Height
Dsbl	Direction-Specific Building Length

Dsbw	Direction-Specific Building Width
Dwsl	Downwind Stack Location
EBR-II	Experimental Breeder Reactor II
EOCR	Experimental Organically-Cooled Reactor
EPA	Environmental Protection Agency
Freon-12	dichlorodifluoromethane
GEP	Good Engineering Practice
ISC2	Industrial Source Complex Version 2
ISCST2	Industrial Source Complex Short-Term Version 2
ISCST2C	Industrial Source Complex Short-Term Version 2 - Cavity and Complex Terrain
ISCST3	Industrial Source Complex Short-Term Version 3
LONGZ	screening urban complex terrain dispersion model for long-term concentration predictions
MPRM	Meteorological Processor for Regulatory Models
MPTER	multiple point source model with terrain adjustments
NRC	Nuclear Regulatory Commission
NWS	National Weather Service
PC	Personal Computer
RAM	refined multiple source urban dispersion model for short-term concentration predictions (named after Robert A. McCormick)
RAMMET	meteorological data preprocessor for the RAM model

RTDM	Rough Terrain Dispersion Model
SCREEN2	screening air dispersion model
SCREEN2C	screening air dispersion model with the Schulman-Scire cavity algorithm
SHORTZ	screening urban complex terrain dispersion model for short-term concentration predictions
SF_6	Sulfur Hexafluoride
TVA	Tennessee Valley Authority
Valley	screening rural complex terrain dispersion model

Symbols

A	linear decay factor
A_F	empirical attenuation factor to simulate the blocking effect of a terrain feature on the air flow
A_p	building cross-sectional area perpendicular to the wind flow
A_s	cross-sectional area of the stack at its exit
A_x	plume cross-sectional area
α	horizontal diffusion coefficient
B_L	larger of the building height and projected building width perpendicular to the wind flow
B_S	smaller of the building height and projected building width perpendicular to the wind flow
B_0	empirical constant for initial dilution
B_1	empirical constant for distance dilution

b	intercept of the regression line
β	entrainment constant
β_a	adiabatic entrainment coefficient
β_j	jet entrainment coefficient
c_p	specific heat of air
χ_{avg}	average pollutant concentration
χ_c	cavity concentration
χ_L	concentration for sampling time t_L
χ_m	measured concentration
$\tilde{\chi}_m$	median measured concentration
χ'_m	maximum measured concentration
χ_p	predicted concentration
$\tilde{\chi}_p$	median predicted concentration
χ'_p	maximum predicted concentration
χ_S	concentration for sampling time t_S
$\chi u/Q$	normalized ground-level concentration along the plume centerline
$\chi u/Q_{max}$	maximum normalized ground-level concentration along the plume centerline
D	plume diameter
D_c	dilution between source and receptor in the cavity
D_s	subsequent dilution due to dispersion as the plume travels along the roof and into the cavity

D_0	initial dilution at roof level near the stack due to increased entrainment of ambient air as the momentum plume is bent over by the wind
d	difference between predicted and measured concentrations
$\bar{d}$	arithmetic mean of the difference between predicted and measured concentrations
$\tilde{d}$	median difference between predicted and measured concentrations
d_s	stack tip diameter
$\partial T_a/\partial z$	vertical temperature gradient
$\partial\theta/\partial z$	potential temperature gradient
ΔE	terrain elevation of the receptor above stack base elevation
ε	power law exponent for sampling time correction
F	buoyancy flux
F_b	buoyancy flux at the source
F_m	momentum flux at the source
F_T	terrain adjustment factors
$f(v)$	normal probability density function of a continuous random variable
f_c	fraction of the plume captured by the cavity
f_s	stack-tip downwash factor
ϕ	wind direction with respect to a line source
g	acceleration due to gravity
Γ	adiabatic lapse rate

γ_1	adiabatic entrainment coefficient
γ_2	stable entrainment coefficient
H	plume height or effective stack height
H_{flat}	plume height for flat terrain
H_m	mixing height
$\overline{H}_m$	average height of the mixing layer
H_{min}	minimum separation distance between the plume centerline and the ground surface
H_{wake}	building wake plume height
h	physical stack height
h_b	building height
h_c	cavity height
h_d	vertical distance of stack-tip downwash of the plume
h_{GEP}	stack height necessary to avoid plume downwash due to building wake effects
h_i	height of the dissipated inversion layer
h_L	alongwind building length
h_r	maximum height of the roof top cavity zone
h_w	projected building width measured from a plane perpendicular to the wind flow
Δh	plume rise
Δh_b	buoyant plume rise

Δh_m	momentum plume rise
φ	vertical diffusion coefficient
k'	ratio of the maximum predicted and measured concentrations
$\tilde{k}$	median ratio of predicted and measured concentrations
L	lesser dimension of either the building height or projected building width
L_0	initial horizontal plume length
L_R	building scaling length
M	momentum flux
M_0	initial momentum flux
MW_a	molecular weight of ambient air
MW_s	molecular weight of the stack gas
m	slope of the regression line
μ	mean of a continuous random variable
n	number of data points in a data set
P, P_1, P_2	integration limits for the normal probability density function
p	wind profile exponent
Q	point source emission rate
Q_I	instantaneous source emission rate
Q_L	line source emission rate
q	net amount of heating of the mixing layer
q_R	net heating rate of the air by solar radiation

R	plume radius
R_0	initial vertical plume radius
r	correlation coefficient
rms_d	root mean square error of the difference between predicted and measured concentrations
r_y	horizontal plume radius
r_z	vertical plume radius
ρ	density of the plume
ρ_a	ambient air density
ρ_s	stack gas density
S	stretched-string distance
S_d	standard deviation of the difference between predicted and measured concentrations
s	stability parameter
σ	standard deviation of a continuous random variable
σ_A	standard deviation of the azimuth angle (or horizontal wind direction) fluctuation
σ_E	standard deviation of the elevation angle (or vertical wind direction) fluctuation
σ_θ	standard deviation of the horizontal wind direction fluctuation
σ_ϕ	standard deviation of the vertical wind direction fluctuation
σ_x	downwind dispersion coefficient (i.e., standard deviation of the concentration distribution in the downwind direction)

σ_y	horizontal dispersion coefficient (i.e., standard deviation of the concentration distribution in the horizontal direction)
σ'_y	modified horizontal dispersion coefficient to account for building wake effects on plume dispersion
$\sigma_{y_{BID}}$	horizontal dispersion coefficient due to buoyancy-induced dispersion
σ_{y_e}	effective horizontal dispersion coefficient due to atmospheric turbulence and buoyancy-induced dispersion
σ_{yF}	horizontal dispersion coefficient for fumigation conditions
σ_{y0}	initial horizontal dispersion coefficient
σ_z	vertical dispersion coefficient (i.e., standard deviation of the concentration distribution in the vertical direction)
σ'_z	modified vertical dispersion coefficient to account for building wake effects on plume dispersion
$\sigma_{z_{BID}}$	vertical dispersion coefficient due to buoyancy-induced dispersion
σ_{z_e}	effective vertical dispersion coefficient due to atmospheric turbulence and buoyancy-induced dispersion
σ_{z0}	initial vertical dispersion coefficient
T_a	ambient air temperature
T_s	stack gas temperature
δT	temperature increase
ΔT	difference between the stack exit gas temperature and the ambient air temperature
ΔT_c	cross-over temperature difference

t	time after an instantaneous emissions release
t_L	long sampling time
t_m	time required for the mixing layer to move from the top of the stack to the top of the plume
t_S	short sampling time
θ_y	horizontal plume spreading angle
θ_z	vertical plume spreading angle
u	transport wind speed
$(u_c)_h$	critical stack height wind speed
u_{ref}	wind speed at the reference measurement height
u_s	wind speed at stack top
V	plume volume flux
V_F	stack exit gas volume flow
v_e	entrainment velocity, i.e., effective speed at which ambient air is drawn into the plume
V_M	exhaust momentum velocity ratio
v_s	stack exit gas velocity
v	continuous random variable
W_A	area source width
W_H	volume source horizontal width
W_P	horizontal plume width
W_V	volume source vertical width

w	plume vertical speed
x	downwind distance or direction
x_c	cavity length
x_F	distance to maximum fumigation
x_f	distance to final plume rise
x_m	downwind distance where the vertical distribution of a plume starts being affected by a mixing lid
x_{max}	distance to the maximum normalized ground-level concentration
x_r	length of the roof top cavity zone
x_{ry}	distance over which rectilinear lateral plume expansion occurs downwind from an ideal point source
x_{SL}	downwind distance from the stack location to the lee edge of the building
x_y	virtual distance to account for the initial horizontal width of a plume
x_z	virtual distance to account for the initial vertical width of a plume
x^*	distance from the stack where the plume begins its final rise
y	horizontal or crosswind distance or direction
z	vertical distance or direction

VOLUME 1

C H A P T E R

1
INTRODUCTION

1.1
OVERVIEW

The focus of this research is air dispersion modeling. Two important deficiencies in the capabilities of current models recommended for regulatory use by the United States Environmental Protection Agency (EPA) have been identified. These deficiencies limit the effectiveness of the models to predict concentrations for conditions that can have the greatest effect on plume dispersion.

The overall research objective is to develop an air dispersion model with the added capabilities of predicting refined concentrations in the cavity region of a building wake and concentrations in complex terrain according to the EPA's intermediate terrain policy. The new model is based on modifications made to the EPA's (1992a) Industrial Source Complex Short-Term (ISCST2) model. It is called the ISCST2C model to denote its capabilities for predicting concentrations in the cavity region of a building wake and complex terrain.

1.2 PROBLEM STATEMENT

A number of Gaussian plume models have been formally accepted for regulatory use by the EPA as described in "Guidelines on Air Quality Models (Revised)" (EPA, 1993a; 1987a; 1986). The purpose of the guideline is to promote consistency and standardization of air dispersion models for regulatory applications. Because of this, most EPA-guideline models are based on common underlying precepts, namely: the Gaussian plume equation as described in Section 2.2.5 of the Literature Review; the Pasquill-Gifford rural dispersion coefficients and the McElroy-Pooler urban dispersion coefficients as described in Section 2.2.7 of the Literature Review; and the plume rise formulas developed by Briggs as described in Section 2.3.1 of the Literature Review.

The differences among the EPA-guideline models are the level of sophistication of their predictive algorithms and the specialized applications for which they were developed. There are two levels of sophistication: screening models and refined models. Screening models are relatively easy and inexpensive to use. They are based on simplified algorithms and worst-case assumptions that tend to overestimate actual concentrations. The second level is refined models. They provide a more detailed treatment of atmospheric processes. Accordingly, refined models require more detailed and precise input data to provide more representative concentration predictions than screening models. Because of this, refined models are more difficult and expensive to use than screening models.

Air dispersion models have been developed by the EPA for specific regulatory applications, including: short-term/long-term concentrations; single/multiple sources; rural/urban dispersion; varying source configurations; plume dispersion in a building wake; plume dispersion in complex terrain; and gravitational settling/deposition. Table 1.1 provides a list of the EPA-guideline Gaussian plume models and their recommended regulatory applications. The models are grouped according to their level of sophistication.

There are two important deficiencies in the capabilities of the EPA-guideline air dispersion models listed in Table 1.1. First, none of the EPA's refined models contain an algorithm for predicting concentrations in the cavity region of a building wake. This is a important deficiency since the EPA (1992b) maintains that a building wake has its greatest effect on plume dispersion when the plume is caught in the cavity. Also, none of the EPA models meet the requirements of a recently adopted EPA policy (1993a) governing the use of air dispersion models for complex terrain applications. This too is an important deficiency since the EPA (1992b) acknowledges that terrain can have its greatest effect on plume dispersion when it rises above plume height. In air dispersion modeling vernacular, terrain that rises above the stack top is referred to as complex terrain; terrain below stack top is referred to as simple terrain. After this research was completed, the EPA (1995) released an update to the ISCST2 model (e.g., ISCST3) which has the capabilities of predicting concentrations in complex terrain according to EPA policy for rural areas but not urban areas.

1.3 OBJECTIVES STATEMENT

The overall research objective is to develop the ISCST2C model which will have the capabilities of predicting refined concentrations in the cavity region of a building wake and concentrations in complex terrain according to EPA policy. From this overall objective statement, five primary objectives have been formulated:

1. develop algorithms for predicting refined cavity concentrations based on the Hosker (1984) formulation from the EPA's screening dispersion model called SCREEN2 (EPA, 1992c) and the Schulman and Scire (1993) formulation from the SCREEN2C model (Sigma Research Corporation, 1994);
2. develop an alternative algorithm to the SCREEN2-based and SCREEN2C-based methods for predicting refined cavity concentrations;
3. develop a computer program based on the Building Profile Input Program (BPIP) (EPA, 1993b) to provide certain direction-specific building dimensions needed for predicting concentrations using the SCREEN2 and SCREEN2C cavity algorithms;
4. test the refined cavity algorithms of the ISCST2C model by comparing predicted concentrations against measured concentrations from a tracer gas release experiment conducted in the wake of a building; and
5. develop algorithms for predicting concentrations in complex terrain according to EPA policy (1993a) based on the EPA's screening rural complex terrain

dispersion model called COMPLEX I (EPA, 1992d) and the EPA's screening urban complex terrain model called SHORTZ (EPA, 1982).

The algorithms developed will be incorporated into the EPA's ISCST2 model, the most widely used of the EPA-guideline Gaussian plume models. The ISCST2 model is popular because it provides refined concentration predictions for a wide variety of applications (refer to Table 1.1). It is frequently used to predict concentrations in the wake regions of a building. The ISCST2 model can be substituted for the EPA's refined single source dispersion model called CRSTER (EPA, 1977a), the EPA's refined multiple source urban dispersion model for short-term concentration predictions called RAM (EPA, 1978), and the EPA's multiple point source model with terrain adjustments (MPTER) (EPA, 1980) for equivalent concentration predictions. The model was recently upgraded to improve the program computer code, user interface, and documentation which increased its popularity.

1.4 ORGANIZATION

This dissertation consists of six chapters. Following the Introduction (Chapter 1) is the Literature Review (Chapter 2). The important components of regulatory air dispersion models are described in the literature review, including: the Gaussian plume equation; dispersion coefficients; plume rise; building wake effects; and complex terrain effects. The development of the ISCST2C model is documented in Chapter 3. Three

elements of model development are discussed, namely: model conception; model formulation and construction; and model testing. The fourth element of model development (i.e., model application) is provided in Chapter 4. Concentrations predicted by the model are compared to concentrations measured in the wake of a building during a tracer gas release experiment. A discussion of results is presented in Chapter 5; conclusions and recommendations for further study are provided in Chapter 6. A list of references and appendices are also provided. Tables are located in Appendix A; figures are located in Appendix B. A quick reference of the pathway/keywords/parameters used to construct the input data files required to run the ISCST2C model is given in Appendix C. A full reference of the pathway/keywords/parameters is given in Appendix D. Following the appendices is a vita about the author.

C H A P T E R

2
LITERATURE REVIEW

2.1
INTRODUCTION

Described in this literature review are the important components of air dispersion modeling based on the Gaussian plume equation. Emphasis is placed on the formulations and procedures incorporated into EPA-guideline air dispersion models. A detailed review of air dispersion modeling basics is presented first. The second topic is a review of the plume rise formulas developed by Briggs. Building wake effects on plume dispersion is then discussed, including the formulations contained in the SCREEN2 model and the SCREEN2C model for predicting concentrations in the cavity region of a building wake. The final section is devoted to complex terrain effects on plume dispersion and EPA-recommended screening procedures for predicting concentrations in rural and urban complex terrain.

2.2
AIR DISPERSION MODELING BASICS

Some of the basic precepts of air dispersion modeling are introduced. Dispersion represents the sum of the transport and diffusion processes of a plume in the atmosphere. Diffusion represents the spreading of a plume caused by turbulent motions in the atmosphere. The relationship between atmospheric turbulence and plume diffusion is examined. Some example plume configurations as a function of atmospheric turbulence are illustrated. These illustrations and the associated discussion demonstrates the need to objectively classify atmospheric turbulence. A few atmospheric stability typing schemes are described.

Air dispersion modeling is based on a simple underlying concept - the ability to predict the dilution rate of pollutants emitted to the atmosphere given the transport wind speed and cross-sectional area of the plume as a function of atmospheric stability. This concept is further delineated by developing a simple geometric plume model. From the simple geometric plume model, the Gaussian plume equation is derived. Most EPA-guideline air dispersion models are based on the Gaussian plume equation. Generalized solutions to the Gaussian plume equation are presented in a series of nomographs. Forms of the Gaussian equation are also given for a number of different source configurations (e.g., area sources, volume sources, line sources, and instantaneous sources).

2.2.1 Atmospheric Turbulence and Plume Diffusion

Some typical patterns of vertical plume diffusion observed in the atmosphere are illustrated in Figure 2.1 (Slade, 1968). Plume diffusion is affected by the vertical movement of air parcels in the atmospheric surface layer. This movement is induced by the turbulence or stability of the atmosphere. A measure of atmospheric stability is the vertical temperature gradient (i.e., temperature change with height) with respect to the dry adiabatic lapse rate. The vertical movement of an air parcel is said to be adiabatic if the process occurs without any exchange of heat between the rising air parcel and its surroundings. The dry adiabatic lapse rate is a 1 °C decrease in temperature for every 100 m increase in height. By comparison, the wet adiabatic lapse rate is a 0.6 °C decrease in temperature for every 100 m increase in height.

Atmospheric turbulence is generally described as unstable, neutral, or stable. When the temperature decreases with height at a rate greater than the dry adiabatic lapse rate (i.e., superadiabatic), the atmosphere is unstable and vertical movement of an air parcel is enhanced. When temperature decreases with height at a rate equal to the dry adiabatic lapse rate, the atmosphere is neutral and vertical movement of an air parcel is in equilibrium. When the temperature decreases with height at a rate less than the dry adiabatic lapse rate (i.e., subadiabatic), the atmosphere is stable and vertical movement of an air parcel is reduced. Stable atmospheres are also characterized by isothermal conditions (i.e., a constant temperature with height) or a temperature increase with height.

The stability criteria based on the vertical temperature gradient with respect to the dry adiabatic lapse rate are illustrated in Figure 2.2.

Other measures of atmospheric turbulence are the standard deviations of the horizontal (σ_θ) and vertical (σ_ϕ) wind direction fluctuations. The standard deviations of the horizontal and vertical wind direction fluctuations are sometimes denoted as σ_A (A for azimuth) and σ_E (E for elevation), respectively. Unstable atmospheric conditions are characterized by large fluctuations of σ_θ and σ_ϕ, whereas, stable atmospheric conditions are characterized by small fluctuations of σ_θ and σ_ϕ. Cramer (1957) has defined unstable, neutral, and stable atmospheres in terms of σ_θ and σ_ϕ values as given in Table 2.1.

Variations of temperature change, σ_θ, and σ_ϕ versus height are depicted in the graphs to the left of the plume sketches in Figure 2.1. In the vertical temperature profile graphs, the dashed curves represent the dry adiabatic lapse rate. In the graphs showing the standard deviations of wind direction versus height, the abscissas (σ_θ and σ_ϕ) represent a range of about 0° to 25°.

The shapes of the plumes vary according to atmospheric stability conditions. Because of their appearance, the plumes are dubbed fanning, fumigating, looping, coning, and lofting plumes. The atmospheric conditions which induce these various plume configurations are described in the following. Similar descriptions have been provided by Slade (1968), Briggs (1969), Wark and Warner (1981), Pendergast (1984), and the EPA (1992b).

Fanning Plume

A fanning plume occurs in a stable atmosphere. Stable atmospheric conditions are characterized by clear or thinly overcast skies at night with a very light meandering wind. Under these conditions, the dilution capacity of the atmosphere is greatly reduced. The plume's vertical spread is restricted, indicative of small σ_ϕ values. Horizontal spreading of the plume is limited, but widens slowly with distance from the stack due to the meandering wind direction. This results in the so-called fanning (horizontal spreading) of a shallow plume. Even though emissions undergo very little vertical dilution in a fanning plume, it is not always an unfavorable dispersion condition. For tall stacks, the plume will spread vertically to the ground under stable conditions only after large transport distances. Large transport distances allow for a large amount of dilution to take place before the plume reaches the ground, thus lowering the ground-level concentration. For short stacks or ground-level sources, a stable atmosphere provides unfavorable dispersion conditions and highest short-term concentrations are likely to occur. In mountainous or hilly areas, high ground-level concentrations can occur during stable atmospheric conditions for tall or short stacks due to plume impingement on the nearby elevated terrain.

Fumigating Plume

Fumigation occurs when a plume that was originally emitted into a stable layer aloft is mixed to ground level. This condition typically occurs when the morning sun

begins warming the ground surface. The air near the ground surface becomes unstable due to thermal turbulence and eventually reaches the plume level. The plume is then mixed rapidly to ground level and can result in high short-term concentrations. This meteorological condition is also referred to as inversion break-up fumigation.

Another form of fumigation can occur because of a source's proximity to a large body of water. When the temperature of the water is cooler than that of the land, the air over the water can become more stable than the air over the land. As the stable air moves over the water to the shore and proceeds over land, it is heated by the ground so that a growing unstable layer is formed over the land with stable air aloft. The unstable layer is called the thermal internal boundary layer. Fumigation can occur when a plume from a source located near the shoreline is emitted into the stable air aloft and is transported downwind until it intersects the top of the well-mixed thermal internal boundary layer. The turbulence within the thermal internal boundary layer can mix the plume rapidly to ground level resulting in high short-term concentrations. This meteorological condition is also known as shoreline fumigation.

Looping Plume

During very unstable atmospheric conditions, a plume can be mixed to the ground relatively close to the stack because of strong atmospheric turbulence. Such a plume is called a looping plume. Unstable atmospheric conditions are represented by bright, sunny afternoons and light winds. A looping plume can result in high short-term

concentrations. Concentrations can be significantly increased when the unstable atmospheric conditions occur in conjunction with a limited mixing condition. Limited mixing occurs when a stable layer aloft (inversion) traps a plume beneath it and limits the vertical dispersion of the plume. The highest concentrations occur when the mixing height is at or slightly above the plume height. If a source is located near a large body of water, inversions will occur due to the effects of sea breezes on the overland mixing layer. Sea breezes typically occur on days when the atmosphere is unstable.

Coning Plume

Neutral or near neutral atmospheric conditions are often characterized by a coning plume. During the day, neutral atmospheric conditions are represented by high wind speeds or overcast skies. At night, neutral atmospheric conditions are represented by moderate wind speeds. High short-term concentrations often occur in conjunction with high wind speeds that limit the plume rise.

Lofting Plume

The lofting condition may be considered the most favorable dispersion situation. The effluent is prevented from reaching the ground due to an inversion layer below the plume height. A lofting plume can occur with the transition from an unstable atmosphere to inversion conditions. This condition is most often observed near sunset and may persist for several hours. Hot effluent from a stack will penetrate an inversion layer and

continue to rise if the plume is warmer than the air above the inversion. Unless the inversion layer is very shallow, the plume is diluted in the layer above the inversion and resulting ground-level concentrations are zero.

2.2.2 Atmospheric Stability Classification Schemes

The most widely used scheme for categorizing atmospheric stability was developed by Pasquill (1961). Pasquill perceived atmospheric turbulence near the ground as consisting of two components: mechanical and thermal. Use of Pasquill's criteria is popular since they are based on relatively simple meteorological measurements of surface wind speeds (at 10 m), daytime insolation (incoming solar radiation), and nighttime cloud cover. Table 2.2 contains the criteria for Pasquill's six stability classes which range from A (the most unstable) through D (neutral) to F (the most stable). Stability class A is associated with a small mechanical component and a large thermal component. Stability class D is all mechanical. Stability class F is associated with a small mechanical component and a small thermal component.

Turner (1964) developed a method of implementing Pasquill's atmospheric stability classification scheme using meteorological observations routinely made at larger U.S. airports by the National Weather Service (NWS) (refer to Table 2.3). The Pasquill stability category using Turner's method is a function of surface wind speed (10 m) and Turner's net radiation index. The steps taken to determine Turner's net radiation index are given in Table 2.4. Turner's net radiation index is dependent on cloud cover, ceiling

height, and the solar insolation class. The solar insolation class is directly related to the solar altitude (refer to Table 2.5). Solar altitude can be determined from the Smithsonian Meteorological Tables (List, 1966) based on location and time. Computer programs have been designed by the EPA (1993c; 1993d) to process NWS meteorological data based on Turner's method for determining Pasquill's atmospheric stability classifications. The data files created by these programs are used as meteorological input to most of the EPA-guideline air dispersion models.

Other criteria have been developed for relating vertical temperature gradient measurements and σ_θ measurements to Pasquill's stability categories. These criteria are given in Table 2.6. The Nuclear Regulatory Commission (NRC) relates Pasquill's atmospheric stability categories to measurements of temperature change with height in NRC Guide 1.23 (1972). A weakness of this method is that it does not consider the mechanical component of atmospheric turbulence. Gifford (1968) presents a relationship between Pasquill's atmospheric stability categories and measurements of the standard deviation of the horizontal wind direction based on an analysis completed by Islitzer and Slade (1968) of approximately 200 individual diffusion experiments.

2.2.3 A Simple Geometric Plume Model

As a prelude to developing the Gaussian plume equation, consider a simple geometric plume model described by Miller (1994) to simulate the atmospheric dispersion of pollutants continuously emitted from an elevated point source (see Figure

2.3). The average pollutant concentration in the plume (units of mass per volume, g/m^3) is determined from the pollutant emission rate (units of mass per time, g/s) divided by the dilution rate of the pollutant in the atmosphere (units of volume per time, m^3/s). The dilution rate is the product of the transport wind speed (units of length per time, m/s) and the plume cross-sectional area (units of length squared, m^2). A simple dimensional analysis yields

$$g/m^3 \triangleq \frac{g/s}{m/s\left(m^2\right)} . \tag{2-1}$$

A mathematical representation of the relationship is

$$\chi_{avg} = \frac{Q}{u\,(A_x)} \tag{2-2}$$

where χ_{avg} is the average pollutant concentration in the plume cross-section, Q is the pollutant emission rate, u is the transport wind speed, and A_x is the plume cross-sectional area.

As illustrated in Figure 2.3, the plume has a cone shape. The cross-sectional area of the plume increases with increasing distance from the source. The horizontal spread of the plume (gauged by the horizontal plume radius, r_y) is not necessarily equal to its vertical spread (gauged by the vertical plume radius, r_z). Therefore, the plume cross-sectional area is equivalent to the area of an ellipse (i.e., $A_x = \pi\, r_y\, r_z$). Making this substitution into Equation (2-2) produces

$$\chi_{avg} = \frac{Q}{u(\pi\, r_y\, r_z)} . \tag{2-3}$$

Equation (2-3) yields the average pollutant concentration within the plume cross-section, e.g., it is assumed the pollutant is equally distributed across the plume cross-section such that the plume centerline concentration is equal to the concentration at the plume edge.

In developing the simple geometric plume model, values of r_y and r_z can be determined from the horizontal and vertical plume spreading angles (θ_y and θ_z), and the distance downwind from the source (x). The following relationships can be determined from the horizontal and vertical plume geometries shown in Figure 2.4:

$$\tan\left(\frac{\theta_y}{2}\right) = \frac{r_y}{x} \tag{2-4}$$

$$r_y = x \tan\left(\frac{\theta_y}{2}\right) \tag{2-5}$$

and

$$\tan\left(\frac{\theta_z}{2}\right) = \frac{r_z}{x} \tag{2-6}$$

$$r_z = x \tan\left(\frac{\theta_z}{2}\right). \tag{2-7}$$

The horizontal and vertical spread of a plume are also a function of atmospheric turbulence. The angular spreading of a plume for an unstable, neutral, or stable atmosphere can be estimated using the values given in Table 2.7.

Values of r_y and r_z increase with increasing distance from the source and with increasing atmospheric turbulence. Hence, the average pollutant concentration in the plume decreases with increasing distance from the source and with increasing atmospheric turbulence.

2.2.4 The Gaussian Distribution

The simple geometric plume model provides a rudimentary representation of plume dispersion in the atmosphere. It serves as the basis for explaining the Gaussian plume model. In the simple geometric plume model, it is assumed that the pollutant is uniformly distributed across the plume cross-section. A more refined assumption is that the pollutant will follow a Gaussian or normal frequency distribution from the plume centerline to the plume edge in both the horizontal (y) and vertical (z) directions. The basis of this assumption comes from an examination of the characteristics of turbulent motion. Wind traces show that the fluctuations of horizontal wind speed and horizontal and vertical wind directions are of a random nature (for an example, see Figure 2.5). The fluctuations of these turbulent quantities can be described by statistical variables contained in the theory of probability.

The Gaussian distribution of a continuous random variable, v, can be depicted by the symmetrical, bell-shaped curve shown in Figure 2.6. The height of the curve, $f(v)$, gives the frequency or density for a given value of the variable. The mathematical equation for the normal probability density function of v depends on its mean (μ) and standard deviation (σ)

$$f(v) = \frac{1}{\sqrt{2\pi}\sigma} \exp\left[-\frac{1}{2}\left(\frac{v-\mu}{\sigma} \right)^2 \right]. \tag{2-8}$$

Another way to represent the Gaussian distribution is by normalizing the frequency distribution of the variable with respect to its mean (refer to Figure 2.7).

Relating this to air dispersion modeling, the center of the distribution represents the plume centerline. The ordinate values of Figure 2.7 represent distances from the plume centerline in units of standard deviation. The abscissa provides the concentration fraction along the plume axis with respect to the plume centerline concentration.

Probability density functions are defined so that the expected frequency of observations falling between two limits is represented by the area under the curve between the two limits. The probability of the variable being exactly equal to a given value cannot be evaluated in a continuous distribution since the area under the curve corresponding to a point on the curve is infinitesimal. The area under the Gaussian curve between two symmetrical limits is determined by integrating Equation (2-8)

$$F(P) = \int_{-P}^{P} \frac{1}{\sqrt{2\pi}} \exp\left[-\frac{1}{2}(P)^2\right] dP \qquad (2\text{-}9)$$

where $P = \frac{v - \mu}{\sigma}$ and $dv = \sigma\, dP$.

Graphical solutions to Equation (2-9) are provided in Figure 2.8. Tabular values are provided in Table 2.8. The solutions provided in Figure 2.8 and Table 2.8 provide the total area under the Gaussian curve between -P and + P. In air dispersion modeling, the area under the Gaussian curve represents the total mass of a pollutant distributed along the plume axis within the two limits. The total area under the curve represents the sum of the expected relative frequencies which is equal to 1.0 (or 100 percent), i.e.,

$$F(P) = \int_{-\infty}^{\infty} \frac{1}{\sqrt{2\pi}} \exp\left[-\frac{1}{2}(P)^2\right] dP = 1.0\ . \qquad (2\text{-}10)$$

By convention, the edge of the plume in the Gaussian plume equation is defined as that point where the pollutant concentration is equal to the 10 percent of the plume centerline concentration. Using the graph of Figure 2.7 and following the line for $f(v) = 0.1$ on the abscissa to the curve and reading the corresponding value of the ordinate, the distance from the plume centerline to the plume edge is 2.15 σ. Therefore, the width of the plume from edge to edge is 4.3 σ. Using the graph of Figure 2.8 and following the line for $P = \pm 2.15$ on the ordinate and reading the corresponding value of the abscissa, the total mass of a pollutant distributed along the plume axis within $\pm$ 2.15 σ is 96.8 percent.

2.2.5 The Gaussian Plume Equation

Consider the atmospheric dispersion of an elevated point source plume as illustrated in Figure 2.9. Pollutants are continuously released at an effective height (H) above the ground equal to the physical stack height (h) plus plume rise (Δh). Dispersion of the plume is tracked from a coordinate system whose origin is located at ground-level at the base of the release point. The x-axis extends horizontally in the direction of the wind such that it tracks the plume centerline. The y-axis is perpendicular to the x-axis and is generally referred to as the cross-wind direction. The z-axis extends vertically to denote receptor height above the ground and/or terrain elevation above stack base elevation.

To develop the Gaussian plume equation (Miller, 1994), consider an equivalent form of the simple geometric plume model

$$\chi_{avg} = \frac{Q}{u\,(\sqrt{\pi}\ r_y)(\sqrt{\pi}\ r_z)}. \tag{2-11}$$

Assuming a Gaussian distribution [refer to Equation (2-8)] from the plume centerline to the plume edge in the horizontal (y) and vertical (z) directions

$$\frac{1}{\sqrt{\pi}\ r_y} = \frac{1}{\sqrt{2\pi}\ \sigma_y} \exp\left[-\frac{1}{2}\left(\frac{y}{\sigma_y}\right)^2\right] \tag{2-12}$$

$$\frac{1}{\sqrt{\pi}\ r_z} = \frac{1}{\sqrt{2\pi}\ \sigma_z} \exp\left[-\frac{1}{2}\left(\frac{z-H}{\sigma_z}\right)^2\right]. \tag{2-13}$$

Substituting Equations (2-12) and (2-13) into Equation (2-11) yields

$$\chi(x,y,z;H) = \frac{Q}{2\pi\, u\, \sigma_y\, \sigma_z} \exp\left[-\frac{1}{2}\left(\frac{y}{\sigma_y}\right)^2\right] \exp\left[-\frac{1}{2}\left(\frac{z-H}{\sigma_z}\right)^2\right]. \tag{2-14}$$

To account for plume reflection off of the ground surface, an image source is located underground (an effective plume height of -H) as illustrated in Figure 2.10. The equation for calculating the concentration due to the image source is given by

$$\chi(x,y,z;-H) = \frac{Q}{2\pi\, u\, \sigma_y\, \sigma_z} \exp\left[-\frac{1}{2}\left(\frac{y}{\sigma_y}\right)^2\right] \exp\left[-\frac{1}{2}\left(\frac{z+H}{\sigma_z}\right)^2\right]. \tag{2-15}$$

Combining Equations (2-14) and (2-15) gives the Gaussian plume equation

$$\chi(x,y,z;H) = \frac{Q}{2\pi\, u\, \sigma_y\, \sigma_z} \exp\left[-\frac{1}{2}\left(\frac{y}{\sigma_y}\right)^2\right] \left\{\exp\left[-\frac{1}{2}\left(\frac{z-H}{\sigma_z}\right)^2\right] + \exp\left[-\frac{1}{2}\left(\frac{z+H}{\sigma_z}\right)^2\right]\right\}. \tag{2-16}$$

2.2.6 Simplified Forms of the Gaussian Plume Equation

Equation (2-16) can be simplified to predict concentrations at ground-level (z = 0)

$$\chi(x,y,0;H)=\frac{Q}{2\pi\, u\, \sigma_y\, \sigma_z}\exp\left[-\frac{1}{2}\left(\frac{y}{\sigma_y}\right)^2\right]\left\{\exp\left[-\frac{1}{2}\left(\frac{0-H}{\sigma_z}\right)^2\right]+\exp\left[-\frac{1}{2}\left(\frac{0+H}{\sigma_z}\right)^2\right]\right\}$$

$$\chi(x,y,0;H)=\frac{Q}{2\pi\, u\, \sigma_y\, \sigma_z}\exp\left[-\frac{1}{2}\left(\frac{y}{\sigma_y}\right)^2\right]\left\{2\exp\left[-\frac{1}{2}\left(\frac{H}{\sigma_z}\right)^2\right]\right\}$$

$$\chi(x,y,0;H)=\frac{Q}{\pi\, u\, \sigma_y\, \sigma_z}\exp\left[-\frac{1}{2}\left(\frac{y}{\sigma_y}\right)^2\right]\exp\left[-\frac{1}{2}\left(\frac{H}{\sigma_z}\right)^2\right]. \qquad (2\text{-}17)$$

The Gaussian plume equation can be simplified further to predict concentrations at ground-level (z = 0) along plume centerline (y = 0)

$$\chi(x,0,0;H)=\frac{Q}{\pi\, u\, \sigma_y\, \sigma_z}\exp\left[-\frac{1}{2}\left(\frac{0}{\sigma_y}\right)^2\right]\exp\left[-\frac{1}{2}\left(\frac{H}{\sigma_z}\right)^2\right]$$

$$\chi(x,0,0;H)=\frac{Q}{\pi\, u\, \sigma_y\, \sigma_z}\exp\left[-\frac{1}{2}\left(\frac{H}{\sigma_z}\right)^2\right]. \qquad (2\text{-}18)$$

For a ground-level source with no plume rise (H = 0), concentrations can be predicted at ground-level (z = 0) along plume centerline (y = 0) using the following equation

$$\chi(x,0,0;0)=\frac{Q}{\pi\, u\, \sigma_y\, \sigma_z}\exp\left[-\frac{1}{2}\left(\frac{0}{\sigma_z}\right)^2\right]$$

$$\chi(x,0,0;0)=\frac{Q}{\pi\, u\, \sigma_y\, \sigma_z}. \qquad (2\text{-}19)$$

2.2.7 Dispersion Coefficients

The parameters σ_y and σ_z in the Gaussian plume equation, generally referred to as the dispersion coefficients, are the standard deviations of the concentration distributions in the horizontal and vertical directions, respectively. They are a function of distance from the source, atmospheric stability, surface roughness, averaging time, and height above the surface. The dispersion coefficients employed in the EPA regulatory Gaussian plume models are empirically derived and partially based on theory.

The Pasquill-Gifford dispersion curves (Pasquill, 1961; Gifford, 1961) as given by Turner (1970) are used in most EPA-guideline models to represent plume dispersion in rural areas (refer to Figures 2.11 and 2.12). These curves are based on the Project Prairie Grass diffusion experiments conducted in the Great Plains near O'Neill, Nebraska during the summer of 1956 (Barad, 1958; Haugen, 1959). The site of the experiments was a large flat field with no upwind obstructions to the wind flow for at least 1.0 km. The site was very smooth (surface roughness < 0.01 m). Seventy field experiments were carried out by releasing sulfur dioxide gas from a point source 0.46 m above the ground for 10 min. To determine the horizontal concentration distribution, the gas was collected at a height of 1.5 m above the ground along semicircular arcs of 1° or 2° intervals at distances of 50 m, 100 m, 200 m, 400 m, and 800 m from the source. To determine the vertical concentration distribution, the gas was collected at six 20 m towers located along the 100 m arc. A synopsis of this and other diffusion experiments is given by Draxler (1984).

Equations that give an approximate fit to the Pasquill-Gifford dispersion curves are of the form (EPA, 1992e)

$$\sigma_y = 465.11628\,(x)\tan(TH) \tag{2-20}$$

and

$$\sigma_z = a\,x^b \tag{2-21}$$

where σ_y and σ_z are in meters, x is in kilometers, and

$$TH = 0.017453293\left[c - d\,\ln(x)\right]. \tag{2-22}$$

The coefficients a and b in Equation (2-21) are listed in Table 2.9; the coefficients c and d in Equation (2-22) are listed in Table 2.10. In Equation (2-22), x is in kilometers.

The Pasquill-Gifford dispersion coefficients are representative of an averaging time of about 10 min. Turner (1970) provides a means for estimating concentrations for averaging times longer than a few minutes (refer to Table 2.11). From an inspection of the data provided in Table 2.11, Turner noted a power law relation of concentration with sampling time. Turner (1970) provides an equation for extrapolating concentration predictions from sampling times on the order of 10 minutes to sampling times up to about 2 hours:

$$\chi_l = \chi_s \left(\frac{t_s}{t_l}\right)^{\varepsilon} \tag{2-23}$$

where χ_l is the concentration estimate for the longer sampling time t_l ($t_l < 2$ hours); χ_s is the concentration estimate for the shorter sampling time t_s (probably 10 minutes); and ε is a power law exponent ($0.17 \le \varepsilon \le 0.20$). No sampling time correction of dispersion coefficient values is used in the EPA Gaussian plume models.

The McElroy-Pooler dispersion curves obtained in the St. Louis, Missouri diffusion study (McElroy and Pooler, 1968) are used in most EPA-guideline models to represent plume dispersion in urban areas (refer to Figures 2.11 and 2.12). A summary of this study is provided by Draxler (1984). The St. Louis study was conducted between 1963 and 1965. It consisted of a series of 42 fluorescent particle tracer releases. Point source releases of 1-hour duration were made at two sites: one at ground level, the other atop a 3-story building. For the ground-level release, downwind sampling arcs were established at distances of 0.8 km, 3.2 km, and 7.3 km with an additional arc added at 16.1 km. For the elevated release, downwind sampling arcs were established at distances of 2.1 km, 4.0 km, and 8.1 km with an additional arc added at 16.1 km. In nine tests, vertical concentration profiles were measured from a tethered balloon. An analysis of the data was inconclusive and σ_z values were computed from the surface sampling data. Briggs (1973) developed the equations given in Table 2.12 as an approximate fit to the McElroy-Pooler dispersion curves.

2.2.8 Transport Wind Speed

Wind speed measurements are typically taken at a height of 10 m for the purpose of determining Pasquill's atmospheric stability category. In practice, the transport wind speed at stack top is used in the Gaussian plume equation for the plume rise and dispersion calculations. As illustrated by Smith (1963) in Figure 2.13, wind speeds are higher at greater distances above the earth's surface. The vertical wind speed profile is

also affected by the mechanical turbulence produced by natural and man-made roughness elements on the earth's surface as illustrated by Davenport (1963) in Figure 2.14. A power law formula can be used to account for the variation of wind speed with height and surface roughness

$$u_s = u_{ref}\left[\frac{\max(h, h_{ref})}{h_{ref}}\right]^p \qquad (2\text{-}24)$$

where u_s = the wind speed at stack height, h; u_{ref} = the wind speed at the reference measurement height, h_{ref} (usually 10 m); and p = the wind profile exponent as a function of surface roughness and stability class. The default values of wind profile exponents used in most EPA-guideline models are given in Table 2.13. Equation (2-24) provides the power law formula as typically employed in EPA-guideline models. That is, the vertical wind speed profile is only considered when the stack height is greater than the reference height. For stack heights less than the reference height, the vertical wind speed profile is not considered and the stack height wind speed is equal to the reference height wind speed.

2.2.9 Plume Trapping

The image source concept used to account for plume reflection off of the ground surface can also be applied to account for plume reflection off of the base of an elevated inversion layer. An infinite series can be added to Equation (2-16) to account for the effects of restricted vertical plume dispersion considering the mixing height (H_m)

$$\chi(x,y,z;H)=\frac{Q}{2\pi u_s \sigma_y \sigma_z}\exp\left[-\frac{1}{2}\left(\frac{y}{\sigma_y}\right)^2\right]\left\{\exp\left[-\frac{1}{2}\left(\frac{z-H}{\sigma_z}\right)^2\right]+\exp\left[-\frac{1}{2}\left(\frac{z+H}{\sigma_z}\right)^2\right]\right\}$$

$$+\sum_{i=1}^{\infty}\left\{\exp\left[-\frac{1}{2}\left(\frac{z-(2iH_m-H)}{\sigma_z}\right)^2\right]+\exp\left[-\frac{1}{2}\left(\frac{z+(2iH_m-H)}{\sigma_z}\right)^2\right]\right.$$

$$\left.+\exp\left[-\frac{1}{2}\left(\frac{z-(2iH_m+H)}{\sigma_z}\right)^2\right]+\exp\left[-\frac{1}{2}\left(\frac{z+(2iH_m+H)}{\sigma_z}\right)^2\right]\right\}. \qquad (2\text{-}25)$$

The use of the method of image sources to account for the multiple reflections of the plume off of the ground surface and off of the top of the mixed layer is illustrated in Figure 2.15.

For long downwind distances, the Gaussian plume equation can be simplified by assuming the vertical distribution of the pollutant is uniform within the surface mixing layer. It is assumed that the vertical distribution of a plume starts being affected by a mixing lid when one-tenth of the plume centerline concentration extends to the height of the stable layer (H_m). At this distance (x_m), $\sigma_z = H_m/2.15$. It is further assumed that by the time the plume travels four times x_m, the plume is uniformly distributed within the surface mixing layer so that $H_m = \sqrt{2\pi}\,\sigma_z$. For downwind distances greater than 4 x_m, the concentration for any height between the ground and the mixing lid can be calculated from

$$\chi(x,y,z;H)=\frac{Q}{\sqrt{2\pi}\,u_s \sigma_y H_m}\exp\left[-\frac{1}{2}\left(\frac{y}{\sigma_y}\right)^2\right]. \qquad (2\text{-}26)$$

A road map for calculating concentrations where the vertical plume growth is restricted due to an inversion layer is given in Table 2.14.

2.2.10 χu/Q Curves

Generalized solutions to the Gaussian plume equation are presented in a series of graphs prepared by Turner (1970) in what is generally referred to as Turner's Workbook. One set of graphs (refer to Figures 2.16 through 2.21) presents the normalized ground-level concentration (χu/Q) along the plume centerline versus downwind distance for various effective plume heights and limits to vertical mixing for stability classes A through F, respectively. The graphs were based on computations made using Equations (2-18) and (2-26) and rural dispersion coefficients (Figures 2.11 and 2.12). Ground-level concentration predictions (χ, g/m^3) can be made by multiplying the normalized ground-level concentration by the appropriate point source emission rate (Q, g/s) and dividing by the appropriate transport wind speed (u, m/s).

Another set of χu/Q curves (refer to Figures 2.22 through 2.25) has been prepared based on urban dispersion coefficients to supplement the generalized solutions presented by Turner. One of the advantages of using χu/Q curves is that they allow for a quick solution of the Gaussian plume equation for a number of conditions. Another advantage is that they allow for the highest ground-level concentration and the distance to the highest ground-level concentration to be readily determined.

An isopleth map is used to illustrate the spatial distribution of ground-level concentrations. Individual isopleths denote the locations where ground-level concentrations equal or exceed a given value. Ground-level concentration isopleths for a single source can be plotted from the ratio of the ground-level off-axis concentration and the ground-level plume centerline concentration:

$$\frac{\chi(x, y,0; H)}{\chi(x,0,0; H)} = \exp\left[-\frac{1}{2}\left(\frac{y}{\sigma_y}\right)^2\right]. \qquad (2\text{-}27)$$

What needs to be determined from Equation (2-27) to draw an isopleth is the off-axis distance y for a number of downwind distances. This can be accomplished by solving for y in Equation (2-27), i.e.,

$$y = \sqrt{2 \ln\left[\frac{\chi(x,0,0; H)}{\chi(x, y,0; H)}\right]}\ \sigma_y . \qquad (2\text{-}28)$$

Values of $\chi(x,0,0;H)$ versus downwind distance can be determined from the $\chi u/Q$ curves (Figures 2.16 through 2.25); $\chi(x,y,0;H)$ represents the isopleth concentration; and values of σ_y versus downwind distance can be determined from Figure 2.11. The off-axis distance can be plotted for a number of downwind distances so that the concentration isopleth can be drawn. Figures 2.26 through 2.31 give the isopleths of normalized ground-level concentrations due to a ground-level source (H = 0 m) for stability classes A through F using rural dispersion coefficients; Figures 2.32 through 2.35 give the isopleths of normalized ground-level concentrations due to a ground-level source (H = 0 m) for stability classes A/B through E/F using urban dispersion coefficients. These graphs can

be used as a tool in emergency response planning to quickly determine the areas (e.g., downwind and crosswind distances) to be evacuated in case of an accidental spill of hazardous chemicals.

The graphs of normalized ground-level concentration versus downwind distance for various effective plume heights and stability classes as provided in Figures 2.16 through 2.25 can be used to develop graphs as suggested by D. O. Martin and prepared by Turner (1970) using rural dispersion coefficients. Figures 2.36 and 2.37 present graphs of the maximum normalized ground-level concentration ($\chi u/Q_{max}$) and the distance (x_{max}) to the maximum normalized ground-level concentration as a function of atmospheric stability and effective plume height using rural and urban dispersion coefficients, respectively. The maximum ground-level concentration can be determined by reading χ u/Q_{max} as a function of effective plume height and stability class and multiplying by Q divided by u. The distance to the maximum ground-level concentration is also of importance and can be read directly from the graph.

2.2.11 Fumigation

The term fumigation was introduced by Hewson and Gill (1944) to characterize the rapid mixing to the ground of a plume initially emitted into a stable layer of the atmosphere. As described in Section 2.2.1, this occurrence is common after dawn when an inversion layer is quickly dissipated by the upward transfer of sensible heat due to solar warming of the ground or when cool, stable air flows over a relatively warm land

mass (e.g., lake or sea breeze). Concentrations due to fumigation can be estimated by integrating the Gaussian plume equation (Equation 2-16) with respect to z from 0 to ∞ and assuming the plume is uniformly distributed from the ground to the height of the dissipated inversion layer (h_i). The resulting equation (Gifford, 1968; Turner, 1970) for the fumigation concentration, χ_F, is

$$\chi_F(x, y, 0; H) = \frac{Q}{\sqrt{2\pi}\, u_s\, \sigma_{yF}\, h_i} \exp\left[-\frac{1}{2}\left(\frac{y}{\sigma_{yF}}\right)^2\right] \qquad (2\text{-}29)$$

where σ_{yF} is horizontal dispersion coefficient for fumigation conditions.

Turner (1970) provides a basis for estimating h_i and σ_{yF} values. For the fumigation condition, since it is assumed that the plume is initially emitted into a stable layer, σ_y and σ_z are characteristic of stable conditions as a function of downwind distance. The maximum concentration resulting from fumigation will occur if the inversion is dissipated up to the top edge of the plume (refer to Figure 2.38). The top edge of the plume is a distance of 2.15 σ_z or approximately 2 σ_z from the plume center (the point where the concentration falls to one-tenth of the plume centerline concentration). The height of the dissipated inversion layer, h_i, up to the top edge of the plume is

$$h_i = H + 2\,\sigma_z(\text{stable}) = h + \Delta h + 2\,\sigma_z(\text{stable})\ . \qquad (2\text{-}30)$$

The value of σ_{yF} is based on an approximation suggested by Bierly and Hewson (1962) that the horizontal edge of the plume spreads outward at an angle of 15° as it fumigates (refer to Figure 2.38)

$$2.15\,\sigma_{yF} = 2.15\,\sigma_y(\text{stable}) + H\tan 15^\circ \tag{2-31}$$

$$\sigma_{yF} = \frac{2.15\,\sigma_y(\text{stable}) + H\,(0.2679)}{2.15} \tag{2-32}$$

$$\sigma_{yF} = \sigma_y(\text{stable}) + \frac{H}{8}\,. \tag{2-33}$$

As noted by Miller (1994), there is an inconsistency in developing the equations used to calculate h_i and σ_{yF}. In calculating h_i, the vertical distance from the plume center to plume edge is based on an approximation of $2.15\,\sigma_z \approx 2\,\sigma_z$; whereas in calculating σ_{yF}, the horizontal distance from the plume center to plume edge is based on $2.15\,\sigma_y$.

To satisfy the assumption that the plume is initially emitted into a stable layer, the downwind distance to the fumigation concentration is based on the time required to dissipate the inversion. Otherwise, if the inversion is dissipated over a distance sufficient to include the entire plume, the appropriate dispersion situation is an unstable atmosphere not fumigation conditions. The distance to maximum fumigation (x_F) is based on the time required for the mixing layer to move from the top of the stack to the top of the plume (t_m) times the mean wind speed within the stable layer (refer to Figure 2.39), e.g.,

$$x_F = t_m\ u\,. \tag{2-34}$$

Pooler (1965) derived an equation for estimating t_m which is dependent on the required net amount of heating of the mixing layer (q) divided by the net heating rate of the air by solar radiation (q_R)

$$t_m = \frac{q}{q_R}\,. \tag{2-35}$$

The required net amount of heating of the mixing layer is proportional to the area above the stack top enclosed between the curves A and B in Figure 2.39 (i.e., $q = \frac{1}{2} b h$). This heating is given by the product of the ambient air density (ρ_a in g/m^3) times the specific heat of air (c_p in cal/g-K) times the temperature increase (δT in K) times the average height of the mixing layer ($\overline{H}_m$ in m)

$$q = \rho_a \, c_p \, \delta T \, \overline{H}_m \, . \tag{2-36}$$

δT is the potential temperature gradient ($\partial\theta/\partial z$) times the thickness of the layer to be heated

$$\delta T = \frac{\partial \theta}{\partial z}\left(h_i - h\right). \tag{2-37}$$

The average height of the mixing layer is

$$\overline{H}_m = \left(\frac{h + h_i}{2}\right). \tag{2-38}$$

Substituting Equations (2-37) and (2-38) into Equation (2-36) yields

$$q = \rho_a \, c_p \, \frac{\partial \theta}{\partial z}\left(h_i - h\right)\left(\frac{h + h_i}{2}\right). \tag{2-39}$$

Dividing q by the net heating rate of the air by solar radiation yields the time required to move the mixing layer from stack top to plume top

$$t_m = \frac{\rho_a \, c_p}{q_R} \frac{\partial \theta}{\partial z}\left(h_i - h\right)\left(\frac{h + h_i}{2}\right). \tag{2-40}$$

Multiplying t_m by the wind speed within the stable layer yields the distance to maximum fumigation

$$x_F = u \frac{\rho_a c_p}{q_R} \frac{\partial \theta}{\partial z} (h_i - h) \left(\frac{h + h_i}{2} \right). \quad (2\text{-}41)$$

2.2.12 Area, Volume, Line, and Instantaneous Sources

Area Source Dispersion

Consider the atmospheric dispersion of pollutants emitted continuously from an area source of equal sides as illustrated in Figure 2.40. The emission rate from an area source is expressed as source strength per unit area, e.g., g/s per m^2. The area source can be simulated as a point source using the Gaussian plume equation to predict the downwind concentrations. This is accomplished by placing a point source a virtual distance (x_y) upwind of the actual area source location so that the lateral spread of the plume accounts for the area source width (W_A). Recall that the distance from the plume centerline to the plume edge in the Gaussian plume equation is 2.15 σ so that the horizontal width of the plume is equal to 4.3 σ_y. The initial horizontal dispersion coefficient (σ_{y0}) can, therefore, be calculated from the area source width

$$\sigma_{y0} = \frac{W_A}{4.3}. \quad (2\text{-}42)$$

A virtual distance can then be determined from Figure 2.11 as that distance associated with the calculated value of σ_{y0} for the appropriate stability class. The horizontal virtual distance x_y is added to the downwind distance x (referenced from the middle of the area

source) to calculate the horizontal dispersion coefficient, i.e., $\sigma_y(x + x_y)$. The vertical dispersion coefficient is calculated as a function of downwind distance, i.e., $\sigma_z(x)$.

There are inherent limitations in the virtual point source algorithm associated with its use in predicting concentrations downwind of an area source. The basic limitation is that while actual emissions across an area source are uniform, the Gaussian plume equation simulates the distribution as higher in the center and lower at the edges. As a result, the Gaussian plume equation does not accurately reflect the crosswind concentration distribution of the area source. This limitation has led the EPA to drop the use of the virtual point source algorithm to predict concentrations downwind of an area source in their air dispersion models. Most notably in the update to the SCREEN2 model (EPA, 1992c), the virtual point source algorithm was replaced with the finite line source equation (refer to Equation 2-45) for area source simulations.

Volume Source Dispersion

A source of emissions with initial horizontal *and* vertical dimensions is referred to as a volume source. An example of a volume source is a coal truck dumping station. In this example, emissions are generated when coal is dumped into a receiving bin displacing air that contains minute coal particles.

A volume source can be simulated based on the virtual point source approach described for area sources, except that two virtual distances are required. A virtual distance x_y is needed so that the lateral spread of the plume accounts for the initial

horizontal width and a virtual distance x_z is needed so that the vertical spread of the plume accounts for the initial vertical width. The respective virtual distances are added to the downwind distance x to calculate the horizontal and vertical dispersion coefficients, i.e., $\sigma_y(x + x_y)$ and $\sigma_z(x + x_z)$.

The virtual distances are determined from Figures 2.11 and 2.12 as those distances associated with the initial horizontal and vertical dispersion coefficients. The initial horizontal dispersion coefficient (σ_{y0}) is calculated from the volume source horizontal width (W_H); refer to Figure 2.41. For a single volume source

$$\sigma_{y0} = \frac{W_H}{4.3} . \tag{2-43}$$

For adjacent volume sources

$$\sigma_{y0} = \frac{W_H}{2.15} . \tag{2-44}$$

As illustrated in Figure 2.41, a series of adjacent volume sources can be used to simulate a line source.

The initial vertical dispersion coefficient (σ_{z0}) is calculated from the volume source vertical width (W_V); refer to Figure 2.42. For a surface-based volume source

$$\sigma_{z0} = \frac{W_V}{2.15} . \tag{2-45}$$

For an elevated volume source on or adjacent to a building of height h_b

$$\sigma_{z0} = \frac{h_b}{2.15} . \tag{2-46}$$

For an elevated volume source not on or adjacent to a building

$$\sigma_{z0} = \frac{W_V}{4.3} . \tag{2-47}$$

Line Source Dispersion

For winds perpendicular to a continuously emitting infinite line source, downwind ground-level concentrations can be predicted using an equation adapted from Sutton (1932) by Turner (1970)

$$\chi(x,0,0;H) = \frac{2\,Q_L}{\sqrt{2\pi}\,\sigma_z\,u} \exp\left[-\frac{1}{2}\left(\frac{H}{\sigma_z}\right)^2\right]. \tag{2-48}$$

The emission rate from a line source (Q_L) is expressed as source strength per unit length, e.g., g/s per m. Equation (2-48) is similar in form to Equation (2-18), the Gaussian plume equation for predicting ground-level, plume centerline concentrations. For an infinite line source there is no lateral dispersion of pollutants, hence the distribution of pollutants is Gaussian in only the z direction. Absent from Equation (2-48) are the lateral dispersion parameter σ_y and the crosswind distance y, since for any downwind distance x the concentration is the same for any value of y along the infinite line source.

For wind directions (ϕ) $\geq 45°$ with respect to the infinite line source, Turner (1970) provides a factor of $(\sin \phi)^{-1}$ which can be applied to Equation (2-48) to approximate downwind concentrations

$$\chi(x,0,0;H) = \frac{2\,Q_L}{\sin\phi\,\sqrt{2\pi}\,\sigma_z\,u}\exp\left[-\frac{1}{2}\left(\frac{H}{\sigma_z}\right)^2\right]. \qquad (2\text{-}49)$$

Consider the atmospheric dispersion of pollutants by winds perpendicular to a continuously emitting finite line source as illustrated in Figure 2.43. The x-axis is defined in the direction of the mean wind and passing through the receptor point. The limits of the finite line source is defined as extending from y_1 to y_2 where $y_1 < y_2$. The equation for predicting the downwind ground-level concentration is given by Sutton (1932)

$$\chi(x,0,0;H) = \frac{2\,Q_L}{\sqrt{2\pi}\,\sigma_z\,u}\exp\left[-\frac{1}{2}\left(\frac{H}{\sigma_z}\right)^2\right]\int_{P_1}^{P_2}\frac{1}{\sqrt{2\pi}}\exp\left(-\frac{1}{2}P^2\right)dP \qquad (2\text{-}50)$$

where $P = \frac{y}{\sigma_y}$; $P_1 = \frac{y_1}{\sigma_y}$; and $P_2 = \frac{y_2}{\sigma_y}$.

The integral in Equation (2-50) provides the area under the Gaussian curve similar in form to Equation (2-9). For the case where the limits of the integral are symmetrical about the mean (i.e., P_1 = -P and P_2 = P), Figure 2.8 or Table 2.8 can be used to provide solutions to Equation (2-50). If the limits of the integral are not symmetrical about the mean, then the area between the mean and the first limit, P_1, can be determined and added to the area between the mean and the second limit, P_2. The area between the mean and P can be determined from most standard statistical tables. A polynomial expression which approximates the area under the Gaussian curve between the mean and P standard deviations is given by Hastings (1955):

$$F(P)-\frac{1}{2}=\frac{1}{2}-\frac{t\left(b_1+t\left(b_2+t\left(b_3+t\left(b_4+t\,b_5\right)\right)\right)\right)}{\sqrt{2\pi}\,\exp\left(-\frac{1}{2}P^2\right)} \tag{2-51}$$

where t = 1/(1 + a P), a = 0.2316419, b_1 = 0.319381530, b_2 = -0.356563782, b_3 = 1.781477937, b_4 = -1.821255978, and b_5 = 1.330274429.

The EPA makes use of the error function to solve the integral in Equation (2-50). The error function is defined as

$$\text{erf}(Z)=\frac{2}{\sqrt{\pi}}\int_0^Z \exp\left(-Z^2\right)dZ\,. \tag{2-52}$$

The error function can be used to determine the area under the Gaussian curve by letting $Z^2 = 1/2\,P^2$ so that $Z = 1/\sqrt{2}\,P$ and $dZ = 1/\sqrt{2}\,dP$. Substituting these values into the integral of Equation (2-50) yields

$$\begin{aligned}\int_{P_1}^{P_2}\frac{1}{\sqrt{2\pi}}\exp\left(-\frac{1}{2}P^2\right)dP &= \frac{2}{2}\frac{1}{\sqrt{2\pi}}\int_0^{Z_1}\exp\left(-Z^2\right)\sqrt{2}\,dZ+\frac{2}{2}\frac{1}{\sqrt{2\pi}}\int_0^{Z_2}\exp\left(-Z^2\right)\sqrt{2}\,dZ\\ &=\frac{1}{2}\left[\frac{2}{\sqrt{\pi}}\int_0^{Z_1}\exp\left(-Z^2\right)dZ\right]+\frac{1}{2}\left[\frac{2}{\sqrt{\pi}}\int_0^{Z_2}\exp\left(-Z^2\right)dZ\right]\\ &=\frac{1}{2}\left[\text{erf}(Z_1)+\text{erf}(Z_2)\right]\end{aligned} \tag{2-53}$$

where $Z_1=\frac{P_1}{\sqrt{2}}$ and $Z_2=\frac{P_2}{\sqrt{2}}$.

Instantaneous Source Dispersion

Consider the dispersion of pollutants emitted instantaneously to the atmosphere. Examples of instantaneous emission releases are explosions, ruptures of gas cylinders,

and flash volatilization of instantaneously spilled liquids. Whereas emissions from a continuous source are generally described as being dispersed in a plume, emissions from an instantaneous source are generally described as being dispersed in a puff. In addition to the lateral and vertical dispersion of emissions in the puff, dispersion in the downwind direction must be considered along with the time (t) since the emission release. This is illustrated in Figure 2.44.

Ground-level concentrations downwind of an instantaneous release of emissions from height, H, can be predicted using an equation adapted from Sutton (1932) by Turner (1970):

$$\chi(x, y, 0; H) = \frac{2\,Q_I}{(2\pi)^{3/2}\,\sigma_x\,\sigma_y\,\sigma_z} \exp\left[-\frac{1}{2}\left(\frac{x - u\,t}{\sigma_x}\right)^2\right] \exp\left[-\frac{1}{2}\left(\frac{y}{\sigma_y}\right)^2\right] \exp\left[-\frac{1}{2}\left(\frac{H}{\sigma_z}\right)^2\right]. \tag{2-54}$$

Emissions from an instantaneous source (Q_I) are expressed as the total mass of the release, e.g., g. Equation (2-54) is similar in form to Equation (2-18), the Gaussian plume equation for predicting ground-level, plume centerline concentrations. For an instantaneous source, the distribution of pollutants is Gaussian in all three directions. An additional term is used to account for the Gaussian distribution in the downwind direction, i.e.,

$$\frac{1}{\sqrt{2\pi}\,\sigma_x} \exp\left[-\frac{1}{2}\left(\frac{x - u\,t}{\sigma_x}\right)^2\right] \tag{2-55}$$

where σ_x = the downwind dispersion coefficient. Absent from the dilution term of Equation (2-54) is the wind speed. Wind speed does not provide dilution in the downwind direction in the dispersion of a puff. In Equation (2-54), the wind speed is used in combination with the time after release (t) to determine the downwind position of the center of the puff with respect to the receptor location.

2.3 PLUME RISE

An important variable in the Gaussian plume equation is the height of the plume above ground (H). Plume height is also referred to as the effective stack height. For an industrial source, the plume height seldom corresponds to the physical stack height (h); rather, it consists of an additional component: the physical stack height plus plume rise (Δh). For industrial sources with high exit gas velocities or temperatures, the major component of the plume height is due to plume rise. For typical elevated buoyant sources, plume rise can increase the plume height by a factor of 2 to 10 times the physical stack height thus reducing the maximum ground-level concentration by a factor of 3 to 100 (Briggs, 1984). Plume rise is, therefore, a significant factor in predicting maximum ground-level concentrations.

A number of equations have been developed for predicting plume rise, some of which are presented in Table 2.15. Factors that are common among these equations include source characteristics such as exit gas velocity, exit gas volume flow, exit gas

temperature, and heat emission rate and meteorological conditions such as air temperature, wind speed, and atmospheric stability. These parameters characterize the physics of plume rise. Exit gas velocity, exit gas volume flow, and heat emission rate describe the momentum of the stack gases released to the atmosphere. Exit gas temperature and exit gas volume flow describe the buoyancy of the stack gases released to the atmosphere.

Typically, stack gases from industrial sources are turbulent at release which causes ambient air to become entrained in the plume. Additional entrainment occurs due to the velocity shear between the stack gases moving vertically and the wind moving horizontally. The entrainment of ambient air within the plume greatly reduces its upward momentum and its buoyancy. As air is entrained, the diameter of the plume increases. The plume bends over as it acquires horizontal momentum from the entrained air and eventually levels off and moves horizontally with the wind.

2.3.1 Briggs' Plume Rise Formulas

The EPA (1993a; 1987a; 1986) recommends the use of the equations developed by Briggs (Briggs, 1975; Hanna, Briggs and Hosker, 1982) to predict plume rise in all air dispersion modeling applications. Consequently, Briggs' plume rise formulas have been incorporated into the EPA-guideline air dispersion models.

The plume rise equations developed by Briggs are semi-empirical. They were developed from fundamental laws of fluid mechanics: conservation of mass (mass is

neither created nor destroyed), conservation of buoyancy (accounts for how the total buoyancy of a plume changes as it rises), and conservation of momentum (describes the effect of forces acting on a plume). To describe the plume trajectory, the conservation equations are integrated over the plume cross-section. The resulting equations are integrated averages of the mass flux, buoyancy flux, and momentum flux in the plume cross-section. The theoretical basis of Briggs' formulas is that plume rise is either buoyancy-dominated or momentum-dominated. In the very early stages of release, plume rise is generally momentum-dominated. Transition to buoyancy domination typically occurs within 5 seconds of release which corresponds to a travel distance of about 50 m (Hanna, Briggs, and Hosker, 1982).

Because of the effects of wind speed, plumes from industrial sources tend to bend-over and follow a gradual increasing trajectory with distance until final plume rise is achieved. For calm wind conditions (i.e., $u < 1$ m/s), a plume is more or less vertical. Briggs has developed a set of equations to predict plume rise for both cases: bent-over plumes and vertical plumes. Since Gaussian plume models cannot predict ground-level concentrations for calm wind conditions, Briggs' plume rise equations for the vertical plume case are not incorporated into the EPA-guideline air dispersion models.

Briggs describes the trajectory of a bent-over plume as consisting of three stages:

- a first stage where entrainment of ambient air into the plume results mostly from self-induced turbulence;

- a transitional stage where entrainment results from a combination of self-induced turbulence and ambient turbulence; and
- a final stage where the plume's vertical velocity has decreased relative to the horizontal wind velocity and entrainment results mostly from ambient turbulence.

The EPA (1993a; 1987a; 1986) does not recommend the general use of gradual plume rise in air dispersion modeling applications. In their view, there is insufficient data to describe the dispersion process during the gradual plume rise phase. There are two exceptions where gradual plume rise is deemed appropriate by the EPA: 1) to account for building wake effects and 2) to account for complex terrain effects for receptors located near a stack. In all other instances, final plume rise is deemed appropriate by the EPA.

Presented in the following is the basis of the Briggs' plume rise formulas incorporated into the EPA-guideline air dispersion models for predicting gradual and final plume rise.

Buoyancy and Momentum Flux

To characterize the inherent buoyancy and momentum of a plume, Briggs introduces buoyancy flux (F) and momentum flux (M) in his equations for predicting plume rise. Both parameters can change with height. The buoyancy flux is a function of the plume volume flux (V) and the density difference between the ambient air (ρ_a) and the plume (ρ). F is defined as

$$F \equiv g\, V\, \frac{\rho_a - \rho}{\rho_a}\, \underline{\Delta}\, \frac{m^4}{s^3} \tag{2-56}$$

where g is the acceleration due to gravity (9.81 m/s^2). Buoyancy flux can be described as a density flow with units of $m^3/s \times g$ ($\underline{\Delta}$ m/s^2). An implicit limit of Equation (2-56) is that $\rho_a \geq \rho$.

Equation (2-56) does not present the buoyancy flux in its most familiar form. The more familiar form of the buoyancy flux is the initial value at the source, denoted as πF_b. F_b is obtained by using the stack exit gas volume flow (V_F) as the initial value of the plume volume flux. V_F is equal to the stack exit gas velocity (v_s) times the cross-sectional area of the stack at its exit (A_s). For a circular stack

$$V_F = v_s \times A_s$$

$$V_F = v_s \times \frac{\pi\, d_s^2}{4} \tag{2-57}$$

where d_s is the stack tip diameter. From the equation of state, gas density is inversely proportional to gas temperature

$$\rho_a = \frac{MW_a}{T_a} \quad \text{and}$$

$$\rho_s = \frac{MW_s}{T_s} \tag{2-58}$$

where MW_a and T_a are the molecular weight and temperature of the ambient air, respectively; and MW_s and T_s are the molecular weight and temperature of the stack gas,

respectively. For $MW_s \cong MW_a$, the inverse of gas temperature can be substituted for gas density yielding

$$\frac{\rho_a - \rho_s}{\rho_a} = \frac{\frac{1}{T_a} - \frac{1}{T_s}}{\frac{1}{T_a}}$$

$$= \frac{T_s - T_a}{T_s}$$

$$\frac{\rho_a - \rho_s}{\rho_a} = \frac{\Delta T}{T_s} \tag{2-59}$$

where $\Delta T = T_s - T_a$. Substituting Equations (2-57) and (2-59) into Equation (2-56) yields the more familiar form, F_b (the buoyancy flux of the source)

$$F_b \equiv g\left(\frac{v_s\, d_s^2}{4}\right)\frac{\Delta T}{T_s}\,. \tag{2-60}$$

An implicit limit of this formula is that $T_s \geq T_a$.

For those cases where the molecular weight of the stack gas is quite different from the molecular weight of ambient air, Equation (2-60) can be rewritten as

$$F_b = g\left(\frac{v_s\, d_s^2}{4}\right)\left(1 - \frac{T_a}{T_s}\frac{MW_s}{MW_a}\right). \tag{2-61}$$

The momentum flux (M) is a function of the plume vertical speed (w), the plume volume flux, and the ratio of plume and ambient air densities. M is defined as

$$M \equiv w\, V \frac{\rho}{\rho_a} \Delta \frac{m^4}{s^3}\,. \tag{2-62}$$

Momentum flux can be described as a velocity (m/s) times a flow rate (m^3/s). The more familiar form of the momentum flux is the initial value at the source, denoted as πF_m. F_m is obtained by using the stack exit gas velocity as the initial value of the plume vertical speed; using the stack exit gas volume flow as the initial value of the plume volume flux; and substituting the inverse of gas temperature for gas density:

$$F_m \equiv v_s \left(\frac{v_s d_s^2}{4} \right) \frac{T_a}{T_s}. \tag{2-63}$$

Equation (2-63) is valid for cases where $MW_s \cong MW_a$. For those cases where the molecular weight of the stack gas is quite different from the molecular weight of ambient air, Equation (2-63) can be rewritten as

$$F_m = v_s \left(\frac{v_s d_s^2}{4} \right) \left(\frac{T_a}{T_s} \frac{MW_s}{MW_a} \right). \tag{2-64}$$

Equations (2-60) and (2-63) are used in the EPA-guideline air dispersion models to calculate the source buoyancy flux and the source momentum flux, respectively. If the molecular weight of the stack gas is significantly less than the molecular weight of ambient air, then the stack gas temperature input into the air dispersion model can be increased by a factor of MW_a/MW_s to properly account for the effect.

Gradual Rise of a Bent-Over Plume

The equations incorporated into the EPA-guideline air dispersion models for predicting gradual plume rise are based on Briggs' formula for predicting gradual rise of a

bent-over plume. This formula was developed to predict plume rise near the source at distances where the plume is still in its first-stage rise, before ambient turbulence has much of an effect. Briggs (1984) shows that ambient turbulence has little effect on plume trajectories for travel times of about 20 s for strong stratification to about 100 s for weak stratification. Briggs (1984) also shows that for buoyant plumes from conventional power plants, the distance to where ambient turbulence retards the rise is approximately 10 stack heights.

The prediction of the trajectory of a bent-over plume is derived directly from the conservation of momentum equation, details of which are given by Briggs (1975). A detailed summary of the derivation and simplifying assumptions required to obtain the derivation are also given by Briggs (1984).

The momentum conservation equation for a bent-over plume whose density approximates ρ_a is (Briggs, 1984)

$$\frac{d(M)}{dz} = \frac{F}{w} . \tag{2-65}$$

The vertical plume velocity, w, represents the rise velocity of the plume centerline moving down the plume axis at a horizontal speed u. The ratio w/u is the slope of the plume axis above the horizontal so that w/u = dz/dx and w = u dz/dx. Incremental travel time of the plume is the incremental travel distance divided by the wind speed (dt = dx/u) so that w = dz/dt. Incremental travel time of the plume in terms of z and w is

$$dt = \frac{dz}{w} . \tag{2-66}$$

Making this substitution into Equation (2-65) and integrating yields

$$\int d(M) = \int F \, dt$$

$$M - M_0 = \pi F_b \, t \, . \tag{2-67}$$

Assuming the initial value of the momentum flux (M_0) is equal to the source value of πF_m and that F is constant and equal to its initial source value of πF_b, Equation (2-67) becomes

$$M = w \, V = \pi F_m + \pi F_b \, t \, . \tag{2-68}$$

A formula relating the change in plume volume flux with distance is derived from the conservation of mass equation (Briggs, 1984)

$$\frac{dV}{dx} = 2 \pi R \, v_e \tag{2-69}$$

where R is the plume radius and v_e is the entrainment velocity. Equation (2-69) introduces a new unknown, v_e, which is the effective speed at which ambient air is drawn into the plume. A closure assumption is made (Briggs, 1984), based on the Taylor entrainment assumption, to relate the entrainment velocity to the plume vertical speed

$$v_e = \beta \, w \tag{2-70}$$

where β is a dimensionless entrainment constant. If a simplifying assumption is made that u is constant with height (i.e., no vertical wind shear), β can also be used to relate the plume radius to its vertical rise (Briggs, 1984)

$$R = \beta \, z \, . \tag{2-71}$$

Recommended values of β are provided following the derivation of Equation (2-73).

Substituting in Equations (2-70) and (2-71) and using the transformation dt = dx/u = dz/w, Equation (2-69) becomes

$$\int dV = \int 2\pi(\beta z)(\beta w)\,dx$$

$$\int \frac{dV}{u} = \int 2\pi\beta^2 z w \frac{dx}{u}$$

$$\int dV = 2\pi\beta^2 u \int z\,dz$$

$$V = \pi\beta^2 u z^2 . \qquad (2\text{-}72)$$

Now Equation (2-68) can be integrated after substituting in Equation (2-72) and the transformations w = u dz/dx and t = x/u to yield the formula for gradual rise of a bent-over plume

$$\int (u)(\pi\beta^2 u z^2)\,dz = \int \pi F_m\,dx + \int \pi F_b \left(\frac{x}{u}\right) dx$$

$$\frac{1}{3}\pi\beta^2 u^2 z^3 = \pi F_m x + \frac{\pi F_b}{2u} x^2$$

$$\Delta h = z = \left(\frac{3}{\beta^2}\frac{F_m}{u^2} x + \frac{3}{2\beta^2}\frac{F_b}{u^3} x^2\right)^{\frac{1}{3}} . \qquad (2\text{-}73)$$

The value of β is different for buoyant plumes and momentum plumes (e.g., jets). Briggs (1975; Hanna, Briggs, and Hosker, 1984) recommends values of $\beta_a = 0.6$ for the buoyancy term (also referred to as the adiabatic entrainment coefficient) and $\beta_j = 0.4 + 1.2\ (u/v_s)$ for the momentum term (also referred to as the jet entrainment coefficient). However, a good fit to a number of data sets was also obtained by Briggs (1975) using Equation (2-75) with $\beta_j = 1 + 1/3\ (u/v_s)$ for the momentum term. It is this value of the jet

entrainment coefficient that is used in the plume rise algorithms of the EPA-guideline air dispersion models.

Gradual Buoyant Plume Rise

The equation used in the EPA-guideline air dispersion models for predicting gradual buoyant plume rise (Δh_b) is derived from Equation (2-73) by dropping the momentum term, using the wind speed at stack top (u_s), and substituting in $\beta_a = 0.6$

$$\Delta h_b = \left[\frac{3}{2\,(0.6)^2} \frac{F_b}{u_s^3} x^2 \right]^{\frac{1}{3}}$$

$$\Delta h_b = \frac{1.6\, F_b^{\frac{1}{3}}\, x^{\frac{2}{3}}}{u_s} . \qquad (2\text{-}74)$$

Equation (2-74) is the well-known $\frac{2}{3}$ power law for buoyant plumes. Briggs (1969) compared the formula with plume rise data from numerous stacks, including Tennessee Valley Authority (TVA) steam plants. A summary of the data is presented in Table 2.16. When evaluating the data, Briggs plotted plume rise versus wind speed as shown in Figure 2.45. The slopes of the lines (Δh versus u) in Figure 2.45 are equal to minus one (i.e., m = -1) for various downwind distances. This view of the data generally supports the relationship that plume rise is inversely proportional to wind speed, i.e.,

$$\Delta h \propto \frac{1}{u} . \qquad (2\text{-}75)$$

The higher the wind speed, the more the plume will bend over due to increased entrainment of ambient air.

Briggs also plotted plume rise times wind speed versus downwind distance (Δh u versus x) as shown in Figure 2.46. In this plot, wind speed effects on plume rise are normalized out. This view of the data suggests a $\frac{2}{3}$ power law with respect to x.

A third plot of the data, as presented in Figure 2.47, shows non-dimensional plume rise $\left[\Delta h / \left(F_b / u\right)^{\frac{1}{3}}\right]$ versus non-dimensional distance downwind $\left(x / \sqrt{u}\right)$. This leads to the formula for gradual rise of buoyant plumes as given by

$$\Delta h_b = \frac{1.6\, F_b^{\frac{1}{3}}\, x^{\frac{2}{3}}}{u} . \qquad (2\text{-}74)$$

Equation (2-74) is valid, regardless of stratification, up to a distance where atmospheric turbulence begins to dominate entrainment (denoted as x*). Equation (2-74) provides a conservative approximation of gradual buoyant plume rise for distances beyond x* up to a distance of 3.5 x* which is considered the distance to final plume rise (x_f).

Gradual Momentum Plume Rise

The equation used in the EPA-guideline air dispersion models for predicting gradual momentum plume rise (Δh_m) for unstable and neutral atmospheric conditions is derived from Equation (2-73) by dropping the buoyancy term and $u = u_s$

$$\Delta h_m = \left(\frac{3}{\beta_j^2} \frac{F_m}{u_s^2} x \right)^{\frac{1}{3}} \tag{2-76}$$

where $\beta_j = 1/3 + u_s/v_s$.

For stable atmospheric conditions, the formula for predicting gradual momentum plume rise is derived from the momentum and buoyancy conservation equations. The rise of a buoyant plume in a stable atmosphere is limited due to the entrainment of negatively-buoyant ambient air. The buoyancy conservation equation for a bent-over plume is given by Briggs (1984) and is used to account for how the total buoyancy of a plume changes as it rises

$$\frac{dF}{dz} = -\frac{s\,V}{S_2} \tag{2-77}$$

where s is the stability parameter and $S_2 \equiv 2.3$ based on laboratory experiments (Briggs, 1984). The stability parameter is the restoring acceleration per unit vertical height of an air parcel adiabatically displaced. Hanna, Briggs, and Hosker (1982) describe the stability parameter as "being proportional to the rate at which stability suppresses the generation of turbulence". It is calculated based on the potential temperature gradient ($\partial\theta/\partial z$)

$$\begin{aligned} s &= \frac{g}{T_a}\left(\frac{\partial T_a}{\partial z} + \Gamma\right) \\ &= \frac{g}{T_a}\frac{\partial \theta}{\partial z} \end{aligned} \tag{2-83}$$

where $\partial T_a/\partial z$ is the vertical temperature gradient, Γ is the adiabatic lapse rate ($\cong$ 1 °C/100 m), and $\partial\theta/\partial z = \partial T_a/\partial z + \Gamma$. Typical values of $\partial\theta/\partial z$ are 0.020 K/m for Pasquill stability category E and 0.035 K/m for Pasquill stability category F.

Using the momentum and buoyancy conservation equations to describe the trajectory of a bent-over plume for a stable atmosphere and assuming s is approximately constant yields the following solution (Briggs, 1984)

$$w\,V = \pi\,F_m \cos\left(\sqrt{\frac{s}{S_2}}\,\frac{x}{u}\right) + \frac{\pi\,F_b}{\sqrt{s/S_2}} \sin\left(\sqrt{\frac{s}{S_2}}\,\frac{x}{u}\right) . \qquad (2\text{-}84)$$

Integrating Equation (2-84) yields

$$\Delta h = z = \left\{ \frac{3\,F_m}{\beta^2\,u\,\sqrt{s/S_2}} \sin\left(\sqrt{\frac{s}{S_2}}\,\frac{x}{u}\right) + \frac{3\,F_b}{\beta^2\,u\,s/S_2}\left[\,1 - \cos\left(\sqrt{\frac{s}{S_2}}\,\frac{x}{u}\right)\right]\right\}^{\frac{1}{3}} . \qquad (2\text{-}85)$$

The equation used in the EPA-guideline air dispersion models for predicting gradual momentum plume rise for stable atmospheric conditions is derived from Equation (2-85) by dropping the buoyancy term, using the stack top wind speed, and omitting the variable S_2

$$\Delta h_m = \left[\frac{3\,F_m}{\beta_j^2\,u_s\,\sqrt{s}} \sin\left(\frac{\sqrt{s}\,x}{u_s}\right)\right]^{\frac{1}{3}} . \qquad (2\text{-}86)$$

where $\beta_j = 1/3 + u_s/v_s$. Equation (2-86) is of the form derived by Briggs (1984) for the rise of vertical plumes (i.e., calm wind) in a stable atmosphere.

Final Buoyant Plume Rise

Briggs (1971) has developed empirical formulas for calculating the distance from the stack to where the plume begins its final stage of rise (x*). During this stage, air entrainment results mostly from atmospheric turbulence. The formulas for calculating x* for unstable or neutral atmospheric conditions are

$$x^* = 14\, F_b^{\frac{5}{8}}\, \underline{\Delta}\ m \qquad \text{for } F_b < 55\ m^4/s^3 \qquad (2\text{-}87)$$

and

$$x^* = 34\, F_b^{\frac{2}{5}}\, \underline{\Delta}\ m \qquad \text{for } F_b \geq 55\ m^4/s^3. \qquad (2\text{-}88)$$

Final plume rise is assumed to be reached at a distance (x_f) of about 3.5 x* downwind (Briggs, 1971).

The form of Equations (2-87) and (2-88), i.e.,

$$\begin{array}{c} \text{slope} \\ \therefore \\ y = b\, x^m \\ \vdots \\ \text{int ercept} \end{array} \qquad (2\text{-}89)$$

indicates they were developed from a least-squares line of best fit of data plotted on log-log paper.

For stable atmospheric conditions, the rise of a buoyant plume is limited due to the entrainment of negatively-buoyant ambient air. Theoretically, according to Equation (2-85), a buoyant plume (F_m = 0) reaches its maximum height at $x_f = \pi\, u_s\, (s/S_2)^{-1/2}$. Empirically, based on many observations including TVA steam plants, the formula to

determine the distance to final rise of a buoyant plume for stable atmospheric conditions is

$$x_f = 2.0715 \frac{u_s}{\sqrt{s}} . \qquad (2\text{-}90)$$

Substituting x_f into Equation (2-74) yields the equations for final buoyant plume rise:

- unstable or neutral atmospheric conditions

$$\Delta h_b = 21.425 \frac{F_b^{\frac{3}{4}}}{u_s} \qquad \text{for } F_b < 55 \text{ m}^4/\text{s}^3 \qquad (2\text{-}91)$$

and

$$\Delta h_b = 38.71 \frac{F_b^{\frac{3}{5}}}{u_s} \qquad \text{for } F_b \geq 55 \text{ m}^4/\text{s}^3 \qquad (2\text{-}92)$$

- stable atmospheric conditions

$$\Delta h_b = 2.6 \left(\frac{F_b}{u_s \, s} \right)^{\frac{1}{3}} . \qquad (2\text{-}93)$$

Final Momentum Plume Rise

The equation used in the EPA-guideline air dispersion models for predicting final momentum plume rise for unstable and neutral atmospheric conditions was empirically derived by Briggs (1969) as a "reasonable value for maximum observed rise"

$$\Delta h_m = 3 \, d_s \frac{v_s}{u_s} . \qquad (2\text{-}94)$$

For stable atmospheric conditions, the equation used in EPA-guideline air dispersion models for predicting final momentum plume rise was derived from theory by Briggs (1969)

$$\Delta h_m = 1.5\left(\frac{F_m}{u_s\sqrt{s}}\right)^{\frac{1}{3}}. \qquad (2\text{-}95)$$

2.3.2 Road Map for Final Plume Rise

A road map providing the equations employed in the EPA-guideline air dispersion models to predict final plume rise is given in Table 2.17. Separate routes are taken depending on atmospheric stability. Different sets of equations are used for unstable and neutral conditions versus stable conditions. Under unstable and neutral conditions, which route to take depends on the value of the buoyancy flux. Different sets of equations are used for $F_b < 55\ m^4/s^3$ and $F_b \geq 55\ m^4/s^3$. Finally, under either unstable and neutral conditions or stable conditions, separate routes are taken depending on whether plume rise is buoyancy-dominated or momentum-dominated. To decide which of these routes to take, a new term is introduced, the cross-over temperature difference (ΔT_c). If the difference between the stack exit gas temperature and the ambient air temperature (ΔT) is greater than or equal to the cross-over temperature difference, then plume rise is assumed to be buoyancy-dominated. If $\Delta T < \Delta T_c$, then plume rise is assumed to be momentum-dominated.

The cross-over temperature difference for each case is obtained by setting the equation for final buoyancy plume rise equal to the equation for final momentum plume rise and solving for ΔT. The resulting ΔT is defined as ΔT_c. So for unstable and neutral conditions and $F_b < 55\ m^4/s^3$, Equation (2-91) is set equal to Equation (2-94) and

$$\Delta T_c = 0.0297\ T_s \frac{v_s^{\frac{1}{3}}}{d_s^{\frac{2}{3}}}\ . \tag{2-96}$$

For unstable and neutral conditions and $F_b \geq 55\ m^4/s^3$, Equation (2-92) is set equal to Equation (2-94) and

$$\Delta T_c = 0.00575\ T_s \frac{v_s^{\frac{2}{3}}}{d_s^{\frac{1}{3}}}\ . \tag{2-97}$$

For stable conditions, Equation (2-93) is set equal to Equation (2-95) and

$$\Delta T_c = 0.019582\ T_s\ v_s \sqrt{s}\ . \tag{2-98}$$

2.3.3 Stack-Tip Downwash

For wind flow around a stack, a slight pressure will develop on the upwind face with a slight vacuum on the downwind face. In some instances, where the vertical stack gas velocity is not high enough with respect to the horizontal wind velocity, the plume will tend to downwash slightly behind the stack. This is referred to as stack-tip downwash. Stack-tip downwash can occur for a poorly designed stack (large exit diameter and low exit gas velocity) or for a process operating at a fraction of its design capacity (reduced exit gas velocity). The stack of a coal-fired boiler generally has the

tell-tale sign of stack-tip downwash with a ring of black soot on the face near the tip. Stack-tip downwash can be avoided by maintaining the stack exit gas velocity to at least 1.5 times the stack top wind speed. For $v_s/u_s < 1.5$, Briggs (Hanna, Briggs, Hosker; 1982) provides a formula for calculating the vertical distance (h_d) the plume will downwash due to wind flow effects around the stack

$$h_d = 2\left(\frac{v_s}{u_s} - 1.5\right)d_s \,. \tag{2-99}$$

Stack tip downwash is one of the components for determining plume height. Plume height is the sum of the physical stack height plus plume rise minus stack tip downwash. The maximum distance the plume will downwash (for $v_s = 0$) is three stack diameters. If $v_s = 1.5\ u_s$, no stack-tip downwash effects are predicted.

2.3.4 Buoyancy-Induced Dispersion

The dispersion coefficients employed in the EPA-guideline air dispersion models are based on the Project Prairie Grass experiment for rural applications and the St. Louis, Missouri experiment for urban applications. In both of these experiments, the tracer gases were released with no plume rise. During the rise of a plume from its source, ambient air mixes into the plume due to the turbulence of the stack gases upon release and due to the velocity shear that exists between the stack gases and the air. Entrainment of ambient air into the plume causes the diameter of the plume to grow as it rises. Thus,

the process of dispersion begins during plume rise. This process is referred to as buoyancy-induced dispersion.

The horizontal and vertical width of a plume during its rise can be defined by its diameter (D). The Gaussian definition of the horizontal and vertical width of a plume from edge to edge is 4.3 σ. By equating these two relationships, the horizontal and vertical dispersion coefficients due to buoyancy-induced dispersion ($\sigma_{y_{BID}}$ and $\sigma_{z_{BID}}$, respectively) are established

$$\sigma_{y_{BID}} = \sigma_{z_{BID}} = \frac{D}{4.3} . \tag{2-100}$$

Briggs provides an equation that relates the plume radius to its vertical rise

$$R = \beta z \tag{2-71}$$

where β = 0.6 for a buoyant plume. Substituting D = 2 R, β = 0.6, and Δh = z into Equation (2-100) yields

$$\sigma_{y_{BID}} = \sigma_{z_{BID}} = \frac{2\,(0.6)\,\Delta h}{4.3}$$

$$\sigma_{y_{BID}} = \sigma_{z_{BID}} \cong \frac{\Delta h}{3.5} . \tag{2-101}$$

Pasquill (1976) provides a method to account for the effect of buoyancy-induced dispersion on atmospheric turbulent dispersion. In the Pasquill method, effective dispersion coefficients (σ_{y_e} and σ_{z_e}) are calculated based on the root mean square of the atmospheric turbulent dispersion coefficients (σ_y and σ_z) and the buoyancy-induced dispersion coefficients ($\sigma_{y_{BID}}$ and $\sigma_{z_{BID}}$), i.e.,

$$\sigma_{y_c} = \sqrt{\sigma_y^2 + \sigma_{y_{BID}}^2} \quad (2\text{-}102)$$

and

$$\sigma_{z_e} = \sqrt{\sigma_z^2 + \sigma_{z_{BID}}^2} \; . \quad (2\text{-}103)$$

An inconsistency may occur in applying Δh in the air dispersion model calculations. For receptors located between the source and the distance to final plume rise (i.e., $x < x_f$), Δh is the distance-dependent gradual plume rise for the purpose of calculating the buoyancy-induced dispersion coefficients when final plume rise is typically used for the purpose of calculating concentration. For receptors located beyond x_f, final plume rise is used in both circumstances.

2.4
BUILDING WAKE EFFECTS

Plume dispersion can be affected by complicated wind flow patterns near buildings, structures, or terrain obstacles. The movement of wind over and around these obstructions to the wind flow produce aerodynamic wakes and eddies. A plume can potentially become trapped in a building wake which could cause the plume to mix rapidly toward the ground (refer to Figure 2.48). This is called plume "downwash". Plume downwash generally causes higher ground-level concentrations near an elevated point source release than would occur otherwise.

As depicted in Figure 2.48, a building wake is generally divided into three regions: 1) a cavity region; 2) a near-wake region; and 3) a far-wake region. In conducting an air quality analysis, the EPA (1993a; 1987a; 1986) recommends that plume

downwash effects be investigated if stacks are less than the Good Engineering Practice (GEP) stack height (EPA, 1985). The methodologies adopted by the EPA for predicting air pollution levels due to plume downwash are based on the results of wind tunnel experiments. To predict concentrations in the cavity and wake regions of nearby buildings, the EPA (1993a; 1987a; 1986) recommends the use of their detailed downwash screening procedures (EPA, 1992b) as implemented in the SCREEN2 air dispersion model (EPA, 1992c). For refined concentration predictions in the near-wake and far-wake regions, the EPA (1993a; 1987a; 1986) recommends the use of their Industrial Source Complex (ISC2) air dispersion model (EPA, 1992a). Presented in the following are the methodologies developed by the EPA for predicting concentrations resulting from plume downwash.

2.4.1 GEP Stack Height

GEP stack height is actually defined by an Act of Congress. In Section 123 of the Clean Air Act, GEP stack height is "the height necessary to insure that emissions from the stack do not result in excessive concentrations of any air pollutant in the immediate vicinity of the source as a result of atmospheric downwash, eddies, and wakes which may be created by the source itself, nearby structures, or nearby terrain obstacles". The height necessary to avoid plume downwash (h_{GEP}) can be calculated based on the formulation proposed by Snyder and Lawson (1976) and adopted by the EPA (1985)

$$h_{GEP} = h_b + 1.5\,L \tag{2-104}$$

where h_b is the height of the nearby building (or obstacle) and L is the lesser of either the building height or projected width (h_w), i.e.

$$L = \text{minimum}\,(h_b, h_w)\,. \tag{2-105}$$

The heights, h_{GEP} and h_b, are measured from the ground-base elevation of the stack. The projected width is measured from a plane perpendicular to the direction of the wind.

In the definition and the equation establishing GEP stack height, "nearby" is the adjective used to describe the scale of influence of a building upon a stack. The maximum extent of a building wake has been established by the EPA (1985) as 5 L, but not greater than 0.8 km downwind. Depending on the type of building, the GEP 5 L area of influence can change as the wind direction changes. This is illustrated in Figure 2.49 for a squat (i.e., $h_b < h_w$) and a tall (i.e., $h_b > h_w$) simple building.

In the case of a squat building where the height is always less than the projected width, the GEP 5 L area of influence is based on the height. The downwind extent of the wake is a constant 5 times the building height as the wind direction changes. In the case of a tall building where the projected width is always less than the height, the GEP 5 L area of influence is based on the projected width. The downwind extent of the wake changes as the projected building width changes with wind direction.

Most industrial facilities consist of multiple stacks and multiple buildings. In this instance, the GEP formula is applied to each stack/building combination. Buildings consisting of multiple tiers are evaluated by applying the GEP formula to each individual tier. For multiple buildings or multiple building tiers, the highest value obtained in

applying the GEP formula is taken to be the GEP stack height. For groups of buildings where the wakes from two buildings are sufficiently close to one another, the wakes from the two buildings act as one wake (EPA, 1985). The GEP formula is applied after assuming the gap between the buildings is filled with a structure equal to the height of the lower building. Sufficiently close means that the distance of separation is less than the L of either building.

Performing a GEP analysis of multiple stacks affected by multiple buildings can be tedious. The EPA (1993b) has developed a computer program, called the Building Profile Input Program (BPIP) to implement the GEP stack height guidelines. BPIP can also be used to calculate the direction-specific build dimensions needed by the ISCST2 model to account for plume downwash within the near-wake and far-wake regions of a building (refer to Section 2.4.3).

2.4.2 Cavity Region

The highest ground-level concentrations due to plume downwash can occur if the plume is caught in the cavity region. The EPA (1992b) recommends that a screening procedure, based on a formulation derived by Hosker (1984) and incorporated into the SCREEN2 air dispersion model (EPA, 1992c), be used to predict cavity concentrations. Recently, an alternative screening procedure for cavity concentration predictions has been developed by Schulman and Scire (1993) and incorporated into the SCREEN2C model (Sigma Research Corporation, 1994).

Hosker Formulation

Hosker (1984) notes from the work of Barry (1964) and Meroney (1982) that equations for predicting concentrations within the cavity region of a building wake are of the general form

$$\chi_c = \frac{Q}{c\ u\ A_p} \tag{2-106}$$

where the coefficient c is typically given a value between 0.5 and 5.0 and A_p is the building cross-sectional area perpendicular to the wind flow (m^2). In this formulation it is assumed that the plume is completely entrained and well-mixed in the cavity.

As for the EPA (1992b) screening procedures, if the plume height equals the cavity height, then the plume is trapped in the cavity. The cavity height (h_c) is determined based on a formula developed by Hosker (1984)

$$h_c = h_b \left[1.0 + 1.6 \exp\left(\frac{-1.3\ h_L}{h_b} \right) \right] \tag{2-107}$$

where h_L is the alongwind building length in m and h_c and h_b are in m. Equation (2-107) was empirically determined from the data of Evans (1957), Lemberg (1973), and others (Arie and Rouse, 1956; Good and Joubert, 1968). As illustrated in Figure 2.50 (Hosker, 1984), there is considerable scatter in the data.

The plume height is determined by the stack height plus gradual momentum plume rise (buoyancy plume rise is not considered) minus stack tip downwash. Gradual momentum plume rise is calculated at a distance of two building heights downwind from

the lee side of the building (i.e., x = 2 h_b) using Equation (2-76) or Equation (2-86). Stack tip downwash is calculated using Equation (2-99). Applying these equations, the minimum wind speed at stack top that causes the plume height to be equal to the cavity height is determined. This is called the critical stack height wind speed, $(u_c)_h$. The dilution wind speed used in Equation (2-106) to predict the cavity concentration is taken to be one-half the critical stack height wind speed. If u < 1 m/s, it is set equal to 1 m/s and if u > 10 m/s, it is set equal to 10 m/s.

An additional check of the wind speed is made to ensure that unrealistically high (i.e., > 20 m/s) wind speeds are not used in the cavity concentration calculation. This is accomplished by adjusting the critical wind speed from stack height to 10 m using the power law formula of Equation (2-24) with a wind profile exponent of 0.2, i.e.,

$$(u_c)_{10m} = (u_c)_h \left(\frac{10\ m}{h}\right)^{0.2} . \qquad (2\text{-}108)$$

The wind profile exponent is representative of neutral conditions in a rural or urban area. If the critical wind speed adjusted to 10 m is greater than 20 m/s, then the cavity concentration is assumed to be zero.

Concentrations within the cavity are predicted using Equation (2-106) with c = 1.5, i.e.,

$$\chi_c = \frac{Q}{1.5\ u\ A_p} . \qquad (2\text{-}109)$$

Substituting in u = 0.5 × $(u_c)_h$, Equation (2-109) becomes

$$\chi_c = \frac{1.33\,Q}{(u_c)_h\,A_p}\,. \tag{2-110}$$

The cavity concentration is assumed to be uniform within the building cross-sectional area for the entire length of the cavity. The cavity length (x_c) is determined based on formulas developed by Hosker (1984). For short block buildings, where $h_L / h_b \leq 2$, Hosker developed a cavity length formula to fit Evans' (1957) data

$$x_c = \frac{A_c\,h_w}{1.0 + B_c\,(h_w / h_b)} \tag{2-111}$$

where x_c is measured from the lee side of the building in m, h_w and h_b are in m, and A_c and B_c are weak functions of h_L / h_b as given by

$$A_c = -2.0 + 3.7\left(\frac{h_L}{h_b}\right)^{-\frac{1}{3}} \tag{2-112}$$

and

$$B_c = -0.15 + 3.05\left(\frac{h_L}{h_b}\right)^{-\frac{1}{3}}\,. \tag{2-113}$$

A plot of Equation (2-111) against Evans' data is provided in Figure 2.51 (Hosker, 1984) for different alongwind length to height ratios. As pointed out by Hosker (1984), the equation fits the data relatively well, generally within ± 15 percent or better.

A cavity length formula for long block buildings, where $h_L / h_b > 2$, was also developed by Hosker to fit Evans' (1957) data

$$x_c = \frac{1.75\,h_w}{1.0 + 0.25\,(h_w / h_b)} \tag{2-114}$$

where x_c is measured from the lee side of the building in m, and h_w and h_b are in m. A plot of Equation (2-114) against Evans' data is provided in Figure 2.52 (Hosker, 1984). As pointed out by Hosker (1984), the agreement between the equation and the data is typically within ± 15 percent or better.

Schulman-Scire Formulation

In the formulation proposed by Schulman and Scire (1993), concentrations in the cavity region of a building wake are based on methodology for estimating contamination of an air intake or receptor as adopted by the American Society of Heating, Refrigerating, and Air-Conditioning Engineers (ASHRAE, 1993). The Schulman-Scire formulation also allows for a fraction of the plume to be captured by the cavity. The equation for predicting the maximum concentration within the cavity region of a building wake is

$$\chi_c = \frac{Q}{v_s A_s} \frac{f_c}{D_c} \tag{2-115}$$

where Q is the source emission rate (g/s); v_s is the stack exit gas velocity (m/s); A_s is the stack exit cross-sectional area (m^2); f_c is the fraction of the plume captured by the cavity; and D_c is the dilution between source and receptor in the cavity (unitless).

The pollutant concentration in the stack gas (χ_s) is represented by the first term, i.e., $\chi_s = Q / (v_s A_s)$. The dilution at the stack is equal to 1.0 and increases with distance from the source to the receptor. D_c consists of two components: an initial dilution (D_0) at roof level near the stack due to increased entrainment of ambient air as the momentum

plume is bent over by the wind and a subsequent dilution (D_s) due to dispersion as the plume travels along the roof and into the cavity. Based on the work of Wilson and Chui (1987), ASHRAE (1993) defines D_c as the square of the sum of the square roots of the two dilution components (i.e., $D_c = \left[\sqrt{D_0} + \sqrt{D_s}\right]^2$). In the Schulman-Scire formulation, D is defined as the sum of the two dilution components (i.e., $D_c = D_0 + D_s$).

D_0 accounts for the initial entrainment of ambient air in the plume by means of crosswind momentum. For a vertically directed uncapped exhaust, a simple empirical equation relating the initial dilution to an exhaust momentum velocity ratio (V_M), refer to Equation (2-117), was developed from wind tunnel simulations by Wilson and Chui (1985)

$$D_0 = 1 + B_0 V_M^2 \qquad (2\text{-}116)$$

where B_0 is an empirical constant for initial dilution (= 7.0). This equation is not valid at distances very near the exhaust. At the exhaust exit, D_0 is unity and not the larger value predicted by Equation (2-116). The initial entrainment of ambient air that is reflected by D_0 occurs while the momentum plume is rising and bending over; it is distributed over some downwind distance. Wind tunnel measurements indicate that this distance is about $10\sqrt{A_s}$. Thus, Equation (2-116) is valid for distances greater than $10\sqrt{A_s}$. In addition, buoyancy plume rise was neglected in developing the equation. Since buoyancy increases the rise of the exhaust gases and produces lower concentrations at roof level, Equation (2-116) contains an inherent safety factor.

The exhaust momentum velocity ratio in Equation (2-116) is given by

$$V_M = \sqrt{\frac{\rho_s}{\rho_a}} \frac{v_s}{u_s} . \tag{2-117}$$

In the plume rise discussion (Section 2.2.1), it was shown that if the molecular weight of the stack gas and ambient air are approximately equal, then the inverse of the gas temperature can be replaced for the gas density. Making the appropriate substitutions, Equation (2-116) becomes

$$D_0 = 1 + 7.0 \frac{T_a}{T_s} \left(\frac{v_s}{u_s} \right)^2 . \tag{2-118}$$

Equation (2-118) was developed for vertically directed uncapped exhausts with stack gas velocities to wind speed ratios ranging from 0 to 2. In the Schulman-Scire formulation, if $v_s / u_s > 2$, then v_s / u_s is set equal to 2.

Dilution due to plume dispersion (D_s) can be calculated based on an equation developed by Wilson and Britter (1982) from wind tunnel experiments

$$D_s = B_1 \left(\frac{u_b}{v_s} \right) \left(\frac{S^2}{A_s} \right) \tag{2-119}$$

where B_1 is an empirical constant for distance dilution; u_b is the upwind wind speed at building roof level; and S is the "stretched-string" distance. S is defined as the shortest length of string connecting the receptor and a point on the stack that intersects the highest roof level (refer to Figure 2.53). In the Schulman-Scire formulation, S is taken to the stretched-string distance from the stack top to the base of the lee wall of the building. Recommended values of B_1 (ASHRAE, 1993) are

- 0.0625 for flat-roofed buildings in low-rise urban surroundings for all wind directions when the exhaust is uncapped and $v_s / u_b > 0.5$ and
- 0.0204 if there is no significant surface roughness such as at roof-level of high rise buildings or in flat rural surroundings, or if the stack is capped and the wind is 45° with respect to the upwind building face, or if $v_s / u_b < 0.5$.

A value of $B_l = 0.0625$ is used in the Schulman-Scire formulation.

Substituting the dilution component formulas into Equation (2-115) yields the equation used in the SCREEN2C model for predicting concentrations in the cavity region of a building wake

$$\chi_c = \frac{Q\, f_c}{v_s\, A_s \left[1 + 7.0 \frac{T_a}{T_s} \left(\frac{v_s}{u_s} \right)^2 + 0.0625 \left(\frac{u_b}{v_s} \right) \left(\frac{S^2}{A_s} \right) \right]}$$

$$= \frac{Q\, f_c}{v_s\, A_s \left[1 + 7.0 \frac{T_a}{T_s} \left(\frac{v_s}{u_s} \right)^2 \right] + 0.0625\, u_b\, S^2} . \qquad (2\text{-}120)$$

The mass fraction of the plume captured by the cavity (f_c) is taken to be the fraction of the plume below the cavity height (h_c) at the end of the cavity ($x = x_c$). The basis for calculating f_c is the assumption that the vertical distribution of the plume is Gaussian (Schulman and Scire, 1993)

$$f_c = 0.5 \left\{ 1 + \mathrm{erf} \left[\frac{(h_c - H)/\sigma_z}{\sqrt{2}} \right] \right\} . \qquad (2\text{-}121)$$

The use of the error function in Equation (2-121) provides the area under the Gaussian curve as described in Section 2.2, Equations (2-52) and (2-53).

The height of the plume (H) is calculated at the end of the cavity using Briggs' equation for gradual rise of a bent-over plume which contains both momentum and buoyancy components; refer to Equation (2-73). The vertical dispersion coefficient (σ_z) is calculated from an empirical relationship established by Wilson and Britter (1982)

$$\sigma_z = 0.21\, L_R^{0.25}\, x^{0.75} \tag{2-122}$$

where L_R is a building scaling length as discussed in the following.

According to Wilson (1976; 1979), the flow patterns around a building can be determined from the height (h_b) and width (h_w) of the upwind building face. The building scaling length (L_R), as defined by Wilson (1979), combines these dimensions and can be used to determine the maximum height (h_c) and length (x_c) of the cavity region of a building wake, as well as, the maximum height (h_r) and length (x_r) of roof top cavity zones. L_R is defined as

$$L_R \equiv B_S^{\frac{2}{3}}\, B_L^{\frac{1}{3}} \tag{2-123}$$

where B_S is the smaller and B_L is the larger of the building height (h_b) and projected building width (h_w) to the wind flow, i.e., $B_S = \min(h_b, h_w)$ and $B_L = \max(h_b, h_w)$. When B_L is larger than 8 B_S, then $B_L = 8\, B_S$ is used in Equation (2-123) (ASHRAE, 1993).

The maximum height of the roof top cavity zone is estimated by (Wilson, 1979)

$$h_r = 0.22\, L_R \tag{2-124}$$

which occurs at a downwind distance of $x = 0.5\ L_R$ from the building face. The length of the roof top cavity zone is estimated as (Wilson, 1979)

$$x_r = 0.9\ L_R . \tag{2-125}$$

If the length of the roof top cavity zone is less than or equal to the along-wind building length (i.e., $x_r \leq h_L$), then the roof cavity will reattach to the building and the height of the cavity region downwind of the lee side of the building is equal to the building height (Wilson and Britter, 1982), i.e.,

$$h_c = h_b . \tag{2-126}$$

If the roof cavity does not reattach to the building (i.e., $x_r > h_L$), then according to Wilson and Britter (1982)

$$h_c = h_b + h_r . \tag{2-127}$$

In the Schulman-Scire formulation, the length of the cavity region measured from the lee side of the building is based on an equation developed by Fackrell (1984) by means of wind tunnel measurements

$$x_c = \frac{1.8\ h_w}{\left(h_L / h_b\right)^{0.3} \left(1.0 + 0.24\ h_w / h_b\right)} . \tag{2-128}$$

In contrast, ASHRAE (1993) recommends an equation suggested by Wilson (1979) to predict the cavity region length

$$x_c = 1.0\ L_R . \tag{2-129}$$

2.4.3 Near-Wake and Far-Wake Regions

High ground-level concentrations due to plume downwash can also occur if the plume is caught in the wake regions. The EPA (1992b) recommends that concentrations within the near-wake and far-wake regions be predicted based on the work of Huber and Snyder (1976) and Schulman and Scire (Schulman and Hanna, 1986). The Huber-Snyder and Schulman-Scire formulations are incorporated into the EPA screening and refined modeling procedures for predicting concentrations in the near-wake and far-wake regions of a building wake.

A plume is assumed to be affected by the building wake if the plume height is less than the GEP stack height as determined using Equation (2-104). Otherwise, the plume is assumed to be unaffected by the building wake. The plume height is determined by the stack height plus gradual momentum plume rise. Neither gradual buoyancy plume rise nor stack tip downwash are considered in the plume height calculation. Gradual momentum plume rise is calculated at a distance of two building heights downwind from the lee side of the building (i.e., $x = 2\ h_b$) using Equation (2-76) or Equation (2-86).

If the plume height is less than the GEP stack height, then one of two algorithms are used to predict concentrations due to building wake effects depending on the building configuration with respect to the stack height. If the stack height is less than the building height plus one-half the lesser of the building height or projected width, then the Schulman-Scire formulation is used. Otherwise, the Huber-Snyder formulation is used. Restated in equation form:

- use the Huber-Snyder formulation if

$$h_b + 0.5\,L \leq h < h_b + 1.5\,L \tag{2-115}$$

- use the Schulman-Scire formulation if

$$h < h_b + 0.5\,L\,. \tag{2-116}$$

Huber-Snyder Formulation

In the Huber-Snyder formulation, the effects of building wakes on plume dispersion are accounted for by modifying the horizontal and vertical dispersion coefficients (σ'_y and σ'_z). These modifications are made for different building configurations to predict concentrations in the near-wake and far-wake regions of the building wake. The building configurations are classified as tall ($h_w < h_b$); squat ($1 \leq h_w / h_b \leq 5$); and very squat ($h_w / h_b > 5$). The cavity region of the building wake is assumed to be within 3 L downwind of the lee side of the building; the near-wake region extends from 3 L to 10 L; and the far-wake region extends beyond 10 L. The Huber-Snyder formulation does not contain an approach for predicting concentrations within the cavity region.

The basis of the Huber-Snyder formulation is the results of wind tunnel experiments (Huber and Snyder, 1976). The experiments are somewhat limited in that a specific atmospheric stability condition (between Pasquill category C and D) and a specific building shape and orientation (a projected building width of twice the building height) were simulated (EPA, 1992e). The wind tunnel experiments yielded the

horizontal and vertical dimensions of the plume for tall, squat, and very squat buildings at the start and end of the near-wake region (i.e., distances of 3 L and 10 L downwind from the lee side of the building, respectively).

Vertical plume dispersion in the near-wake. The vertical width of the plume was observed to be 1.5 L at the start of the near-wake region and 2.5 L at the end of the near-wake region for each building configuration (refer to Figure 2.54). The vertical dimension of a plume released near the ground can be roughly estimated as a plume half-width so that the Gaussian distribution is approximated by 2.15 σ. The enhanced vertical dispersion coefficient of the plume (σ'_z) is then given by

- at x = 3 L

$$\begin{aligned} 2.15\,\sigma'_z &= 1.5\,L \\ \sigma'_z &= 0.7\,L \end{aligned} \qquad (2\text{-}117)$$

- and at x = 10 L

$$\begin{aligned} 2.15\,\sigma'_z &= 2.5\,L \\ \sigma'_z &= 1.16\,L\,. \end{aligned} \qquad (2\text{-}118)$$

Interpolating for distances between 3 L and 10 L downwind leads to the formulation

$$\sigma'_z = 0.7\,L + 0.067\,(x - 3\,L)\,. \qquad (2\text{-}119)$$

For a tall building, L is defined by the building width (h_w) and for squat and very-squat buildings, L is defined by the building height (h_b). Making these substitutions into Equation (2-119) yields the Huber-Snyder formulas for calculating σ_z within the near-wake region of a building wake for tall, squat, and very-squat buildings

- tall building ($h_b > h_w$)

$$\sigma'_z = 0.7\, h_w + 0.067\,(x - 3\, h_w) \quad \text{for } 3\, h_w \le x < 10\, h_w \tag{2-120}$$

- squat building ($1 \le h_w / h_b \le 5$) and very-squat building ($h_w / h_b > 5$)

$$\sigma'_z = 0.7\, h_b + 0.067\,(x - 3\, h_b) \quad \text{for } 3\, h_b \le x < 10\, h_b\,. \tag{2-121}$$

The vertical dispersion coefficient is modified to account for building wake effects on plume dispersion if the plume height to building height ratio is less than 2.5 (i.e., $H / h_b < 2.5$).

Horizontal plume dispersion in the near-wake. The horizontal width of the plume for a tall and squat building was observed to be one and one-half times the building width ($1.5\ h_w$) at the start of the near-wake region (refer to Figure 2.55). For a very squat building, the height is quite small compared to the width and there is less resistance to air flow over the building than around the building. Consequently, for a stack located away from the ends of the building, the horizontal width of the plume at the start of the near-wake region was observed to be one and one-half times the building height ($1.5\ h_b$). By locating the stack within $2.5\ h_b$ of the ends of a very squat building, the horizontal width of the plume was observed to be seven and one-half times the building height ($7.5\ h_b$). At the end of the near-wake region (i.e., 10 L downwind), the horizontal width of the plume was observed to be $3.5\ h_w$ for a tall building; $1.5\ h_w + 2.0\ h_b$ for a squat building; $3.5\ h_b$ for a very squat building if the stack is located away from the ends of the building; and $9.5\ h_b$ for a very squat building if the stack is within $2.5\ h_b$ of the ends of the building.

Interpolating for distances between 3 L and 10 L downwind and using the Gaussian definition of the horizontal width of a plume from edge to edge as 4.3 σ yields the Huber-Snyder formulas for calculating enhanced σ_y within the near-wake region of a building wake for tall, squat, and very-squat buildings

- tall building ($h_b > h_w$)

$$\sigma'_y = 0.35\, h_w + 0.067\,(x - 3\, h_w) \quad \text{for } 3\, h_w \le x < 10\, h_w \tag{2-122}$$

- squat building ($1 \le h_w / h_b \le 5$)

$$\sigma'_y = 0.35\, h_w + 0.067\,(x - 3\, h_b) \quad \text{for } 3\, h_b \le x < 10\, h_b \tag{2-123}$$

- very-squat building ($h_w / h_b > 5$)

$$\sigma'_y = 0.35\, h_b + 0.067\,(x - 3\, h_b) \quad \text{for } 3\, h_b \le x < 10\, h_b \tag{2-124}$$

denoted as the "upper bound" estimate, applicable if the stack is located away from the ends of the building or

$$\sigma'_y = 1.75\, h_b + 0.067\,(x - 3\, h_b) \quad \text{for } 3\, h_b \le x < 10\, h_b \tag{2-125}$$

denoted as the "lower bound" estimate, applicable if the stack is located within 2.5 h_b of the ends of the building.

The horizontal dispersion coefficient is modified to account for building wake effects on plume dispersion if the plume height to building height ratio is less than or equal to 1.2 (i.e., $H / h_b \le 1.2$).

Plume dispersion in the far-wake. In the far-wake region of a building wake, plume dispersion is simulated by a volume source (refer to Section 2.2.12). The

enhanced plume growth caused by the building wake is accounted for by initializing the horizontal and vertical plume width to values at 10 L downwind. A virtual distance x_y is calculated so that the lateral spread of the plume accounts for the initial horizontal width and a virtual distance x_z is calculated so that the vertical spread of the plume accounts for the initial vertical width. The respective virtual distances are added to the downwind distance x to calculate the enhanced horizontal and vertical dispersion coefficients, i.e.,

$$\sigma'_y = \sigma_y\left(x + x_y\right) \tag{2-126}$$

and

$$\sigma'_z = \sigma_z\left(x + x_z\right) \tag{2-127}$$

for $x \geq 10$ L.

Schulman-Scire Formulation

Schulman and Hanna (1986) proposed three refinements to the Huber-Snyder building wake algorithm as implemented by the EPA, namely: 1) compute σ'_z as a linear decreasing function of plume height; 2) account for reduced plume rise due to the large initial plume dilution; and 3) account for the building height and projected width as a function of wind direction. The most significant of these refinements is plume rise during downwash conditions based on the work of Schulman and Scire (1980). Because of this, the implementation of all three refinements is generally referred to as the Schulman-Scire formulation.

Vertical plume dispersion. Regarding the first refinement, Schulman and Hanna (1986) concluded that it is important to compute σ'_z as a continuous function of plume height. The attempt is to improve a perceived flaw in the Huber-Snyder formulation that assumes the full effect of the building wake on plume dispersion occurs abruptly at a plume height less than the GEP stack height. This assumption leads to a discontinuity that had not been observed in the wind tunnel experiment conducted by Huber and Snyder (1982). To improve the computation of σ'_z, Schulman and Hanna developed a linear decay factor (A) to be incorporated in Equations (2-119) and (2-127), i.e.,

$$\sigma'_z = A\left[\, 0.7\,L + 0.067\,(x - 3\,L)\,\right] \quad \text{for } 3\,L \le x < 10\,L \tag{2-128}$$

and

$$\sigma'_z = A\left[\, \sigma_z(x + x_z)\,\right] \quad \text{for } x \ge 10\,L\,. \tag{2-129}$$

The linear decay factor ranges from 1 when the plume height is less than or equal to the building height (i.e., A = 1 for $H \le h_b$) to 0 when the plume height is greater than or equal to the building height plus twice the lesser of the building height or projected width (i.e., A = 0 for $H > h_b + 2\,L$). For plume heights between h_b and $h_b + 2\,L$, A is given by

$$A = \frac{h_b - H}{2\,L} + 1\,. \tag{2-130}$$

A graph of the linear decay factor as a function of plume height for a squat building (i.e., $L = h_b$) is given in Figure 2.56. The graph provides a comparison of the Huber-Snyder and Schulman-Scire formulations in computing σ'_z. There is a practical limit on the value of A since the EPA implements the Schulman-Scire formulation only

when $h < h_b + 0.5\ L$. For $h_b + 0.5\ L \leq h < h_b + 0.5\ L$, the Huber-Snyder formulation is used and effectively, A = 1. Consider a source with minimal plume rise (i.e., h = H) in the wake of a squat building. Substituting $H < h_b + 0.5\ L$ into Equation (2-130) yields the lower applicable limit for A of 0.75. Because of the way the Schulman-Sire formulation is implemented by the EPA, the original discontinuity Schulman and Hanna attempted to correct still exists. An additional discontinuity is introduced for stack heights near the cross-over point between the wake formulations, i.e., $h \cong h_b + 0.5\ L$ (refer to Figure 2.56).

Reduced plume rise due to building wake effects. The increased mechanical turbulence in a building wake enlarges the horizontal and vertical dimensions of a plume. The result of this enhanced dispersion is a large initial entrainment of ambient air into the plume which reduces the buoyancy and thus the rise of the plume. The increased mechanical turbulence caused by the building decays rapidly with distance downwind. Consequently, the effect of the building is to initially increase entrainment of ambient air into the plume but not change the subsequent rate of entrainment.

If $\sigma_y > \sigma_z$, then the initial shape of the plume can be approximated by a finite line source of horizontal length L_0 and vertical width 2 R_0 with half-circular ends (refer to Figure 2.57). Otherwise, if there is little or no enhancement of horizontal dispersion or if $\sigma_z > \sigma_y$, then the initial shape of the plume can be represented by a circle of radius R_0. The initial dimensions of the downwashed plume are related to the horizontal and vertical dispersion coefficients, i.e.,

$$R_0 = \sqrt{2}\ \sigma_z \text{ and} \qquad (2\text{-}131)$$

$$L_0 = \sqrt{2\,\pi}\left(\sigma_y - \sigma_z\right) \quad \text{for } \sigma_y > \sigma_z \quad \text{or}$$
$$L_0 = 0 \qquad\qquad\qquad\quad \text{for } \sigma_y \le \sigma_z \,. \tag{2-132}$$

The factor $\sqrt{2}$ in Equation (2-131) converts the Gaussian σ_z to an equivalent uniform circular distribution and the factor $\sqrt{2\,\pi}$ in Equation (2-132) converts the Gaussian σ_y to an equivalent uniform rectangular distribution. Both σ_y and σ_z are evaluated at x = 3 L and are taken as the larger of the building enhanced sigmas and the rural or urban sigmas. The linear decay factor (A) is used in computing the building enhanced σ_z.

The plume rise of a downwashed finite line source was solved by Schulman and Scire (1980) in the Buoyant Line and Point Source (BLP) model. Several terms were added to the Briggs plume rise formula to account for the rise of a buoyant finite line source plume; the rise of a buoyant point source plume with downwash; and the rise of a buoyant finite line source plume with downwash.

The rise of the rectangular portion of a buoyant finite line source plume of length L_0 for neutral atmospheric conditions is given by Schulman and Scire (1980)

$$z^2 = \frac{1}{2\,\beta_a\,L_0}\frac{\pi\,F_b}{u^3}\,x^2 \,. \tag{2-133}$$

Equation (2-133) is for the rectangular portion of the plume only and neglects the horizontal entrainment of ambient air at the edges of the plume as denoted by the two half-circular ends in Figure 2.57. The equation establishes a linear dependence of rectangular plume rise with distance which reflects a decreased ability of a rectangular plume to entrain ambient air.

The solution of the plume rise equation given by Schulman and Scire (1980) for a buoyant finite line source with entrainment at the edges of the plume for neutral atmospheric conditions is

$$z^3 + \frac{3\,L_0}{\pi\,\beta_a}\,z^2 = \frac{3}{2\,\beta_a^2}\,\frac{F_b}{u^3}\,x^2 \,. \tag{2-134}$$

With $L_0 = 0$, the equation reduces to the Briggs formula for gradual rise of a buoyant point source plume. The second term in Equation (2-134) accounts for the rise of the rectangular portion of the buoyant finite line source plume. The coefficient $(3L_0/\pi\beta_a)$ represents the ratio of the point source and rectangular source buoyancy components, i.e.,

$$\left[\frac{\dfrac{3}{2\,\beta_a^2}\,\dfrac{F_b}{u^3}\,x^2}{\dfrac{1}{2\,\beta_a\,L_0}\,\dfrac{\pi\,F_b}{u^3}\,x^2}\right] z^2 = \frac{3\,L_0}{\pi\,\beta_a}\,z^2 \,. \tag{2-135}$$

Similar terms were developed by Schulman and Scire (1980) to account for downwash of a buoyant point source plume, i.e.,

$$\frac{3\,R_0}{\beta_a}\,z^2 + \frac{3\,R_0^2}{\beta_a^2}\,z \tag{2-136}$$

and downwash of a buoyant finite line source plume, i.e.,

$$\frac{6\,R_0\,L_0}{\pi\,\beta_a^2}\,z \,. \tag{2-137}$$

In implementing the Schulman and Scire formula to compute the gradual rise of a downwashed finite line source plume for unstable and neutral atmospheric conditions, the

EPA (1992e) incorporated all of the terms developed by Schulman and Scire into an equation that also takes into account the momentum component, i.e.,

$$z^3 + \frac{3\,L_0}{\pi\,\beta_a}\,z^2 + \left(\frac{3\,R_0}{\beta_a}\,z^2 + \frac{3\,R_0^2}{\beta_a^2}\,z\right) + \frac{6\,R_0\,L_0}{\pi\,\beta_a}\,z = \frac{3\,F_b}{2\,\beta_a^2\,u^3}\,x^2 + \frac{3\,F_m}{\beta_j^2\,u^2}\,x \quad . \quad (2\text{-}138)$$

Equation (2-138) reduces to the Briggs formula for gradual rise of a bent-over plume when the line source length and downwash effects are negligible (i.e., L_0 and R_0 approach zero).

The formula for gradual rise of a downwashed finite line source plume for stable atmospheric conditions is (EPA, 1992e)

$$z^3 + \frac{3\,L_0}{\pi\,\beta_a}\,z^2 + \left(\frac{3\,R_0}{\beta_a}\,z^2 + \frac{3\,R_0^2}{\beta_a^2}\,z\right) + \frac{6\,R_0\,L_0}{\pi\,\beta_a}\,z = \frac{3\,F_b}{2\,\beta_a^2\,u^3}\,x^2 + \frac{3\,F_m}{\beta_j^2\,u\,\sqrt{s}}\,\sin\left(\frac{\sqrt{s}\,x}{u}\right) \quad (2\text{-}139)$$

with a maximum stable buoyant rise given by (EPA, 1992e)

$$z^3 + \frac{3\,L_0}{\pi\,\beta_a}\,z^2 + \left(\frac{3\,R_0}{\beta_a}\,z^2 + \frac{3\,R_0^2}{\beta_a^2}\,z\right) + \frac{6\,R_0\,L_0}{\pi\,\beta_a}\,z = \frac{6\,F_b}{\beta_a^2\,u\,s} \quad . \quad (2\text{-}140)$$

The larger of the buoyant and moment rise is selected for the plume height calculations in the Schulman-Scire formulation as implemented by the EPA. This is determined separately by alternately setting F_b or F_m equal to zero and solving the cubic equation for z (i.e., Δh).

Direction-specific building dimensions. Schulman and Hanna (1986) also noted the importance specifying building height and projected width as a function of wind direction in refined modeling applications. This importance was reflected for an example

building configuration of an east-west width of 15 m, a north-south width of 30 m, and a height of 20 m. For winds out of the east or west, the dispersion enhancement calculations are for a tall building since the building height (20 m) is greater than the projected width (15 m). For winds out of the north or south, the dispersion enhancement calculations are for a squat building since the building height (20 m) is less than the projected width (30 m). Schulman and Hanna recommended that the building height and projected width be specified for each 10 degrees of wind direction so that the appropriate set of dispersion enhancement equations are matched with the building configuration. EPA implemented this recommendation in the Schulman-Scire formulation *and* the Huber-Snyder formulation of the ISCST2 model (EPA, 1992e). The EPA (1993b) has developed the computer program BPIP to calculate the direction-specific building heights and direction-specific building widths needed as input to the ISCST2 model.

2.4.4 Road Map for Enhanced Dispersion Due to Building Wake Effects

Table 2.18 provides a road map of the equations employed in the EPA-guideline air dispersion models for predicting enhanced horizontal and vertical dispersion coefficients (σ'_y and σ'_z) in the near-wake region of a building. Different sets of equations are used depending on the building configuration. The horizontal dispersion coefficient is modified if the building wake plume height (H_{wake}) is less than or equal to 1.2 times the building height (h_b). The building wake plume height is the stack height (h) plus the momentum plume rise at two building heights downwind (Δh_m at $x = 2\ h_b$). The vertical

dispersion coefficient is modified if the building wake plume height is less than 2.5 times the building height. The vertical dispersion coefficient is further modified for building wake plume heights between h_b and $h_b + 0.5$ L.

2.5 COMPLEX TERRAIN

Complex terrain refers to terrain that extends above the stack top. Complex terrain is an important consideration in air dispersion modeling because under stable atmospheric conditions high concentrations can occur due to plume impingement on elevated terrain.

The EPA's general method for predicting ground-level concentrations in complex terrain is to modify the flat terrain Gaussian plume model. This provides a very simple approximation of the complicated interactions between plume dispersion and elevated terrain. The fundamental hypothesis of the method allows for the plume centerline to approach and partially or fully intercept elevated terrain. The basic formulations only account for plume interception of elevated terrain and not the flow about the terrain feature. The more complicated formulations predict whether the plume intercepts the terrain to some degree and/or flows over and around the terrain feature.

Presented in this section are the rudimentary concepts of plume dispersion in complex terrain. The recommendations adopted by the EPA for predicting concentrations in complex terrain are discussed.

2.5.1 EPA Recommendations

There are a number of screening techniques currently recommended by the EPA (1993a; 1987a; 1986) for predicting concentrations in complex terrain. These include: 1) the Valley screening technique (EPA, 1977b); 2) the CTSCREEN model (EPA, 1990); 3) the COMPLEX I model (EPA, 1992d); 4) the SHORTZ and LONGZ models (EPA, 1982); and 5) the Rough Terrain Dispersion Model (RTDM) (Environmental Research and Technology, 1987). For refined concentration predictions, the EPA recommends the use of an air dispersion model called CTDMPLUS (EPA, 1989) which was developed from their Complex Terrain Model Development (CTDM) project (EPA, 1987b).

According to EPA recommendations, the Valley screening technique may be used to predict 24-hour average concentrations for both rural and urban applications. The Valley screening technique utilizes built-in worst-case assumptions for meteorology. The model accounts for plume interception of elevated terrain but not the flow about the terrain feature. Comparable concentration predictions can be obtained by using the Valley-equivalent option contained in the COMPLEX I model or the SCREEN2 model (EPA, 1992c).

The CTSREEN model is a screening version of the CTDMPLUS model. It utilizes built-in worst-case assumptions for meteorology. The model requires the terrain data to be digitized and preprocessed so that flow about the terrain feature can be predicted.

The COMPLEX I model combines the terrain adjustment assumptions of the MPTER model (EPA, 1980) and Valley model. The EPA recommends using the COMPLEX I model for predicting concentrations in rural areas for all averaging times. The COMPLEX I model accesses one year of sequential hourly meteorology.

The SHORTZ and LONGZ models are recommended by the EPA for predicting concentrations in urban areas for short-term averages and long-term averages, respectively. Like the Valley model, SHORTZ and LONGZ account for plume interception of elevated terrain but not the flow about the terrain feature. The SHORTZ model accesses one year of sequential hourly meteorology; the LONGZ model accepts meteorology compiled in statistical data summaries.

RTDM is recommended by the EPA for predicting concentrations in rural areas for all averaging times. The model accesses one year of sequential hourly meteorology. Like the CTSCREEN model, RTDM can account for flow about the terrain feature.

The EPA has defined three terrain regimes that need to be considered when performing air dispersion modeling: complex terrain, intermediate terrain, and simple terrain. Complex terrain refers to terrain higher than stack top. Intermediate terrain is a subset of complex terrain and refers to terrain higher than stack top but lower than plume height. Simple terrain refers to terrain lower than stack top. A depiction of complex, intermediate, and simple terrain regimes is given in Figure 2.58.

The EPA (1993a) has adopted a policy governing the use of air dispersion models in these three terrain regimes:

> "The Valley model, COMPLEX I, SHORTZ/LONGZ, and RTDM should be used only to estimate concentrations at receptors whose elevations are greater than or equal to plume height. For receptors at or below stack height, a simple terrain model should be used. Receptors between stack height and plume height present a unique problem since none of the above models were designed to handle receptors in this narrow regime, the definition of which will vary hourly as meteorological conditions vary. CTSCREEN may be used to estimate concentrations under all stability conditions at all receptors located 'on terrain' above stack top, but has limited applicability in multi-source situations. As a result, the estimation of concentrations at receptors between stack height and plume height should be considered on a case-by-case basis after consultation with the EPA Regional Office; the most appropriate technique may be a function of the actual source(s) and terrain configuration unique to that application. One technique that will be generally acceptable, but is not necessarily preferred for any specific application, involves applying both a complex terrain model (except for the Valley model) and a simple terrain model. The Valley model should not be used for any intermediate terrain receptor. For each receptor located between stack height and plume height, an hour-by-hour comparison of concentration estimates from both models is made. The higher of the two modeled concentrations should be chosen to represent the impact at that receptor for that hour, and then used to compute the concentration for the appropriate averaging time(s). For the simple terrain models, terrain may have to be 'chopped off' at stack height, since these models are frequently limited to receptors no greater than stack height."

This policy has become to be known as the EPA's intermediate terrain policy. Even though the EPA has implemented the intermediate terrain policy, there is currently no EPA-guideline air dispersion model that meets the explicit requirements of the policy for all types of land use.

To better understand the EPA's methods for predicting ground-level concentrations in complex terrain, the basic formulations of the Valley model, the COMPLEX I model, and the SHORTZ model are described.

2.5.2 Valley Model

The Valley model was developed to predict the likely maximum 24-hour average ground-level concentrations that would occur during a year due to isolated sources in rural complex terrain. The model does not characterize the flow of the plume about the terrain feature rather it links a particular set of meteorological conditions with high short-term concentrations on complex terrain. According to the Valley formulation, short-term concentrations on complex terrain are highest when light winds and stable atmospheric conditions occur for several hours of the day. The algorithm represents a fanning plume where the horizontal spread of the plume far exceeds its vertical spread (refer to Section 2.1.1). Although the Valley model has the capability of predicting long-term concentrations based on meteorology compiled in statistical data summaries, the EPA (1993a; 1987a; 1986) recommends that the model be used only to predict 24-hour average concentrations.

The Valley model was developed to predict the dispersion of pollutants from large non-ferrous smelters located in the mountainous terrain of the Western U.S. The basis for the meteorological conditions built into the Valley model was, therefore, an analysis of upper air summaries of wind speed and atmospheric stability for the Western U.S. From plume rise calculations, it was determined that the heights of smelter plumes in a stable atmosphere would not likely exceed 400 m. Wind speeds aloft of 2.5 m/s ± 1.0 m/s were found to occur a third of the time or more at most of the upper air stations examined. A wind speed of 2.5 m/s and F stability are taken to represent the worst-case meteorological

conditions for plume dispersion in rural complex terrain. Furthermore, it is assumed that the 2.5 m/s wind speed and F stability will persist for any given wind direction for any 6 hours of a 24-hour period. No adjustments for wind speed variation with height are made in the model.

With respect to its treatment of terrain effects on plume dispersion, the Valley model assumes that the plume height with respect to the stack base elevation remains constant for stable atmospheric conditions after final rise is achieved. It is further assumed that the plume can approach elevated terrain but that the plume centerline can come no closer than 10 m to the ground surface. If the terrain extends above the original plume height, the plume centerline is adjusted so that it remains 10 m above the ground. Figure 2.59 provides an illustration of the concept. If a plume height is initially within 10 m of the ground, it is assumed to remain at its initial height above the ground regardless of the downwind terrain elevation.

Once a plume has encountered a terrain feature, it is assumed to have a blocking effect on the air flow. The plume is assumed to be deflected upward and to the sides of the ridge. An empirical attenuation factor is used to reduce the predicted concentration as a function of height above the point where the plume centerline initially intercepts the terrain feature. The factor has a value of one at and below this point and decreases linearly with increasing height to zero at and beyond 400 m above this point; refer to Figure 2.59.

The dispersion equations used in the Valley model were developed from the Gaussian plume equations that account for plume trapping. To depict a fanning plume, the horizontal distribution of the plume is assumed to be uniform (i.e., non-Gaussian) over a 22.5° wind sector. Wind direction data is commonly referenced to 16 points of a compass (i.e., N, NNE, NE, etc.) thus explaining the sector width of 22.5° (i.e., 360°/16). The vertical distribution of the plume in the Valley model is based on the Pasquill-Gifford vertical dispersion coefficients as illustrated in Figure 2.12.

The plume rise equations used in the Valley model are based on Briggs' formulas for gradual and final rise of buoyant plumes. Momentum plume rise is not considered in the Valley model; neither is stack-tip downwash. The model contains an option for accounting for vertical buoyancy-induced dispersion ($\sigma_{z_{BID}}$).

When using the Valley screening technique for urban areas, the EPA recommends that E stability be substituted for F stability in the concentration predictions. Urban dispersion coefficients are not contained in the Valley model; as a result, concentration predictions for urban areas are based on rural dispersion coefficients.

2.5.3 COMPLEX I Model

The COMPLEX I model is a modification of MPTER model that includes the Valley assumption for plume impingement on complex terrain. MPTER is an acronym for Multiple Point source with TERrain adjustments. MPTER is the EPA's first air dispersion model to provide concentration predictions for multiple sources accounting for

small changes in terrain elevations. The MPTER model is limited to terrain applications where the receptor ground-level elevations are no higher than the elevation of the lowest stack top. The Valley formulation was incorporated into the MPTER model to provide the capability of predicting concentrations at receptors located on terrain higher than stack top.

One of the main advantages of the COMPLEX I model over the Valley model is that it does not have to rely on built-in worst-case assumptions of meteorology for the concentration predictions. Instead, the model can provide concentration predictions based on hour-by-hour measurements of meteorology representative of the dispersion conditions of the area. When used with a year of sequential hourly meteorological measurements, the COMPLEX I model provides concentration predictions for short-term (i.e., 1-hour to 24-hour) as well as long-term (i.e., annual) averaging times.

The COMPLEX I model combines the MPTER and Valley formulations to account for terrain effects on plume dispersion. From the MPTER formulation, the COMPLEX I model simulates plume behavior in the vicinity of complex terrain through the use of terrain adjustment factors. Terrain adjustment factors (F_T) are used to alter the plume height with respect to the terrain elevation. They are entered as a function of atmospheric stability and range from 0 for the plume to fully intercept elevated terrain to 1 for no terrain effects.

A value of $F_T = 1$ is equivalent to assuming flat terrain. It simulates a plume that remains at a constant height with respect to the terrain elevation so that the plume fully

rises over the elevated terrain. A value of $F_T = 0$ simulates a plume that levels off; remains at a constant height with respect to the stack base elevation; and fully intercepts terrain that rises above the plume centerline. When $F_T = 0$, the minimum separation distance between the plume centerline and the ground surface (H_{min}) can be specified (adapted from the Valley formulation). The EPA (1993a; 1987a; 1986) recommends using $F_T = 0.5$ for stability classes A through D; $F_T = 0$ for stability classes E and F; and $H_{min} = 10$ m.

The plume height used in the dispersion equations of the COMPLEX I model is adjusted to account for terrain effects. Two methods are used. First, from the MPTER model, the plume height (H) is determined by

$$H = H_{flat} - \Delta E(1 - F_T) \tag{2-141}$$

where H_{flat} is the plume height for flat terrain (i.e., stack height plus plume rise) and ΔE is the terrain elevation of the receptor above the stack base elevation. The MPTER method of altering the plume height with respect to the terrain elevation is depicted in Figure 2.60 for three values of F_T. Next, the plume height is determined by the product of the plume height for flat terrain and the terrain adjustment factor. The maximum value of plume height from the two calculations is used in the dispersion equations, i.e.,

$$H = \max\left\{ \left(H_{flat} \times F_T\right), \left[H_{flat} - \Delta E(1 - F_T) \right] \right\}. \tag{2-142}$$

The attenuation factor from the Valley model is employed by the COMPLEX I model to account for the blocking effect of the terrain on the air flow. The attenuation factor is used to predict hourly concentrations for stable atmospheric conditions. The

effect of the attenuation factor is to reduce the predicted concentration as a function of plume height above the point where the plume centerline intercepts the elevated terrain. The attenuation factor (A_F) is given by

$$A_F = \frac{400 - (\Delta E + z - H_{flat})}{400} . \quad (2\text{-}143)$$

where z is the receptor height above the ground. For $H_{flat} \geq (\Delta E + z)$, $A_F = 1.0$ and for $(\Delta E + z - H_{flat}) \geq 400$, $A_F = 0$.

The dispersion equations used in the COMPLEX I model were developed from the Gaussian plume equations that account for plume trapping. The horizontal distribution of the plume is assumed to be uniform (i.e., non-Gaussian) over a 22.5° wind sector. This assumption was used in the Valley model to simulate a fanning plume which is indicative of stable atmospheric conditions. In the COMPLEX I model, however, the horizontal plume width (W_P) is based on the crosswind arc length of a 22.5° wind sector for all atmospheric conditions.

By assuming the plume is uniformly distributed in the horizontal, W_P can be substituted for $\sqrt{2\pi}\,\sigma_y$ in the Gaussian plume equations so that

- for distances of $x < x_m$

$$\chi(x, y, z; H) = \frac{Q}{\sqrt{2\pi}\, u\, W_P\, \sigma_z} \left\{ \exp\left[-\frac{1}{2}\left(\frac{z - H}{\sigma_z} \right)^2 \right] + \exp\left[-\frac{1}{2}\left(\frac{z + H}{\sigma_z} \right)^2 \right] \right\} \quad (2\text{-}144)$$

- for distances of $x_m \le x < 4\ x_m$

$$\chi(x,y,z;H) = \frac{Q}{\sqrt{2\pi}\,u\,W_p\,\sigma_z}\left\{\exp\left[-\frac{1}{2}\left(\frac{z-H}{\sigma_z}\right)^2\right]+\exp\left[-\frac{1}{2}\left(\frac{z+H}{\sigma_z}\right)^2\right]\right\}$$

$$+\sum_{i=1}^{\infty}\left\{\exp\left[-\frac{1}{2}\left(\frac{z-(2i\,H_m-H)}{\sigma_z}\right)^2\right]+\exp\left[-\frac{1}{2}\left(\frac{z+(2i\,H_m-H)}{\sigma_z}\right)^2\right]\right.$$

$$\left.+\exp\left[-\frac{1}{2}\left(\frac{z-(2i\,H_m+H)}{\sigma_z}\right)^2\right]+\exp\left[-\frac{1}{2}\left(\frac{z+(2i\,H_m+H)}{\sigma_z}\right)^2\right]\right\} \qquad (2\text{-}145)$$

- and for distances of $x \ge 4\ x_m$

$$\chi(x,y,z;H) = \frac{Q}{u\,W_p\,H_m}\ . \qquad (2\text{-}146)$$

The crosswind arc length of a 22.5° wind sector is $2\pi/16$ x which defines the horizontal plume width as a function of downwind distance. Figure 2.61 depicts how the horizontal plume widths of the COMPLEX I model compare to the Pasquill-Gifford horizontal dispersion coefficients (i.e., σ_y). The vertical distribution of the plume is based on the Pasquill-Gifford vertical dispersion coefficients as provided in Figure 2.12 and Table 2.10. The transport wind speed is calculated using Equation (2-24) considering the variation of wind speed with height.

The plume rise equations used in the COMPLEX I model are based on Briggs' formulas for gradual and final plume rise. Both buoyancy and momentum plume rise are considered based on the equations summarized in Table 2.17. The model also contains

options for accounting for stack-tip downwash using Equation (2-99) and vertical buoyancy-induced dispersion using Equations (2-101) and (2-103).

The COMPLEX I model contains a Valley-equivalent mode where 24-hour average concentrations are predicted in a manner similar to the short-term screening mode of the Valley model. The main assumptions employed by the COMPLEX I model in the Valley screening mode are:

- worst-case short-term meteorological conditions are represented by a wind speed of 2.5 m/s and F stability and will persist for any given wind direction for any 6 hours of a 24 hour period;
- no adjustments for wind speed variation with height and surface roughness are made;
- after final rise is achieved, the plume height remains constant with respect to the stack base elevation and the plume centerline can approach complex terrain but come no closer than 10 m to the ground surface; and
- deflection of the plume by the terrain is simulated by an attenuation factor that ranges from 1 at and below the point where the plume centerline initially intercepts the terrain to 0 at and beyond 400 m above this point.

2.5.4 SHORTZ Model

The SHORTZ model is similar to the COMPLEX I model in that concentration predictions can be based on hour-by-hour measurements of meteorology representative of

the dispersion conditions of the area. When used with a year of sequential hourly meteorological measurements, the SHORTZ model provides concentration predictions for short-term as well as long-term averaging times. Although the model has both rural and urban modes for simple and complex terrain, the EPA (1993a; 1987a; 1986) recommends that the SHORTZ model be used only to predict concentrations for urban complex terrain applications.

The SHORTZ model simulates the interaction of the plume and complex terrain in a manner similar to that of the Valley model. The plume is assumed to remain at the constant height of final plume rise and fully intercept terrain that rises above the plume centerline. Unlike the Valley model, there is no minimum separation distance between the plume centerline and the ground. The plume centerline is allowed to intercept the ground surface.

The dispersion equations used in the SHORTZ model were developed from the Gaussian plume equations that account for plume trapping as summarized in Table 2.14. The dispersion coefficients used in the SHORTZ model are based on the work of Cramer (1957, 1976). The horizontal and vertical dispersion coefficients (σ_y and σ_z) are directly related to the standard deviations of the horizontal (σ_A) and vertical (σ_E) wind direction fluctuations, respectively. A simple power law expression with distance that includes the effects of the initial source dimensions is used. The horizontal dispersion coefficient is given by

$$\sigma_y = \sigma_A \, x_{ry} \left[\frac{x + x_y - x_{ry}(1-\alpha)}{\alpha \, x_{ry}} \right]^{\alpha} \tag{2-147}$$

where σ_y is in m; σ_A is in radians; x_{ry} is specified by Cramer et al. (1972) as the distance in m over which rectilinear lateral plume expansions occurs downwind from an ideal point source (= 50 m based on diffusion experiments); x is in m; x_y is the virtual distance in m to account for the initial horizontal source dimension (= 0 for a point source); and α is specified by Cramer et al. (1972) as the horizontal diffusion coefficient (= 0.9). The vertical dispersion coefficient is given by

$$\sigma_z = \sigma_E (x + x_z)^{\varphi} \tag{2-148}$$

where σ_z is in m; σ_E is in radians; x is in m; x_z is the virtual distance in m to account for the initial vertical source dimension (= 0 for a point source); and φ is specified by Cramer et al. (1972) as the vertical diffusion coefficient (= 1).

The SHORTZ model is designed to read hourly σ_A and σ_E measurements calculate the appropriate σ_y and σ_z values. If measurements of only σ_A or σ_E are available, then the missing parameter can be based on the measured parameter by the following approximate relationship (EPA, 1982)

$$\sigma_A \cong 1.43 \, \sigma_E \, . \tag{2-149}$$

If σ_A and σ_E measurements are not available, values can be approximated based on the Pasquill stability category. Default values of σ_A and σ_E as a function of Pasquill stability category are provided in Table 2.19 for rural and urban areas. The default σ_A and σ_E

values for urban areas are based on the rural values but for the stability category one step more unstable than the indicated stability category.

Rural σ_y and σ_z curves used in the SHORTZ model based on the default values of σ_A and σ_E are provided in Figures 2.62 and 2.63, respectively. Also plotted for comparative purposes are the Pasquill-Gifford dispersion curves. In a similar manner, urban σ_y and σ_z curves used in the SHORTZ model based on the default values of σ_A and σ_E are provided in Figures 2.64 and 2.65, respectively. Plotted for comparative purposes are the McElroy-Pooler dispersion curves.

Using Equation (2-24), the observed mean wind speed is adjusted from the measurement height to the source height for the plume rise calculations and to the final plume height for the concentration predictions. Default values of the wind profile exponents built into the SHORTZ model are given in Table 2.20.

The plume rise equations of the SHORTZ model are derived from the buoyancy terms of Briggs' formulas, namely:

- for unstable and neutral atmospheric conditions

$$\Delta h = \left(\frac{3}{2\beta^2} \frac{F_b}{u^3} x^2 \right)^{\frac{1}{3}} \tag{2-150}$$

- for stable atmospheric conditions

$$\Delta h = \left\{ \frac{3 F_b}{\beta^2 u \, s/S_2} \left[1 - \cos\left(\sqrt{\frac{s}{S_2}} \frac{x}{u} \right) \right] \right\}^{\frac{1}{3}}. \tag{2-151}$$

Buoyancy effects alone are considered in calculating plume rise in the SHORTZ model; momentum effects on plume rise are not considered. In addition, only final plume rise is calculated in the model and assumed to be attained at the stack location. Gradual plume rise is not considered; neither is buoyancy-induced dispersion.

To obtain the equations used in the SHORTZ model for final plume rise, it is assumed that final rise is attained at a distance of ten stack heights downwind (i.e., x = 10 h). The distance to final rise of 10 h was originally proposed by Briggs (1969). This assumption is different than subsequently recommended by Briggs (1971) and generally adopted in other EPA air dispersion models as discussed in Section 2.2.1. Moreover, in the SHORTZ model different values of β are used for unstable/neutral atmospheric conditions versus stable atmospheric conditions. For unstable/neutral atmospheric conditions, β is denoted as γ_1 (the adiabatic entrainment coefficient) and is taken to equal 0.6 (Briggs, 1972); for stable atmospheric conditions, β is denoted as γ_2 (the stable entrainment coefficient) and is taken to equal 0.66 (Briggs, 1972). Incorporated into the plume rise equation for unstable and neutral atmospheric conditions is a factor (f_s) that accounts for stack-tip downwash. Omitted from the plume rise equation for stable atmospheric conditions is the term S_2. The resulting equations for final plume rise are:

- for unstable and neutral atmospheric conditions (i.e., $\partial\theta/\partial z \leq 0$)

$$\Delta h = \left[\frac{3}{2\,\gamma_1^2} \frac{F_b}{u^3} (10\,h)^2 \right]^{\frac{1}{3}} f_s \qquad (2\text{-}152)$$

where f_s is the Cramer et al. (1975) stack-tip downwash correction factor that is used to limit the plume rise as the mean wind speed at stack height approaches or exceeds the exit gas velocity, i.e.,

$$f_s = 1 \qquad \text{if } u \le \frac{v_s}{1.5}$$

$$f_s = \frac{3\,v_s - 3\,u}{v_s} \qquad \text{if } \frac{v_s}{1.5} < u < v_s \qquad (2\text{-}153)$$

$$f_s = 0 \qquad \text{if } u \ge v_s$$

- for stable atmospheric conditions (i.e., $\partial\theta/\partial z > 0$)

$$\Delta h = \left\{ \frac{3\,F_b}{\gamma_2^2\,u\,s}\left[1 - \cos\left(\frac{\sqrt{s}}{u} 10\,h \right) \right] \right\}^{\frac{1}{3}} \qquad \text{if } \frac{\pi\,u}{\sqrt{s}} \ge 10\,h \qquad (2\text{-}154)$$

$$\Delta h = \left(\frac{6\,F_b}{\gamma_2^2\,u\,s} \right)^{\frac{1}{3}} \qquad \text{if } \frac{\pi\,u}{\sqrt{s}} < 10\,h. \qquad (2\text{-}155)$$

C H A P T E R

3
DEVELOPMENT OF THE ISCST2C MODEL

3.1
OVERVIEW

The conception, formulation and construction, and testing of the ISCST2C model are presented herein. These are three of the four primary elements of model development (Smoot, 1993). The fourth element, application of the ISCST2C model, is documented in the next chapter.

3.2
MODEL CONCEPTION

Model conception consists of defining the problem and determining modeling needs. As intimated in the problem statement of Chapter 1, there are important deficiencies in the capabilities of currently available EPA-guideline models to predict concentrations for conditions that can have the greatest effect on plume dispersion. The capability to predict refined concentrations in the cavity region of a building wake needs

to be developed and the capability to predict concentrations for complex terrain applications according to the EPA's intermediate terrain policy needs to be developed.

Presently, the EPA's ISCST2 model accounts for plume downwash within the near-wake and far-wake regions of a building but not within the cavity region. To predict concentrations in the cavity, the EPA (1993a; 1987a; 1986) recommends the use of their detailed downwash screening procedures (EPA, 1992b) as implemented in the SCREEN2 model (EPA, 1992c). The SCREEN2 model is limited in that it only provides screening predictions of short-term (i.e., 1-hour average) concentrations. The model is restricted to information for a single stack located on a single tiered building. Calculations are performed for only two orientations of the wind with respect to the building: 1) the wind aligned with the minimum building length and 2) the wind aligned with the maximum building length. The resulting concentration predictions are based on theoretical worst-case conditions of meteorology. The ISCST2C model has been developed with the capability of providing refined cavity concentration predictions for averaging times ranging from 1-hour to 1-year; for multiple stacks affected by multiple buildings with multiple tiers; for building configuration as a function of wind direction; for overlapping adjacent cavities by superposition; and for representative hourly meteorology.

Complex terrain is an important consideration in air dispersion modeling because under stable atmospheric conditions high concentrations can occur due to plume impingement on terrain higher than stack top. Currently, there is no EPA-guideline model that complies with the EPA's recently implemented policy for predicting

concentrations in complex terrain for all types of land use. This policy calls for a complex terrain model to be used only for predicting concentrations at receptors whose elevations are greater than or equal to plume height and a simple terrain model to be used only for predicting concentrations at receptors whose elevations are at or below stack top. For receptors whose elevations are between stack top and plume height, both a complex terrain model and a simple terrain model can be applied. An hour-by-hour comparison of the concentration predictions from both models is made with the higher of the two selected as the result for the hour. After this research was completed, the EPA (1995) finished the development of the ISCST3 model which incorporates the COMPLEX I model into the ISCST2 model. This provides a model that implements the intermediate terrain policy for rural complex terrain applications only. The ISCST2C model has been developed with the capability of implementing the EPA's intermediate terrain policy for both rural *and* urban complex terrain applications.

3.3
MODEL FORMULATION AND CONSTRUCTION

Model formulation and construction is accomplished in three steps (Smoot, 1993): a) determining the governing equations; b) determining the solution scheme; and c) writing the computer code. Each of these steps are described for the formulation and construction of the ISCST2C model. The product is a working computer program. A description of the setup and execution of the ISCST2C model is also provided.

3.3.1 Governing Equations

The primary formulations implemented in the ISCST2C model include the Hosker formulation of the SCREEN2 model for predicting cavity concentrations; the Schulman-Scire formulation of the SCREEN2C model for predicting cavity concentrations; an alternative formulation developed as part of this research for predicting cavity concentrations; the formulation of the COMPLEX I model for predicting concentrations in rural complex terrain; and the formulation of the SHORTZ model for predicting concentrations in urban complex terrain.

The Hosker formulation, the Schulman-Scire formulation, the COMPLEX I model, and the SHORTZ model are described in some detail in the Literature Review (Chapter 2). A summary of the important equations is provided here. A description of the alternative cavity formulation developed in this research is also provided.

Hosker Formulation

The primary calculation routines of the Hosker formulation are listed. None of these equations are contained in the existing ISCST2 model but have been added to the ISCST2C model for predicting concentrations in the cavity region of a building wake.

- Concentrations in the cavity region (χ_c) are predicted using the following equation as described in Section 2.4.2

$$\chi_c = \frac{Q}{1.5\ u\ (h_b \times h_w)} \tag{3-1}$$

where Q is the emission rate in g/s; u is the dilution wind speed for the hour in m/s; h_b is the direction-specific building height in m; and h_w is the direction-specific building width in m.

- An inherent assumption of Equation (3-1) is that the plume is completely entrained in the cavity. This assumption is satisfied if the plume height is less than or equal to the cavity height. The cavity height (h_c in m) is determined by

$$h_c = h_b \left[1.0 + 1.6 \exp\left(\frac{-1.3\, h_L}{h_b} \right) \right] \qquad (3\text{-}2)$$

where h_L is the direction-specific along-wind building length in m. As for the implementation of the Hosker algorithm in the ISCST2C model, if the plume height is greater than or equal to the GEP stack height, then it is assumed there are no building wake effects on plume dispersion and cavity concentrations are not computed.

- The plume height (H) is determined by the stack height (h) plus gradual momentum plume rise (Δh_m) at a distance of two building heights downwind minus stack tip downwash (h_d), i.e.,

$$H = h + \Delta h_m - h_d \,. \qquad (3\text{-}3)$$

Gradual momentum plume rise is a function of stack top wind speed (u_s) and is calculated using Equation (2-76) for unstable and neutral conditions or Equation (2-86) for stable conditions, refer to Section 2.3.1. Stack tip downwash is also a function of stack top wind speed and is calculated using

Equation (2-99), refer to Section 2.3.3. Making these substitutions, Equation (3-3) becomes (for unstable and neutral conditions),

$$H = h + \left[\frac{3}{\beta_j^2}\frac{F_m}{u_s^2}(2\,h_b)\right]^{\frac{1}{3}} - 2\left(\frac{v_s}{u_s} - 1.5\right)d_s \qquad (3\text{-}4)$$

or for stable conditions,

$$H = h + \left\{\frac{3\,F_m}{\beta_j^2\,u_s\,\sqrt{s}}\sin\left[\frac{\sqrt{s}\,(2\,h_b)}{u_s}\right]\right\} - 2\left(\frac{v_s}{u_s} - 1.5\right)d_s \qquad (3\text{-}5)$$

where F_m is the momentum flux in m^4/s^3; β_j is the jet entrainment coefficient; v_s is the stack exit gas velocity in m/s; d_s is the stack tip diameter in m; and s is the stability parameter in $1/m^2$.

- By setting h_c = H in Equation (3-4) or (3-5), the minimum stack top wind speed that causes the plume to be entrained in the cavity is computed. This is called the critical stack height wind speed, $(u_c)_h$. The solution for $(u_c)_h$ is obtained by iteration.
- The hourly wind speed is adjusted to the stack height accounting for the effects of surface roughness and stability class using the power law formula of Equation (2-24); refer to Section 2.2.8. If the hourly stack top wind speed is greater than or equal to the critical stack height wind speed, then Equation (3-1) is employed to predict the cavity concentration. The dilution wind speed used in Equation (3-1) is one-half the critical stack height wind speed but not less than 1 m/s, i.e.,

$$1 \le u = 0.5 \times (u_c)_h \ . \tag{3-6}$$

- The cavity concentration is assumed to be uniform within the building cross-sectional area for the entire length of the cavity. As for the implementation of the Hosker algorithm in the ISCST2C model, the cavity length (x_c) is taken to be 3 L, i.e.,

$$x_c = 3\,L \tag{3-7}$$

where x_c is in m and is measured from the stack location.

Schulman-Scire Formulation

The primary calculation routines of the Schulman-Scire formulation are listed. None of these equations are contained in the existing ISCST2 model but have been added to the ISCST2C model for predicting concentrations in the cavity region of a building wake.

- Concentrations in the cavity region are predicted using the following equation as described in Section 2.4.2

$$\chi_c = \frac{Q\, f_c}{v_s\, A_s \left[1 + 7.0 \frac{T_a}{T_s}\left(\frac{v_s}{u_s}\right)^2\right] + 0.0625\, u_b\, S^2} \tag{3-8}$$

where f_c is the mass fraction of the plume captured in the cavity; A_s is the stack tip cross-sectional area in m^2; T_a is the ambient air temperature in K; T_s

is the stack exit gas temperature in K; u_b is the building roof top wind speed in m/s; and S is the stretched-string distance in m.

- f_c is taken to be fraction of the plume below the cavity height at the end of the cavity. Assuming a vertical Gaussian distribution of the plume, f_c is the area under the Gaussian curve between the cavity height and the plume edge (refer to Section 2.2.4). Making use of the error function (refer to Section 2.2.12), f_c is calculated from the following equation

$$f_c = 0.5\left\{1 + \text{erf}\left[\frac{(h_c - H)/\sigma_z}{\sqrt{2}}\right]\right\}. \qquad (3\text{-}9)$$

- The stack top wind speed and the building roof top wind speed are determined considering the variation of wind speed with height. The power law formula of Equation (2-24) is used to determine wind speed versus height as a function of surface and stability class (refer to Section 2.2.8).
- As implemented in the Schulman-Scire formulation, S is the stretched-string distance from the top of the stack to the base of the lee wall of the building. An illustration is provided in Figure 3.1. The stretched-string distance is calculated by

$$S = h_b + \sqrt{(h - h_b)^2 + x_{SL}^2} \qquad (3\text{-}10)$$

where $(h - h_b)$ is the height of the stack above the roof and x_{SL} is the downwind distance from the stack location to the lee edge of the building. If

the top of the stack is lower than the roof, then (h - h_b) is set equal to zero when calculating the stretched-string distance.

- A so-called building scaling length (L_R) is used in the computation of a number of parameters, including the maximum height of the roof top cavity zone, the location and length of the roof top cavity zone, and the vertical dispersion coefficient. L_R is defined as

$$L_R \equiv B_S^{\frac{2}{3}} B_L^{\frac{1}{3}} \tag{3-11}$$

where B_S is the smaller and B_L is the larger of the building height and projected building width.

- The maximum height (h_r) and length (x_r) of the roof top cavity zone are estimated as functions of the building scaling length

$$h_r = 0.22\, L_R \tag{3-12}$$

and

$$x_r = 0.9\, L_R\,. \tag{3-13}$$

The location of h_r is a distance of 0.5 L_R downwind from the building face.

- If the roof top cavity zone reattaches to the building (indicated by $x_r < h_L$), then the height of the cavity region downwind of the lee side of the building is equal to the building height, i.e.,

$$h_c = h_b\,. \tag{3-14}$$

Otherwise, if the roof cavity does not reattach to the building (indicated by $x_r > h_L$); then the cavity height is equal to the building height plus the height of the roof cavity, i.e.,

$$h_c = h_b + h_r \,. \tag{3-15}$$

- The plume height at the end of the cavity is calculated based on the stack height plus the gradual rise of a bent-over plume. Gradual plume rise is calculated using Briggs' formula that contains both momentum and buoyancy components; refer to Section 2.3.1, Equation (2-73). Stack tip downwash is not considered. The formulation for computing plume height is

$$\begin{aligned} H &= h + \Delta h \\ &= h + \left(\frac{3}{\beta_j^2} \frac{F_m}{u_s^2} x_c + \frac{3}{2\,\beta_a^2} \frac{F_b}{u_s^3} x_c^2 \right)^{\frac{1}{3}} \end{aligned} \tag{3-16}$$

- If the plume height is greater than or equal to the GEP stack height, then it is assumed there are no building wake effects on plume dispersion and cavity concentrations are not computed.
- The vertical dispersion coefficient is calculated from the following empirical relationship

$$\sigma_z = 0.21\, L_R^{0.25}\, x^{0.75} \,. \tag{3-17}$$

- Like the Hosker formulation, the cavity concentration is assumed to be uniform within the building cross-sectional area for the entire length of the cavity. As for the implementation of the Schulman-Scire algorithm in the ISCST2C model, the cavity length is taken to be 3 L.

Gaussian Cavity Formulation

One of the objectives of this research is to develop an alternative algorithm to the SCREEN2-based and SCREEN2C-based methods for predicting refined cavity concentrations. A Gaussian formulation has been developed and incorporated in the ISCST2C model as described in the following.

The Gaussian cavity algorithm is based on the hypothesis that plume dispersion within the cavity region of a building wake generally follows a Gaussian distribution. It is assumed that the concentrations at the lee wall of the building (e.g., the source) can be described by the equation presented by Hosker (1984), Equation (2-106), with c = 1, i.e.,

$$\chi = \frac{Q}{u\left(A_p\right)} . \tag{3-18}$$

Equation (3-18) is equivalent to the simple geometric plume model described in Section 2.2.3. And as in the geometric plume model, it is assumed that the cross-sectional area of the plume in the cavity increases with increasing distance from the source. Initial dispersion is represented by a volume source with a plume cross-sectional area based on the building dimensions perpendicular to the wind flow. At 3 L downwind, the cross-sectional area of the plume is based on the measurements made by Huber and Snyder (1976) in a wind tunnel. The Gaussian cavity formulation is best described as a Gaussian volume source plume formulation with dispersion coefficients based on extrapolations of the Huber-Snyder building wake sigmas.

Vertical plume dispersion in the cavity. The vertical width of the volume source plume for tall, squat, and very squat building configurations is assumed to be 1.0 L at the start of the cavity and 1.5 L at the end of the cavity which is assumed to correspond to the beginning of the near-wake at 3 L downwind (refer to Figure 3.2). The vertical dimension of a volume source released near the ground can be roughly estimated as a plume half-width so that the Gaussian distribution is approximated by 2.15 σ. The enhanced vertical dispersion coefficient of the plume (σ'_z) in the cavity is then given by

- at x = 0

$$\begin{aligned} 2.15\,\sigma'_z &= 1.0\ \mathrm{L} \\ \sigma'_z &= 0.47\ \mathrm{L} \end{aligned} \qquad (3\text{-}19)$$

- and at x = 3 L

$$\begin{aligned} 2.15\,\sigma'_z &= 1.5\ \mathrm{L} \\ \sigma'_z &= 0.7\ \mathrm{L}\,. \end{aligned} \qquad (3\text{-}20)$$

Interpolating for distances between 0 and 3 L downwind, leads to the formulation

$$\sigma'_z = 0.47\ \mathrm{L} + 0.0767\ \mathrm{x}\,. \qquad (3\text{-}21)$$

A linear decay factor (A) is used in the ISCST2 wake algorithm to calculate σ'_z for distances of 3 L and beyond; refer to Equation (2-130). The linear decay was not incorporated into the Gaussian cavity algorithm based on results from a tracer gas release experiment conducted in the wake of a building as presented in Chapter 4.

For a tall building, L is defined by the building width (h_w) and for squat and very-squat buildings, L is defined by the building height (h_b). Making these substitutions into

Equation (3-21) yields the formulas for calculating σ_z within the cavity region of a building wake for tall, squat, and very-squat buildings

- tall building ($h_b > h_w$)

$$\sigma'_z = 0.47\, h_w + 0.0767\, x \quad \text{for } 0 \le x < 3\, h_w \tag{3-22}$$

- squat building ($1 \le h_w / h_b \le 5$) and very-squat building ($h_w / h_b > 5$)

$$\sigma'_z = 0.47\, h_b + 0.0767\, x \quad \text{for } 0 \le x < 3\, h_b\,. \tag{3-23}$$

The vertical dispersion coefficient is modified to account for building wake effects on plume dispersion if the plume height to building height ratio (i.e., H / h_b) is less than 2.5.

Horizontal plume dispersion in the cavity. The horizontal width of the volume source plume is assumed to be the building width at the start of the cavity and 1.5 h_w at the end of the cavity for a tall and squat building (refer to Figure 3.3). For a very squat building, the height is quite small compared to the width and there is less resistance to air flow over the building than around the building. Consequently, for a stack located away from the ends of the building, the horizontal width of the volume source plume at the start of the cavity is assumed to be 1.0 h_b and at the end of the cavity it is assumed to be 1.5 h_b. If the stack is located within 2.5 h_b of the ends of a very squat building, the horizontal width of the volume source plume is assumed to be 7.5 h_b at the end of the cavity.

Interpolating for distances between 0 and 3 L downwind and using the Gaussian definition of the horizontal width of a plume from edge to edge as 4.3 σ yields the formulas for calculating enhanced σ_y within the cavity region of a building wake for tall, squat, and very-squat buildings

- tall building ($h_b > h_w$)

$$\sigma'_y = 0.23\, h_w + 0.04\, x \quad \text{for } 0 \le x < 3\, h_w \tag{3-24}$$

- squat building ($1 \le h_w / h_b \le 5$)

$$\sigma'_y = 0.23\, h_w + \frac{0.12\, h_w\, x}{3\, h_b} \quad \text{for } 0 \le x < 3\, h_b \tag{3-25}$$

- very-squat building ($h_w / h_b > 5$)

$$\sigma'_y = 0.23\, h_b + 0.04\, x \quad \text{for } 0 \le x < 3\, h_b \tag{3-26}$$

denoted as the "upper bound" estimate, applicable if the stack is located away from the ends of the building or

$$\sigma'_y = 0.23\, h_b + 0.507\, x \quad \text{for } 0 \le x < 3\, h_b \tag{3-27}$$

denoted as the "lower bound" estimate, applicable if the stack is located within 2.5 h_b of the ends of the building.

The horizontal dispersion coefficient is modified to account for building wake effects on plume dispersion within the cavity if the plume height is less than the GEP stack height (i.e., $H < h_b + 1.5\, L$). This criteria is based on results from a comparison of predicted and measured concentrations as presented in Chapter 4 and is different from the Huber-Snyder wake algorithm where σ_y is modified if the plume height is less than or equal to 1.2 h_b (i.e., $H \le 1.2\, h_b$).

The concept of total or partial plume capture in the cavity as contained in the Hosker and Schulman-Scire formulations is not emulated in the Gaussian cavity algorithm. The Gaussian cavity algorithm accounts for the horizontal, vertical, and

downwind variations in cavity concentrations which the other algorithms do not. The downwind extent of the cavity region is taken to be 3 L. If the plume height is greater than or equal to the GEP stack height, then it is assumed there are no building wake effects on plume dispersion and cavity concentrations are not computed.

The hypothesis of Gaussian plume dispersion within the cavity is tested with an analysis of tracer gas measurement data collected in the cavity region of a building wake. Also, the Gaussian cavity formulation is tested against the Hosker and Schulman-Scire formulations in comparisons of model predictions to tracer gas measurements. These results are presented in Chapter 4.

COMPLEX I Model

The primary calculation routines of the COMPLEX I model are listed. Some of these routines are contained in the existing ISCST2 model. Algorithms that were developed and implemented in the ISCST2C model are those for calculating horizontal plume width; pollutant concentrations assuming a uniform, non-Gaussian horizontal distribution of the plume; plume height in rural complex terrain; and the attenuation factor to account for the blocking effect of the terrain on the air flow.

- The horizontal distribution of the plume is assumed to be uniform over a 22.5° wind sector for all stability categories as discussed in Section 2.5.3. Since the crosswind distribution is assumed to be non-Gaussian, the horizontal

plume width (W_P) can be substituted for $\sqrt{2\pi}\,\sigma_y$ in the Gaussian plume equations so that for distances of $x < x_m$

$$\chi(x,y,z;H) = \frac{Q}{\sqrt{2\pi}\,u_s\,W_P\,\sigma_z}\left\{\exp\left[-\frac{1}{2}\left(\frac{z-H}{\sigma_z}\right)^2\right]+\exp\left[-\frac{1}{2}\left(\frac{z+H}{\sigma_z}\right)^2\right]\right\}; \quad (3\text{-}28)$$

for distances of $x_m \le x < 4\,x_m$

$$\chi(x,y,z;H) = \frac{Q}{\sqrt{2\pi}\,u_s\,W_P\,\sigma_z}\left\{\exp\left[-\frac{1}{2}\left(\frac{z-H}{\sigma_z}\right)^2\right]+\exp\left[-\frac{1}{2}\left(\frac{z+H}{\sigma_z}\right)^2\right]\right\}$$

$$+\sum_{i=1}^{\infty}\left\{\exp\left[-\frac{1}{2}\left(\frac{z-(2iH_m-H)}{\sigma_z}\right)^2\right]+\exp\left[-\frac{1}{2}\left(\frac{z+(2iH_m-H)}{\sigma_z}\right)^2\right]\right.$$

$$\left.+\exp\left[-\frac{1}{2}\left(\frac{z-(2iH_m+H)}{\sigma_z}\right)^2\right]+\exp\left[-\frac{1}{2}\left(\frac{z+(2iH_m+H)}{\sigma_z}\right)^2\right]\right\}; \quad (3\text{-}29)$$

and for distances of $x \ge 4\,x_m$

$$\chi(x,y,z;H) = \frac{Q}{u_s\,W_P\,H_m}. \quad (3\text{-}30)$$

- The horizontal plume width is given by the crosswind arc length of a 22.5° wind sector, i.e.,

$$W_P = (2\pi/16)\,x. \quad (3\text{-}31)$$

- The vertical dispersion coefficients are based on the Pasquill-Gifford dispersion curves presented in Section 2.2.7. The parameters used to calculate σ_z values are presented in Table 2.9.

- The wind speed at stack top is used for the plume rise and concentration predictions and is determined considering the variation of wind speed with height (refer to Section 2.2.8). The power law formula of Equation (2-24) is used to perform the calculations. The formula employs a wind profile exponent as a function of surface roughness and stability class. Default values of wind profile exponents for rural areas are presented in Table 2.13 (EPA, 1993a; 1987a; 1986).
- The plume rise equations are based on Briggs' formulas for gradual and final plume rise considering both the buoyancy and momentum terms as described in Section 2.3.1. Gradual buoyant plume rise is calculated using Equation (2-74). Gradual momentum plume rise is calculated using Equation (2-76) for unstable and neutral conditions or Equation (2-86) for stable conditions. A road map for performing the calculations for final plume rise is presented in Table 2.17.
- There is an option to account for stack tip downwash as described in Section 2.3.3. Stack tip downwash is calculated using Equation (2-99).
- There is an option to account for vertical buoyancy-induced dispersion as described in Section 2.3.4. Horizontal buoyancy-induced dispersion is not considered. Vertical buoyancy-induced dispersion is calculated using Equations (2-101) and (2-103).

- Plume behavior in the vicinity of complex terrain is simulated through the use of terrain adjustment factors as described in Section 2.4.3. Terrain adjustment factors (F_T) are used to calculate a plume height adjusted for terrain effects (H) according to the following formulation

$$H = \max\left\{ \left(H_{flat} \times F_T\right), \left[H_{flat} - \Delta E(1 - F_T) \right] \right\} \qquad (3\text{-}32)$$

where H_{flat} is the plume height for flat terrain and ΔE is the terrain elevation of the receptor above the stack base elevation. Values for F_T are entered as a function of atmospheric stability and range from 0 to indicate a plume fully intercepts terrain that rises above the plume centerline up to 1 to indicate no terrain effects. Default values of F_T are 0.5 for stability classes A through D and 0 for stability classes E and F (EPA, 1993a; 1987a; 1986). When a value of 0 is specified for F_T, a minimum separation distance between the plume centerline and the ground surface (H_{min}) can be designated. The default value for H_{min} is 10 m (EPA, 1993a; 1987a; 1986).

- An empirical attenuation factor is employed to account for the blocking effect of the terrain on the air flow under stable atmospheric conditions. The effect of the attenuation factor is to reduce the predicted concentration as a function of plume height above the point where the plume centerline intercepts the elevated terrain. The attenuation factor (A_F) is given by

$$A_F = \frac{400 - \left(\Delta E + z - H_{flat}\right)}{400}. \qquad (3\text{-}33)$$

A_F equals 1.0 if the unadjusted plume height is greater than or equal to the receptor height (i.e., $A_F = 1.0$ for $H_{flat} \geq \Delta E + z$) and A_F equals 0 if the difference between the receptor height and the unadjusted plume height is greater than or equal to 400 m (i.e., $A_F = 0$ for $\Delta E + z - H_{flat} \geq 400$).

SHORTZ Model

The primary calculation routines of the SHORTZ model are listed. Most of these calculations routines were developed and implemented in the ISCST2C model. The algorithms developed and added to the ISCST2C model were those for calculating σ_y and σ_z values; for calculating wind speed at stack height and plume height using wind profile exponents recommended for urban complex terrain applications; and for calculating plume rise.

- Concentration predictions are based on the Gaussian plume equation accounting for plume trapping (refer to Section 2.2.9). A road map for performing the concentration calculations is presented in Table 2.14.
- The horizontal dispersion coefficient (σ_y, in m) is a function of the standard deviation of the horizontal wind direction (σ_A, in radians)

$$\sigma_y = \sigma_A \, x_{ry} \left[\frac{x + x_y - x_{ry}(1-\alpha)}{\alpha \, x_{ry}} \right]^{\alpha} \qquad (3\text{-}34)$$

where x_{ry} is a parameter referred to as the distance in m over which rectilinear lateral plume expansion occurs downwind of an ideal point source

(empirically determined to equal 50 m); x is the downwind distance in m; x_y is the virtual distance in m for the initial horizontal source dimension (= 0 for a point source); and α is referred to as the horizontal diffusion coefficient (empirically determined to equal 0.9).

- The vertical dispersion coefficient (σ_z, in m) is a function of the standard deviation of the vertical wind direction (σ_E, in radians)

$$\sigma_z = \sigma_E \left(x + x_z\right)^{\varphi} \tag{3-35}$$

where x_z is the virtual distance in m for the initial vertical source dimension (= 0 for a point source) and φ is referred to as the vertical diffusion coefficient (empirically determined to equal 1.0).

- The wind speed at stack top is used for the plume rise calculations; the wind speed at plume height is used for the concentration predictions. The variation of wind speed with height is determined using the power law formula of Equation (2-24), refer to Section 2.2.8. In Equation (2-24), a wind profile exponent is employed. For urban complex terrain applications, wind profile exponents are a function of stability class and wind speed. Default values are presented in Table 2.20 (EPA, 1993a; 1987a; 1986).

- The plume rise formulas are derived from the Briggs formulas as described in Section 2.5.4. Only final buoyant plume rise is calculated including a factor (f_s) to account for stack tip downwash. For unstable and neutral atmospheric conditions

$$\Delta h = \left[\frac{3}{2\,\gamma_1^2} \frac{F_b}{u_s^3} (10\,h)^2 \right]^{\frac{1}{3}} f_s \qquad (3\text{-}36)$$

where Δh is the plume rise in m and γ_1 is the adiabatic entrainment coefficient (= 0.6). For stable atmospheric conditions

$$\Delta h = \left\{ \frac{3\,F_b}{\gamma_2^2\,u_s\,s} \left[1 - \cos\left(\frac{\sqrt{s}}{u_s} 10\,h \right) \right] \right\}^{\frac{1}{3}} \qquad \text{if } \frac{\pi\,u_s}{\sqrt{s}} \geq 10\,h \text{ or} \qquad (3\text{-}37)$$

$$\Delta h = \left(\frac{6\,F_b}{\gamma_2^2\,u_s\,s} \right)^{\frac{1}{3}} \qquad \text{if } \frac{\pi\,u_s}{\sqrt{s}} < 10\,h \qquad (3\text{-}38)$$

where γ_2 is the stable entrainment coefficient (= 0.66).

3.3.2 Solution Scheme

Refined Cavity Concentrations

Two new input parameters are implemented in the ISCST2C model to enable concentration predictions in the cavity region of a building wake: 1) the projected along-wind length of the building (Dsbl) and 2) the distance from the upwind edge of the building to the stack (i.e., referred to as the downwind stack location or Dwsl).

The building length is used in the Hosker formulation to calculate the cavity height; refer to Equation (3-2). In the Schulman-Scire formulation, the building length is used to calculate the building scaling length; refer to Equation (3-11). The building scaling length is used to calculate the cavity height and the vertical dispersion parameter.

The downwind stack location is used in the Schulman-Scire formulation to calculate the stretched-string distance. Negative values of Dwsl denote the stack is located upwind of the building. Positive values of Dwsl denote the stack is located on the building, to the side but within the influence of the building, or downwind of the building. If Dwsl $\leq$ 0, then the stack is located upwind of the building. If 0 $\leq$ Dwsl $\leq$ Dsbl, then the stack is located on or to the side of the building. If Dwsl > Dsbl, then the stack is located downwind of the building. The range of downwind stack location is fixed at 0 $\leq$ Dwsl $\leq$ Dsbl. So if Dwsl < 0, Dwsl is set to 0 and if Dwsl > Dsbl, Dwsl is set to Dsbl for consistency with the Schulman-Scire formulation in calculating the stretched-string distance.

Values of Dsbl and Dwsl can change with the orientation of the wind. These changes are accounted for in order to predict refined cavity concentrations. Dsbl values are entered as an array of 36 projected along-wind lengths (m) of the building beginning with the 10° flow vector (e.g., the direction toward which the wind is blowing) and incrementing 10° clockwise. Similarly, Dwsl values are entered as an array of 36 distances (m) from the upwind edge of the building to the stack beginning with the 10° flow vector and incrementing 10° clockwise. A computer program was developed as part of this research to provide the direction-specific projected along-wind lengths of the building and the direction-specific distances from the upwind edge of the building to the stack needed by the ISCST2C model to account for plume downwash within the cavity region of a building.

Input of hourly meteorology based on local measurements allows for the prediction of refined cavity concentrations. In the Hosker formulation, the critical stack height wind speed needed for complete plume capture in the cavity region is determined. If the hourly wind speed adjusted to stack height is less than the critical stack height wind speed, then it is assumed that the plume is not completely captured within the cavity and the cavity concentration is zero (EPA, 1992b). If the hourly wind speed adjusted to stack height is greater than or equal to the critical stack height wind speed, then a refined cavity concentration is predicted based on a dilution wind speed equal to one-half of the hourly stack top wind speed but not less than 1 m/s (EPA, 1992b).

The downwind extent of the cavity region of a building wake is defined differently in the Hosker formulation, the Schulman-Scire formulation, and the ISCST2 wake algorithm and contradictory results from these algorithms can be expected. The ability to choose either the Hosker formulation or the Schulman-Scire formulation is programmed into the ISCST2C model. The selected cavity formulation is used to predict concentrations for receptors located within 3 L of the stack location; the ISCST2 wake algorithm is used to predict concentrations for receptors located at 3 L and beyond.

Complex Terrain

The key to implementing the EPA's intermediate terrain policy is to identify the terrain regime of each receptor location. The stack height marks the boundary between simple and complex terrain regimes. The ISCST2 algorithm is used in the ISCST2C

model to predict concentrations in simple terrain (e.g., receptors located on terrain elevations lower than the stack height). The COMPLEX I and SHORTZ algorithms are used to predict concentrations in complex terrain (e.g., receptors located on terrain elevations higher than stack top). The COMPLEX I algorithm is applicable to rural land use and the SHORTZ algorithm is applicable to urban land use.

Intermediate terrain is a subset of complex terrain and includes the region bounded by the stack height and the plume height. For applications in rural areas, both the ISCST2 and COMPLEX I algorithms are used to predict concentrations in intermediate terrain. For applications in urban areas, both the ISCST2 and SHORTZ algorithms are used to predict concentrations in intermediate terrain. The higher value of the ISCST2 prediction or the COMPLEX I/SHORTZ prediction is taken to represent the concentration prediction at the specific intermediate terrain receptor for the specific hour of meteorology.

The plume height is defined differently in the ISCST2 and SHORTZ algorithms and contradictory results can be expected. The plume rise calculations performed by the ISCST2 algorithm is used in the ISCST2C model to define the plume height which is the upper boundary of the intermediate terrain regime.

3.3.3 Computer Code

The core computer code of the ISCST2C model is from the current regulatory version of the EPA's ISCST2 model (dated 93109). The computer code is written in

FORTRAN and was developed on an IBM®-compatible personal computer using the Lahey F77L-EM/32 FORTRAN Compiler, Version 5.2 and the Microsoft® FORTRAN PowerStation Compiler, Version 1.0. Both compilers produce executable programs for a 32-bit Microsoft® Disk Operating System (DOS) extended memory environment.

The governing equations and solution schemes of the Hosker cavity formulation, the Schulman-Scire cavity formulation, the Gaussian cavity formulation, the COMPLEX I model, and the SHORTZ model were programmed as new subroutines or modifications to existing subroutines of the ISCST2 model. In addition, new subroutines and modifications to existing subroutines were written to input the data required for the supplementary algorithms. Subroutines that control output of data and results, quality control checks, and program execution were also created as new or modified computer code. Table 3.1 provides a list of new and modified subroutines of the ISCST2C model with a description of their purpose.

3.3.4 Setup and Execution of the ISCST2C Model

Input Data File Setup

Construction of the input data files required to run the ISCST2C model is essentially the same as required for the ISCST2 model (EPA, 1992a). Program options and input data are entered via five functional pathways as established in the ISCST2 model:

- the **CO** pathway for specifying overall job **CO**ntrol options;
- the **SO** pathway for specifying **SO**urce information;
- the **RE** pathway for specifying **RE**ceptor information;
- the **ME** pathway for specifying **ME**teorology information; and
- the **OU** pathway for specifying **OU**tput options.

Minor modifications have been made to the CO, SO, and ME pathways of the ISCST2 model. No modifications have been made to the RE or OU pathways. Presented in Appendix C is a Quick Reference Table of the keywords and parameters that can be used for each pathway of an ISCST2C input data file. A complete reference of keywords and parameters is presented in Appendix D.

Modifications Made to the CO Pathway

In the CO pathway, the MODELSEL keyword has been added and the TERRHGTS keyword has been modified to control options for predicting concentrations in the cavity region of a building wake and on elevated terrain. The new MODELSEL keyword is used to select the dispersion algorithms to be employed in an ISCST2C model run. The ISCST2 parameter and/or the HOSKER or SCHULM or CAVITY parameters and/or the CMPLXI or SHORTZ parameters can be used in combination. The syntax and type of the MODELSEL keyword are summarized below:

Syntax:	CO	MODELSEL	ISCST2	HOSKER or SCHULM or CAVITY	CMPLXI or SHORTZ
Type:	Optional, Non-repeatable				

If only the ISCST2 parameter is specified, then results from the ISCST2C model are based on the ISCST2 algorithm (e.g., an ISCST2 model equivalent run). If the HOSKER parameter is specified, then results from the ISCST2C model are based on the Hosker cavity formulation contained in the SCREEN2 model. If the SCHULM parameter is specified, then results from the ISCST2C model are based on the Schulman-Scire cavity formulation contained in the SCREEN2C model. If the CAVITY parameter is specified, then results from the ISCST2C model are based on the Gaussian cavity formulation. If only the CMPLXI parameter is specified, then results from the ISCST2C model are based on the COMPLEX I algorithm (e.g., COMPLEX I model equivalent run). Note that the RURAL parameter (for rural dispersion) must be specified with the MODELOPT keyword for the COMPLEX I algorithm to be invoked. If only the SHORTZ parameter is specified, then results from the ISCST2C model are based on the SHORTZ algorithm (e.g., SHORTZ model equivalent run). Note that the URBAN parameter (for urban dispersion) must be specified with the MODELOPT keyword for the SHORTZ algorithm to be invoked.

The ISCST2 and HOSKER or SCHULM or CAVITY parameters can be specified to predict concentrations in a building wake. For sources subject to building wake effects, the ISCST2 model is used to predict concentrations in the near-wake and far-

wake regions (3 L and beyond downwind) and the specified cavity algorithm is used to predict concentrations within 3 L.

The ISCST2 and CMPLXI or SHORTZ parameters can be specified to predict concentrations in complex terrain according to the EPA's intermediate terrain policy. If ISCST2 is specified in conjunction with CMPLXI or SHORTZ, then the ISCST2 algorithm is used to predict concentrations on elevated terrain up to plume height (with terrain elevations higher than stack top "chopped-off" at the stack top elevation) and the COMPLEX I or SHORTZ algorithm is used to predict concentrations on elevated terrain higher than stack top. For those receptors located on terrain between stack top and plume height (intermediate terrain), the higher of the ISCST2 and COMPLEX I or SHORTZ predictions is used. This evaluation is performed for each source-receptor-hour combination input to the model. Also note that the RURAL parameter must be specified with the MODELOPT keyword for the COMPLEX I algorithm to be invoked and the URBAN parameter must be specified with the MODELOPT keyword for the SHORTZ algorithm to be invoked.

If the HOSKER or SCHULM or CAVITY parameter is specified in the MODELSEL keyword in combination with the ISCST2 and/or CMPLXI or SHORTZ parameter(s), then the selected cavity algorithm is also used to predict concentrations on elevated terrain up to plume height. In this case, the higher of the ISCST2, cavity, and CMPLXI or SHORTZ predictions is used for receptors located on intermediate terrain.

For the TERRHGTS keyword, if the ELEV secondary keyword is set, then two new optional parameters can be specified. The new syntax and type of the TERRHGTS keyword/ELEV secondary keyword are summarized below:

Syntax:	CO TERRHGTS ELEV (Taf(i), i=1,6 Hmin)
Type:	Optional, Non-repeatable

where the ELEV secondary keyword specifies that receptor heights on elevated terrain are allowed on the REceptor pathway; Taf(1) through Taf(6) are terrain adjustment factors for each of the six stability categories; and Hmin is the minimum separation distance in m between the plume centerline and the ground surface. If elevated terrain is assumed and a receptor height is not specified, then it is assumed to have a value of 0.0 meters. Default values of Taf are 0.5, 0.5, 0.5, 0.5, 0.0, and 0.0 for stability categories A through F, respectively. The default value for Hmin is 10 m.

Modifications Made to the SO Pathway

Modifications have been made to the SO pathway that allow additional direction-specific building dimensions to be input for use in the SCREEN2 and SCREEN2C cavity algorithms via two new keywords: BUILDLNG and BUILDSTK. The use of these keywords is similar to the existing BUILDHGT and BUILDWID keywords of the ISCST2 model.

The BUILDLNG keyword is used to input optional direction-specific along-wind building lengths. The syntax and type of this keyword are summarized below:

Syntax:	SO BUILDLNG Srcid (or Srcrng) Dsbl(i), i=1,36
Type:	Optional, Repeatable
Order:	Must follow the LOCATION card for each source input

where Srcid is the source identification code; Srcrng is the range of sources (inclusive) for which building dimensions apply (entered as two alphanumeric strings separated by a '-'); and Dsbl is an array of direction-specific along-wind building lengths (m) beginning with the 10° flow vector and incrementing 10° clockwise. The use of the BUILDLNG keyword is optional. If HOSKER or SCHULM cavity concentration predictions are requested and no values of Dsbl are input to the program, then the direction-specific along-wind building length is set equal to the maximum direction-specific building width (Dsbw) for the complement angle to the flow vector, i.e., Dsbl(i) = Max [Dsbw(i+9) , Dsbw(i-9)].

The BUILDSTK keyword is used to input optional direction-specific distances from the upwind edge of the building to the stack. The syntax and type of this keyword are summarized below:

Syntax:	SO BUILDSTK Srcid (or Srcrng) Dwsl(i), i=1,36
Type:	Optional, Repeatable
Order:	Must follow the LOCATION card for each source input

where Srcid is the source identification code; Srcrng is the range of sources (inclusive) for which building dimensions apply (entered as two alphanumeric strings separated by a '-'); and Dwsl is an array of direction-specific distances (m) from the upwind edge of the building to the stack beginning with the 10° flow vector and incrementing 10° clockwise.

Like the BUILDLNG keyword, the use of the BUILDSTK keyword is optional. If SCHULM cavity concentration predictions are requested and no values of Dwsl are input to the program, then the stack is assumed to be located on the roof in the center of the building.

Values of Dwsl and Dsbl are used in the ISCST2C model to determine the stack location with respect to the building location. Negative values of Dwsl denote that the stack is located upwind of the building. For $0 \leq$ Dwsl $\leq$ Dsbl, the stack is located on or to the side of the building. Values of Dwsl > Dsbl denote that the stack is located downwind of the building.

The Building Profile Input Program (BPIP) was designed by the EPA (1993b) to implement its guidelines for determining Good Engineering Practice (GEP) stack height (EPA, 1985). BPIP calculates direction-specific building heights (Dsbh) and widths (Dsbw) needed by the ISCST2 model to account for plume downwash effects within the near-wake and far-wake regions of a building wake. Modification have been made to BPIP so that the program also calculates values of Dsbl and Dwsl needed by the ISCST2C model to account for plume downwash effects within the cavity region of a building wake. The modified program is called Building Profile Input Program - Cavity (BPIPC). BPIPC uses a data file in the same format required by BPIP. Output from BPIPC includes 36 values of Dsbh, Dsbw, Dsbl, and Dwsl in the proper pathway/keyword/parameter format required by the ISCST2C model.

Modifications Made to the ME Pathway

Modifications have been made to the ME pathway that allow σ_E and σ_A values to be input for use in the SHORTZ calculations with the use of two new keywords: SIGMAELV and SIGMAAZM. The ISCST2C model retains the five format options for the meteorological data file as established in the ISCST2 model:

1. the default ASCII format for a sequential hourly data file;
2. the user-specified ASCII format for a sequential hourly data file;
3. the free-format ASCII sequential hourly data file;
4. the unformatted sequential hourly data file generated by the Meteorological Processor for Regulatory Models (MPRM) (EPA, 1993c) or the RAMMET meteorological data preprocessor program (EPA, 1993d); and
5. the card image ASCII format for a sequential hourly data file.

For the first four options, σ_E and σ_A values are assigned as a function of atmospheric stability category. The default values of σ_E and σ_A built into the ISCST2C model are given in Table 3.2 (EPA, 1982). The user can specify non-default values of σ_E and σ_A with the use of the keywords SIGMAELV and SIGMAAZM.

The SIGMAELV keyword is used to input optional σ_E values as a function of atmospheric stability category. The syntax and type of this keyword are summarized below:

Syntax:	ME SIGMAELV SigE1 SigE2 SigE3 SigE4 SigE5 SigE6
Type:	Optional, Non-repeatable

where SigE1 through SigE6 are the σ_E values for each of the six stability categories. Values of σ_E can be input in radians or degrees. If $\sigma_E < 1.0$, then σ_E is assumed to be in radians; if $\sigma_E > 1.0$, then σ_E is assumed to be in degrees.

The SIGMAAZM keyword is used to input optional σ_A values as a function of atmospheric stability category. The syntax and type of this keyword are summarized below:

Syntax:	ME SIGMAAZM SigA1 SigA2 SigA3 SigA4 SigA5 SigA6
Type:	Optional, Non-repeatable

where SigA1 through SigA6 are the σ_A values for each of the six stability categories. Values of σ_A can be input in radians or degrees. If $\sigma_A < 1.0$, then σ_A is assumed to be in radians; if $\sigma_A > 1.0$, then σ_A is assumed to be in degrees.

Using the fifth format option allows hourly σ_E and σ_A values to be input to the ISCST2C model. The following command syntax is used to access a sequential hourly data file in the card image ASCII format:

```
ME  INPUTFIL  Metfil  CARD
```

where Metfil is the filename for the meteorological input file and the secondary keyword of CARD specifies the use of card image data using a default ASCII format. The default card format used in the ISCST2 model has been modified by the addition of hourly σ_E and σ_A values in the input data file. The order of the meteorological variables and the default card image ASCII format of the ISCST2C model are provided in Table 3.3.

The ME pathway has also been modified to allow the new keyword ANEMELEV to be used to input the ground elevation above mean sea level of the anemometer measurement location for use in the SHORTZ calculations. By default, the anemometer height for wind speed measurements is assumed to be the height above the stack base elevation. The syntax and type of this keyword are summarized below:

Syntax:	ME ANEMELEV ZA (ZAunit)
Type:	Optional, Non-repeatable

where ZA is the ground elevation above mean sea level of the anemometer measurement location and the optional parameter ZAunit is the units of ZA in METERS or FEET (default is METERS).

Model Execution

The ISCST2C model was developed on an IBM-compatible personal computer (PC) with certain minimum hardware requirements: 1) 80386, 80486, or Pentium® processor; 2) math co-processor; 3) 8 MB of random access memory; 4) and Microsoft®-DOS Version 3.2 or higher. The program is an extended memory version using static storage allocations. The limits on the number of receptors, sources, source groups, and averaging periods are initially set as follows:

Number of Receptors	2500
Number of x-coordinates or distances	250
Number of y-coordinates or directions	250
Number of Sources	300
Number of Source Groups	5
Number of Short-Term Averages	4

To run the program, the following command line is entered at the command prompt:

```
ISCST2C   inputfile   outputfile
```

where "inputfile" is the name of the input data file and "outputfile" is the name of the file to hold the model results. As the program runs, it writes updates on the status of processing to the PC's screen. If processing proceeds with no errors, the program first indicates that the setup information is being processed, i.e.,

```
Now Processing SETUP Information
```

and then gives the Julian day of meteorology currently being processed, i.e.,

```
Now Processing Data For Day No.    1
```

When all days of meteorological data have been processed, the program indicates that the output options are being processed, i.e.,

```
Now Processing Output Options
```

Model results are contained in an output file named at the time the program was executed.

If the command line was entered but the first status message is not seen, then the program did not load into memory properly and a DOS error message will be visible on the screen. If the program stops after completing the setup processing and before any meteorological data is processed, then a fatal error was encountered during the setup processing or the RUNORNOT option in the CO pathway was set to NOT run. Check the output file. Listings of the input file and fatal error messages are provided.

3.4 MODEL TESTING

The ISCST2C model was tested to verify the computer code. Essentially, this is a quality assurance/quality control task to ensure the ISCST2C model is predicting the correct concentrations. Computer code verification was accomplished in two ways. First, FORTRAN write statements were added during the development of the ISCST2C model to print calculated values of the key variables used in the prediction of concentrations. Verification of the calculations were performed using a calculator and using a spreadsheet.

The ISCST2C was programmed with the capability to produce equivalent concentration predictions of the ISCST2 model, SCREEN2 model, the SCREEN2C model, the COMPLEX I model, and the SHORTZ model. The computer code of the ISCST2C model was verified by running example test files supplied with these models and comparing the results. These comparisons are presented in the following.

3.4.1 Comparison of ISCST2 and ISCST2C Predictions

The ISCST2C model was run using the EPA's example input data file named TEST-ST.INP supplied with the ISCST2 model. Comparisons of the 50 predicted maximum 3-hr and 24-hr average concentrations are presented in Tables 3.4 and 3.5, respectively. As demonstrated by the tables, the results obtained from the ISCST2C model are the same as those obtained from the EPA's ISCST2 model.

3.4.2 Comparison of SCREEN2 Cavity and ISCST2C Cavity Predictions

Presented in the SCREEN2 model user's guide (EPA, 1992c) is an example run for predicting cavity concentrations. The ISCST2C model was run using an equivalent data set. Comparisons of the predicted concentrations are presented in Table 3.6. As demonstrated by the table, the results obtained from the ISCST2C model are equivalent to those obtained from the EPA's SCREEN2 model.

3.4.3 Comparison of SCREEN2C Cavity and ISCST2C Cavity Predictions

The ISCST2C model was run using an input data file equivalent to the file named TEST-S2.DAT supplied with the SCREEN2C model. Comparisons of the predicted concentrations are presented in Table 3.7. The results obtained from the ISCST2C model are different from those obtained from the SCREEN2C model. These differences are due to an error discovered in the SCREEN2C computer code for calculating plume rise.

The SCREEN2C model is a modification of the EPA's SCREEN2 model. Instead of relying on existing subroutines in the SCREEN2 model to calculate plume rise, the SCREEN2C model contains a new additional subroutine to perform the calculations. The new plume rise subroutine does not calculate plume rise correctly which significantly affects the cavity concentration predictions. After making the appropriate corrections to the SCREEN2C computer code, the results obtained from the ISCST2C model are equivalent to those obtained from the SCREEN2C model.

The SCREEN2C model also contains a new additional subroutine to solve the error function when an existing subroutine in the SCREEN2 model serves the same purpose. The SCREEN2C model contains duplicate subroutines for calculating plume rise and for computing the error function.

3.4.4 Comparison of COMPLEX I and ISCST2C Predictions

The ISCST2C model was run using an input data file equivalent to the EPA's example data file named TEST-ST.INP supplied with the COMPLEX I model. Comparisons of the predicted concentrations are presented in Table 3.8. With the exception of hour 12 for distances of 2500 m and beyond, the results obtained from the ISCST2C model are equivalent to those obtained from the EPA's COMPLEX I model.

The differences in the two models' predictions for hour 12 are due to differences in defining unlimited mixing. For stable or unlimited mixing conditions, plume trapping is not considered in either model's concentration predictions. Unlimited mixing is defined as a mixing height of 10,000 m or greater in the ISCST2C model (which is consistent with the ISCST2 model) and 5,000 m or greater in the COMPLEX I model. The meteorological conditions for hour 12 are characterized by Pasquill stability category A and a mixing height of 5,000 m which exemplifies the differences between the two models. In the ISCST2C model, a mixing height of 5,000 m represents limited mixing conditions and plume trapping is considered in the concentration predictions. Equation (3-29) is employed to account for multiple plume reflections of off the ground surface and

the top of the mixed layer. In the COMPLEX I model, a mixing height of 5,000 m represents unlimited mixing conditions and plume trapping is not considered in the concentration predictions. Equation (3-28) is employed and multiple plume reflections of off the ground surface and the top of the mixed layer are ignored. As demonstrated by Table 3.8, the differences in the definitions of unlimited mixing between the two models only matters for extremely unstable atmospheric conditions and receptor locations far from the source.

3.4.5 Comparison of SHORTZ and ISCST2C Predictions

The ISCST2C model was run using an input data file equivalent to the EPA's example data file named SHORTZ.RUN supplied with the SHORTZ model. Comparisons of the 50 predicted maximum 24-hr average concentrations for all sources combined are presented in Table 3.9. Most of the ISCST2C model predictions vary by 0.02 percent or less from the SHORTZ model predictions. The maximum variation is a 0.66 percent higher concentration predicted by the ISCST2C model compared to the SHORTZ model. According to the EPA (1993a, 1987a, 1986), an alternative model is equivalent to a regulatory model if the maximum concentrations or the highest, second highest concentrations from the models are within 2 percent. As demonstrated by Table 3.9, the results obtained from the ISCST2C model are equivalent to those obtained from the EPA's SHORTZ model.

C H A P T E R

4
APPLICATION OF THE ISCST2C MODEL

4.1
INTRODUCTION

Subsequent to producing a working air dispersion model and verifying its concentration predictions, an application of the ISCST2C model was performed for the conditions of a field experiment conducted in the wake of a building. Meteorological and concentration measurements were made during the experiment providing an opportunity to compare measured concentrations to predicted concentrations using the ISCST2C model. A review of experiments conducted in the wakes of buildings is presented in this chapter along with a discussion of the data set selected for use in evaluating the cavity, near-wake, and far-wake algorithms of the ISCST2C model.

Model application actually consists of a number of intermediate steps which include data collection and compilation, model runs, summarizing model results, sensitivity analysis, comparing model predictions against measured concentrations, interpreting results, and preparing a report (adapted from Smoot, 1993). Each of these

steps were employed in the application of the ISCST2C model. Documentation of the application of the ISCST2C model is presented in this chapter.

4.2
REVIEW OF BUILDING WAKE MEASUREMENT STUDIES

A comprehensive review of experimental data sets collected in the wakes of buildings is provided by Ramsdell (1988; 1990). A list of 29 data sets along with the appropriate references was compiled and organized according to the type of experiment, i.e., wind tunnel studies, field studies, or a combination of wind tunnel and field studies.

Questions regarding the quantitative use of wind tunnel data to estimate the flow and diffusion around buildings have been raised by Ramsdell (1988). Wind tunnel data are limited due to inherent model scaling assumptions and the inability of wind tunnels to fully simulate a meandering wind or a full range of atmospheric stabilities. Similar concerns are raised by Dickson, Start, and Markee (1969). At the Rancho Seco reactor site, wind tunnel and field experiments were conducted in the wake of the reactor building. Poor correlation between corresponding plume centerline concentrations measured in the wind tunnel and in the field was observed (Ramsdell, 1988). For these reasons, only data sets obtained from field studies were considered for use in the evaluation of the ISCST2C model.

A list of field data sets along with some release characteristics and meteorological conditions is provided in Table 4.1 (adapted from Ramsdell, 1988; 1990). Data were collected in the cavity region of the building wake in three of the seven field experiments

listed, i.e., the Experimental Breeder Reactor II (EBR-II) tests (Dickson, Start, and Markee; 1969), the Rancho Seco tests (Start, et al.; 1978), and the Experimental Organically-Cooled Reactor (EOCR) tests (Start, et al.; 1980). These data sets were obtained and evaluated further.

The EBR-II tests were conducted at a fairly complex site consisting of multiple buildings. The data set is somewhat limited in that only plume centerline concentrations are readily available as provided by Ramsdell (1988) and concentrations in the cavity region of the building wake are not available for six of the fifteen tests conducted. In addition, only ground-level releases were made during the experiment. For these reasons, the EBR-II data set was not selected for use in evaluating the ISCST2C model.

The Rancho Seco tests were conducted at a site consisting of many large structures, including a 43 m high reactor building. Tracer gases were released within the influence of the reactor building, but the site is dominated by two 146 m high hyperbolic, natural draft cooling towers located within the air sampling grid. Because of the complicating effects of the cooling tower wakes upon measured tracer gas concentrations, this data set was not selected for use in evaluating the ISCST2C model.

The EOCR tests were conducted at a relatively uncomplicated site characterized by flat desert terrain and a reasonably simple building configuration. Tracer gas releases were made at several representative heights, i.e., ground level, roof vent level, and elevated stack level. A broad set of meteorological conditions was observed during the experiment with wind speeds ranging from 0.5 to 8.0 m/s and atmospheric stabilities

ranging from A to F. Concentration measurements were made from about 10 m to 1200 m from the release points. Crosswind concentration measurements were also made during the tests. The EOCR data set is seemingly the best of the field measurement studies available and was selected for use in evaluating the ISCST2C model.

4.3 DATA COLLECTION AND COMPILATION

The data needed to predict concentrations using the ISCST2C model include source parameters, meteorology, and receptor locations. These data, as collected during the EOCR field measurement study, are compiled and presented in the following. The air concentration measurements made during the study are also compiled and presented. The methods employed for each type of measurement are described.

4.3.1 Source Parameters

The source parameters required by the ISCST2C model include pollutant emission rates, location coordinates, emission release heights, and terrain elevations at the base of the source. Additional data are required depending on the configuration of the source (i.e., point, area, or volume source). Tracer gases were released as point sources during the EOCR experiment. For point sources, exit gas temperatures, exit gas velocities, and stack tip diameters are needed for the plume rise calculations. Also, the locations and dimensions of nearby structures are needed to account for possible building wake effects on plume dispersion.

A total of 24 tests were conducted during the experiment. The first two tests were discarded due to various equipment and weather problems. During each test, three different tracer gases were released at three different heights on the EOCR building. The tracer gases employed were sulfur hexafluoride (SF_6), dichlorodifluoromethane (Freon-12), and dibromodifluoromethane (12B2). These gases were chosen as tracers because they are inert, non-toxic at the concentrations used, and have naturally low background concentrations.

The tracer gases were released at ground-level (1 m), roof-level (23 m), and stack-level (30 m) on or adjacent to the EOCR building. Ground-level releases were from one of three locations adjacent to the building: the northeast face, the northwest face, or the southwest face. Ground-level releases were generally from the windward side of the building. The roof-level release was from the center of the highest tier of the EOCR building. The stack-level release was through the existing EOCR building stack. A plot plan of the EOCR building showing the locations and providing the coordinates of the tracer gas release points is presented in Figure 4.1.

Tracer gas releases from the three different heights were started simultaneously. The tracer gas plumes were allowed to extend to the outermost sampling arc before the air sampling grid was activated. Typically, the duration of the air sampling was one hour at which time the tracer gas releases were also terminated. Table 4.2 provides a summary of the emission rates, duration, locations, and heights of the tracer gas releases for each test.

The tracer gases were released at the ambient air temperature with no upward velocity so as to ensure no plume rise. Likewise, to ensure no plume rise would be calculated in the ISCST2C model runs, stack gas temperatures and ambient air temperatures were set at 294 K. Small exit gas velocities (i.e., 0.001 m/s) and stack tip diameters (i.e., 0.001 m) were also used.

The EOCR building is located on flat, level, desert terrain. The ground cover is primarily sagebrush. There are no terrain effects on plume dispersion at the site so the stack base elevations were set at 0 m.

The BPIPC computer program was used to process the location coordinates of the sources and building corners (refer to Figure 4.1) to calculate the direction-specific building dimensions required by the ISCST2C model. Output from BPIPC includes direction-specific building heights, widths, lengths, and distances from the windward face of the building to the stack location. Results from BPIPC are summarized in Tables 4.3, 4.4, and 4.5 for the ground-level releases on the northeast, northwest, and southwest building faces, respectively, and Tables 4.6 and 4.7 for the roof-level and stack-level releases, respectively.

4.3.2 Meteorology

The meteorological data required by the ISCST2C model include wind speed, wind direction, atmospheric stability category, ambient air temperature, and mixing height. Wind speeds and atmospheric stability categories used in the ISCST2C model

runs were based on hourly measurements made during the tests. These measurements were made from an instrumented tower located 150 m northwest of the center of the sampling grid. Wind sensors were located at 4 m, 10 m, and 30 m levels. During the tests, the tower was out of the influence of the building wake.

Direct measurements of atmospheric stability category cannot be made. Atmospheric stability categories for the EOCR tests were determined using the turbulence-based Sigma-A method recommended by the EPA (1987c). The Sigma-A method uses the standard deviation of the horizontal wind direction (σ_A) measured at 10 m in combination with the mean wind speed measured at 10 m and time of day to establish the stability category. The criteria for determining the atmospheric stability category according to the Sigma-A method are presented in Tables 4.8 and 4.9.

Air flow measurements within the building wake were not made during the study. The flow vectors used in the ISCST2C model runs were based on the direction of plume transport indicated by a straight line between the tracer gas release location and the location where the plume centerline (e.g., maximum) concentration was measured in the sampling grid. Flow vectors were determined as a function of release height and sampling arc location (i.e., cavity, near-wake, and far-wake; refer to Section 4.3.3).

As discussed in Section 4.3.1, the tracer gases were released at the ambient air temperature with no upward velocity so as to ensure no plume rise. To ensure no plume rise would be calculated in the ISCST2C model runs, ambient air temperatures and stack gas temperatures were set at 294 K.

Mixing heights are not a significant meteorological factor affecting measured or predicted concentrations at distances in close proximity to a source. The farthest receptor location used in the evaluation of the ISCST2C model is approximately 400 m. Mixing heights were not determined during the EOCR experiment, so the effects of a mixing lid were ignored in the modeling. An unlimited mixing height (i.e., 10,000 m) was used in the meteorological input data files.

Summaries of the meteorological parameter values used in the ISCST2C model runs are presented in Tables 4.10, 4.11, and 4.12 for the ground-level, roof-level, and stack-level releases, respectively.

4.3.3 Receptor Locations

The receptor location data required by the ISCST2C model include location coordinates, terrain elevations, and the vertical height above the ground. A polar sampling grid was employed during the EOCR tests. Air sampling was performed along six circular arcs with radii of 37.4 m, 87.7 m, 386.3 m, 793.6 m, 1200 m, and 1600 m centered on the roof-level tracer release location. However, only the sampling data from the first three arcs were used to evaluate the ISCST2C model. The 37.4 m, 87.7 m, and 386.3 m arcs are representative of plume dispersion in the cavity, near-wake, and far-wake regions of the EOCR building, respectively. The remaining arcs are located well into the far-wake region, where the building's influence on plume dispersion is minimal. The first three arcs had sampling positions every 6 degrees. Consequently, a polar

receptor grid defined by 3 rings and 60 radials, as illustrated in Figure 4.2, was used in the ISCST2C model runs.

The terrain within the first three sampling arcs rises by no more than 10 feet above the base elevation of the EOCR building. Accordingly, flat terrain was assumed in the ISCST2C model runs. Air samples were collected at a height of 1 m which was accounted for in the ISCST2C model runs.

4.3.4 Measured Concentrations

Ambient air samples were collected in sampling bags filled by a calibrated, battery-operated pump. Each bag contained an integrated air sample over the test period (usually one-hour duration). Collected air samples were analyzed with an electron capture gas chromatography system. The simultaneous analysis of tracer gases in a bag sample was accomplished by using parallel columns.

Air samplers were not operated at every sampling grid position during the tracer gas releases. The locations where measurable tracer gas were found during the ground-level releases are given in Tables 4.13, 4.14, and 4.15 for each of the three regions of the building wake. Similarly, Tables 4.16, 4.17, and 4.18 provide the locations where measurable tracer gas were found during the roof-level releases; and Tables 4.19, 4.20, and 4.21 provide the locations where measurable tracer gas were found during the stack-level releases. These tables reveal that for some tests no concentrations, very few concentrations, or large gaps in the crosswind concentration distributions occur along a

sampling arc. In these cases, it is questionable whether or not the plume centerline was actually detected during the test. The problem is further illustrated in Figures 4.3, 4.4, and 4.5 which show the crosswind concentration distributions in the cavity region of the building wake for the ground-level, roof-level, and stack-level releases, respectively.

A test segment (e.g., the concentration distribution along a particular sampling arc for a particular release height) is deemed invalid if there are less than two crosswind concentrations on either side of the maximum concentration. Furthermore, the test segment is considered invalid if there is a gap of more than 18 degrees between the locations of the maximum concentration and either of the adjacent crosswind concentrations. Using these criteria, the following test segments are invalid:

- Ground-level release

Cavity	Tests 9, 10
Near-wake	Test 21
Far-wake	Tests 7, 11, 13, 21

- Roof-level release

Cavity	Tests 6, 8, 9, 10, 14, 20, 21, 23
Near-wake	Tests 3, 6
Far-wake	Tests 3, 4, 5, 7, 8, 9, 10, 14, 15, 22, 23

- Stack-level release

Cavity	Tests 9, 10, 12, 15, 16, 17, 18, 19, 20, 21, 22, 24
Near-wake	Tests 20, 21
Far-wake	Tests 4, 7, 8, 11, 20, 21, 22

4.4 MODEL RUNS

The ISCST2C model is a batch-type computer program that requires the data to be keyed for disk storage. Two input data files are required for a model run. One file contains control options, source data, receptor data, certain meteorological information, and output options. The other file contains the hourly meteorological data. Multiple model runs were made to obtain the predicted concentrations. A total of fifteen sets of input data files were constructed for the ISCST2C model runs: nine sets of files for the cavity region (three cavity algorithms times three release heights), three sets of files for the near-wake region (one for each release height), and three sets of files for the far-wake region (one for each release height). An example control data file is given in Figure 4.6.

4.5 SUMMARIZING MODEL RESULTS

The results of the air dispersion modeling runs were summarized in a spreadsheet. The results were arranged for ready comparison with ambient air concentration measurements. Concurrent pairs of measured versus predicted concentrations were compiled in the spreadsheet allowing the data to be sorted into various categories based on release height, meteorology, and sampling location.

4.6 SENSITIVITY ANALYSIS

The sensitivity of the ISCST2C model predictions to changes in input parameter values were analyzed by preparing curves of the normalized ground-level concentrations ($\chi u/Q$) along the plume centerline versus downwind distance (refer to Section 2.1.10). These curves can be used to interpret the concentration predictions of the different algorithms incorporated into the ISCST2C model.

For the cavity, near-wake, and far-wake algorithms, curves were prepared showing concentration predictions as a function of building configuration (i.e., tall, squat, and very squat) and plume height. These curves are presented as Figures 4.7, 4.8, and 4.9 for the Hosker cavity algorithm, the Schulman-Scire cavity algorithm, and the Gaussian cavity algorithm, respectively. The near-wake and far-wake concentrations presented in the figures were predicted using the EPA's wake algorithms of the ISCST2 model.

For the complex terrain algorithms, curves were prepared showing concentration predictions as a function of plume height above terrain height and atmospheric stability. These curves are presented as Figures 4.10 through 4.15 for stability classes A through F, respectively, using the COMPLEX I algorithm and Figures 4.16 through 4.19 for stability classes A through D, respectively, using the SHORTZ algorithm.

4.7 MEASURED VERSUS PREDICTED CONCENTRATIONS

4.7.1 Crosswind Concentration Distributions

A series of 20 figures (Figures 4.20 through 4.39) were prepared showing the crosswind concentration distributions observed in the cavity region of the building wake for each tracer gas release. Each figure provides the results from one test showing the crosswind concentration distributions in the cavity for the ground-level, roof-level, and stack-level releases. From these plots, σ_y values can be determined. Values of σ_y were not determined for those crosswind concentration distributions that contain multiple peaks indicating dramatically variable wind direction or for those crosswind concentrations distributions where the minimum number of samples and minimum spacing criteria are not satisfied (refer to Section 4.3). These measured σ_y values are plotted with downwind distance from the release point in Figure 4.40. Also plotted in Figure 4.40 are predicted σ_y values versus distance using the Gaussian cavity algorithm. Values were predicted for the wind aligned with the minimum width and maximum width of the EOCR building. This provides the minimum and maximum limits of predicted σ_y values using the Gaussian cavity algorithm. Also plotted are bands showing ± 50 percent of the predicted σ_y values.

4.7.2 Testing Model Performance

The ISCST2C model is evaluated for its ability to predict measured concentrations. The appropriate input data required by the ISCST2C model was obtained and compiled for the EOCR experiment; the ISCST2C model was run; and the results summarized in a spreadsheet.

The first test of the model is its ability to predict measured concentrations in the cavity region of the building wake. Three different cavity algorithms are tested: the Hosker formulation, the Schulman-Scire formulation, and the Gaussian cavity formulation. Concurrent pairs of measured versus predicted concentrations at the plume centerline locations as well as crosswind locations ($\pm$ 1 σ_y) within the cavity are included in the data set. This tests the algorithms' ability to simulate concentrations at a particular location at a particular time within the cavity. It provides the most stringent test of the algorithms.

Cumulative frequency distribution plots of unpaired measured and predicted concentrations in the cavity region have been prepared. Profiles of measured and predicted plume centerline concentrations with distance have also been prepared. The cumulative frequency distribution plots and downwind concentration profiles test the model's ability to simulate the distribution of concentrations unpaired in time. These provide the least stringent tests of the algorithms.

4.7.3 Performance Measures

Two general types of performance measures are used in the analysis (Fox, 1981): 1) difference measures to quantify the magnitude of the differences between predicted and measured concentrations and 2) correlation measures to quantify the association or agreement between predicted and measured concentrations. Difference measures include the median of the difference between predicted and measured concentrations; the standard deviation of the concentration difference; the root mean square error of the concentration difference; the median ratio of predicted and measured concentrations; and the ratio of the maximum predicted and maximum measured concentrations. Correlation measures include the regression equation (e.g., slope and intercept) and the correlation coefficient. Difference measures provide an indication of model accuracy; correlation measures provide an indication of model precision.

The median, standard deviation, and root mean square error of the concentration difference and the median ratio of predicted and measured concentrations are computed from concurrent values. These statistics provide an indication of model accuracy at a particular location at a particular time. The ratio of the maximum predicted and maximum measured concentrations are computed from unpaired values and provide an indication of model accuracy in predicting the distribution of measured concentrations. The regression equation and correlation coefficient are computed from concurrent pairs of measured and predicted concentrations and provide an indication of model precision at a particular location at a particular time.

4.7.4 Presentation of Results

The results of the statistical analyses of concurrent pairs of measured concentration (χ_m) and predicted concentration (χ_p) within the cavity region of the EOCR building are presented in Tables 4.22, 4.23, and 4.24 for the Hosker, the Schulman-Scire, and the Gaussian cavity algorithms, respectively. The overall data set consists of 175 pairs of measured and predicted concentrations. This data set has been sorted and further evaluated according to release height, atmospheric stability, wind speed group, and crosswind location. A four digit code is used to describe the data set. The first digit indicates the release height: 0 = all release heights, 1 = ground-level releases (1 m), 2 = roof-level releases (23 m), and 3 = stack-level releases (30 m). The second digit indicates atmospheric stability: 0 = all stabilities, 1 = unstable (A, B, and C), 2 = neutral (D), and 3 = stable (E and F). The third digit indicates the wind speed group: 0 = all wind speeds, 1 = release height wind speeds less than 1 m/s, 2 = release height wind speeds between 1 and 3 m/s, 3 = release height wind speeds between 3 and 5 m/s, and 4 = release height wind speeds greater than 5 m/s. The last digit indicates the crosswind location of the sampler ($\pm$ 1 σ_y) within the cavity: 0 = all locations, 1 = locations on the plume centerline, and 2 = locations off of the plume centerline. The following statistics are summarized in the tables:

n - the number of data points in the data set;

$\tilde{\chi}_m$ - the median measured concentration ($\mu g/m^3$);

$\tilde{\chi}_p$ - the median predicted concentration ($\mu g/m^3$);

χ'_m - the maximum measured concentration ($\mu g/m^3$);

χ'_p - the maximum predicted concentration ($\mu g/m^3$);

$\tilde{d}$ - the median difference between predicted and measured concentrations ($\mu g/m^3$)

$$\tilde{d} = \text{middle value of } d_1, d_2, d_3, \ldots, d_n \tag{4-1}$$

where $d = \chi_p - \chi_m$ (the concentration difference);

S_d - the standard deviation of the concentration difference ($\mu g/m^3$)

$$S_d = \sqrt{\frac{1}{n-1}\sum(d-\bar{d})^2} \tag{4-2}$$

where $\bar{d} = \frac{1}{n}\sum d$ (the arithmetic mean concentration difference);

rms_d - the root mean square error of the concentration difference ($\mu g/m^3$)

$$rms_d = \sqrt{\frac{1}{n}\sum d^2}\ ; \tag{4-3}$$

$\tilde{k}$ - the median ratio of the predicted and measured concentrations

$$\tilde{k} = \text{middle value of} \left(\frac{\chi_p}{\chi_m}\right)_1, \left(\frac{\chi_p}{\chi_m}\right)_2, \left(\frac{\chi_p}{\chi_m}\right)_3, \ldots, \left(\frac{\chi_p}{\chi_m}\right)_n ; \tag{4-4}$$

k' - the ratio of the maximum predicted and maximum measured concentrations

$$k' = \frac{\chi'_p}{\chi'_m}; \tag{4-5}$$

m - the slope of the regression line

$$m = \frac{\sum \chi_m \chi_p - \sum \chi_m \sum \chi_p / n}{\sum \chi_m^2 - (\sum \chi_m)^2 / n}; \tag{4-6}$$

b - the intercept of the regression line

$$b = \frac{\sum \chi_p - m\sum \chi_m}{n}; \text{ and} \tag{4-7}$$

r - the correlation coefficient

$$r = m\sqrt{\frac{1}{n-1}\sum(\chi_m - \bar{\chi}_m)^2} \Big/ \sqrt{\frac{1}{n-1}\sum(\chi_p - \bar{\chi}_p)^2}. \tag{4-8}$$

The results of the regression analysis are depicted in a series of scatter diagrams. The scatter diagrams were prepared from the overall data set which consists of concentrations at the plume centerline locations as well as crosswind locations ($\pm$ 1 σ_y) within the cavity. Concurrent values of measured and predicted concentrations within the cavity are plotted in the scatter diagrams with the least-squares line of best fit drawn through the data. Each figure contains three graphs to present and readily compare the results from the Hosker cavity algorithm, the Schulman-Scire cavity algorithm, and the Gaussian cavity algorithm. A figure is provided for each of the thirteen data sort categories (i.e., all data combined and the data sorted by release height, atmospheric stability, wind speed, and crosswind sampling location).

Figure 4.41 presents the scatter diagrams of measured versus predicted concentrations for all data combined. Figures 4.42, 4.43, and 4.44 are scatter diagrams of measured versus predicted concentrations for the data sorted by ground-level, roof-level, and stack-level releases, respectively. Scatter diagrams of measured versus predicted concentrations for the data sorted by unstable, neutral, and stable atmospheric stabilities are given in Figures 4.45, 4.46, and 4.47, respectively. Scatter diagrams of measured

versus predicted concentrations for the data sorted by wind speeds less than 1 m/s; wind speeds between 1 and 3 m/s; wind speeds between 3 and 5 m/s; and wind speeds greater than 5 m/s are plotted in Figures 4.48, 4.49, 4.50, and 4.51, respectively. Figures 4.52 and 4.53 are scatter diagrams of measured versus predicted concentrations for the data sorted by plume centerline and off-centerline locations, respectively.

Cumulative frequency distribution plots of measured and predicted concentrations within the cavity are presented in Figures 4.54 through 4.66. Each figure contains three plots to present and readily compare the results from the Hosker cavity algorithm, the Schulman-Scire cavity algorithm, and Gaussian cavity algorithm. A figure is provided for each of thirteen data sort categories (i.e., all data combined and the data sorted by release height, atmospheric stability, wind speed, and crosswind sampling location). The figures were prepared from the overall data set which consists of concentrations at the plume centerline locations as well as crosswind locations ($\pm$ 1 σ_y) within the cavity.

Since air dispersion models are generally used to predict the highest concentrations expected at a receptor, data sets consisting of concurrent pairs of measured and predicted concentrations at the plume centerline in the cavity, near-wake, and far-wake regions of the EOCR building were compiled. This tests the ISCST2C model's ability to simulate maximum concentrations in a building wake and provides an opportunity to compare the performance of the cavity algorithms against the performance of the EPA-adopted methods for predicting concentrations in the near-wake and far-wake regions of the building.

The results of the statistical analyses of concurrent pairs of measured and predicted concentrations at the plume centerline within the cavity region of the EOCR building are presented in Tables 4.25, 4.26, and 4.27 for the Hosker, the Schulman-Scire, and the Gaussian cavity algorithms, respectively. Tables 4.28 and 4.29 present the results of the statistical analyses of concurrent pairs of measured and predicted concentrations at the plume centerline within the near-wake and far-wake regions, respectively. The data sets have been sorted and further evaluated according to release height, atmospheric stability, and wind speed group. A four digit code is used to describe the data set where the first digit indicates the release height, the second digit indicates atmospheric stability, the third digit indicates the wind speed group, and the fourth digit indicates the crosswind location. The groupings used in the data sort and the statistics summarized in the tables are the same as those defined for Tables 4.22 through 4.24.

The results of the statistical analyses of maximum measured versus predicted concentrations within the cavity, near-wake, and far-wake regions are depicted in the scatter diagrams of Figure 4.67. Cumulative frequency distribution plots of maximum measured and predicted concentrations within the cavity, near-wake, and far-wake regions are presented in Figure 4.68. The scatter diagrams and cumulative frequency distribution plots were prepared from the data set which consists of plume centerline concentrations within the cavity, near-wake, and far-wake regions. Plume centerline concentrations in the cavity region were predicted using the Gaussian cavity algorithm;

plume centerline locations in the near-wake and far-wake regions were predicted using the EPA's wake algorithm.

Figures 4.69, 4.70, and 4.71 were prepared to illustrate the rate of pollutant dispersion downwind of the EOCR building for the ground-level, roof-level, and stack-level tracer gas releases, respectively. Profiles of measured and predicted plume centerline concentrations with distance are plotted in the figures. Each figure contains three graphs to present and readily compare the results from the Hosker, Schulman-Scire, and Gaussian cavity algorithms. Near-wake and far-wake concentrations presented in the figures were predicted using the EPA's wake algorithm.

4.8 INTERPRETING RESULTS

The performance measures of the ISCST2C model cannot be compared to any standards of performance because such standards do not exist. Rather, the performance of the ISCST2C model has to be referenced against currently recommended EPA-guideline models. Therefore, the performances of the Schulman-Scire algorithm and the Gaussian cavity algorithm are compared to the performance of the EPA-recommended Hosker cavity algorithm. The performances of all three cavity algorithms are also compared against the performance of the ISCST2 model in predicting concentrations in the near-wake and far wake regions of the building. A discussion of the results obtained from the application of the ISCST2C model is provided in Chapter 5.

C H A P T E R

5
DISCUSSION OF RESULTS

5.1
INTRODUCTION

This chapter is devoted to a discussion of results obtained from the application of the ISCST2C model as described in Chapter 4. An important part of the discussion is the sensitivity analysis of model predictions in the cavity, near-wake, and far-wake regions of a building and model predictions in rural and urban complex terrain. Another important part of the discussion is the analysis of the crosswind concentration profiles measured in the cavity region of the EOCR building. The major part of the discussion, however, is the statistical analysis of measured versus predicted concentrations in the cavity region of the EOCR building. The criteria used to interpret the results of the statistical analysis are described followed by discussions on the performance of the Hosker, Schulman-Scire, and Gaussian cavity algorithms. Next, the abilities of the three cavity algorithms to accurately and precisely predict measured plume centerline concentrations are examined. The final two sections of the chapter present performance comparisons of the three cavity

algorithms and performance comparisons of the cavity algorithms with the ISCST2 wake algorithms.

5.2 SENSITIVITY ANALYSIS

5.2.1 Cavity, Near-Wake, and Far-Wake Algorithms

The Hosker cavity algorithm predicts a constant concentration within the cavity region of a building wake (refer to Figure 4.7). In the ISCST2C model, the cavity region extends from the stack location out to 3 L downwind. Cavity concentrations predicted by the Hosker algorithm are insensitive to changes in plume height up to the cavity height or the GEP stack height, whichever is less. When the plume height is greater than the cavity height or greater than or equal to the GEP stack height, cavity concentrations are predicted to be zero. The lesser of the cavity height or the GEP stack height for the representative tall, squat, and very squat building configurations used in the sensitivity analysis are 45 m, 10 m, and 10 m, respectively. The differences in $\chi u/Q$ for the various building configurations are a direct function of the differences in the cross-sectional areas of the buildings. At the end of the cavity region and beginning of the near-wake region there are large discontinuities between the concentration predictions of the Hosker cavity algorithm and the ISCST2 near-wake algorithm.

The Schulman-Scire cavity algorithm also predicts a constant concentration within the cavity region of a building wake (refer to Figure 4.8). Cavity concentrations predicted by the Schulman-Scire algorithm are sensitive to changes in plume height up to the GEP stack height. When the plume height is greater than or equal to the GEP stack height, cavity concentrations are predicted to be zero. The GEP stack heights for the representative tall, squat, and very squat building configurations used in the sensitivity analysis are 45 m, 25 m, and 25 m, respectively. The differences in $\chi u/Q$ for the various plume heights are a direct function of the differences in the stretched-string distance. As with the Hosker algorithm, at the end of the cavity region and the beginning of the near-wake region there are large discontinuities between the concentration predictions of the Schulman-Scire cavity algorithm and the ISCST2 near-wake algorithm.

Unlike the Hosker and Schulman-Scire algorithms, the Gaussian cavity algorithm predicts concentrations which vary with downwind distance within the cavity region of a building wake (refer to Figure 4.9). Cavity concentrations predicted by the Gaussian algorithm are sensitive to changes in plume height up to the GEP stack height. When the plume height is greater than or equal to the GEP stack height, cavity concentrations are predicted to be zero. The differences in $\chi u/Q$ for the various plume heights are a direct function of the differences in the effects of the term

$$\exp\left[-\frac{1}{2}\left(\frac{H}{\sigma_z}\right)^2\right] \qquad (5\text{-}1)$$

in the Gaussian plume equation; refer to Equation (2-17). There are fewer discontinuities between the concentration predictions of the Gaussian cavity algorithm and the ISCST2 near-wake algorithm. For plume heights less than or equal to 1.2 h_b, the concentration predictions at the end of the cavity region and the beginning of the near-wake region are continuous. For plume heights greater than 1.2 h_b, there are discontinuities between the concentration predictions of the Gaussian cavity algorithm and the ISCST2 near-wake algorithm at the end of the cavity region and the beginning of the near-wake region. These discontinuities occur because σ_y is modified in the Gaussian cavity algorithm if the plume height is less than the GEP stack height (i.e., $H < h_b + 1.5\ L$); whereas, σ_y is modified in the ISCST2 wake algorithm if the plume height is less than or equal to 1.2 h_b (i.e., $H \leq 1.2\ h_b$). Another influence on the discontinuities between the two algorithms is that the linear decay factor of the ISCST2 wake algorithm is not incorporated into the Gaussian cavity algorithm. The linear decay factor is used to further modify σ_z if $h < h_b + 0.5\ L$. The effects of the linear decay factor on near-wake and far-wake concentrations are noted for the tall building configuration where higher concentrations are predicted for a plume height of 40 m compared to a plume height of 35 m at distances ranging from 70 to 250 m (refer to Figure 4.7, 4.8, or 4.9).

For the conditions reflected in the sensitivity analysis, the Schulman-Scire algorithm tends to predict higher cavity concentrations than either the Hosker or Gaussian cavity algorithms. The conditions emulated in the sensitivity analysis are representative of the EOCR experiment where tracer gases were released at the ambient air temperature

with no upward velocity so as to ensure no plume rise. The exit gas velocity is an important parameter affecting the calculation of the dilution component in the Schulman-Scire formulation. The lower the exit gas velocity, the lower the dilution between source and receptor, and the higher the predicted cavity concentration. The results presented in the sensitivity analysis depict the highest concentrations expected to be predicted with the Schulman-Scire cavity algorithm.

5.2.2 Complex Terrain Algorithms

Concentrations predicted by the COMPLEX I algorithm (refer to Figures 4.10 to 4.15) tend to be more sensitive to changes in plume height above terrain height than concentrations predicted by the SHORTZ algorithm (refer to Figures 4.16 to 4.19). Higher concentrations are generally predicted by the SHORTZ algorithm compared to concentrations predicted by the COMPLEX I algorithm. This indicates that a source located in urban complex terrain could potentially have a greater predicted effect on ambient air concentrations than if it were located in rural complex terrain.

5.3 CROSSWIND CONCENTRATION DISTRIBUTIONS

One of the fundamental differences between the Gaussian cavity algorithm and the Hosker or Schulman-Scire cavity algorithms is the assumption regarding the crosswind distribution of the pollutant within the cavity. In the Hosker and Schulman-

Scire algorithms, the horizontal and vertical concentration profiles are assumed to emulate a top-hat distribution, e.g., a constant concentration across the width and height of the cavity with zero concentration outside of the cavity. As indicated by its name, the horizontal and vertical concentration profiles in the Gaussian algorithm are assumed to follow a Gaussian distribution.

In the EOCR tracer gas release experiment, concentration measurements were made along an arc passing across the width of the cavity. The resulting crosswind concentration profiles tend to support the hypothesis that horizontal plume dispersion within the cavity region of a building wake generally follow a Gaussian distribution (refer to Figures 4.20 through 4.39). The existence of a flat crosswind concentration profile in the cavity was not observed during the field experiment.

From some of the crosswind concentration distributions, measured σ_y values were determined and plotted against predicted σ_y values by the Gaussian cavity algorithm. Although there is considerable scatter in the data, the results suggest that horizontal dispersion in the cavity region of the EOCR building is relatively independent of downwind distance (refer to Figure 4.40). The results also indicate that the Gaussian cavity algorithm provides reasonable predictions of σ_y. All but one of the measured values fall within $\pm$ 50 percent of the range of predicted values for the EOCR building.

5.4
MEASURED VERSUS PREDICTED CONCENTRATIONS

5.4.1 Criteria Used to Interpret Results

Several key statistical parameters are used as the basis for interpreting model performance in predicting measured concentrations in the wake of the EOCR building. These are the number of data points in the data set (n); the median ratio of predicted to measured concentrations ($\tilde{k}$); and the correlation coefficient of the regression analysis (r). Values of n, $\tilde{k}$, and r are provided in the statistical summary diagrams of Figures 5.1, 5.2, and 5.3 for the Hosker, Schulman-Scire, and Gaussian cavity algorithms, respectively. Statistics are provided for the data set as a whole and the data sorted by release height (i.e., ground-level, roof-level, and stack-level releases); by stability (i.e., unstable, neutral, and stable atmospheric conditions); by wind speed (i.e., 1.0 m/s $\leq u_h$, 1.0 m/s $< u_h \leq$ 3.0 m/s, 3.0 m/s $< u_h \leq$ 5.0 m/s, and $u_h >$ 5.0 m/s); and by location (i.e., plume centerline and crosswind locations).

Since air dispersion models are generally used to predict the highest concentrations at a receptor, another series of statistical summary diagrams are provided to help interpret the performance of the models in predicting plume centerline concentrations within the cavity. Figures 5.4, 5.5, and 5.6 summarize n, $\tilde{k}$, and r values from the statistical analysis of measured versus predicted plume centerline concentrations for the Hosker, Schulman-Scire, and Gaussian cavity algorithms, respectively. Statistics

are provided for the plume centerline data set and the data further sorted according to release height, atmospheric stability, and wind speed group.

To put the performance of the three cavity algorithms in perspective, the performance of the ISCST2 model in predicting concentrations in the wake regions of the EOCR building is tested. Figures 5.7 and 5.8 summarize n, $\tilde{k}$, and r values from the statistical analysis of measured versus predicted plume centerline concentrations for the near-wake and far-wake regions, respectively. Statistics are provided for the plume centerline data set and the data further sorted according to release height, atmospheric stability, and wind speed group.

When comparing model performance for the various conditions, the median ratio of predicted to measured concentrations is used as an index of relative model accuracy and the correlation coefficient is used an index of relative model precision. Values of $\tilde{k}$ greater than one indicate the model tends to overpredict the measured concentration; whereas, $\tilde{k}$-values less than one indicate the model tends to underpredict the measured concentration. The correlation coefficient is a measure of how closely model predictions and measured concentrations are associated. Whenever the correlation coefficient is high, the model performs well for the conditions represented in the data set. Low correlation coefficients indicate a large magnitude in the variability between model predictions and measured concentrations.

The relationship among n, $\tilde{k}$, and r must also be considered when interpreting model performance. Inferences drawn from the statistical summary diagrams are usually

based on comparisons of unbalanced data sets (i.e., variable n). The size of the data set (n) is important when evaluating the significance of $\tilde{k}$ and r values. It is also important to note that model accuracy is dependent on model precision to the extent that $\tilde{k}$-values tend to be meaningless when correlation coefficients are quite low. Most of the discussion in the preceding sections is based on an interpretation of n, $\tilde{k}$, and r provided in the statistical summary diagrams.

5.4.2 Performance of the Hosker Cavity Algorithm

The overall accuracy and precision of the Hosker cavity algorithm are reflected in a $\tilde{k}$-value of 1.90 (i.e., 90 % overprediction) and a correlation coefficient of 0.43 (refer to Figure 5.1). Accuracy and precision of the model are not significantly improved when the data are sorted by release height. The model tends to predict measured concentrations more accurately for ground-level releases ($\tilde{k}$ = 0.64) than for roof-level releases ($\tilde{k}$ = 8.60) or stack-level releases ($\tilde{k}$ = 0.00). A $\tilde{k}$-value of 0.00 for the stack-level releases indicates that in more than half of the instances the model predicts zero concentration. This is because the Hosker algorithm predicts that the plume height is greater than the cavity height for these cases and thus the plume does not become entrained in the cavity. The algorithm tends to predict measured concentrations more precisely for ground-level and stack-level releases (r = 0.44) than for roof-level releases (r = 0.31).

As for atmospheric stability, the accuracy and precision of the Hosker algorithm are generally better for stable conditions ($\tilde{k}$ = 1.42 and r = 0.52) than for unstable ($\tilde{k}$ = 2.75 and r = 0.52) or neutral conditions ($\tilde{k}$ = 2.51 and r = 0.27).

When the data are sorted by wind speed group, the Hosker algorithm tends to underpredict measured concentrations for wind speeds greater than 5.0 m/s and significantly overpredict measured concentrations for wind speeds between 3.0 and 5.0 m/s. The error ranges from 104 percent underprediction for $u_h > 5.0$ m/s to 625 percent overprediction for $3.0 < u_h \leq 5.0$ m/s - about a factor of 14.8. There is also a large variation in the precision of the model to predict measured concentrations sorted by wind speed as reflected in the correlation coefficients which range from 0.30 for $3.0 < u_h \leq 5.0$ m/s to 0.73 for $u_h > 5.0$ m/s. The correlation coefficient obtained for the data sorted by wind speeds greater than 5.0 m/s (i.e., r = 0.73) represents the highest r-value obtained in the statistical analysis of measured versus predicted concentrations for the Hosker algorithm.

The Hosker algorithm performs similarly for centerline and crosswind receptor locations. There is a median 41 percent overprediction of measured concentrations for plume centerline receptors and a median 97 percent overprediction of measured concentrations for receptors at crosswind locations. Correlation coefficients are 0.44 and 0.43 for the data sorted by plume centerline and crosswind locations, respectively.

5.4.3 Performance of the Schulman-Scire Cavity Algorithm

Overall, the Schulman-Scire cavity algorithm tends to overpredict measured concentrations as reflected in a $\tilde{k}$-value of 12.32. The overall precision of the algorithm is reflected in a correlation coefficient of 0.45. Refer to Figure 5.2. The model tends to significantly overpredict measured concentrations for each of the release heights. The range of the error is 282 percent overprediction for ground-level releases to 2442 percent overprediction for roof-level releases. There is also a wide range in the precision of the model to predict measured concentrations by release height. The algorithm tends to predict measured concentrations more precisely for stack-level releases (r = 0.73) than for roof-level (r = 0.43) or ground-level releases (r = 0.28).

As for atmospheric stability, the accuracy of the Schulman-Scire algorithm is generally better for neutral conditions ($\tilde{k}$ = 7.05) than for unstable ($\tilde{k}$ = 18.20) or stable conditions ($\tilde{k}$ = 14.98); whereas the precision tends to be better for unstable conditions (r = 0.83) than for neutral (r = 0.64) or stable conditions (r = 0.36).

The Schulman-Scire algorithm tends to significantly overpredict measured concentrations for each of the data sets grouped by wind speeds. The accuracy and precision of the model is best for wind speeds greater than 5.0 m/s as reflected in a $\tilde{k}$-value of 1.98 and a r-value of 0.83. These represent the highest values obtained in the statistical analysis of measured versus predicted concentrations for the Schulman-Scire algorithm. For those data sort groups of wind speeds less than or equal to 5.0 m/s, the model tends to overpredict measured concentrations by a factor of 13 to 14.5. The model

tends to predict measured concentrations fairly precisely for wind speeds between 1.0 and 3.0 m/s (r = 0.78) and wind speeds between 3.0 and 5.0 m/s (r = 0.70), but poorly for wind speeds less than 1.0 m/s (r = 0.31).

Although significantly overpredicting measured concentrations for the data sorted by receptor location, the Schulman-Scire algorithm performs slightly better for centerline locations than for crosswind locations. There is a median 661 percent overprediction of measured concentrations on the plume centerline and a median 1328 percent overprediction of measured concentrations at crosswind locations. Correlation coefficients are 0.52 and 0.43 for the data sorted by centerline and crosswind locations, respectively.

5.4.4 Performance of the Gaussian Cavity Algorithm

The overall accuracy and precision of the Gaussian cavity algorithm are reflected in a $\tilde{k}$-value of 1.11 (i.e., 11 % overprediction) and a correlation coefficient of 0.73 (refer to Figure 5.3). Accuracy and precision of the model are somewhat mixed for the data sorted by release height. For stack-level releases, the model tends to predict measured concentrations fairly accurately and precisely ($\tilde{k}$ = 0.90 and r = 0.90). Accuracy and precision of the model are reduced for ground-level ($\tilde{k}$ = 0.78 and r = 0.64) and roof-level releases ($\tilde{k}$ = 1.83 and r = 0.53).

The Gaussian algorithm performs well for the data sorted by atmospheric stability. The accuracy and precision of the model are generally better for neutral conditions ($\tilde{k}$ =

0.90 and r = 0.89) than for unstable ($\tilde{k}$ = 1.61 and r = 0.71) or stable conditions ($\tilde{k}$ = 1.37 and r = 0.69).

When the data are sorted by wind speed group, the Gaussian algorithm tends to underpredict measured concentrations for wind speeds greater than 5.0 m/s and overpredict measured concentrations for wind speeds less than 1.0 m/s. The error ranges from 127 percent underprediction for u_h > 5.0 m/s to 47 percent overprediction for 1.0 m/s ≤ u_h - about a factor of 3.3. The model is relatively precise in predicting measured concentrations sorted by wind speed as reflected in the correlation coefficients which range from 0.66 for 1.0 m/s ≤ u_h to 0.95 for u_h > 5.0 m/s. The correlation coefficients obtained for the data sorted by wind speeds between 3.0 and 5.0 m/s and wind speeds greater than 5.0 m/s (i.e., r = 0.95 for both groups) represent the highest r-values obtained in the statistical analysis of measured versus predicted concentrations for the Gaussian algorithm.

The Gaussian algorithm performs similarly for centerline and crosswind receptor locations. There is a median 46 percent overprediction of measured concentrations for plume centerline receptors and a median 4 percent overprediction of measured concentrations for receptors at crosswind locations. Correlation coefficients are 0.75 and 0.73 for the data sorted by plume centerline and crosswind locations, respectively.

5.4.5 Predicting Plume Centerline Concentrations

The accuracy and precision of the Hosker algorithm in predicting plume centerline concentrations measured in the cavity region of the EOCR building is mixed (refer to Figure 5.4). The algorithm tends to underpredict measured concentrations for the conditions that typically represent worst-case dispersion. These include a median 89 percent underprediction for ground-level releases; a median 37 percent underprediction for stable atmospheric conditions; and a median 49 percent underprediction for wind speeds less than or equal to 1.0 m/s. The model underpredicts the maximum plume centerline concentration measured during the study by 138 percent (i.e., $k' = 0.42$; refer to Table 4.25). The precision of the Hosker algorithm in predicting measured plume centerline concentrations is generally poorer than either the Schulman-Scire or Gaussian cavity algorithms. Correlation coefficients from the statistical analysis of measured versus predicted plume centerline concentrations range from 0.30 to 0.80 for the Hosker algorithm with all but one of the data sort categories having r-values below 0.70.

The tendency of the Schulman-Scire algorithm is to significantly overpredict plume centerline concentrations measured in the cavity region of the EOCR building (refer to Figure 5.5). The error ranges from 219 to 1790 percent overprediction with seven of the eleven data sort categories having $\tilde{k}$-values greater than 7.0 (i.e., > 700 % overprediction). The model overpredicts the maximum plume centerline concentration measured during the study by 145 percent (i.e., $k' = 2.45$; refer to Table 4.26). The precision of the Schulman-Scire algorithm in predicting measured plume centerline

concentrations is generally good as reflected in correlation coefficients which range from 0.35 to 0.96 (refer to Figure 5.5). A majority of the data sort categories have r-values above 0.70. However, the poorest precision of the Schulman-Scire algorithm in predicting measured plume centerline concentrations is for the data sort categories that represent worst-case dispersion (i.e., ground-level releases, stable atmospheric conditions, and low wind speeds).

The Gaussian algorithm tends to predict plume centerline concentrations measured in the cavity region of the EOCR building relatively accurately (refer to Figure 5.6). The tendency of the algorithm is to slightly overpredict measured concentrations. For seven of the eleven data sort categories, the model tends to predict measured concentrations within 50 percent. For the conditions that typically represent worst-case dispersion, the algorithm tends to predict measured concentrations within 25 percent. These include a median 22 percent overprediction for ground-level releases; a median 22 percent overprediction for stable atmospheric conditions; and a median 12 percent overprediction for wind speeds less than or equal to 1.0 m/s. The model accurately predicts the maximum plume centerline concentration measured during the study as reflected in a k′-value of 0.99 (refer to Table 4.27). The precision of the Gaussian algorithm in predicting measured plume centerline concentrations is generally good as reflected in correlation coefficients which range from 0.44 to 0.98 (refer to Figure 5.6). A majority of the data sort categories have r-values above 0.70.

5.4.6 Performance Comparison of the Cavity Algorithms

The Gaussian cavity algorithm generally predicts measured concentrations in the cavity region of the EOCR building more accurately and more precisely than either the Hosker cavity algorithm or the Schulman-Scire cavity algorithm. For the data set as a whole, all of the cavity algorithms tend to overpredict measured concentrations. The Gaussian algorithm tends to predict measured concentrations relatively accurately with a $\tilde{k}$-value reflecting only an 11 percent overprediction. The Hosker algorithm tends to overpredict measured concentrations by 90 percent and the Schulman-Scire algorithm tends to significantly overpredict measured concentrations with a $\tilde{k}$-value reflecting an 1132 percent overprediction. Model precision is highest for the Gaussian algorithm as reflected in an overall correlation coefficient of 0.73 compared with 0.43 for the Hosker algorithm and 0.45 for the Schulman-Scire algorithm. Inferences regarding the accuracy and precision of the Hosker, Schulman-Scire, and Gaussian cavity algorithms can also be made from the cumulative frequency distribution plots of Figure 4.54. The Gaussian algorithm is able to correctly simulate the distribution of measured concentrations unpaired in time. The Hosker algorithm overpredicts measured concentrations for most of the distribution, but underpredicts the distribution of the highest measured concentrations. The Schulman-Scire algorithm overpredicts the entire distribution of measured concentrations.

The performance of the Gaussian algorithm is also better than the Hosker and Schulman-Scire algorithms for the data sorted by release height. The accuracy of the

Gaussian algorithm is reflected in $\tilde{k}$-values which range from 0.78 to 1.83. For the Hosker algorithm $\tilde{k}$-values range from 0.00 to 8.60 and for the Schulman-Scire algorithm $\tilde{k}$-values range from 3.82 to 25.42. The precision of the Gaussian algorithm is reflected in r-values which range from 0.53 to 0.90. For the Hosker algorithm r-values range from 0.31 to 0.44 and for the Schulman-Scire algorithm r-values range from 0.28 to 0.73. The cumulative frequency distribution plots of Figures 4.55, 4.56, and 4.57 also provide insights into the accuracy and precision of the three cavity algorithms for the data sorted by ground-level, roof-level, and stack-level releases, respectively. The Gaussian algorithm more correctly simulates the distributions of measured concentrations sorted by release heights than either the Hosker or Schulman-Scire algorithms.

Similar observations are noted for the data sorted by atmospheric stability. The accuracy and precision of the Gaussian algorithm are reflected in $\tilde{k}$-values which range from 0.90 to 1.61 and r-values which range from 0.69 to 0.89. For the Hosker algorithm $\tilde{k}$-values range from 1.42 to 2.75 and r-values range from 0.27 to 0.52. For the Schulman-Scire algorithm $\tilde{k}$-values range from 7.05 to 18.20 and r-values range from 0.36 to 0.83. The distributions of measured concentrations sorted by atmospheric stability are more correctly simulated by the Gaussian algorithm than either the Hosker or Schulman-Scire algorithms (refer to Figures 4.58, 4.59, and 4.60 for unstable, neutral, and stable conditions, respectively).

The trend continues for the data sorted by wind speed group. The Gaussian algorithm tends to predict measured concentrations with median errors ranging from 127

percent underprediction to 47 percent overprediction. These compare with median errors ranging from 104 percent underprediction to 625 overprediction for the Hosker algorithm and median errors ranging from 282 to 2442 percent overprediction for the Schulman-Scire algorithm. The Gaussian algorithm is also relatively precise in predicting measured concentrations sorted by wind speed as reflected in correlation coefficients which range from 0.66 to 0.95. These compare with correlation coefficients ranging from 0.30 to 0.73 for the Hosker algorithm and correlation coefficients ranging from 0.31 to 0.83 for the Schulman-Scire algorithm. The cumulative frequency distribution plots of Figures 4.61, 4.62, 4.63, and 4.64 support the general notion that the Gaussian algorithm more correctly simulates the distributions of measured concentrations sorted by wind speeds than either the Hosker or Schulman-Scire algorithms. However, the Gaussian algorithm does a poor job in predicting the distribution of measured concentrations for wind speeds greater than 5.0 m/s (refer to Figure 4.64). Arguably, the Schulman-Scire algorithm provides better results for the data in the $u_h > 5.0$ m/s grouping.

The trend is completed with the data sorted by receptor location. The Gaussian algorithm performs similarly for centerline and crosswind locations. There is a median 46 percent overprediction of measured concentrations with a correlation coefficient of 0.75 for centerline locations and a median 4 percent overprediction of measured concentrations with a correlation coefficient of 0.73 for crosswind locations. These compare with the Hosker algorithm results of a median 41 and 97 percent overprediction of measured concentrations and correlation coefficients of 0.44 and 0.43 for centerline

and crosswind locations, respectively. The results for the Schulman-Scire algorithm are a median 661 and 1328 percent overprediction of measured concentrations and correlation coefficients of 0.52 and 0.43 for centerline and crosswind locations, respectively. The Gaussian algorithm is able to correctly simulate the distributions of measured concentrations sorted by centerline and crosswind locations as illustrated in the cumulative frequency distribution plots of Figure 4.65 and 4.66, respectively. The Hosker algorithm overpredicts measured concentrations for most of both distributions, but underpredicts both distributions for the highest measured concentrations. The Schulman-Scire algorithm overpredicts both distributions of measured concentrations.

5.4.7 Performance Comparison with the ISCST2 Wake Algorithms

The performance of the three cavity algorithms are as good as or in many cases better than the performance of the ISCST2 wake algorithms. The ISCST2 model tends to significantly overpredict plume centerline concentrations measured in the near-wake and far-wake regions of the EOCR building (refer to Figures 5.7 and 5.8). Median errors of 100 to 200 percent overprediction or more are typical for the data sort categories. The model significantly overpredicts the maximum plume centerline concentration measured in the near-wake during the study as reflected in a k′-value of 3.08 (refer to Table 4.28) but accurately predicts the maximum plume centerline concentration measured in the far-wake region as reflected in a k′-value of 1.09 (refer to Table 4.29). The precision of the ISCST2 model predicting plume centerline concentrations measured in the near-wake

region is generally poor as reflected in correlation coefficients which range from 0.19 to 0.84 (refer to Figure 5.7). Nine of the eleven data sort categories have r-values below 0.70. The precision of the ISCST2 model predicting plume centerline concentrations measured in the far-wake region is only slightly better. The correlation coefficients range from -0.19 to 0.86 with five of the eleven data sort categories having r-values below 0.70 (refer to Figure 5.8).

C H A P T E R

6
CONCLUSIONS

6.1
INTRODUCTION

Presented in this chapter are the major findings of the research. The implications of the EPA's recent release of the ISCST3 model on the completed research is also considered. The final section is the recommendations for further research.

6.2
RESEARCH FINDINGS

The objectives of this research were met. A new model that overcomes two important deficiencies in the capabilities of the EPA-guideline air dispersion models has been developed. It is called the ISCST2C model. The model is capable of predicting refined concentrations in the cavity region of a building wake and concentrations in complex terrain according to EPA policy. The ISCST2C model contains three algorithms for predicting refined cavity concentrations and three algorithms for predicting complex terrain concentrations.

One of the cavity algorithms of the ISCST2C model is based on the Hosker formulation of the EPA's SCREEN2 model. The EPA recommends the use of the screening procedures contained in the SCREEN2 model for predicting concentrations in a building cavity. Another of the cavity algorithms is based on a more recent formulation developed by Schulman and Scire as implemented in the SCREEN2C model. The third cavity algorithm is based on a Gaussian formulation that was developed as part of this research. The Gaussian cavity algorithm is consistent with current EPA methods and guidance for predicting concentrations due to plume downwash. The ISCST2C model contains the ISCST2 algorithms for predicting concentrations in the near-wake and far-wake regions of a building. To provide certain direction-specific building dimensions needed for predicting refined cavity concentrations using the Hosker and Schulman-Scire algorithms, the BPIPC computer program has been developed.

The ISCST2C model contains both simple and complex terrain algorithms to predict concentrations on intermediate and complex terrain. These algorithms are based on the ISCST2 model (simple terrain) and the COMPLEX I and SHORTZ models (complex terrain). The ISCST2C model has been developed with the capability of implementing the EPA's intermediate terrain policy for both rural and urban complex terrain applications.

The sensitivity of the ISCST2C model predictions to changes in input parameter values was analyzed by preparing curves of $\chi u/Q$ along the plume centerline versus downwind distance. There are large discontinuities between the concentration predictions

of the Hosker cavity algorithm and the ISCST2 near-wake algorithm at the boundary of the cavity and near-wake regions. There are also large discontinuities between the concentration predictions of the Schulman-Scire cavity algorithm and the ISCST2 near-wake algorithm at the cavity and near-wake boundary. There are fewer discontinuities in the concentration predictions of the Gaussian cavity algorithm and the ISCST2 near-wake algorithm. For plume heights less than or equal to 1.2 times the building height, the concentration predictions at the end of the cavity region and the beginning of the near-wake region are continuous. For greater plume heights, there are discontinuities between the concentration predictions of the Gaussian cavity algorithm and the ISCST2 near-wake algorithm because of differences in the criteria for modifying σ_y and σ_z adopted in the algorithms. The methods adopted in the Gaussian cavity algorithm was based on results from a comparison of measured and predicted concentrations.

In the SHORTZ model, the plume centerline is allowed to fully intercept elevated terrain for all stability categories. In the COMPLEX I model, the plume centerline is allowed to intercept elevated terrain with a minimum separation distance for stable conditions only. For unstable and neutral conditions, the plume centerline is slightly altered to follow the terrain feature and not allowed to intercept elevated terrain. As a result, higher concentrations are generally predicted by the SHORTZ algorithm compared to concentrations predicted by the COMPLEX I algorithm. This indicates that a source located in urban complex terrain could potentially have a greater predicted effect on ambient air concentrations than if it were located in rural complex terrain.

The most important part of this research effort was to test the refined cavity algorithms of the ISCST2C model by comparing predicted concentrations against measured concentrations from the field experiment conducted in the wake of the EOCR building. Tracer gas was released from three different levels during the experiment: on the ground, on the building roof top, and from an elevated stack. A broad set of meteorological conditions were observed during the experiment with wind speeds ranging from 0.5 to 8.0 m/s and atmospheric stabilities ranging from A to F. Concentration measurements were made along an arc traversing the width of the building cavity. The resulting crosswind concentration profiles tend to support the hypothesis of the Gaussian cavity algorithm that horizontal plume dispersion within the cavity region of a building wake generally follow a Gaussian distribution. The existence of a top-hat crosswind concentration profile in the cavity as assumed in the Hosker and Schulman-Scire cavity algorithms was not observed during the field experiment. The Gaussian cavity algorithm provides reasonable predictions of measured σ_y values.

The Gaussian cavity algorithm generally predicts measured concentrations in the cavity region of the EOCR building more accurately and more precisely than either the Hosker cavity algorithm or the Schulman-Scire cavity algorithm. The Gaussian algorithm tends to predict measured concentrations relatively accurately as reflected in an overall 11 percent overprediction. Overall, the Hosker algorithm tends to overpredict measured concentrations by 90 percent. In more than half of the instances for the stack-level releases, the Hosker algorithm predicts the plume does not become entrained in the cavity

and the cavity concentration is zero. This result was disproved by the measurements. Overall, the Schulman-Scire algorithm tends to significantly overpredict measured concentrations by 1132 percent. Model precision is generally highest for the Gaussian algorithm compared with the Hosker algorithm and the Schulman-Scire algorithm. The Gaussian algorithm is usually able to correctly simulate the distribution of measured concentrations unpaired in time. The Hosker algorithm tends to overpredict measured concentrations for most of the distribution, but underpredict the distribution of the highest measured concentrations. The Schulman-Scire algorithm tends to overpredict the entire distribution of measured concentrations.

The Hosker algorithm tends to underpredict measured plume centerline concentrations for conditions that typically represent worst-case dispersion (i.e., ground-level releases, stable atmospheric conditions, and low wind speeds). The algorithm underpredicts the maximum plume centerline concentration measured during the study by 138 percent. The precision of the Schulman-Scire algorithm is poorest when predicting measured plume centerline concentrations for the data sort categories that represent worst-case dispersion. The algorithm overpredicts the maximum plume centerline concentration measured during the study by 145 percent. The Gaussian cavity algorithm tends to predict measured plume centerline concentrations within 25 percent for the worst-case dispersion conditions. The algorithm accurately predicts the maximum plume centerline concentration measured during the study (within 1 percent).

The performance of the three cavity algorithms is as good as or in many cases better than the performance of the ISCST2 wake algorithms. The ISCST2 model tends to significantly overpredict plume centerline concentrations measured in the near-wake and far-wake regions of the EOCR building. The precision of the ISCST2 model predicting plume centerline concentrations measured in the near-wake and far-wake regions is generally poor.

6.3 RECENT RELEASE OF THE ISCST3 MODEL

Since this research was completed, the EPA (1995) released the ISCST3 model which incorporates several new features into the ISCST2 model. However, the two important deficiencies in the capabilities of other EPA-guideline models as identified in the Problem Statement of Chapter 1 are shared by the ISCST3 model. The ISCST3 model does not contain an algorithm for predicting concentrations in the cavity region of a building wake. Neither does the ISCST3 model implement the EPA's intermediate terrain policy for urban complex terrain applications, although it does for rural complex terrain applications.

The new features of the ISCST3 model include: 1) a revised area source algorithm; 2) a revised dry deposition algorithm; 3) a new wet deposition algorithm; 4) a new algorithm for modeling impacts of particulate emissions from open pit sources such as surface coal mines; and 5) incorporating the COMPLEX I algorithm for use in

predicting concentrations in rural complex terrain according to EPA policy. Only one of the new features of the ISCST3 model (i.e., item #5) partially fulfills one of the objectives of this research. The ISCST3 model implements the EPA's intermediate terrain policy for rural complex terrain applications only. The SHORTZ algorithm was not incorporated into the ISCST3 model and thus cannot be used for predicting concentrations in urban complex terrain. The ISCST2C model has the capability of implementing the intermediate terrain policy for both rural *and* urban complex terrain applications. An additional quality assurance/quality control task was completed to ensure the results obtained from the ISCST2C model are the same as those obtained from the ISCST3 model. An input data file equivalent to the EPA's example data file supplied with the COMPLEX I model was used for this task. The same results were produced by both models.

The recent update to the ISCST3 model did not revise the wake algorithms of the ISCST2 model. Neither was an algorithm for predicting concentrations in the cavity region of a building wake added to the ISCST3 model. To address this deficiency, the Gaussian cavity algorithm developed in this research was incorporated into the ISCST3 model. In a statistical analysis of measured versus predicted concentrations, the performance of the Gaussian cavity algorithm was generally better than either the Hosker or the Schulman-Scire cavity algorithms.

6.4 RECOMMENDATIONS FOR FURTHER RESEARCH

The performance of the Gaussian cavity algorithm in predicting measured concentrations in the wake of the EOCR building is favorable, but additional studies are recommended. The model tends to predict measured concentrations relatively accurately and precisely. However, these results are empirical and should be investigated using another data set. There are differences in the criteria used by the Gaussian cavity algorithm and the ISCST2 algorithm for modifying σ_y and σ_z to account for building wake effects. These differences cause discontinuities in the concentration predictions of the two algorithms at the cavity and near-wake boundary (e.g., 3 L downwind). This discrepancy between the Gaussian cavity algorithm and the ISCST2 wake algorithm requires further study.

The Gaussian cavity algorithm is precise but inaccurate in predicting measured concentrations for high wind speed conditions (i.e., $u_h > 5.0$ m/s). There is a median error of 127 percent underprediction. The same relative error is observed in predicting plume centerline concentrations and the maximum measured concentration in the data sort category. This suggests a systematic error in predicting concentrations for high wind speed conditions that should be substantiated using another data set. However, low measured concentrations are associated with high wind speeds.

In the EOCR experiment, tracer gases were released with no upward velocity so as to ensure no plume rise. The exit gas velocity is an important parameter affecting the

calculation of the dilution component in the Schulman-Scire algorithm. The lower the exit gas velocity, the lower the dilution between source and receptor, and the higher the predicted cavity concentration. The EOCR experiment represents the worst-case dilution conditions and the highest concentrations expected to be predicted with the Schulman-Scire cavity algorithm. Additional studies are recommended to test the algorithm over a range of dilution conditions including those with appreciable plume rise.

The Hosker algorithm is used in the EPA's SCREEN2 model to predict the maximum concentration likely to occur in the cavity region of a building wake. However, the results of this research indicate that the Hosker algorithm tends to underpredict measured concentrations for the conditions that represent worst-case dispersion. For these cases, the Gaussian cavity algorithm tends to predict higher concentrations that more accurately and precisely reflect measured concentrations. These results suggest that the SCREEN2 model may underestimate not overestimate actual concentrations in a building cavity. Additional studies are recommended to examine worst-case plume dispersion in the cavity region of a building wake.

LIST OF REFERENCES

LIST OF REFERENCES

1. Arie, M. M., and H. Rouse, 1956, " Experiments on Two-Dimensional Flow Over a Normal Wall", *Journal of Fluid Mechanics*, Vol. 1, Pt. 2, pp. 129-141.

2. ASHRAE, 1993, "Air Flow Around Buildings", Chapter 14 in *ASHRAE Handbook - 1993 Fundamentals*, American Society of Heating, Refrigerating, and Air Conditioning Engineers, Inc., Atlanta, Georgia.

3. Barad, M. L. (Editor), 1958, *Project Prairie Grass, A Field Program in Diffusion*, Geophysical Research Papers, No. 59, Vols. I and II, Report AFCRC-TR-58-235, Air Force Cambridge Research Center, Cambridge, Massachusetts.

4. Barry, P. J., 1964, "Estimation of Downwind Concentration of Airborne Effluents Discharged in the Neighborhood of Buildings", AECL Report 2043, Atomic Energy of Canada, Ltd., Chalk River, Ontario, Canada.

5. Bierly, E. W., and E. W. Hewson, 1962, "Some Restrictive Meteorological Conditions to be Considered in the Design of Stacks", *Journal of Applied Meteorology*, Vol. 1, No. 3, pp. 383-390.

6. Briggs, G. A., 1984, "Plume Rise and Buoyancy Effects", in *Atmospheric Science and Power Production*, D. Randerson (Editor), DOE/TIC-27601, U.S. Department of Energy, Technical Information Center, Oak Ridge, Tennessee, pp. 327-366.

7. Briggs, G. A., 1975, "Plume Rise Predictions", in *Lectures on Air Pollution and Environmental Impact Analyses*, AMS Workshop on Meteorology and Environmental Assessment, American Meteorological Society, Boston, Massachusetts 02108.

8. Briggs, G. A., 1973, "Diffusion Estimation for Small Emissions", ATDL Contribution File No. 79, Atmospheric Turbulence and Diffusion Laboratory, Oak Ridge, Tennessee.

9. Briggs, G. A., 1972, "Chimney Plumes in Neutral and Stable Surroundings", *Atmospheric Environment*, Vol. 6, No. 7, pp. 507-510.

10. Briggs, G. A., 1971, "Some Recent Analyses of Plume Rise Observations", in Proceedings of the Second International Clean Air Congress, Academic Press, New York, New York, pp. 1029-1032.

11. Briggs, G. A., 1969, *Plume Rise*, AEC Critical Review Series, U.S. Atomic Energy Commission, Office of Information Services, Oak Ridge, Tennessee.

12. Cramer, H. E., 1976, "Improved Techniques for Modeling the Dispersal of Tall Stack Plumes", *Proceedings 7th Meeting of the Expert Panel on Air Pollution Modeling*, NATO Committee on the Challenges of Modern Society, Arlie, Virginia, pp. 731-780.

13. Cramer, H. E., 1957, "A Practical Method for Estimating the Dispersal of Atmospheric Contaminants", *Proceedings of the First National Conference on Applied Meteorology*, American Meteorological Society, Hartford, Connecticut, pp. C-33 - C-55.

14. Cramer, H. E., H. V. Geary, and J. F. Bowers, 1975, "Diffusion Model Calculations of Long-Term and Short-Term Ground-Level SO_2 Concentrations in Allegheny County, Pennsylvania", EPA-903/9-75-018, EPA Region III, Philadelphia, Pennsylvania.

15. Cramer, H. E., et al., 1972, "Development of Dosage Models and Concepts", Desert Test Center Report DTC-TR-72-609, U.S. Army, Fort Douglas, Utah.

16. Davenport, A. G., 1963, "The Relationship of Wind Structure to Wind Loading", presented at the International Conference on the Wind Effects on Buildings and Structures, June 26-28, National Physical Laboratory, Teddington, Middlesex, England.

17. Dickson, C. R., G. E. Start, and E. H. Markee, 1969, "Aerodynamic Effects of the EBR-II Reactor Complex on Effluent Concentration", *Nuclear Safety*, Vol. 10, No. 3, pp. 228-242.

18. Draxler, R. A., 1984, "Diffusion and Transport Experiments", in *Atmospheric Science and Power Production*, D. Randerson (Editor), DOE/TIC-27601, U.S. Department of Energy, Technical Information Center, Oak Ridge, Tennessee, pp. 367-422.

19. EPA, 1995, "User's Guide for the Industrial Source Complex (ISC3) Dispersion Models; Volume I - User Instructions", EPA-454/B-95-003a, Office of Air Quality Planning and Standards, Research Triangle Park, North Carolina 27711.

20. EPA, 1993a, "Supplement B to the Guideline on Air Quality Models (Revised)", EPA-450/2-78-027R, Office of Air Quality Planning and Standards, Research Triangle Park, North Carolina 27711.

21. EPA, 1993b, "User's Guide to the Building Profile Input Program", Office of Air Quality Planning and Standards, Research Triangle Park, North Carolina 27711.

22. EPA, 1993c, "Meteorological Processor for Regulatory Models (MPRM) User's Guide", EPA-600/3-88-043, Office of Air Quality Planning and Standards, Research Triangle Park, North Carolina 27711.

23. EPA, 1993d, "PCRAMMET User's Guide", Office of Air Quality Planning and Standards, Research Triangle Park, North Carolina 27711.

24. EPA, 1992a, "User's Guide for the Industrial Source Complex (ISC2) Dispersion Models; Volume I - User Instructions", EPA-450/4-92-008a, Office of Air Quality Planning and Standards, Research Triangle Park, North Carolina 27711.

25. EPA, 1992b, "Screening Procedures for Estimating the Air Quality Impact of Stationary Sources, Revised", EPA-454/R-92-019, Office of Air Quality Planning and Standards, Research Triangle Park, North Carolina 27711.

26. EPA, 1992c, "SCREEN2 Model User's Guide", EPA-450/4-92-006, Office of Air Quality Planning and Standards, Research Triangle Park, North Carolina 27711.

27. EPA, 1992d, COMPLEX I Model Program Listing, Version 92290, Support Center for Regulatory Air Models (SCRAM) Bulletin Board System (BBS), Research Triangle Park, North Carolina 27711.

28. EPA, 1992e, "User's Guide for the Industrial Source Complex (ISC2) Dispersion Models; Volume II - Description of Model Algorithms", EPA-450/4-92-008b, Office of Air Quality Planning and Standards, Research Triangle Park, North Carolina 27711.

29. EPA, 1990, "User's Guide to the Complex Terrain Dispersion Model Plus Algorithms for Unstable Situations (CTDMPLUS): Volume II. The Screening Model (CTSCREEN)", EPA-600/8-90-087, Office of Research and Development, Research Triangle Park, North Carolina 27711.

30. EPA, 1989, "User's Guide to the Complex Terrain Dispersion Model Plus Algorithms for Unstable Situations (CTDMPLUS): Volume I. Model Description and User Instructions", EPA-600/8-89-041, Atmospheric Research and Exposure Assessment Laboratory, Research Triangle Park, North Carolina 27711.

31. EPA, 1987a, "Supplement A to the Guideline on Air Quality Models (Revised)", EPA-450/2-78-027R, Office of Air Quality Planning and Standards, Research Triangle Park, North Carolina 27711.

32. EPA, 1987b, "EPA Complex Terrain Model Development: Final Report", EPA-600/3-88-006, Research Triangle Park, North Carolina 27711.

33. EPA, 1987c, "On-Site Meteorological Program Guidance for Regulatory Modeling Applications", EPA-450/4-87-013, Office of Air Quality Planning and Standards, Research Triangle Park, North Carolina 27711.

34. EPA, 1986, "Guideline on Air Quality Models (Revised)", EPA-450/2-78-027R, Office of Air Quality Planning and Standards, Research Triangle Park, North Carolina 27711.

35. EPA, 1985, "Guideline for Determination of Good Engineering Practice Stack Height (Technical Support Document for the Stack Height Regulations) (Revised)", EPA-450/4-80-023R, Office of Air Quality Planning and Standards, Research Triangle Park, North Carolina 27711.

36. EPA, 1982, "User's Instructions for the SHORTZ and LONGZ Computer Programs - Volume I", EPA-903/9-82-004a, Region III, Philadelphia, Pennsylvania 19106.

37. EPA, 1980, "User's Guide for MPTER, A Multiple Gaussian Dispersion Algorithm with Optional Terrain Adjustment", EPA-600/8-80-016, Environmental Sciences Research Laboratory, Research Triangle Park, North Carolina 27711.

38. EPA, 1978, "User's Guide for RAM; Volume I. Algorithm Description and Use", EPA-600/8-78-016a, Environmental Sciences Research Laboratory, Research Triangle Park, North Carolina 27711.

39. EPA, 1977a, "User's Manual for Single Source (CRSTER) Model", EPA-450/2-77-013, Research Triangle Park, North Carolina 27711.

40. EPA, 1977b, "Valley Model User's Guide", 1977, EPA-450/2-77-018, Office of Air Quality Planning and Standards, Research Triangle Park, North Carolina 27711.

41. Environmental Research and Technology, 1987, "User's Guide to the Rough Terrain Diffusion Model (RTDM)", ERT Document No. P-D-535-585, Concord, Massachusetts.

42. Evans, B. H., 1957, "Natural Air Flow Around Buildings", Texas Engineering Experimental Station Research Report No. 59, Texas A&M University, College Station, Texas.

43. Fackrell, J. E., 1984, "Parameters Characterizing Dispersion in the Near Wake of Buildings", *Journal of Wind Engineering and Industrial Aerodynamics*, Vol. 16, pp. 97-118.

44. Fox, D. G., 1981, "Judging Air Quality Model Performance", *Bulletin American Meteorological Society*, Vol. 62, No. 5, pp. 599-609.

45. GPUSC, 1972, "Atmospheric Dispersion Experiments with SF_6 Tracer Gas at Three Mile Island Nuclear Station Under Low Wind Speed Inversion Conditions", Amendment #24, Docket No. 50-289, General Public Utilities Service Corporation.

46. Gifford, F. A. Jr., 1968, "An Outline of Theories of Diffusion in the Lower Atmosphere", in *Meteorology and Atomic Energy*, D. H. Slade (Editor), U.S. Atomic Energy Commission, Division of Technical Information, Oak Ridge, Tennessee, pp. 65-116.

47. Gifford, F. A. Jr., 1961, "Use of Routine Meteorological Observations for Estimating Atmospheric Dispersion", *Nuclear Safety*, Vol. 2, No. 4, pp. 47-51.

48. Good, M. C., and P. N. Joubert, 1968, "The Form Drag of Two-Dimensional Bluff-Plates Immersed in Turbulent Boundary Layers", *Journal of Fluid Mechanics*, Vol. 31, Pt. 3, pp. 547-582.

49. Hanna, S. R., G. A. Briggs, and R. P. Hosker, Jr., 1982, *Handbook on Atmospheric Diffusion*, DOE/TIC-11223, U.S. Department of Energy, Technical Information Center, Oak Ridge, Tennessee.

50. Hastings, C., 1955, *Approximations for Digital Computers*, Princeton University Press.

51. Haugen, D. A. (Editor), 1959, *Project Prairie Grass, A Field Program in Diffusion*, Geophysical Research Papers, No. 59, Vol. III, Report AFCRC-TR-58-235, Air Force Cambridge Research Center, Cambridge, Massachusetts.

52. Hewson, E. W., and G. C. Gill, 1944, "Meteorological Investigations in the Columbia River Valley Near Trail, B. C." U.S. Bureau of Mines Bulletin 453, U.S. Government Printing Office, Washington, D.C.

53. Hosker, R. P., 1984, "Flow and Diffusion Near Obstacles" in *Atmospheric Science and Power Production*, D. Randerson (Editor), DOE/TIC-27601, U.S. Department of Energy, Technical Information Center, Oak Ridge, Tennessee., pp. 241-326.

54. Huber, A. H., and W. H. Snyder, 1982, "Wind Tunnel Investigation of the Effects of a Rectangular-Shaped Building on Dispersion of Effluents from Short Adjacent Stacks", *Atmospheric Environment*, Vol. 16, No. 12, pp. 2837-2848.

55. Huber, A. H., and W. H. Snyder, 1976, "Building Wake Effects on Short Stack Effluents", *Preprint Volume for the Third Symposium on Atmospheric Diffusion and Air Quality*, American Meteorological Society, Boston, Massachusetts.

56. Islitzer, N. F., and D. H. Slade, 1968, "Diffusion and Transport Experiments", in *Meteorology and Atomic Energy*, D. H. Slade (Editor), U.S. Atomic Energy Commission, Division of Technical Information, Oak Ridge, Tennessee, pp. 117-188.

57. Islitzer, N. F., 1965, "Aerodynamic Effects of Large Reactor Complexes Upon Atmospheric Turbulence and Diffusion", IDO-12041, U.S. Atomic Energy Commission, Idaho Falls, Idaho.

58. Kao, S. K., 1984, "Theories of Atmospheric Transport and Diffusion" in *Atmospheric Science and Power Production*, D. Randerson (Editor), DOE/TIC-27601, U.S. Department of Energy, Technical Information Center, Oak Ridge, Tennessee., pp. 189-239.

59. Lemberg, R., 1973, "On the Wakes Behind Bluff Bodies in a Turbulent Boundary Layer", Ph.D. Thesis and Boundary Layer Wind Tunnel Report No. BLWT-3-73, University of Western Ontario, London, Ontario, Canada.

60. List, R. J., 1966, *Smithsonian Meteorological Tables*, Sixth Revised Edition, Smithsonian Institution, Washington, D. C.

61. McElroy, J. L., and F. Pooler, 1968, "The St. Louis Dispersion Study", U.S. Public Health Service, National Air Pollution Control Administration, AP-53.

62. Meroney, R. N., 1982, "Turbulent Diffusion Near Buildings", in *Engineering Meteorology*, E. J. Plate (Editor), Elsevier Scientific Publishing Company, Amsterdam, Netherlands, pp. 481-525.

63. Miller, T. L., 1994, "Lectures on Air Dispersion Modeling", Department of Civil and Environmental Engineering, The University of Tennessee, Knoxville, Tennessee 37996.

64. NRC, 1972, "Meteorological Programs in Support of Nuclear Power Plants", Regulatory Guide 1.23, Office of Standards and Development, Washington, D. C.

65. Pasquill, F., 1976, "Atmospheric Dispersion Parameters in Gaussian Plume Modeling, Part II: Possible Requirements for Change in the Turner Workbook Values", EPA-600/4-76-030b, Office of Air Quality Planning and Standards, Research Triangle Park, North Carolina 27711.

66. Pasquill, F., 1961, "The Estimation of the Dispersion of Windborne Material", *The Meteorological Magazine*, Vol. 90, No. 1063, pp. 33-49.

67. Pendergast, M. M., 1984, "Meteorological Fundamentals", in *Atmospheric Science and Power Production*, D. Randerson (Editor), DOE/TIC-27601, U.S. Department of Energy, Technical Information Center, Oak Ridge, Tennessee, pp. 33-79.

68. Pooler, F., 1965, "Potential Dispersion of Plumes from Large Power Plants", U.S. Public Health Service, Publication No. 999-AP-16.

69. Ramsdell, J. V. Jr., 1990, "Diffusion in Building Wakes for Ground-Level Releases", *Atmospheric Environment*, Vol. 24B, No. 3, pp. 377-388.

70. Ramsdell, J. V. Jr., 1988, "Atmospheric Diffusion for Control Room Habitability Assessments", NUREG/CR-5055, U.S. Nuclear Regulatory Commission, Washington, D. C.

71. Sagendorf, J. F., N. R. Ricks, G. E. Start, and C. R. Dickson, 1980, "Diffusion Near Buildings as Determined from Atmospheric Tracer Experiments", NUREG/CR-1394, U.S. Nuclear Regulatory Commission, Washington, D. C.

72. Schulman, L. L., and S. R. Hanna, 1986, "Evaluation of Downwash Modifications to the Industrial Source Complex Model", *Journal of the Air Pollution Control Association*, Vol. 36, No. 3, pp. 258-264.

73. Schulman, L. L., and J. S. Scire, 1993, "Building Downwash Screening Modeling for the Downwind Recirculation Cavity", *Journal of the Air & Waste Management Association*, Vol. 43, No. 8, pp. 1122-1127.

74. Schulman, L. L., and J. S. Scire, 1980, "Buoyant Line and Point Source (BLP) Dispersion Model User's Guide", Document P-7304B, Environmental Research and Technology, Inc., Concord, Massachusetts.

75. Sigma Research Corporation, 1994, "Revisions to SCREEN2 Model User's Guide", from the EPA's Support Center for Regulatory Air Models (SCRAM) Bulletin Board System (BBS), Research Triangle Park, North Carolina 27711.

76. Slade, D. H., 1968, "Meteorological Fundamentals for Atmospheric Transport and Diffusion Studies", in *Meteorology and Atomic Energy*, D. H. Slade (Editor), U.S. Atomic Energy Commission, Division of Technical Information, Oak Ridge, Tennessee, pp. 13-63.

77. Smith, M. E., 1963, "The Use and Misuse of the Atmosphere", Brookhaven Lecture Series, No. 24, BNL 784 (T-298), Brookhaven National Laboratory, p. 15.

78. Smoot, J. L., 1993, "Lectures on Hydrology", Department of Civil and Environmental Engineering, The University of Tennessee, Knoxville, Tennessee 37996.

79. Snyder, W. H., and R. E. Lawson, Jr., 1976, "Determination of a Necessary Height for a Stack Close to a Building - A Wind Tunnel Study", *Atmospheric Environment*, Vol. 10, No. 9, pp. 683-691.

80. Start, G. E., N. F. Hukari, J. F. Sagendorf, J. H. Cate, and C. R. Dickson, 1980, "EOCR Building Wake Effects on Atmospheric Diffusion", NUREG/CR-1395, U.S. Nuclear Regulatory Commission, Washington, D.C.

81. Start, G. E., J. H. Cate, C. R. Dickson, N. R. Ricks, G. R. Ackerman, and J. F. Sagendorf, 1978, "Rancho Seco Building Wake Effects on Atmospheric Diffusion", ARL-69, Air Resources Laboratory, National Oceanic and Atmospheric Administration, Idaho Falls, Idaho.

82. Sutton, O. G., 1932, "A Theory of Eddy Diffusion in the Atmosphere", *Proc. R. Soc. (London) Ser. A*, Vol. 135, pp. 143-165.

83. Thuillier, R. H., 1988, "Diffusion in Building Wakes", *Proceedings of the ANS Topical Meeting on Emergency Response - Planning, Technologies, and Implementation*, Charleston, South Carolina, CONF-880913, U.S. Department of Energy, Washington, D.C.

84. Thuillier, R. H., 1982, "Dispersion Characteristics in the Lee of Complex Structures", *Journal of the Air Pollution Control Association*, Vol. 32, No. 5, pp. 526-532.

85. Thuillier, R. H., and R. M. Mancuso, 1980, "Building Effects on Effluent Dispersion from Roof Vents at Nuclear Power Plants", EPRI NP-1380, Electric Power Research Institute, Palo Alto, California.

86. Turner, D. B., 1970, "Workbook of Atmospheric Dispersion Estimates", U.S. Environmental Protection Agency, AP-26, Office of Air Programs, Research Triangle Park, North Carolina 27711.

87. Turner, D. B., 1964, "A Diffusion Model for an Urban Area", *Journal of Applied Meteorology*, Vol. 3, No. 1, pp. 83-91.

88. Wark, K., and C. F. Warner, 1981, *Air Pollution: Its Origin and Control*, Second Edition, Harper & Row, Publishers, New York, New York 10022.

89. Wilson, D. J., 1979, "Flow Patterns Over Flat Roofed Buildings and Application to Exhaust Stack Design", *ASHRAE Transactions*, Vol. 85, pp. 284-295.

90. Wilson, D. H., 1976, "Contamination of Air Intakes from Roof Exhaust Vents", *ASHRAE Transactions*, Vol. 82, pp. 1024-1038.

91. Wilson, D. J., and R. E. Britter, 1982, "Estimates of Building Surface Concentrations from Nearby Point Sources", *Atmospheric Environment*, Vol. 16, No. 11, pp. 2631-2646.

92. Wilson, D. J., and E. H. Chui, 1987, "Effect of Turbulence from Upwind Buildings on Dilution of Exhaust Gases", *ASHRAE Transactions*, Vol. 93, No. 2, pp. 2186-2197.

93. Wilson, D. J., and E. H. Chui, 1985, "Influence of Exhaust Velocity and Wind Incidence Angle on Dilution from Roof Vents", *ASHRAE Transactions*, Vol. 91, No. 2b, pp. 1693-1706.

DEVELOPING A NEW DISPERSION MODEL FOR PREDICTING AIR POLLUTION LEVELS IN THE CAVITY REGION OF A BUILDING WAKE AND COMPLEX TERRAIN

A Dissertation

Presented for the

Doctor of Philosophy

Degree

The University of Tennessee, Knoxville

Steven Michael Claggett

May 1996

VOLUME 2

APPENDICES

APPENDIX A

TABLES

TABLE 1.1 Regulatory Gaussian Plume Models

EPA-Recommended Application	Refined Models							Screening Model	Complex Terrain Screening Models	
	CRSTER	RAM	MPTER	ISCST2	BLP	CDM 2.0	ISCLT2	SCREEN2	COMPLEX I	SHORTZ
Short-Term Concentrations	•	•	•	•	•			•	•	•
Long-Term Concentrations	•	•	•	•	•	•	•		•	•
Single Source	•	•	•	•	•	•	•	•	•	•
Multiple Sources		•	•	•	•	•	•		•	•
Rural Dispersion Coefficients	•		•	•	•		•	•	•	
Urban Dispersion Coeff.	•	•	•	•		•	•	•		•
Point Sources	•	•	•	•	•	•	•	•	•	•
Area Sources		•		•		•	•	•		•
Volume Sources				•			•	•		•
Buoyant Industrial Line Src.					•					
Flares								•		
Building Wake Effects				•	•		•	•		
Cavity Concentrations								•		
Flat Terrain	•	•	•	•	•	•	•	•		
Simple Terrain	•		•	•	•		•	•		
Complex Terrain								•	•	•
Intermediate Terrain										
Gravitational Settling				•			•			
Pollutant Deposition				•			•			
Pollutant Decay	•	•	•	•	•	•	•		•	•
Fumigation								•		

TABLE 2.1 Cramer's Classifications of Atmospheric Stability

Atmospheric Stability	σ_θ (degrees)	σ_ϕ (degrees)
Extremely Unstable	30	10
Near Neutral (rough surface; trees, buildings)	15	5
Near Neutral (very smooth surface; grass)	6	2
Extremely Stable	3	1

TABLE 2.2 Key to Pasquill's Atmospheric Stability Categories

A: Extremely unstable conditions
B: Moderately unstable conditions
C: Slightly unstable conditions
D: Neutral conditions
E: Slightly stable conditions
F: Moderately stable conditions

Surface Wind Speed at 10 m (m/s)	Daytime Insolation			Nighttime Conditions	
	Strong	Moderate	Slight	Thinly Overcast or ≥ 4/8 Low Cloud	≤ 3/8 Cloudiness
<2	A	A-B	B		
2	A-B	B	C	E	F
4	B	B-C	C	D	E
6	C	C-D	D	D	D
>6	C	D	D	D	D

Notes: Night refers to the period from 1 hour before sunset to 1 hour after sunrise.

D stability should be used, regardless of wind speed, for overcast conditions during day or night, and for any sky conditions during the hour preceding or following night as defined above.

According to Turner (1970), "strong" daytime insolation corresponds to a solar altitude > 60° with clear skies; "slight" insolation corresponds to a solar altitude from 15° to 35° with clear skies. Cloudiness will decrease insolation and should be considered along with solar altitude in determining insolation. Insolation that would be strong with clear skies can be expected to be reduced to moderate with broken (5/8 to 7/8) middle clouds and to slight with broken low clouds.

TABLE 2.3 Turner's Key to Pasquill's Stability Categories

Wind Speed (knots)	Net Radiation Index (refer to Table 3.4)						
	4	3	2	1	0	-1	-2
0, 1	A	A	B	C	D	F	G*
2, 3	A	B	B	C	D	F	G
4, 5	A	B	C	D	D	E	F
6	B	B	C	D	D	E	F
7	B	B	C	D	D	D	E
8, 9	B	C	C	D	D	D	E
10	C	C	D	D	D	D	E
11	C	C	D	D	D	D	D
≥ 12	C	D	D	D	D	D	D

*Note: class G is considered as Pasquill class F.

TABLE 2.4 Steps in Determining Turner's Net Radiation Index

Time of Day[a]	Total Cloud Cover (CC)[b]	Ceiling Height (CH) (feet)	Net Radiation Index
Daytime or Nighttime	10/10	< 7000	0
Nighttime	≤ 4/10	-	-2
	> 4/10	-	-1
Daytime	≤ 5/10	-	insolation class number (refer to Table 3.5)
	5/10 < CC < 10/10	< 7000	insolation class number - 2[c]
	5/10 < CC < 10/10	7000 ≥ CH > 16000	insolation class number - 1[c]
	10/10	≥ 7000	insolation class number - 1[c]
	5/10 < CC < 10/10	≥ 16000	insolation class number[c]

[a]Nighttime refers to the period from 1 hour before sunset to 1 hour after sunrise.
[b]Opaque cloud cover is preferred.
[c]For these 4 cases, if the Net Radiation Index < 1, set it equal to 1.

TABLE 2.5 Insolation Class Number

Solar Altitude (ϕ) (degrees)	Insolation	Insolation Class Number
$60 < \phi$	strong	4
$35 < \phi \leq 60$	moderate	3
$15 < \phi \leq 35$	slight	2
$\phi \leq 15$	weak	1

TABLE 2.6 Relationships of the Vertical Temperature Gradient and the Standard Deviation of the Horizontal Wind Direction Fluctuations to Pasquill's Stability Categories

Pasquill Stability Category	Condition	Description	Wind Speed (m/s)	Temperature Change with Height (°C/100 m)	σ_θ (degrees)
A	Extremely Unstable	very sunny, summer weather	1	-1.9	25.0
B	Moderately Unstable	sunny and warm	2	-1.9 to -1.7	20.0
C	Slightly Unstable	average day	5	-1.7 to -1.5	15.0
D	Neutral	overcast day or nighttime	5	-1.5 to -0.5	10.0
E	Slightly Stable	average night	3	-0.5 to 1.5	5.0
F	Moderately Stable	clear night	2	1.5 to 4.0	2.5
	Extremely Stable		-	> 4.0	-

TABLE 2.7 Plume Spreading Angles

Atmospheric Stability	Horizontal Spreading Angle (degrees)	Vertical Spreading Angle (degrees)
Unstable	40	20
Neutral	20	10
Stable	10	5

TABLE 2.8 Areas of the Normal Curve

Standard Deviation Units	0	1	2	3	4	5	6	7	8	9	Standard Deviation Units
0.0	.0000	.0080	.0160	.0239	.0319	.0399	.0478	.0558	.0638	.0717	0.0
0.1	.0797	.0876	.0955	.1034	.1113	.1192	.1271	.1350	.1428	.1507	0.1
0.2	.1585	.1663	.1741	.1819	.1897	.1974	.2051	.2128	.2205	.2282	0.2
0.3	.2358	.2434	.2510	.2586	.2661	.2737	.2812	.2886	.2961	.3035	0.3
0.4	.3108	.3182	.3255	.3328	.3401	.3473	.3545	.3616	.3688	.3759	0.4
0.5	.3829	.3899	.3969	.4039	.4108	.4177	.4245	.4313	.4381	.4448	0.5
0.6	.4515	.4581	.4647	.4713	.4778	.4843	.4907	.4971	.5035	.5098	0.6
0.7	.5161	.5223	.5285	.5346	.5407	.5467	.5527	.5587	.5646	.5705	0.7
0.8	.5763	.5821	.5878	.5935	.5991	.6047	.6102	.6157	.6211	.6265	0.8
0.9	.6319	.6372	.6424	.6476	.6528	.6579	.6629	.6680	.6729	.6778	0.9
1.0	.6827	.6875	.6923	.6970	.7017	.7063	.7109	.7154	.7199	.7243	1.0
1.1	.7287	.7330	.7373	.7415	.7457	.7499	.7540	.7580	.7620	.7660	1.1
1.2	.7699	.7737	.7775	.7813	.7850	.7887	.7923	.7959	.7995	.8029	1.2
1.3	.8064	.8098	.8132	.8165	.8198	.8230	.8262	.8293	.8324	.8355	1.3
1.4	.8385	.8415	.8444	.8473	.8501	.8529	.8557	.8584	.8611	.8638	1.4
1.5	.8664	.8690	.8715	.8740	.8764	.8789	.8812	.8836	.8859	.8882	1.5
1.6	.8904	.8926	.8948	.8969	.8990	.9011	.9031	.9051	.9070	.9090	1.6
1.7	.9109	.9127	.9146	.9164	.9181	.9199	.9216	.9233	.9249	.9265	1.7
1.8	.9281	.9297	.9312	.9328	.9342	.9357	.9371	.9385	.9399	.9412	1.8
1.9	.9426	.9439	.9451	.9464	.9476	.9488	.9500	.9512	.9523	.9534	1.9
2.0	.9545	.9556	.9566	.9576	.9586	.9596	.9606	.9615	.9625	.9634	2.0
2.1	.9643	.9651	.9660	.9668	.9676	.9684	.9692	.9700	.9707	.9715	2.1
2.2	.9722	.9729	.9736	.9743	.9749	.9756	.9762	.9768	.9774	.9780	2.2
2.3	.9786	.9791	.9797	.9802	.9807	.9812	.9817	.9822	.9827	.9832	2.3
2.4	.9836	.9840	.9845	.9849	.9853	.9857	.9861	.9865	.9869	.9872	2.4
2.5	.9876	.9879	.9883	.9886	.9889	.9892	.9895	.9898	.9901	.9904	2.5
2.6	.9907	.9909	.9912	.9915	.9917	.9920	.9922	.9924	.9926	.9929	2.6
2.7	.9931	.9933	.9935	.9937	.9939	.9940	.9942	.9944	.9946	.9947	2.7
2.8	.9949	.9950	.9952	.9953	.9955	.9956	.9958	.9959	.9960	.9961	2.8
2.9	.9963	.9964	.9965	.9966	.9967	.9968	.9969	.9970	.9971	.9972	2.9
3.0	.9973	.9974	.9975	.9976	.9976	.9977	.9978	.9979	.9979	.9980	3.0
3.1	.9981	.9981	.9982	.9983	.9983	.9984	.9984	.9985	.9985	.9986	3.1
3.2	.9986	.9987	.9987	.9988	.9988	.9988	.9989	.9989	.9990	.9990	3.2
3.3	.9990	.9991	.9991	.9991	.9992	.9992	.9992	.9992	.9993	.9993	3.3
3.4	.9993	.9994	.9994	.9994	.9994	.9994	.9995	.9995	.9995	.9995	3.4
3.5	.9995										
3.6	.9996										
3.7	.9997										
3.8	.9998										
3.9	.9999										

TABLE 2.9 Parameters Used to Calculate Pasquill-Gifford Rural σ_y

Pasquill Stability Category	$\sigma_y = 465.11628\,(x)\tan(TH)$ $TH = 0.017453293\,[c - d\ln(x)]$	
	c	d
A	24.1670	2.5334
B	18.3330	1.8096
C	12.5000	1.0857
D	8.3330	0.72382
E	6.2500	0.54287
F	4.1667	0.36191

Note: σ_y is in meters and x is in kilometers

TABLE 2.10 Parameters Used to Calculate Pasquill-Gifford Rural σ_z

Pasquill Stability Category	x (km)	$\sigma_z(\text{meters}) = a\ x^b$ (x in km)	
		a	b
A	< 0.10	122.800	0.94470
	0.10 - 0.15	158.080	1.05420
	0.16 - 0.20	170.220	1.09320
	0.21 - 0.25	179.520	1.12620
	0.26 - 0.30	217.410	1.26440
	0.31 - 0.40	258.890	1.40940
	0.41 - 0.50	346.750	1.72830
	0.51 - 3.11	453.850	2.11660
	> 3.11	σ_z = 5000 m	
B	< 0.20	90.673	0.93198
	0.21 - 0.40	98.483	0.98332
	> 0.40	109.300	1.09710
C	All	61.141	0.91465
D	< 0.30	34.459	0.86974
	0.31 - 1.00	32.093	0.81066
	1.01 - 3.00	32.093	0.64403
	3.01 - 10.00	33.504	0.60486
	10.01 - 30.00	36.650	0.56589
	> 30.00	44.053	0.51179

Note: For A, B, and C stability categories, if the calculated value of σ_z > 5000 m, set σ_z = 5000 m.

TABLE 2.10 (continued)

Pasquill Stability Category	x (km)	$\sigma_z(\text{meters}) = a\ x^b$ (x in km)	
		a	b
E	< 0.10	24.260	0.83660
	0.10 - 0.30	23.331	0.81956
	0.31 - 1.00	21.628	0.75660
	1.01 - 2.00	21.628	0.63077
	2.01 - 4.00	22.534	0.57154
	4.01 - 10.00	24.703	0.50527
	10.01 - 20.00	26.970	0.46713
	20.01 - 40.00	35.420	0.37615
	> 40.00	47.618	0.29592
F	< 0.20	15.209	0.81558
	0.21 - 0.70	14.457	0.78407
	0.71 - 1.00	13.953	0.68465
	1.01 - 2.00	13.953	0.63227
	2.01 - 3.00	14.823	0.54503
	3.01 - 7.00	16.187	0.46490
	7.01 - 15.00	17.836	0.41507
	15.01 - 30.00	22.651	0.32681
	30.01 - 60.00	27.074	0.27436
	> 60.00	34.219	0.21716

TABLE 2.11 Variation of Calculated Concentration with Sampling Time

Sampling Time	Ratio of Calculated Concentration to 3-min Concentration
3-min	1.00
15-min	0.82
1-hr	0.61
3-hr	0.51
24-hr	0.36

TABLE 2.12 Briggs' Formulas to Calculate McElroy-Pooler Urban Dispersion Coefficients

Pasquill Stability Category	σ_y (m)	σ_z (m)
A - B	$\frac{0.32\,x}{\sqrt{1.0+0.0004\,x}}$	$0.24\,x\sqrt{1.0+0.001\,x}$
C	$\frac{0.22\,x}{\sqrt{1.0+0.0004\,x}}$	$0.20\,x$
D	$\frac{0.16\,x}{\sqrt{1.0+0.0004\,x}}$	$\frac{0.14\,x}{\sqrt{1.0+0.0003\,x}}$
E - F	$\frac{0.11\,x}{\sqrt{1.0+0.0004\,x}}$	$\frac{0.08\,x}{\sqrt{1.0+0.0015\,x}}$

Note: x is in meters.

TABLE 2.13 Wind Profile Exponents

Surface Roughness	Stability Class					
	A	B	C	D	E	F
Urban	0.15	0.15	0.20	0.25	0.30	0.30
Rural	0.07	0.07	0.10	0.15	0.35	0.55

TABLE 2.14 Road Map for Calculating Concentrations Due to Plume Trapping

Downwind Distance	Equation
$x < x_m$	$\chi(x,y,z;H) = \frac{Q}{2\pi u \sigma_y \sigma_z} \exp\left[-\frac{1}{2}\left(\frac{y}{\sigma_y}\right)^2\right] \left\{\exp\left[-\frac{1}{2}\left(\frac{z-H}{\sigma_z}\right)^2\right] + \exp\left[-\frac{1}{2}\left(\frac{z+H}{\sigma_z}\right)^2\right]\right\}$ (2-16)
$x_m \le x < 4\,x_m$	$\chi(x,y,z;H) = \frac{Q}{2\pi u \sigma_y \sigma_z} \exp\left[-\frac{1}{2}\left(\frac{y}{\sigma_y}\right)^2\right] \left\{\exp\left[-\frac{1}{2}\left(\frac{z-H}{\sigma_z}\right)^2\right] + \exp\left[-\frac{1}{2}\left(\frac{z+H}{\sigma_z}\right)^2\right]\right\}$ $+\sum_{i=1}^{\infty}\left\{\exp\left[-\frac{1}{2}\left(\frac{z-(2iH_m-H)}{\sigma_z}\right)^2\right] + \exp\left[-\frac{1}{2}\left(\frac{z+(2iH_m-H)}{\sigma_z}\right)^2\right]\right.$ $\left. + \exp\left[-\frac{1}{2}\left(\frac{z-(2iH_m+H)}{\sigma_z}\right)^2\right] + \exp\left[-\frac{1}{2}\left(\frac{z+(2iH_m+H)}{\sigma_z}\right)^2\right]\right\}$ (2-25)
$x \ge 4\,x_m$	$\chi(x,y,z;H) = \frac{Q}{\sqrt{2\pi}\, u \sigma_y H_m} \exp\left[-\frac{1}{2}\left(\frac{y}{\sigma_y}\right)^2\right]$ (2-26)

TABLE 2.15 Comparison of Plume Rise Formulas

Holland	$\Delta h = \frac{1}{u}\left(1.5\, v_s\, d_s + 0.04\, Q_H\right)$
Stumke	$\Delta h = \frac{1}{u}\left[1.5\, v_s\, d_s + 65\, d_s^{3/2}\left(\frac{\Delta T}{T_s}\right)^{1/4}\right]$
Concawe #1	$\Delta h = \frac{2.58\, Q_H^{0.58}}{u^{0.70}}$
Concawe #2	$\Delta h = \frac{5.53\sqrt{Q_H}}{u^{3/4}}$
Lucas, Moore, and Spurr	$\Delta h = \frac{135\, Q_H^{1/4}}{u}$
Rauch	$\Delta h = \frac{47.2\, Q_H^{1/4}}{u}$
Stone and Clark	$\Delta h = \frac{1}{u}\left[\left(104.2 + 0.171\, h\right) Q_H^{1/4}\right]$
Bryant-Davidson	$\Delta h = d_s\left(\frac{v_s}{u}\right)^{1.4}\left(1 + \frac{\Delta T}{T_s}\right)$
ASME	
Momentum Sources	$\Delta h = d_s\left(\frac{v_s}{u}\right)^{1.4}$
Neutral and Unstable	$\Delta h = \frac{5.7\, Q_H}{u^3}$
Stable	$\Delta h = 0.672\left[Q_H \Big/ \left(u\, \frac{g}{T_a} \times \frac{\partial \theta}{\partial z}\right)\right]^{1/3}$

TABLE 2.15 (continued)

Moses and Carson	
All Data	$\Delta h = \frac{1}{u}\left(-0.029\ v_s\ d_s + 5.35\sqrt{Q_H}\right)$
Unstable	$\Delta h = \frac{1}{u}\left(3.47\ v_s\ d_s + 10.53\sqrt{Q_H}\right)$
Neutral	$\Delta h = \frac{1}{u}\left(0.35\ v_s\ d_s + 5.41\sqrt{Q_H}\right)$
Stable	$\Delta h = \frac{1}{u}\left(-1.04\ v_s\ d_s + 4.58\sqrt{Q_H}\right)$
Csanady	$\Delta h = \frac{9.5\ Q_H}{u^3}$

Definitions:

Δh = plume rise (m)
u = wind speed (m/s)
v_s = stack gas exit velocity (m/s)
d_s = stack exit diameter (m)
Q_H = heat emissions (kcal/s)
ΔT = temperature difference (K) between the stack gas and ambient air
T_s = stack gas temperature (K)
T_a = ambient air temperaure (K)
h = stack height (m)
g = acceleration due to gravity (9.81 m/s^2)
$\partial\theta/\partial z$ = potential temperature gradient (K/m)

TABLE 2.16 Comparison of Predicted Plume Rise with Observations for Neutral Conditions

Source	Code[a]	No. of Stacks	h (ft)	d_s (ft)	v_s (ft/s)	Range of u (ft/s)	Q_H/Stack (10^6 cal/s)	x* [b] (ft)	x (ft)	u Δh (ft-ft/s)
Ball	B					2 to 14	0.0096	14	60	112
Harwell A	HA	1	200	11.3	32.6	14 to 30	1.10	370	2950	4430
Harwell B	HB	1	200	11.3	32.6	17 to 38	1.10	370	1900	3980
Bosanquet	BO	1		6.5	31.9	14 to 33	1.54	485	600	2450
Darmstadt	DS	1	246	7.5	15.7	16 to 25	0.855	380	820	2150
Duisburg	DB	1	410	11.5	28.0	15 to 29	1.88	705	1150	3400
Tallawarra	T	1	288	20.5	12.0	20 to 23	2.93	680	1000	5500
Lakeview	L	1	493	19.5	65.0	25 to 49	11.6	1630	3250	22100
CEGB[c] Plants										
Earley	E	2	250	12.0	18.3	14 to 35	1.54	485	4800	5580
Earley	E	2	250	12.0	56.0	14 to 35	4.72	760	4800	8150
Castle Donington	CD	2	425	23.0	40.9	10 to 26	11.95	1510	4800	14800
Castle Donington	CD	2	425	23.0	54.7	10 to 35	16.0	1700	4800	18600
Northfleet	N	2	492	19.7	46.3	13 to 52	7.9	1400	5900	10900
Northfleet	N	2	492	19.7	70.0	13 to 52	11.95	1660	5900	11150
TVA[d] Plants										
Shawnee	S	8	250	14.0	48.7	8 to 29	5.45	805	2500	6210
Colbert	C	3	300	16.5	42.9	10 to 17	6.74	975	1000	7200
Johnsonville	J	2	400	14.0	94.8	6 to 22	10.8	1400	2500	10100
Widows Creek	WC	1	500	20.8	71.5	8 to 21	16.8	1910	2500	8000
Gallatin	G	1	500	25.0	52.4	7 to 34	16.9	1920	3000	14250
Gallatin	G	2	500	25.0	23.7	5 to 39	8.55	1460	2000	7850
Paradise	P	1	600	26.0	51.3	6 to 55	20.2	2300	4500	21200
Paradise	P	2	600	26.0	57.2	12 to 34	21.9	2380	4500	20000

Notes: [a]Codes referenced to Figure 2.46
[b]Calculated value from the equation, $x^* = 0.52\, F^{2/5}\, h^{3/5}$
[c]Central Electricity Generating Board
[d]Tennessee Valley Authority

TABLE 2.17 Road Map for Calculating Final Plume Rise

Unstable or Neutral Atmospheric Conditions				Stable Atmospheric Conditions	
for $F_b < 55\frac{m^4}{s^3}$, $(\Delta T)_c = 0.0297\, T_s \frac{v_s^{1/3}}{d_s^{2/3}}$		for $F_b \geq 55\frac{m^4}{s^3}$, $(\Delta T)_c = 0.00575\, T_s \frac{v_s^{2/3}}{d_s^{1/3}}$		$(\Delta T)_c = 0.019582\, T_s\, v_s \sqrt{s}$	
if $\Delta T < (\Delta T)_c$, momentum dominated	if $\Delta T \geq (\Delta T)_c$, buoyancy dominated	if $\Delta T < (\Delta T)_c$, momentum dominated	if $\Delta T \geq (\Delta T)_c$, buoyancy dominated	if $\Delta T < (\Delta T)_c$, momentum dominated	if $\Delta T \geq (\Delta T)_c$, buoyancy dominated
$\Delta h = 3\, d_s \frac{v_s}{u}$	$\Delta h = 21.425 \frac{F_b^{3/4}}{u}$	$\Delta h = 3\, d_s \frac{v_s}{u}$	$\Delta h = 38.71 \frac{F_b^{3/5}}{u}$	$\Delta h = 1.5\left(\frac{F_m}{u\sqrt{s}}\right)^{1/3}$ or $\Delta h = 3\, d_s \frac{v_s}{u}$ whichever is lower	$\Delta h = 2.6\left(\frac{F_b}{u\, s}\right)^{1/3}$

TABLE 2.18 Road Map to Account for Plume Downwash within the Near-Wake Region of a Building (for $3\,L \le x < 10\,L$)

Building Configuration	σ_y modifications (if $H \le 1.2\,h_b$)	σ_z modifications (if $H < 2.5\,h_b$)	further σ_z modifications (if $h_b \le H \le h_b + 0.5\,L$)
Tall Building $(h_b > h_w)$	$\sigma_y' = 0.35\,h_w + 0.067(x - 3\,h_w)$	$\sigma_z' = 0.7\,h_w + 0.067(x - 3\,h_w)$	$\sigma_z' = A[0.7\,h_w + 0.067(x - 3\,h_w)]$
Squat Building $(h_b \le h_w \le 5\,h_b)$	$\sigma_y' = 0.35\,h_w + 0.067(x - 3\,h_b)$	$\sigma_z' = 0.7\,h_b + 0.067(x - 3\,h_b)$	$\sigma_z' = A[0.7\,h_b + 0.067(x - 3\,h_b)]$
Very Squat Building $(h_w > 5\,h_b)$	$\sigma_y' = 0.35\,h_b + 0.067(x - 3\,h_b)$ or $\sigma_y' = 1.75\,h_b + 0.067(x - 3\,h_b)$ if the stack is within $2.5\,h_b$ of the ends of the building	$\sigma_z' = 0.7\,h_b + 0.067(x - 3\,h_b)$	$\sigma_z' = A[0.7\,h_b + 0.067(x - 3\,h_b)]$

Note: $A = \dfrac{h_b - H}{2\,L} + 1$ for $h_b \le H \le h_b + 0.5\,L$

TABLE 2.19 Default Values of σ_A and σ_E as a Function of Pasquill Stability Category

Pasquill Stability Category	σ_A (radians)		σ_E (radians)	
	Rural Areas	Urban Areas	Rural Areas	Urban Areas
A	0.2495	0.2495	0.1745	0.1745
B	0.1544	0.2495	0.1080	0.1745
C	0.1051	0.1544	0.0735	0.1080
D	0.0665	0.1051	0.0465	0.0735
E	0.0501	0.0665	0.0350	0.0465
F	0.0336	0.0665	0.0235	0.0465

TABLE 2.20 Default Values of the Wind Profile Exponents Built Into the SHORTZ Model

Pasquill Stability Category	Wind Speed (m/s)					
	0 - 1.5	1.6 - 3.0	3.1 - 5.1	5.2 - 8.2	8.3 - 10.8	> 10.8
A	0.10	0.10	0.10	0.10	0.10	0.10
B	0.15	0.10	0.10	0.10	0.10	0.10
C	0.20	0.15	0.10	0.10	0.10	0.10
D	0.25	0.20	0.15	0.10	0.10	0.10
E	0.30	0.25	0.20	0.15	0.10	0.10
F	0.40	0.30	0.20	0.15	0.10	0.10

TABLE 3.1 ISCST2C Model Subroutines that Support the Cavity and Complex Terrain Concentration Predictions

Subroutine Name	New or Modified	Purpose
ISCST2C	New	To control program execution.
INIT block data	Modified	To include the additional optional keyword MODELSEL for selecting the ISCST2, Hosker, Schulman-Scire, Gaussian cavity, COMPLEX I, and/or SHORTZ dispersion algorithms. To include the additional optional keywords ANEMELEV, SIGMAELV, and SIGMAAZM to support the SHORTZ algorithm predictions. To provide SHORTZ algorithm default values of: the power law exponents as a function of stability class and wind speed class; the vertical wind direction fluctuations (σ_E) as a function of stability class; and the horizontal wind direction fluctuations (σ_A) as a function of stability class. To include additional error messages for the Hosker algorithm.
SETUP	Modified	To provide default values of direction-specific building lengths for the Hosker and Schulman-Scire algorithms if not entered by the user. To provide default values of direction-specific distances from the upwind edge of the building to the stack for the Schulman-Scire algorithm if not entered by the user.
VARINI	Modified	To initialize MODELSEL parameters. To initialize control variables and computation variables for the Hosker and SHORTZ algorithms.
COCARD	Modified	To add the MODELSEL keyword for selecting the dispersion algorithms.
MODSEL	New	To process MODELSEL options with error handling (i.e., check for too few or too many options, check for invalid options, and check for conflicting or missing options).

TABLE 3.1 (continued)

Subroutine Name	New or Modified	Purpose
SOCARD	Modified	To add the two new keywords, BUILDLNG and BUILDSTK for inputting direction-specific building lengths (along-wind) and direction-specific distances from the upwind edge of the building to the stack for use in the Hosker and Schulman-Scire cavity algorithms.
DSFILL	Modified	To allow input of direction-specific building lengths (along-wind) and direction-specific distances from the upwind edge of the building.
MECARD	Modified	To process optional meteorological input data for use in the SHORTZ algorithm via three new keywords in the ME pathway: 1) SIGMAELV is used to input optional σ_E values as a function of atmospheric stability category; 2) SIGMAAZM is used to input optional σ_A values as a function of atmospheric stability category; and 3) ANEMELEV is used to input the ground elevation above mean sea level of the anemometer measurement location.
ANMELV	New	To read the optional anemometer base elevation.
SIGMAE	New	To read user-supplied σ_E values.
SIGMAA	New	To read user-supplied σ_A values.
PRTOPT	Modified	To print out the MODELSEL options. To print out options associated with the Hosker, Schulman-Scire, COMPLEX I, and SHORTZ algorithms.

TABLE 3.1 (continued)

Subroutine Name	New or Modified	Purpose
PRTSRC	Modified	To print out direction-specific building lengths (along-wind) and direction-specific distances from the upwind edge of the building to the stack.
PRTMET	Modified	To print out ISCST2 default, SHORTZ default, or user-supplied wind profile exponents. To print out SHORTZ default or user-supplied σ_E and σ_A values.
METEXT	Modified	To read and set appropriate meteorological data for use in the SHORTZ algorithm. These include: reading σ_E and σ_A values as part of hourly records from an ASCII file using the CARD format; selecting appropriate (i.e., default or user-supplied) values of σ_E and σ_A as a function of stability class if hourly values are not available; and selecting appropriate (i.e., default or user-supplied) values of wind speed power law exponents as a function of stability class and wind speed class if hourly values are not available.
METDAT	Modified	To read and print out σ_E and σ_A values as part of the summary of the meteorological data if SHORTZ predictions are to be made.
PCALC	Modified	To control the execution of the Hosker, Schulman-Scire, and Gaussian cavity algorithms and the execution of the COMPLEX I and SHORTZ complex terrain algorithms. If intermediate terrain is requested, PCALC performs the comparison of ISCST2 and COMPLEX I concentration predictions for rural areas or ISCST2 and SHORTZ concentration predictions for urban areas and the higher value is used.

TABLE 3.1 (continued)

Subroutine Name	New or Modified	Purpose
SETSRC	Modified	To set direction-specific building lengths (along-wind) and direction-specific distances from the upwind edge of the building to the stack for use in the Hosker and Schulman-Scire algorithms.
PHEFCX	New	To calculate effective plume height for the COMPLEX I algorithm.
PHEFSZ	New	To calculate effective plume height for the SHORTZ algorithm.
PDIS	Modified	To calculate dispersion parameters for the Gaussian cavity algorithm.
PDISCX	New	To calculate dispersion parameters for the COMPLEX I algorithm.
PDISSZ	New	To calculate dispersion parameters for the SHORTZ algorithm.
PCHICX	New	To calculate hourly point source concentrations using the Gaussian plume equation for the COMPLEX I algorithm.
PCHISZ	New	To calculate hourly point source concentrations using the Gaussian plume equation for the SHORTZ algorithm.
WSAJSZ	New	To adjust wind speed from anemometer height to stack height for use in the plume rise calculations for the SHORTZ algorithm. To adjust wind speed from anemometer height to plume height for use in the dispersion calculations for the SHORTZ algorithm.

TABLE 3.1 (continued)

Subroutine Name	New or Modified	Purpose
VERTCX	New	To calculate the vertical term for use in the Gaussian plume equation of the COMPLEX I algorithm.
VERTSZ	New	To calculate the vertical term for use in the Gaussian plume equation of the SHORTZ algorithm.
DELHSZ	New	To calculate final plume rise for the SHORTZ algorithm.
SYENH	Modified	To calculate building enhanced σ_y in the cavity region of a building wake for use in the Gaussian cavity algorithm.
SZENH	Modified	To calculate building enhanced σ_z in the cavity region of a building wake for use in the Gaussian cavity algorithm.
CAVTY1	New	To predict concentrations in the cavity region of a building wake based on the Hosker algorithm.
UCRIT	New	To compute the critical wind speed needed to trap the plume within the building cavity for use in the Hosker algorithm.
DISTFC	New	To calculate the distance to final plume rise in the computation of the critical wind speed for use in the Hosker algorithm.
DHPMOC	New	To calculate distance-dependent momentum plume rise in the computation of the critical wind speed for use in the Hosker algorithm.
HSPRMC	New	To calculate stack height adjusted for stack tip downwash in the computation of the critical wind speed for use in the Hosker algorithm.

TABLE 3.1 (continued)

Subroutine Name	New or Modified	Purpose
CAVTY2	New	To predict concentrations in the cavity region of a building wake based on the Schulman-Scire algorithm.
MAIN1.INC	Modified	To increase the limits on the number of error/warning/ information messages allowed in the ISCST2C program.
MAIN4.INC	New	To supply array names, array limits, and named common blocks to support the Hosker, Schulman-Scire, and Gaussian cavity algorithms and the COMPLEX I and SHORTZ complex terrian algorithms.

TABLE 3.2 ISCST2C Model Default Values for Hourly Turbulent Intensities

Pasquill Stability Category	σ_E (radians)	σ_A (radians)
A	0.1745	0.2495
B	0.1745	0.2495
C	0.1080	0.1544
D	0.0735	0.1051
E	0.0465	0.0665
F	0.0465	0.0665

TABLE 3.3 Default Card Image Format Available as an Option to Access an ASCII Meteorological Data File

Meteorological Variable	FORTRAN Format	Columns
Year (last 2 digits)	I2	1-2
Month	I2	3-4
Day	I2	5-6
Hour	I2	7-8
Flow Vector (degrees)	F9.4	9-17
Wind Speed (m/s)	F9.4	18-26
Ambient Temperature (K)	F6.1	27-32
Stability Class (A=1, B=2, . . . F =6)	I2	33-34
Rural Mixing Height (m)	F7.1	35-41
Urban Mixing Height (m)	F7.1	42-48
Wind Profile Exponent (CARD only)	F8.4	49-56
Vertical Potential Temperature Gradient (K/m) (CARD only)	F8.4	57-64
σ_E (radians, if <1.0; degrees, if ≥ 1.0) (CARD only)	F8.0	65-72
σ_A (radians, if <1.0; degrees, if ≥ 1.0) (CARD only)	F8.0	73-80

TABLE 3.4 Comparison of ISCST2C Model and ISCST2 Model Predictions, 3-Hour Average Concentrations

Rank	ISCST2C Conc. ($\mu g/m^3$)	ISCST2 Conc. ($\mu g/m^3$)	Percent Difference (%)	Rank	ISCST2C Conc. ($\mu g/m^3$)	ISCST2 Conc. ($\mu g/m^3$)	Percent Difference (%)
1	58.49796	58.49796	0.00	26	23.46712	23.46712	0.00
2	44.44987	44.44987	0.00	27	23.46605	23.46605	0.00
3	42.91793	42.91793	0.00	28	23.36448	23.36448	0.00
4	39.77713	39.77713	0.00	29	23.20899	23.20899	0.00
5	39.74929	39.74929	0.00	30	22.48893	22.48893	0.00
6	38.87197	38.87197	0.00	31	21.58885	21.58885	0.00
7	38.86485	38.86485	0.00	32	20.75264	20.75264	0.00
8	38.23961	38.23961	0.00	33	20.54257	20.54257	0.00
9	36.78835	36.78835	0.00	34	20.49381	20.49381	0.00
10	34.85760	34.85760	0.00	35	20.34694	20.34694	0.00
11	34.63943	34.63943	0.00	36	19.90563	19.90563	0.00
12	33.48913	33.48913	0.00	37	19.86664	19.86664	0.00
13	33.00018	33.00018	0.00	38	19.40333	19.40333	0.00
14	30.24433	30.24433	0.00	39	19.22923	19.22923	0.00
15	29.01512	29.01512	0.00	40	19.12111	19.12111	0.00
16	28.91837	28.91837	0.00	41	19.01548	19.01548	0.00
17	28.23046	28.23046	0.00	42	18.85819	18.85819	0.00
18	27.91387	27.91387	0.00	43	18.79751	18.79751	0.00
19	27.62766	27.62766	0.00	44	18.78396	18.78396	0.00
20	27.19272	27.19272	0.00	45	18.69016	18.69016	0.00
21	26.94443	26.94443	0.00	46	18.68435	18.68435	0.00
22	26.57828	26.57828	0.00	47	18.62641	18.62641	0.00
23	25.77849	25.77849	0.00	48	18.58105	18.58105	0.00
24	24.52643	24.52643	0.00	49	18.34548	18.34548	0.00
25	23.62175	23.62175	0.00	50	18.06474	18.06474	0.00

TABLE 3.5 Comparison of ISCST2C Model and ISCST2 Model Predictions, 24-Hour Average Concentrations

Rank	ISCST2C Conc. ($\mu g/m^3$)	ISCST2 Conc. ($\mu g/m^3$)	Percent Difference (%)	Rank	ISCST2C Conc. ($\mu g/m^3$)	ISCST2 Conc. ($\mu g/m^3$)	Percent Difference (%)
1	19.16219	19.16219	0.00	26	6.11606	6.11606	0.00
2	17.05618	17.05618	0.00	27	6.06938	6.06938	0.00
3	14.96334	14.96334	0.00	28	6.00619	6.00619	0.00
4	12.96035	12.96035	0.00	29	5.86348	5.86348	0.00
5	11.80088	11.80088	0.00	30	5.66910	5.66910	0.00
6	11.28550	11.28550	0.00	31	5.65172	5.65172	0.00
7	10.82985	10.82985	0.00	32	5.59537	5.59537	0.00
8	9.96251	9.96251	0.00	33	5.44591	5.44591	0.00
9	9.40921	9.40921	0.00	34	5.29404	5.29404	0.00
10	8.87260	8.87260	0.00	35	5.17007	5.17007	0.00
11	8.72792	8.72792	0.00	36	5.13712	5.13712	0.00
12	8.20316	8.20316	0.00	37	5.02653	5.02653	0.00
13	8.00629	8.00629	0.00	38	5.01194	5.01194	0.00
14	7.67080	7.67080	0.00	39	5.00498	5.00498	0.00
15	7.60356	7.60356	0.00	40	4.98424	4.98424	0.00
16	7.42794	7.42794	0.00	41	4.90845	4.90845	0.00
17	7.40934	7.40934	0.00	42	4.90821	4.90821	0.00
18	7.31224	7.31224	0.00	43	4.85900	4.85900	0.00
19	7.14673	7.14673	0.00	44	4.83446	4.83446	0.00
20	7.13027	7.13027	0.00	45	4.53527	4.53527	0.00
21	7.12761	7.12761	0.00	46	4.46501	4.46501	0.00
22	6.86429	6.86429	0.00	47	4.41879	4.41879	0.00
23	6.82080	6.82080	0.00	48	4.40116	4.40116	0.00
24	6.39990	6.39990	0.00	49	4.37727	4.37727	0.00
25	6.34529	6.34529	0.00	50	4.23232	4.23232	0.00

TABLE 3.6 Comparison of ISCST2C Model and SCREEN2 Model Cavity Algorithm Predictions

Building Cavity	ISCST2C Conc. ($\mu g/m^3$)	SCREEN2 Conc. ($\mu g/m^3$)	Percent Difference (%)
1	3167	3168	-0.03
2	1691	1691	0.00

TABLE 3.7 Comparison of ISCST2C Model and SCREEN2C Model Cavity Algorithm Predictions

Building Cavity	ISCST2C Conc. ($\mu g/m^3$)	SCREEN2C Conc. ($\mu g/m^3$)	Percent Difference (%)
Shorter Side Along Flow	203	1189	-83
Longer Side Along Flow	170	1077	-84

TABLE 3.8 Comparison of ISCST2C Model and COMPLEX I Model Predictions

Hour	x (m)	Source 1			Source 2			Source 3			All Sources		
		ISCST2C Conc. ($\mu g/m^3$)	COMPLEX I Conc. ($\mu g/m^3$)	Percent Diff. (%)	ISCST2C Conc. ($\mu g/m^3$)	COMPLEX I Conc. ($\mu g/m^3$)	Percent Diff. (%)	ISCST2C Conc. ($\mu g/m^3$)	COMPLEX I Conc. ($\mu g/m^3$)	Percent Diff. (%)	ISCST2C Conc. ($\mu g/m^3$)	COMPLEX I Conc. ($\mu g/m^3$)	Percent Diff. (%)
12	1319	1400.494	1400.483	0.00	1404.855	1404.844	0.00	738.533	738.528	0.00	3543.883	3543.855	0.00
	1710	661.284	661.279	0.00	661.990	661.985	0.00	357.629	357.626	0.00	1680.903	1680.889	0.00
	2500	210.714	207.822	1.39	210.749	207.862	1.39	115.230	113.612	1.42	536.693	529.296	1.40
	2940	146.079	125.723	16.19	146.083	125.735	16.18	80.023	68.815	16.29	372.185	320.272	16.21
	3240	129.324	101.568	27.33	129.325	101.575	27.32	70.862	55.609	27.43	329.511	258.752	27.35
	5560	75.373	59.249	27.21	75.373	59.241	27.23	41.302	32.451	27.27	192.047	150.951	27.22
13	1319	1585.296	1585.288	0.00	1571.451	1571.444	0.00	564.933	564.931	0.00	3721.680	3721.663	0.00
	1710	1432.426	1432.417	0.00	1426.259	1426.250	0.00	595.893	595.890	0.00	3454.578	3454.557	0.00
	2500	1049.738	1049.730	0.00	1048.48	1048.473	0.00	513.456	513.453	0.00	2611.675	2611.656	0.00
	2940	811.419	811.413	0.00	810.815	810.809	0.00	411.082	411.079	0.00	2033.316	2033.301	0.00
	3240	692.590	692.585	0.00	692.232	692.226	0.00	357.324	357.322	0.00	1742.146	1742.133	0.00
	5560	244.273	244.271	0.00	244.275	244.273	0.00	132.751	132.750	0.00	621.299	621.294	0.00
14	1319	664.044	664.042	0.00	598.930	598.929	0.00	159.992	159.992	0.00	1422.966	1422.963	0.00
	1710	797.745	797.741	0.00	746.005	746.002	0.00	240.251	240.250	0.00	1784.001	1783.994	0.00
	2500	1103.134	1103.127	0.00	1074.398	1074.391	0.00	456.106	456.104	0.00	2633.639	2633.622	0.00
	2940	968.432	968.425	0.00	950.796	950.789	0.00	432.185	432.182	0.00	2351.413	2351.397	0.00
	3240	901.449	901.442	0.00	889.180	889.174	0.00	421.012	421.009	0.00	2211.640	2211.625	0.00
	5560	389.171	389.168	0.00	388.510	388.507	0.00	207.717	207.715	0.00	985.397	985.390	0.00
3-hr Avg.	1319	1216.611	1216.604	0.00	1191.746	1191.739	0.00	487.819	487.817	0.00	2896.177	2896.161	0.00
	1710	963.818	963.812	0.00	944.751	944.746	0.00	397.924	397.922	0.00	2306.494	2306.480	0.00
	2500	787.862	786.893	0.12	777.876	776.909	0.12	361.598	361.056	0.15	1927.336	1924.585	0.14
	2940	641.977	635.187	1.07	635.898	629.111	1.08	307.763	304.025	1.23	1585.638	1568.323	1.10
	3240	574.454	565.198	1.64	570.246	560.992	1.65	283.066	277.980	1.83	1427.766	1404.170	1.68
	5560	236.272	230.896	2.33	236.053	230.677	2.33	127.256	124.305	2.37	599.581	585.878	2.34

TABLE 3.8 (continued)

Hour	x (m)	Source 1 ISCST2C Conc. ($\mu g/m^3$)	Source 1 COMPLEX I Conc. ($\mu g/m^3$)	Source 1 Percent Diff. (%)	Source 2 ISCST2C Conc. ($\mu g/m^3$)	Source 2 COMPLEX I Conc. ($\mu g/m^3$)	Source 2 Percent Diff. (%)	Source 3 ISCST2C Conc. ($\mu g/m^3$)	Source 3 COMPLEX I Conc. ($\mu g/m^3$)	Source 3 Percent Diff. (%)	All Sources ISCST2C Conc. ($\mu g/m^3$)	All Sources COMPLEX I Conc. ($\mu g/m^3$)	All Sources Percent Diff. (%)
15	1319	35.884	35.884	0.00	25.494	25.494	0.00	3.507	3.507	0.00	64.885	64.885	0.00
	1710	58.284	58.284	0.00	44.740	44.740	0.00	7.036	7.036	0.00	110.060	110.060	0.00
	2500	546.287	546.285	0.00	483.276	483.275	0.00	118.470	118.470	0.00	1148.034	1148.030	0.00
	2940	706.137	706.133	0.00	644.070	644.067	0.00	183.213	183.212	0.00	1533.419	1533.413	0.00
	3240	911.234	911.229	0.00	849.419	849.414	0.00	271.168	271.167	0.00	2031.821	2031.811	0.00
	5560	670.534	670.529	0.00	660.968	660.963	0.00	319.015	319.013	0.00	1650.517	1650.505	0.00
16	1319	1.116	1.116	0.00	0.507	0.507	0.00	0.132	0.132	0.00	1.755	1.755	0.00
	1710	1.047	1.047	0.00	0.524	0.524	0.00	0.131	0.131	0.00	1.702	1.702	0.00
	2500	821.413	821.409	0.00	632.975	632.972	0.00	187.484	187.484	0.00	1641.872	1641.865	0.00
	2940	1631.136	1631.127	0.00	1363.867	1363.861	0.00	457.676	457.674	0.00	3452.679	3452.663	0.00
	3240	3078.488	3078.469	0.00	2791.971	2791.955	0.00	1095.325	1095.320	0.00	6965.784	6965.744	0.00
	5560	1020.252	1020.243	0.00	1048.695	1048.686	0.00	601.270	601.265	0.00	2670.217	2670.195	0.00
17	1319	0.007	0.007	0.00	0.004	0.004	0.00	0.002	0.002	0.00	0.013	0.013	0.00
	1710	0.003	0.003	0.00	0.002	0.002	0.00	0.001	0.001	0.00	0.006	0.006	0.00
	2500	284.037	284.036	0.00	226.875	226.875	0.00	59.992	59.992	0.00	570.904	570.902	0.00
	2940	1160.807	1160.801	0.00	996.160	996.157	0.00	283.294	283.293	0.00	2440.261	2440.251	0.00
	3240	4455.594	4455.571	0.00	4113.536	4113.517	0.00	1379.132	1379.126	0.00	9948.262	9948.214	0.00
	5560	2266.513	2266.494	0.00	2298.074	2298.055	0.00	1286.882	1286.871	0.00	5851.469	5851.420	0.00
3-hr	1319	12.336	12.336	0.00	8.668	8.668	0.00	1.214	1.214	0.00	22.217	22.217	0.00
Avg.	1710	19.778	19.778	0.00	15.089	15.089	0.00	2.389	2.389	0.00	37.256	37.256	0.00
	2500	550.579	550.577	0.00	447.709	447.707	0.00	121.982	121.982	0.00	1120.270	1120.266	0.00
	2940	1166.026	1166.021	0.00	1001.366	1001.361	0.00	308.061	308.060	0.00	2475.453	2475.442	0.00
	3240	2815.105	2815.089	0.00	2584.975	2584.962	0.00	915.209	915.204	0.00	6315.289	6315.256	0.00
	5560	1319.100	1319.089	0.00	1335.912	1335.901	0.00	735.722	735.716	0.00	3390.734	3390.706	0.00

TABLE 3.9 Comparison of ISCST2C Model and SHORTZ Model Predictions

Rank	ISCST2C Conc. ($\mu g/m^3$)	SHORTZ Conc. ($\mu g/m^3$)	Percent Difference (%)	Rank	ISCST2C Conc. ($\mu g/m^3$)	SHORTZ Conc. ($\mu g/m^3$)	Percent Difference (%)
1	978.69867	978.86304	-0.02	26	81.16267	81.16995	-0.01
2	769.51813	769.58472	-0.01	27	77.57705	77.41260	0.21
3	757.56036	757.68433	-0.02	28	74.69930	74.70448	-0.01
4	444.75333	444.80811	-0.01	29	74.66181	74.66954	-0.01
5	374.68436	374.72485	-0.01	30	72.34868	72.30989	0.05
6	315.09995	315.14185	-0.01	31	71.17039	71.13933	0.04
7	266.12741	266.14941	-0.01	32	69.13321	69.06831	0.09
8	204.94763	204.97279	-0.01	33	65.39411	65.37700	0.03
9	198.65126	198.65639	0.00	34	61.63354	61.63518	0.00
10	178.77501	178.77472	0.00	35	60.01960	60.02385	-0.01
11	176.58746	176.56883	0.01	36	58.52979	58.32220	0.36
12	160.13594	160.14735	-0.01	37	57.23189	57.24533	-0.02
13	144.91896	144.89710	0.02	38	56.77550	56.76241	0.02
14	144.68800	144.68823	0.00	39	56.54599	56.54976	-0.01
15	137.07574	137.08533	-0.01	40	54.93892	54.94768	-0.02
16	120.05204	120.04817	0.00	41	54.03186	53.89925	0.25
17	115.84912	115.82636	0.02	42	52.71075	52.69847	0.02
18	114.11768	114.11478	0.00	43	50.70673	50.55800	0.29
19	104.67840	104.60376	0.07	44	49.47418	49.48622	-0.02
20	103.94363	103.90326	0.04	45	48.40836	48.31277	0.20
21	92.41021	92.40195	0.01	46	47.58395	47.53464	0.10
22	90.98980	90.97162	0.02	47	46.88060	46.88268	0.00
23	89.10958	89.09845	0.01	48	42.58626	42.58925	-0.01
24	87.53722	87.44235	0.11	49	41.82878	41.55421	0.66
25	82.98872	82.97292	0.02	50	41.61232	41.60017	0.03

TABLE 4.1 Field Experiments Conducted in Building Wakes

Site	Building Area (m^2)	Release Ht. (m)	No. of Releases	Air Sampling Locations (m)		10 m Wind Speed (m/s)		Atmospheric Stability Class	
				Min.	Max.	Min.	Max.	Min.	Max.
Materials Test Reactor (Islitzer, 1965)	1700	1	13	100	850	2.1	5.9	1	6
Experimental Breeder Reactor-II (Dickson et al., 1969)	665	1	15	30	600	4.4	11.6	1	6
Three Mile Island Nuclear Power Station (GPUSC, 1972)	2000	1	5	149	244	0.6	1.8	5	6
Millstone	1950	27.6 48.3	26 36	350	800	2.9	11.2	1	6
Rancho Seco Nuclear Power Station (Start, et al., 1978; Sagendorf, et al., 1980)	2050	4 18.5 43	27 12 5	62	800	0.5	5.3	1	6
Experimental Organically Cooled Reactor (Start, et al., 1980; Sagendorf, et al., 1980)	1090	1 23 30	22 22 20	8	1200	0.5	8.0	1	6
Duane Arnold Energy Center (Thuillier and Mancuso, 1980; Thuillier, 1982)	1850	1 23.5 45.7	11 16 12	300	1000	0.3	4.6	1	6
Diablo Canyon Power Plant (Thuillier, 1988)	1600		38	840	840	1.0	11.4	1	4

TABLE 4.2 Release Characteristics of the EOCR Tacer Gas Experiment

Test Number	Date	Start Time (MST)	Duration (min.)	SF_6 Release			Freon-12 Release			12B2 Release		
				Location	H (m)	Q (g/s)	Location	H (m)	Q (g/s)	Location	H (m)	Q (g/s)
3	7/08/75	0606	60	Stack	30	0.0462	SW Face	1	0.9945	Roof	23	0.0982
4	7/09/75	0559	50	Stack	30	0.0599	SW Face	1	0.9490	Roof	23	0.1322
5	7/18/75	1007	60	Stack	30	0.0750	SW Face	1	0.6696	Roof	23	0.1346
6	7/21/75	0624	60	Stack	30	0.1086	SW Face	1	0.6178	Roof	23	0.1346
7	7/22/75	0543	47	Stack	30	0.0898	NE Face	1	0.6233	Roof	23	0.1393
8	7/24/75	0348	29	Stack	30	0.0933	NE Face	1	0.6269	Roof	23	0.1354
9	7/28/75	0503	60	Stack	30	0.1016	NE Face	1	0.6274	Roof	23	0.1371
10	7/31/75	1024	43	Stack	30	0.1113	NE Face	1	0.6200	Roof	23	0.1388
11	8/12/75	1008	27	Stack	30	0.2104	Roof	23	0.5940	NE Face	1	0.0905
12	8/13/75	0642	30	Stack	30	0.0619	Roof	23	0.6204	NE Face	1	0.1338
13	8/14/75	1017	60	Stack	30	0.0581	Roof	23	0.5880	NE Face	1	0.1321
14	5/06/76	0619	60	NW Face	1	0.0529	Stack	30	2.1438	Roof	23	0.1459
15	5/12/76	0618	60	NE Face	1	0.1533	Stack	30	1.5907	Roof	23	0.1706
16	5/18/76	0616	60	NE Face	1	0.1593	Stack	30	1.6086	Roof	23	0.6959
17	5/21/76	0451	60	NE Face	1	0.1688	Stack	30	1.2874	Roof	23	0.6289
18	6/23/76	0435	60	NE Face	1	0.1557	Stack	30	1.2831	Roof	23	0.6246
19	6/29/76	0329	60	NE Face	1	0.1566	Stack	30	1.2582	Roof	23	0.6192
20	6/30/76	0344	58	NE Face	1	0.1585	Stack	30	1.2446	Roof	23	0.6226
21	7/15/76	0344	60	NE Face	1	0.1539	Stack	30	1.2419	Roof	23	0.6088
22	7/16/76	0742	60	NE Face	1	0.1479	Stack	30	1.2288	Roof	23	0.6286
23	7/21/76	0748	58	NE Face	1	0.1573	Stack	30	1.8364	Roof	23	0.6356
24	7/22/76	0814	60	NE Face	1	0.1543	Stack	30	1.8242	Roof	23	0.6005

TABLE 4.3 Direction-Specific Building Dimensions of the EOCR Building for Ground-Level Releases on the Northeast Face

Flow Vector (° from N)	Height (m)	Width (m)	Length (m)	Stack Location (m)	Flow Vector (° from N)	Height (m)	Width (m)	Length (m)	Stack Location (m)
10	22.86	29.50	30.27	36.41	190	22.86	29.50	30.27	-6.14
20	22.86	27.76	29.27	38.48	200	22.86	27.76	29.27	-9.20
30	22.86	25.18	27.38	39.37	210	22.86	25.18	27.38	-11.99
40	22.86	21.83	24.66	39.07	220	22.86	21.83	24.66	-14.41
50	22.86	21.84	24.65	39.31	230	22.86	21.84	24.65	-14.66
60	22.86	25.18	27.37	40.10	240	22.86	25.18	27.37	-12.73
70	22.86	27.77	29.26	39.67	250	22.86	27.77	29.26	-10.41
80	22.86	29.51	30.26	38.03	260	22.86	29.51	30.26	-7.77
90	22.86	30.35	30.34	35.24	270	22.86	30.35	30.34	-4.90
100	22.86	30.27	29.50	31.38	280	22.86	30.27	29.50	-1.88
110	22.86	29.27	27.76	26.56	290	22.86	29.27	27.76	1.20
120	14.63	33.94	26.94	20.94	300	14.63	33.94	26.94	6.00
130	6.40	41.55	41.10	14.68	310	6.40	41.55	41.10	26.42
140	6.40	41.55	41.10	11.32	320	6.40	41.55	41.10	29.78
150	14.63	33.93	26.95	8.74	330	14.63	33.93	26.95	18.20
160	22.86	29.26	27.77	3.77	340	22.86	29.26	27.77	23.99
170	22.86	30.26	29.51	0.45	350	22.86	30.26	29.51	29.06
180	22.86	30.34	30.35	-2.89	360	22.86	30.34	30.35	33.24

TABLE 4.4 Direction-Specific Building Dimensions of the EOCR Building for Ground-Level Releases on the Northwest Face

Flow Vector (° from N)	Height (m)	Width (m)	Length (m)	Stack Location (m)	Flow Vector (° from N)	Height (m)	Width (m)	Length (m)	Stack Location (m)
10	22.86	29.50	30.27	17.73	190	22.86	29.50	30.27	12.54
20	22.86	27.76	29.27	15.38	200	22.86	27.76	29.27	13.89
30	22.86	25.18	27.38	12.56	210	22.86	25.18	27.38	14.82
40	22.86	21.83	24.66	9.36	220	22.86	21.83	24.66	15.30
50	22.86	21.84	24.65	7.61	230	22.86	21.84	24.65	17.04
60	22.86	25.18	27.37	7.36	240	22.86	25.18	27.37	20.01
70	22.86	27.77	29.26	6.89	250	22.86	27.77	29.26	22.36
80	22.86	29.51	30.26	6.22	260	22.86	29.51	30.26	24.04
90	22.86	30.35	30.34	5.35	270	22.86	30.35	30.34	24.99
100	22.86	30.27	29.50	4.32	280	22.86	30.27	29.50	25.18
110	22.86	29.27	27.76	3.16	290	22.86	29.27	27.76	24.60
120	22.86	27.38	25.18	1.90	300	22.86	27.38	25.18	23.28
130	22.86	24.66	21.83	0.59	310	22.86	24.66	21.83	21.25
140	22.86	24.65	21.84	1.26	320	22.86	24.65	21.84	20.57
150	22.86	27.37	25.18	3.90	330	22.86	27.37	25.18	21.28
160	22.86	29.26	27.77	6.42	340	22.86	29.26	27.77	21.34
170	22.86	30.26	29.51	8.75	350	22.86	30.26	29.51	20.76
180	22.86	30.34	30.35	10.81	360	22.86	30.34	30.35	19.54

TABLE 4.5 Direction-Specific Building Dimensions of the EOCR Building for Ground-Level Releases on the Southwest Face

Flow Vector (° from N)	Height (m)	Width (m)	Length (m)	Stack Location (m)	Flow Vector (° from N)	Height (m)	Width (m)	Length (m)	Stack Location (m)
10	22.86	29.50	30.27	5.71	190	22.86	29.50	30.27	24.56
20	22.86	27.76	29.27	4.21	200	22.86	27.76	29.27	25.06
30	22.86	25.18	27.38	2.58	210	22.86	25.18	27.38	24.80
40	22.86	21.83	24.66	0.87	220	22.86	21.83	24.66	23.79
50	22.86	21.84	24.65	0.87	230	22.86	21.84	24.65	23.78
60	22.86	25.18	27.37	2.58	240	22.86	25.18	27.37	24.79
70	22.86	27.77	29.26	4.21	250	22.86	27.77	29.26	25.05
80	22.86	29.51	30.26	5.71	260	22.86	29.51	30.26	24.55
90	22.86	30.35	30.34	7.04	270	22.86	30.35	30.34	23.30
100	22.86	30.27	29.50	8.16	280	22.86	30.27	29.50	21.34
110	22.86	29.27	27.76	9.02	290	22.86	29.27	27.76	18.74
120	22.86	27.38	25.18	9.62	300	22.86	27.38	25.18	15.56
130	22.86	24.66	21.83	9.92	310	22.86	24.66	21.83	11.92
140	22.86	24.65	21.84	11.92	320	22.86	24.65	21.84	9.91
150	22.86	27.37	25.18	15.57	330	22.86	27.37	25.18	9.61
160	22.86	29.26	27.77	18.75	340	22.86	29.26	27.77	9.02
170	22.86	30.26	29.51	21.35	350	22.86	30.26	29.51	8.15
180	22.86	30.34	30.35	23.31	360	22.86	30.34	30.35	7.04

TABLE 4.6 Direction-Specific Building Dimensions of the EOCR Building for the Roof-Level Releases

Flow Vector (° from N)	Height (m)	Width (m)	Length (m)	Stack Location (m)	Flow Vector (° from N)	Height (m)	Width (m)	Length (m)	Stack Location (m)
10	22.86	29.50	30.27	15.13	190	22.86	29.50	30.27	15.14
20	22.86	27.76	29.27	14.63	200	22.86	27.76	29.27	14.64
30	22.86	25.18	27.38	13.69	210	22.86	25.18	27.38	13.70
40	22.86	21.83	24.66	12.33	220	22.86	21.83	24.66	12.34
50	22.86	21.84	24.65	12.32	230	22.86	21.84	24.65	12.33
60	22.86	25.18	27.37	13.68	240	22.86	25.18	27.37	13.69
70	22.86	27.77	29.26	14.63	250	22.86	27.77	29.26	14.63
80	22.86	29.51	30.26	15.13	260	22.86	29.51	30.26	15.13
90	22.86	30.35	30.34	15.17	270	22.86	30.35	30.34	15.17
100	22.86	30.27	29.50	14.75	280	22.86	30.27	29.50	14.75
110	22.86	29.27	27.76	13.88	290	22.86	29.27	27.76	13.88
120	22.86	27.38	25.18	12.59	300	22.86	27.38	25.18	12.59
130	22.86	24.66	21.83	10.92	310	22.86	24.66	21.83	10.91
140	22.86	24.65	21.84	10.92	320	22.86	24.65	21.84	10.91
150	22.86	27.37	25.18	12.60	330	22.86	27.37	25.18	12.59
160	22.86	29.26	27.77	13.89	340	22.86	29.26	27.77	13.88
170	22.86	30.26	29.51	14.76	350	22.86	30.26	29.51	14.75
180	22.86	30.34	30.35	15.18	360	22.86	30.34	30.35	15.17

TABLE 4.7 Direction-Specific Building Dimensions of the EOCR Building for the Stack-Level Releases

Flow Vector (° from N)	Height (m)	Width (m)	Length (m)	Stack Location (m)	Flow Vector (° from N)	Height (m)	Width (m)	Length (m)	Stack Location (m)
10	22.86	29.50	30.27	19.34	190	22.86	29.50	30.27	10.93
20	22.86	27.76	29.27	21.33	200	22.86	27.76	29.27	7.95
30	22.86	25.18	27.38	22.66	210	22.86	25.18	27.38	4.72
40	22.86	21.83	24.66	23.31	220	22.86	21.83	24.66	1.35
50	22.86	21.84	24.65	24.98	230	22.86	21.84	24.65	-0.33
60	22.86	25.18	27.37	27.63	240	22.86	25.18	27.37	-0.26
70	22.86	27.77	29.26	29.44	250	22.86	27.77	29.26	-0.18
80	22.86	29.51	30.26	30.36	260	22.86	29.51	30.26	-0.10
90	22.86	30.35	30.34	30.35	270	22.86	30.35	30.34	-0.01
100	22.86	30.27	29.50	29.42	280	22.86	30.27	29.50	0.08
110	22.86	29.27	27.76	27.60	290	22.86	29.27	27.76	0.16
120	22.86	27.38	25.18	24.94	300	22.86	27.38	25.18	0.24
130	22.86	24.66	21.83	21.52	310	22.86	24.66	21.83	0.31
140	22.86	24.65	21.84	19.45	320	22.86	24.65	21.84	2.38
150	22.86	27.37	25.18	18.80	330	22.86	27.37	25.18	6.38
160	22.86	29.26	27.77	17.58	340	22.86	29.26	27.77	10.19
170	22.86	30.26	29.51	15.82	350	22.86	30.26	29.51	13.69
180	22.86	30.34	30.35	13.58	360	22.86	30.34	30.35	16.77

TABLE 4.8 Initial Estimate of Stability Category as a Function of the Standard Deviation of the Horizontal Wind Direction

σ_A (degrees)	Initial Stability Category Estimate
$22.5° \leq \sigma_A$	A
$17.5° \leq \sigma_A < 22.5°$	B
$12.5° \leq \sigma_A < 17.5°$	C
$7.5° \leq \sigma_A < 12.5°$	D
$3.8° \leq \sigma_A < 7.5°$	E
$\sigma_A < 3.8°$	F

TABLE 4.9 Wind Speed Adjustment for Determining the Pasquill Stability Category from the Standard Deviation of the Horizontal Wind Direction

Time of Day	Initial Stability Category Estimate (from Table 4.8)	10 m Scalar Wind Speed, u (m/s)	Pasquill Stability Category
Daytime	A	$u < 3$ m/s	A
		$3 \text{ m/s} \le u < 4$ m/s	B
		$4 \text{ m/s} \le u < 6$ m/s	C
		$6 \text{ m/s} \le u$	D
	B	$u < 4$ m/s	B
		$4 \text{ m/s} \le u < 6$ m/s	C
		$6 \text{ m/s} \le u$	D
	C	$u < 6$ m/s	C
		$6 \text{ m/s} \le u$	D
	D, E, or F	ANY	D
Nighttime	A	$u < 2.9$ m/s	F
		$2.9 \text{ m/s} \le u < 3.6$ m/s	E
		$3.6 \text{ m/s} \le u$	D
	B	$u < 2.4$ m/s	F
		$2.4 \text{ m/s} \le u < 3.0$ m/s	E
		$3.0 \text{ m/s} \le u$	D
	C	$u < 2.4$ m/s	E
		$2.4 \text{ m/s} \le u$	D
	D	ANY	D
	E	$u < 5.0$ m/s	E
		$5.0 \text{ m/s} \le u$	D
	F	$u < 3.0$ m/s	F
		$3.0 \text{ m/s} \le u < 5.0$ m/s	E
		$5.0 \text{ m/s} \le u$	D

TABLE 4.10 Meteorological Conditions During the EOCR Tracer Gas Release Experiment, Ground-Level Releases

Test Number	Flow Vector (° from N)			Wind Speed (m/s)	Stability Class	Air Temp. (K)	Mixing Height (m)
	Cavity	Near-Wake	Far-Wake				
3	238	222	216	0.5	6	293	10000
4	221	201	185	3.1	4	293	10000
5	126	85	71	7.4	4	293	10000
6	212	187	148	1.8	1	293	10000
7	27	90	200	0.5	6	293	10000
8	113	90	154	0.9	6	293	10000
9	999*	150	183	1.9	6	293	10000
10	999	39	326	0.8	2	293	10000
11	122	200	999	1.5	1	293	10000
12	142	210	211	2.3	3	293	10000
13	122	138	999	2.1	1	293	10000
14	218	215	220	1.9	4	293	10000
15	136	191	206	2.0	3	293	10000
16	69	166	189	3.1	2	293	10000
17	69	150	171	1.1	6	293	10000
18	69	205	217	4.1	4	293	10000
19	69	144	171	1.0	4	293	10000
20	69	200	217	1.5	4	293	10000
21	69	150	160	1.3	4	293	10000
22	69	186	200	2.4	4	293	10000
23	113	191	206	1.9	3	293	10000
24	69	196	217	1.8	2	293	10000

*999 denotes missing data.

TABLE 4.11 Meteorological Conditions During the EOCR Tracer Gas Release Experiment, Roof-Level Releases

Test Number	Flow Vector (° from N)			Wind Speed (m/s)	Stability Class	Air Temp. (K)	Mixing Height (m)
	Cavity	Near-Wake	Far-Wake				
3	210	216	216	1.3	6	293	10000
4	186	192	186	4.5	4	293	10000
5	78	72	66	8.8	4	293	10000
6	96	138	258	2.6	1	293	10000
7	96	90	306	0.6	6	293	10000
8	336	168	144	1.8	6	293	10000
9	999*	174	120	3.9	6	293	10000
10	999	348	30	3.7	2	293	10000
11	114	84	108	1.5	1	293	10000
12	204	210	216	3.4	3	293	10000
13	168	96	120	1.9	1	293	10000
14	216	216	222	3.3	4	293	10000
15	198	192	204	4.8	3	293	10000
16	180	186	210	3.6	2	293	10000
17	90	132	126	2.4	6	293	10000
18	198	210	216	6.5	4	293	10000
19	162	174	198	4.2	4	293	10000
20	216	216	222	5.3	4	293	10000
21	144	174	174	3.8	4	293	10000
22	198	198	198	4.6	4	293	10000
23	162	192	198	3.2	3	293	10000
24	180	192	216	3.1	2	293	10000

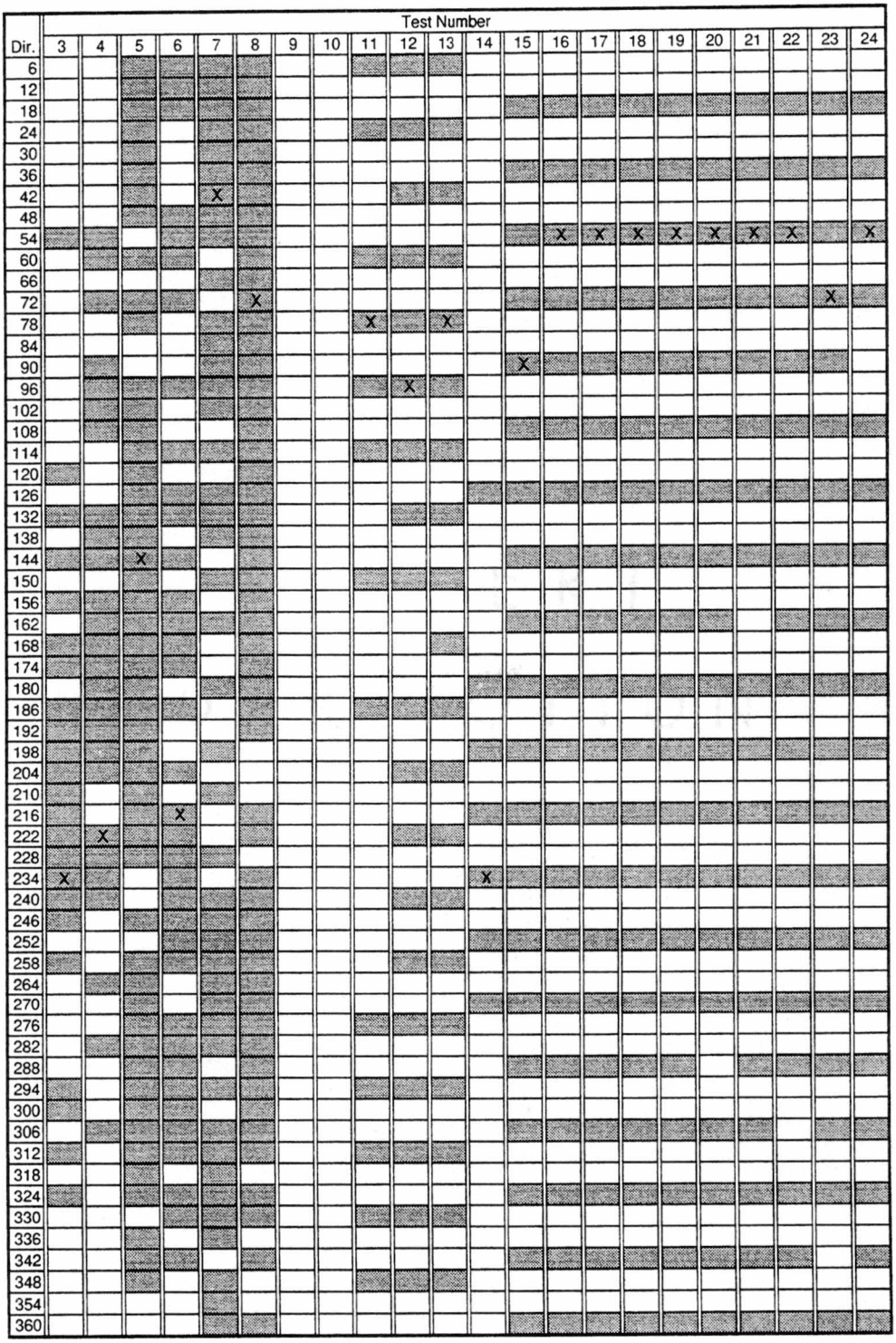
*999 denotes missing data.

TABLE 4.12 Meteorological Conditions During the EOCR Tracer Gas Release Experiment, Stack-Level Releases

Test Number	Flow Vector (° from N)			Wind Speed (m/s)	Stability Class	Air Temp. (K)	Mixing Height (m)
	Cavity	Near-Wake	Far-Wake				
3	225	223	218	1.3	6	293	10000
4	216	201	188	4.4	4	293	10000
5	74	55	59	9.0	4	293	10000
6	196	195	188	2.8	1	293	10000
7	104	84	305	0.7	6	293	10000
8	84	91	134	1.8	6	293	10000
9	999*	190	140	4.1	6	293	10000
10	999	48	358	3.8	2	293	10000
11	206	254	194	1.5	1	293	10000
12	220	217	212	3.5	3	293	10000
13	191	269	229	2.1	1	293	10000
14	322	238	200	3.4	4	293	10000
15	216	184	206	4.9	3	293	10000
16	354	206	206	3.7	2	293	10000
17	308	254	121	2.5	6	293	10000
18	123	217	218	6.9	4	293	10000
19	168	190	218	4.5	4	293	10000
20	322	153	140	5.6	4	293	10000
21	234	184	146	4.0	4	293	10000
22	354	206	194	4.7	4	293	10000
23	201	201	206	3.3	3	293	10000
24	201	195	218	3.2	2	293	10000

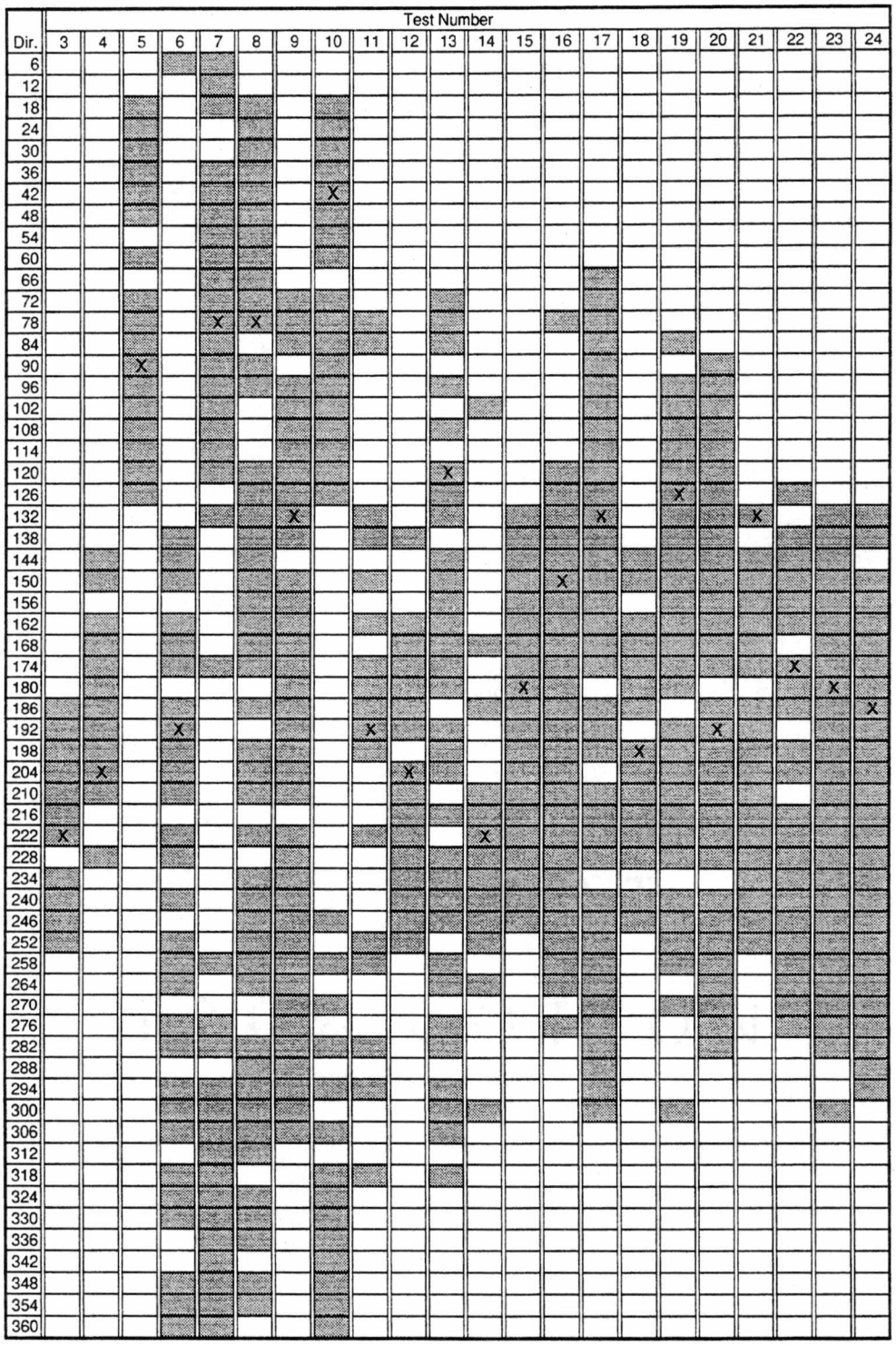
*999 denotes missing data.

TABLE 4.13 Sampling Locations Within the Cavity Region of the EOCR Building During the Ground-Level Tracer Gas Releases



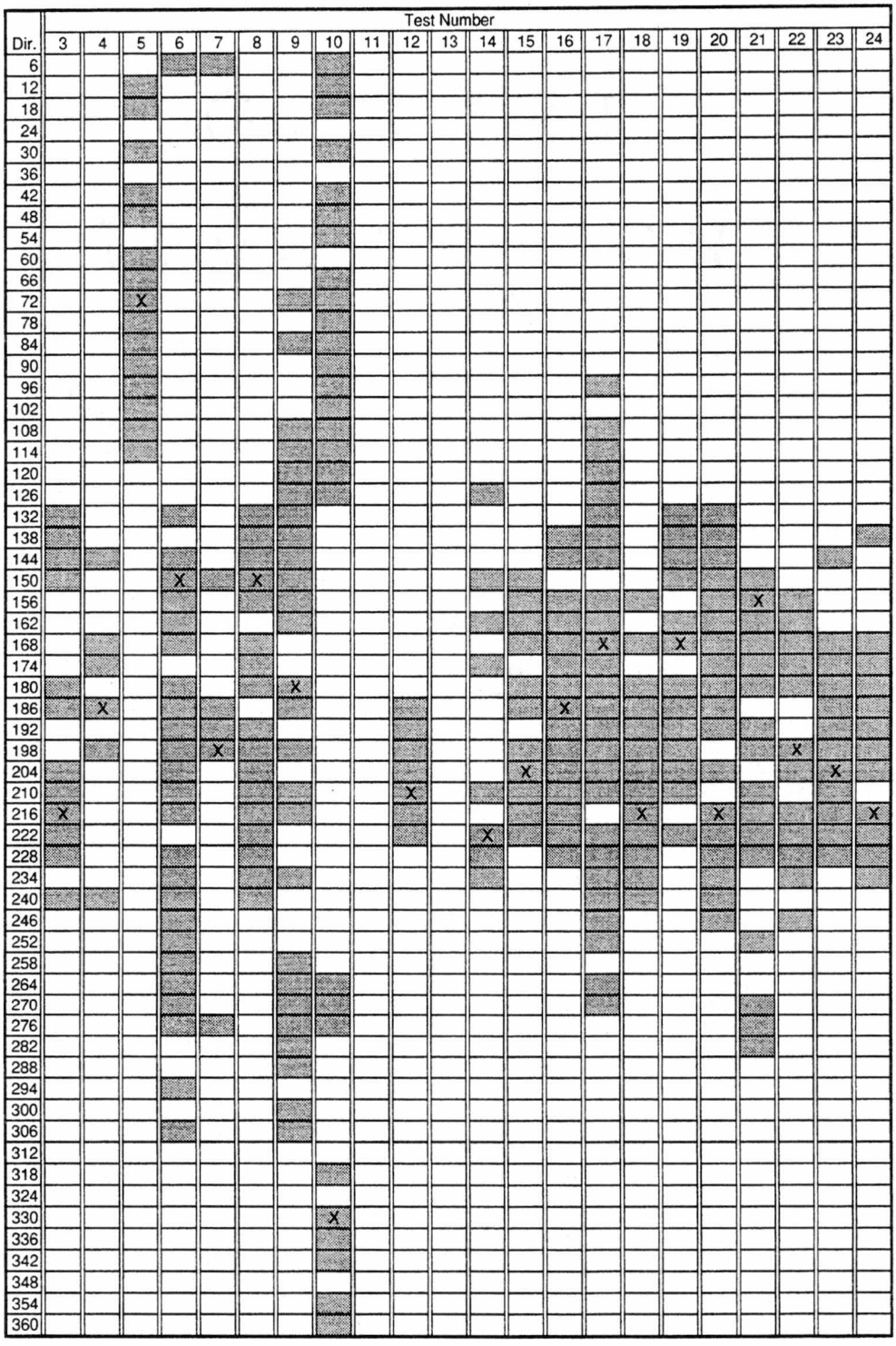
- Concentration measurement obtained.
X - Maximum measured concentration for the test.

TABLE 4.14 Sampling Locations Within the Near-Wake Region of the EOCR Building During the Ground-Level Tracer Gas Releases



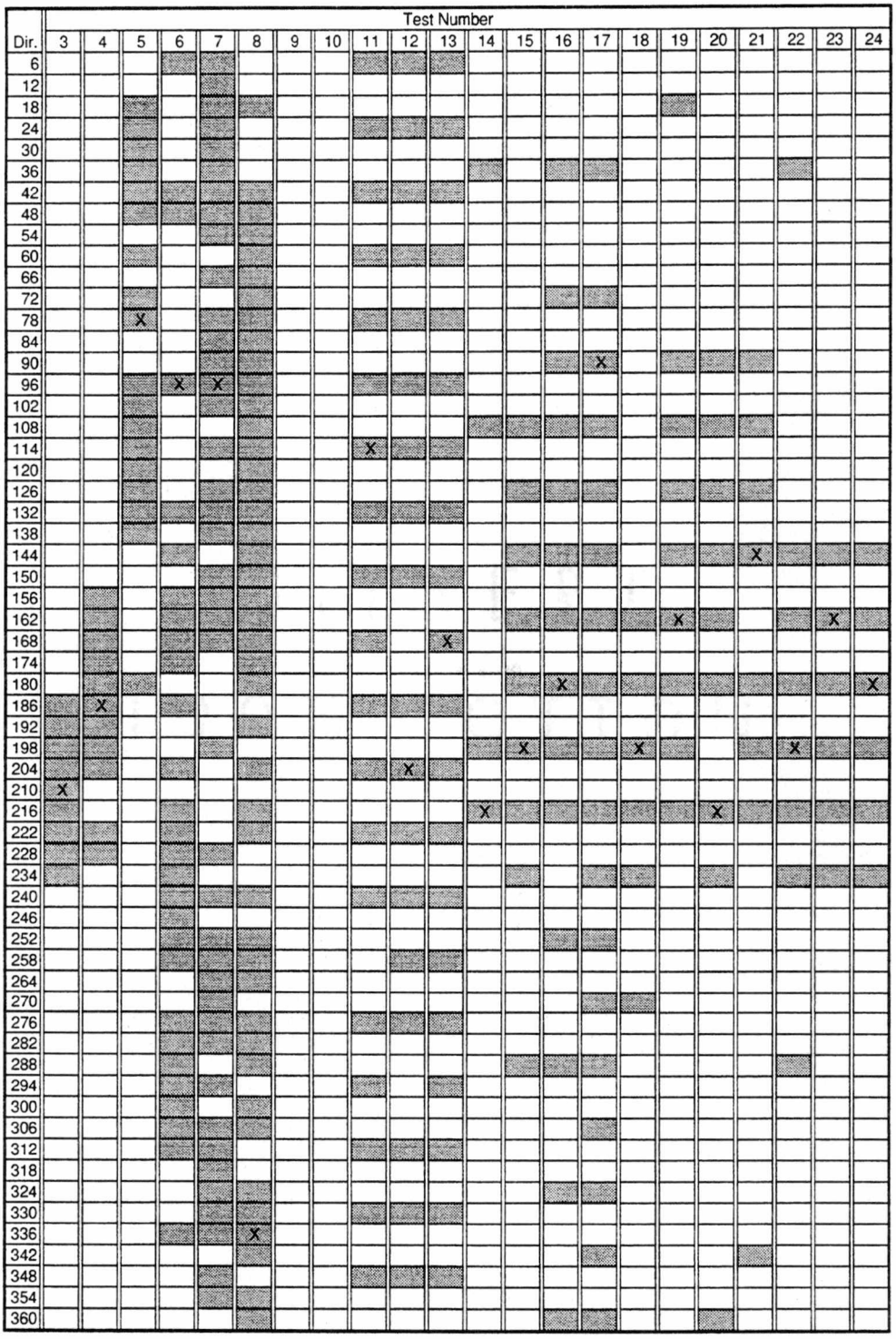
- Concentration measurement obtained.
X - Maximum measured concentration for the test.

TABLE 4.15 Sampling Locations Within the Far-Wake Region of the EOCR Building During the Ground-Level Tracer Gas Releases



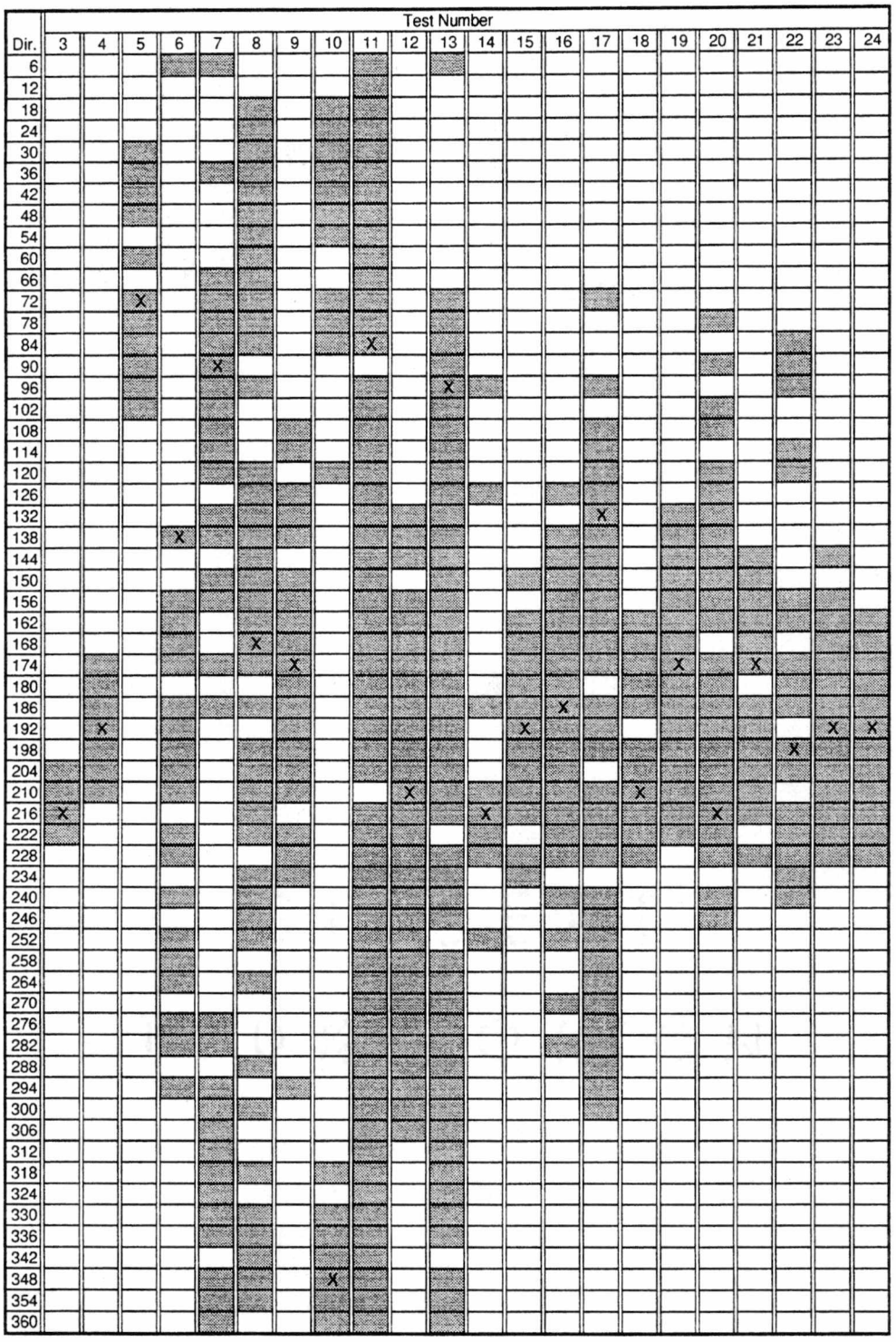
- Concentration measurement obtained.
X - Maximum measured concentration for the test.

TABLE 4.16 Sampling Locations Within the Cavity Region of the EOCR Building During the Roof-Level Tracer Gas Releases



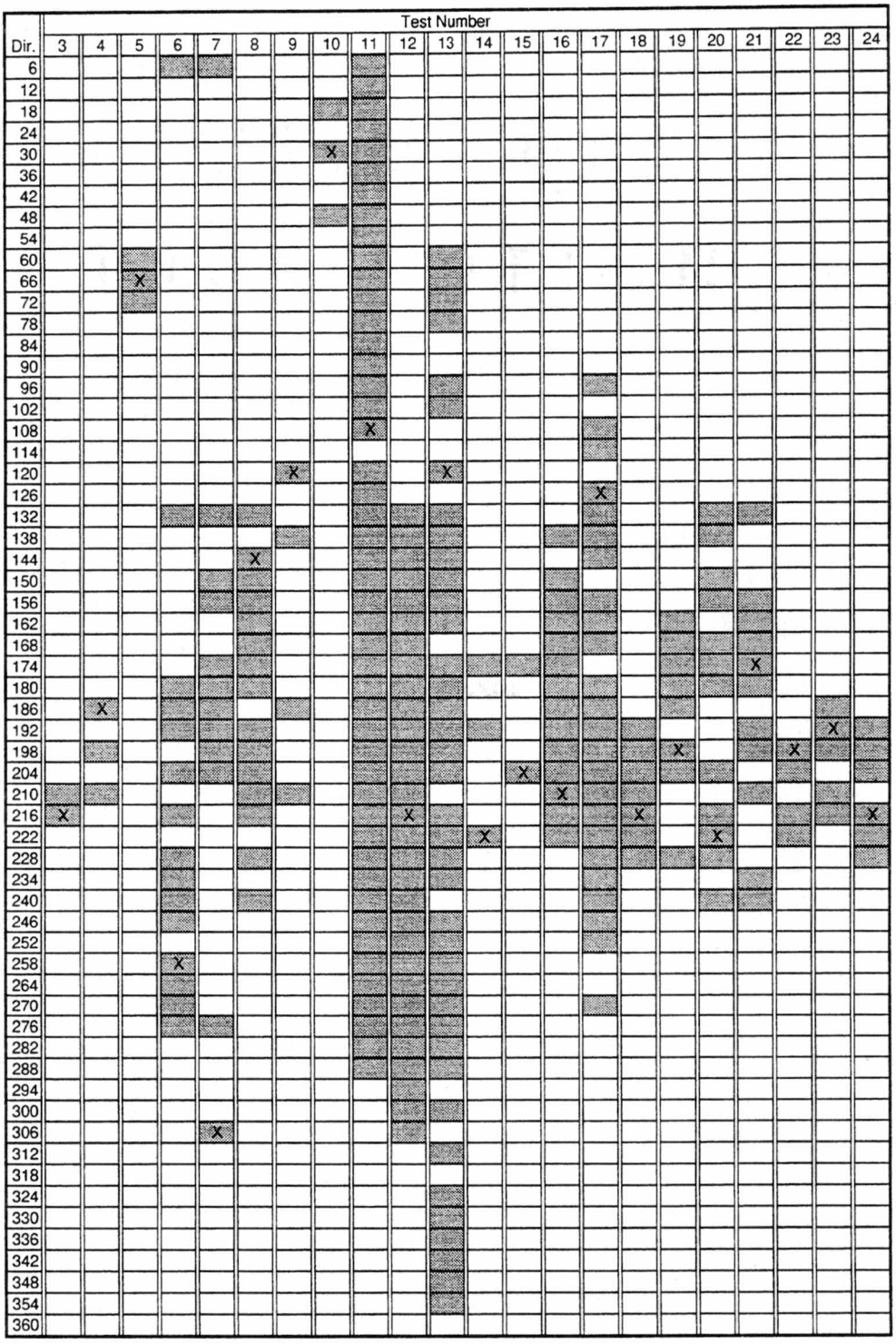
- Concentration measurement obtained.
X - Maximum measured concentration for the test.

TABLE 4.17 Sampling Locations Within the Near-Wake Region of the EOCR Building During the Roof-Level Tracer Gas Releases



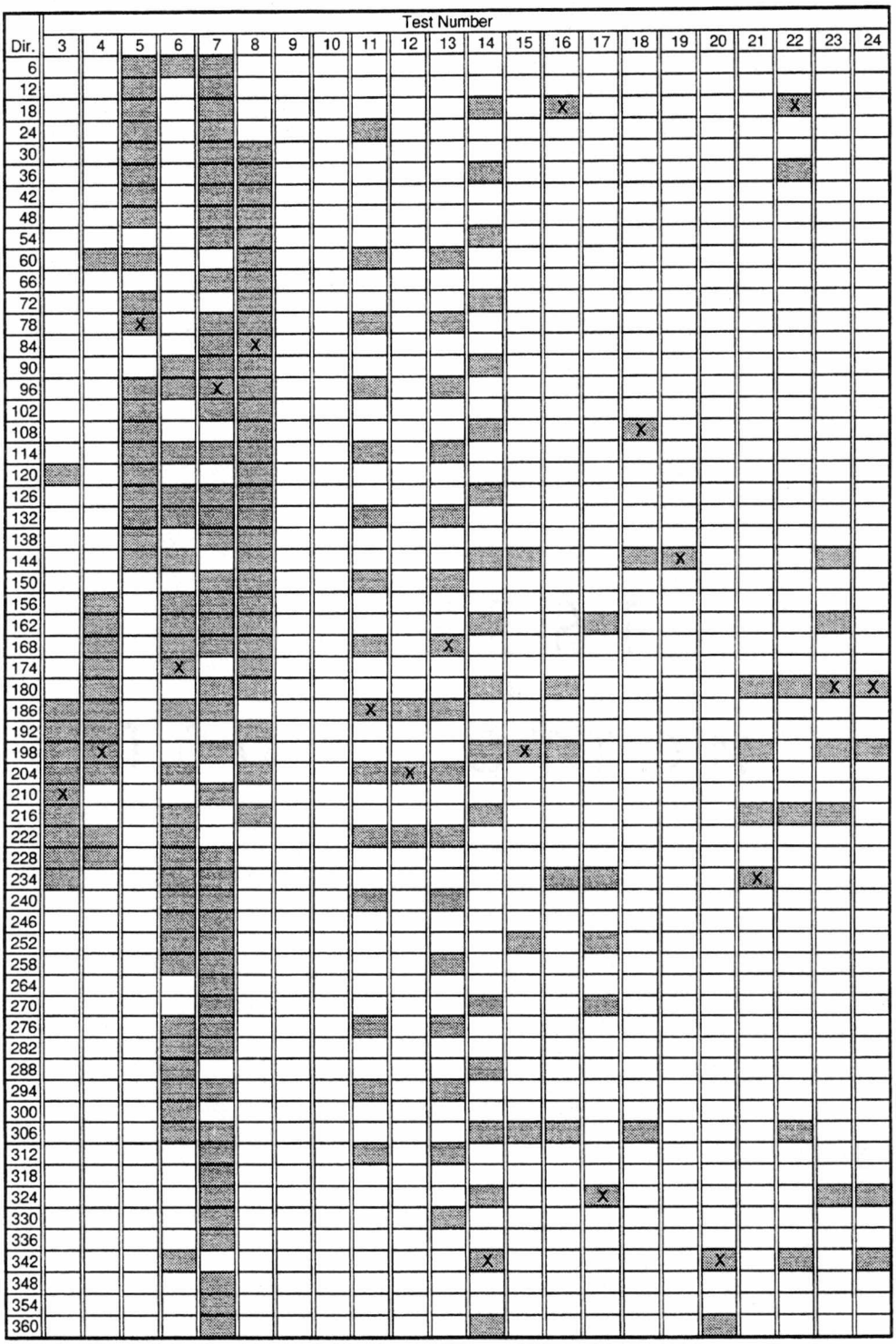
- Concentration measurement obtained.
X - Maximum measured concentration for the test.

TABLE 4.18 Sampling Locations Within the Far-Wake Region of the EOCR Building During the Roof-Level Tracer Gas Releases



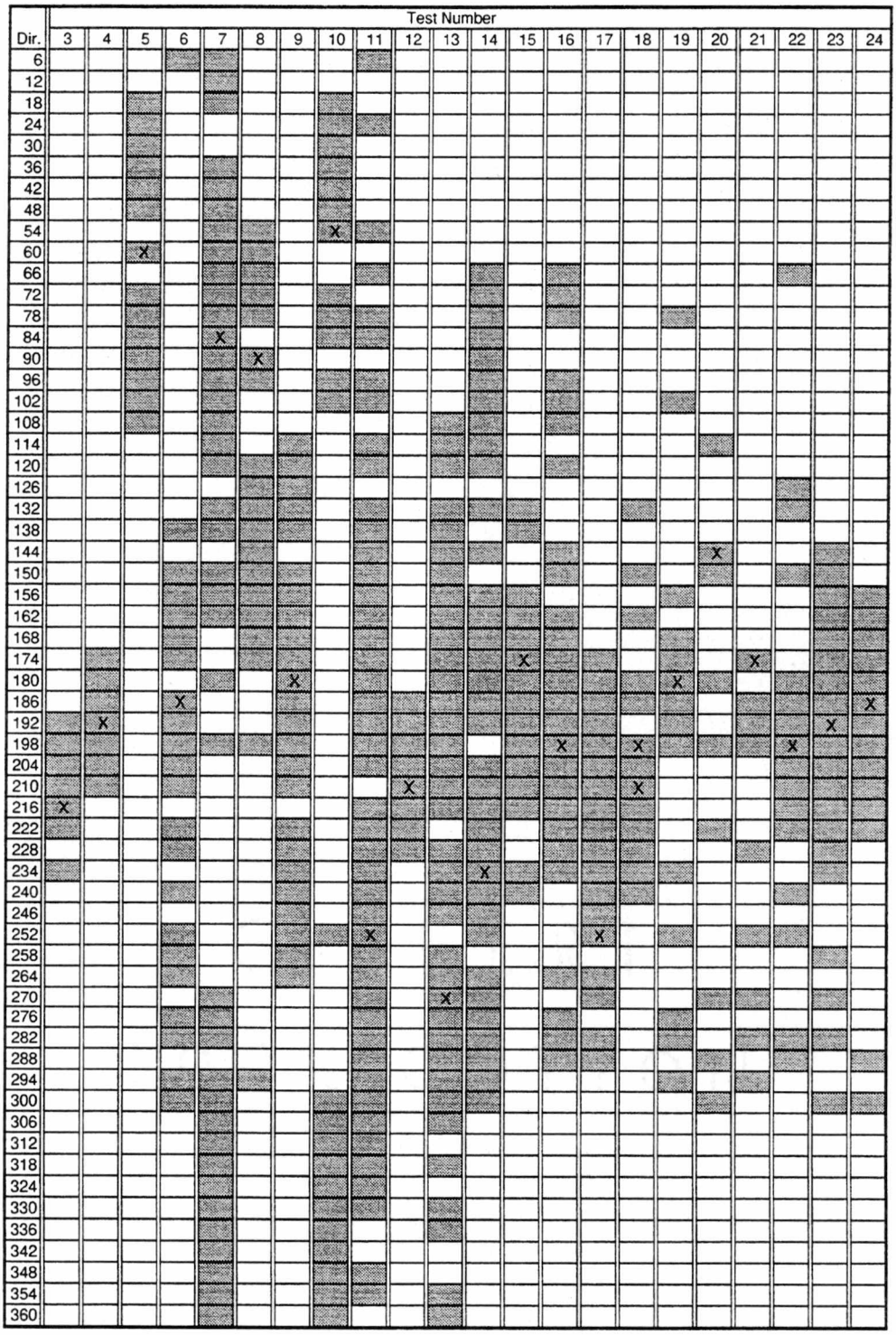
- Concentration measurement obtained.
X - Maximum measured concentration for the test.

TABLE 4.19 Sampling Locations Within the Cavity Region of the EOCR Building During the Stack-Level Tracer Gas Releases



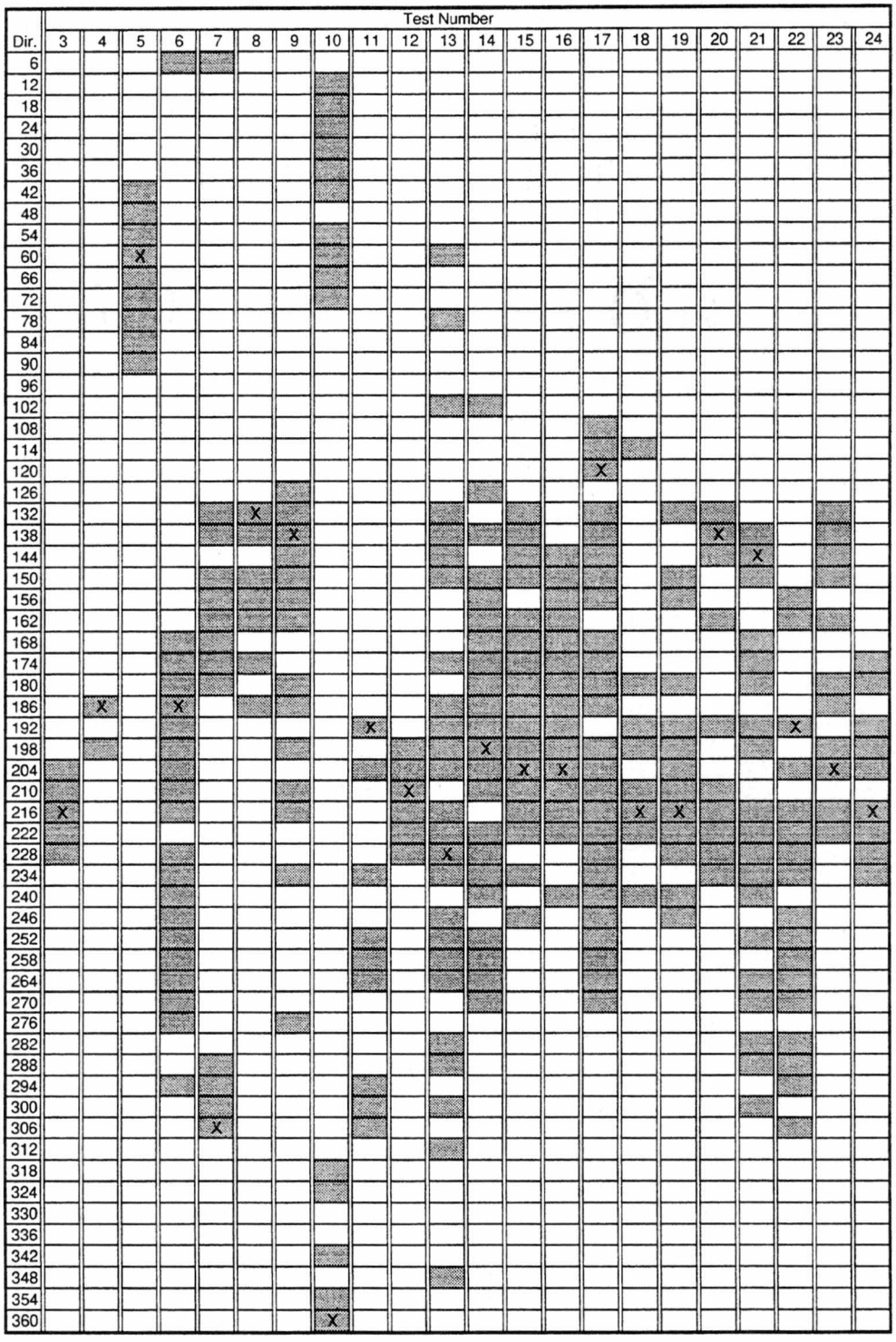
- Concentration measurement obtained.
X - Maximum measured concentration for the test.

TABLE 4.20 Sampling Locations Within the Near-Wake Region of the EOCR Building During the Stack-Level Tracer Gas Releases



- Concentration measurement obtained.
X - Maximum measured concentration for the test.

TABLE 4.21 Sampling Locations Within the Far-Wake Region of the EOCR Building During the Stack-Level Tracer Gas Releases



- Concentration measurement obtained.
X - Maximum measured concentration for the test.

TABLE 4.22 Statistical Data Summary of Measured Versus Predicted Concentrations, Hosker Cavity Algorithm

Data Set (H-S-W-L)[1]	n	$\tilde{\chi}_m$ ($\mu g/m^3$)	$\tilde{\chi}_p$ ($\mu g/m^3$)	χ'_m ($\mu g/m^3$)	χ'_p ($\mu g/m^3$)	$\tilde{d}$ ($\mu g/m^3$)	S_d ($\mu g/m^3$)	rms_d ($\mu g/m^3$)	$\tilde{k}$	k′	m	b	r
0-0-0-0	175	42.6	162	3587	1492	34.6	619	618	1.90	0.42	0.20	220	0.43
1-0-0-0	76	334	214	3587	1152	-113	820	864	0.64	0.32	0.16	295	0.44
2-0-0-0	54	22.0	168	138	592	139	175	274	8.60	4.30	2.08	180	0.31
3-0-0-0	45	9.15	0	231	1492	-7.31	357	369	0.00	6.45	3.99	38.4	0.44
0-1-0-0	58	42.4	206	1091	716	110	234	261	2.75	0.66	0.47	199	0.52
0-2-0-0	60	33.2	162	1491	1492	22.8	382	383	2.51	1.00	0.34	178	0.27
0-3-0-0	57	62.7	134	3587	1152	58.7	943	975	1.42	0.32	0.18	231	0.52
0-0-1-0	47	70.8	134	3587	1152	59.0	1013	1069	1.67	0.32	0.17	255	0.50
0-0-2-0	64	42.4	164	1091	716	-1.00	232	242	0.82	0.66	0.47	159	0.53
0-0-3-0	46	31.8	108	1491	1492	50.5	401	438	7.25	1.00	0.44	255	0.30
0-0-4-0	18	21.1	202	631	214	-17.8	182	192	0.49	0.34	0.30	63.9	0.73
0-0-0-1	44	81.3	165	3587	1492	24.9	653	649	1.41	0.42	0.19	215	0.44
0-0-0-2	131	31.3	162	3525	1492	41.3	610	608	1.97	0.42	0.21	221	0.43

[1](H-S-W-L): a 4-digit code is used to describe the various data sets of measured versus predicted concentrations in which the digits indicate

H - release height [0 = all release heights; 1 = ground release (1 m); 2 = roof release (23 m); and 3 = stack release (30 m)]

S - atmospheric stability [0 = all stabilities; 1 = unstable (A, B, and C); 2 = neutral (D); and 3 = stable (E and F)]

W - wind speed [0 = all wind speeds; 1 = $u_h \leq 1.0$ m/s; 2 = $1.0 < u_h \leq 3.0$ m/s; 3 = $3.0 < u_h \leq 5.0$ m/s; and 4 = 5 m/s < u_h]

L - receptor location [0 = all locations; 1 = plume centerline location (y = 0 m); and 2 = crosswind location (y > 0 m)].

TABLE 4.23 Statistical Data Summary of Measured Versus Predicted Concentrations, Schulman-Scire Cavity Algorithm

Data Set (H-S-W-L)[1]	n	$\tilde{\chi}_m$ ($\mu g/m^3$)	$\tilde{\chi}_p$ ($\mu g/m^3$)	χ'_m ($\mu g/m^3$)	χ'_p ($\mu g/m^3$)	$\tilde{d}$ ($\mu g/m^3$)	S_d ($\mu g/m^3$)	rms_d ($\mu g/m^3$)	$\tilde{k}$	k'	m	b	r
0-0-0-0	175	42.6	746	3587	8788	445	1817	2131	12.3	2.45	1.31	1024	0.45
1-0-0-0	76	334	1416	3587	8788	682	2499	3103	3.82	2.45	0.79	2010	0.28
2-0-0-0	54	22.0	826	138	2346	800	605	1015	25.4	17.0	10.8	528	0.48
3-0-0-0	45	9.15	69.7	231	1182	60.6	322	395	13.9	5.11	6.21	116	0.73
0-1-0-0	58	42.4	1019	1091	6811	966	1584	2048	18.2	6.24	5.90	587	0.83
0-2-0-0	60	33.2	557	1491	5439	311	1142	1322	7.05	3.65	2.97	308	0.64
0-3-0-0	57	62.7	452	3587	8788	441	2451	2798	15.0	2.45	0.89	1459	0.36
0-0-1-0	47	70.8	1312	3587	8788	446	2631	3072	13.1	2.45	0.75	1824	0.31
0-0-2-0	64	42.4	776	1091	6811	505	1566	1939	13.0	6.24	5.44	425	0.78
0-0-3-0	46	31.8	778	1491	5439	754	1258	1540	14.5	3.65	3.73	565	0.70
0-0-4-0	18	21.1	547	631	746	157	189	277	1.98	1.18	1.14	180	0.83
0-0-0-1	44	81.3	826	3587	8788	434	1531	1790	7.61	2.45	1.27	859	0.52
0-0-0-2	131	31.3	746	3525	8788	445	1905	2234	14.3	2.49	1.33	1077	0.43

[1](H-S-W-L): a 4-digit code is used to describe the various data sets of measured versus predicted concentrations in which the digits indicate

H - release height [0 = all release heights; 1 = ground release (1 m); 2 = roof release (23 m); and 3 = stack release (30 m)]

S - atmospheric stability [0 = all stabilities; 1 = unstable (A, B, and C); 2 = neutral (D); and 3 = stable (E and F)]

W - wind speed [0 = all wind speeds; 1 = $u_h \leq 1.0$ m/s; 2 = $1.0 < u_h \leq 3.0$ m/s; 3 = $3.0 < u_h \leq 5.0$ m/s; and 4 = 5 m/s < u_h]

L - receptor location [0 = all locations; 1 = plume centerline location (y = 0 m); and 2 = crosswind location (y > 0 m)].

TABLE 4.24 Statistical Data Summary of Measured Versus Predicted Concentrations, Gaussian Cavity Algorithm

Data Set (H-S-W-L)[1]	n	$\tilde{\chi}_m$ ($\mu g/m^3$)	$\tilde{\chi}_p$ ($\mu g/m^3$)	χ'_m ($\mu g/m^3$)	χ'_p ($\mu g/m^3$)	$\tilde{d}$ ($\mu g/m^3$)	S_d ($\mu g/m^3$)	rms_d ($\mu g/m^3$)	$\tilde{k}$	k′	m	b	r
0-0-0-0	175	42.6	69.5	3587	3556	1.54	492	491	1.11	0.99	0.70	110	0.73
1-0-0-0	76	334	249	3587	3556	-97.1	749	744	0.78	0.99	0.60	291	0.64
2-0-0-0	54	22.0	45.9	138	205	15.0	39.2	46.9	1.83	1.49	0.89	29.6	0.53
3-0-0-0	45	9.15	6.24	231	196	-0.96	18.4	18.4	0.90	0.85	0.82	1.19	0.90
0-1-0-0	58	42.4	92.3	1091	1393	8.80	208	209	1.61	1.28	0.80	66.6	0.71
0-2-0-0	60	33.2	61.3	1491	1304	-0.57	128	136	0.90	0.87	0.77	-4.15	0.89
0-3-0-0	57	62.7	60.8	3587	3556	4.12	828	822	1.37	0.99	0.63	282	0.69
0-0-1-0	47	70.8	81.1	3587	3556	5.15	914	906	1.47	0.99	0.60	357	0.66
0-0-2-0	64	42.4	105	1091	1393	2.38	205	206	1.18	1.28	0.79	65.9	0.71
0-0-3-0	46	31.8	47.8	1491	1304	4.19	81.8	81.1	1.18	0.87	0.89	8.82	0.95
0-0-4-0	18	21.1	24.2	631	289	-16.9	149	185	0.44	0.46	0.40	3.32	0.95
0-0-0-1	44	81.3	156	3587	3556	22.6	524	524	1.46	0.99	0.77	164	0.75
0-0-0-2	131	31.3	52.6	3525	3050	0.76	481	479	1.04	0.87	0.67	92.4	0.73

[1](H-S-W-L): a 4-digit code is used to describe the various data sets of measured versus predicted concentrations in which the digits indicate

H - release height [0 = all release heights; 1 = ground release (1 m); 2 = roof release (23 m); and 3 = stack release (30 m)]

S - atmospheric stability [0 = all stabilities; 1 = unstable (A, B, and C); 2 = neutral (D); and 3 = stable (E and F)]

W - wind speed [0 = all wind speeds; 1 = $u_h \leq 1.0$ m/s; 2 = $1.0 < u_h \leq 3.0$ m/s; 3 = $3.0 < u_h \leq 5.0$ m/s; and 4 = 5 m/s < u_h]

L - receptor location [0 = all locations; 1 = plume centerline location (y = 0 m); and 2 = crosswind location (y > 0 m)].

TABLE 4.25 Statistical Data Summary of Measured Versus Predicted Concentrations, Hosker Cavity Algorithm, Plume Centerline Locations Within the Cavity

Data Set (H-S-W-L)[1]	n	$\tilde{\chi}_m$ ($\mu g/m^3$)	$\tilde{\chi}_p$ ($\mu g/m^3$)	χ'_m ($\mu g/m^3$)	χ'_p ($\mu g/m^3$)	$\tilde{d}$ ($\mu g/m^3$)	S_d ($\mu g/m^3$)	rms_d ($\mu g/m^3$)	$\tilde{k}$	k′	m	b	r
0-0-0-1	44	81.3	165	3587	1492	24.9	653	649	1.41	0.42	0.19	215	0.44
1-0-0-1	20	360	168	3587	1152	-193	815	885	0.53	0.32	0.19	191	0.61
2-0-0-1	14	43.6	291	138	592	251	182	295	6.76	4.30	1.61	208	0.30
3-0-0-1	10	11.4	0	231	1492	-5.90	407	409	0.00	6.45	4.84	-50.3	0.80
0-1-0-1	18	52.0	206	1091	716	92.8	260	269	2.32	0.66	0.34	205	0.42
0-2-0-1	16	89.9	163	1491	1492	4.92	428	415	1.54	1.00	0.37	161	0.38
0-3-0-1	10	123	156	3587	1152	-6.89	1170	1204	0.73	0.32	0.16	216	0.57
0-0-1-1	8	297	149	3587	1152	-37.1	1258	1341	0.67	0.32	0.17	203	0.58
0-0-2-1	19	95.4	166	1091	716	-1.43	271	266	0.95	0.66	0.31	178	0.41
0-0-3-1	13	50.8	287	1491	1492	48.1	449	449	6.45	1.00	0.40	251	0.39
0-0-4-1	4	26.6	116	631	214	-1.59	249	225	1.23	0.34	0.23	71.1	0.63

[1](H-S-W-L): a 4-digit code is used to describe the various data sets of measured versus predicted concentrations in which the digits indicate

H - release height [0 = all release heights; 1 = ground release (1 m); 2 = roof release (23 m); and 3 = stack release (30 m)]

S - atmospheric stability [0 = all stabilities; 1 = unstable (A, B, and C); 2 = neutral (D); and 3 = stable (E and F)]

W - wind speed [0 = all wind speeds; 1 = $u_h \leq 1.0$ m/s; 2 = $1.0 < u_h \leq 3.0$ m/s; 3 = $3.0 < u_h \leq 5.0$ m/s; and 4 = 5 m/s < u_h]

L - receptor location [0 = all locations; 1 = plume centerline location (y = 0 m); and 2 = crosswind location (y > 0 m)].

TABLE 4.26 Statistical Data Summary of Measured Versus Predicted Concentrations, Schulman-Scire Cavity Algorithm, Plume Centerline Locations Within the Cavity

Data Set (H-S-W-L)[1]	n	$\tilde{\chi}_m$ ($\mu g/m^3$)	$\tilde{\chi}_p$ ($\mu g/m^3$)	χ'_m ($\mu g/m^3$)	χ'_p ($\mu g/m^3$)	$\tilde{d}$ ($\mu g/m^3$)	S_d ($\mu g/m^3$)	rms_d ($\mu g/m^3$)	$\tilde{k}$	k'	m	b	r
0-0-0-1	44	81.3	826	3587	8788	434	1531	1790	7.61	2.45	1.27	859	0.52
1-0-0-1	20	360	1033	3587	8788	424	2138	2479	3.19	2.45	1.03	1319	0.42
2-0-0-1	14	43.6	956	138	2346	917	626	1075	18.9	17.0	9.43	488	0.51
3-0-0-1	10	11.4	107	231	1182	95.3	352	428	7.98	5.11	5.31	58.9	0.96
0-1-0-1	18	52.0	1019	1091	6811	932	1332	1731	13.9	6.24	4.69	533	0.80
0-2-0-1	16	89.9	651	1491	5439	424	946	1113	4.61	3.65	2.95	100	0.90
0-3-0-1	10	123	882	3587	8788	216	2464	2592	10.2	2.45	0.81	1278	0.40
0-0-1-1	8	297	1364	3587	8788	370	2728	2878	7.38	2.45	0.69	1646	0.35
0-0-2-1	19	95.4	955	1091	6811	426	1342	1666	6.24	6.24	3.95	423	0.72
0-0-3-1	13	50.8	874	1491	5439	839	1014	1291	8.34	3.65	3.18	382	0.93
0-0-4-1	4	26.6	316	631	746	92.7	230	265	3.57	1.18	0.89	195	0.76

[1](H-S-W-L): a 4-digit code is used to describe the various data sets of measured versus predicted concentrations in which the digits indicate

H - release height [0 = all release heights; 1 = ground release (1 m); 2 = roof release (23 m); and 3 = stack release (30 m)]

S - atmospheric stability [0 = all stabilities; 1 = unstable (A, B, and C); 2 = neutral (D); and 3 = stable (E and F)]

W - wind speed [0 = all wind speeds; 1 = $u_h \leq 1.0$ m/s; 2 = $1.0 < u_h \leq 3.0$ m/s; 3 = $3.0 < u_h \leq 5.0$ m/s; and 4 = 5 m/s < u_h]

L - receptor location [0 = all locations; 1 = plume centerline location (y = 0 m); and 2 = crosswind location (y > 0 m)].

TABLE 4.27 Statistical Data Summary of Measured Versus Predicted Concentrations, Gaussian Cavity Algorithm, Plume Centerline Locations Within the Cavity

Data Set (H-S-W-L)[1]	n	$\tilde{\chi}_m$ ($\mu g/m^3$)	$\tilde{\chi}_p$ ($\mu g/m^3$)	χ'_m ($\mu g/m^3$)	χ'_p ($\mu g/m^3$)	$\tilde{d}$ ($\mu g/m^3$)	S_d ($\mu g/m^3$)	rms_d ($\mu g/m^3$)	$\tilde{k}$	k′	m	b	r
0-0-0-1	44	81.3	156	3587	3556	22.6	524	524	1.46	0.99	0.77	164	0.75
1-0-0-1	20	360	442	3587	3556	56.9	781	775	1.22	0.99	0.65	398	0.67
2-0-0-1	14	43.6	96.7	138	205	55.3	53.1	71.7	2.25	1.49	0.74	62.7	0.44
3-0-0-1	10	11.4	10.5	231	196	0.34	24.5	23.9	1.02	0.85	0.86	1.06	0.95
0-1-0-1	18	52.0	181	1091	1393	48.9	318	342	2.55	1.28	0.90	163	0.60
0-2-0-1	16	89.9	129	1491	1304	1.66	132	129	1.22	0.87	0.81	36.3	0.95
0-3-0-1	10	123	129	3587	3556	3.78	1032	986	1.22	0.99	0.71	365	0.71
0-0-1-1	8	297	353	3587	3556	-19.8	1168	1101	1.12	0.99	0.67	478	0.67
0-0-2-1	19	95.4	243	1091	1393	86.9	309	339	1.79	1.28	0.84	190	0.61
0-0-3-1	13	50.8	124	1491	1304	1.77	91.9	89.0	1.15	0.87	0.83	25.2	0.98
0-0-4-1	4	26.6	38.6	631	289	-10.9	174	172	0.58	0.46	0.43	16.2	0.98

[1](H-S-W-L): a 4-digit code is used to describe the various data sets of measured versus predicted concentrations in which the digits indicate

H - release height [0 = all release heights; 1 = ground release (1 m); 2 = roof release (23 m); and 3 = stack release (30 m)]

S - atmospheric stability [0 = all stabilities; 1 = unstable (A, B, and C); 2 = neutral (D); and 3 = stable (E and F)]

W - wind speed [0 = all wind speeds; 1 = $u_h \leq 1.0$ m/s; 2 = $1.0 < u_h \leq 3.0$ m/s; 3 = $3.0 < u_h \leq 5.0$ m/s; and 4 = 5 m/s < u_h]

L - receptor location [0 = all locations; 1 = plume centerline location (y = 0 m); and 2 = crosswind location (y > 0 m)].

TABLE 4.28 Statistical Data Summary of Measured Versus Predicted Concentrations, ISCST2 Wake Algorithm, Plume Centerline Locations Within the Near-Wake

Data Set (H-S-W-L)[1]	n	$\tilde{\chi}_m$ ($\mu g/m^3$)	$\tilde{\chi}_p$ ($\mu g/m^3$)	χ'_m ($\mu g/m^3$)	χ'_p ($\mu g/m^3$)	$\tilde{d}$ ($\mu g/m^3$)	S_d ($\mu g/m^3$)	rms_d ($\mu g/m^3$)	$\tilde{k}$	k'	m	b	r
0-0-0-1	61	28.1	82.5	763	2352	33.4	307	311	2.43	3.08	0.74	88.4	0.32
1-0-0-1	21	53.4	106	406	2352	49.3	481	508	2.35	5.79	1.76	109	0.39
2-0-0-1	20	25.5	88.6	287	203	46.0	85.8	88.2	2.74	0.71	0.12	73.8	0.19
3-0-0-1	20	18.6	49.0	763	385	2.55	129	130	1.35	0.50	0.40	30.4	0.84
0-1-0-1	26	34.2	71.9	267	303	14.4	64.2	64.9	2.15	1.13	0.50	44.5	0.56
0-2-0-1	21	28.0	95.5	763	808	41.9	207	210	2.62	1.06	0.41	104	0.35
0-3-0-1	14	110	147	520	2352	20.1	587	590	2.78	4.52	0.84	193	0.24
0-0-1-1	8	86.1	181	406	2352	29.7	774	803	3.18	5.79	1.35	299	0.25
0-0-2-1	21	28.1	82.5	520	528	44.9	112	116	2.66	1.02	0.65	69.6	0.66
0-0-3-1	26	30.1	82.6	763	570	13.1	134	131	1.93	0.75	0.38	59.1	0.53
0-0-4-1	6	20.0	67.3	96.8	132	36.6	33.6	43.3	1.90	1.36	1.14	26.0	0.74

[1](H-S-W-L): a 4-digit code is used to describe the various data sets of measured versus predicted concentrations in which the digits indicate

H - release height [0 = all release heights; 1 = ground release (1 m); 2 = roof release (23 m); and 3 = stack release (30 m)]

S - atmospheric stability [0 = all stabilities; 1 = unstable (A, B, and C); 2 = neutral (D); and 3 = stable (E and F)]

W - wind speed [0 = all wind speeds; 1 = $u_h \leq 1.0$ m/s; 2 = $1.0 < u_h \leq 3.0$ m/s; 3 = $3.0 < u_h \leq 5.0$ m/s; and 4 = 5 m/s < u_h]

L - receptor location [0 = all locations; 1 = plume centerline location (y = 0 m); and 2 = crosswind location (y > 0 m)].

TABLE 4.29 Statistical Data Summary of Measured Versus Predicted Concentrations, ISCST2 Wake Algorithm, Plume Centerline Locations Within the Far-Wake

Data Set (H-S-W-L)[1]	n	$\tilde{\chi}_m$ ($\mu g/m^3$)	$\tilde{\chi}_p$ ($\mu g/m^3$)	χ'_m ($\mu g/m^3$)	χ'_p ($\mu g/m^3$)	$\tilde{d}$ ($\mu g/m^3$)	S_d ($\mu g/m^3$)	rms_d ($\mu g/m^3$)	$\tilde{k}$	k′	m	b	r
0-0-0-1	44	8.34	26.3	404	440	10.0	95.7	97.6	3.35	1.09	0.40	42.7	0.35
1-0-0-1	18	9.46	23.2	39.8	440	16.5	117	130	3.96	11.1	6.26	-13.5	0.68
2-0-0-1	11	5.62	25.0	147	84.7	16.3	50.5	48.9	3.63	0.58	-0.08	30.7	-0.17
3-0-0-1	15	8.44	39.3	404	223	2.18	78.7	76.9	2.21	0.55	0.42	22.8	0.86
0-1-0-1	21	5.08	15.3	147	80.6	2.84	35.3	34.9	2.30	0.55	0.16	19.8	0.22
0-2-0-1	15	8.49	33.5	404	139	16.9	75.5	73.0	2.85	0.34	0.29	30.1	0.82
0-3-0-1	8	19.5	110	322	440	67.1	173	198	8.45	1.36	0.37	148	0.24
0-0-1-1	5	27.8	71.3	37.8	440	40.3	193	239	3.07	11.6	11.4	-84.0	0.72
0-0-2-1	17	2.59	15.3	322	223	7.06	54.1	52.8	3.77	0.69	0.54	21.3	0.75
0-0-3-1	17	8.44	35.8	404	139	9.87	72.5	70.4	3.82	0.34	0.29	30.0	0.75
0-0-4-1	5	8.79	27.6	33.7	40.3	16.3	9.62	15.6	2.59	1.20	0.84	14.9	0.75

[1](H-S-W-L): a 4-digit code is used to describe the various data sets of measured versus predicted concentrations in which the digits indicate

H - release height [0 = all release heights; 1 = ground release (1 m); 2 = roof release (23 m); and 3 = stack release (30 m)]

S - atmospheric stability [0 = all stabilities; 1 = unstable (A, B, and C); 2 = neutral (D); and 3 = stable (E and F)]

W - wind speed [0 = all wind speeds; 1 = $u_h \leq 1.0$ m/s; 2 = $1.0 < u_h \leq 3.0$ m/s; 3 = $3.0 < u_h \leq 5.0$ m/s; and 4 = 5 m/s < u_h]

L - receptor location [0 = all locations; 1 = plume centerline location (y = 0 m); and 2 = crosswind location (y > 0 m)].

APPENDIX B

FIGURES

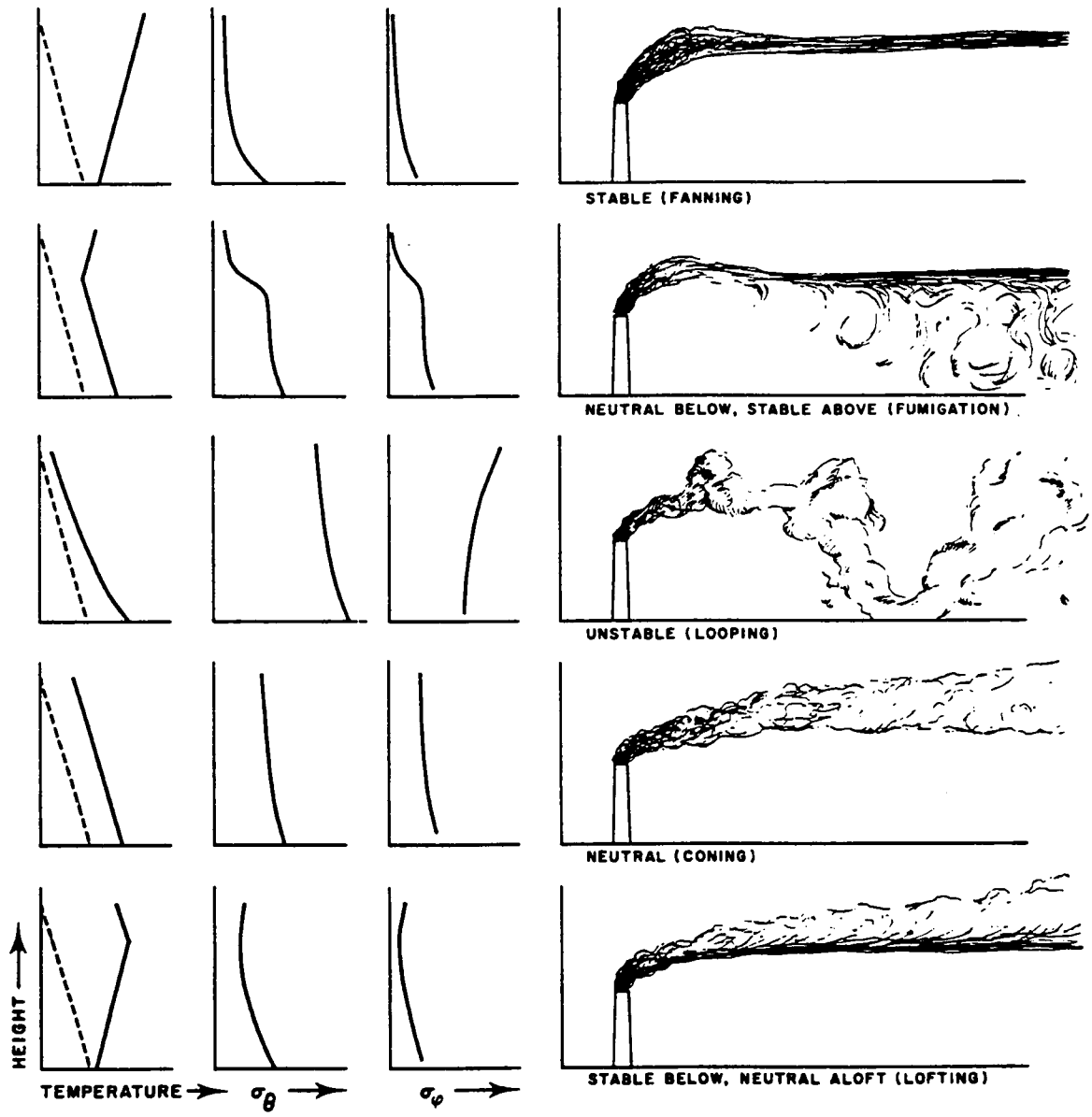


FIGURE 2.1 Various Types of Smoke Plume Patterns Observed in the Atmosphere (Slade, 1968)

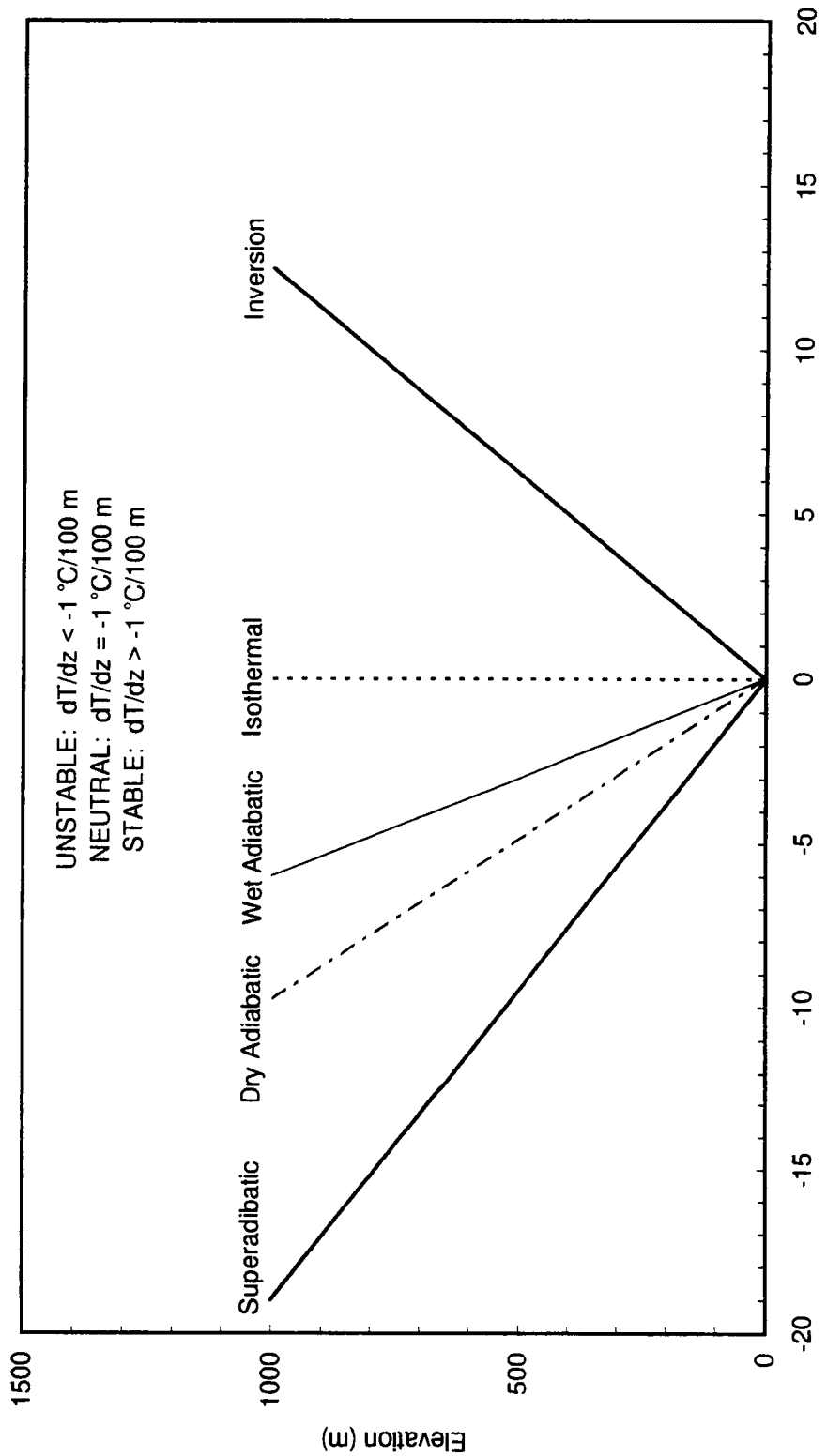


FIGURE 2.2 Unstable, Neutral, and Stable Atmospheres Based on Temperature Change with Height

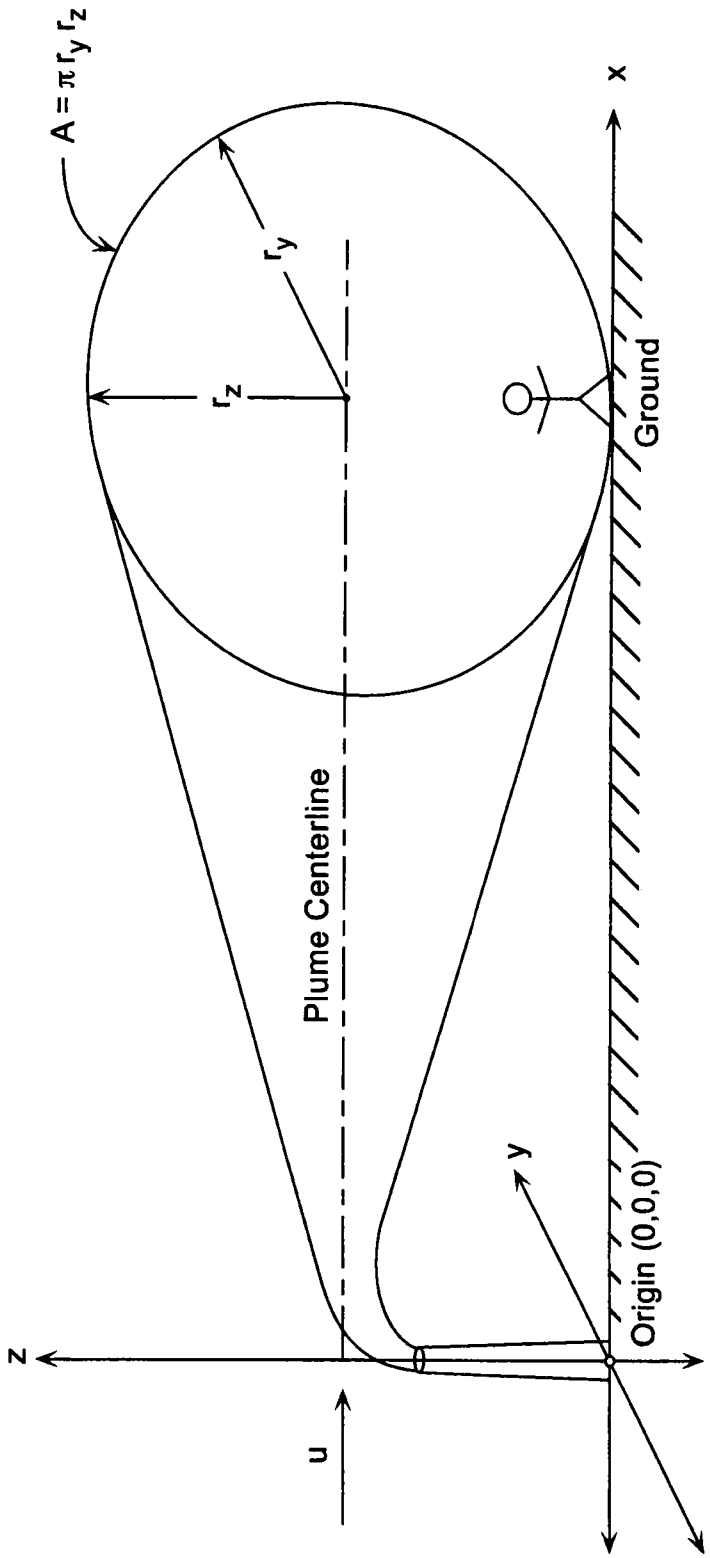


FIGURE 2.3 Illustration of Dispersion for a Simple Geometric Plume

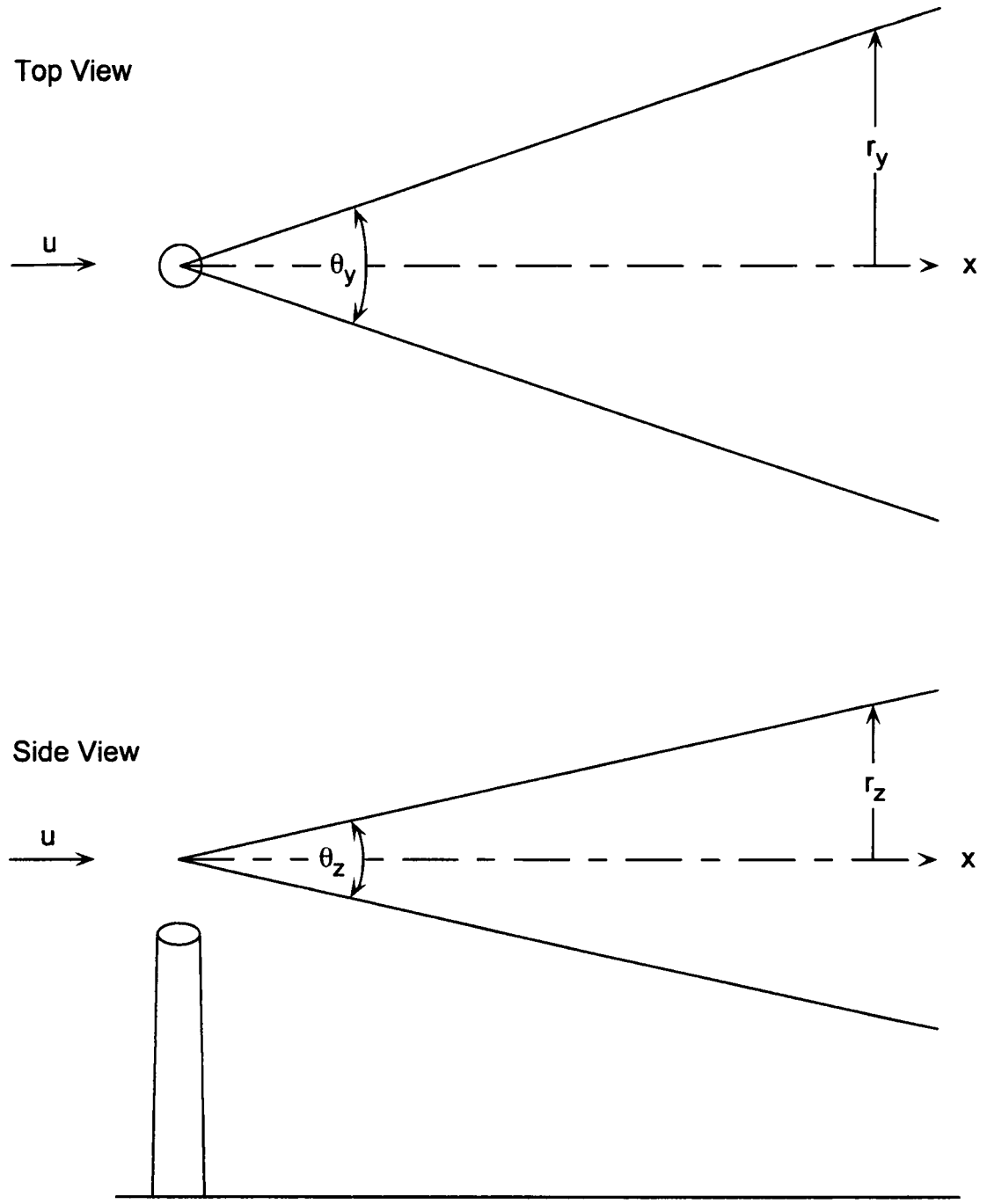
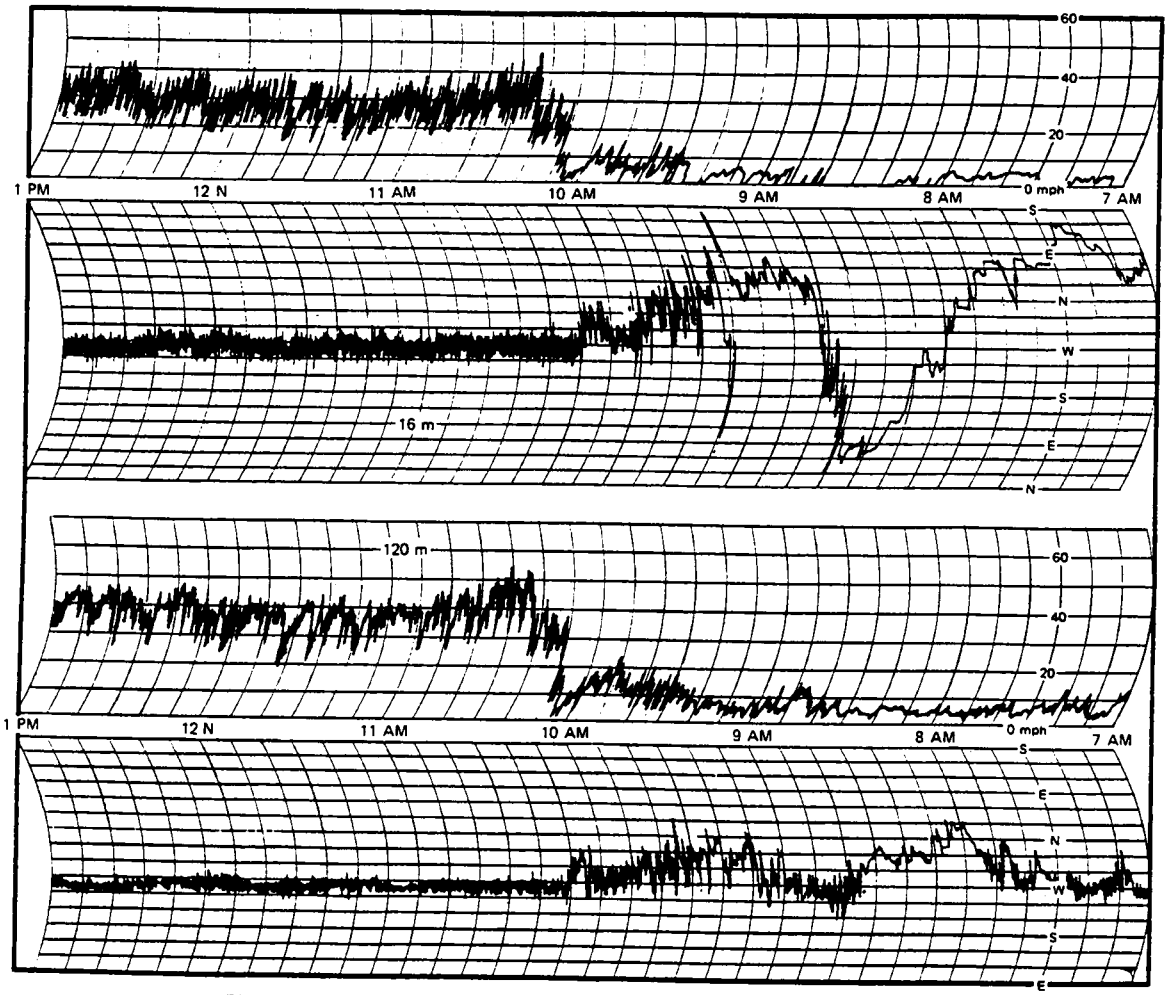
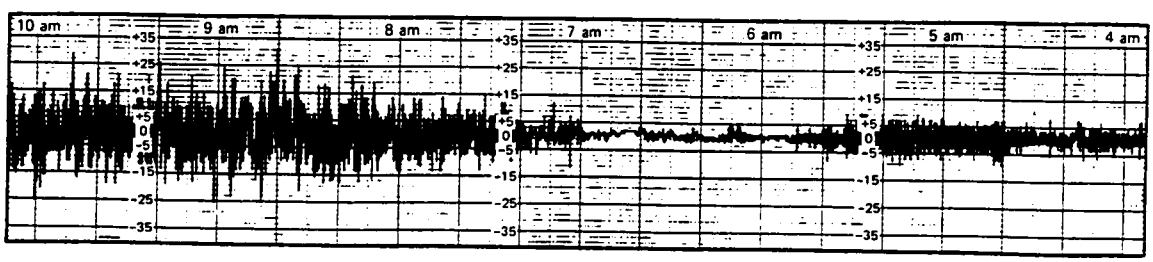


FIGURE 2.4 Trigonometric Relationships of a Simple Geometric Plume



Horizontal wind speed and direction traces at 16 m and 120 m heights



Vertical wind direction trace at 10 m height

FIGURE 2.5 Typical Wind Speed and Wind Direction Traces (Kao, 1984)

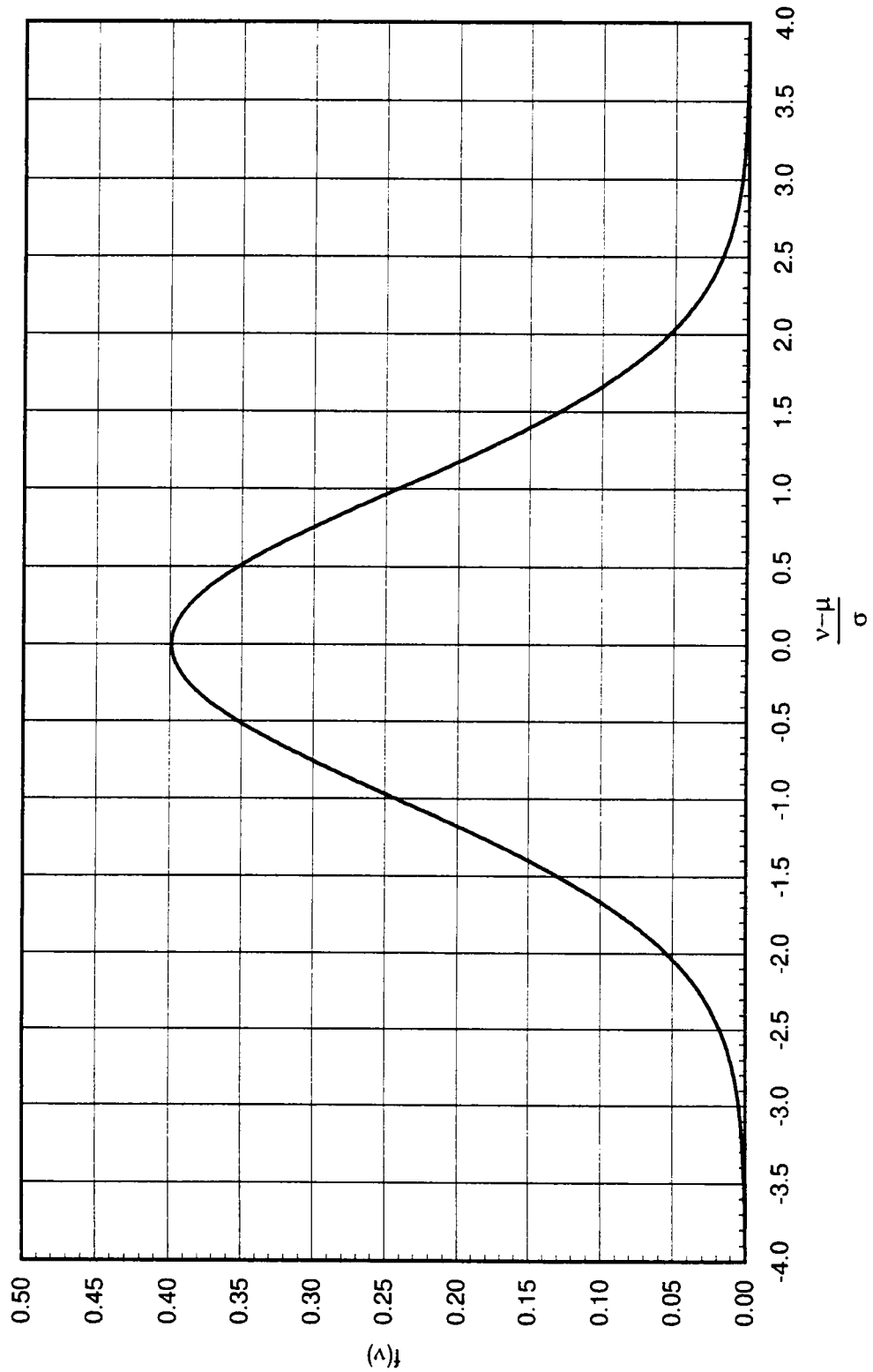


FIGURE 2.6 Gaussian Distribution

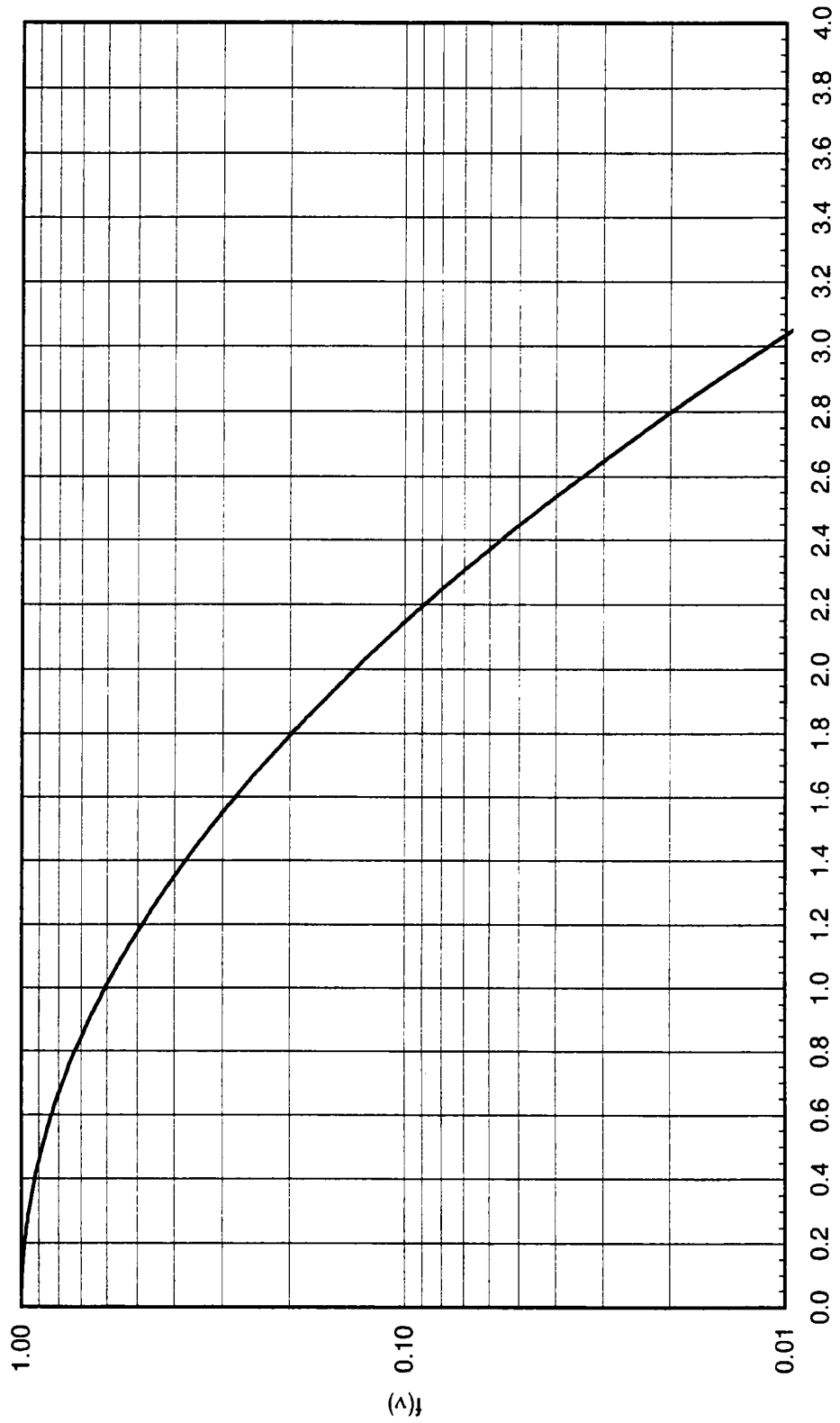


FIGURE 2.7 Normalized Gaussian Distribution

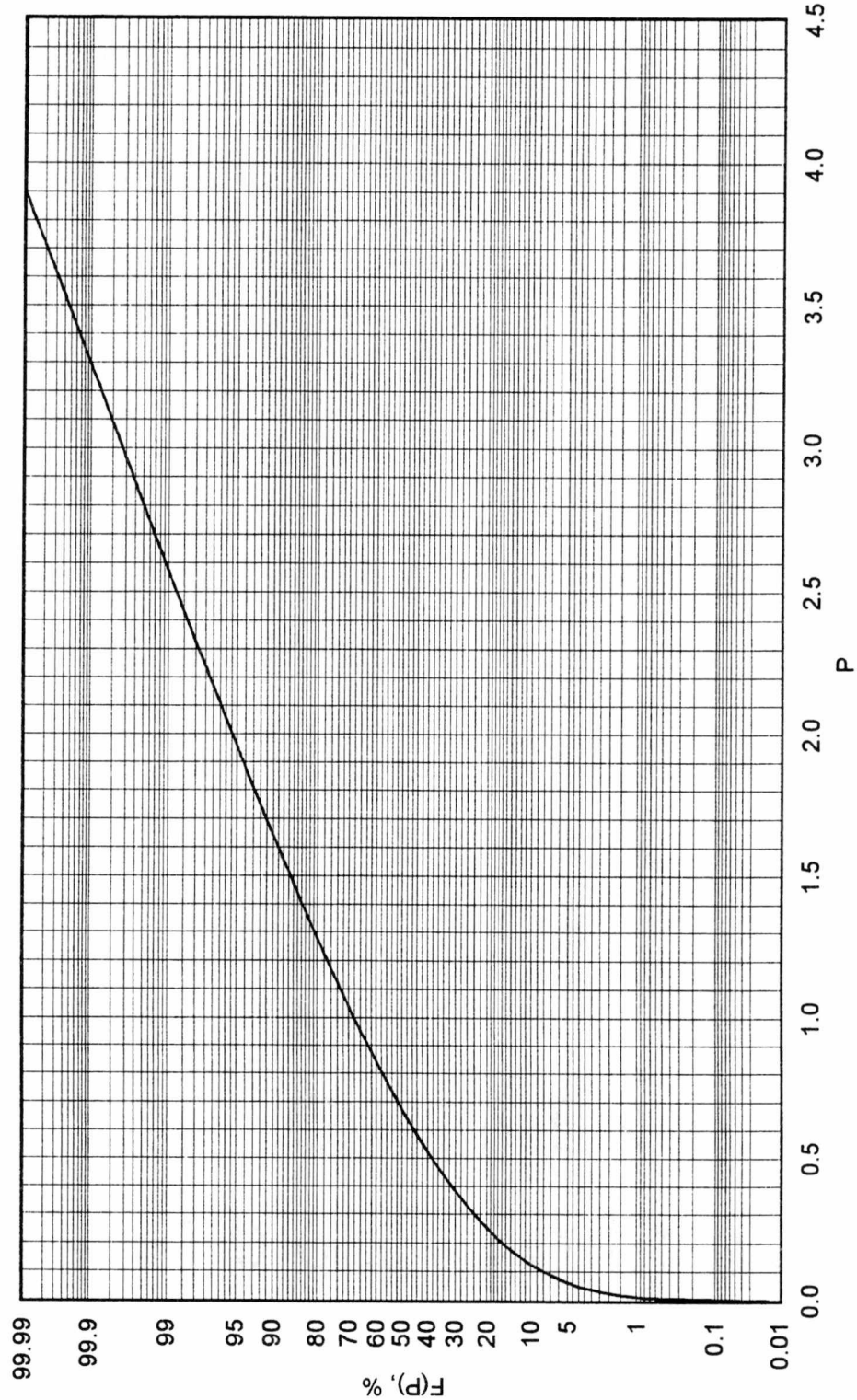


FIGURE 2.8 Area Under the Gaussian Distribution Curve

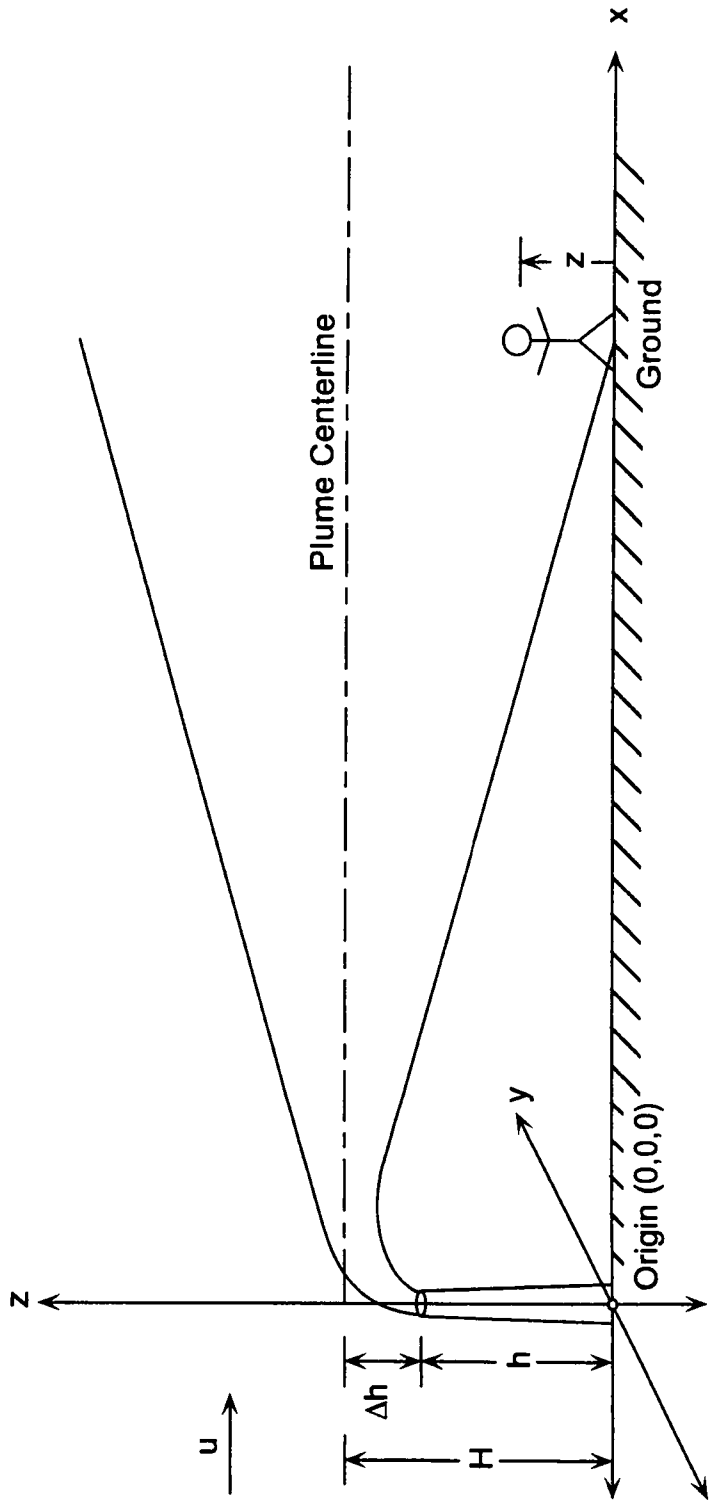


FIGURE 2.9 Illustration of Plume Dispersion from an Elevated Point Source

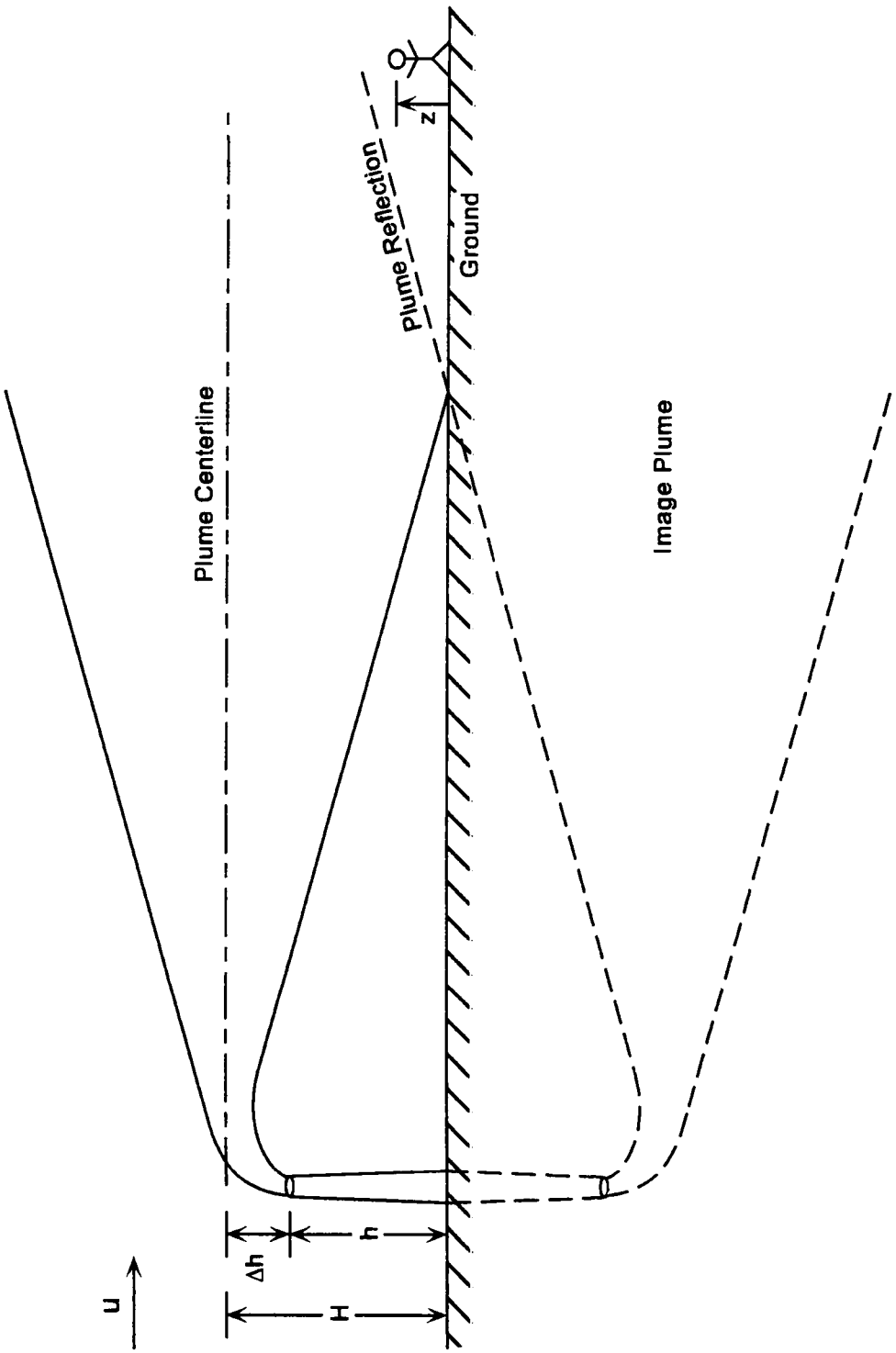


FIGURE 2.10 Illustration of Plume Reflection Using an Image Plume

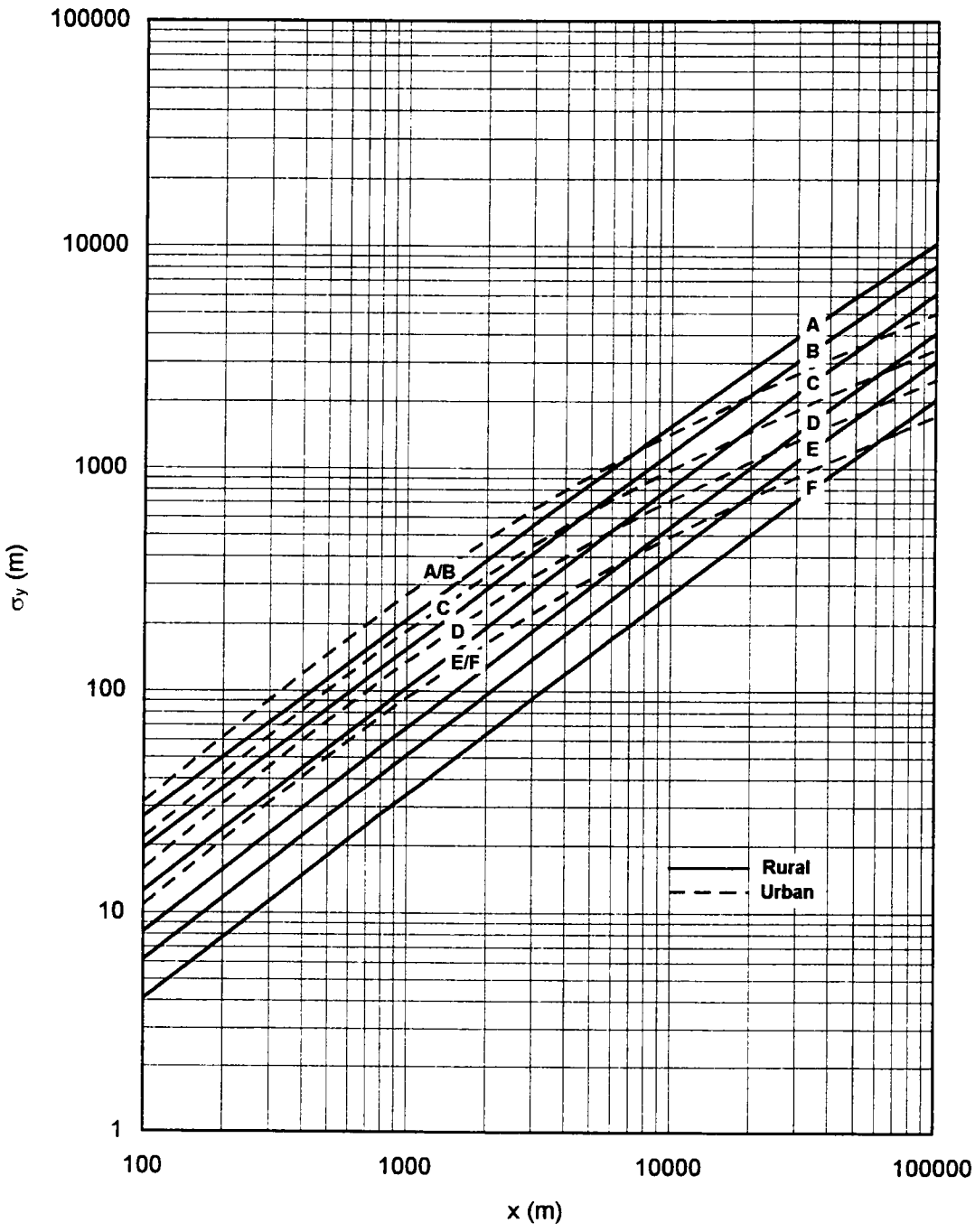


FIGURE 2.11 Rural and Urban Horizontal Dispersion Coefficients (σ_y) as a Function of Stability Category

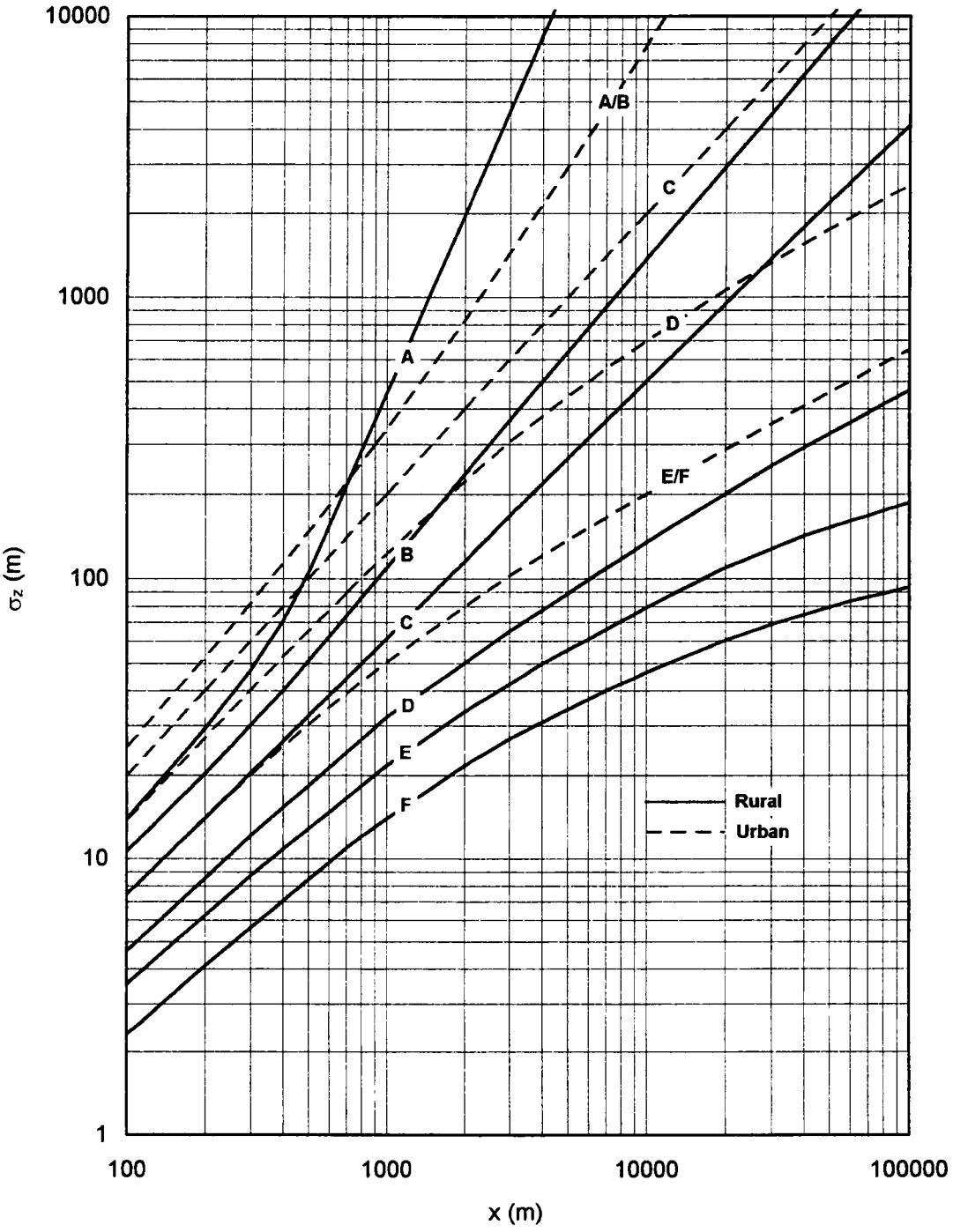


FIGURE 2.12 Rural and Urban Vertical Dispersion Coefficients (σ_z) as a Function of Stability Category

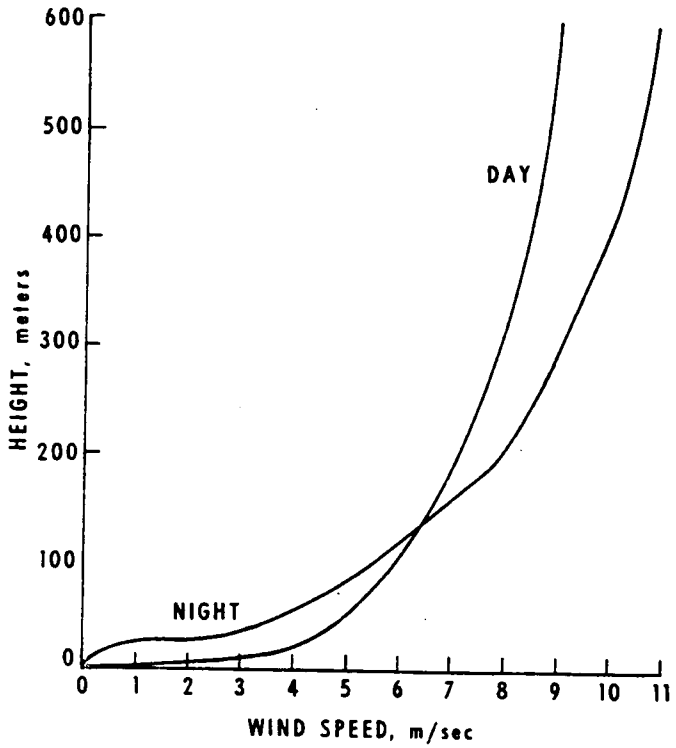


FIGURE 2.13 Typical Variation of Wind Speed with Height (Smith, 1963)

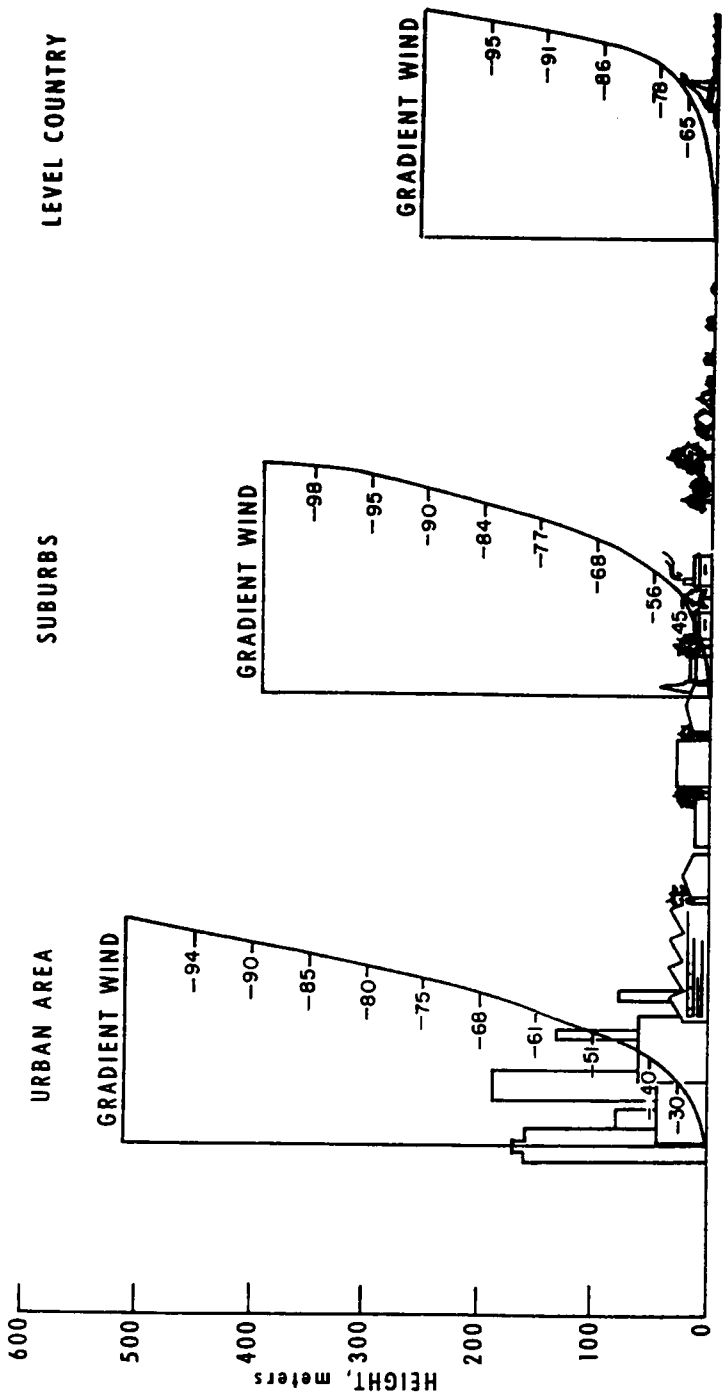


FIGURE 2.14 Variation of Wind Speed with Surface Roughness (Davenport, 1963)

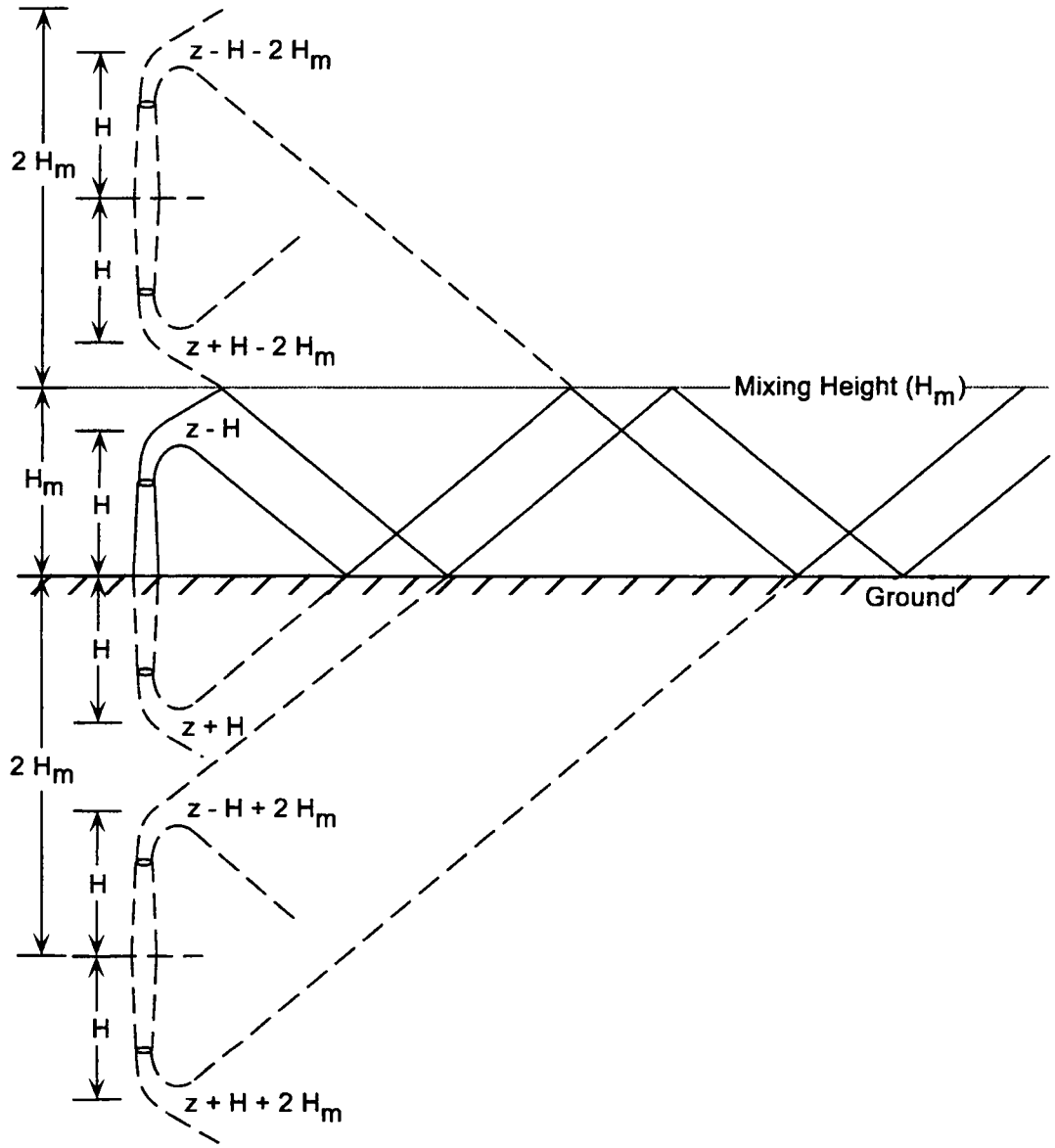


FIGURE 2.15 Multiple Image Sources for Plume Reflection

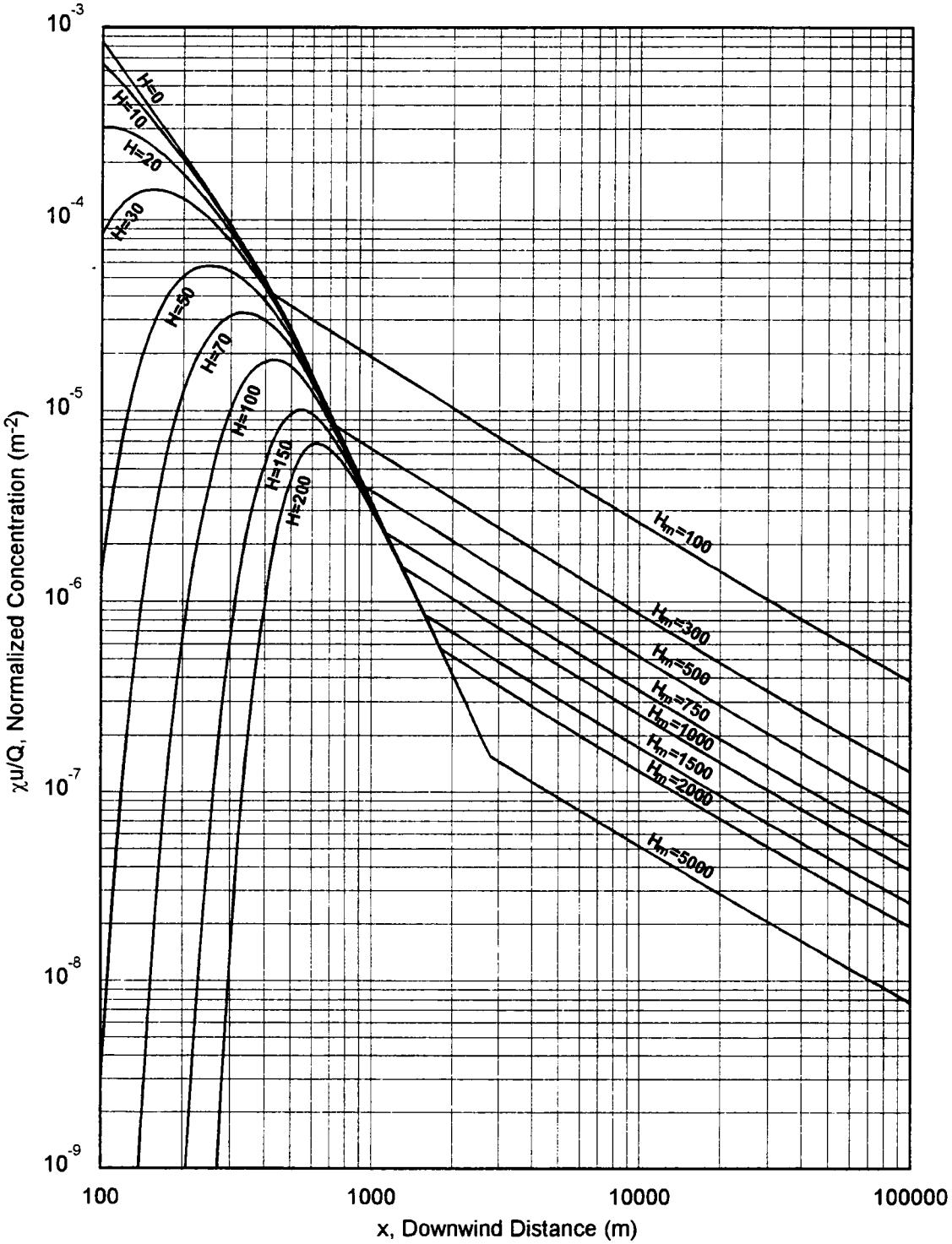


FIGURE 2.16 $\chi u/Q$ with Distance for Various Plume Heights (H in m) and Limits to Vertical Mixing (H_m in m), A Stability, Rural Dispersion Coefficients

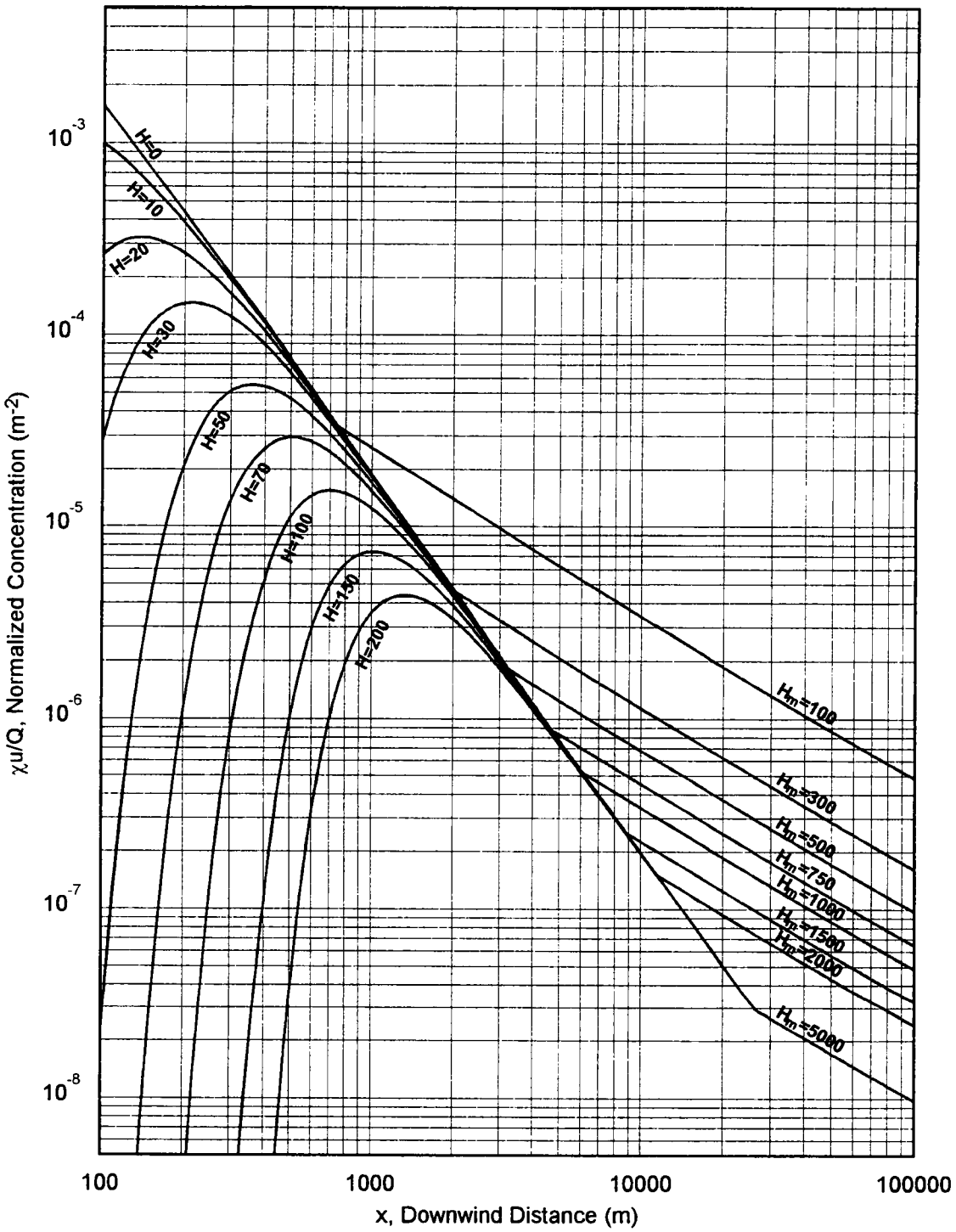


FIGURE 2.17 $\chi u/Q$ with Distance for Various Plume Heights (H in m) and Limits to Vertical Mixing (H_m in m), B Stability, Rural Dispersion Coefficients

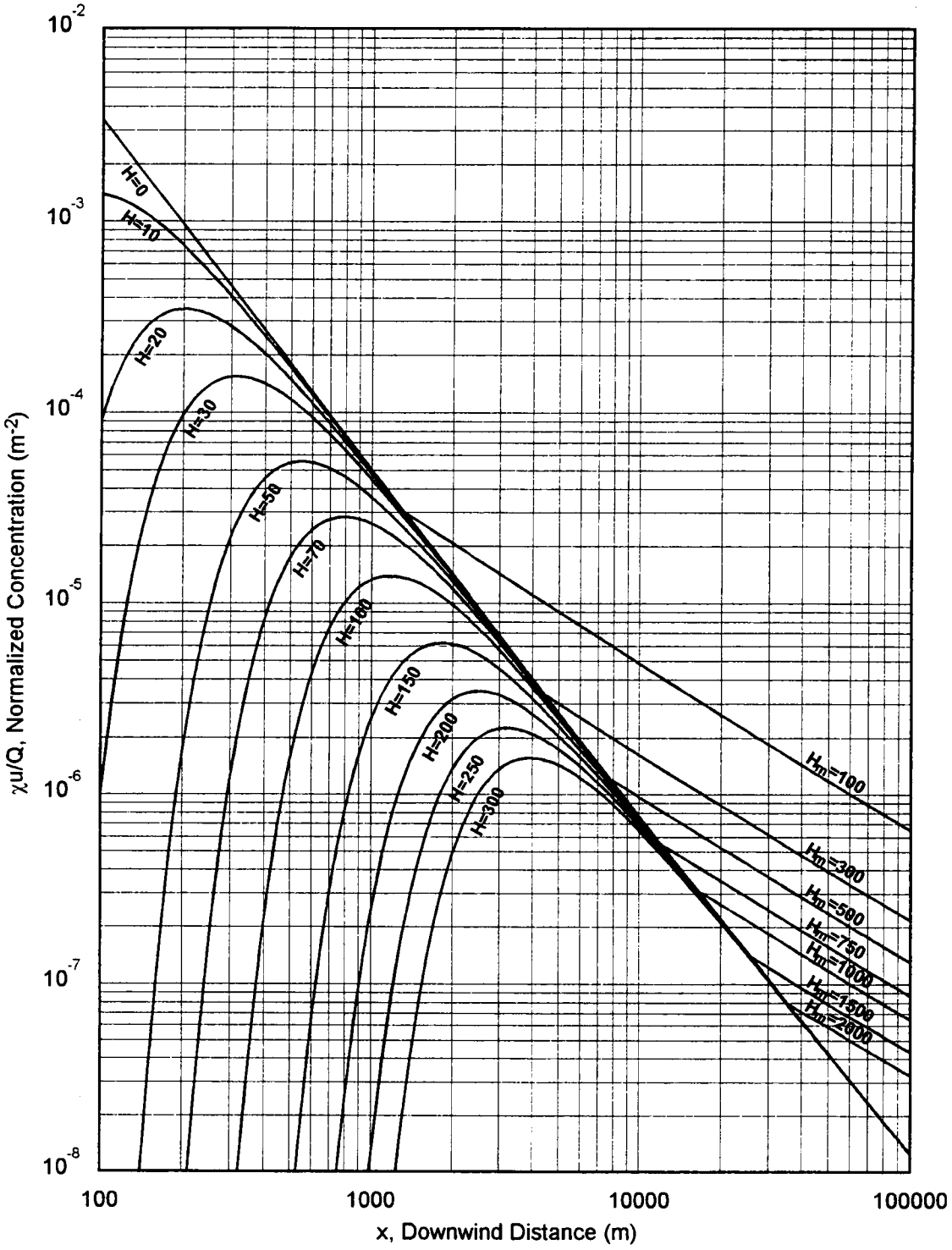


FIGURE 2.18 χu/Q with Distance for Various Plume Heights (H in m) and Limits to Vertical Mixing (H_m in m), C Stability, Rural Dispersion Coefficients

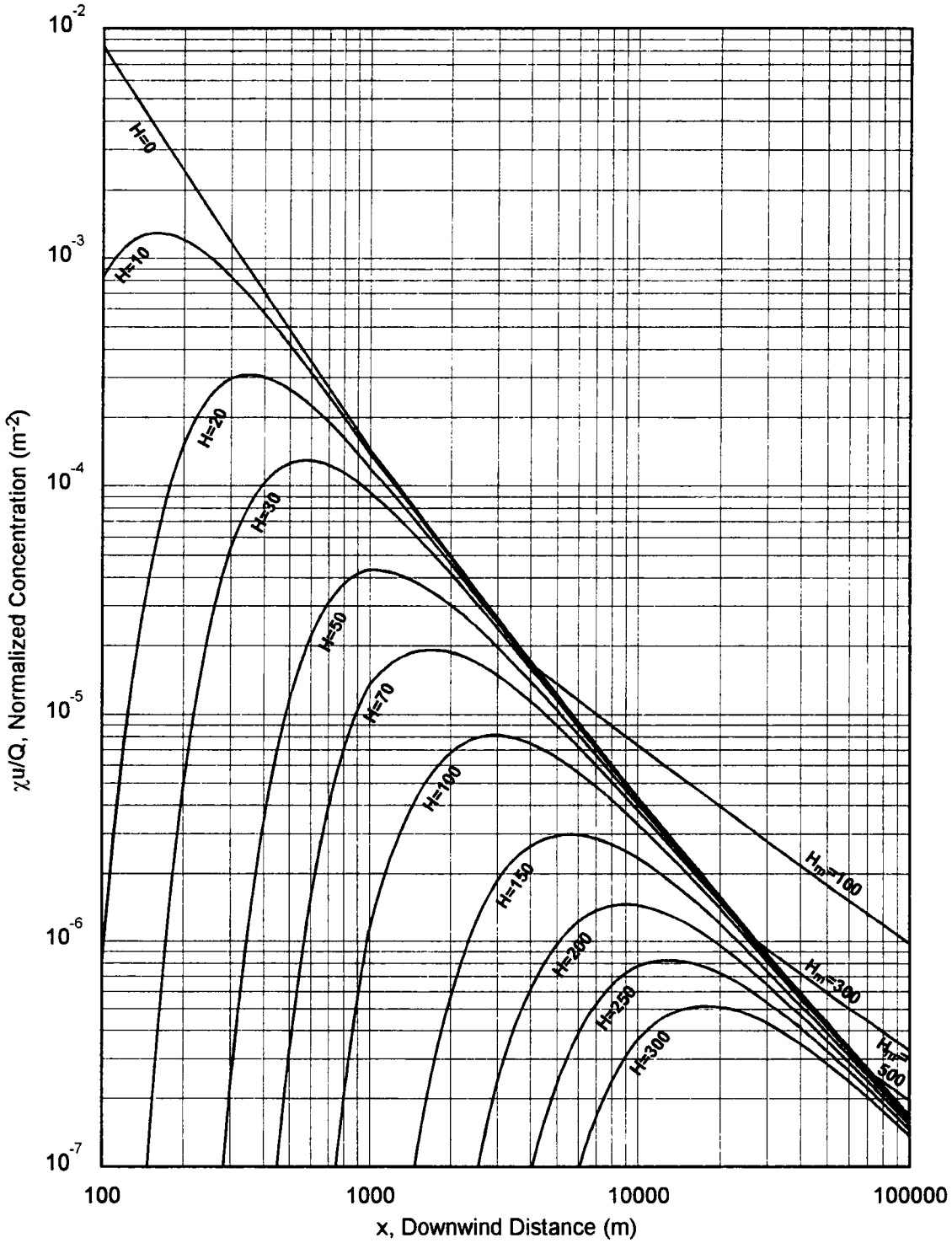


FIGURE 2.19 χu/Q with Distance for Various Plume Heights (H in m) and Limits to Vertical Mixing (H_m in m), D Stability, Rural Dispersion Coefficients

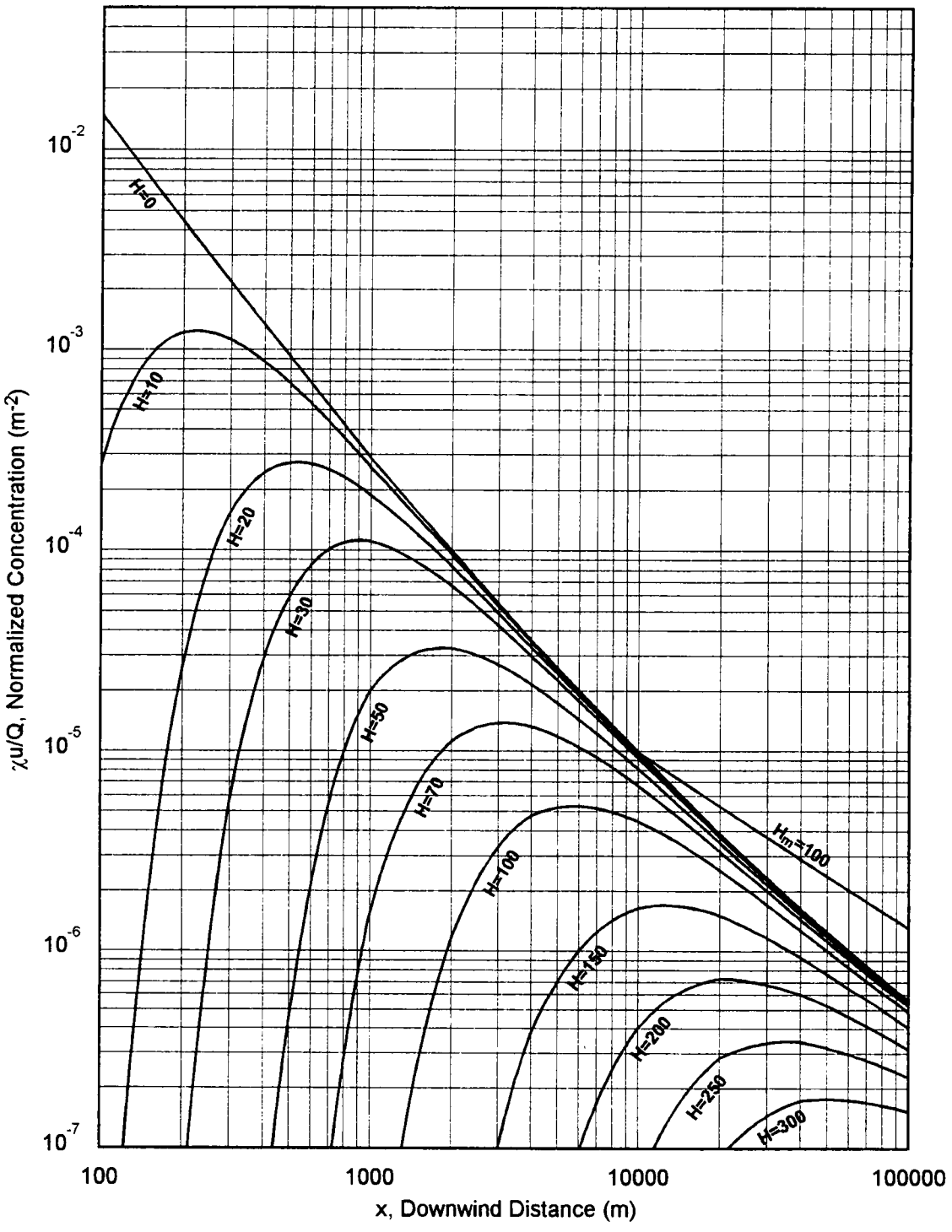


FIGURE 2.20 $\chi u/Q$ with Distance for Various Plume Heights (H in m) and Limits to Vertical Mixing (H_m in m), E Stability, Rural Dispersion Coefficients

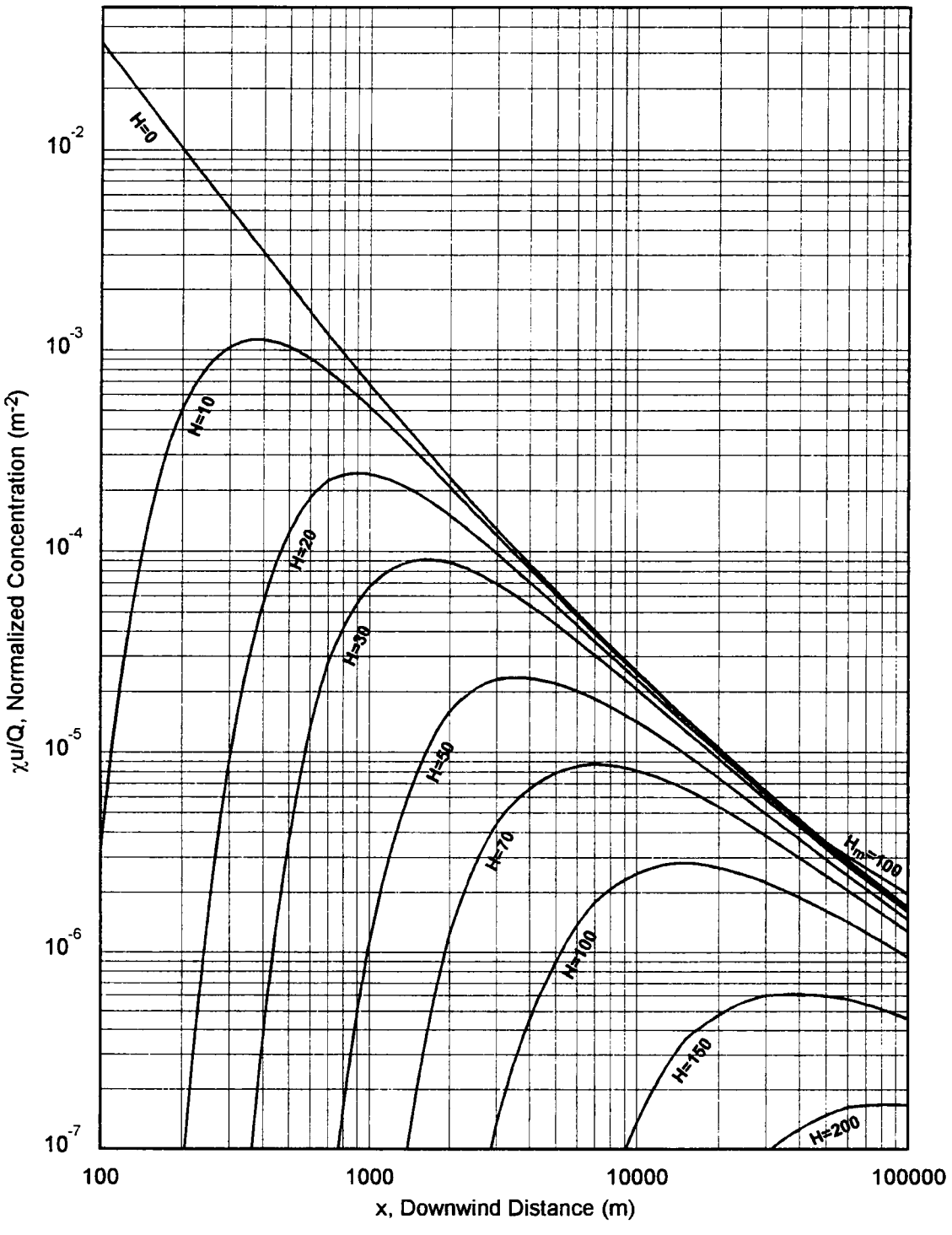


FIGURE 2.21 $\chi u/Q$ with Distance for Various Plume Heights (H in m) and Limits to Vertical Mixing (H_m in m), F Stability, Rural Dispersion Coefficients

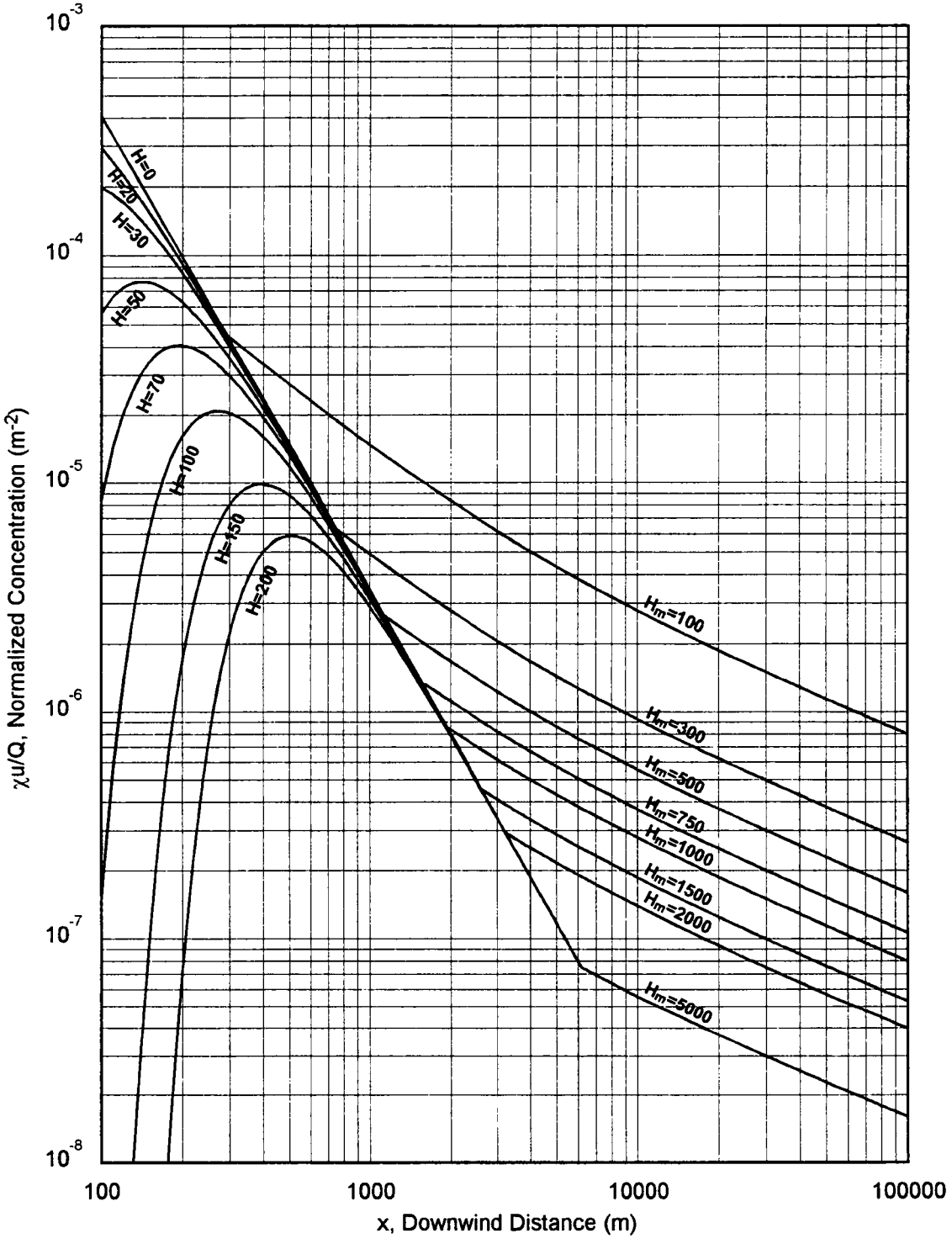


FIGURE 2.22 $\chi u/Q$ with Distance for Various Plume Heights (H in m) and Limits to Vertical Mixing (H_m in m), A/B Stability, Urban Dispersion Coefficients

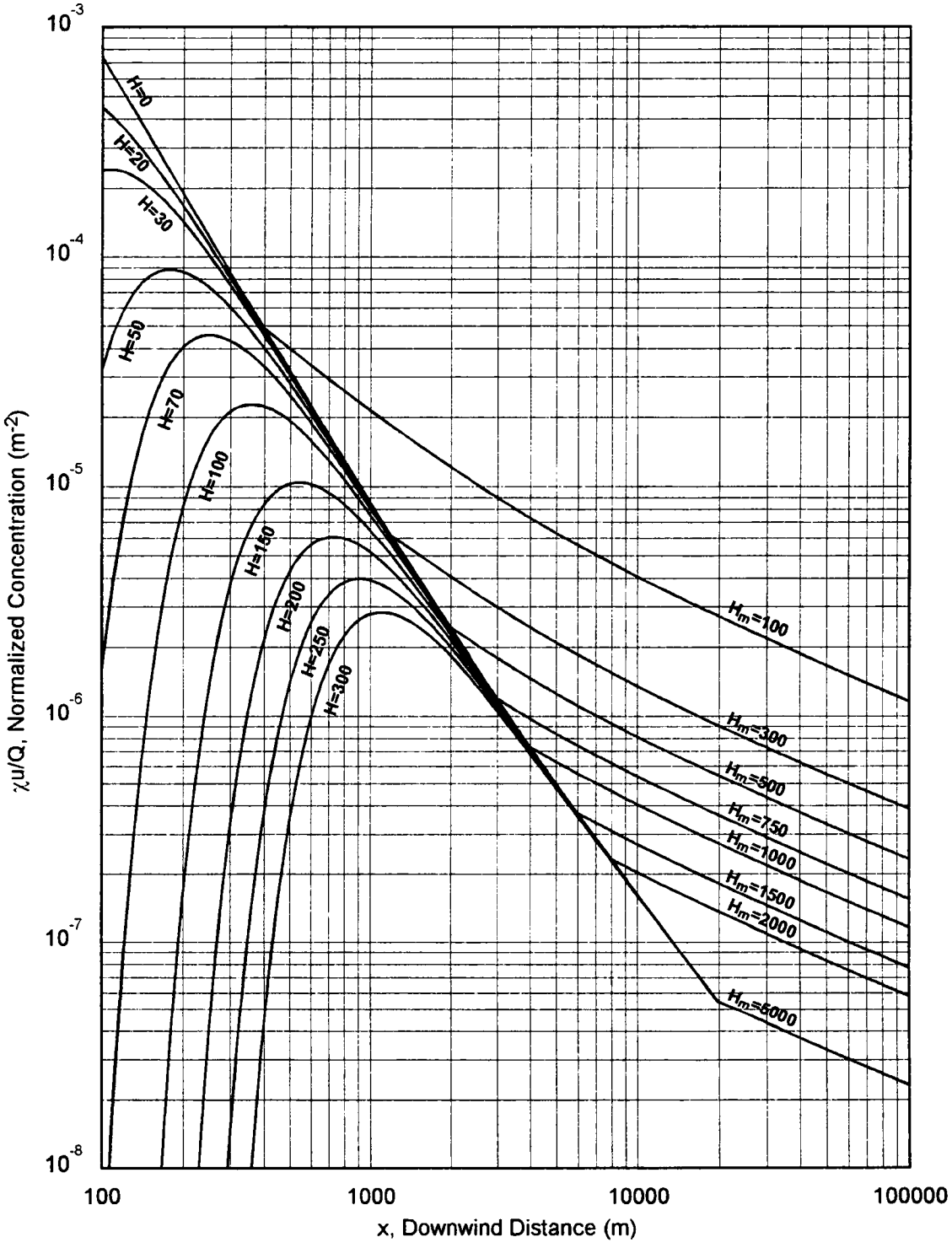


FIGURE 2.23 χu/Q with Distance for Various Plume Heights (H in m) and Limits to Vertical Mixing (H_m in m), C Stability, Urban Dispersion Coefficients

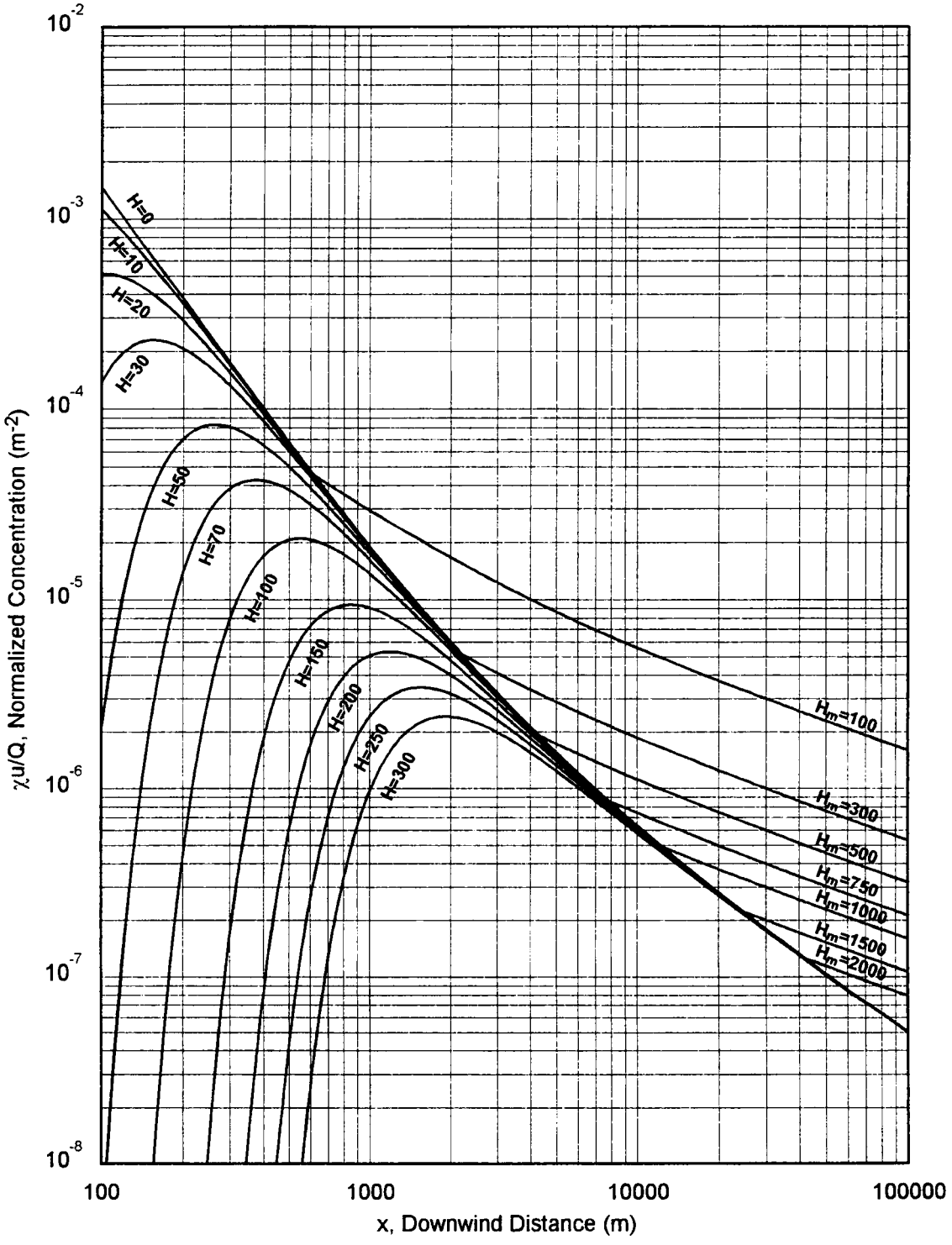


FIGURE 2.24 χu/Q with Distance for Various Plume Heights (H in m) and Limits to Vertical Mixing (H_m in m), D Stability, Urban Dispersion Coefficients

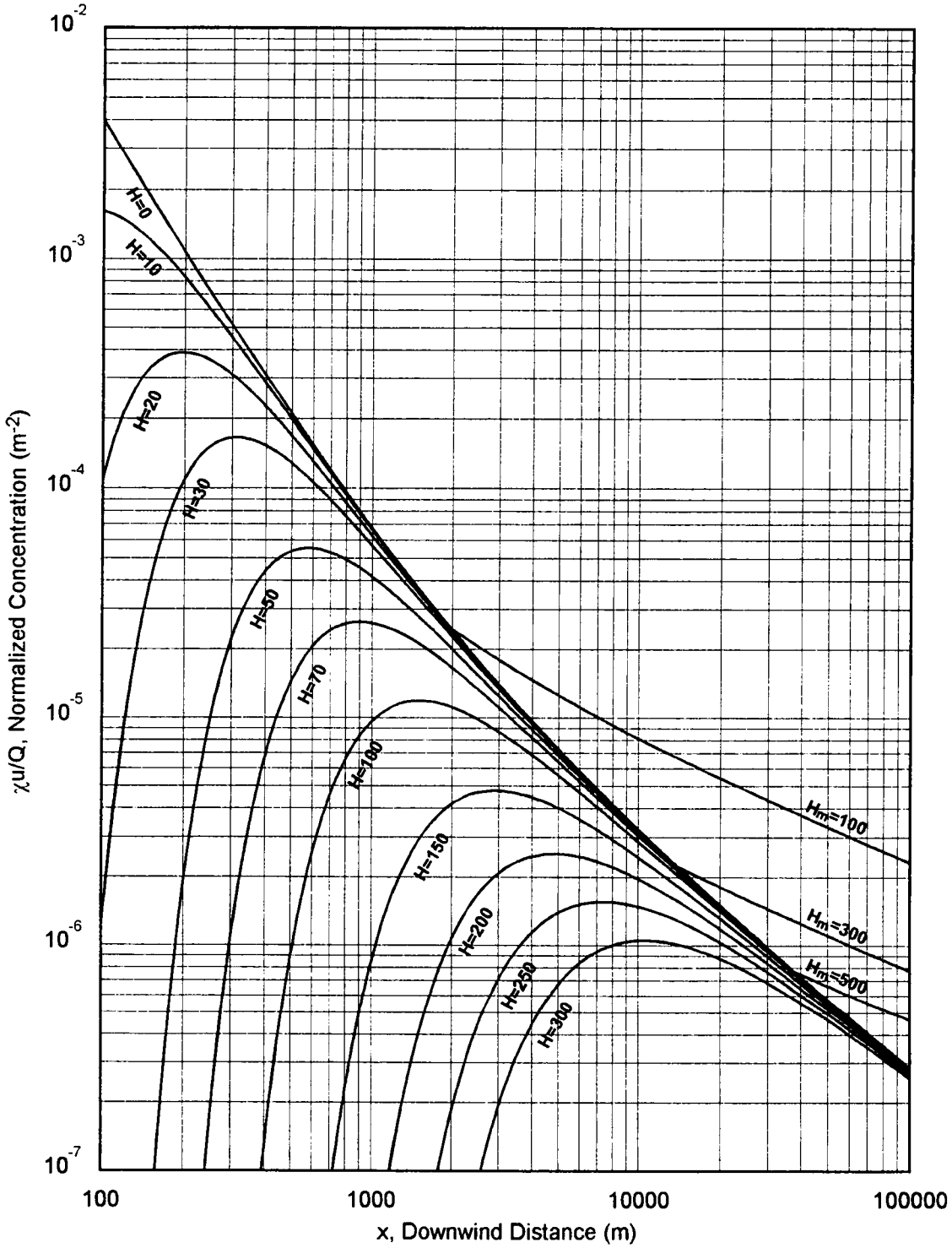


FIGURE 2.25 $\chi u/Q$ with Distance for Various Plume Heights (H in m) and Limits to Vertical Mixing (H_m in m), E/F Stability, Urban Dispersion Coefficients

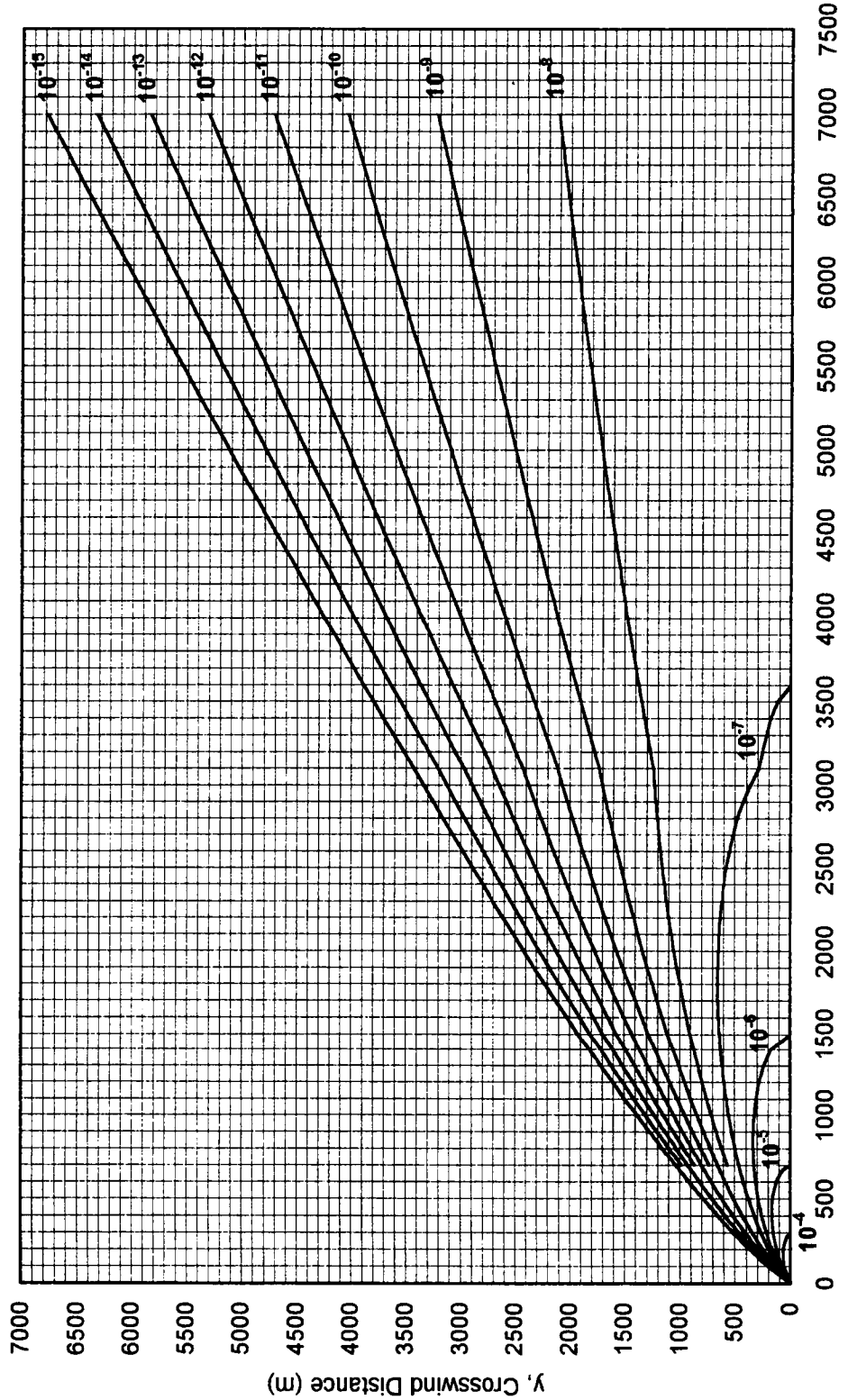


FIGURE 2.26 Isopleths of $\chi u/Q$ (m^{-2}) for a Ground-Level Source, A Stability, Rural Dispersion Coefficients

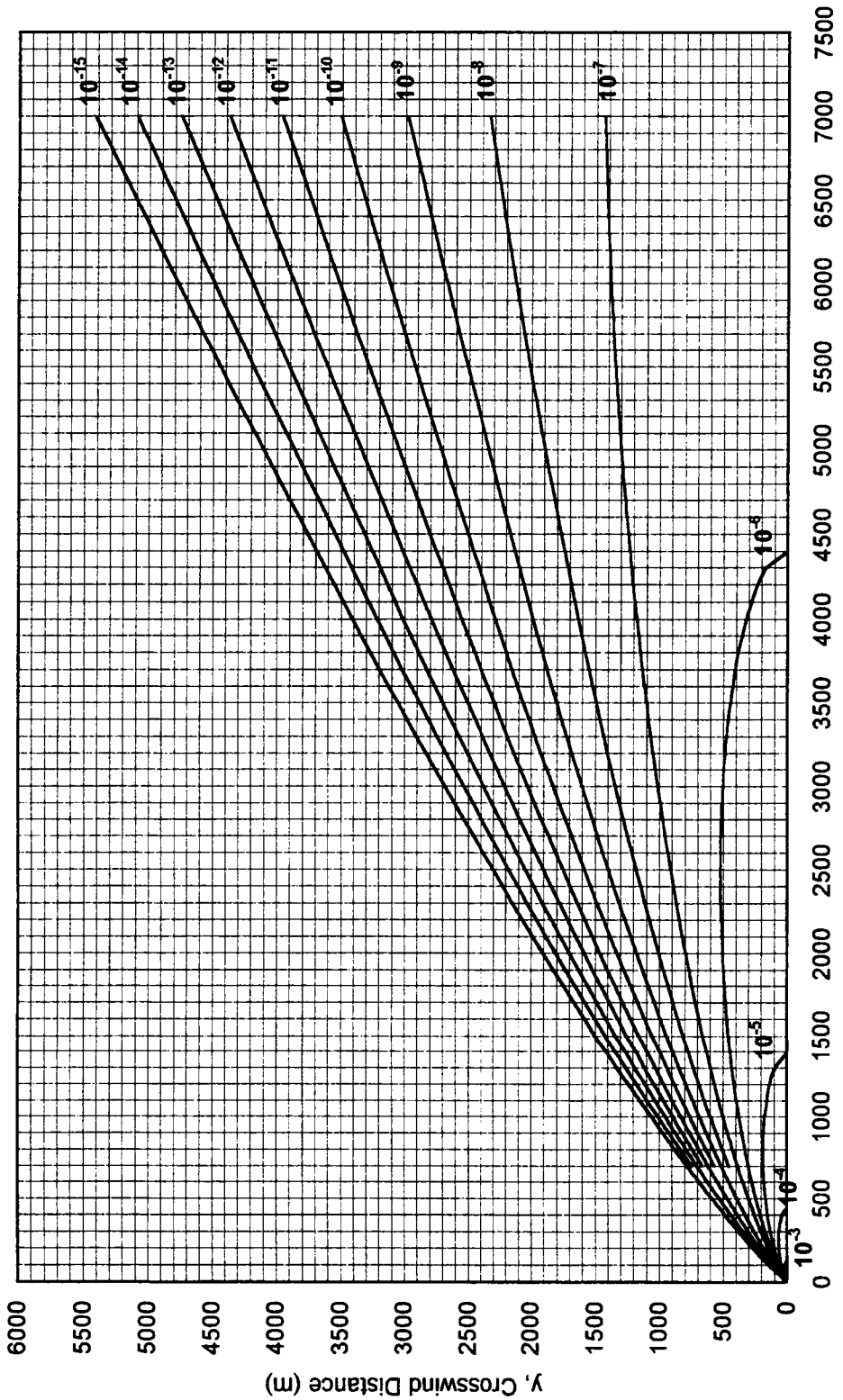


FIGURE 2.27 Isopleths of $\chi u/Q$ (m^{-2}) for a Ground-Level Source, B Stability, Rural Dispersion Coefficients

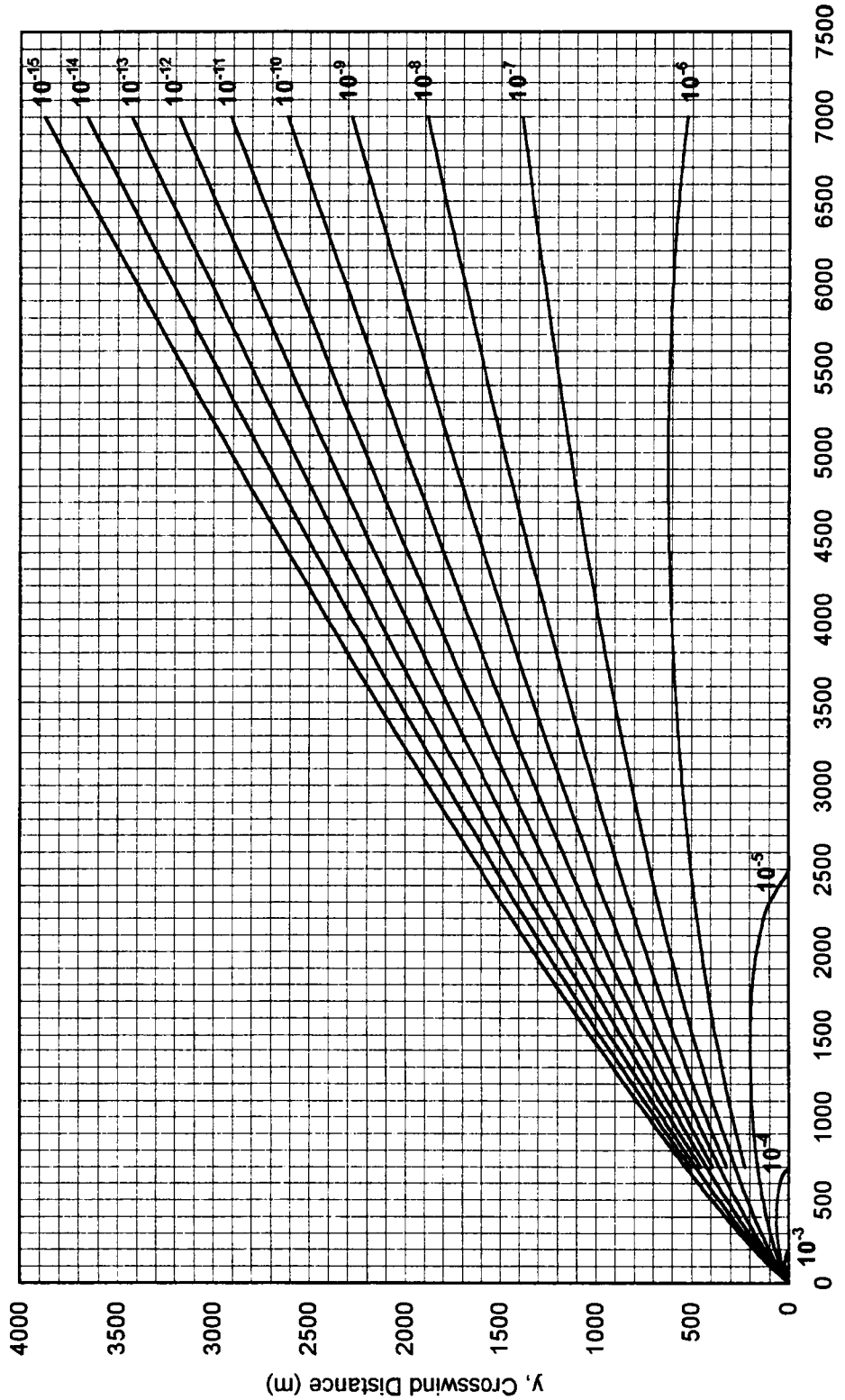


FIGURE 2.28 Isopleths of $\chi u/Q$ (m^{-2}) for a Ground-Level Source, C Stability, Rural Dispersion Coefficients

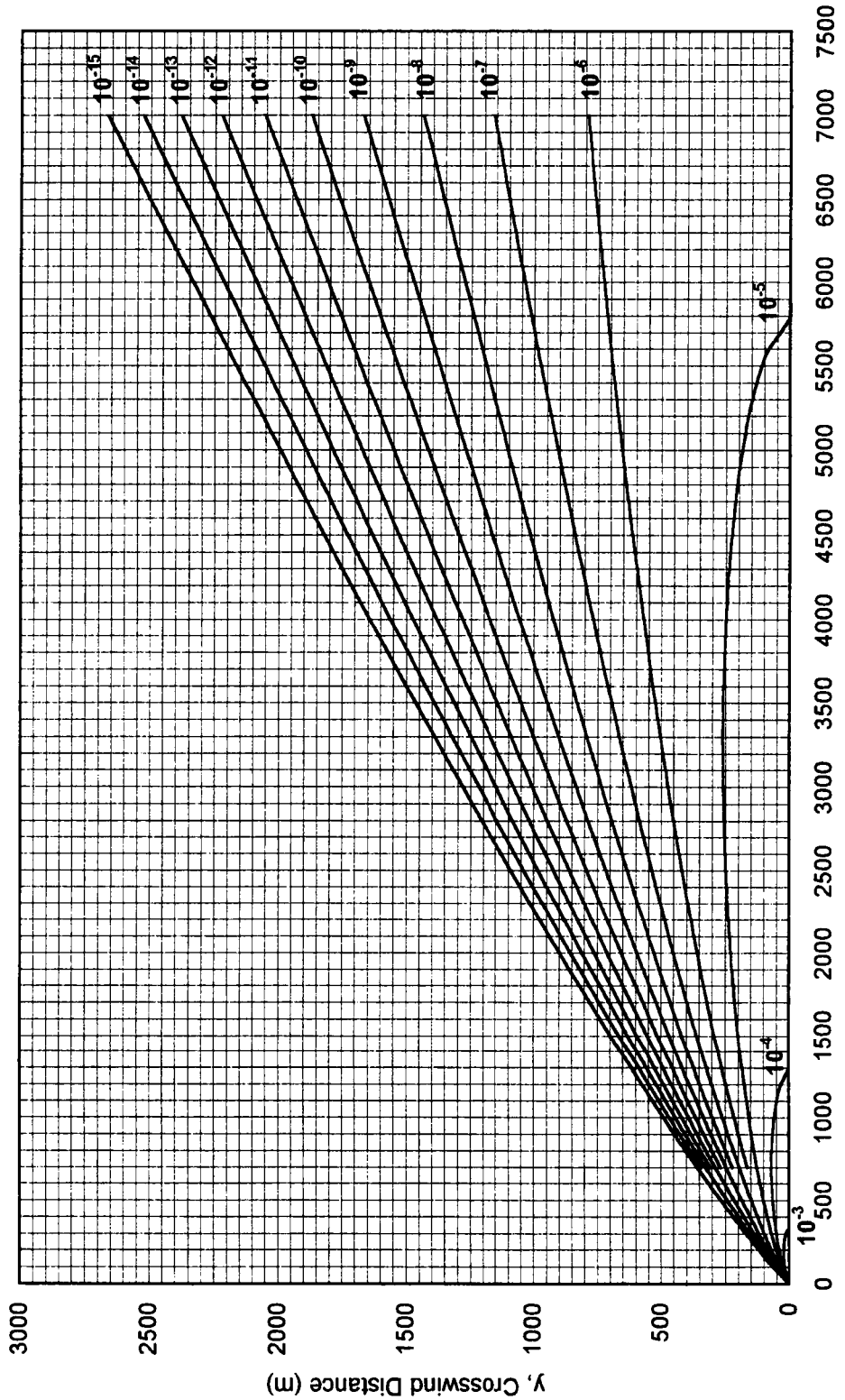


FIGURE 2.29 Isopleths of $\chi u/Q$ (m^{-2}) for a Ground-Level Source, D Stability, Rural Dispersion Coefficients

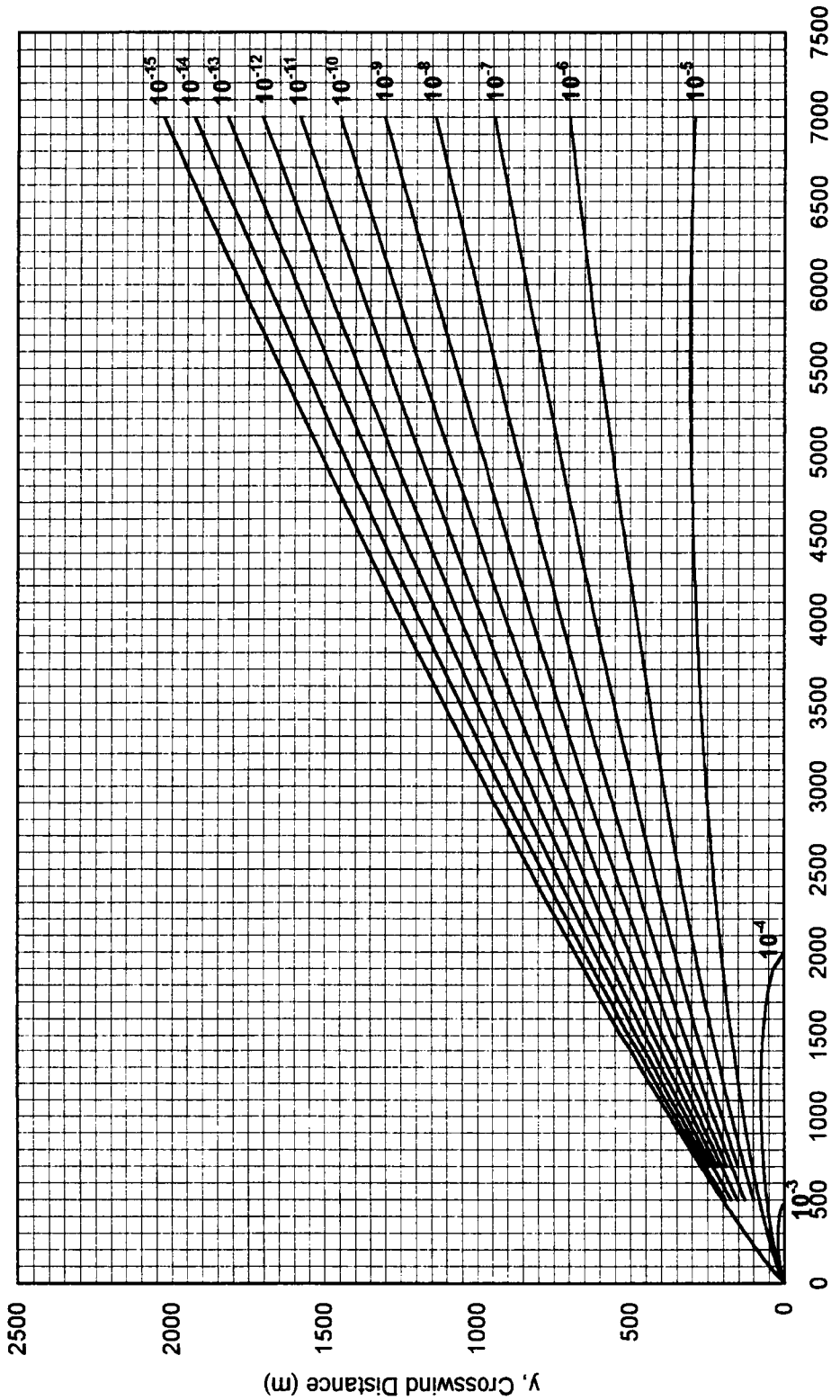


FIGURE 2.30 Isopleths of $\chi u/Q$ (m^{-2}) for a Ground-Level Source, E Stability, Rural Dispersion Coefficients

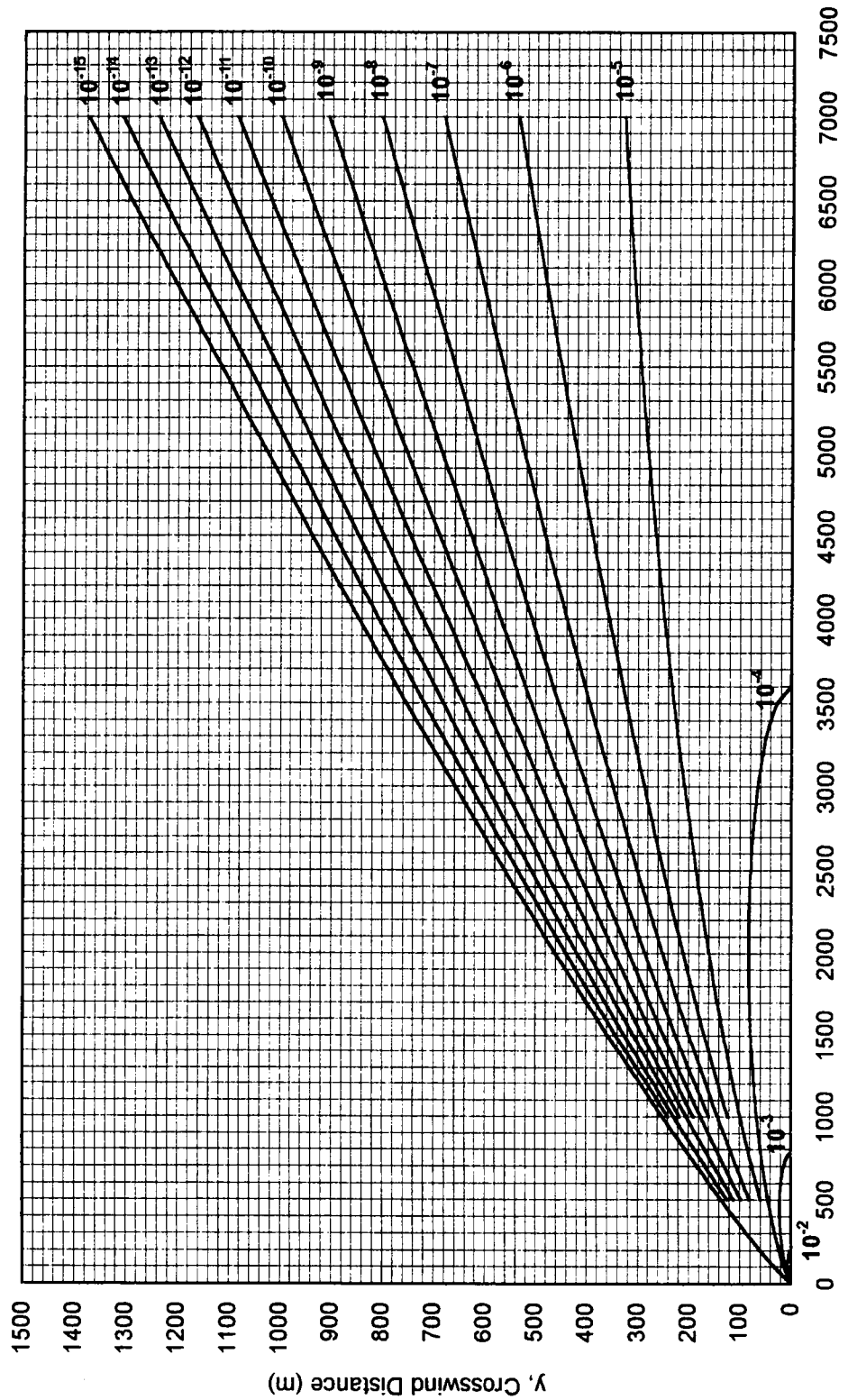


FIGURE 2.31 Isopleths of $\chi u/Q$ (m^{-2}) for a Ground-Level Source, F Stability, Rural Dispersion Coefficients

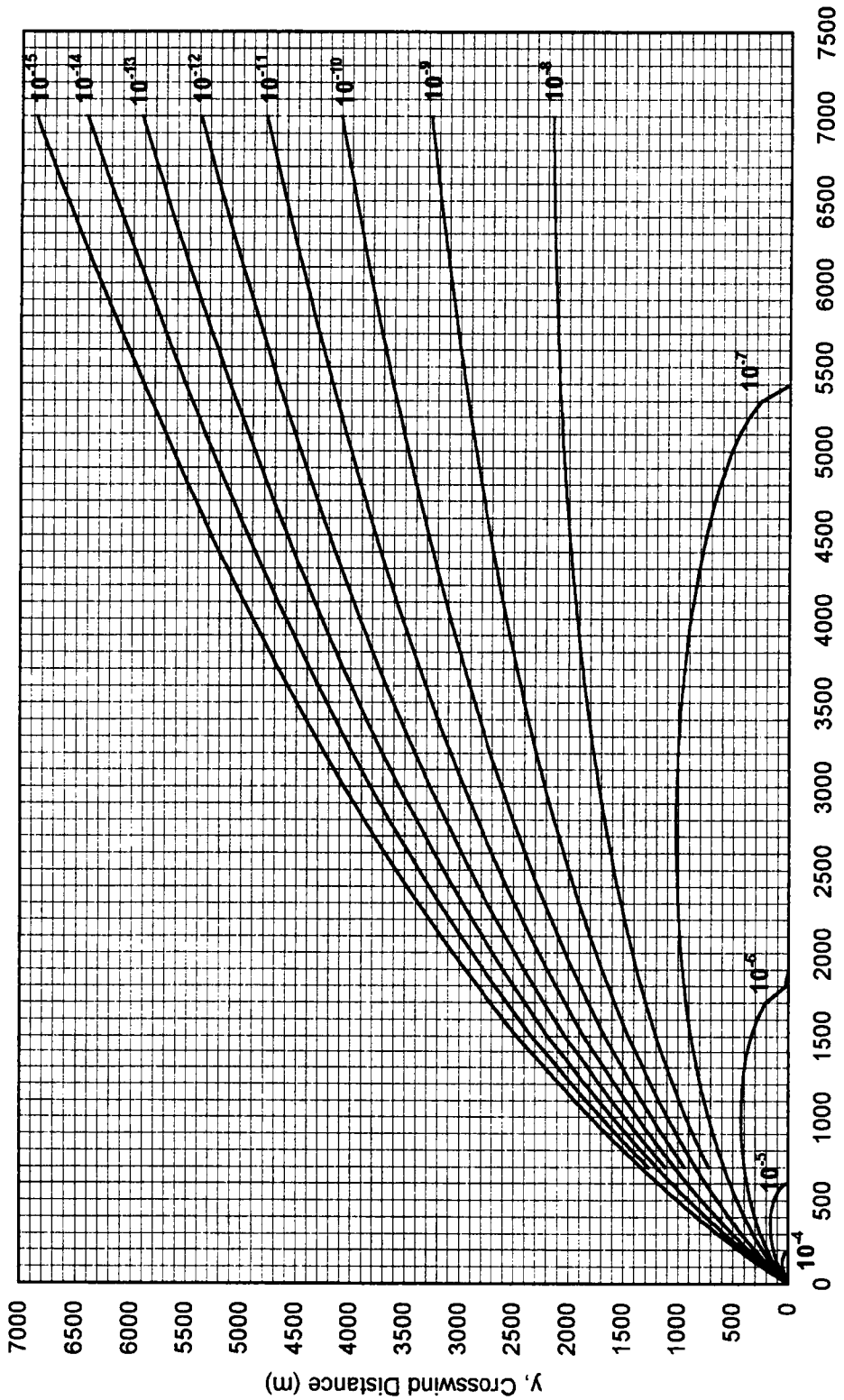


FIGURE 2.32 Isopleths of $\chi u/Q$ (m^{-2}) for a Ground-Level Source, A/B Stability, Urban Dispersion Coefficients

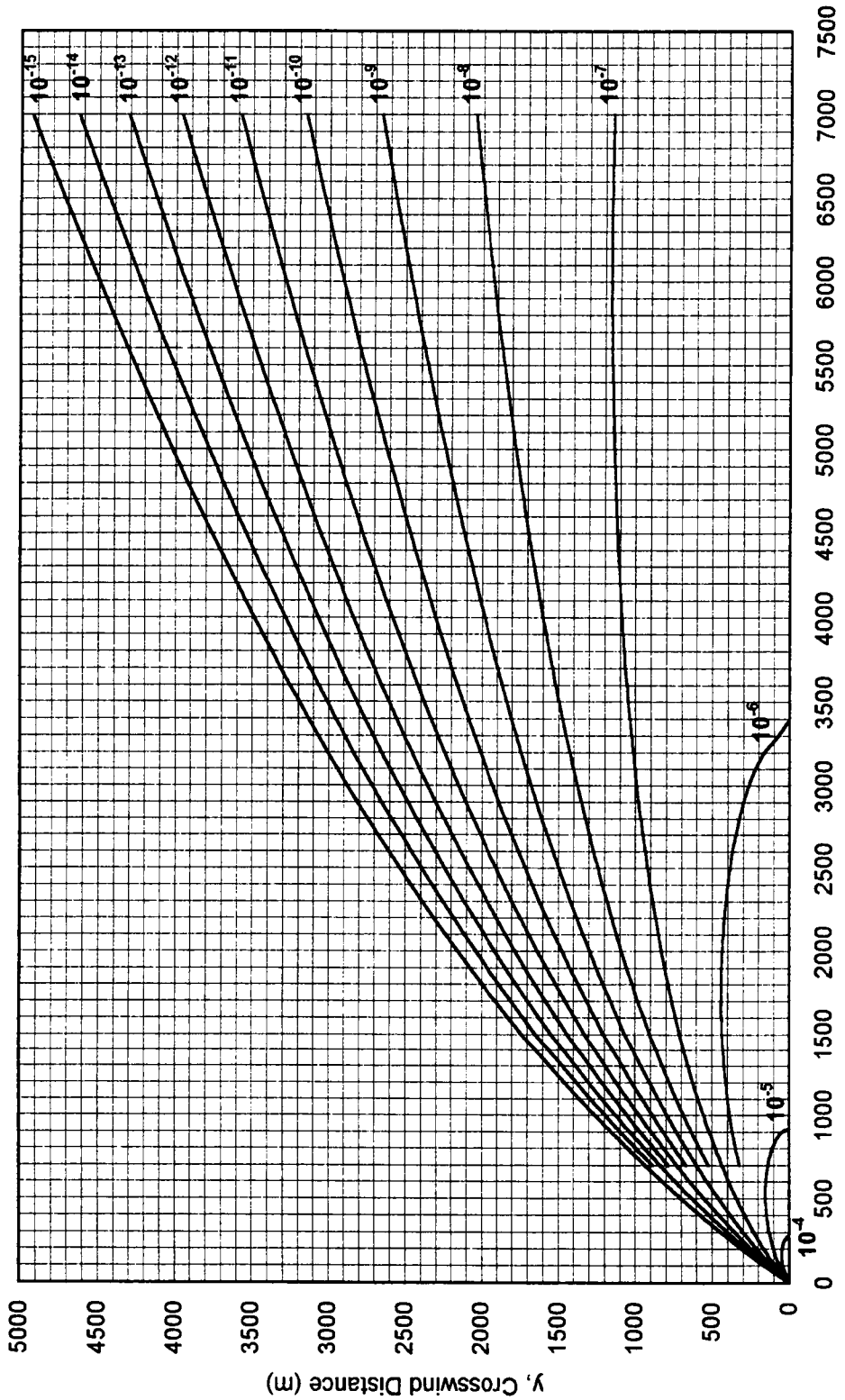


FIGURE 2.33 Isopleths of $\chi u/Q$ (m^{-2}) for a Ground-Level Source, C Stability, Urban Dispersion Coefficients

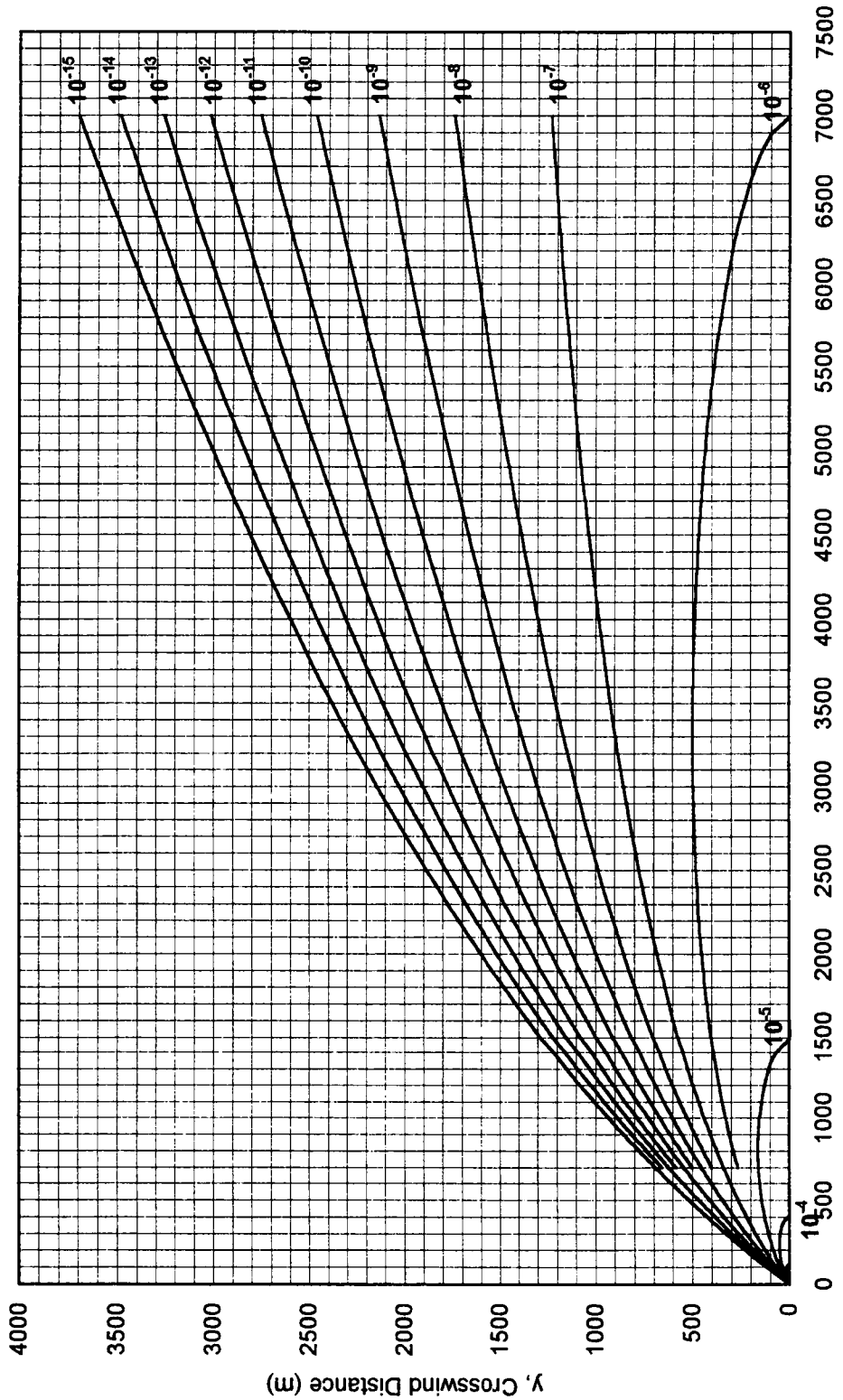


FIGURE 2.34 Isopleths of $\chi u/Q$ (m^{-2}) for a Ground-Level Source, D Stability, Urban Dispersion Coefficients

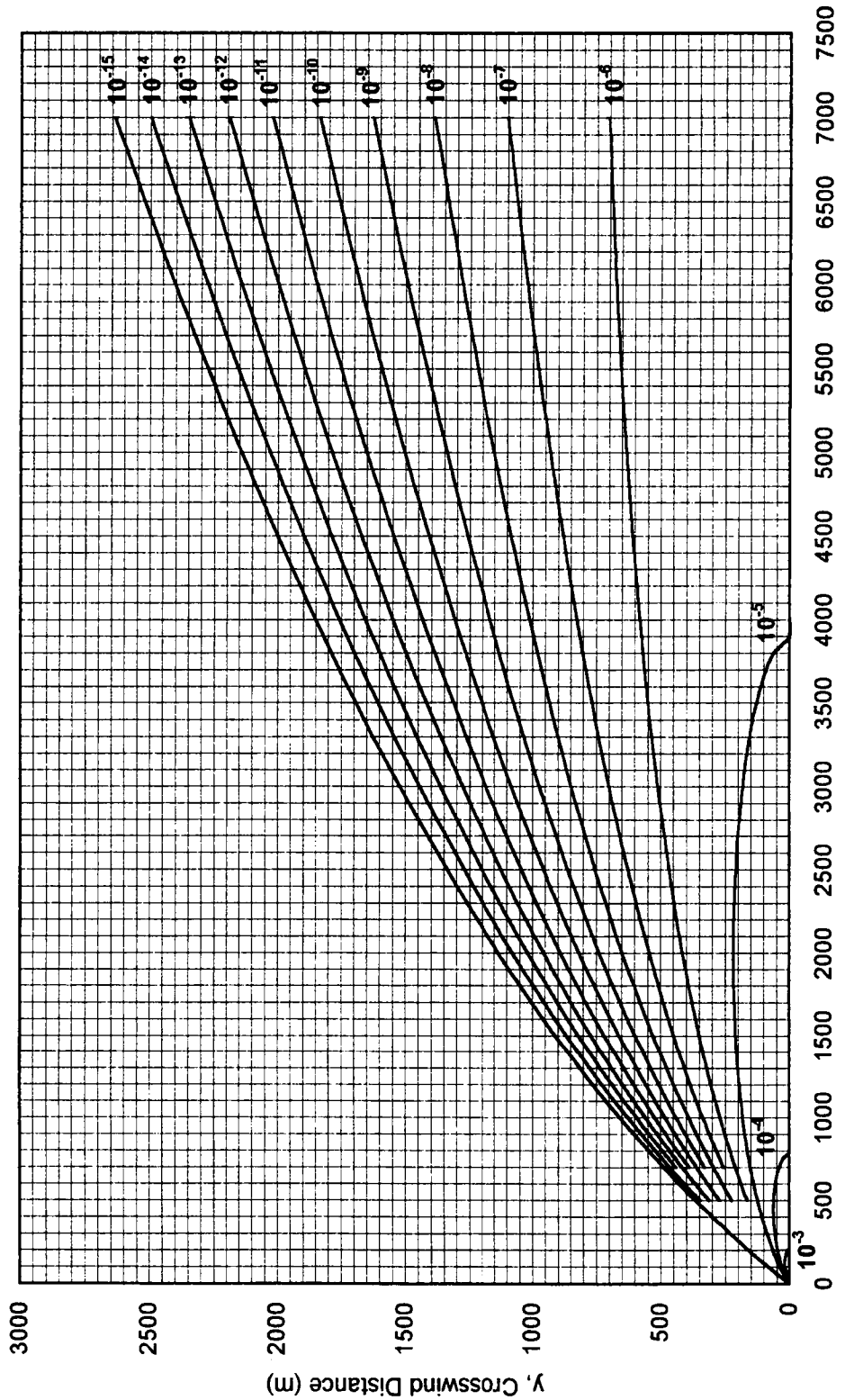


FIGURE 2.35 Isopleths of $\chi u/Q$ (m^{-2}) for a Ground-Level Source, E/F Stability, Urban Dispersion Coefficients

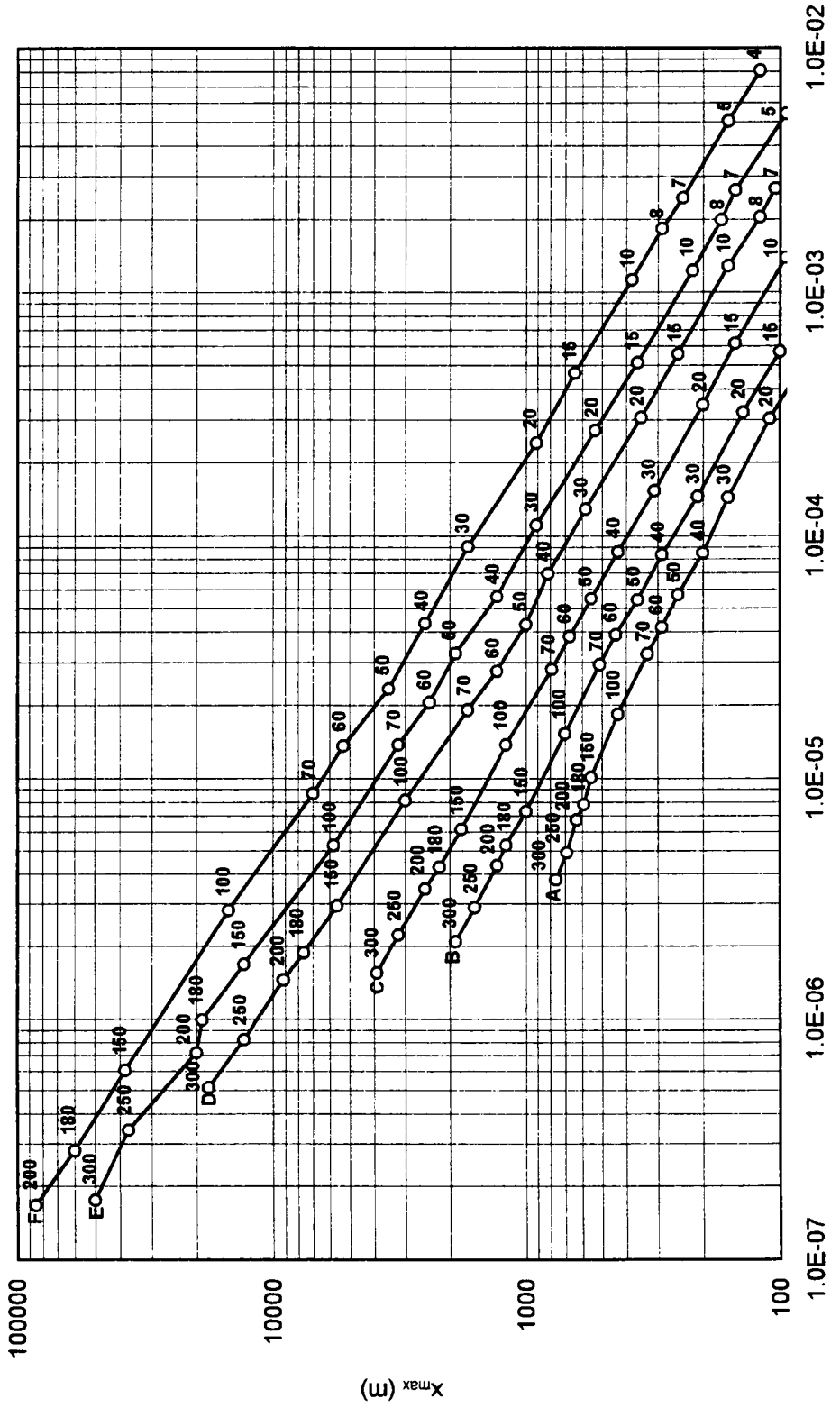


FIGURE 2.36 Distance to Maximum Concentration Versus Maximum $\chi u/Q$ as a Function of Stability and Plume Height (m), Rural Dispersion Coefficients

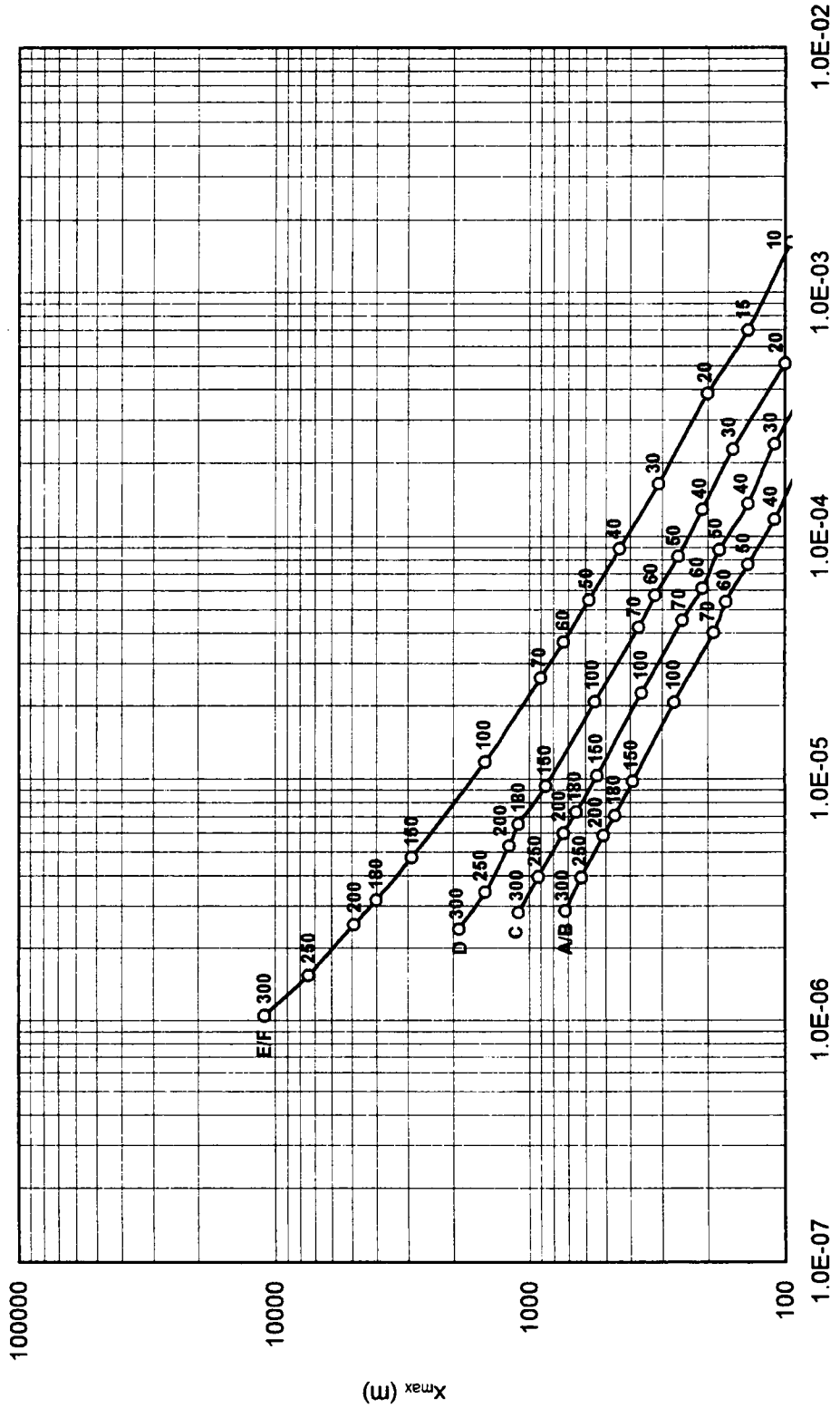


FIGURE 2.37 Distance to Maximum Concentration Versus Maximum $\chi u/Q$ as a Function of Stability and Plume Height (m), Urban Dispersion Coefficients

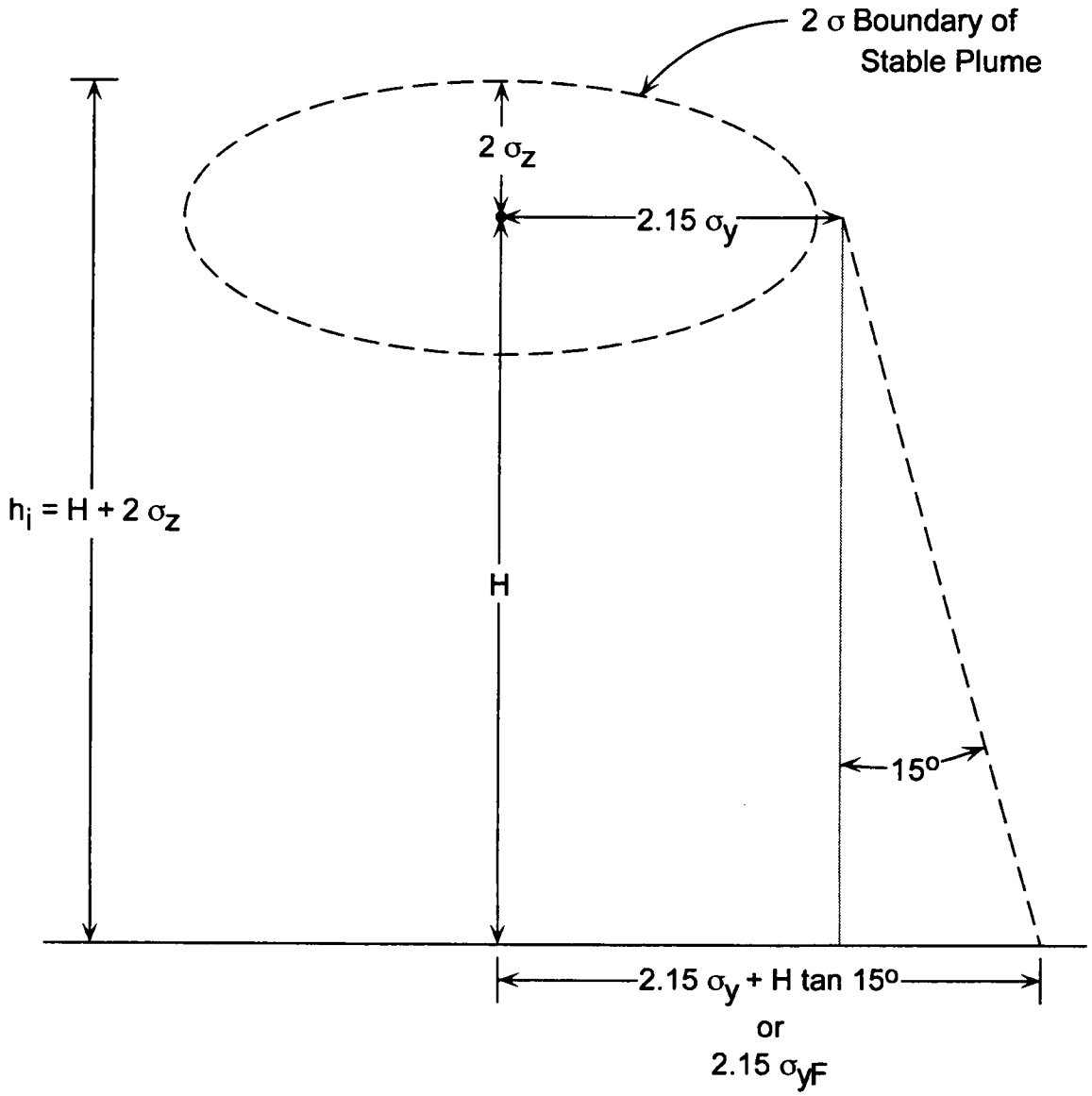


FIGURE 2.38 Cross-Section of a Fumigating Plume

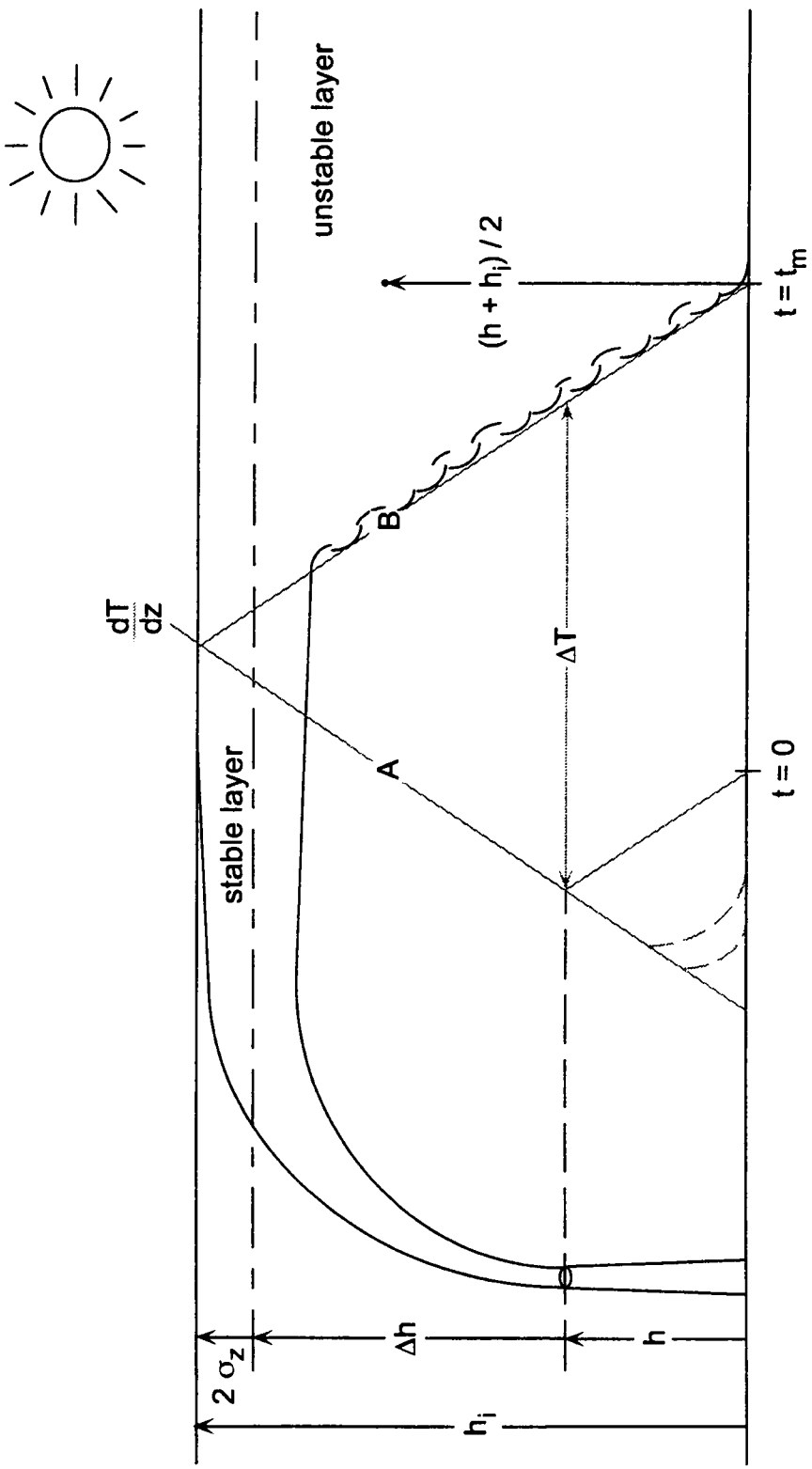


FIGURE 2.39 Profile of a Fumigating Plume

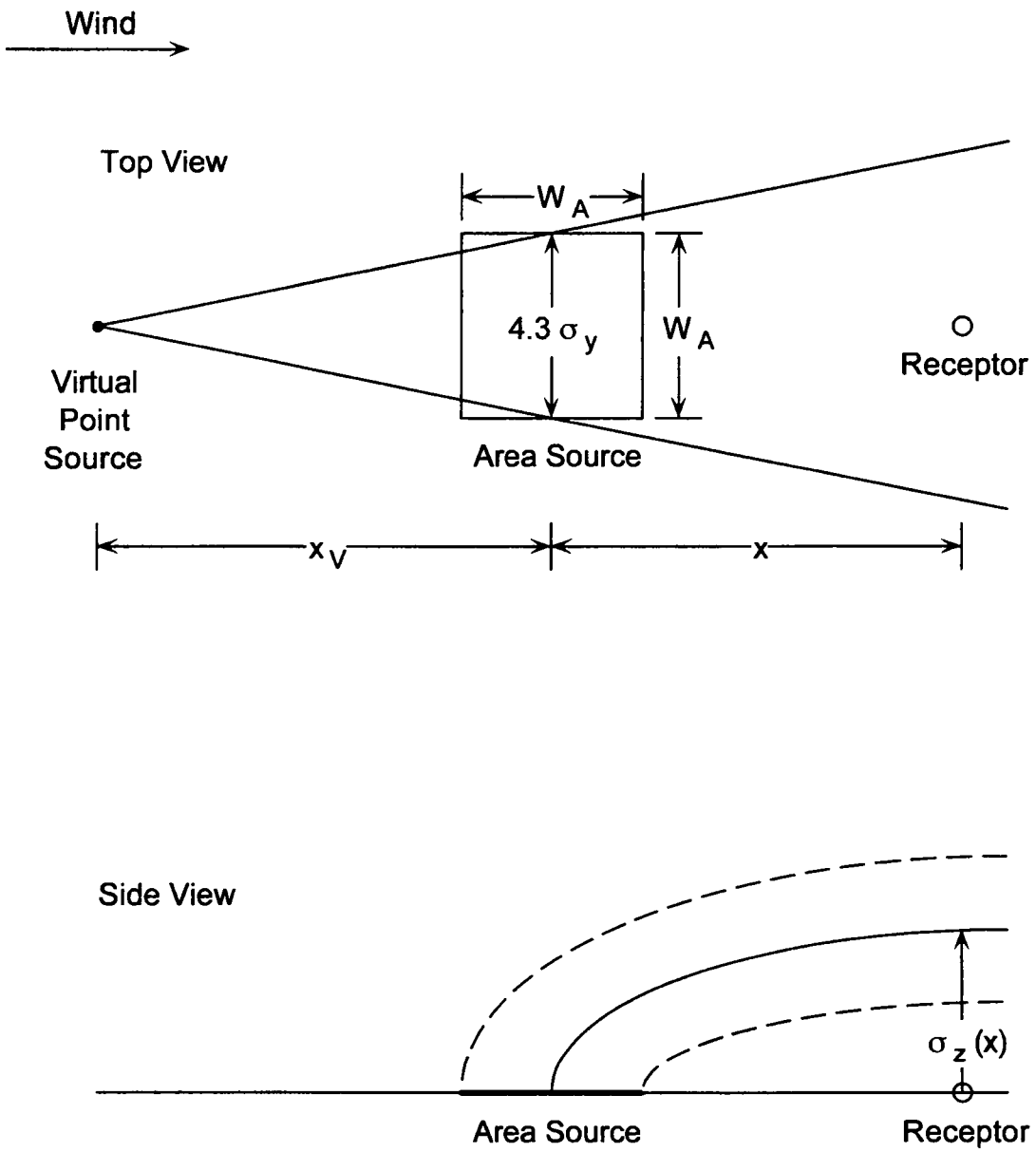


FIGURE 2.40 Illustration of Plume Dispersion From an Area Source

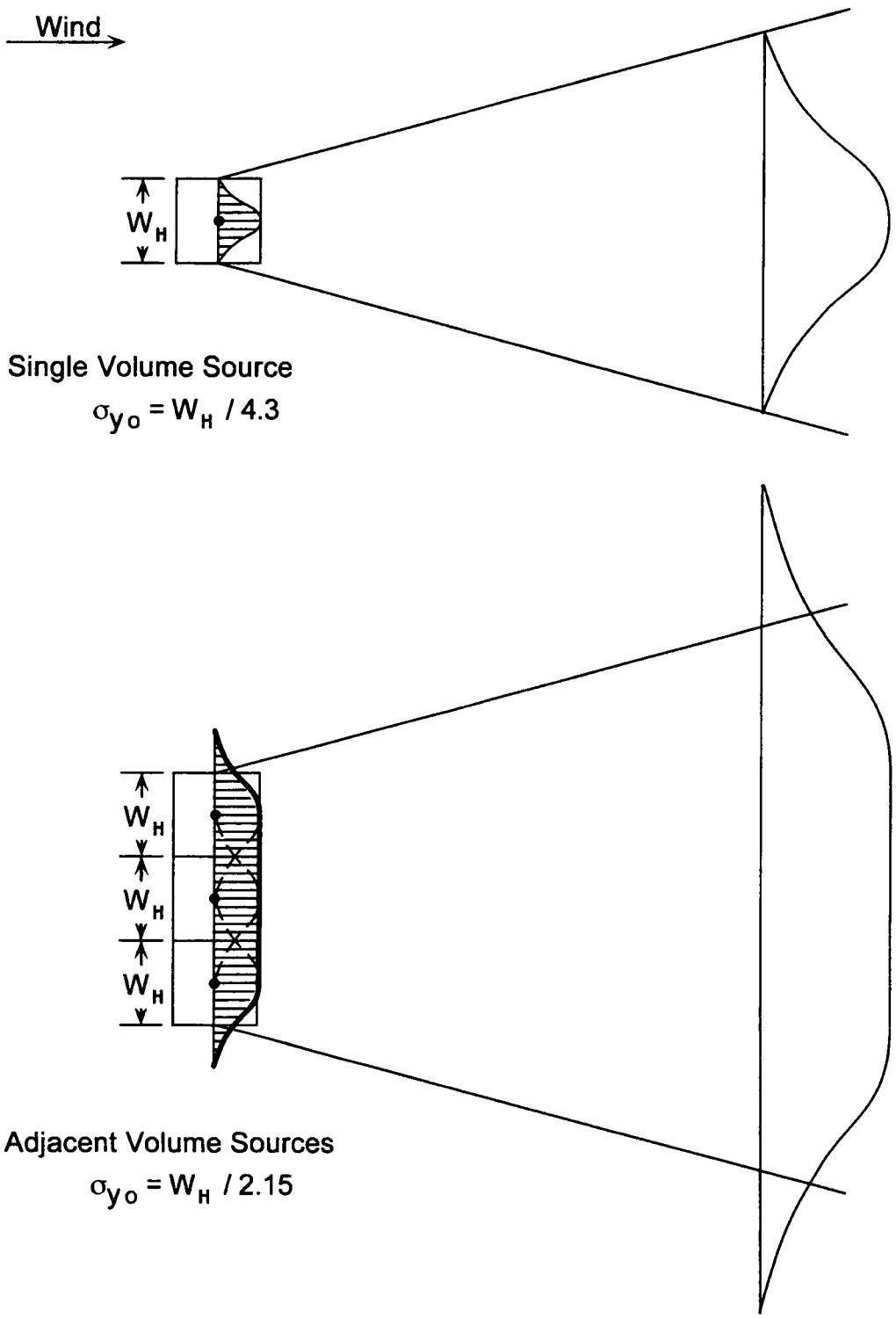
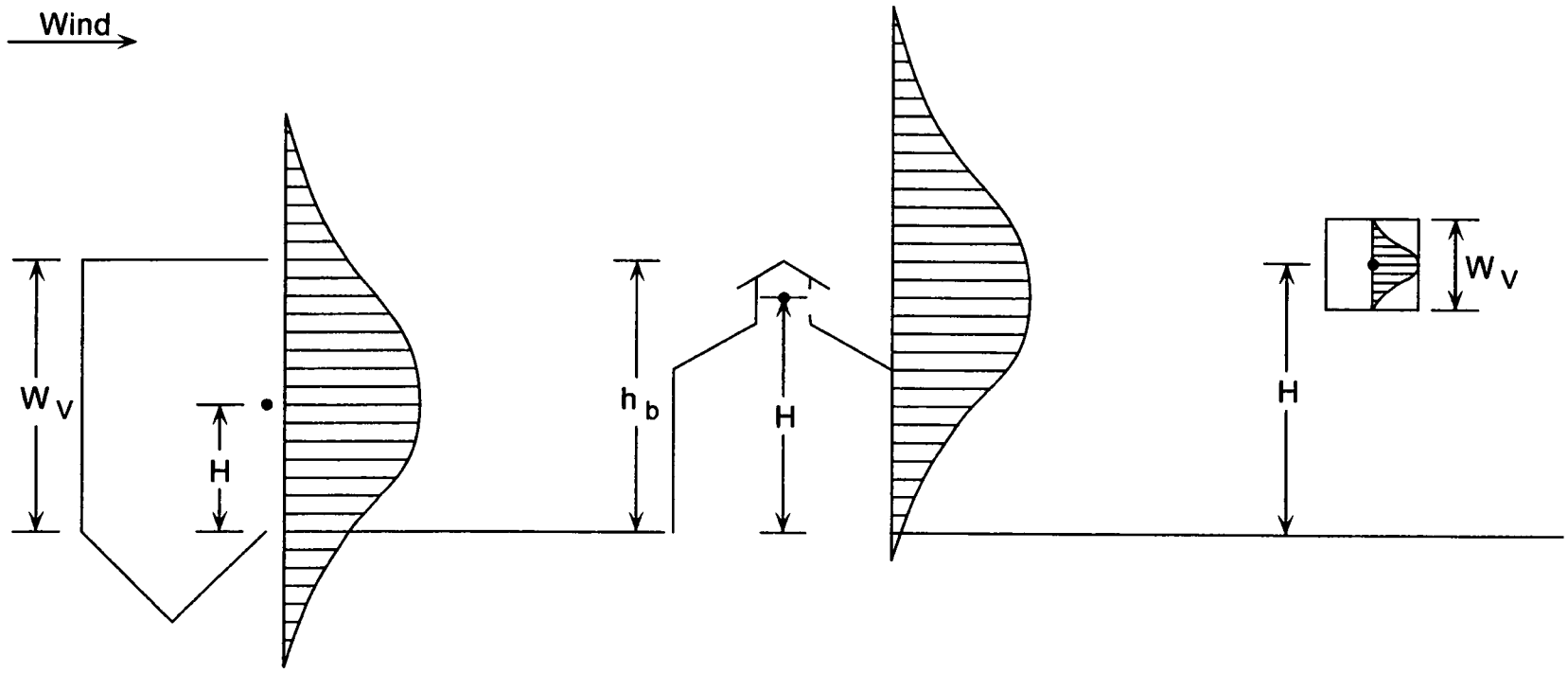


Figure 2.41 Illustration of Plume Dispersion from a Volume Source (Top View)



Suface-Based Source
$\sigma_{z\,o} = W_V / 2.15$

Elevated Source On or Adjacent to a Building
$\sigma_{z\,o} = h_b / 2.15$

Elevated Source Not On or Adjacent to a Building
$\sigma_{z\,o} = W_V / 4.3$

FIGURE 2.42 Illustration of Plume Dispersion From a Volume Source (Side View)

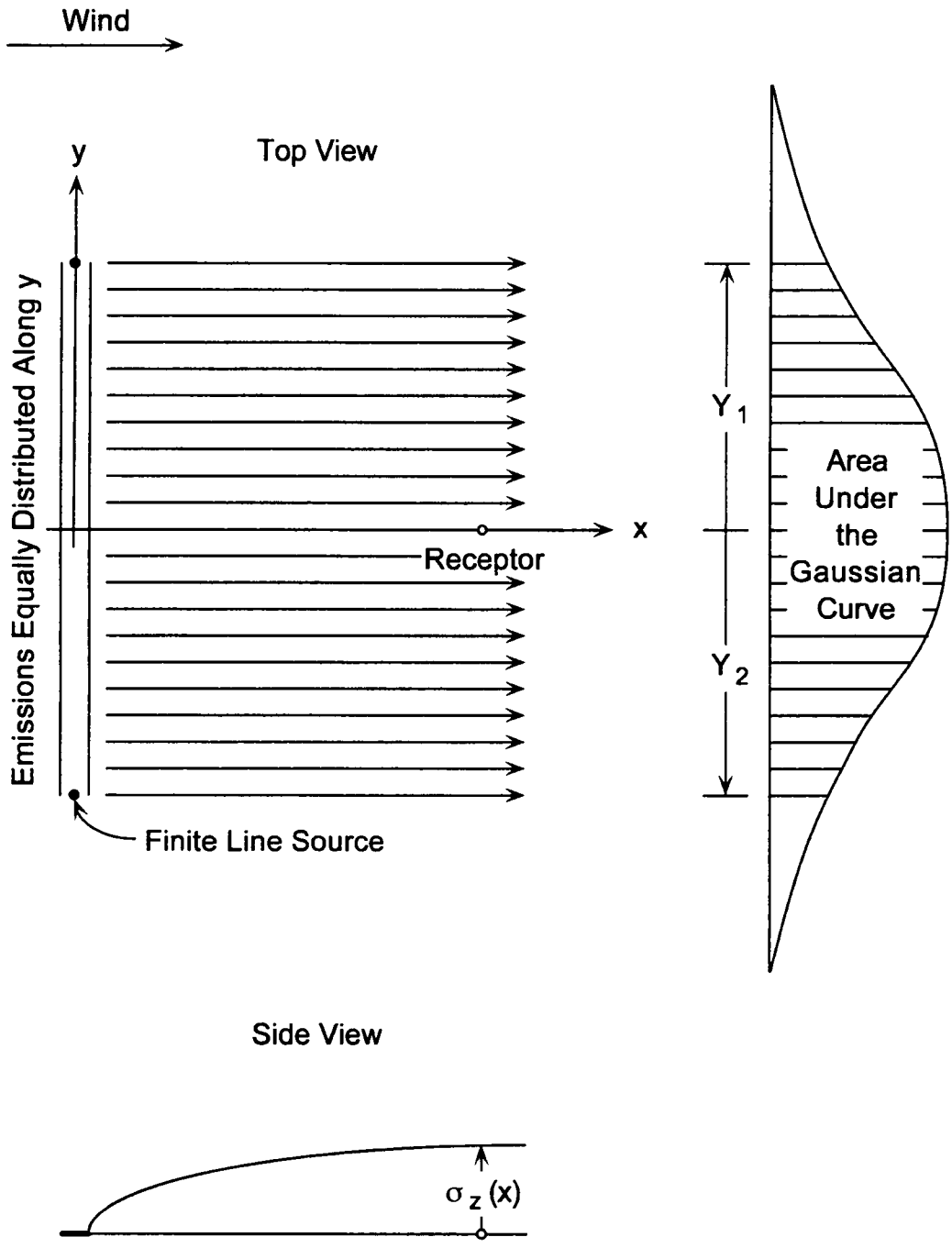


FIGURE 2.43 Illustration of Plume Dispersion From a Finite Line Source

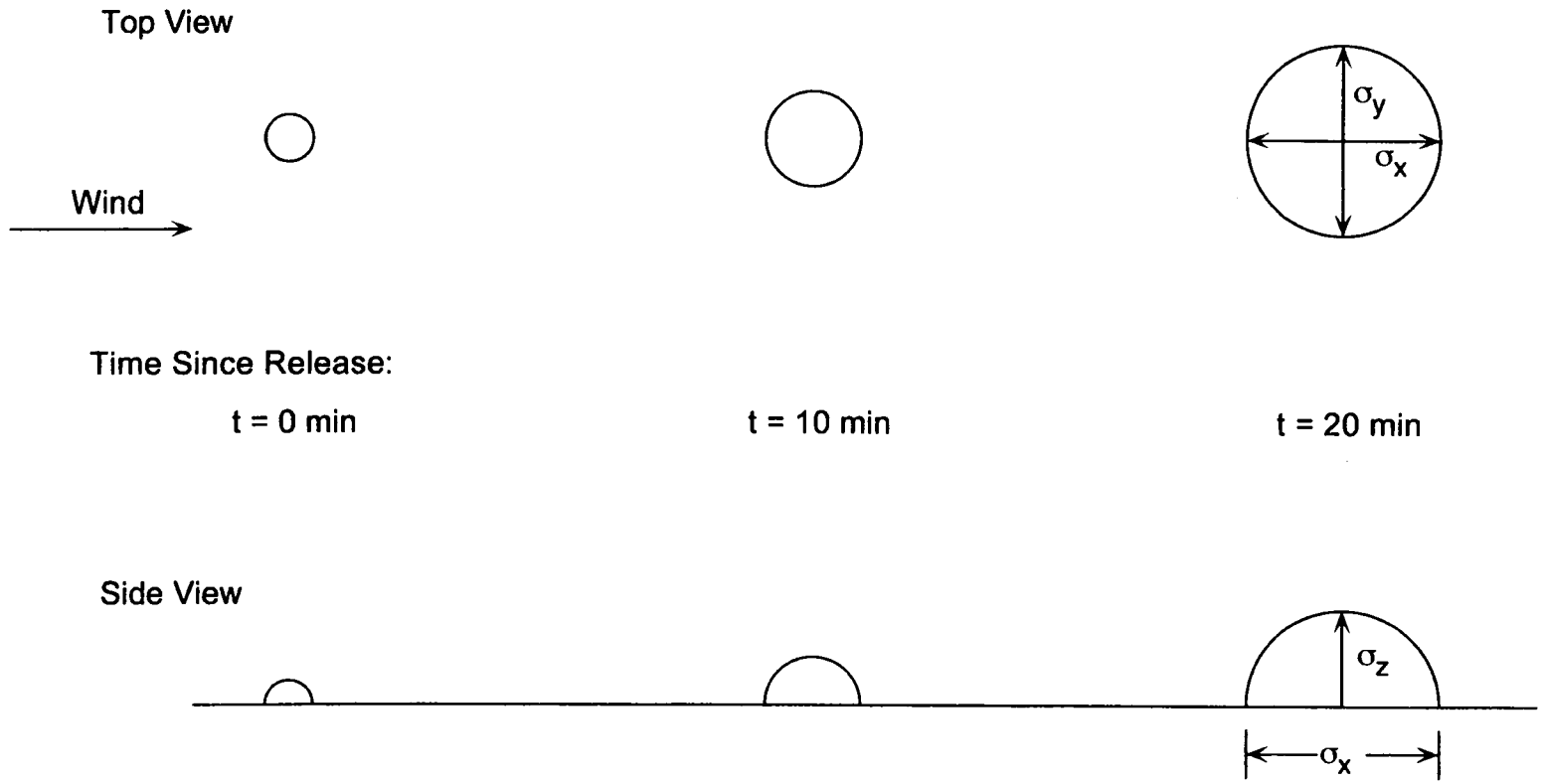


FIGURE 2.44 Illustration Of Puff Dispersion From an Instantaneous Source

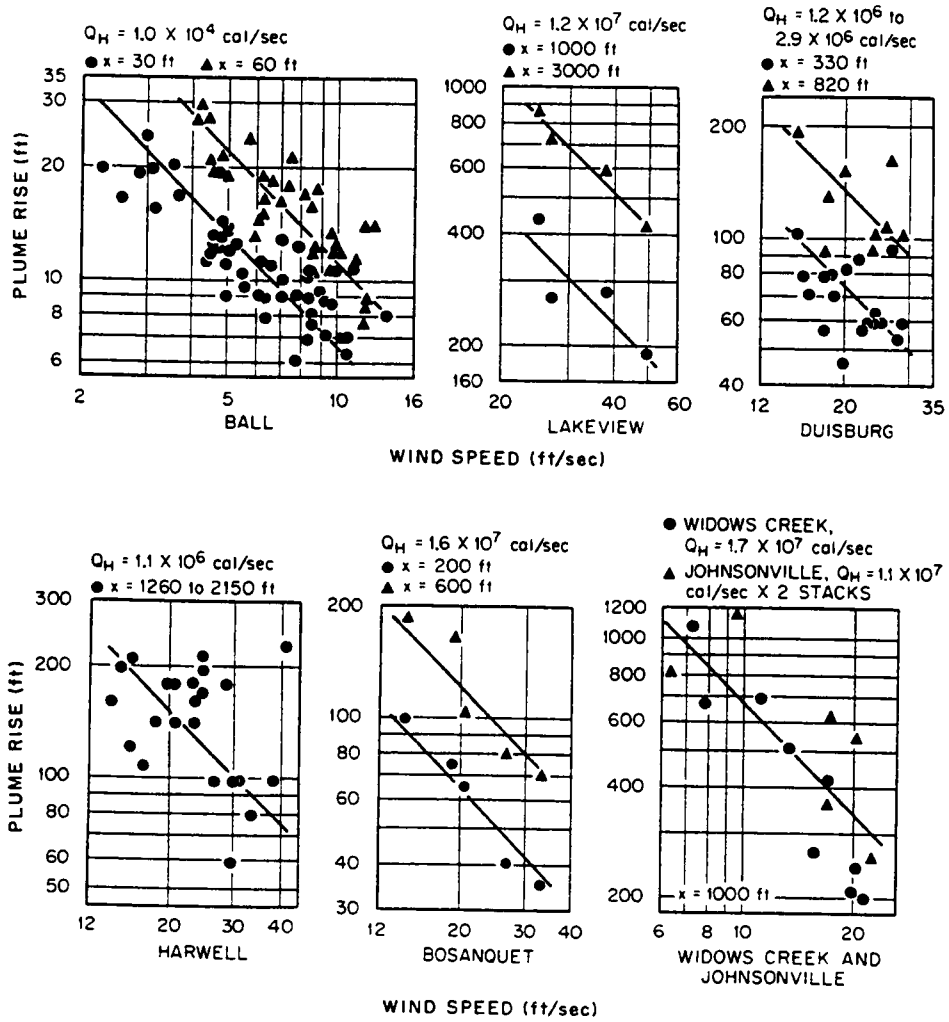


FIGURE 2.45 Plume Rise Versus Wind Speed in Near-Neutral Conditions (Briggs, 1969)

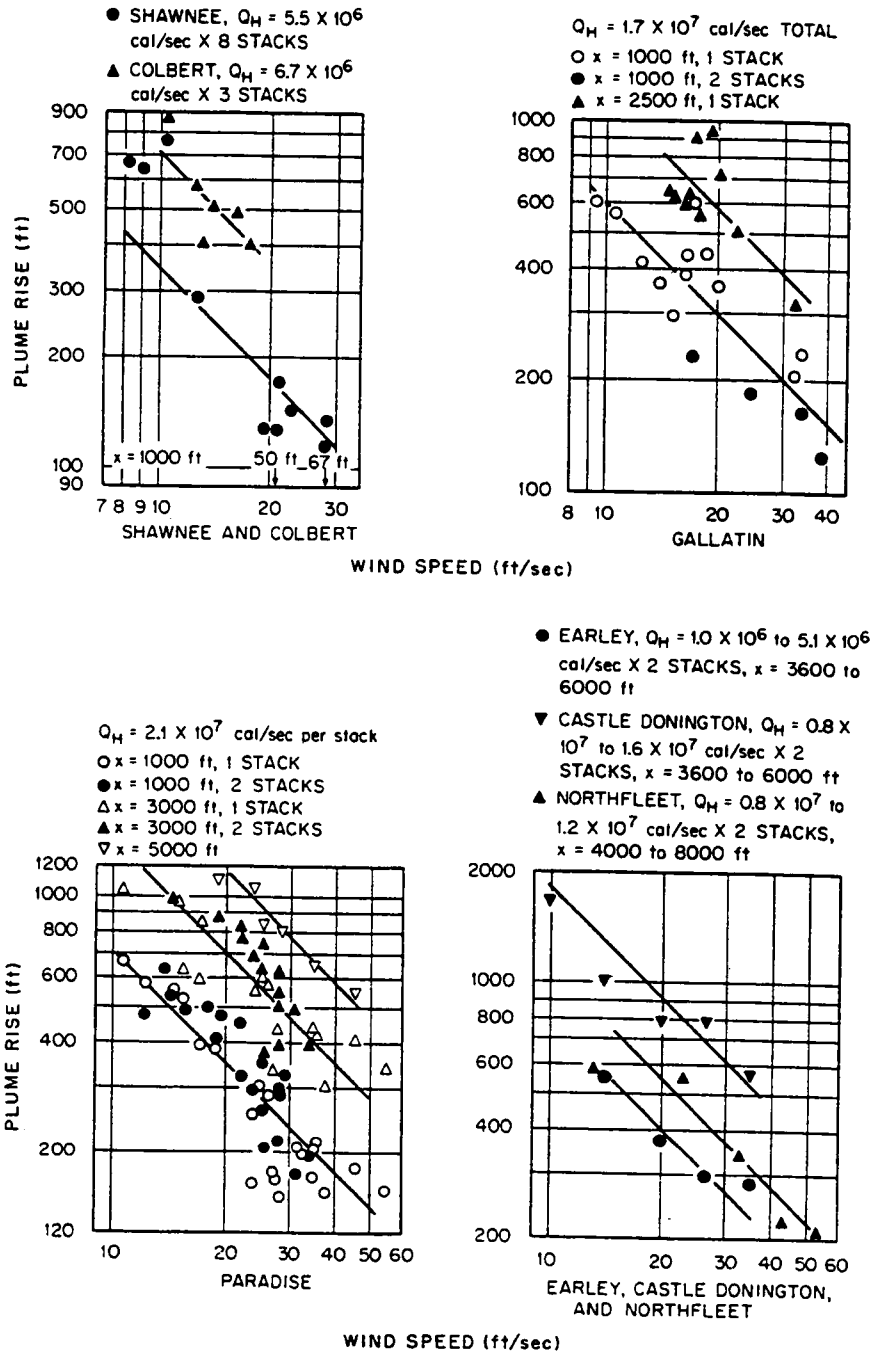


FIGURE 2.45 (continued)

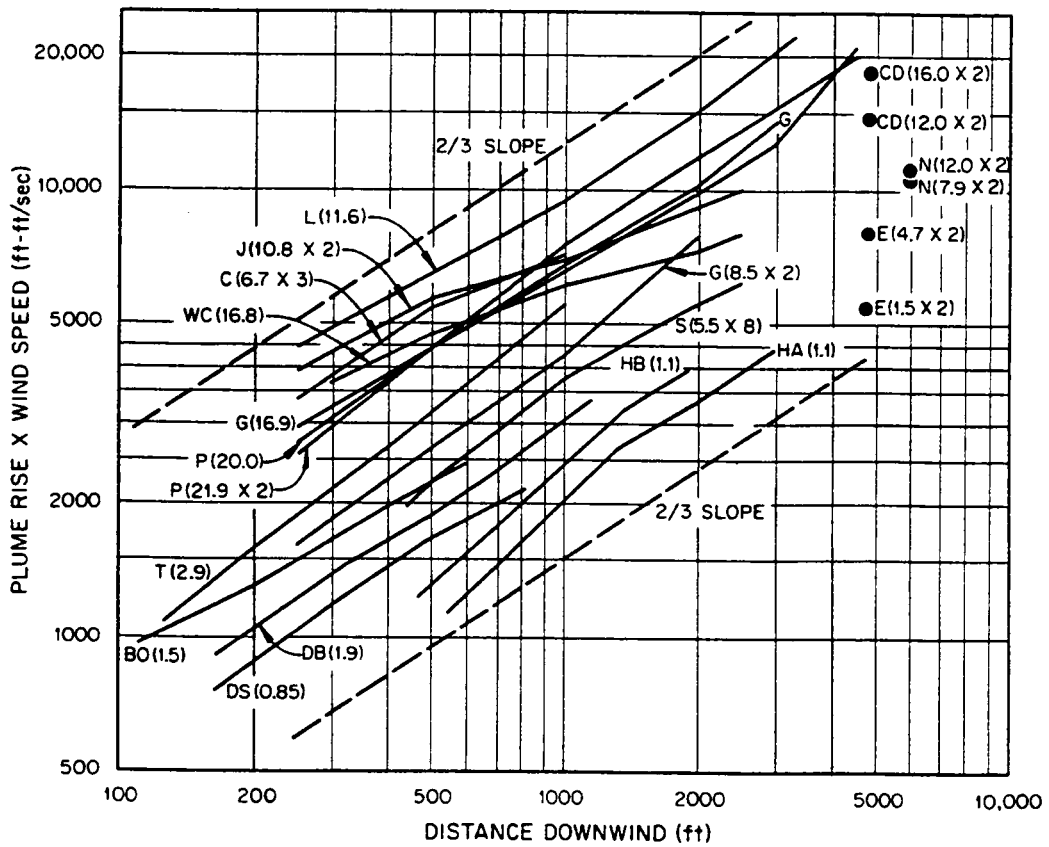


FIGURE 2.46 Plume Rise Times Wind Speed Versus Downwind Distance in Near-Neutral Conditions (Briggs, 1969)

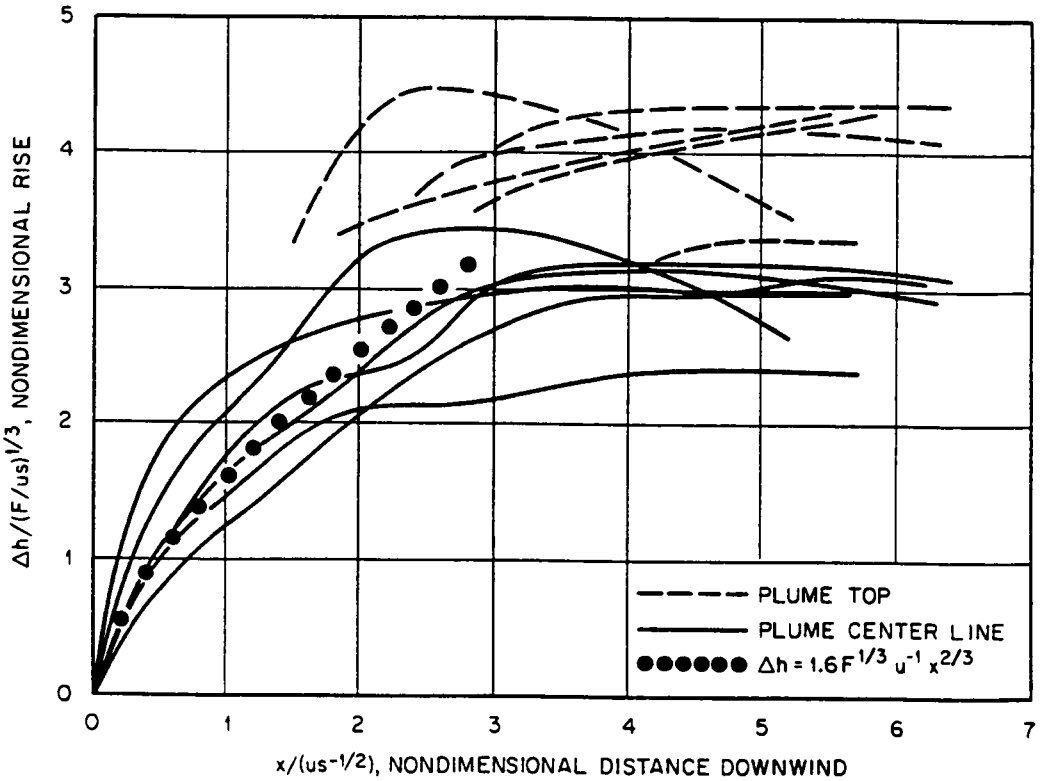
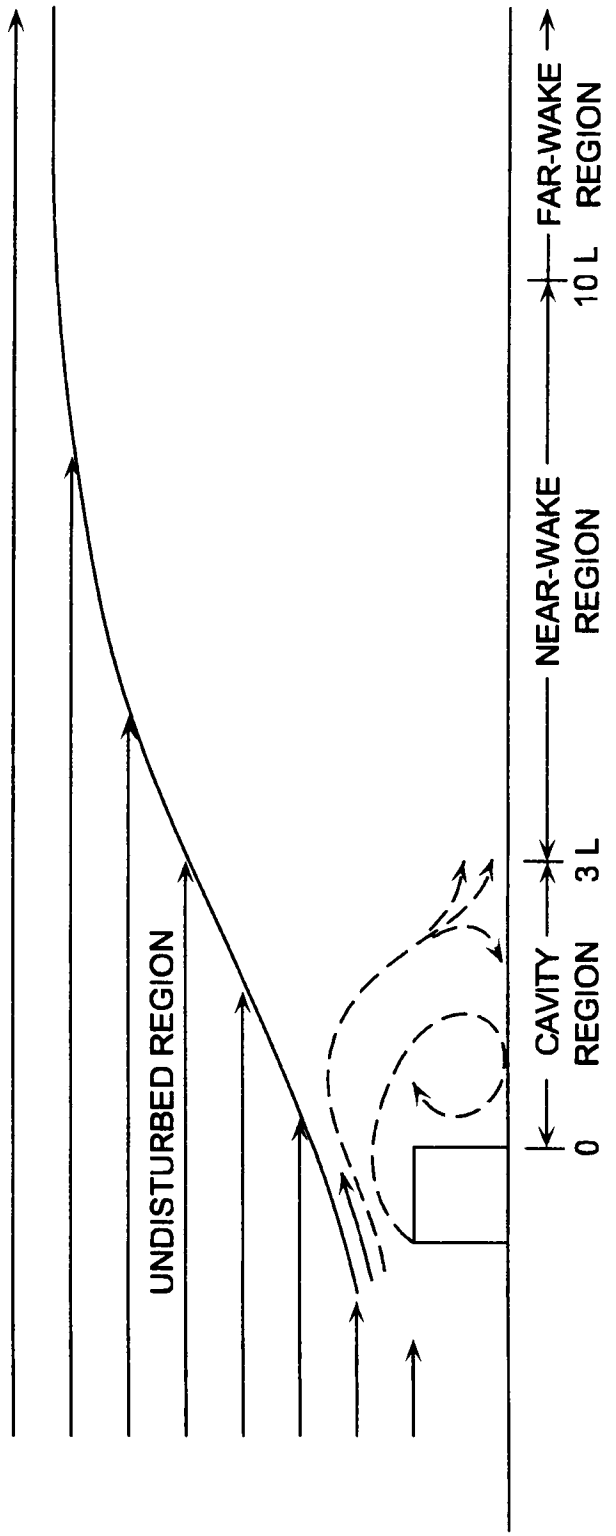


FIGURE 2.47 Rise of Buoyant Plumes in Stable Air in Cross-Wind at the TVA Paradise and Gallatin Plants (Briggs, 1969)



Note: L is the Lesser Dimension of the Building Height (h_b) or the Projected Building Width (h_w)

FIGURE 2.48 Cavity, Near-Wake, and Far-Wake Regions of a Building Wake

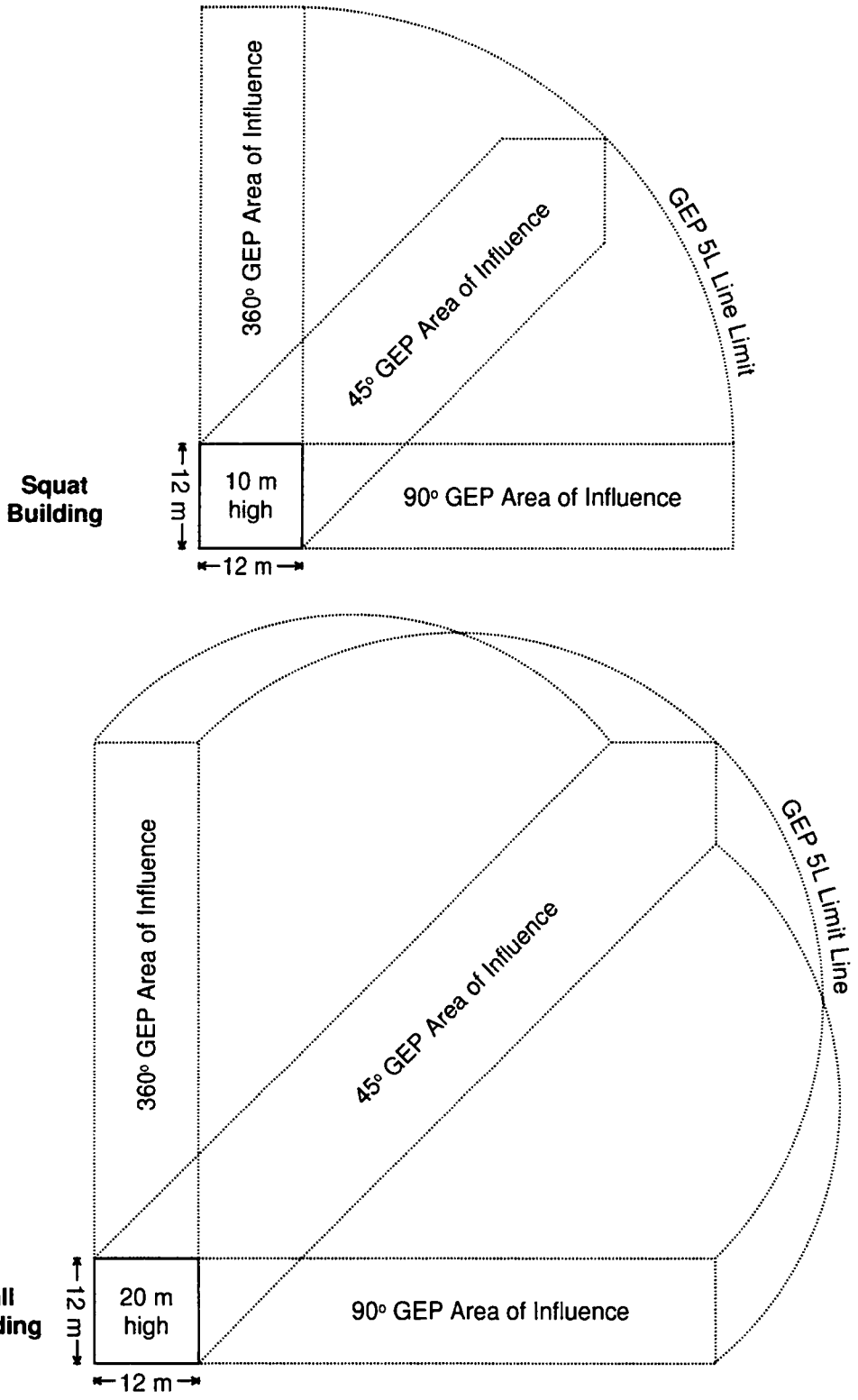


FIGURE 2.49 GEP Areas of Influence

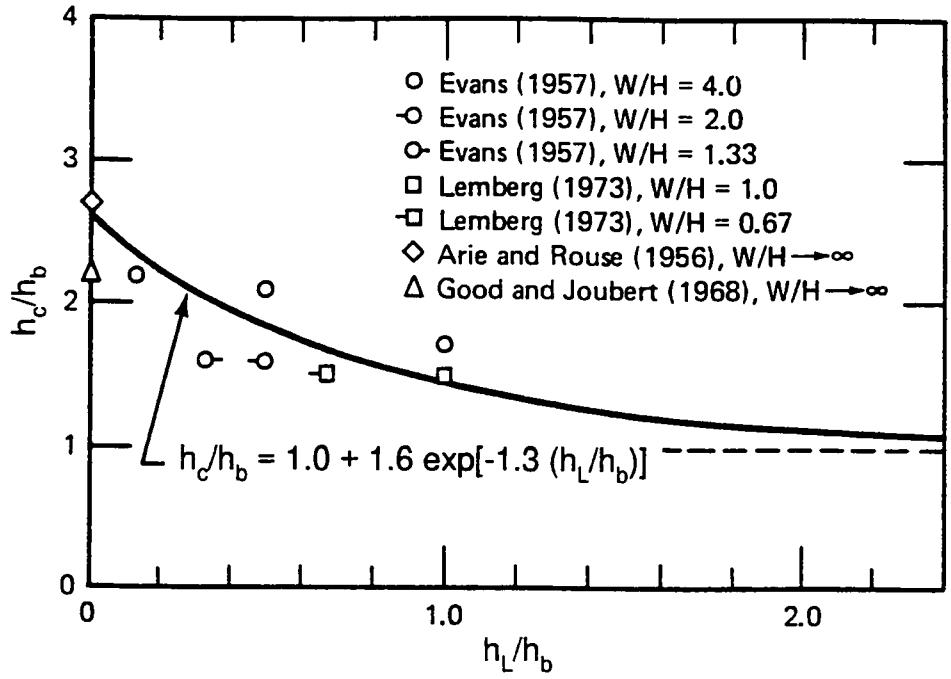


FIGURE 2.50 Maximum Wake Cavity Height Behind Block-Type Obstacles in Near-Uniform Flow (Hosker, 1984)

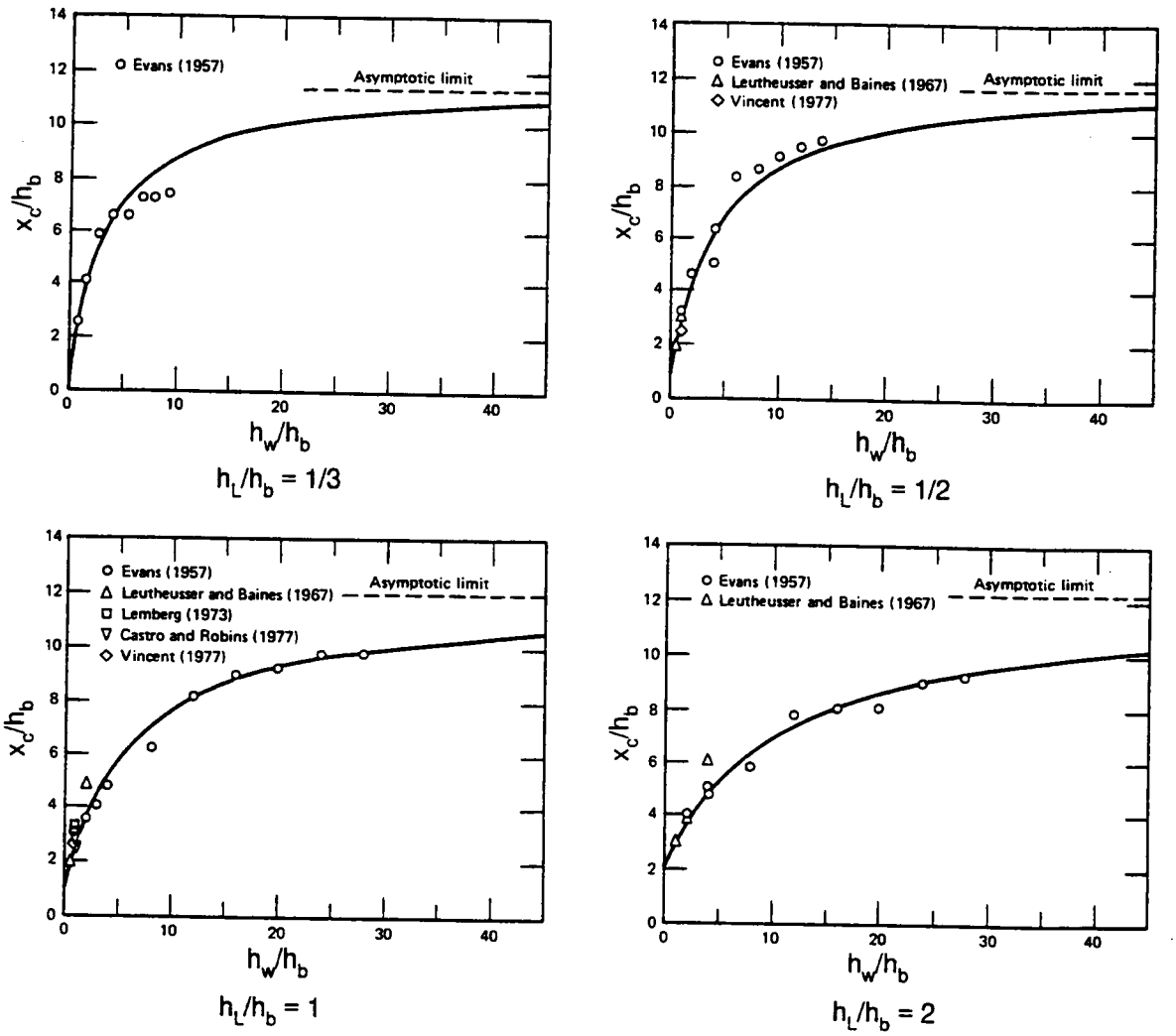


FIGURE 2.51 Empirical Expression for Wake Cavity Length Compared to Data on Rectangular Prisms in Nearly Uniform Flow ($h_L/h_b \leq 2$) (Hosker, 1984)

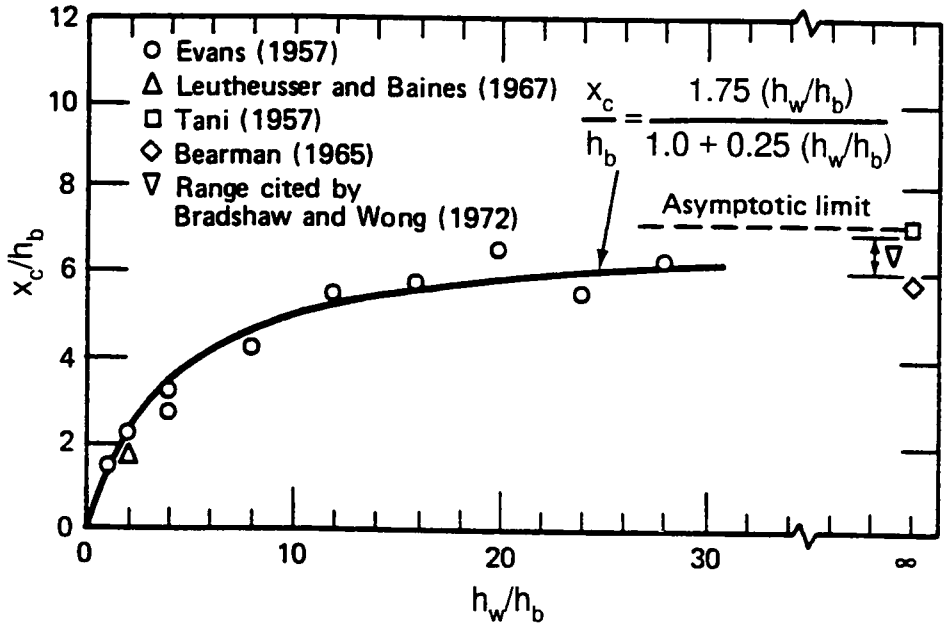


FIGURE 2.52 Empirical Expression for Wake Cavity Length Compared to Data on Rectangular Prisms in Nearly Uniform Flow ($h_L/h_b > 2$) (Hosker, 1984)

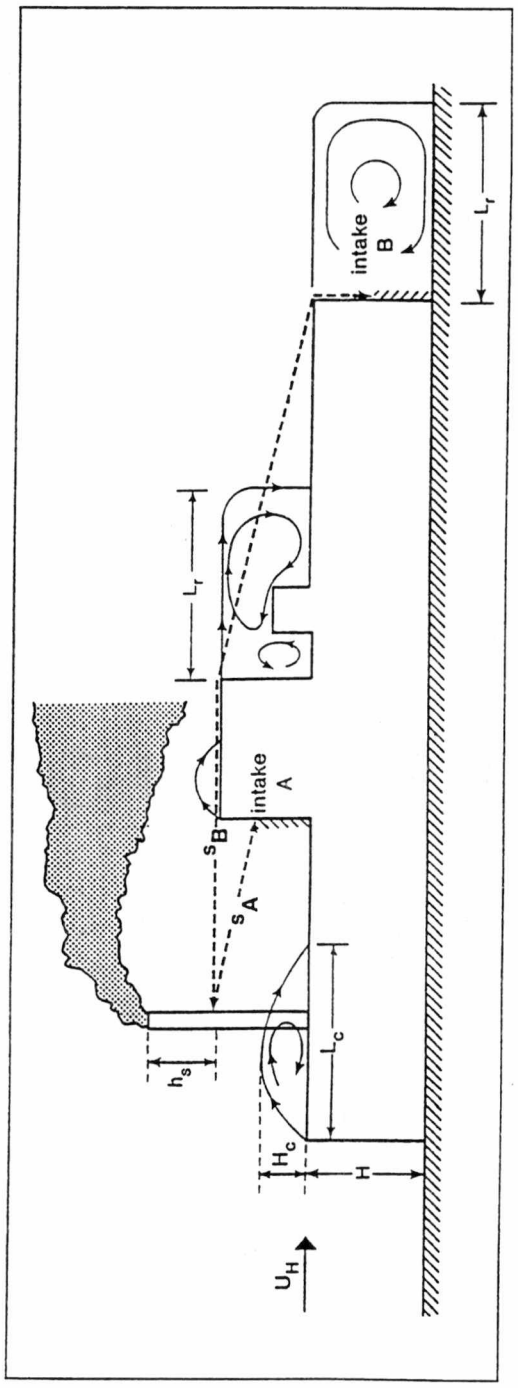


FIGURE 2.53 Illustration of Stretched-String Distance (ASHRAE, 1993)

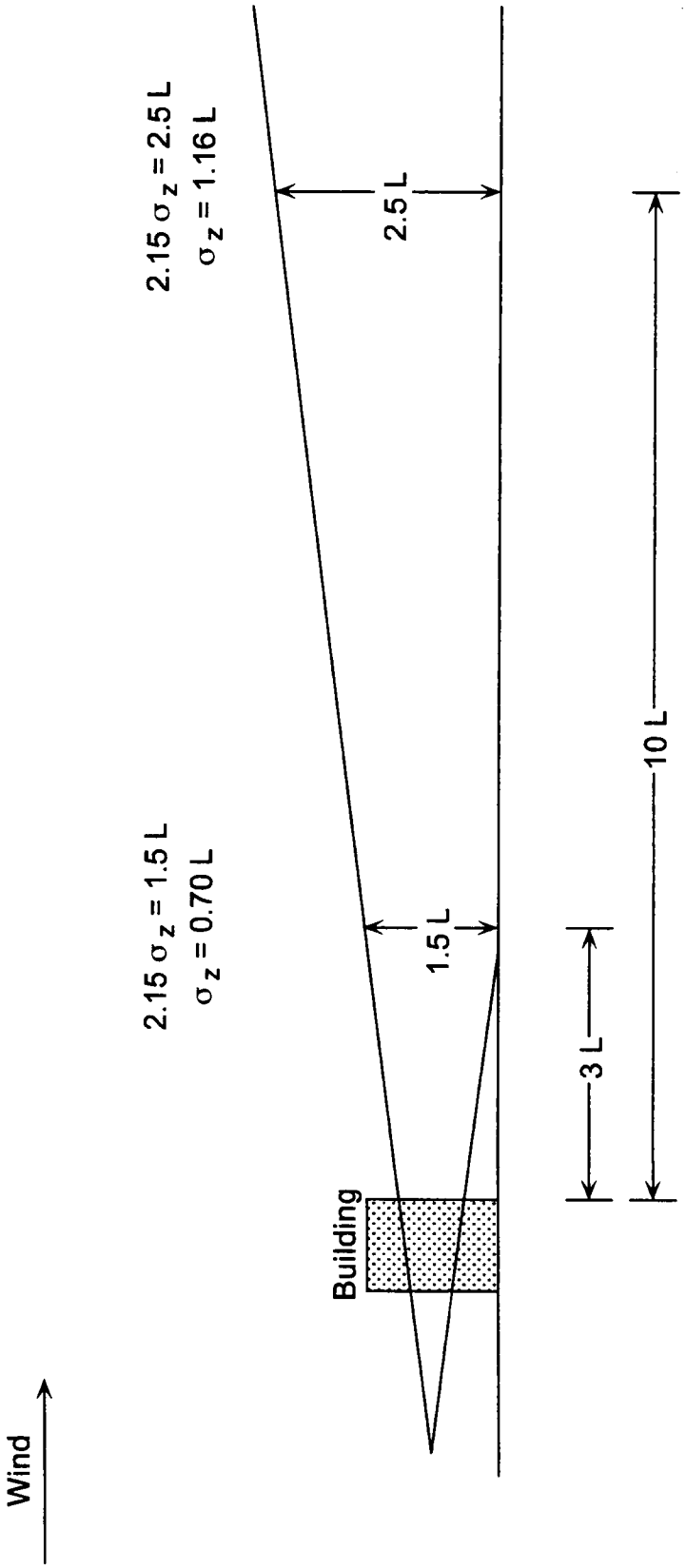


FIGURE 2.54 Vertical Width of the Plume in the Wake Region

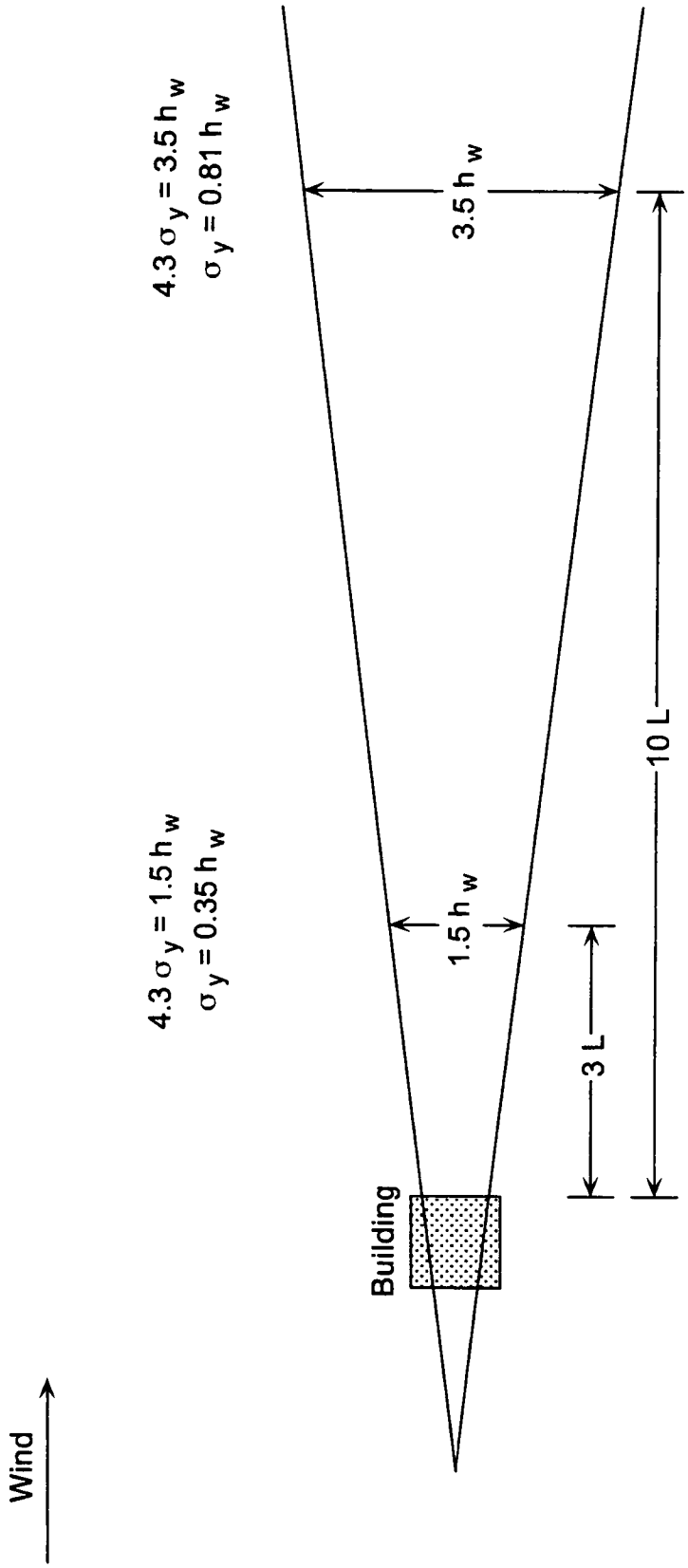


FIGURE 2.55 Horizontal Width of the Plume in the Wake Region

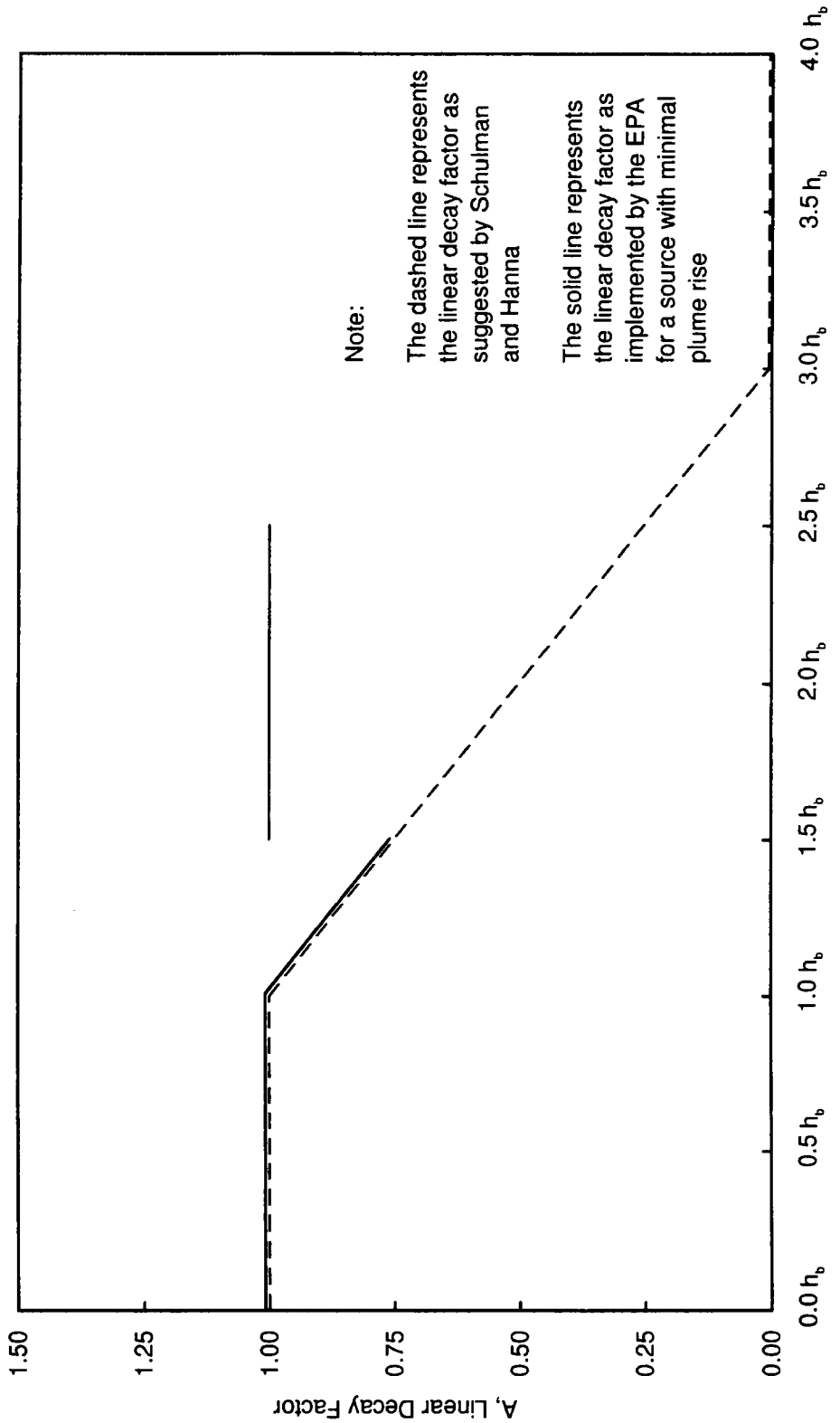


FIGURE 2.56 Linear Decay Factor Used in the Schulman-Scire Wake Algorithm

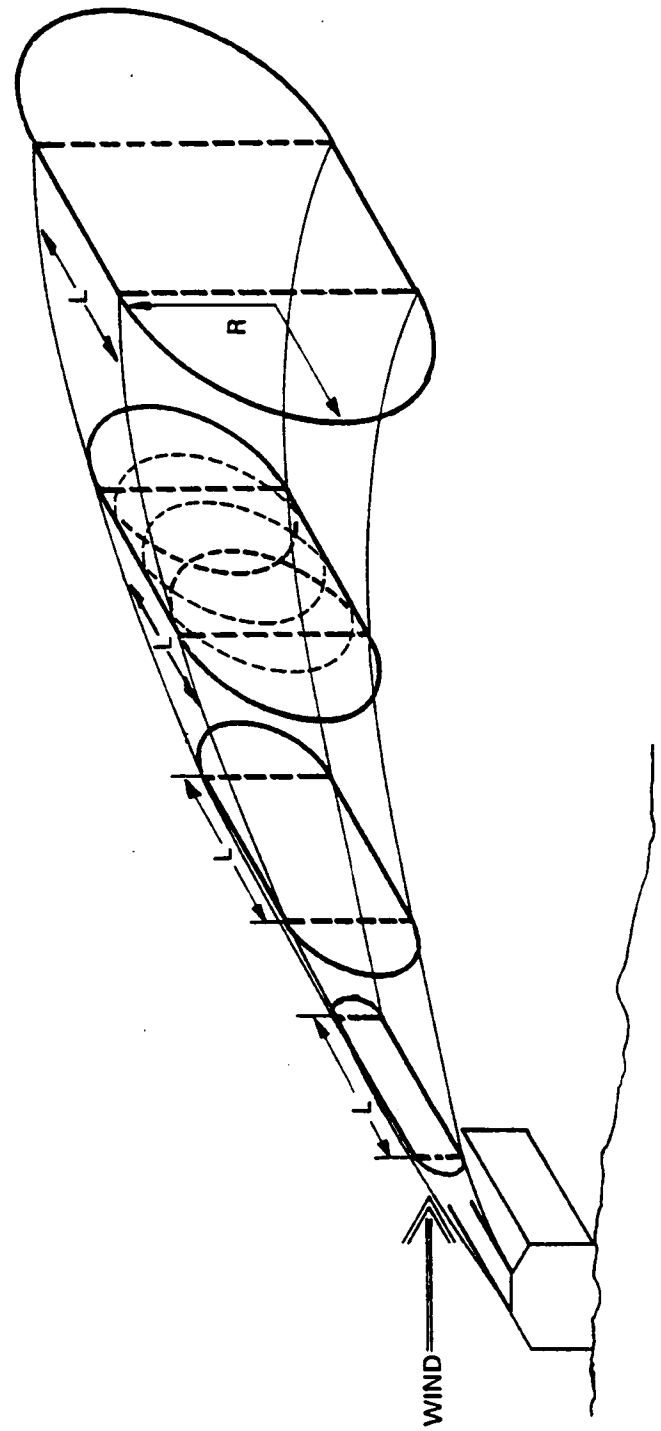


FIGURE 2.57 Initial Shape of a Plume Emitted Close to the Roof of a Building (Schulman and Scire, 1980)

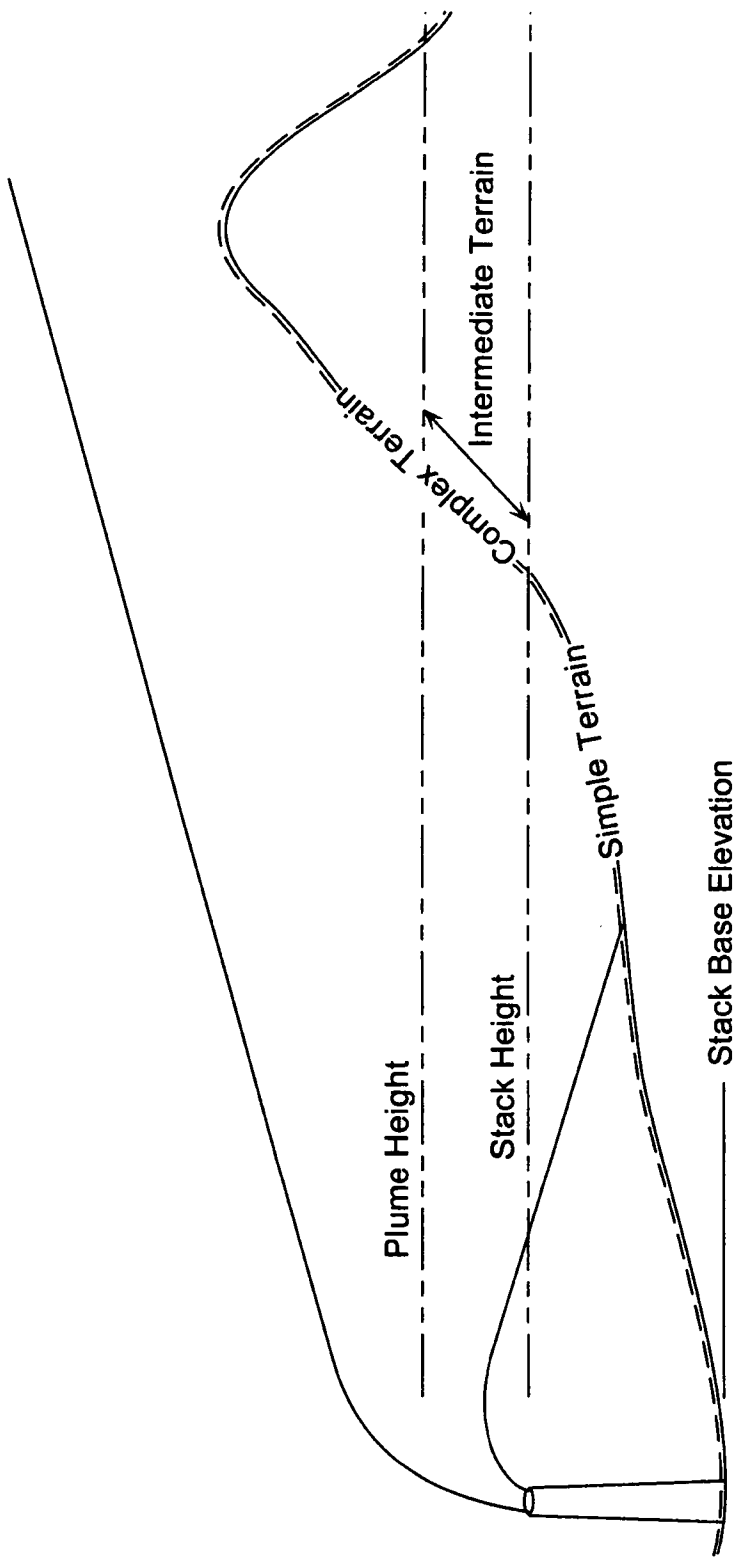


FIGURE 2.58 Simple, Intermediate, and Complex Terrain Regimes

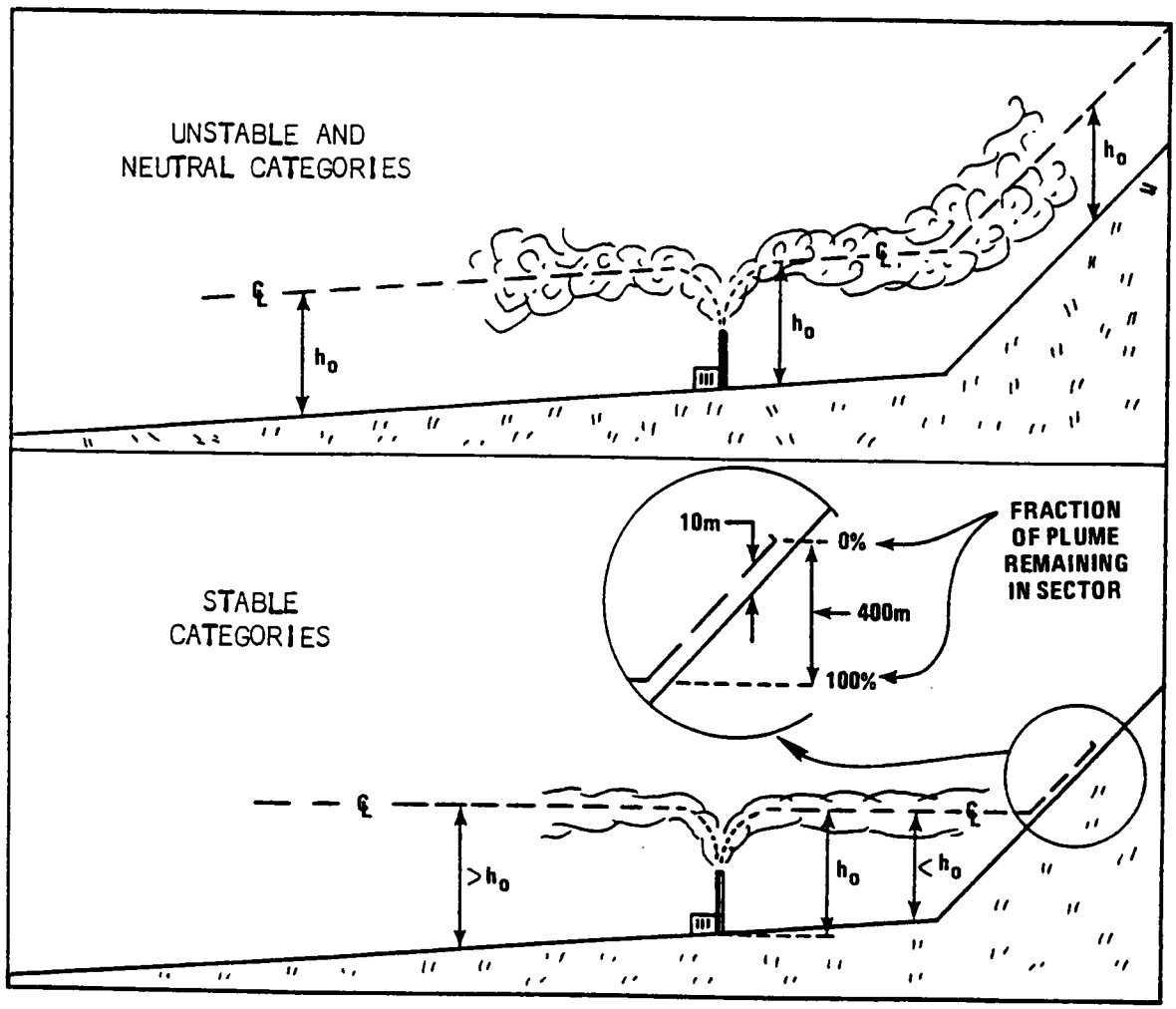


FIGURE 2.59 Plume Interception of Elevated Terrain in the Valley Model (EPA, 1977b)

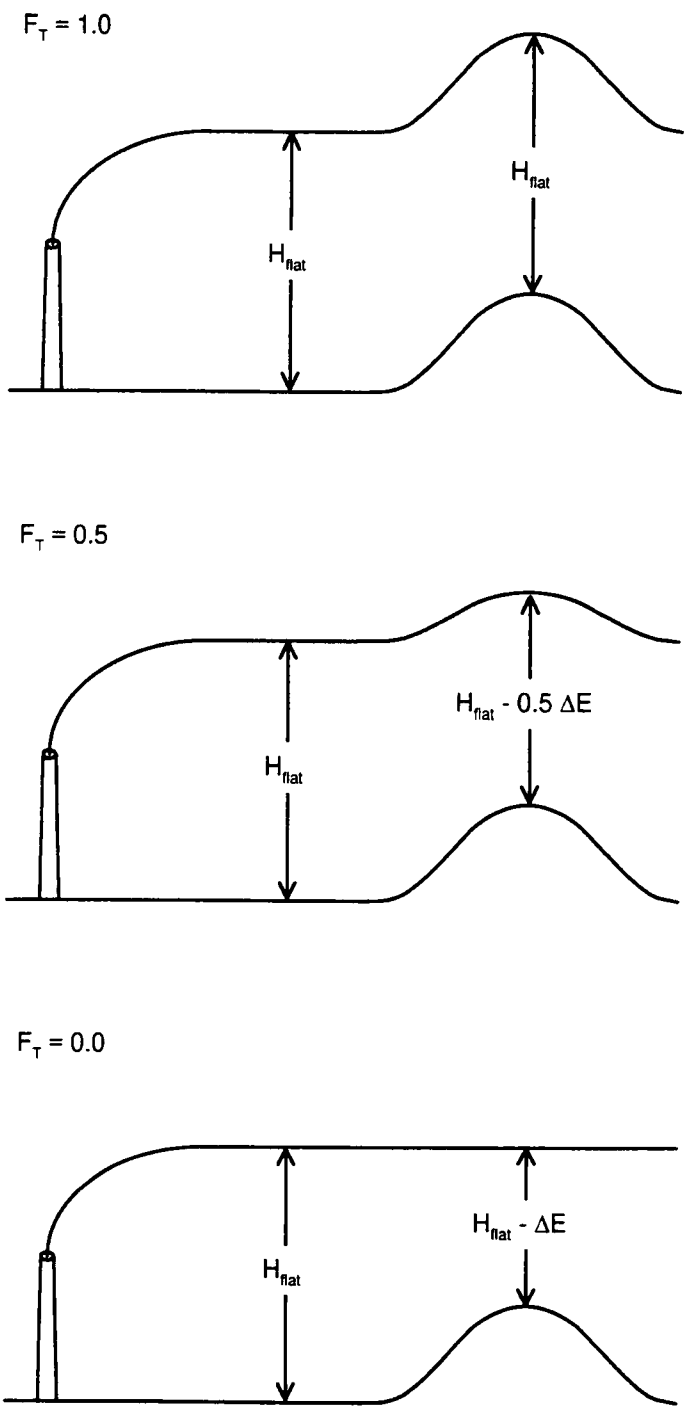


FIGURE 2.60 Use of Terrain Adjustment Factors to Alter Plume Height in the COMPLEX I Model

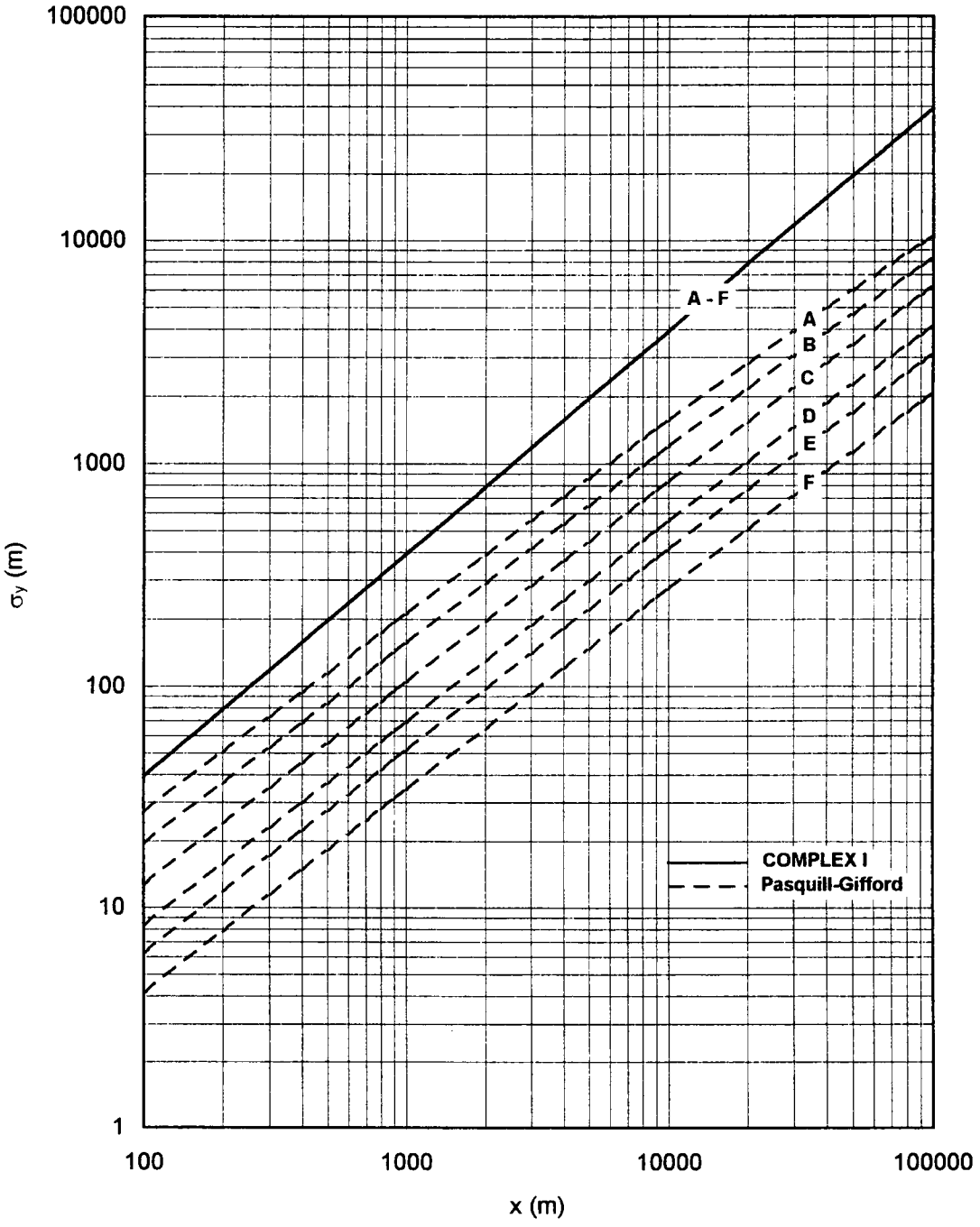


FIGURE 2.61 Horizontal Plume Widths of the COMPLEX I Model Compared with Pasquill-Gifford σ_y Values

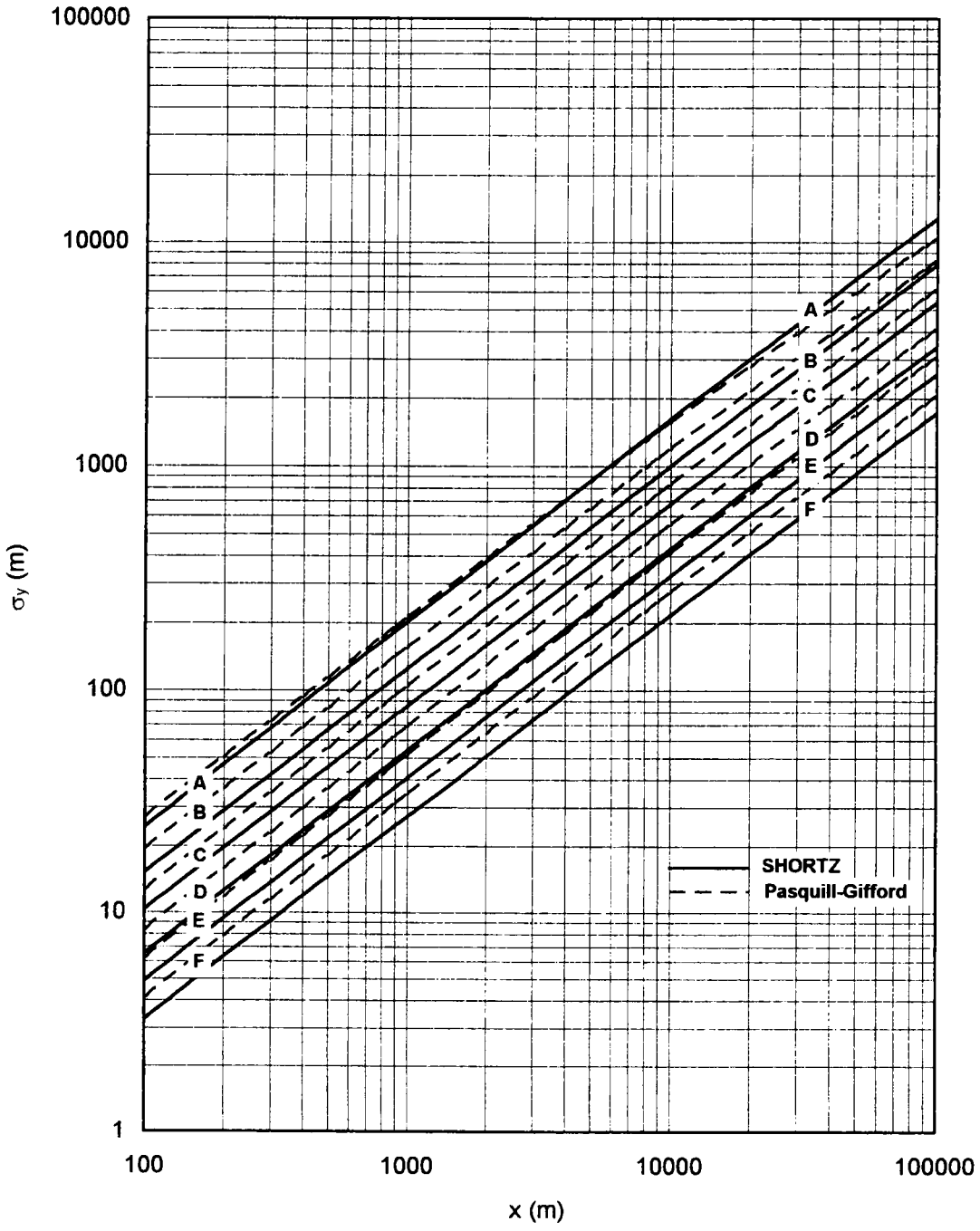


FIGURE 2.62 Default Rural Horizontal Dispersion Coefficients (σ_y) Used in the SHORTZ Model

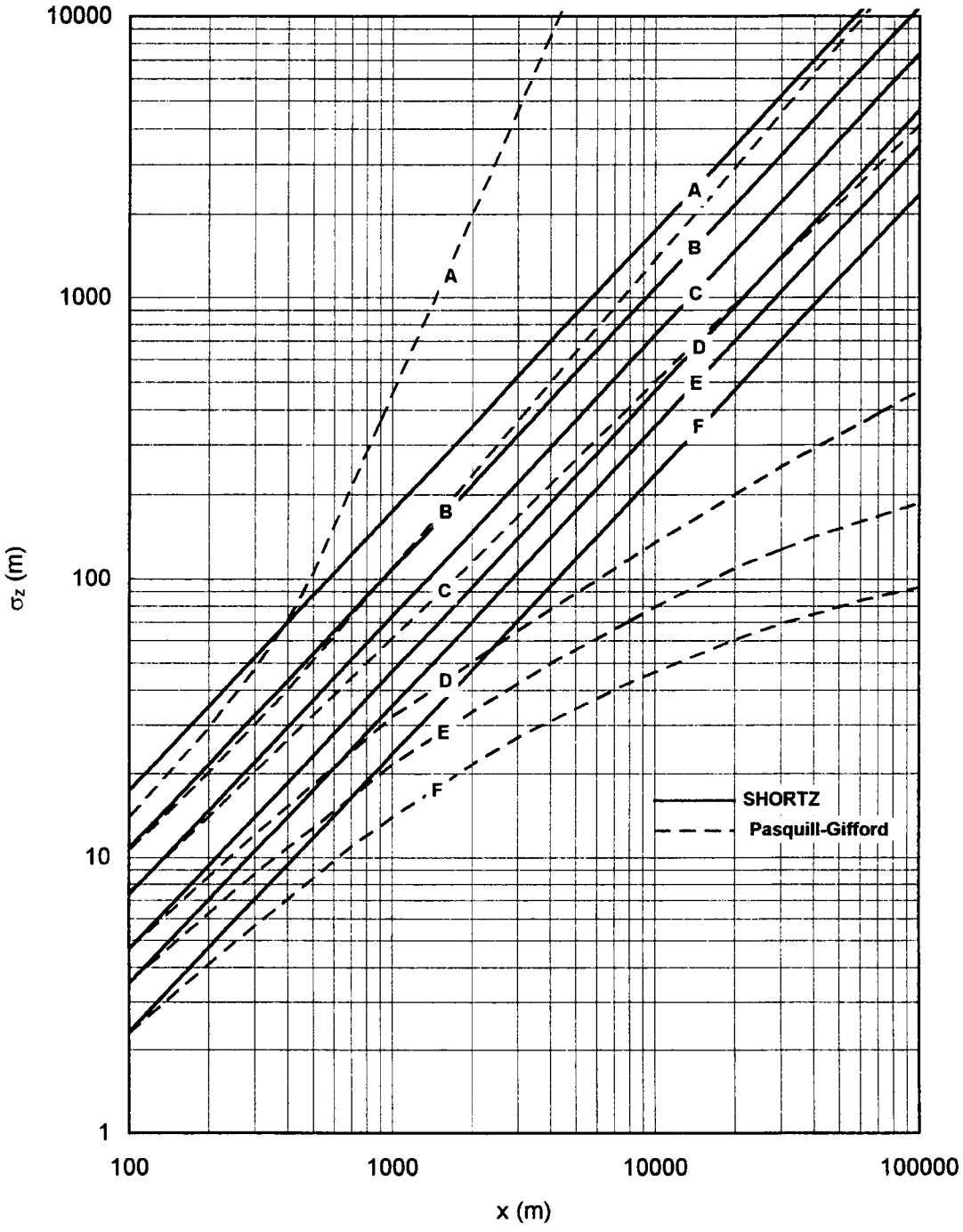


FIGURE 2.63 Default Rural Vertical Dispersion Coefficients (σ_z) Used in the SHORTZ Model

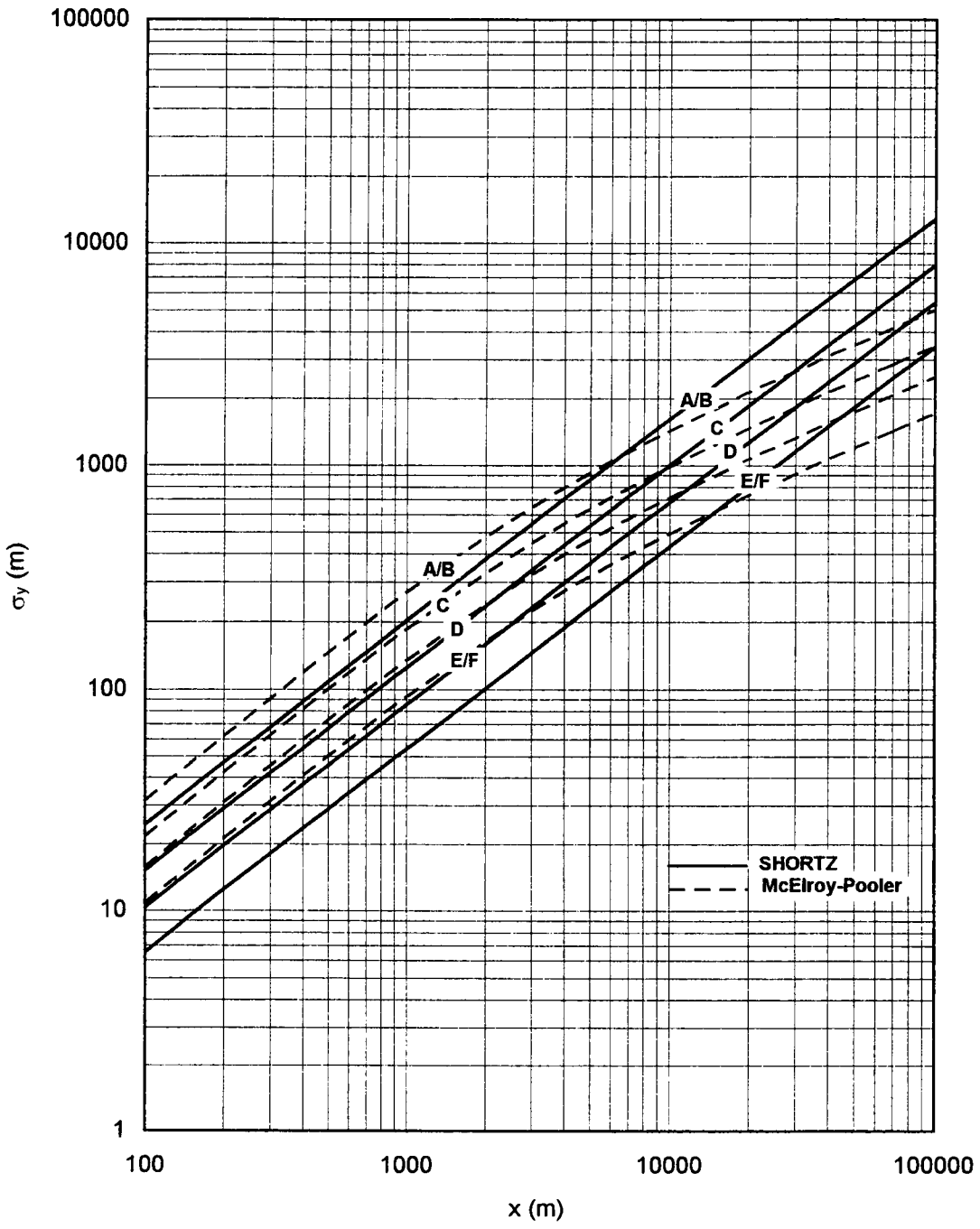


FIGURE 2.64 Default Urban Horizontal Dispersion Coefficients (σ_y) Used in the SHORTZ Model

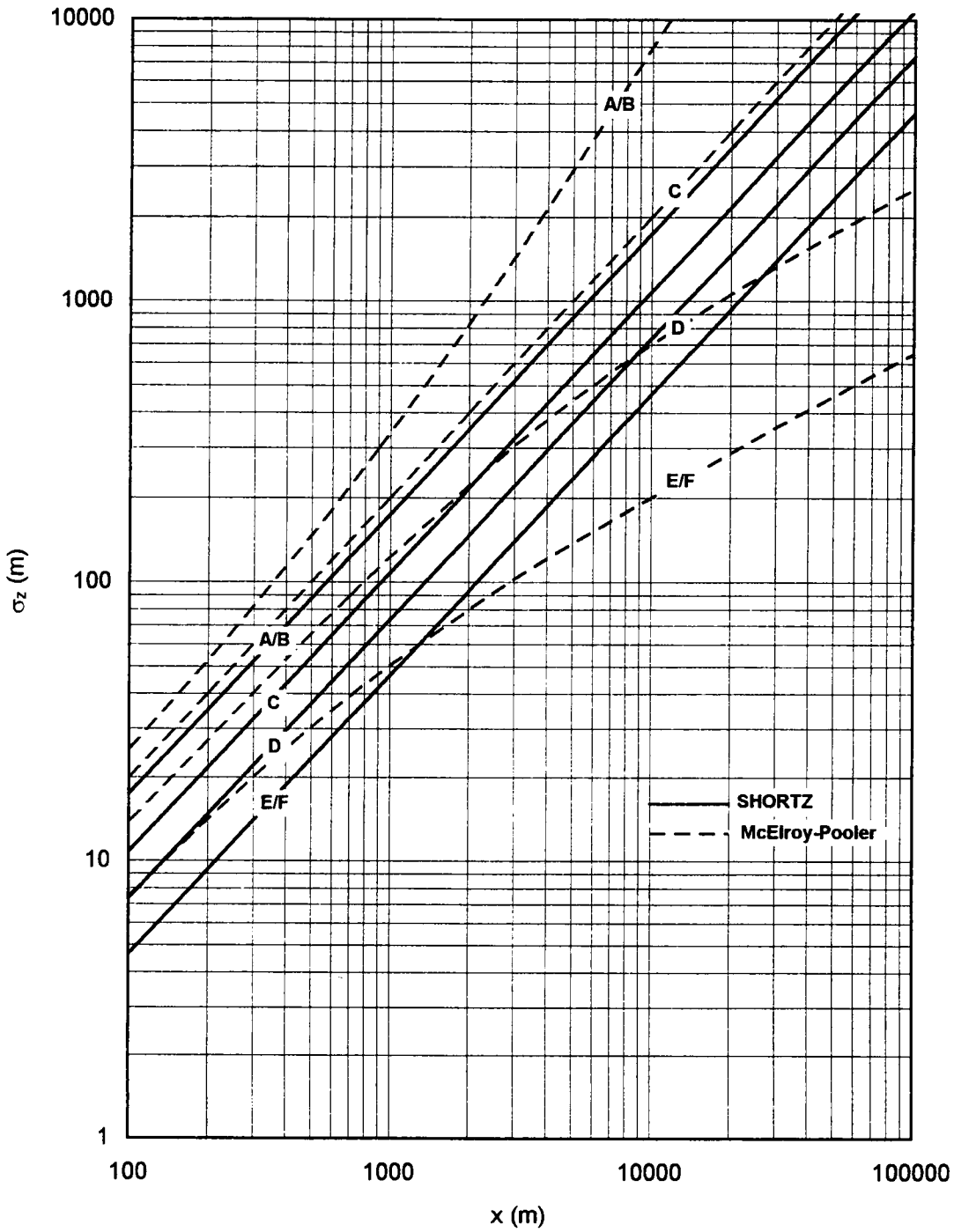


FIGURE 2.65 Default Urban Vertical Dispersion Coefficients (σ_z) Used in the SHORTZ Model

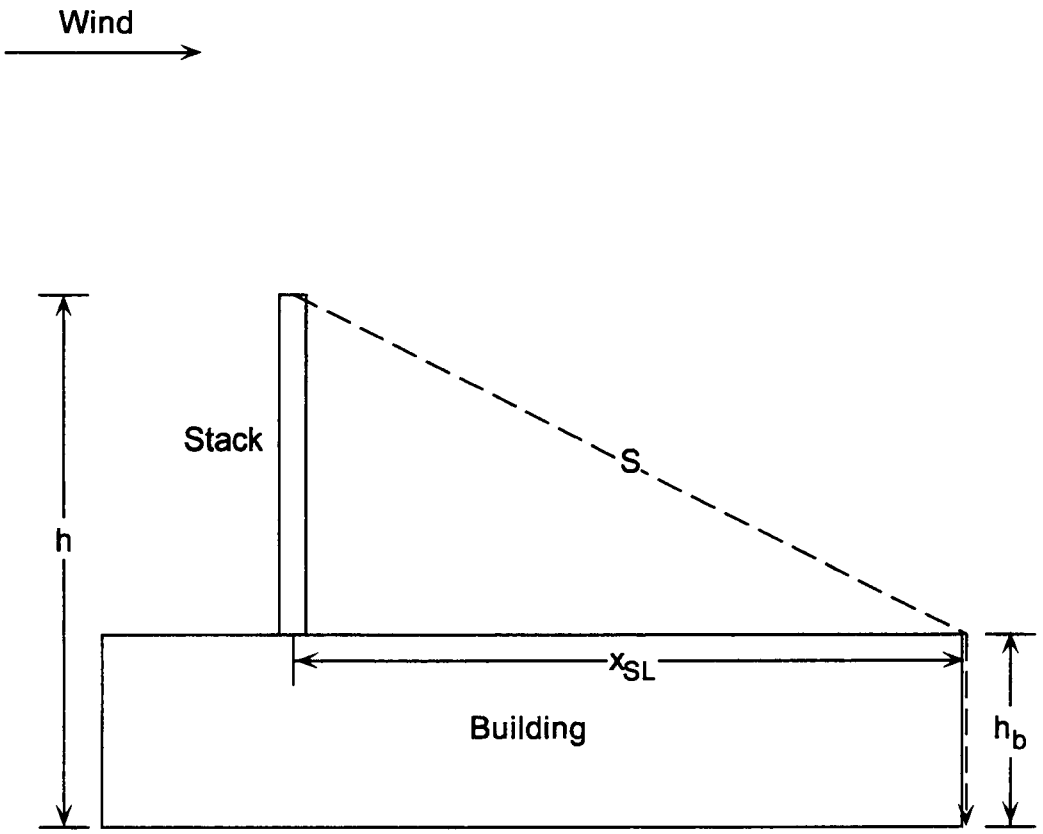


FIGURE 3.1 Stretched-String Distance as Defined in the Schulman-Scire Cavity Algorithm

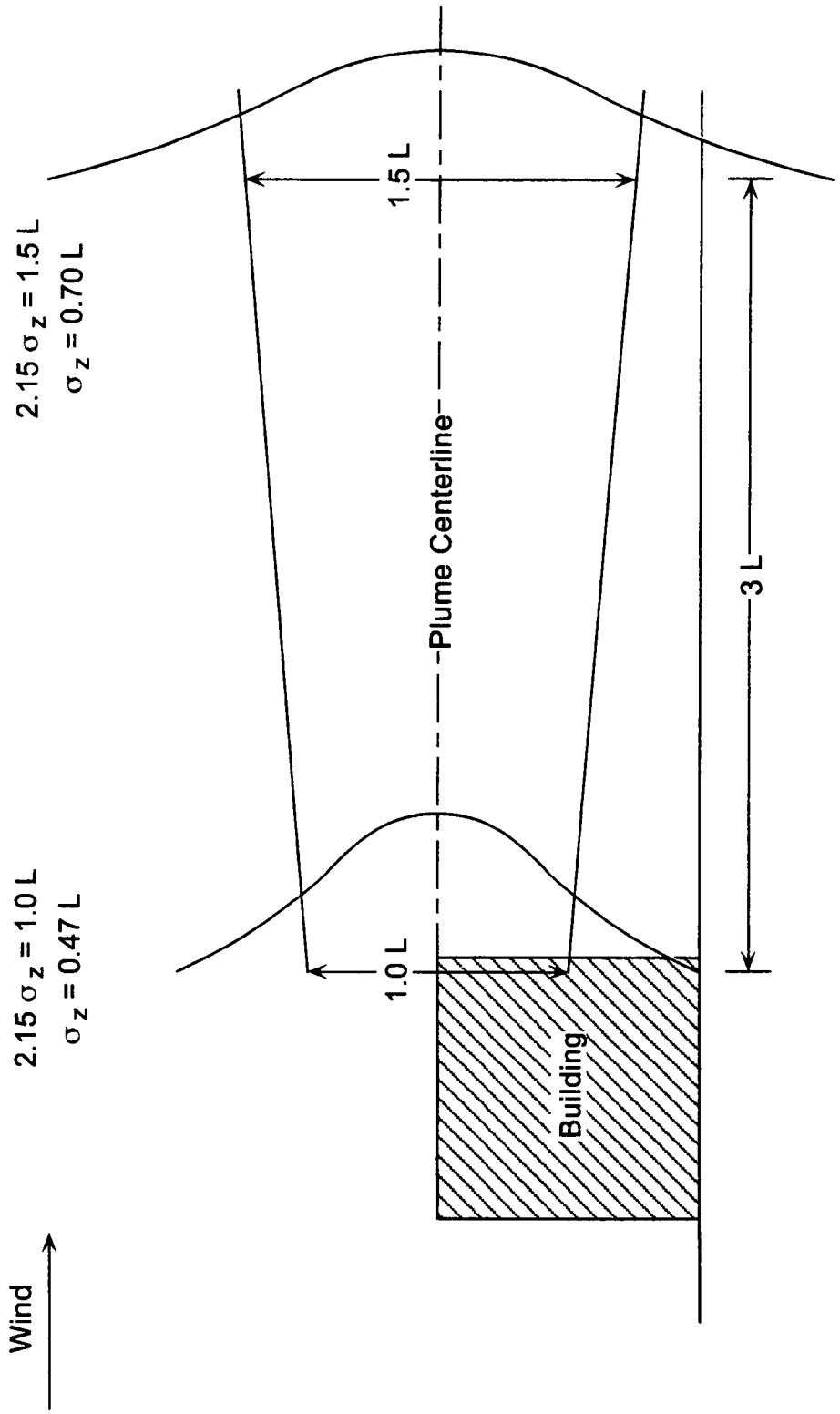


FIGURE 3.2 Vertical Width of the Plume in the Cavity Region (Roof-Level Release)

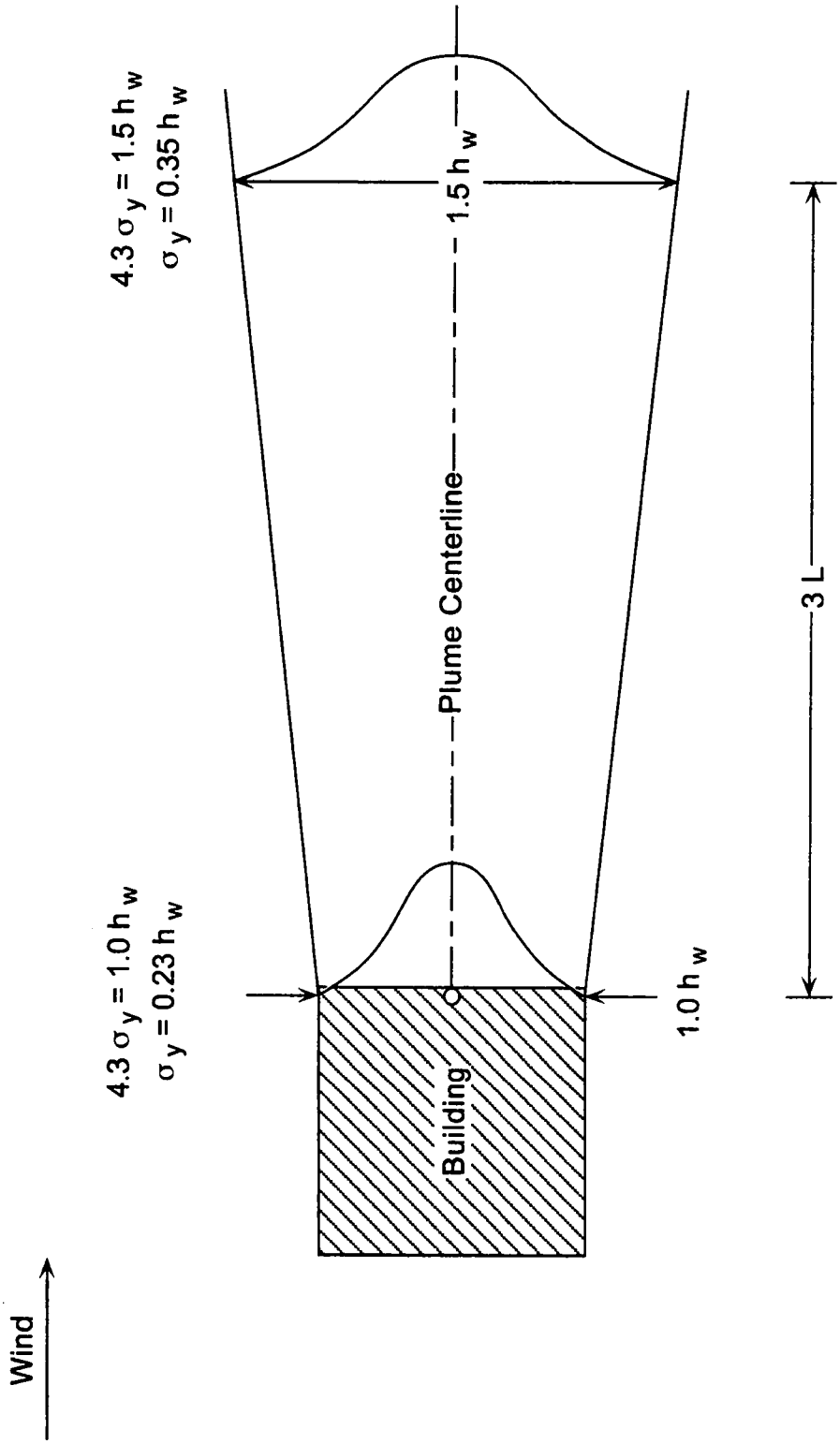


FIGURE 3.3 Horizontal Width of the Plume in the Cavity Region

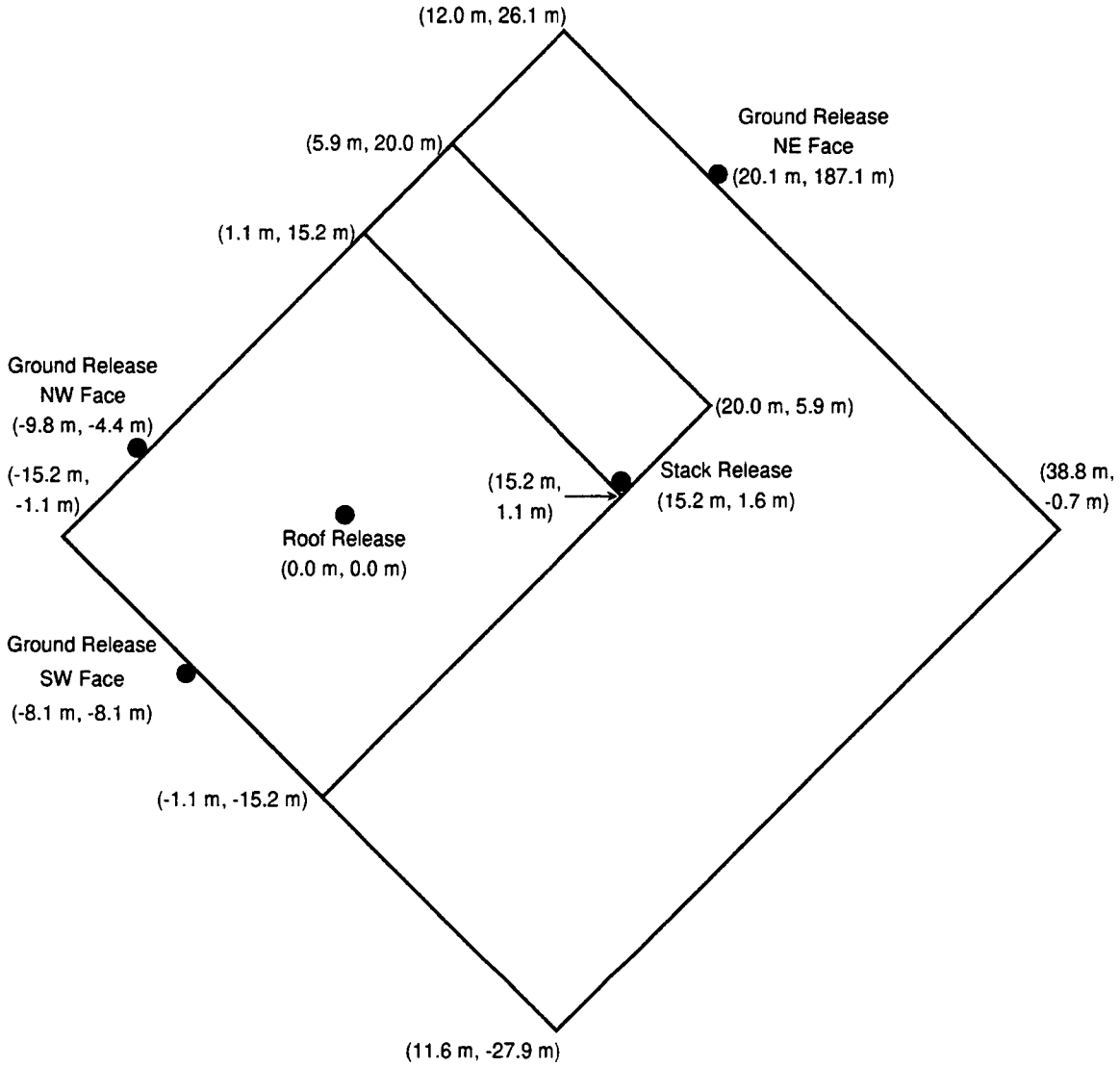


FIGURE 4.1 EOCR Building Plot Plan

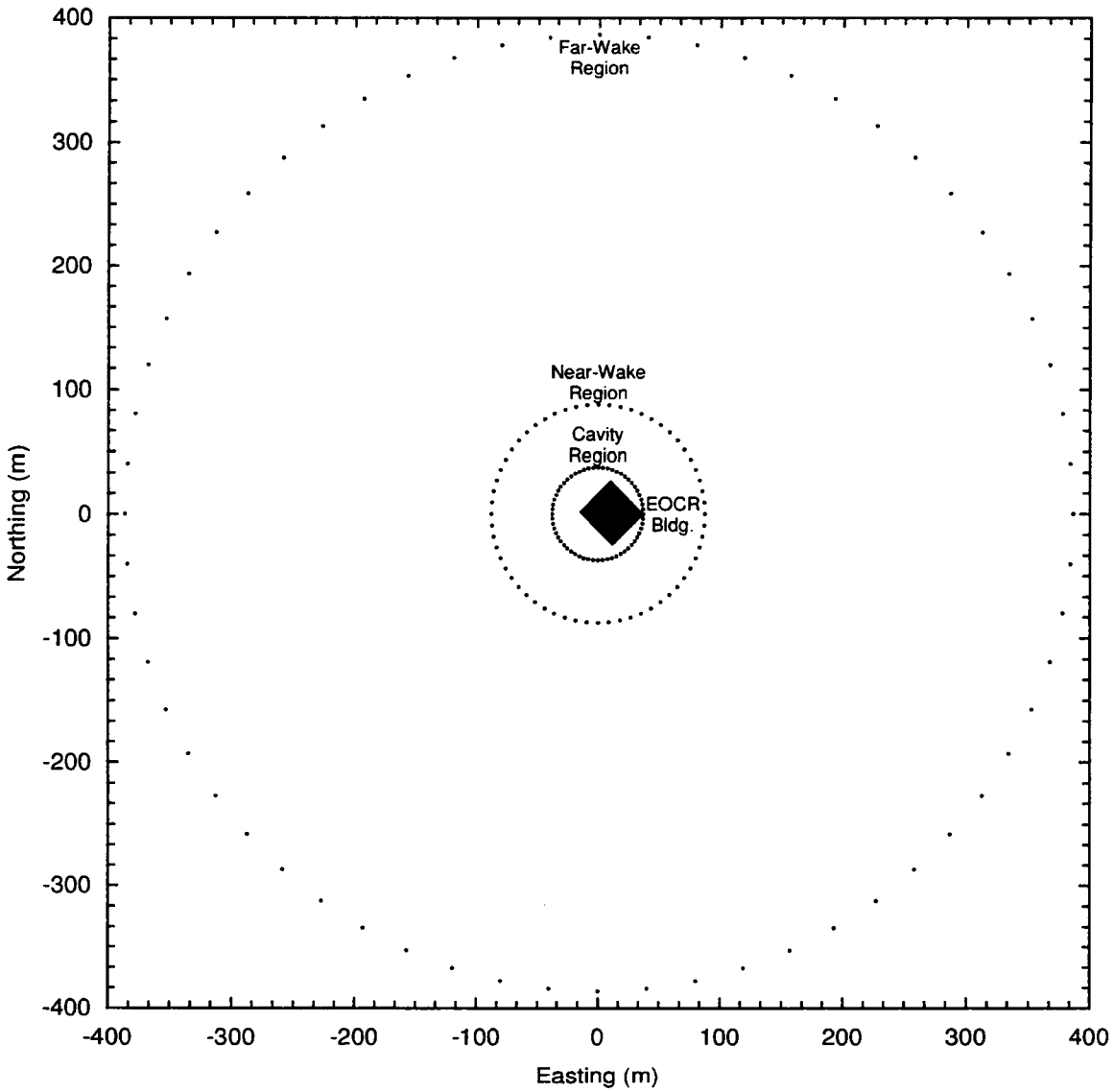


FIGURE 4.2 Sampling Grid Used During the EOCR Tracer Gas Release Experiment

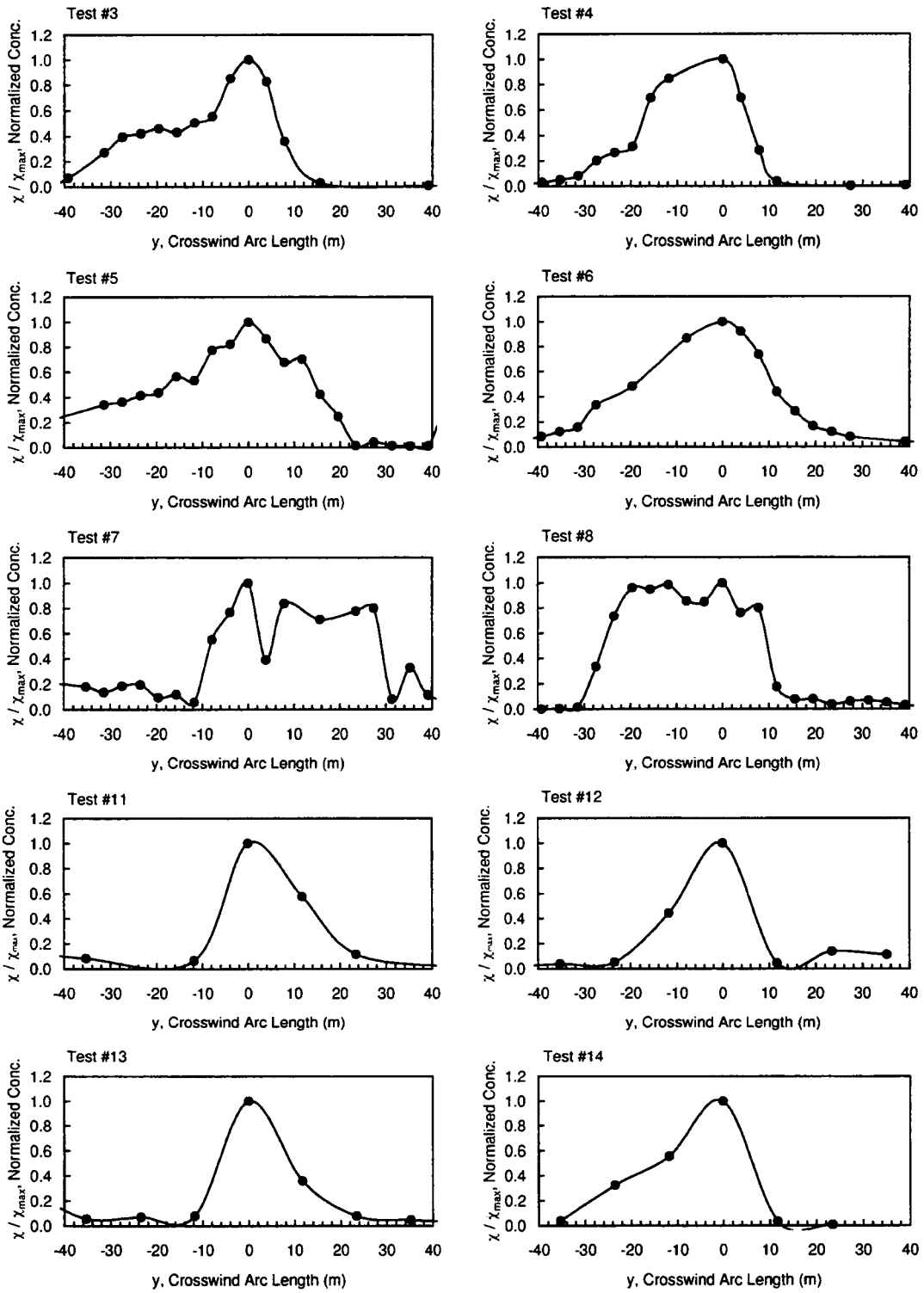


FIGURE 4.3 Crosswind Concentration Distributions Within the Cavity Region of the EOCR Building During the Ground-Level Tracer Gas Releases

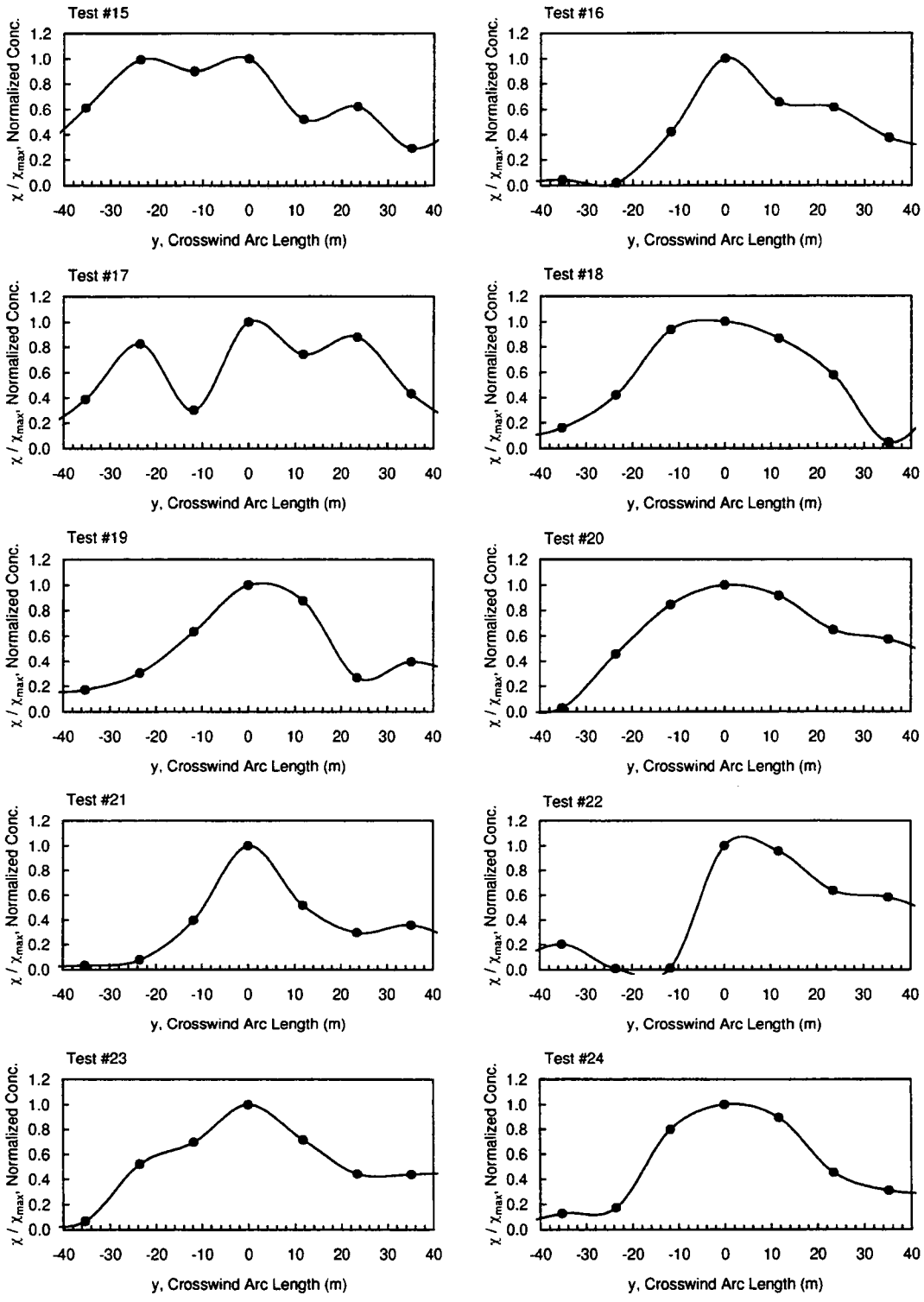


FIGURE 4.3 (continued)

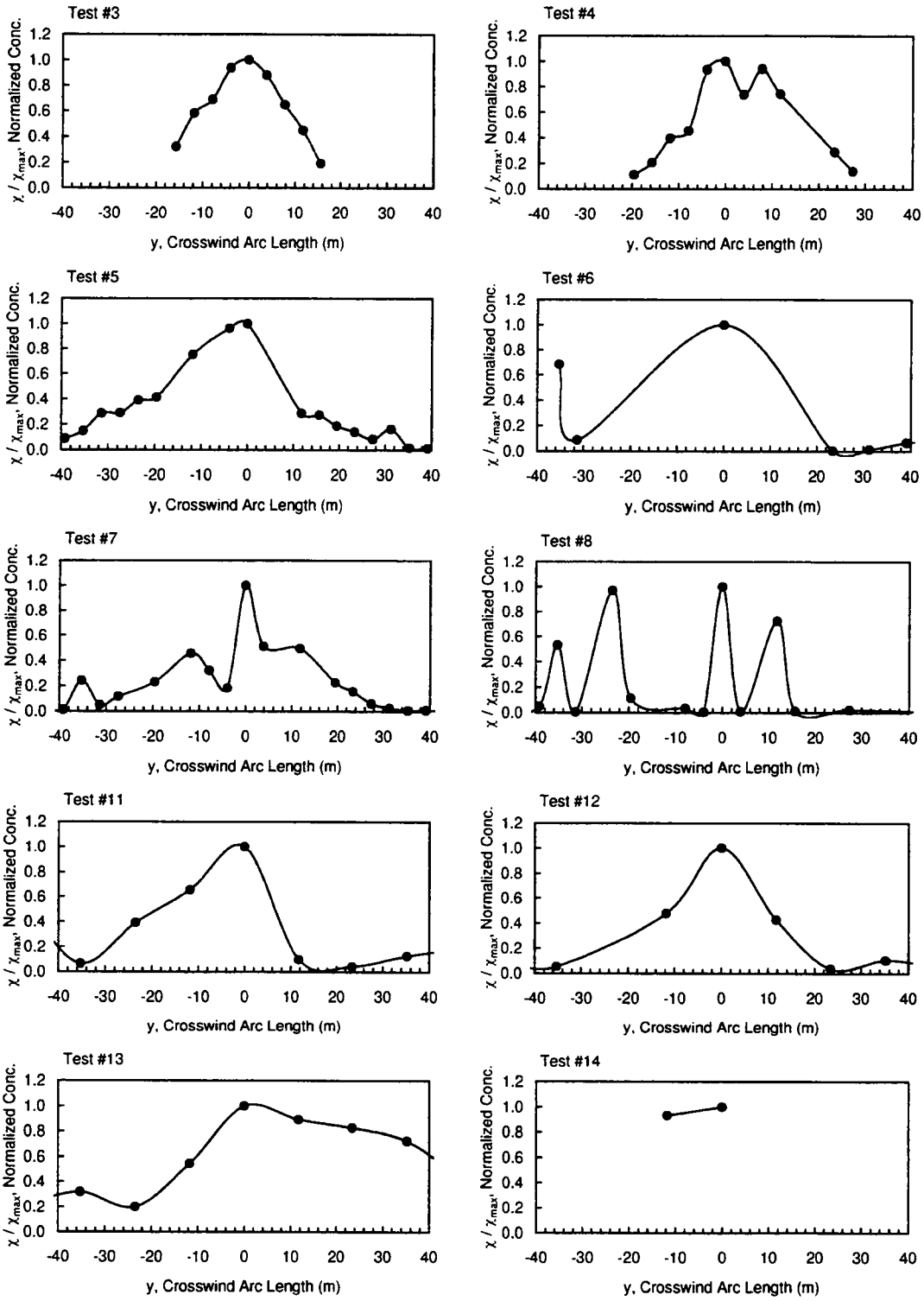


FIGURE 4.4 Crosswind Concentration Distributions Within the Cavity Region of the EOCR Building During the Roof-Level Tracer Gas Releases

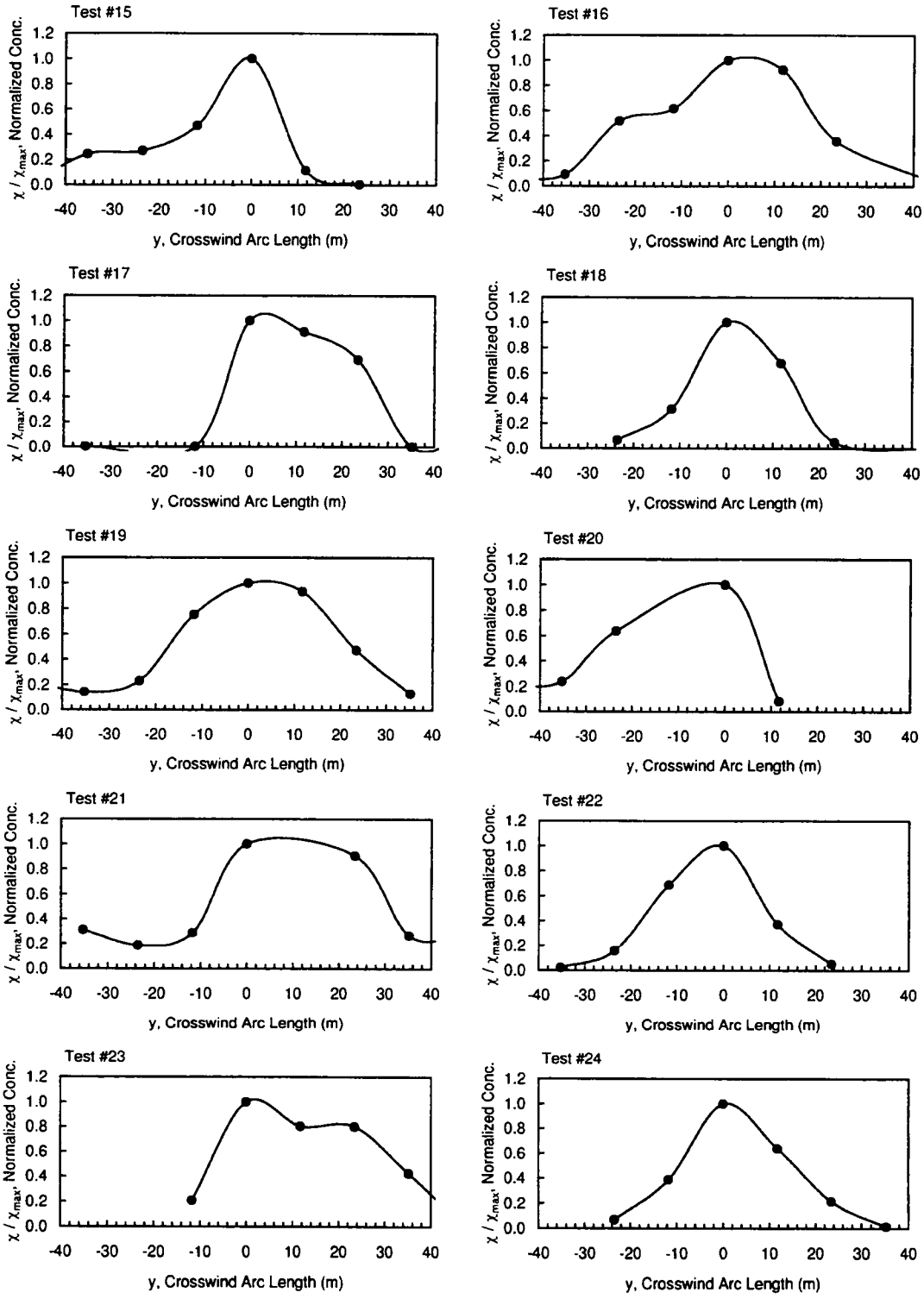


FIGURE 4.4 (continued)

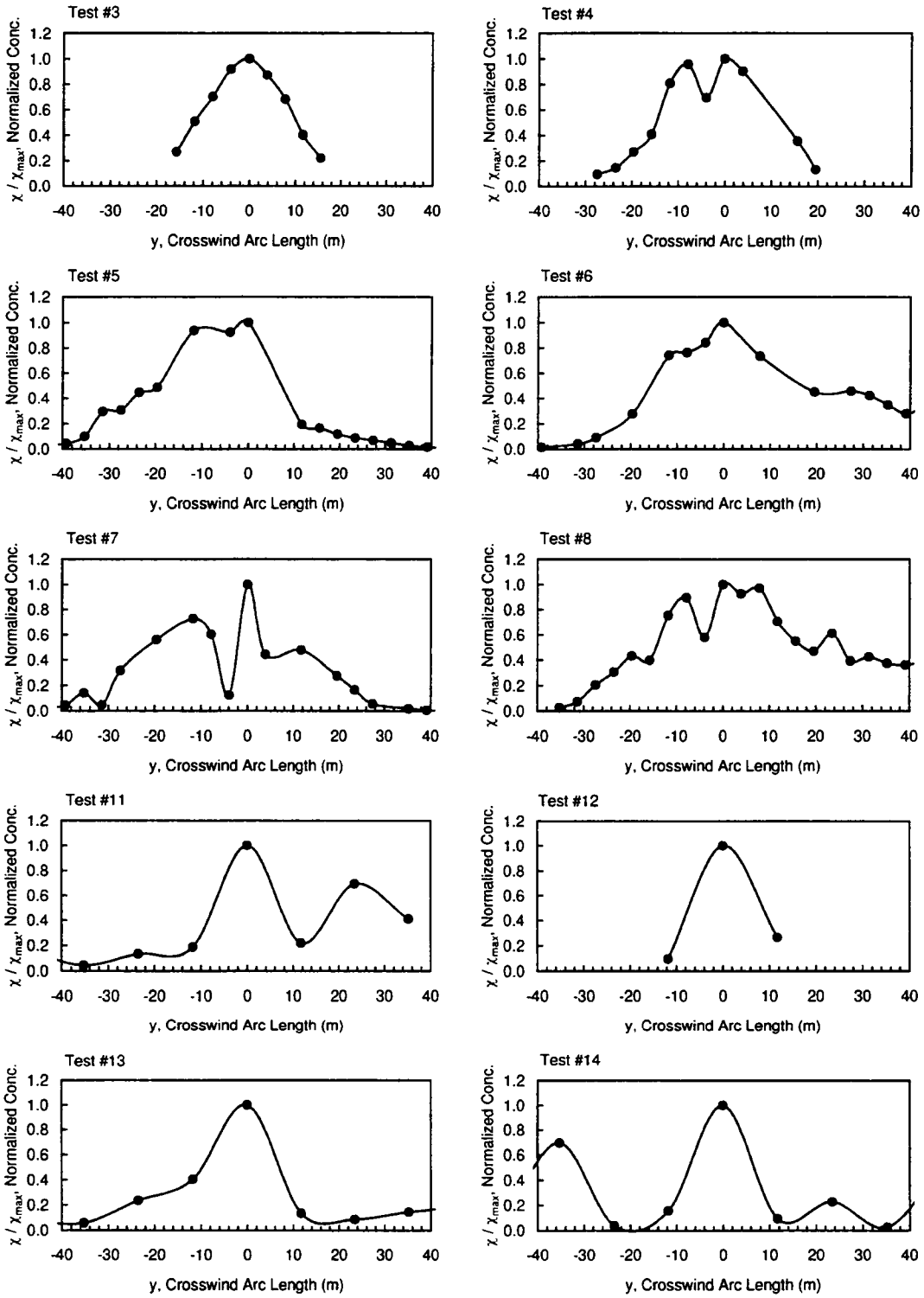


FIGURE 4.5 Crosswind Concentration Distributions Within the Cavity Region of the EOCR Building During the Stack-Level Tracer Gas Releases

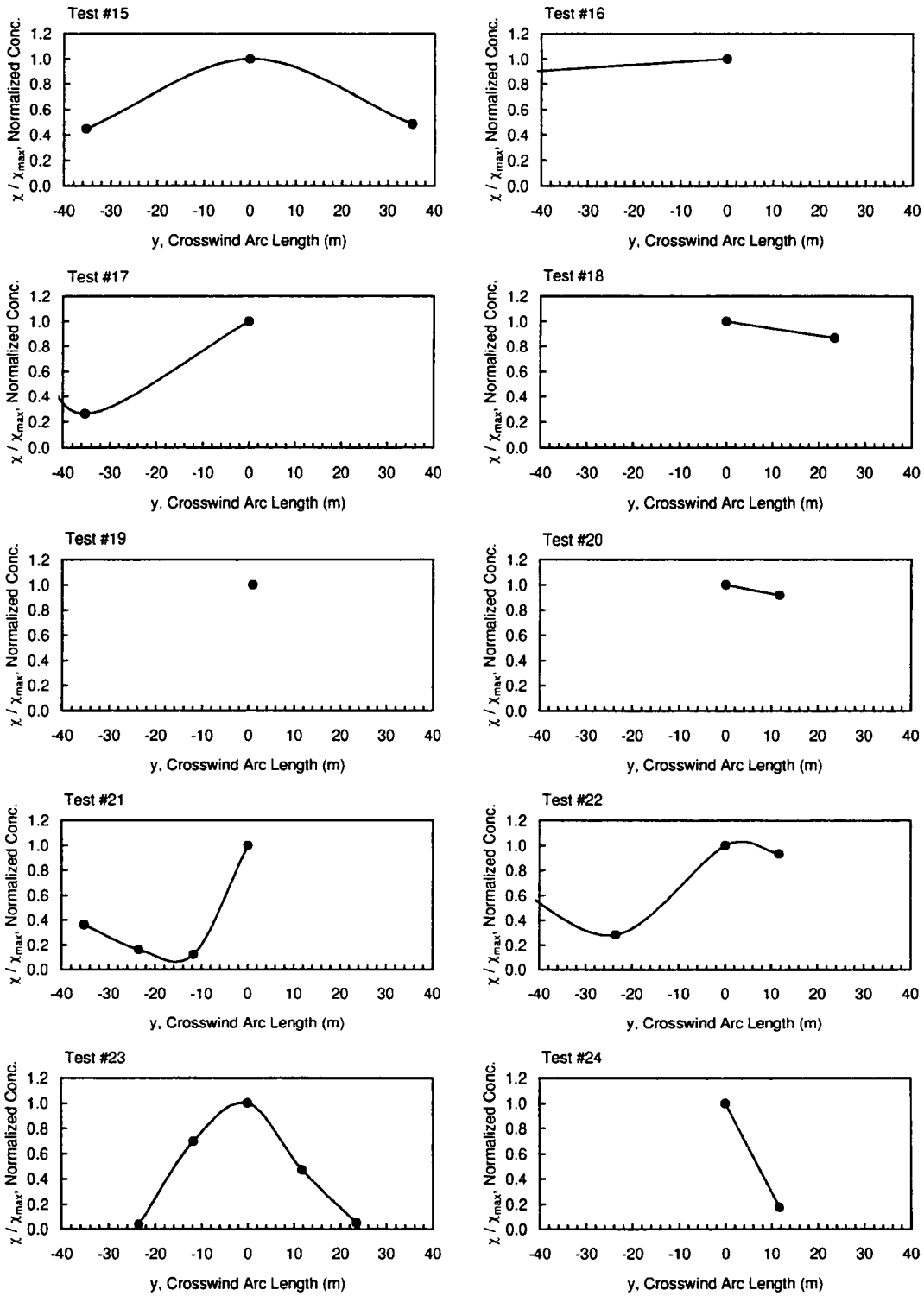


FIGURE 4.5 (continued)

```
CO STARTING
CO TITLEONE EOCR Reactor Building   Dissertation Research   M. Claggett
CO TITLETWO Predicted SCHULM Conc.    ROOF Release     Cavity Receptors
CO MODELOPT CONC RURAL NOCALM MSGPRO
CO MODELSEL SCHULM
CO AVERTIME 1
CO POLLUTID OTHER
CO FLAGPOLE 1.0
CO RUNORNOT RUN
CO FINISHED

SO STARTING
**                              X       Y       Z
**              ID     TYPE     (m)     (m)     (m)
**            -----  ------  -----   -----   -----
SO LOCATION   ROOF    POINT    0.      0.      0.
**
** Point Source           QS      HS      TS       VS       DS
** Parameters:     ID    (g/s)    (m)     (K)     (m/s)     (m)
**              -----  -----   -----   -----   ------   ------
SO SRCPARAM      ROOF   1.0    22.86   293.   0.0001   0.0001
**
** Stack gas temperature set to ambient and low stack gas velocity and
** stack exit diameter for no plume rise
**
** Direction-Specific Building Dimensions from BPIPC
**
SO BUILDHGT ROOF      22.86   22.86   22.86   22.86   22.86   22.86
SO BUILDHGT ROOF      22.86   22.86   22.86   22.86   22.86   22.86
SO BUILDHGT ROOF      22.86   22.86   22.86   22.86   22.86   22.86
SO BUILDHGT ROOF      22.86   22.86   22.86   22.86   22.86   22.86
SO BUILDHGT ROOF      22.86   22.86   22.86   22.86   22.86   22.86
SO BUILDHGT ROOF      22.86   22.86   22.86   22.86   22.86   22.86
SO BUILDWID ROOF      29.50   27.76   25.18   21.83   21.84   25.18
SO BUILDWID ROOF      27.77   29.51   30.35   30.27   29.27   27.38
SO BUILDWID ROOF      24.66   24.65   27.37   29.26   30.26   30.34
SO BUILDWID ROOF      29.50   27.76   25.18   21.83   21.84   25.18
SO BUILDWID ROOF      27.77   29.51   30.35   30.27   29.27   27.38
SO BUILDWID ROOF      24.66   24.65   27.37   29.26   30.26   30.34
SO BUILDLNG ROOF      30.27   29.27   27.38   24.66   24.65   27.37
SO BUILDLNG ROOF      29.26   30.26   30.34   29.50   27.76   25.18
SO BUILDLNG ROOF      21.83   21.84   25.18   27.77   29.51   30.35
SO BUILDLNG ROOF      30.27   29.27   27.38   24.66   24.65   27.37
SO BUILDLNG ROOF      29.26   30.26   30.34   29.50   27.76   25.18
SO BUILDLNG ROOF      21.83   21.84   25.18   27.77   29.51   30.35
SO BUILDSTK ROOF      15.13   14.63   13.69   12.33   12.32   13.68
SO BUILDSTK ROOF      14.63   15.13   15.17   14.75   13.88   12.59
SO BUILDSTK ROOF      10.92   10.92   12.60   13.89   14.76   15.18
SO BUILDSTK ROOF      15.14   14.64   13.70   12.34   12.33   13.69
SO BUILDSTK ROOF      14.63   15.13   15.17   14.75   13.88   12.59
SO BUILDSTK ROOF      10.91   10.91   12.59   13.88   14.75   15.17
```

FIGURE 4.6 Control Data File for an ISCST2C Model Run, EOCR Tests, Roof-Level Release, Cavity Region Receptors

```
** Tracer Gas Emission Rates (g/s) During Each Test:
**
**     Test Number --->     1       2       3       4       5       6
SO EMISFACT ROOF HROFDY  0.0000  0.0000  0.0982  0.1322  0.1346  0.1346
**     Test Number --->     7       8       9      10      11      12
SO EMISFACT ROOF HROFDY  0.1393  0.1354  0.1371  0.1388  0.5940  0.6204
**     Test Number --->    13      14      15      16      17      18
SO EMISFACT ROOF HROFDY  0.5880  0.1459  0.1706  0.6959  0.6289  0.6246
**     Test Number --->    19      20      21      22      23      24
SO EMISFACT ROOF HROFDY  0.6192  0.6226  0.6088  0.6286  0.6356  0.6005

SO SRCGROUP ALL
SO FINISHED

RE STARTING
**
** Polar grid defined by one ring with a radius of 37.4 m and
** 60 radials, one placed every 6 degrees.
**
RE GRIDPOLR PGRID STA
RE GRIDPOLR PGRID ORIG  0.0  0.0
RE GRIDPOLR PGRID DIST  37.4
RE GRIDPOLR PGRID GDIR  60  6.  6.
RE GRIDPOLR PGRID END
RE FINISHED

ME STARTING
ME INPUTFIL ROOFC.MET
ME ANEMHGHT 22.86
ME SURFDATA 99999 1975
ME UAIRDATA 99999 1975
ME FINISHED

OU STARTING
OU DAYTABLE 1
OU FINISHED
```

FIGURE 4.6 (continued)

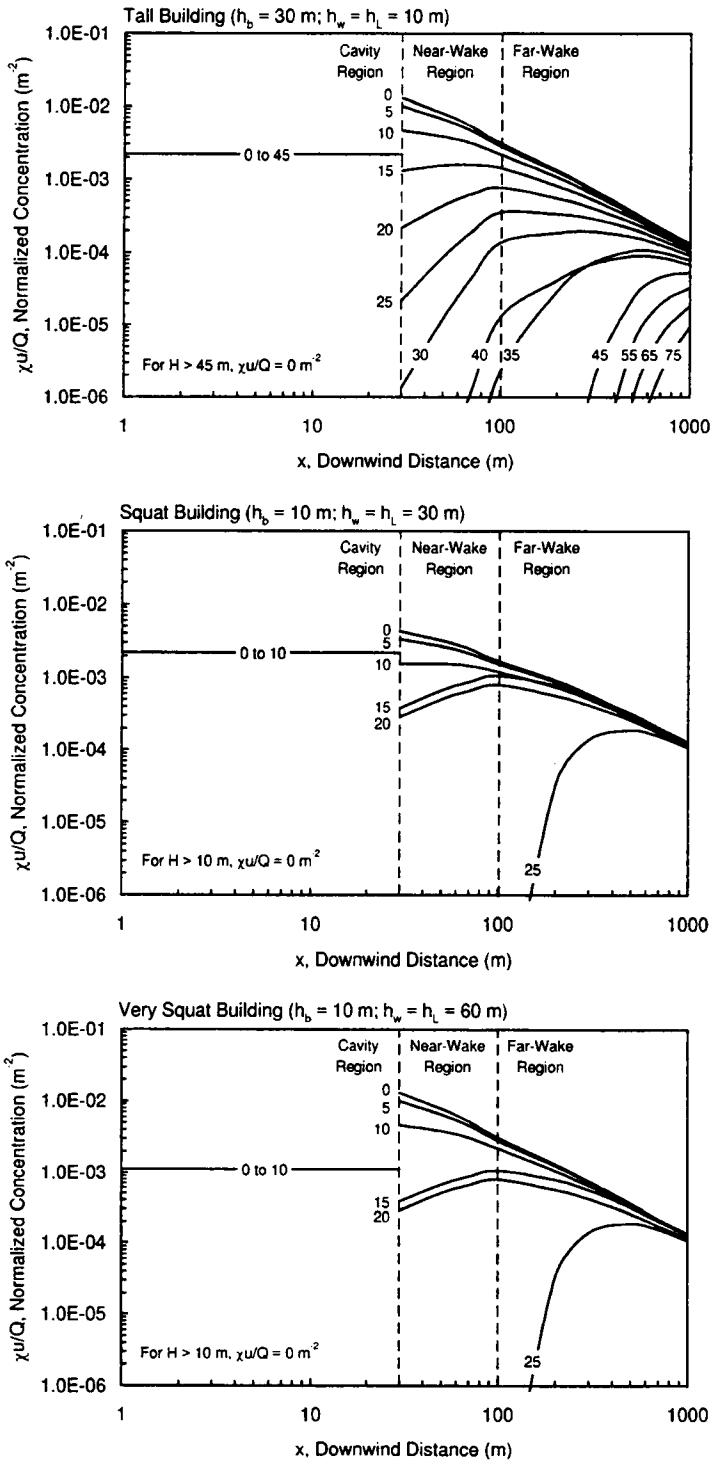


FIGURE 4.7 χu/Q with Distance for Various Plume Heights (m) and Representative Building Configurations, Hosker Cavity Algorithm

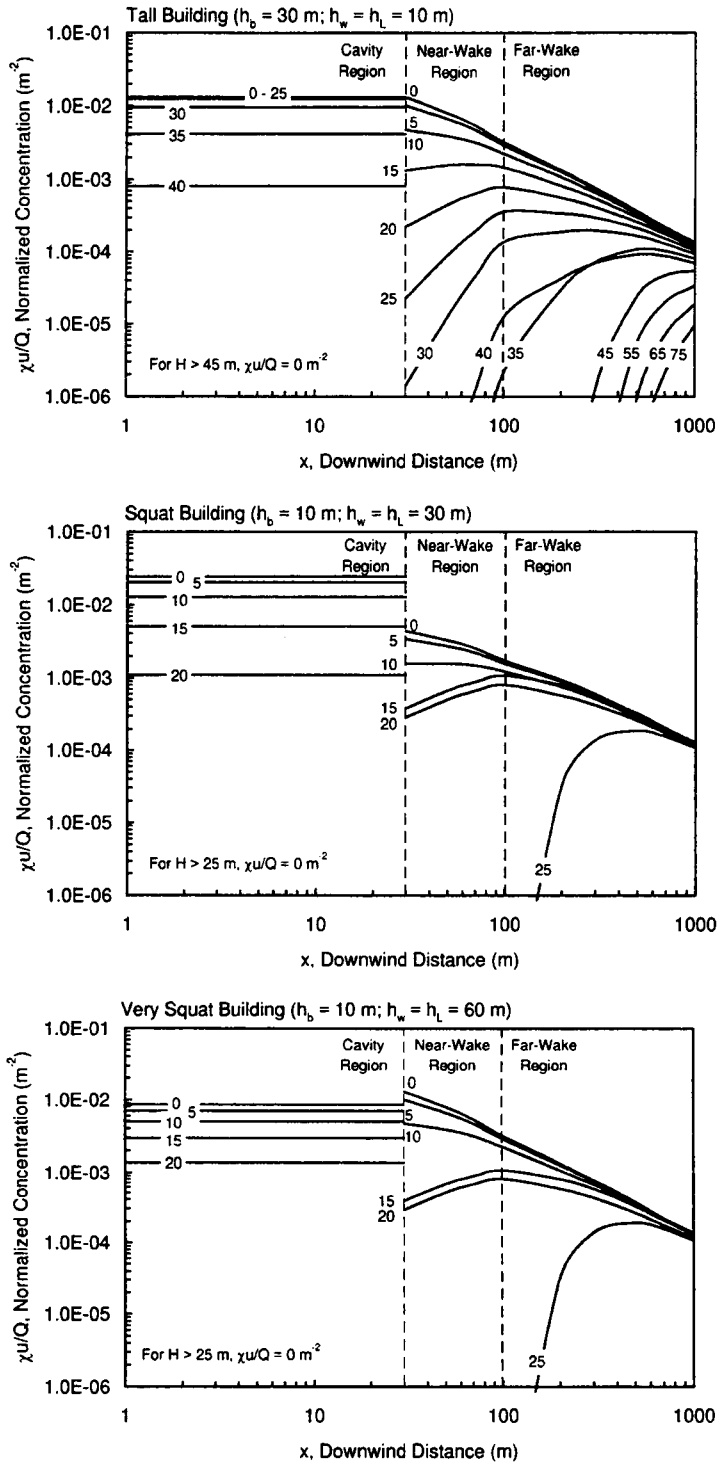


FIGURE 4.8 χu/Q with Distance for Various Plume Heights (m) and Representative Building Configurations, Schulman-Scire Cavity Algorithm

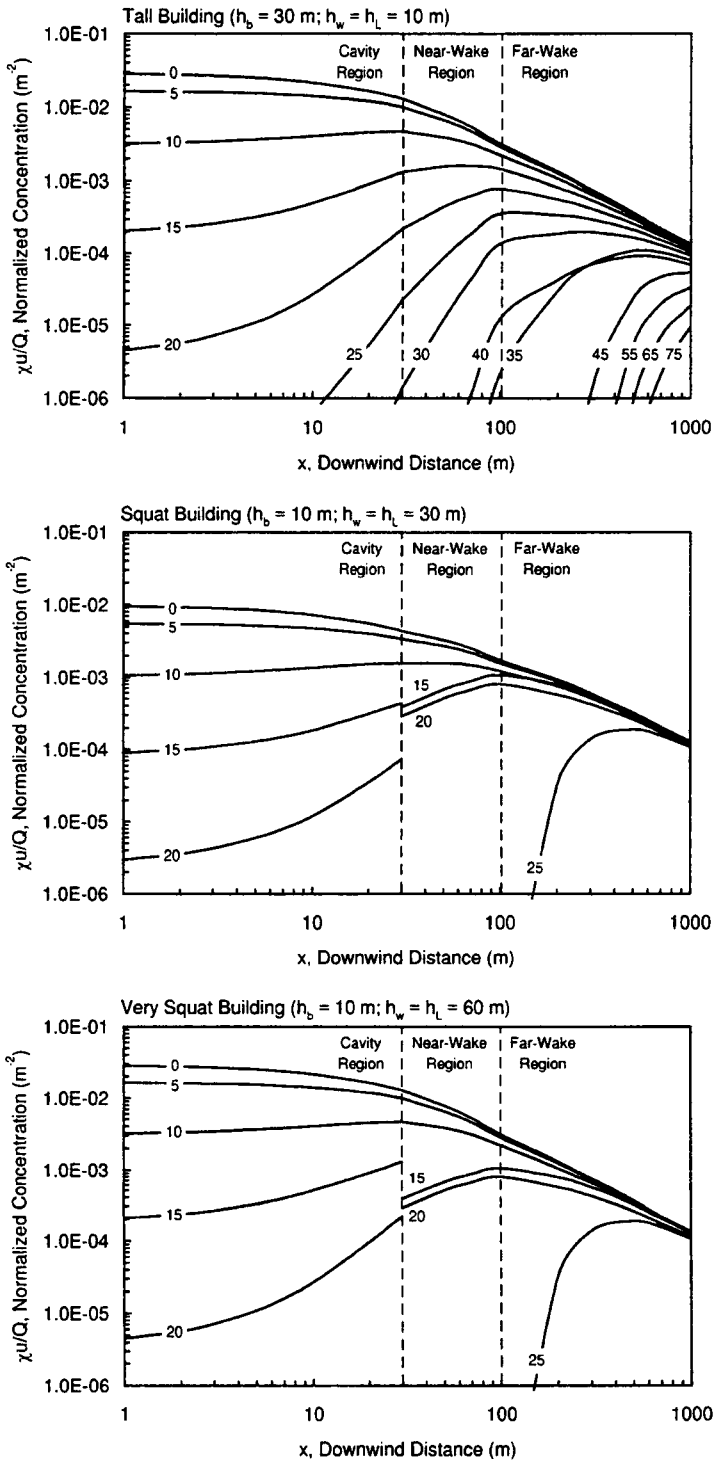


FIGURE 4.9 χu/Q with Distance for Various Plume Heights (m) and Representative Building Configurations, Gaussian Cavity Algorithm

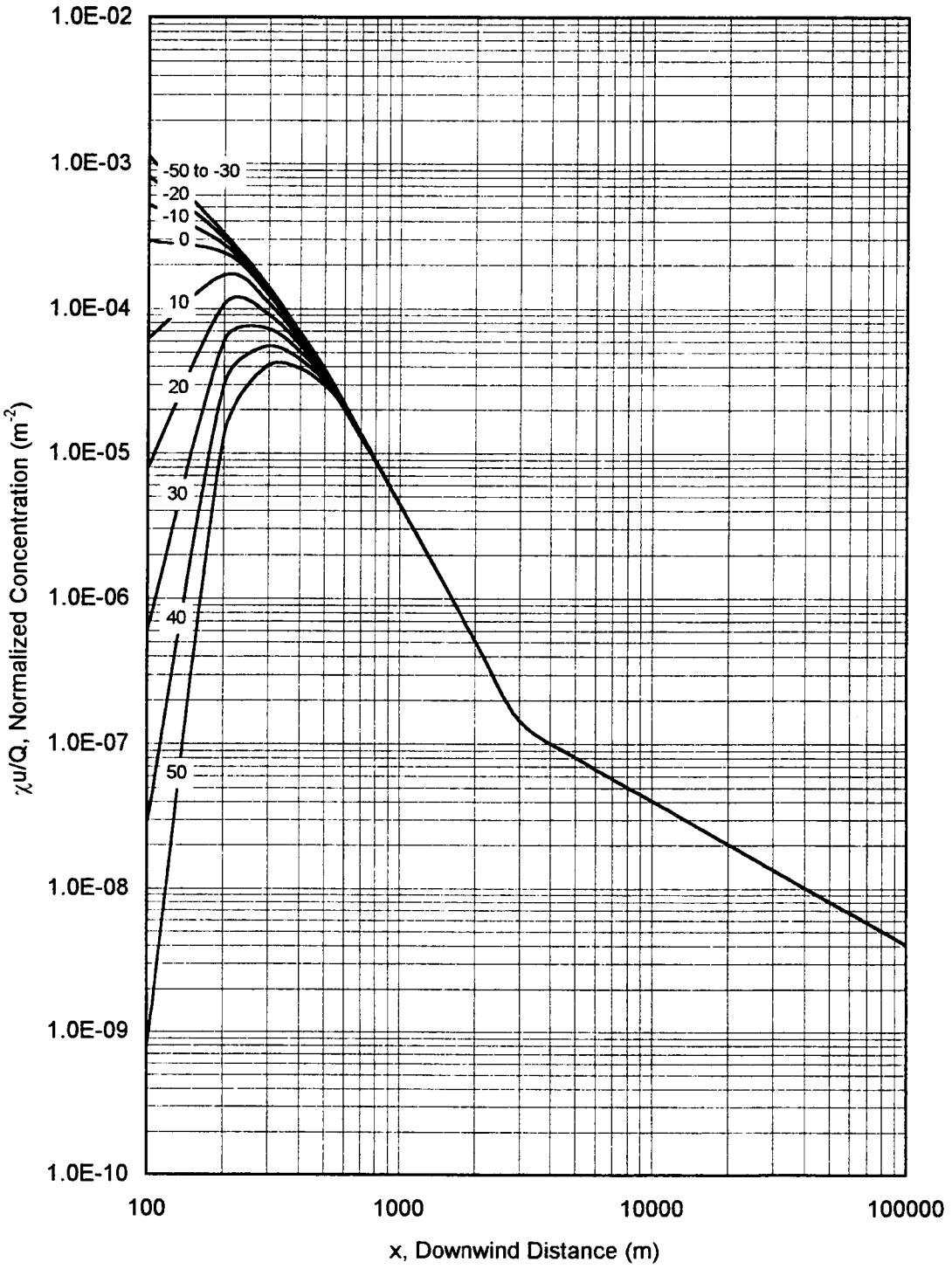


FIGURE 4.10 $\chi u/Q$ with Distance for Various Plume Heights Above Terrain Height (H - H_T, in m), A Stability, COMPLEX I Algorithm

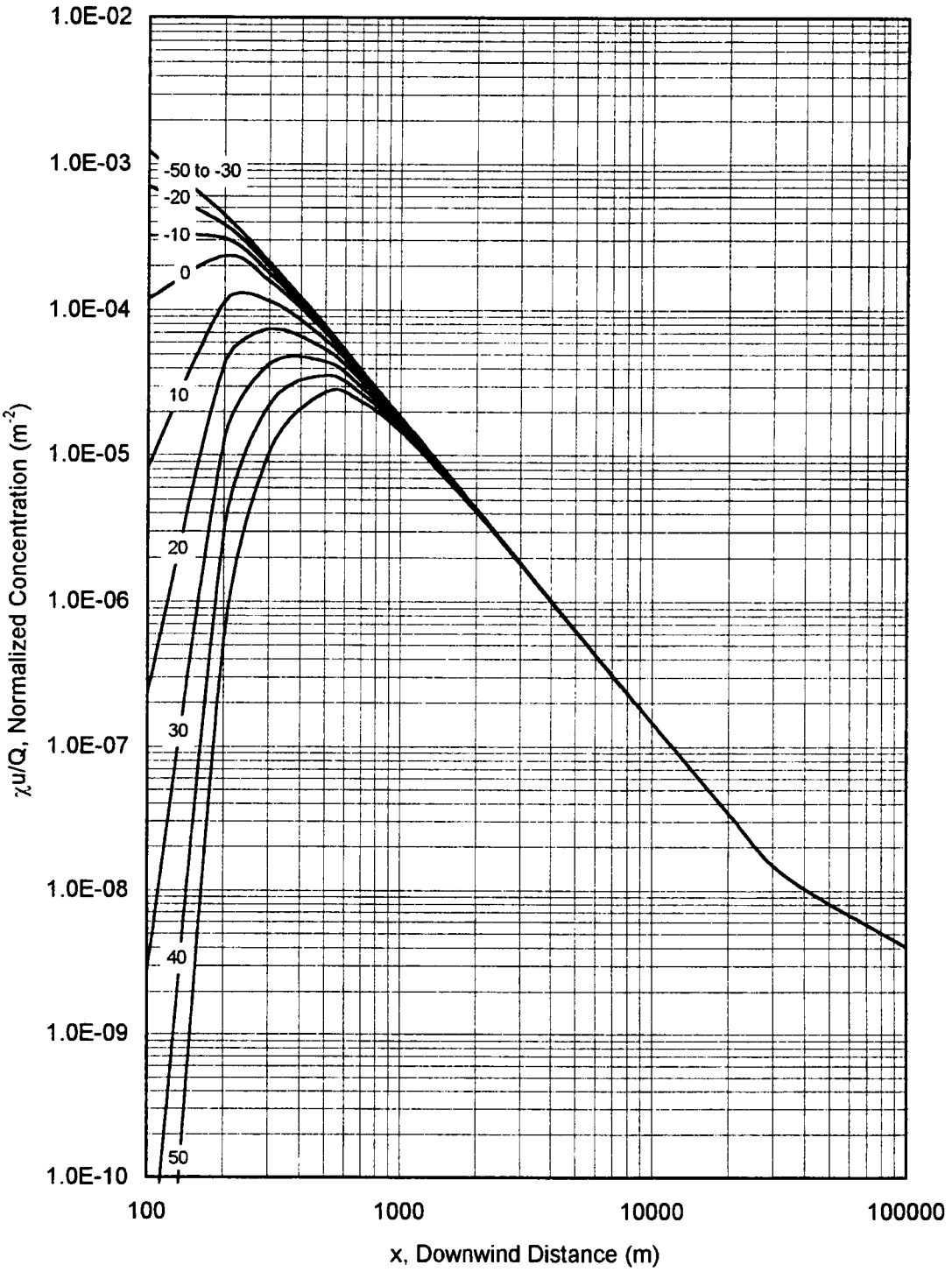


FIGURE 4.11 $\chi u/Q$ with Distance for Various Plume Heights Above Terrain Height ($H - H_T$, in m), B Stability, COMPLEX I Algorithm

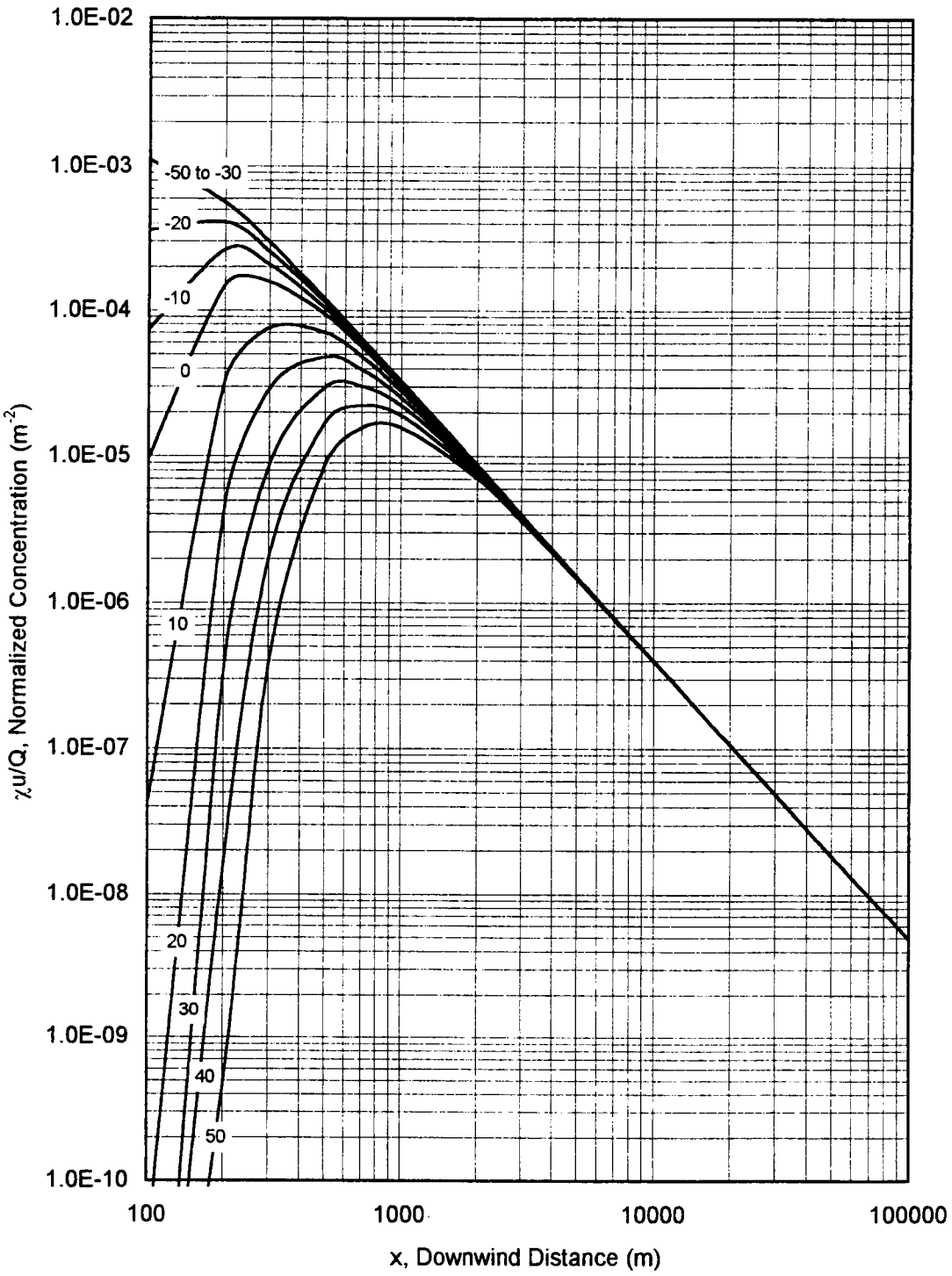


FIGURE 4.12 χu/Q with Distance for Various Plume Heights Above Terrain Height (H - H_T, in m), C Stability, COMPLEX I Algorithm

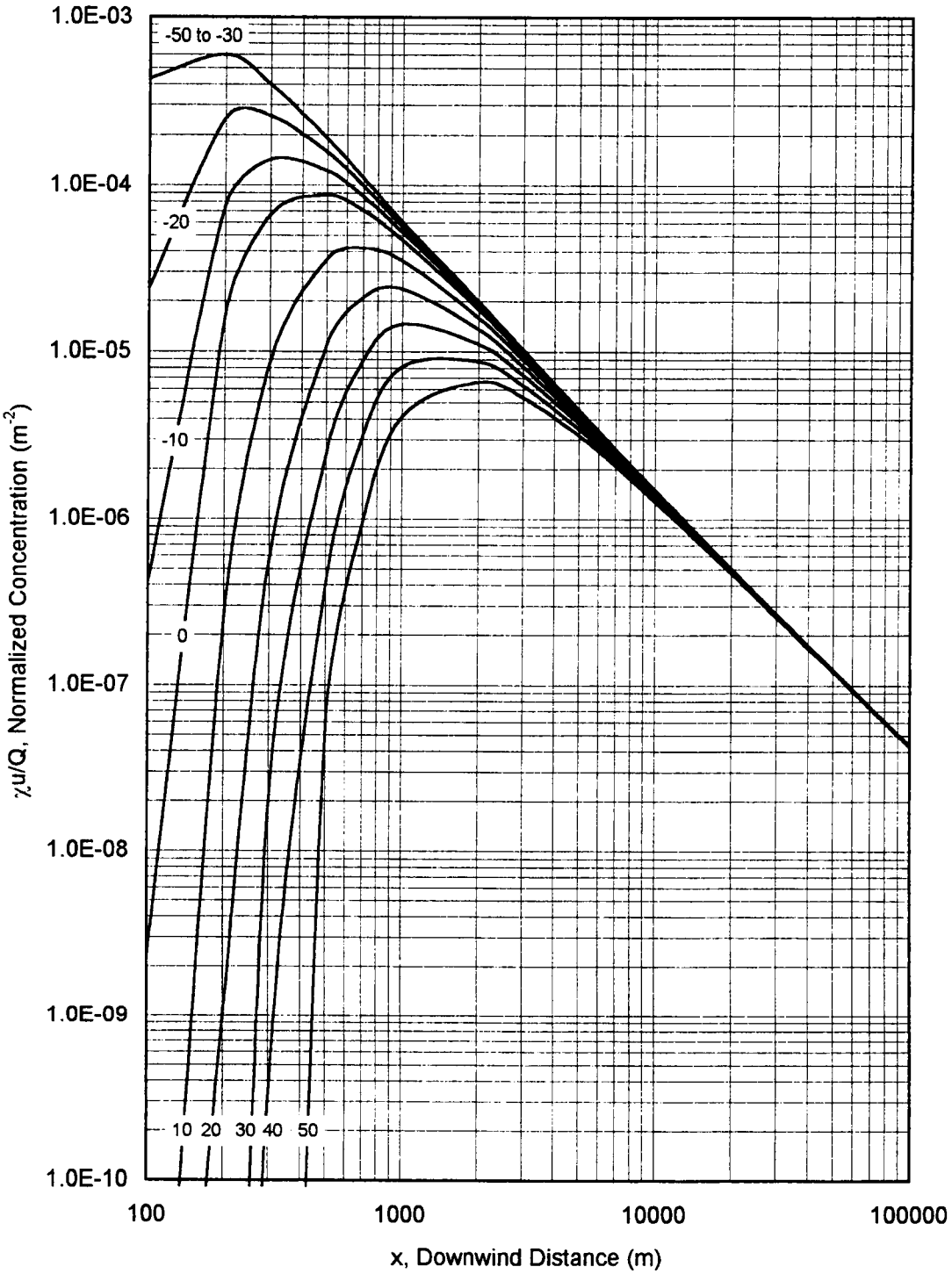


FIGURE 4.13 χu/Q with Distance for Various Plume Heights Above Terrain Height (H - H_T, in m), D Stability, COMPLEX I Algorithm

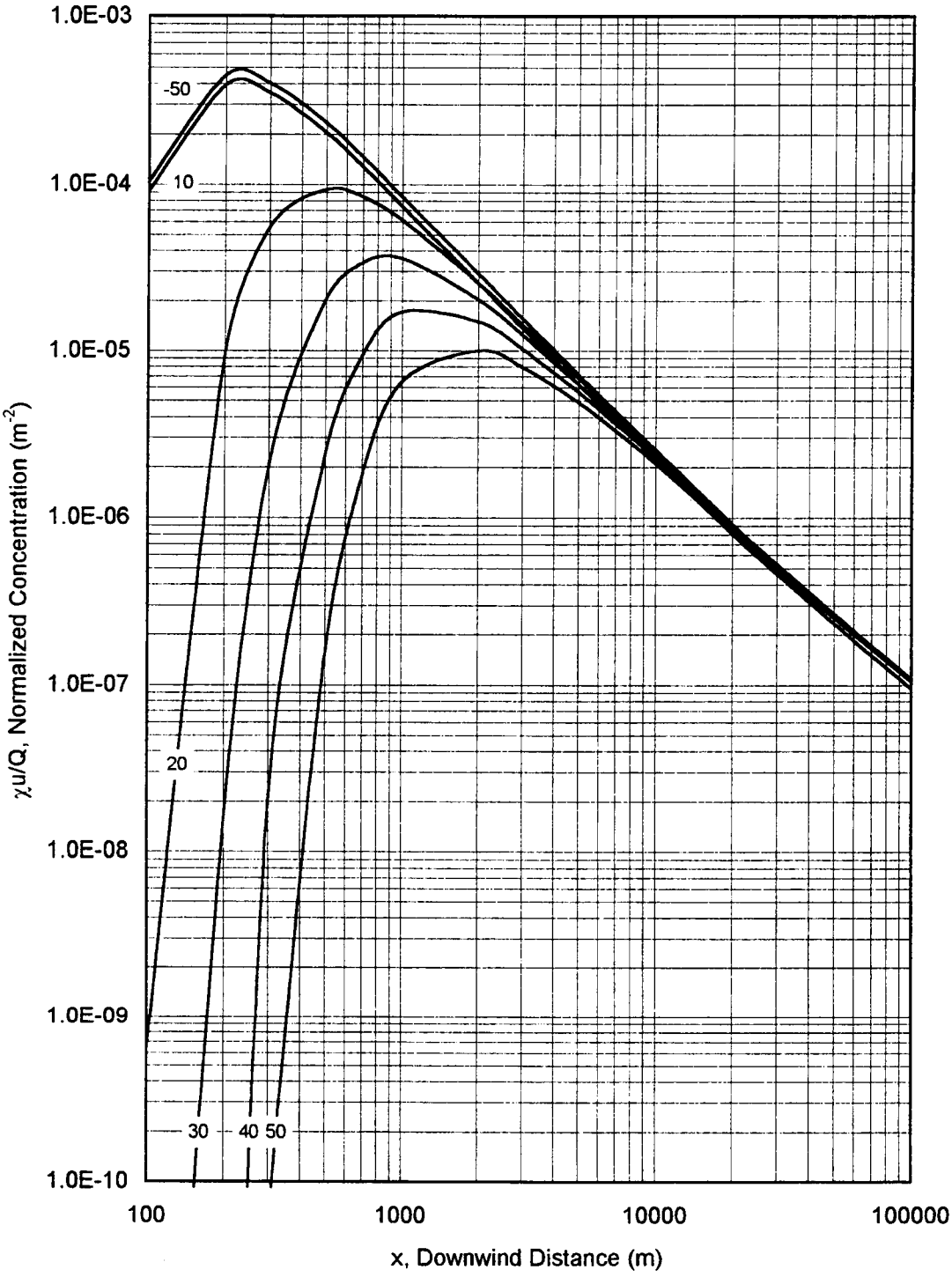


FIGURE 4.14 $\chi u/Q$ with Distance for Various Plume Heights Above Terrain Height ($H - H_T$, in m), E Stability, COMPLEX I Algorithm

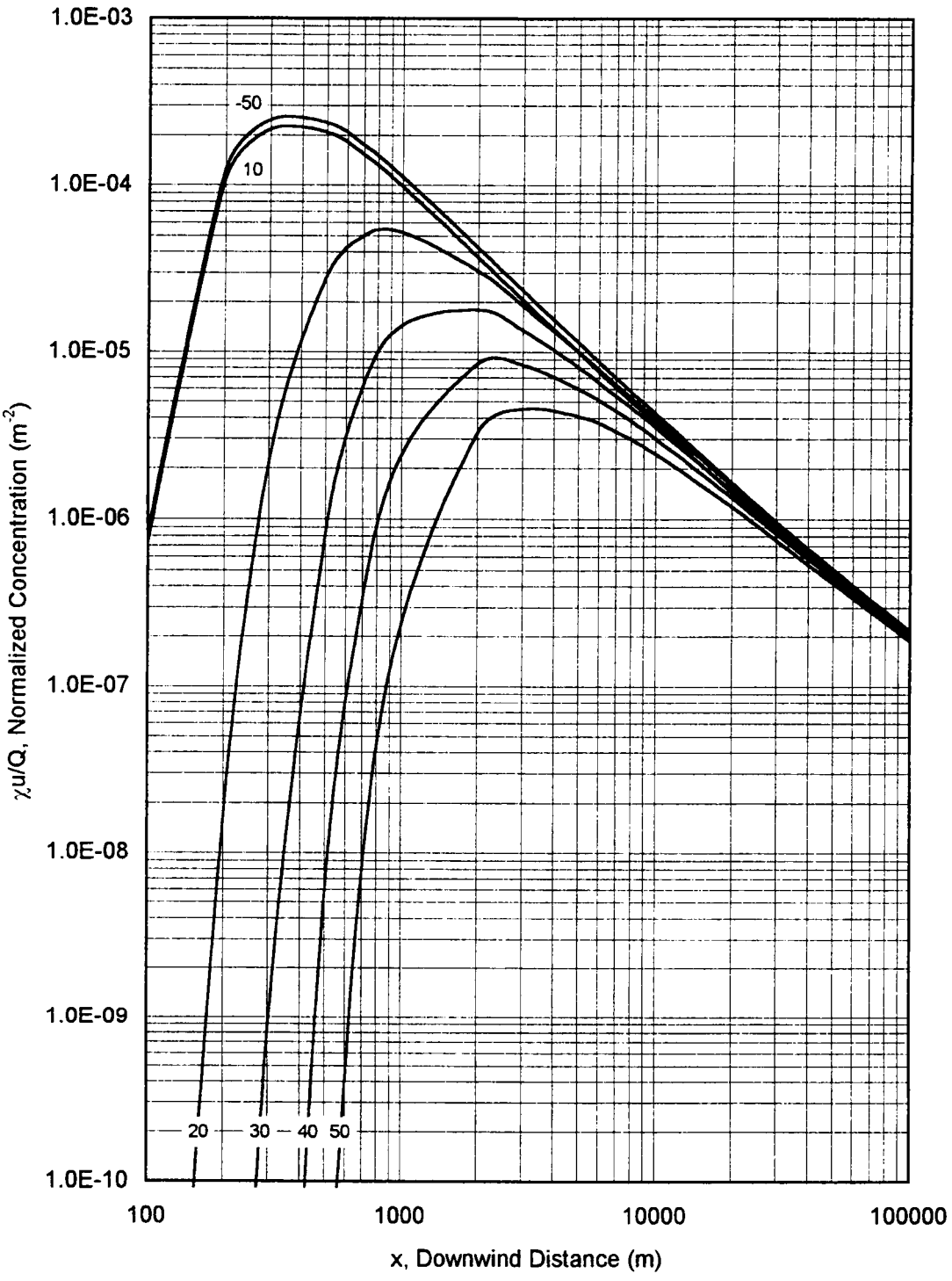


FIGURE 4.15 $\chi u/Q$ with Distance for Various Plume Heights Above Terrain Height ($H - H_T$, in m), F Stability, COMPLEX I Algorithm

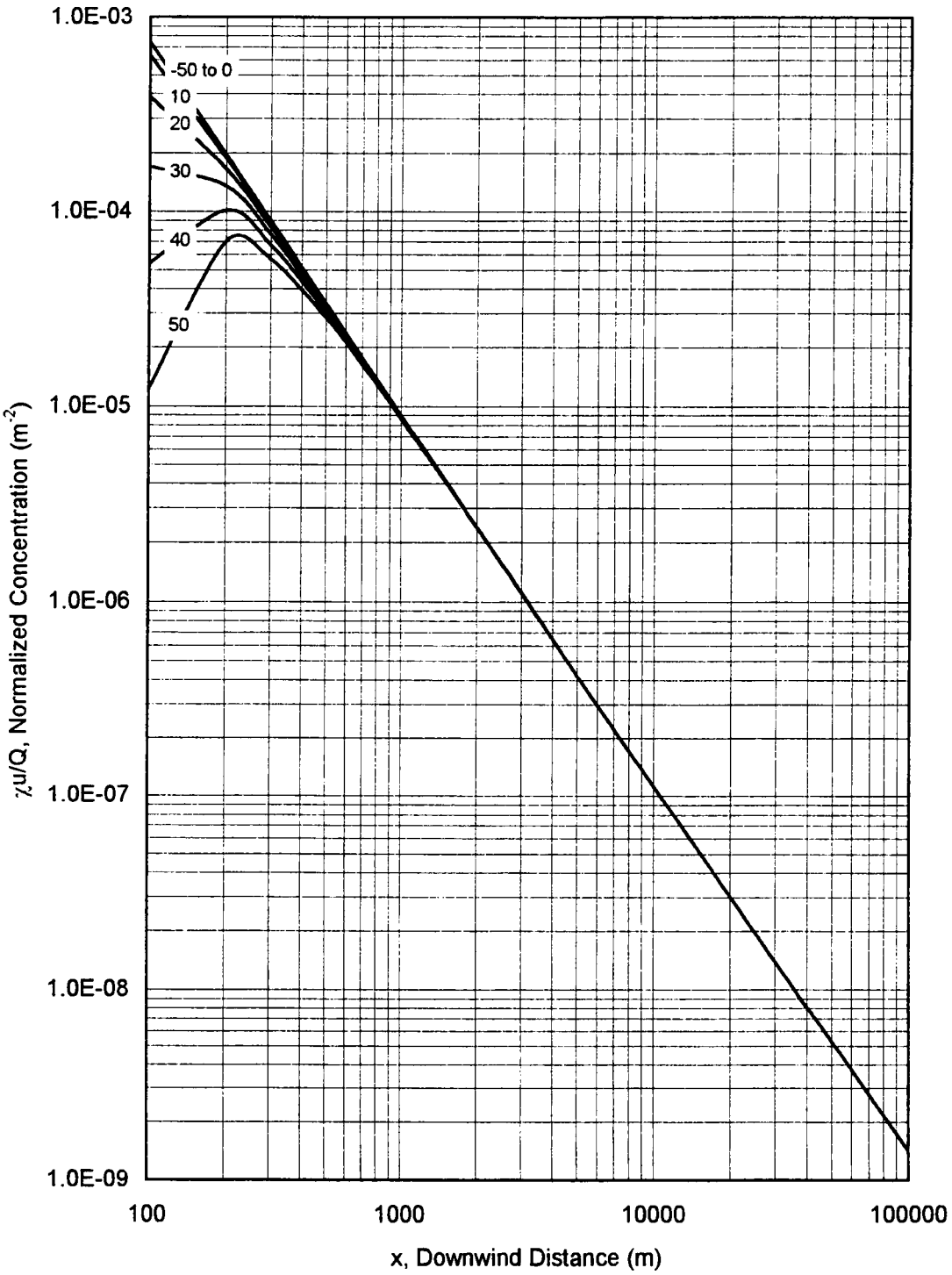


FIGURE 4.16 $\chi u/Q$ with Distance for Various Plume Heights Above Terrain Height ($H - H_T$, in m), A Stability, SHORTZ Algorithm

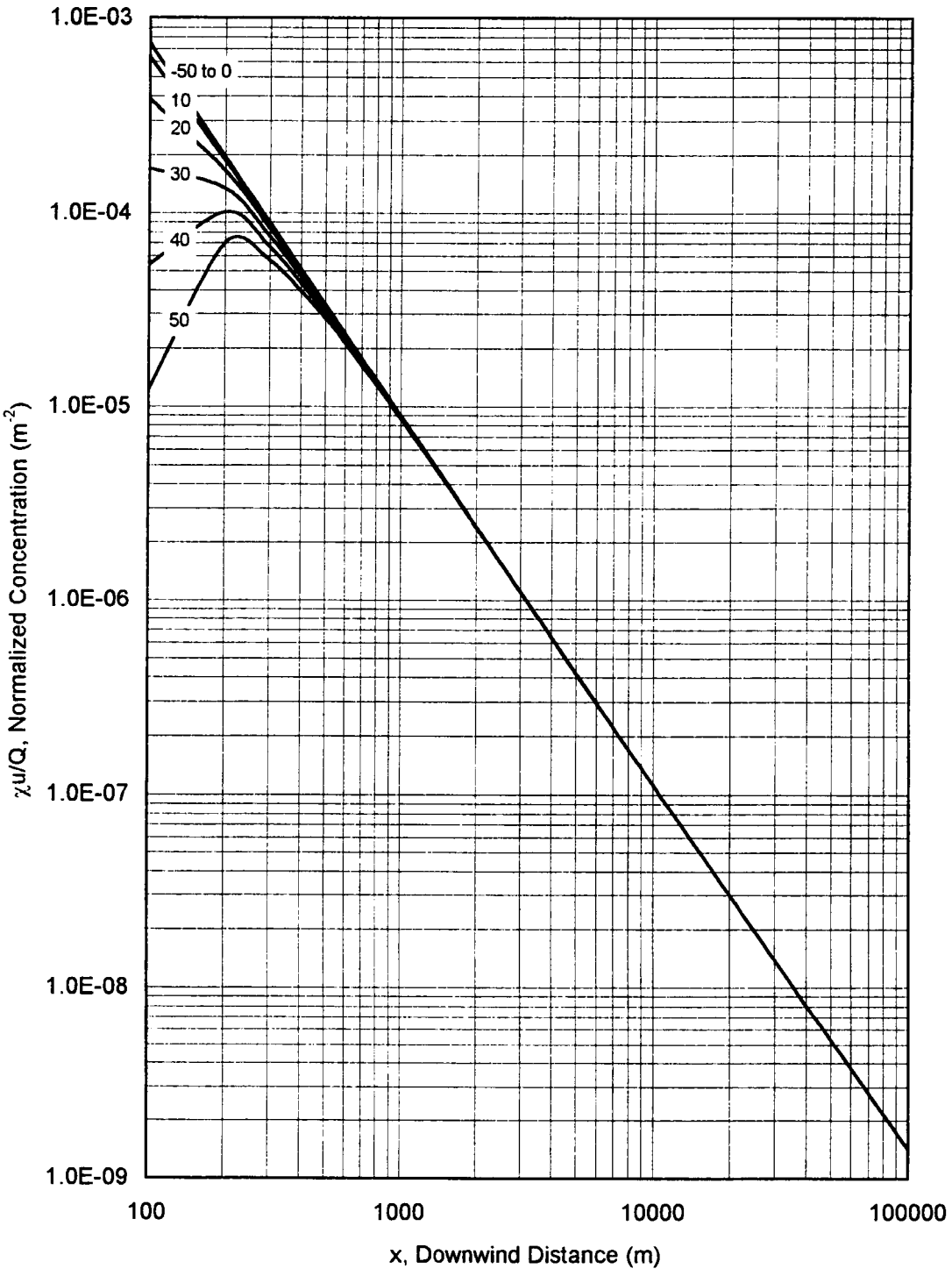


FIGURE 4.17 $\chi u/Q$ with Distance for Various Plume Heights Above Terrain Height ($H - H_T$, in m), B Stability, SHORTZ Algorithm

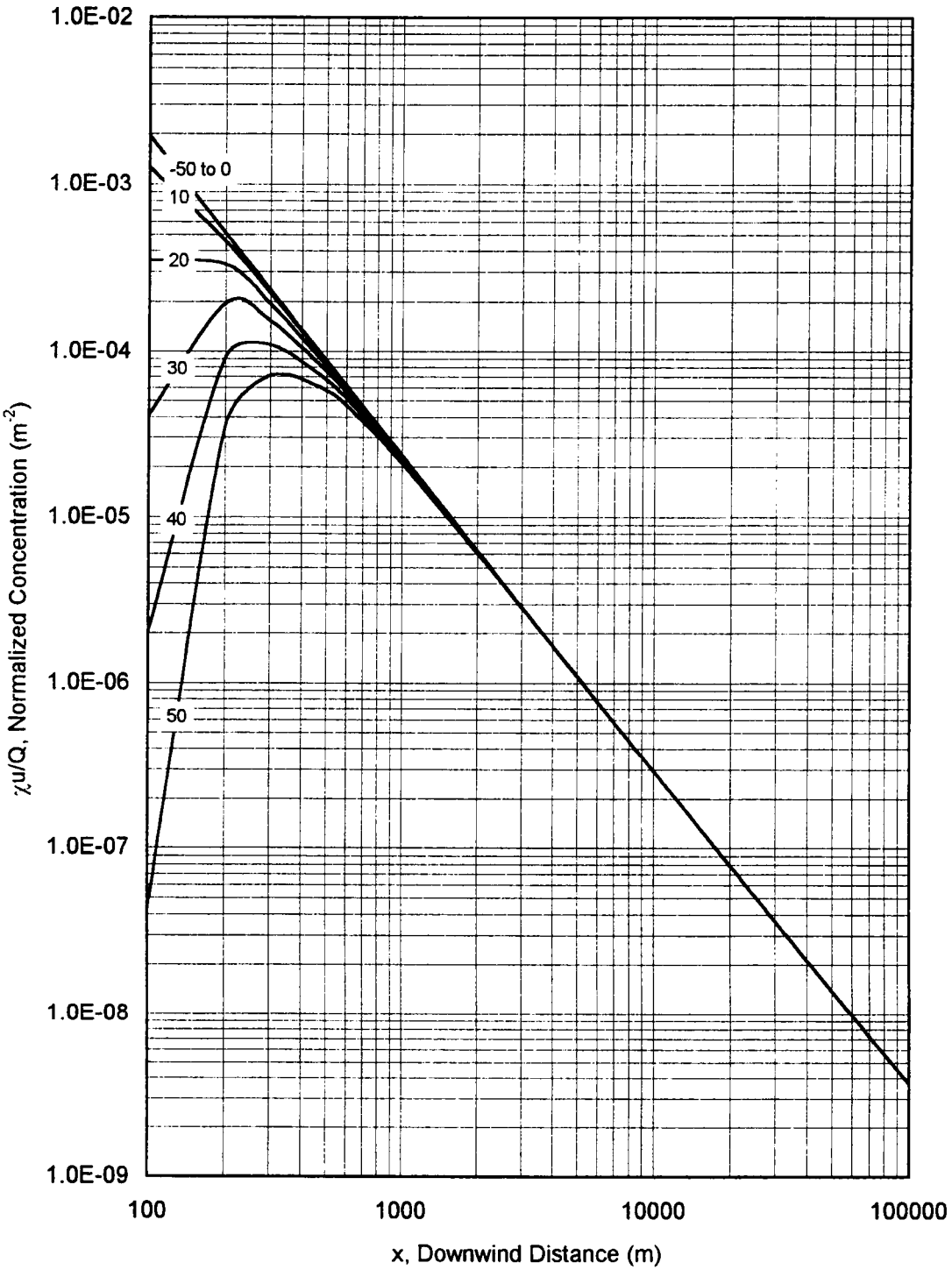


FIGURE 4.18 $\chi u/Q$ with Distance for Various Plume Heights Above Terrain Height ($H - H_T$, in m), C Stability, SHORTZ Algorithm

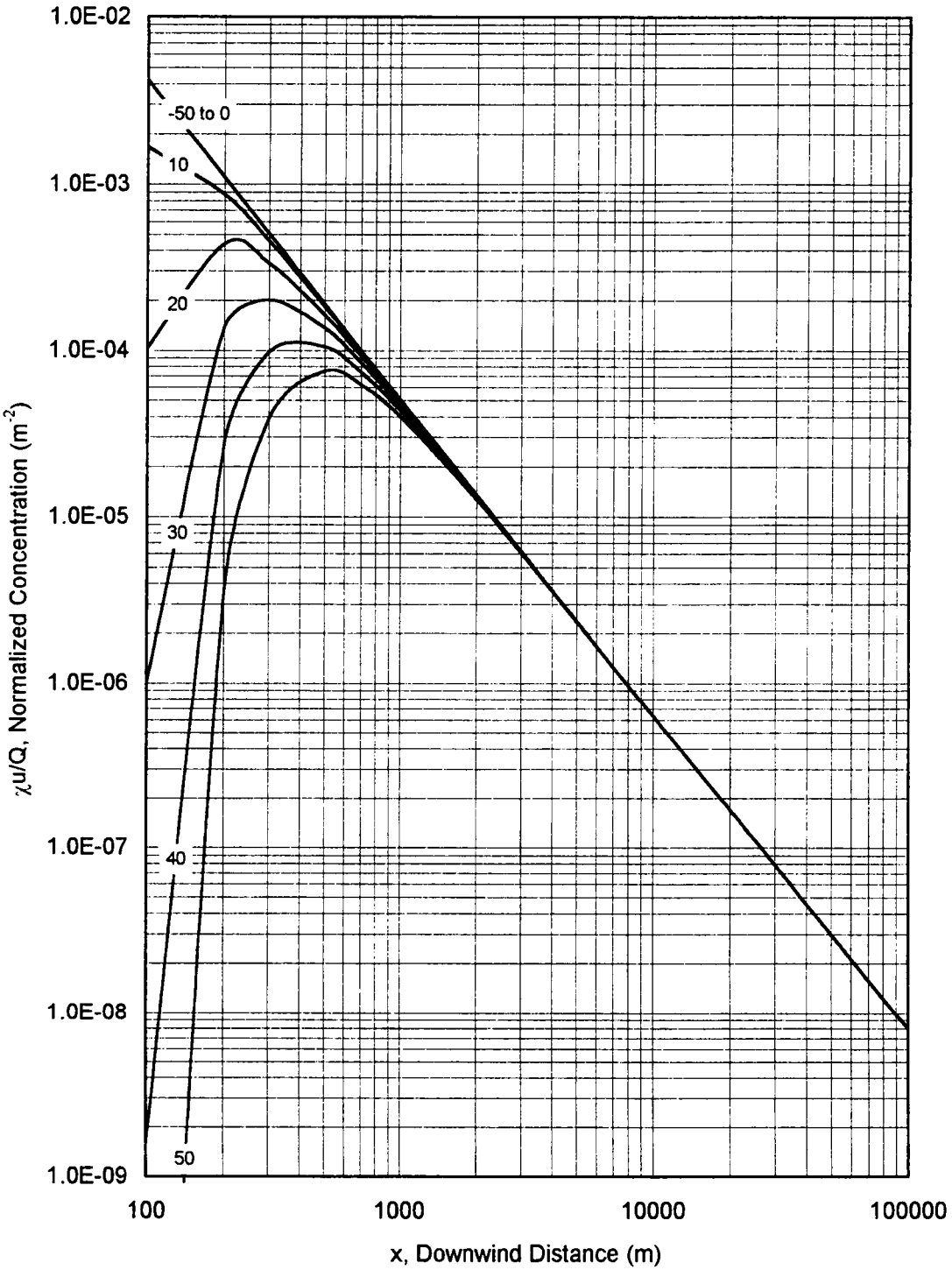


FIGURE 4.19 $\chi u/Q$ with Distance for Various Plume Heights Above Terrain Height ($H - H_T$, in m), D Stability, SHORTZ Algorithm

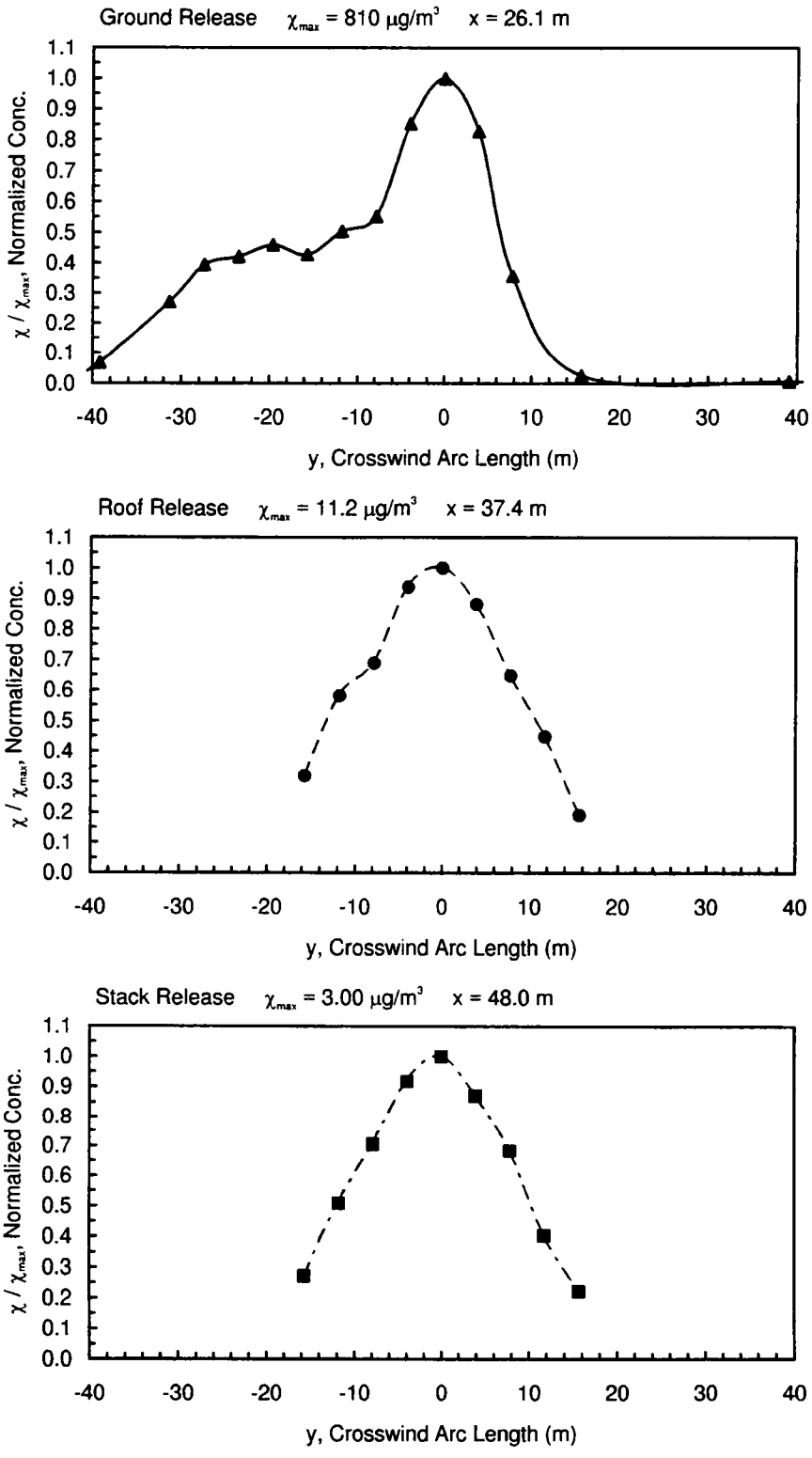


FIGURE 4.20 Crosswind Concentration Distributions Within the Cavity Region of the EOCR Building During Tracer Gas Release Test #3

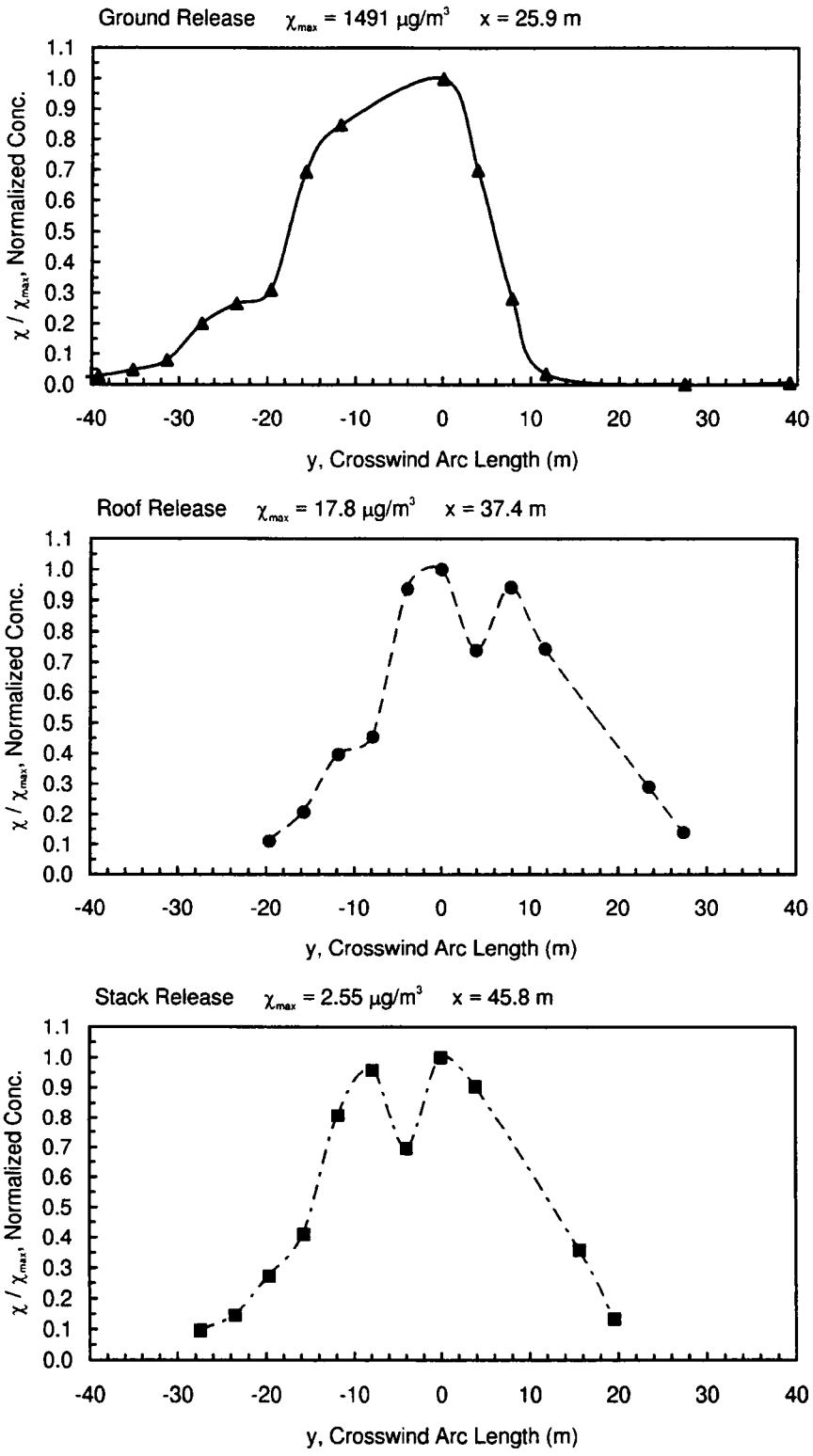


FIGURE 4.21 Crosswind Concentration Distributions Within the Cavity Region of the EOCR Building During Tracer Gas Release Test #4

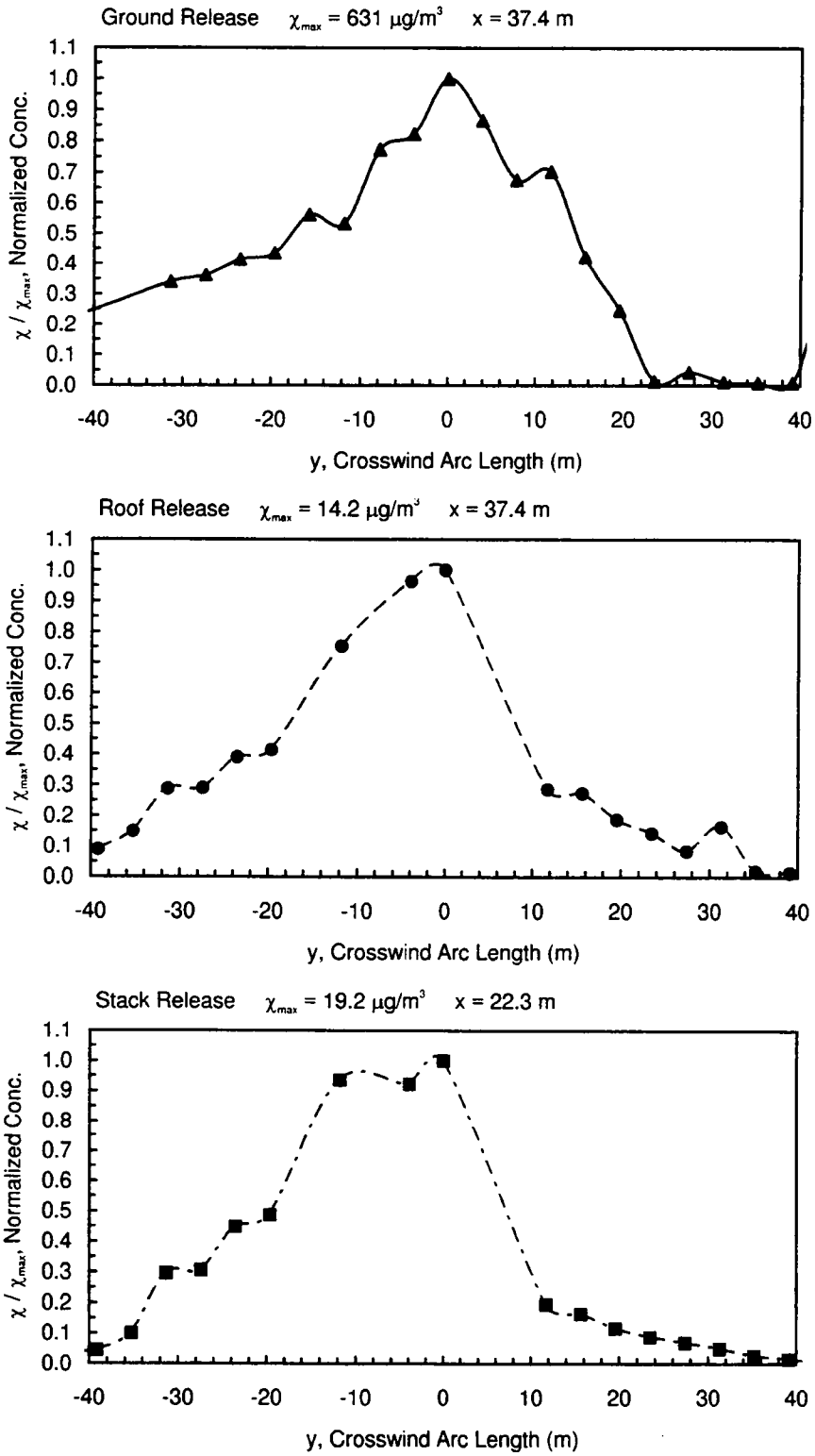


FIGURE 4.22 Crosswind Concentration Distributions Within the Cavity Region of the EOCR Building During Tracer Gas Release Test #5

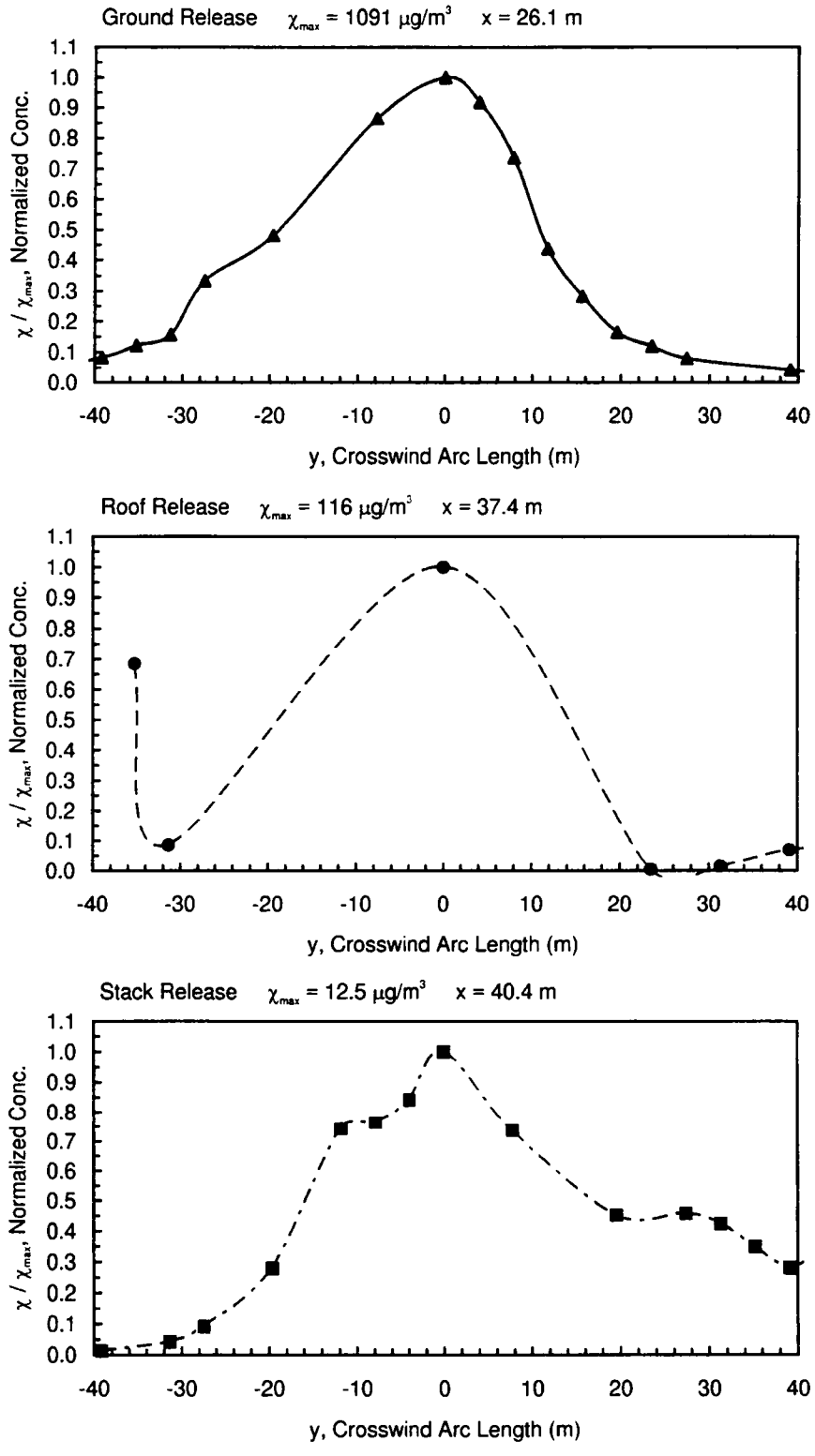


FIGURE 4.23 Crosswind Concentration Distributions Within the Cavity Region of the EOCR Building During Tracer Gas Release Test #6

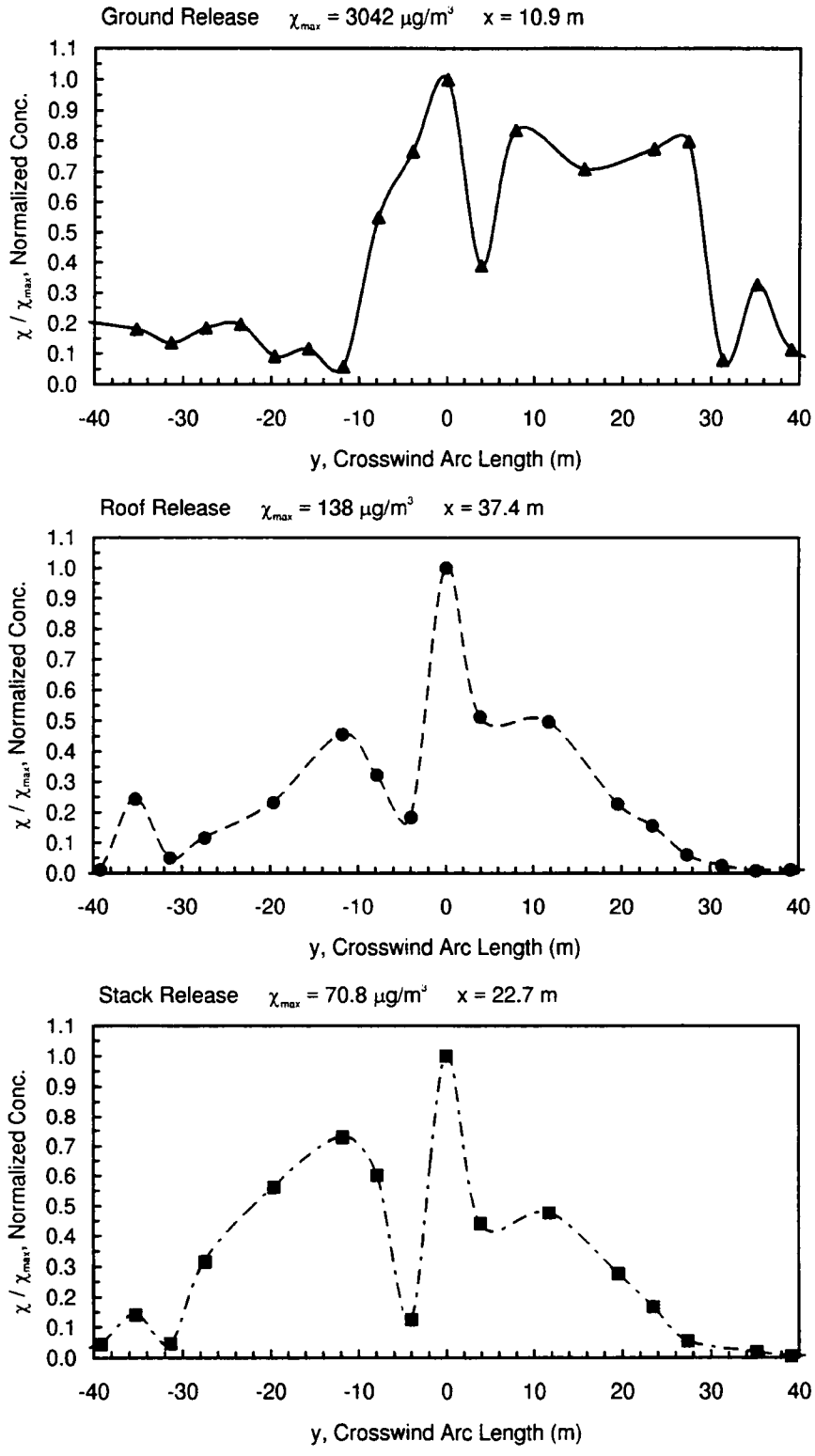


FIGURE 4.24 Crosswind Concentration Distributions Within the Cavity Region of the EOCR Building During Tracer Gas Release Test #7

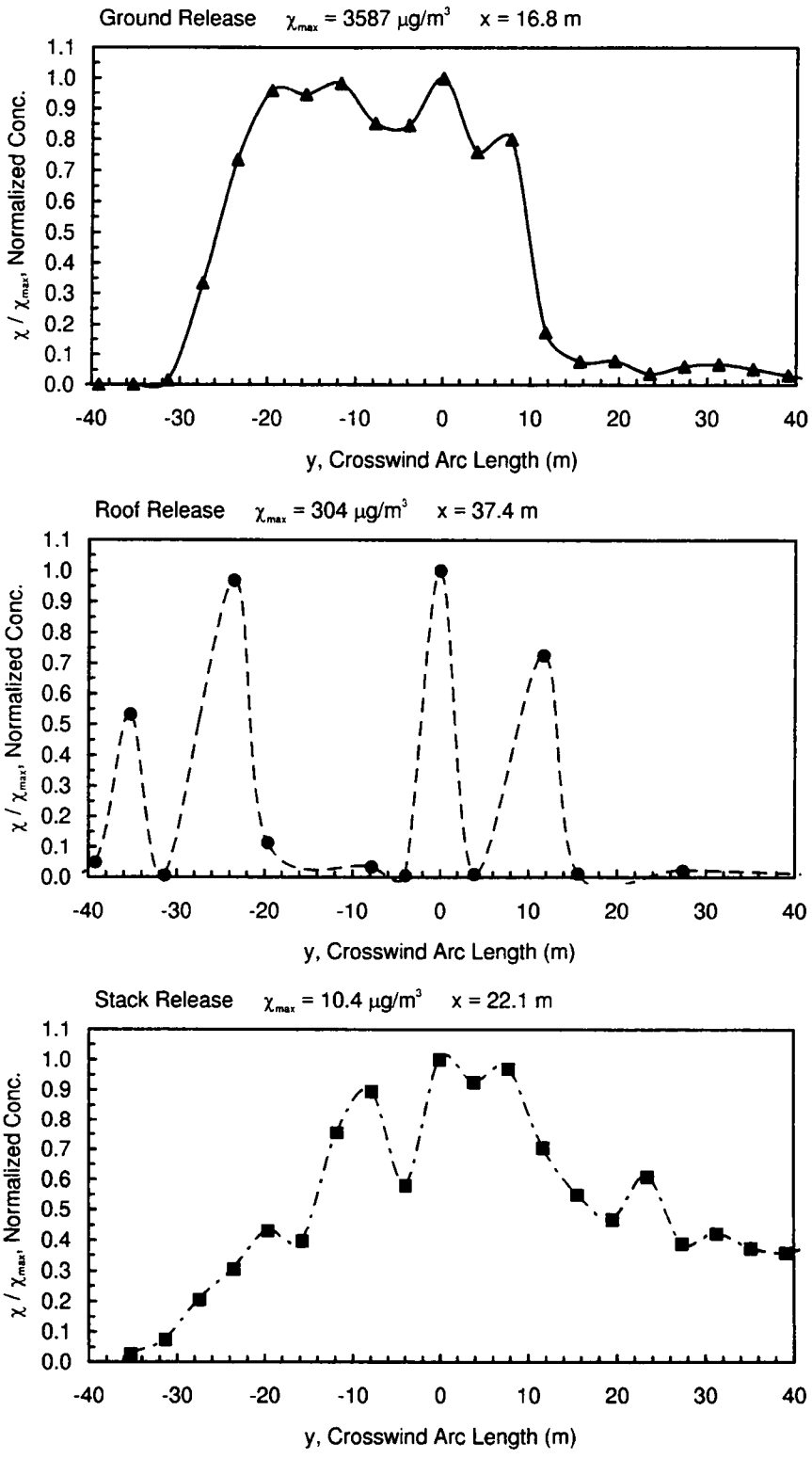


FIGURE 4.25 Crosswind Concentration Distributions Within the Cavity Region of the EOCR Building During Tracer Gas Release Test #8

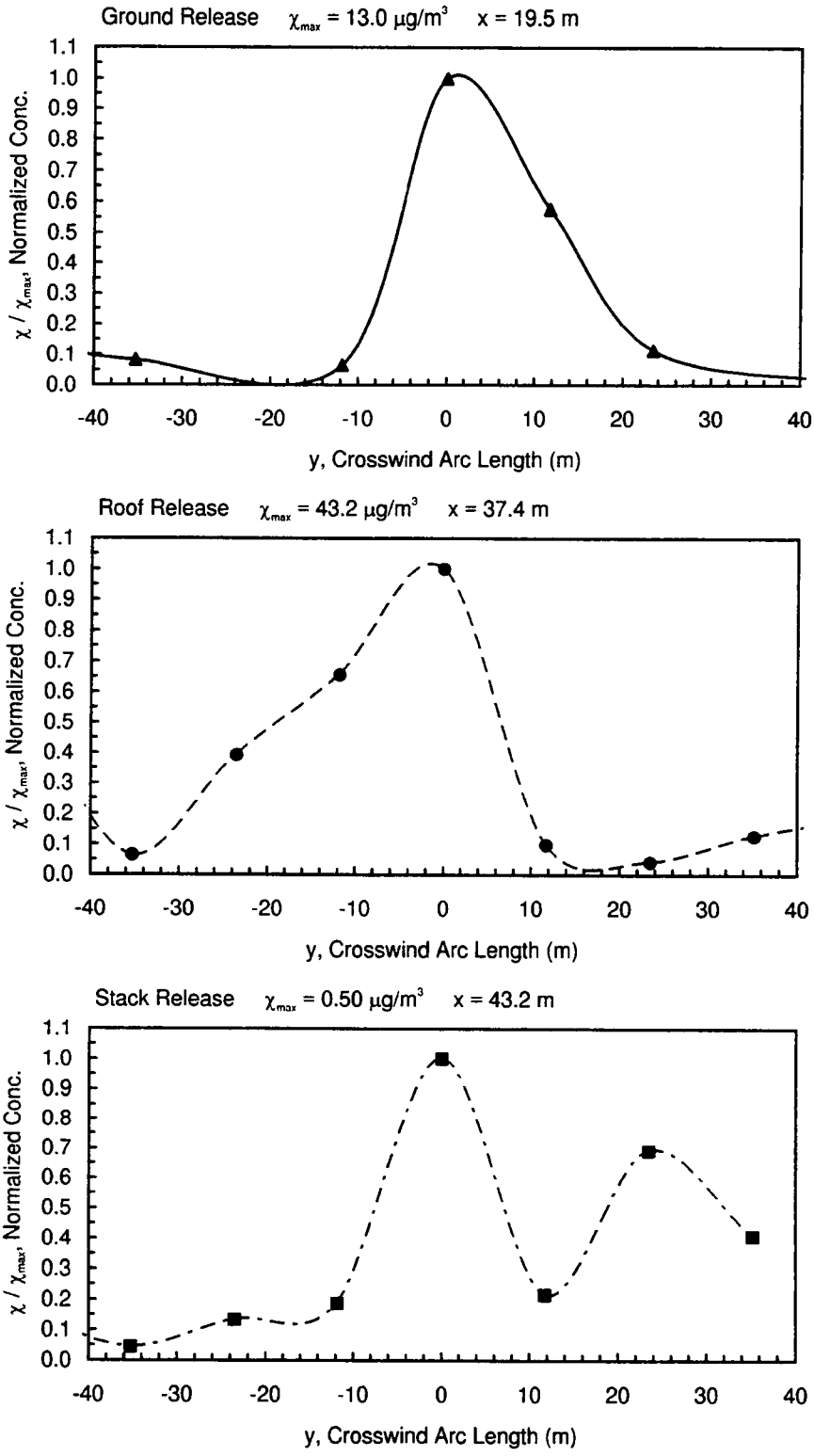


FIGURE 4.26 Crosswind Concentration Distributions Within the Cavity Region of the EOCR Building During Tracer Gas Release Test #11

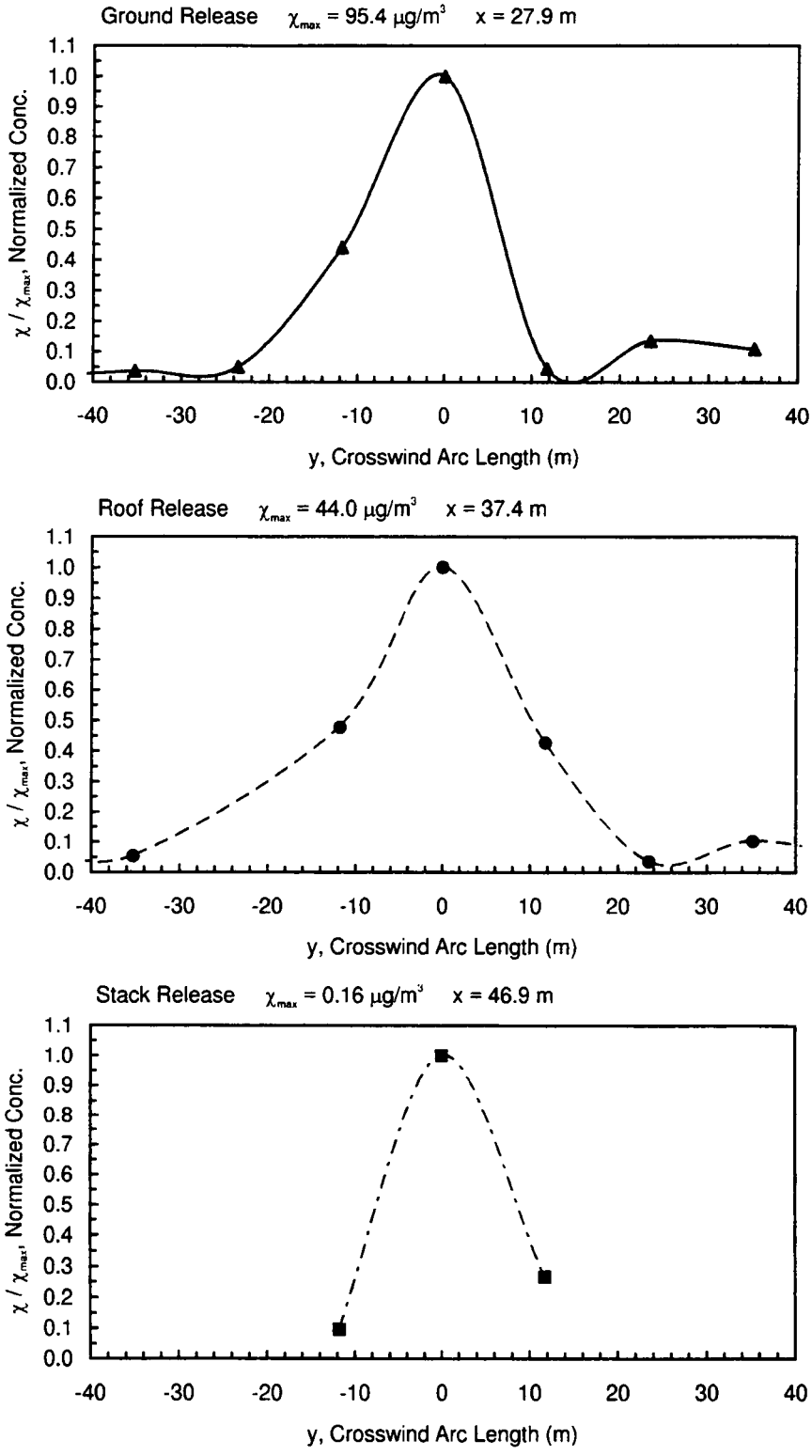


FIGURE 4.27 Crosswind Concentration Distributions Within the Cavity Region of the EOCR Building During Tracer Gas Release Test #12

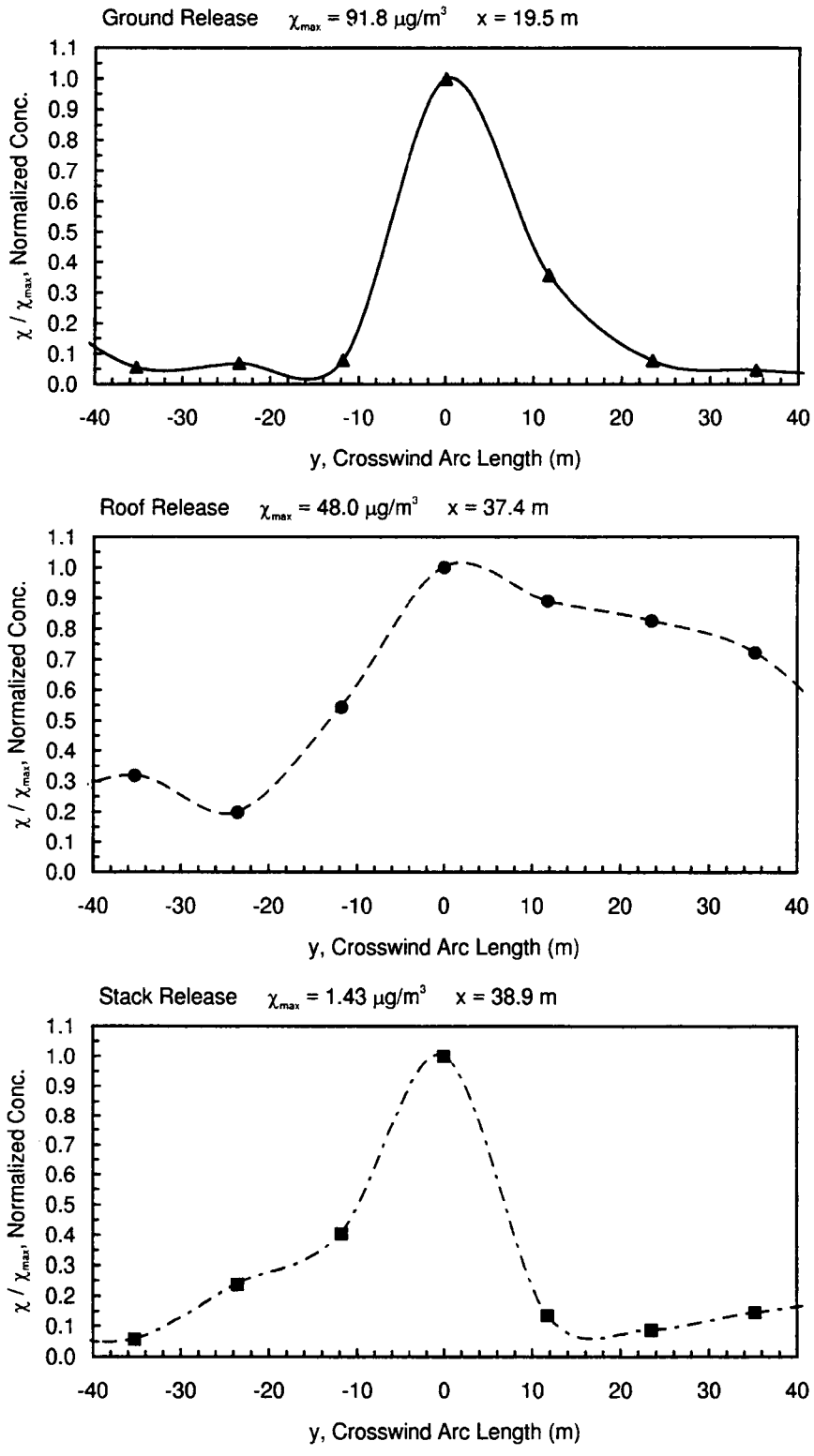


FIGURE 4.28 Crosswind Concentration Distributions Within the Cavity Region of the EOCR Building During Tracer Gas Release Test #13

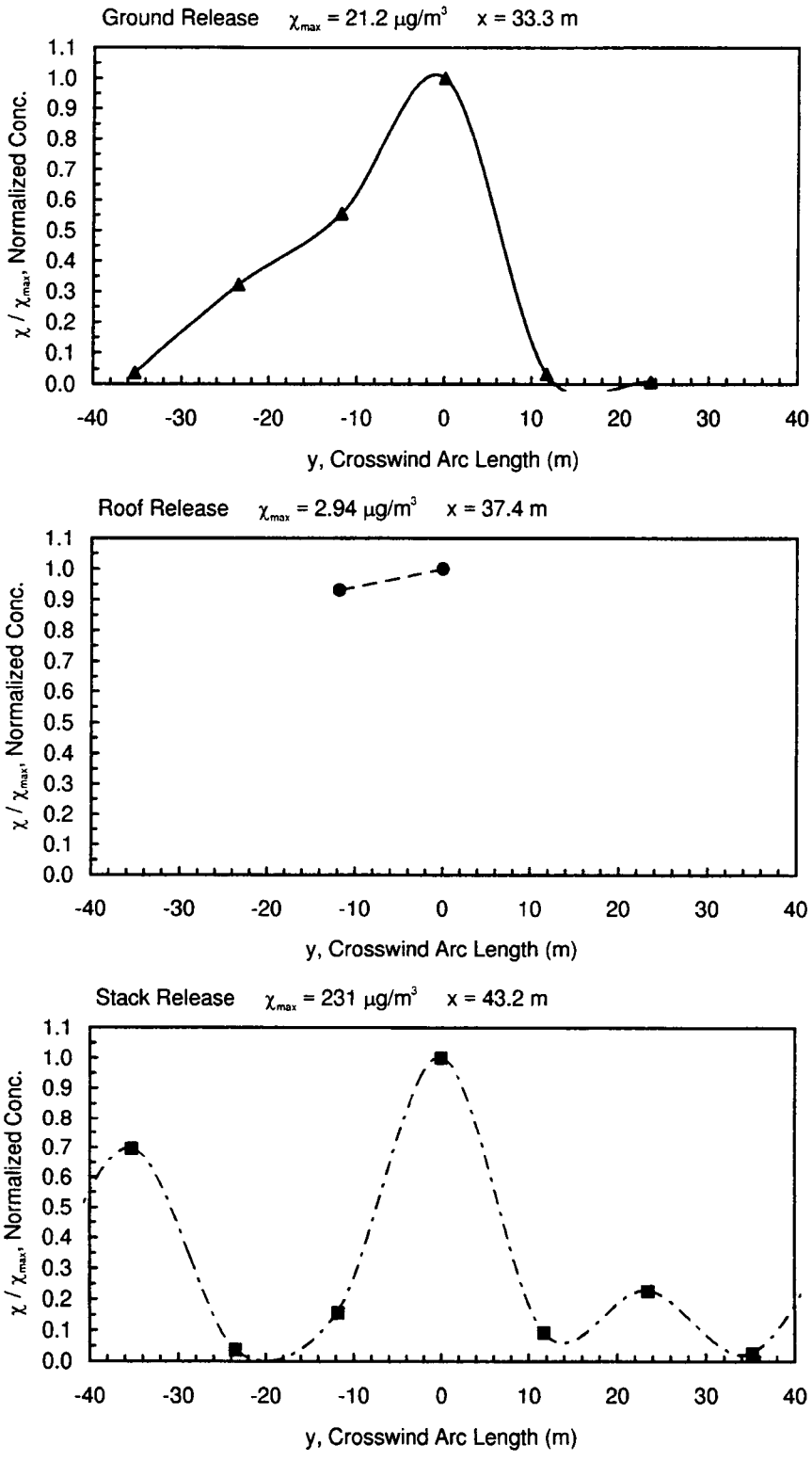


FIGURE 4.29 Crosswind Concentration Distributions Within the Cavity Region of the EOCR Building During Tracer Gas Release Test #14

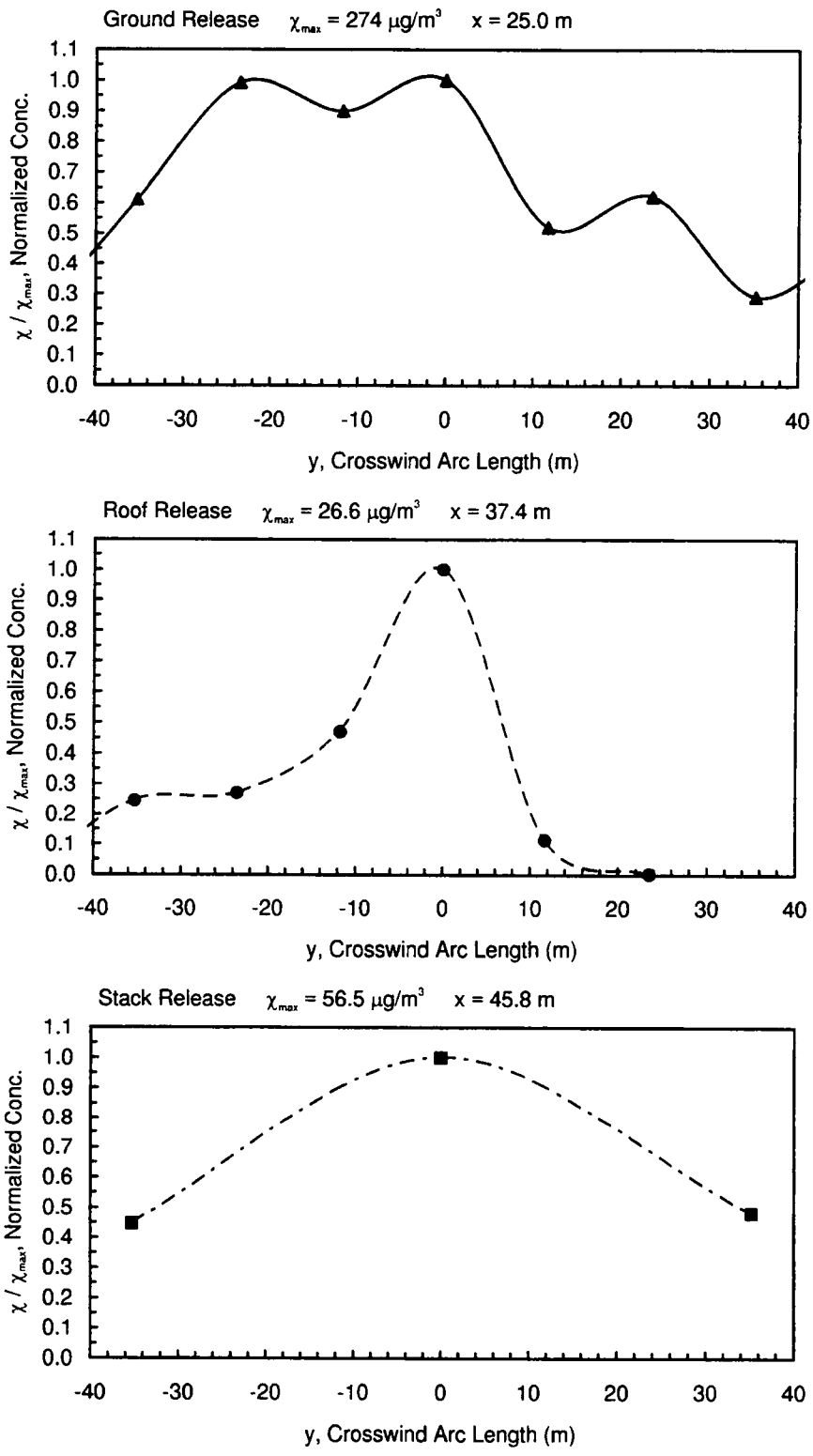


FIGURE 4.30 Crosswind Concentration Distributions Within the Cavity Region of the EOCR Building During Tracer Gas Release Test #15

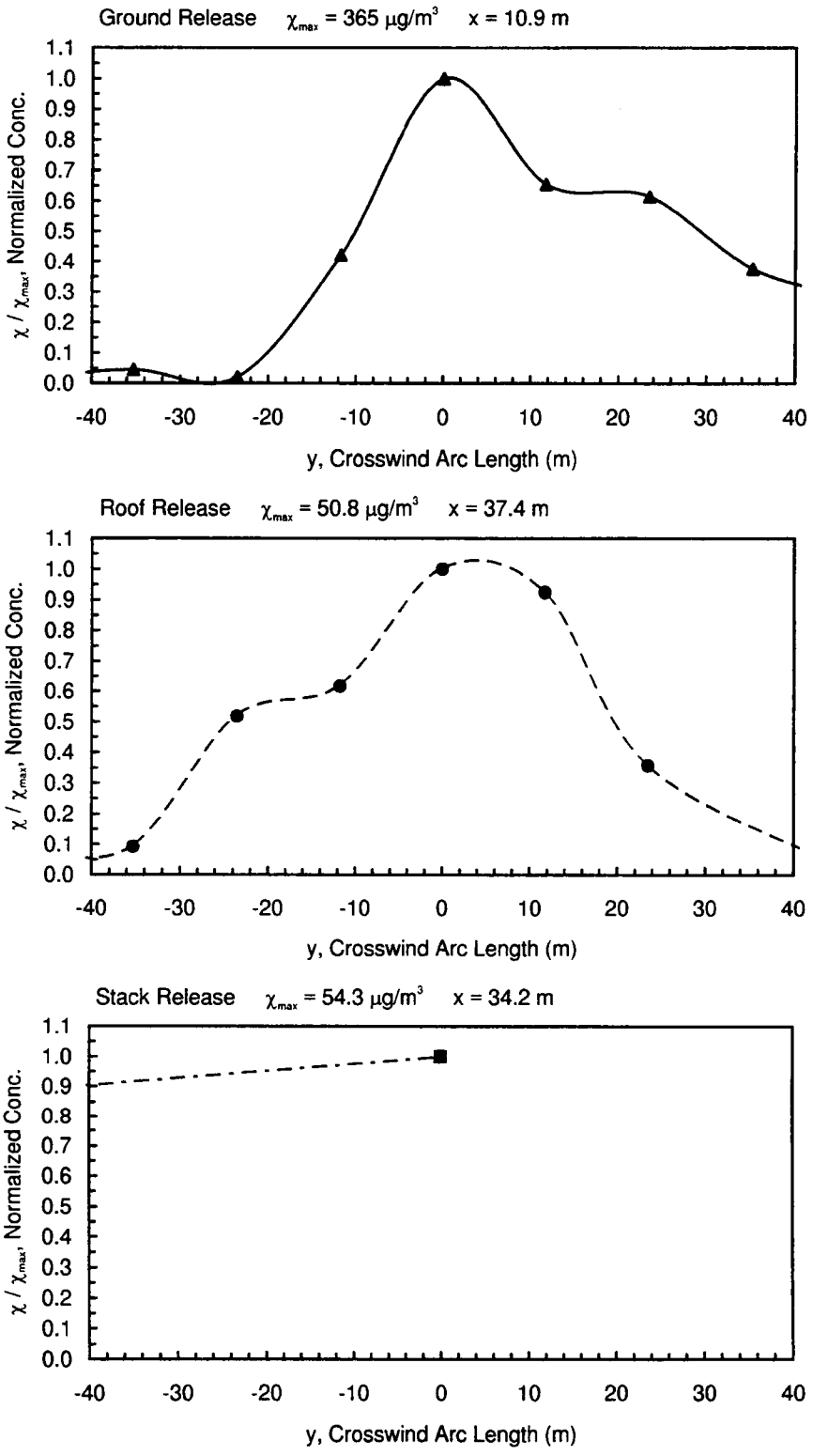


FIGURE 4.31 Crosswind Concentration Distributions Within the Cavity Region of the EOCR Building During Tracer Gas Release Test #16

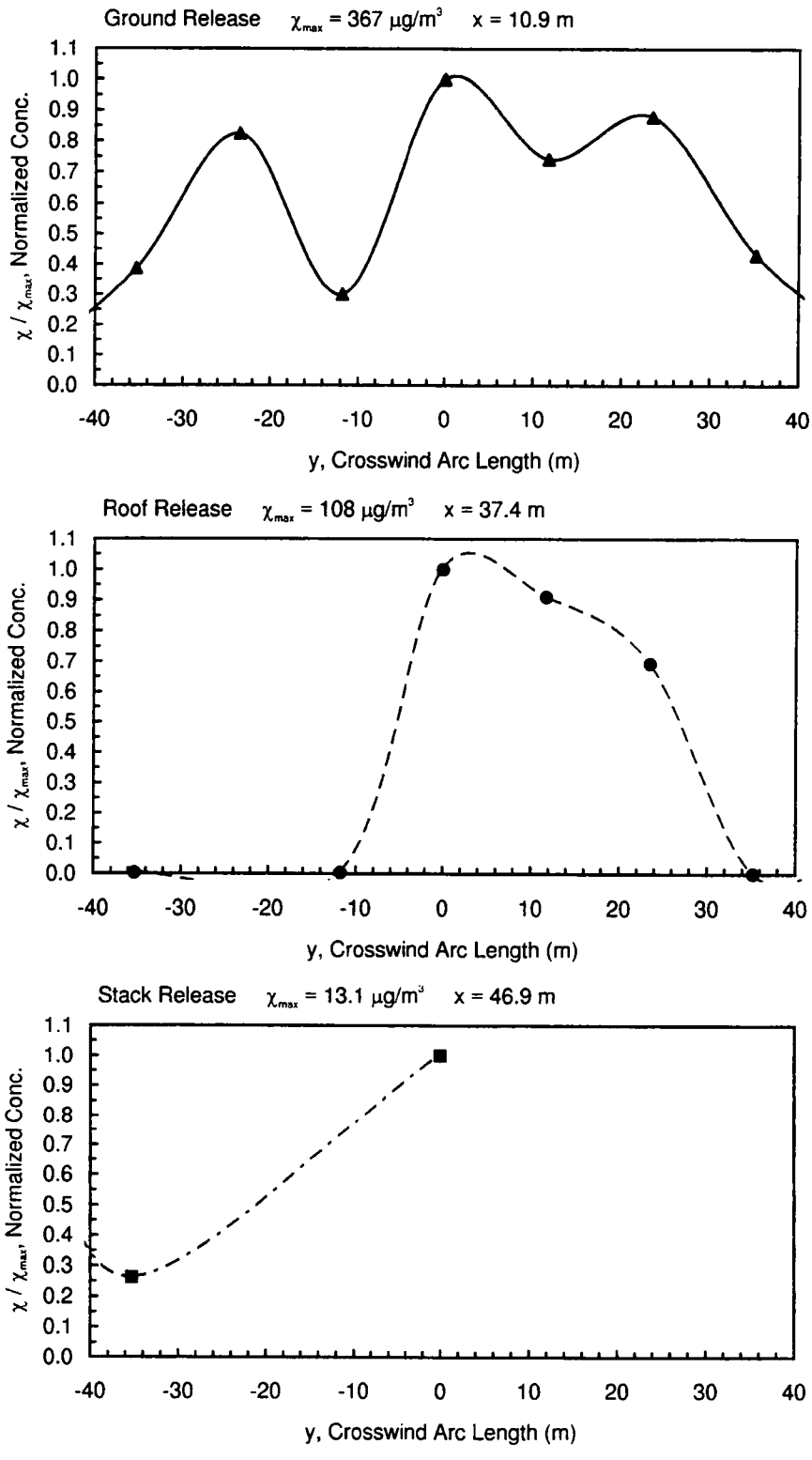


FIGURE 4.32 Crosswind Concentration Distributions Within the Cavity Region of the EOCR Building During Tracer Gas Release Test #17

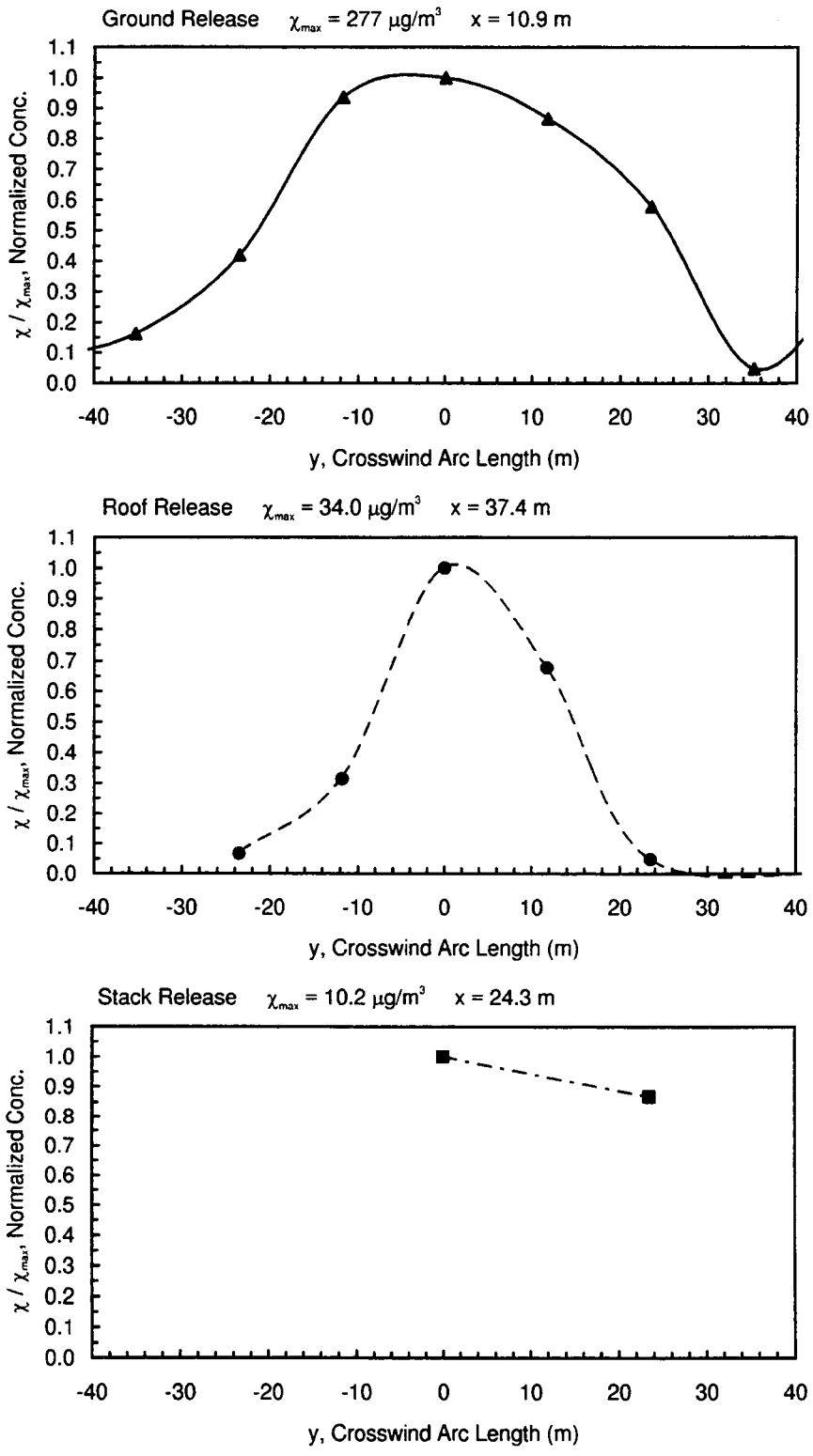


FIGURE 4.33 Crosswind Concentration Distributions Within the Cavity Region of the EOCR Building During Tracer Gas Release Test #18

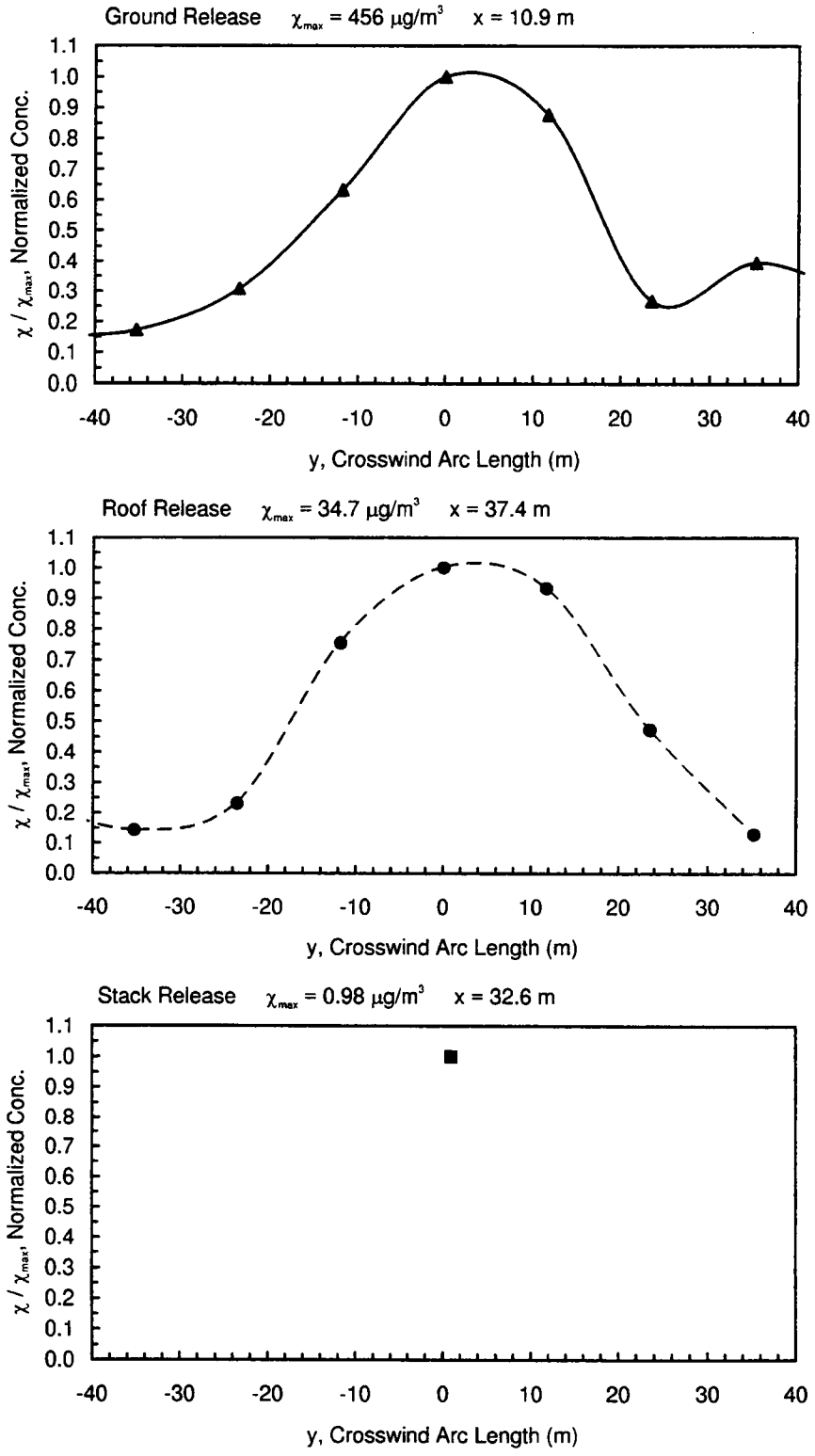


FIGURE 4.34 Crosswind Concentration Distributions Within the Cavity Region of the EOCR Building During Tracer Gas Release Test #19

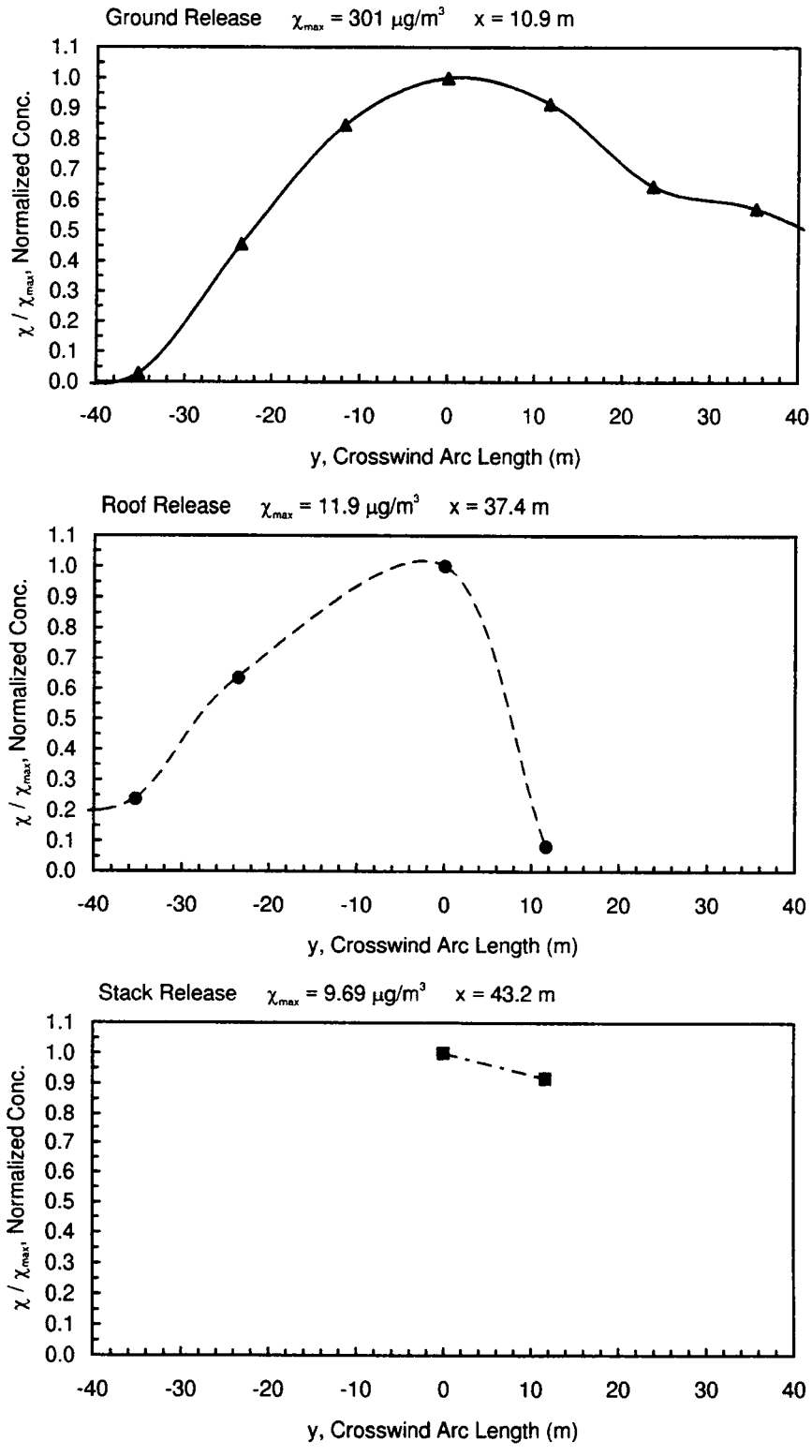


FIGURE 4.35 Crosswind Concentration Distributions Within the Cavity Region of the EOCR Building During Tracer Gas Release Test #20

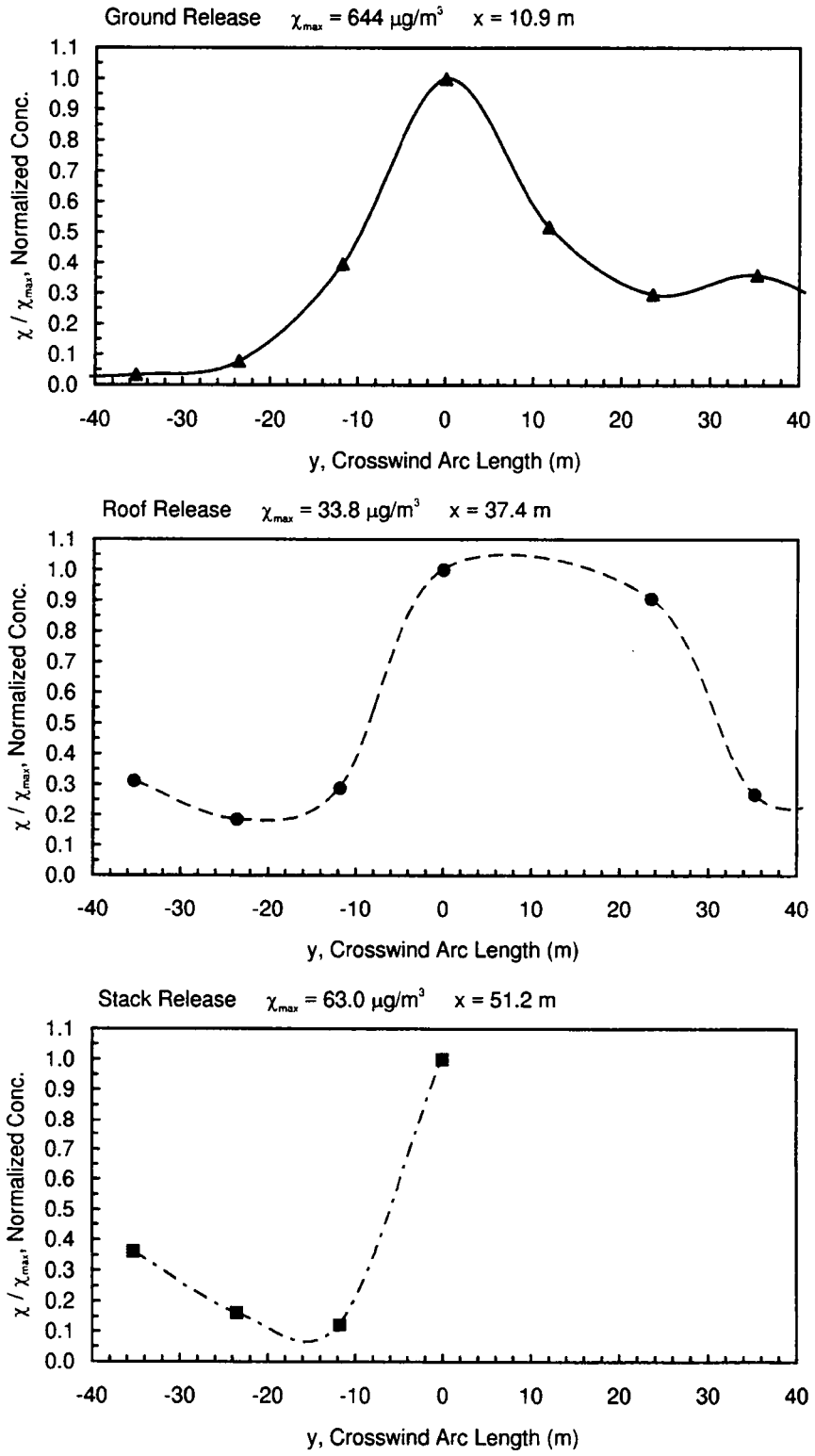


FIGURE 4.36 Crosswind Concentration Distributions Within the Cavity Region of the EOCR Building During Tracer Gas Release Test #21

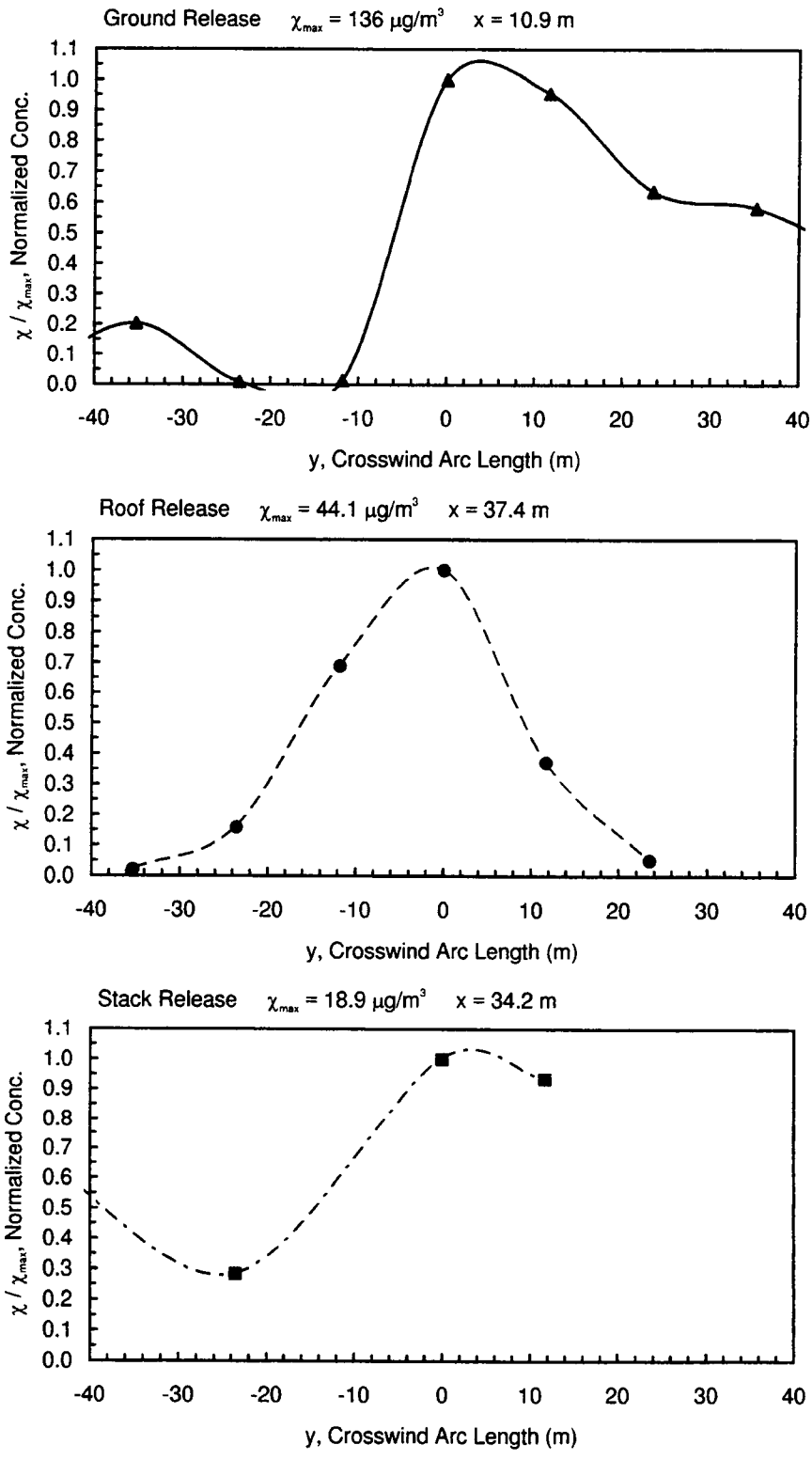


FIGURE 4.37 Crosswind Concentration Distributions Within the Cavity Region of the EOCR Building During Tracer Gas Release Test #22

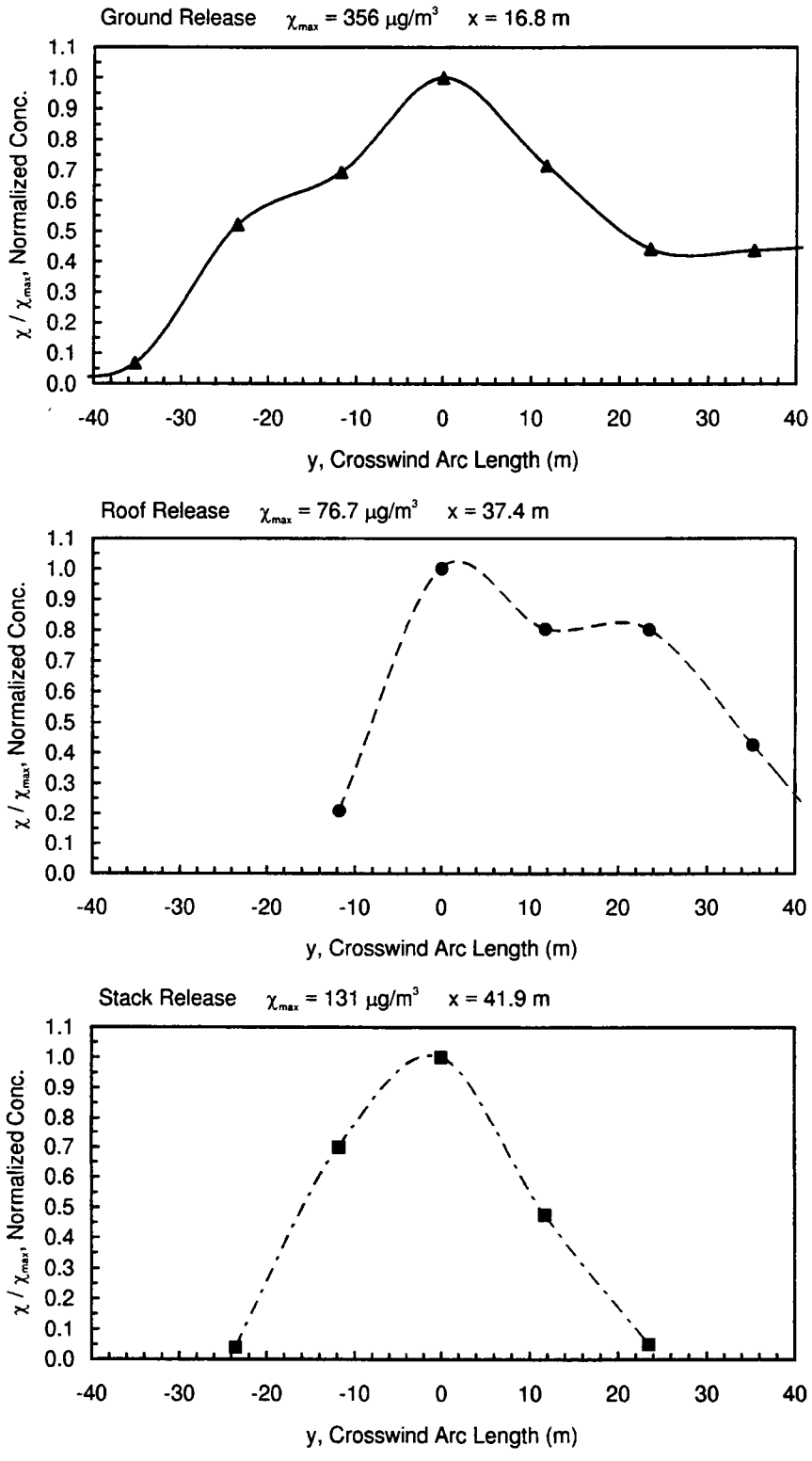


FIGURE 4.38 Crosswind Concentration Distributions Within the Cavity Region of the EOCR Building During Tracer Gas Release Test #23

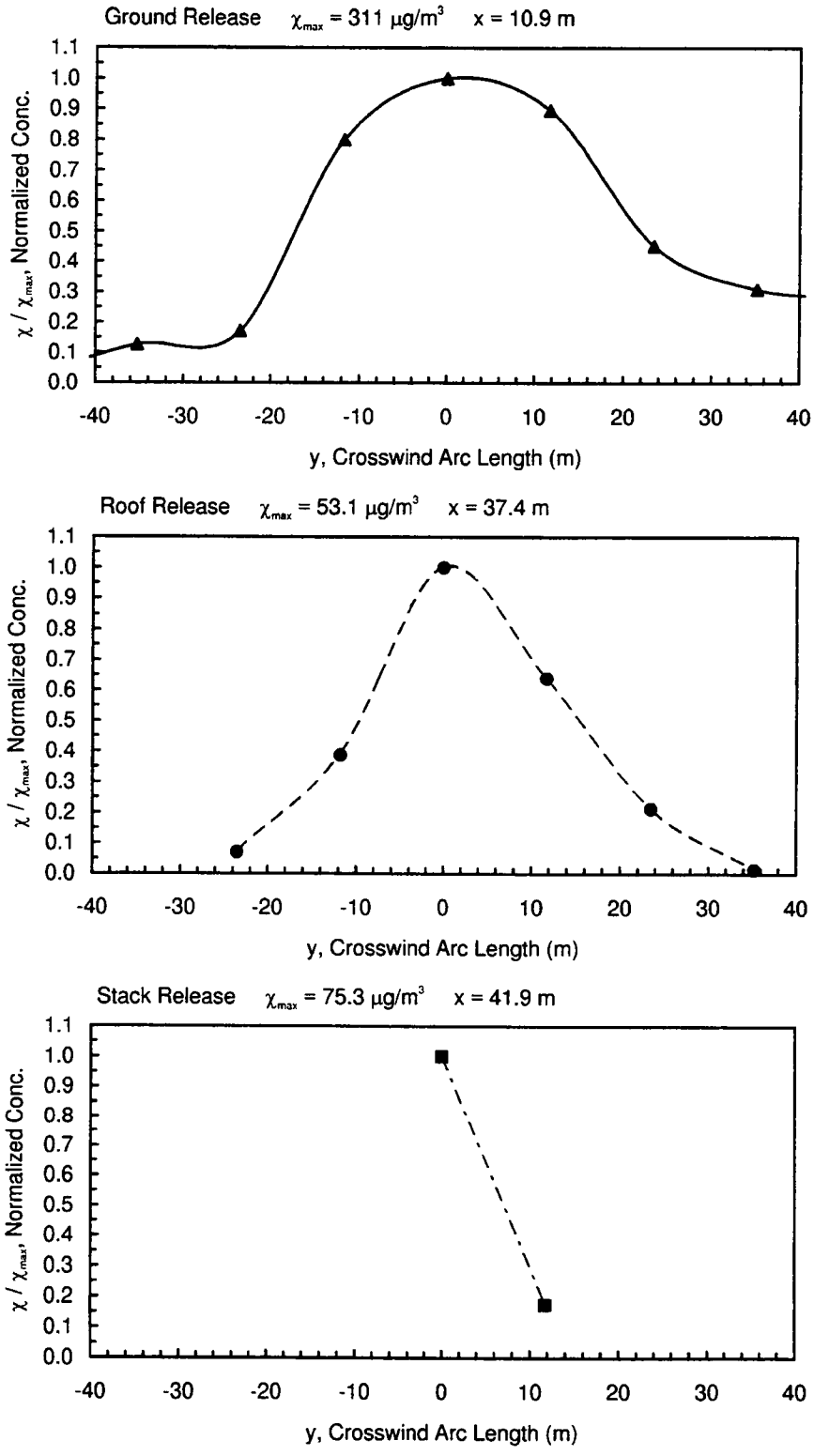


FIGURE 4.39 Crosswind Concentration Distributions Within the Cavity Region of the EOCR Building During Tracer Gas Release Test #24

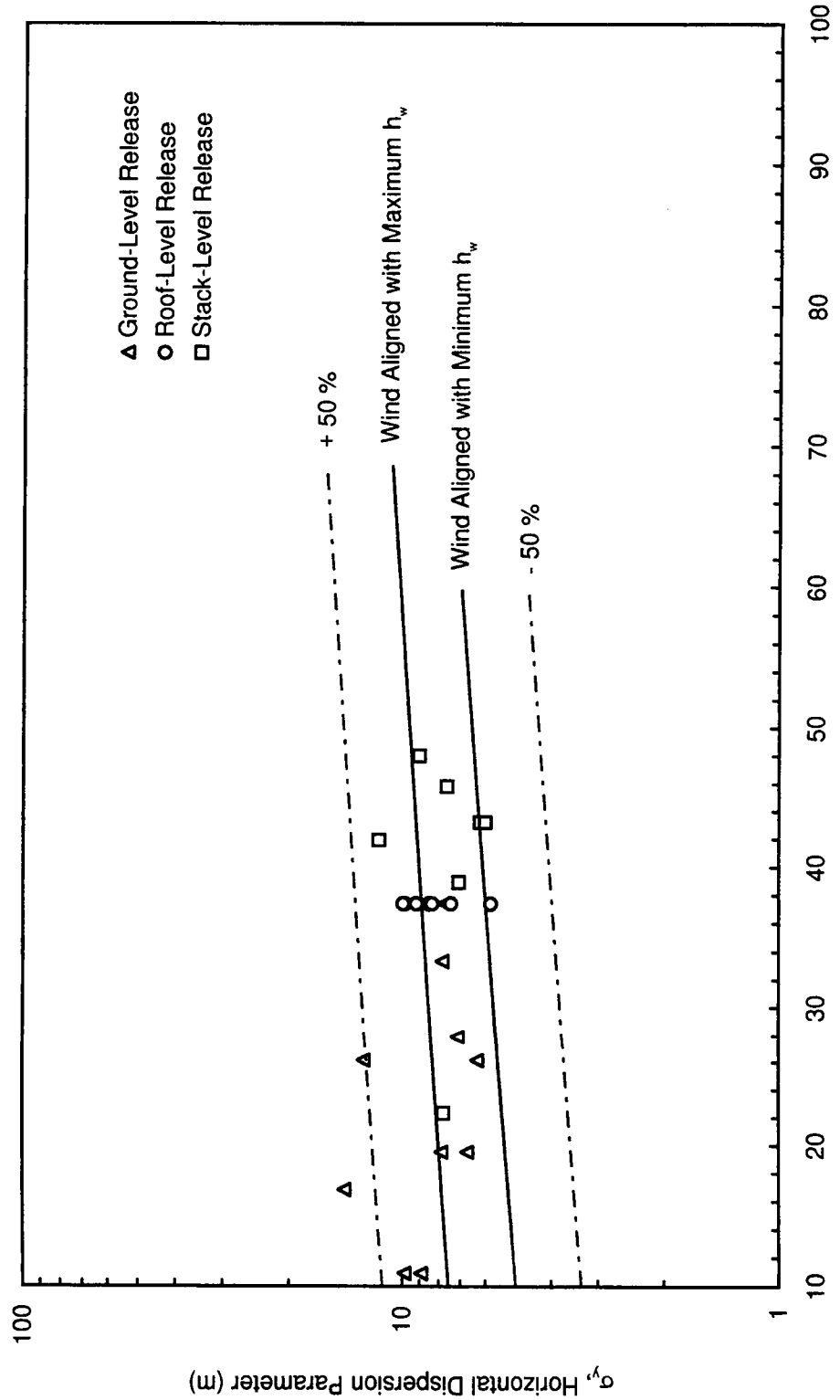


FIGURE 4.40 Observed σ_y Values During the EOCR Tracer Gas Release Experiment

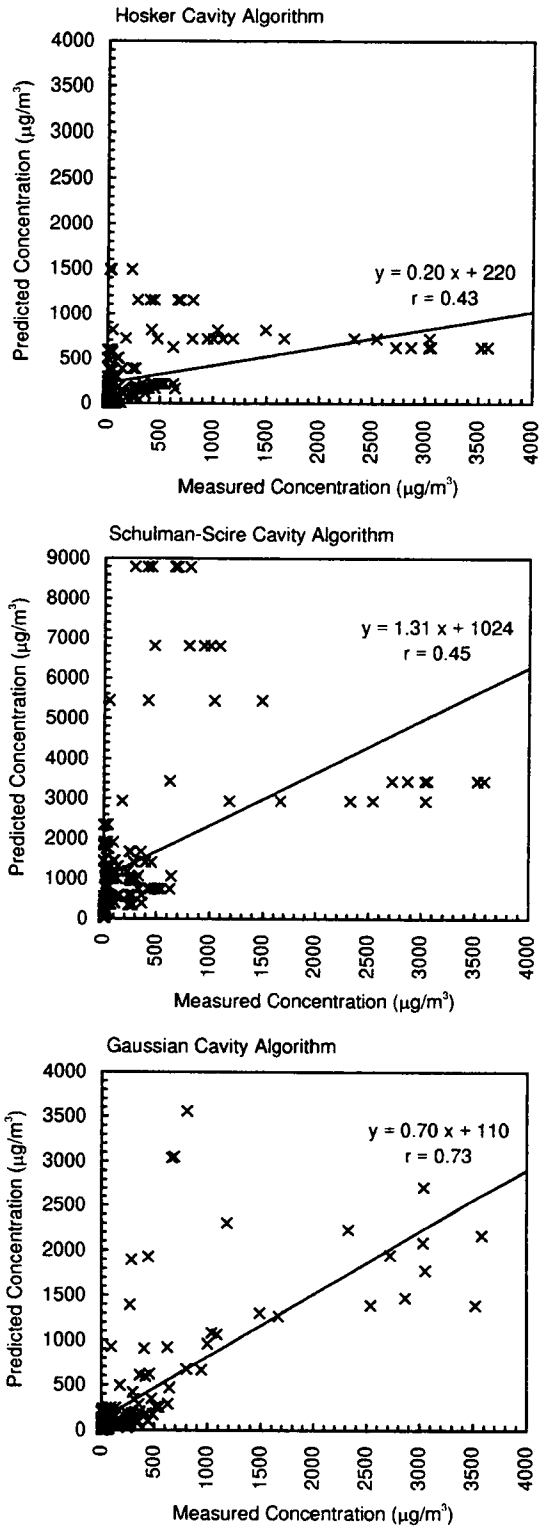


FIGURE 4.41 Scatter Diagrams of Measured Versus Predicted Concentrations Within the Cavity Region of the EOCR Building, All Data

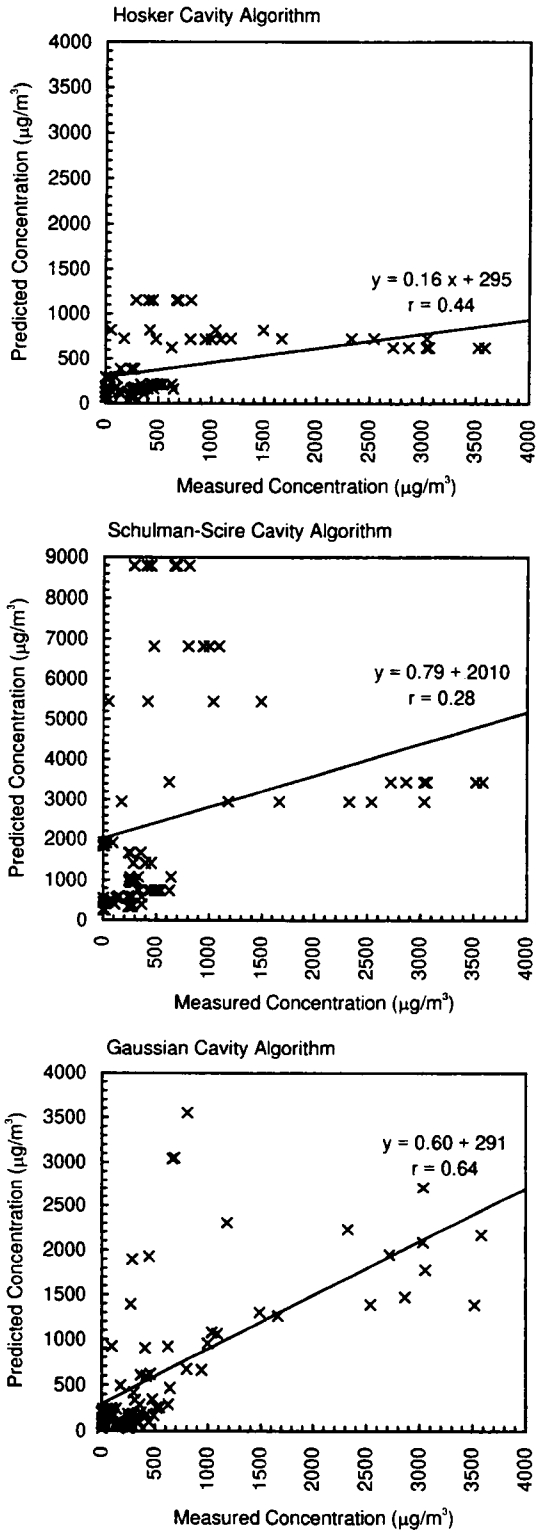


FIGURE 4.42 Scatter Diagrams of Measured Versus Predicted Concentrations Within the Cavity Region of the EOCR Building, Ground-Level Release

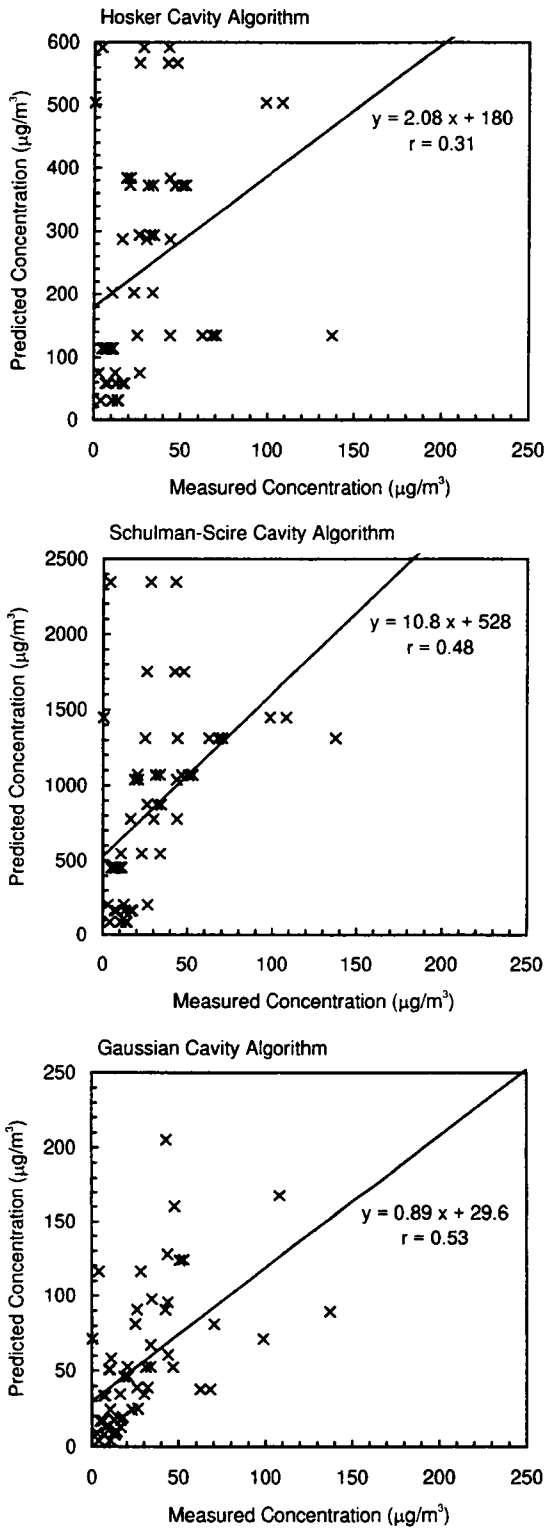


FIGURE 4.43 Scatter Diagrams of Measured Versus Predicted Concentrations Within the Cavity Region of the EOCR Building, Roof-Level Release

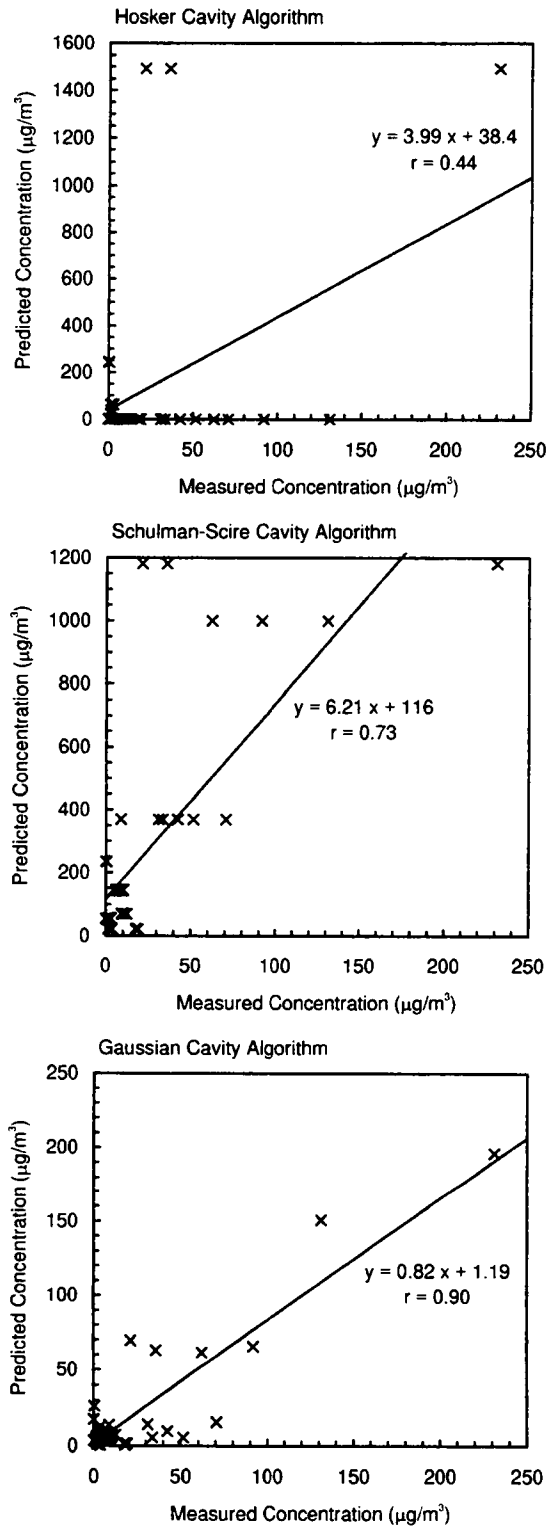


FIGURE 4.44 Scatter Diagrams of Measured Versus Predicted Concentrations Within the Cavity Region of the EOCR Building, Stack-Level Release

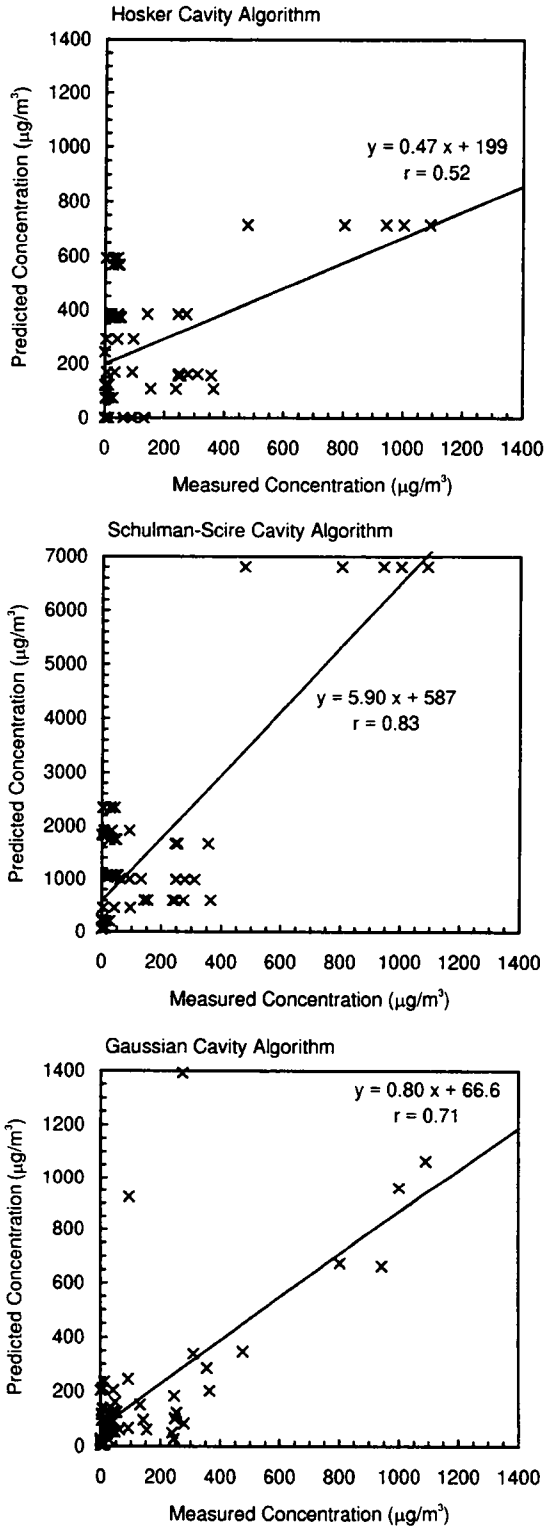


FIGURE 4.45 Scatter Diagrams of Measured Versus Predicted Concentrations Within the Cavity Region of the EOCR Building, Unstable Atmosphere

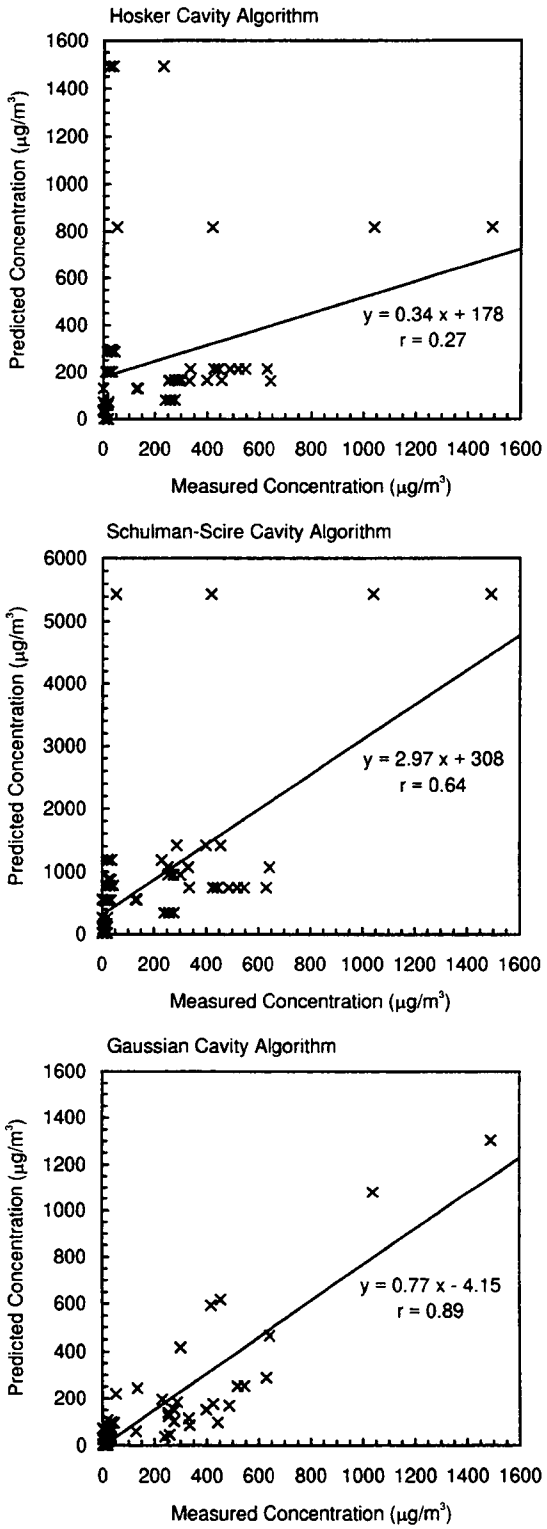


FIGURE 4.46 Scatter Diagrams of Measured Versus Predicted Concentrations Within the Cavity Region of the EOCR Building, Neutral Atmosphere

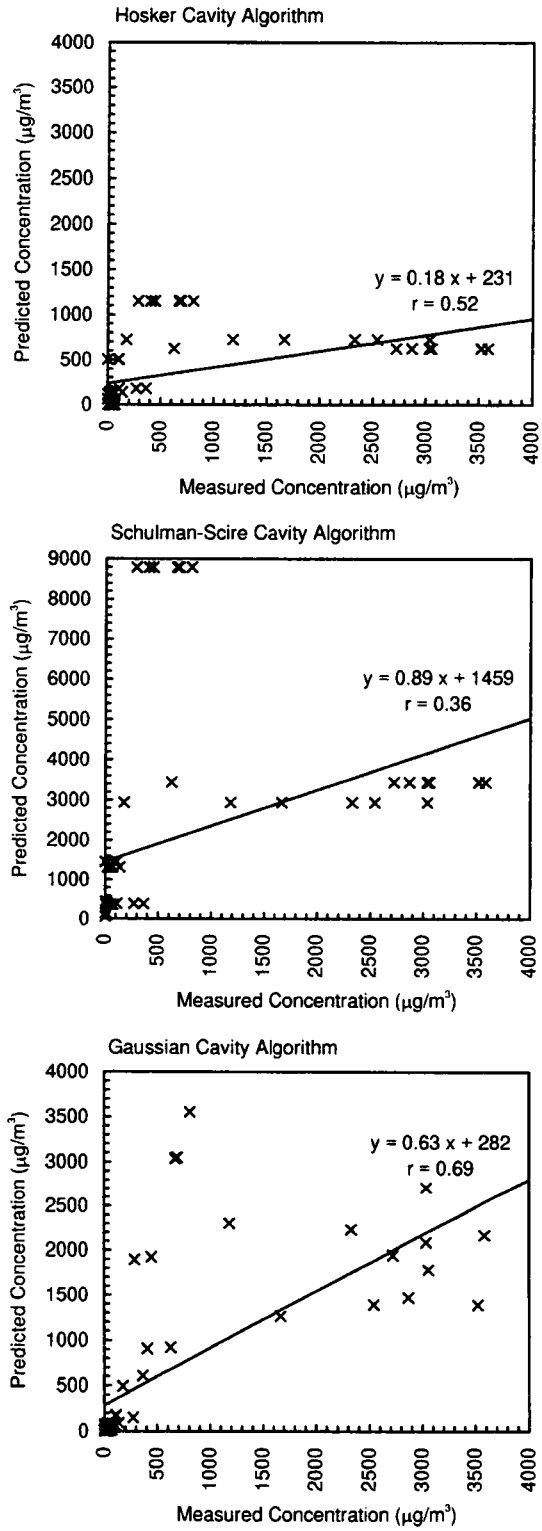


FIGURE 4.47 Scatter Diagrams of Measured Versus Predicted Concentrations Within the Cavity Region of the EOCR Building, Stable Atmosphere

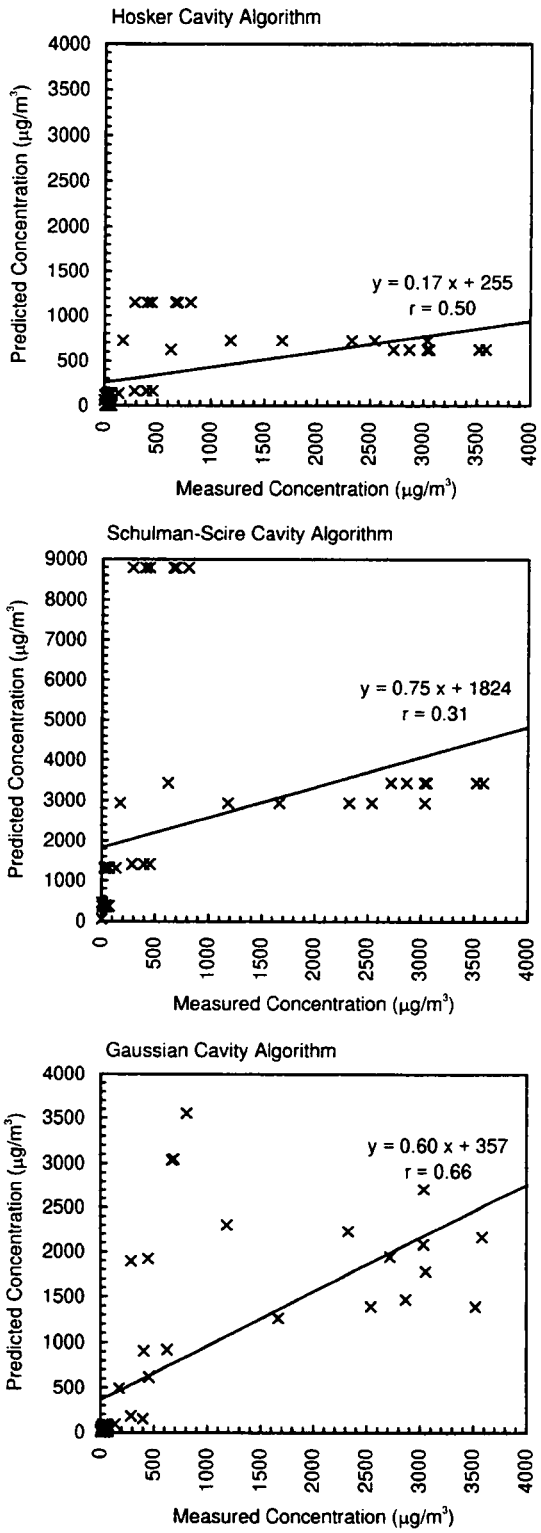


FIGURE 4.48 Scatter Diagrams of Measured Versus Predicted Concentrations Within the Cavity Region of the EOCR Building, $u_h \leq 1.0$ m/s

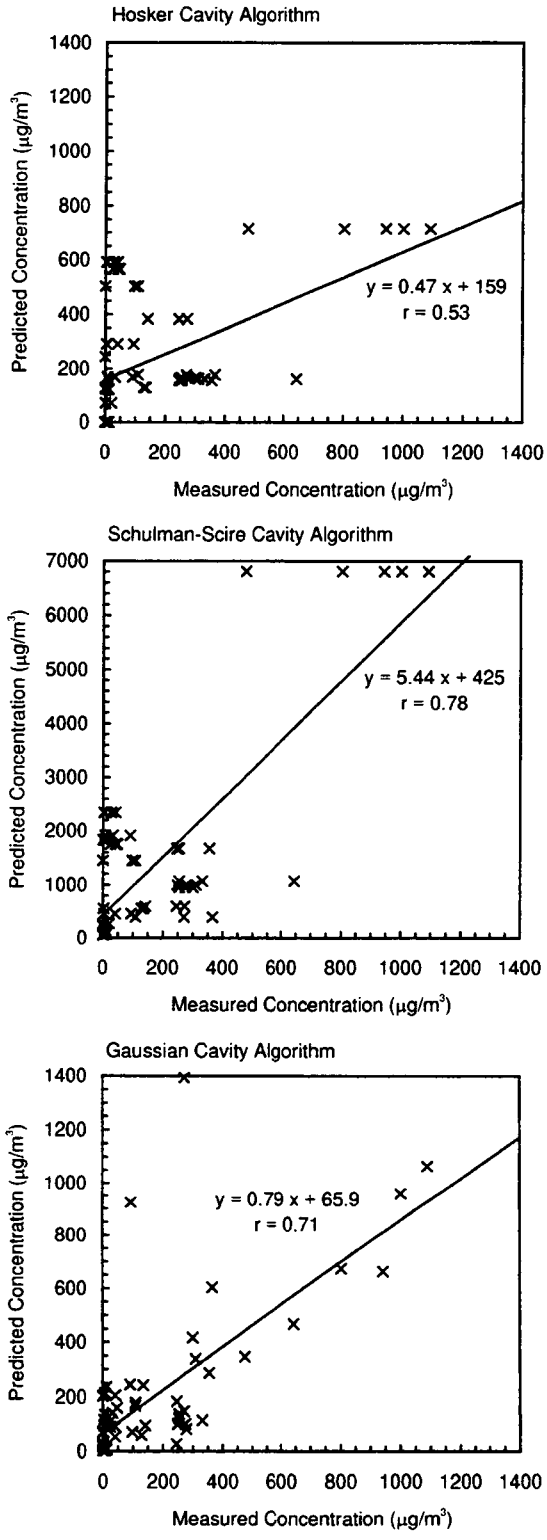


FIGURE 4.49 Scatter Diagrams of Measured Versus Predicted Concentrations Within the Cavity Region of the EOCR Building, 1.0 m/s $\leq u_h <$ 3.0 m/s

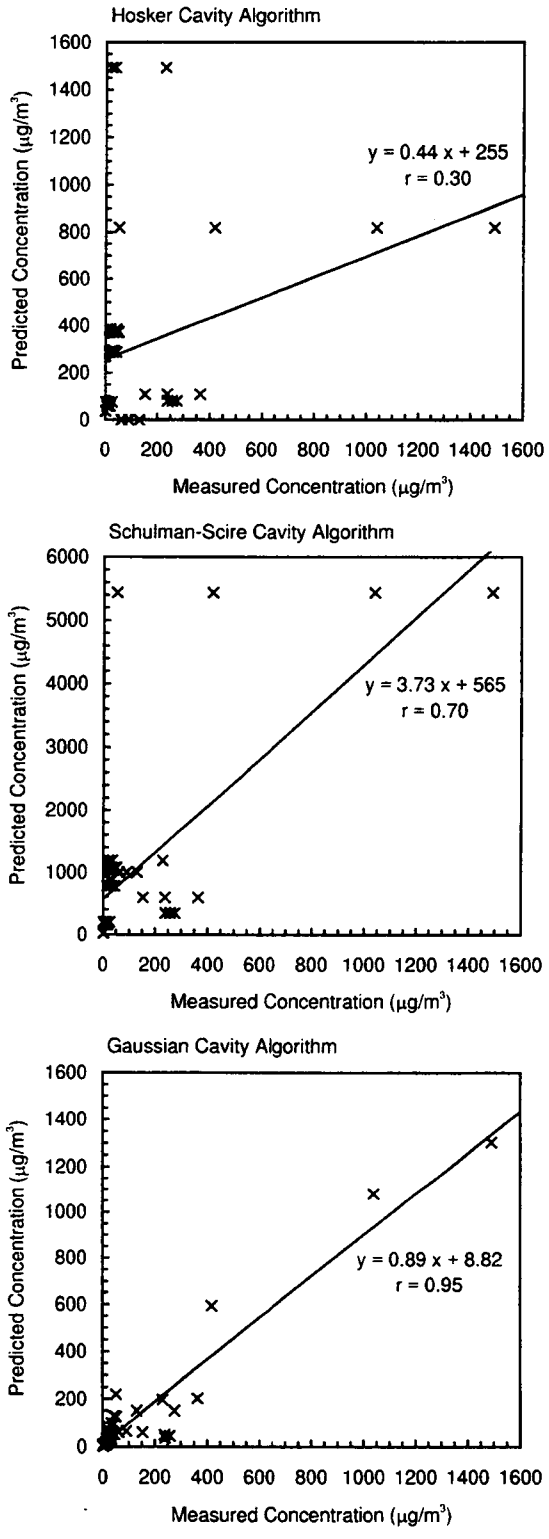


FIGURE 4.50 Scatter Diagrams of Measured Versus Predicted Concentrations Within the Cavity Region of the EOCR Building, 3.0 m/s $\leq u_h <$ 5.0 m/s

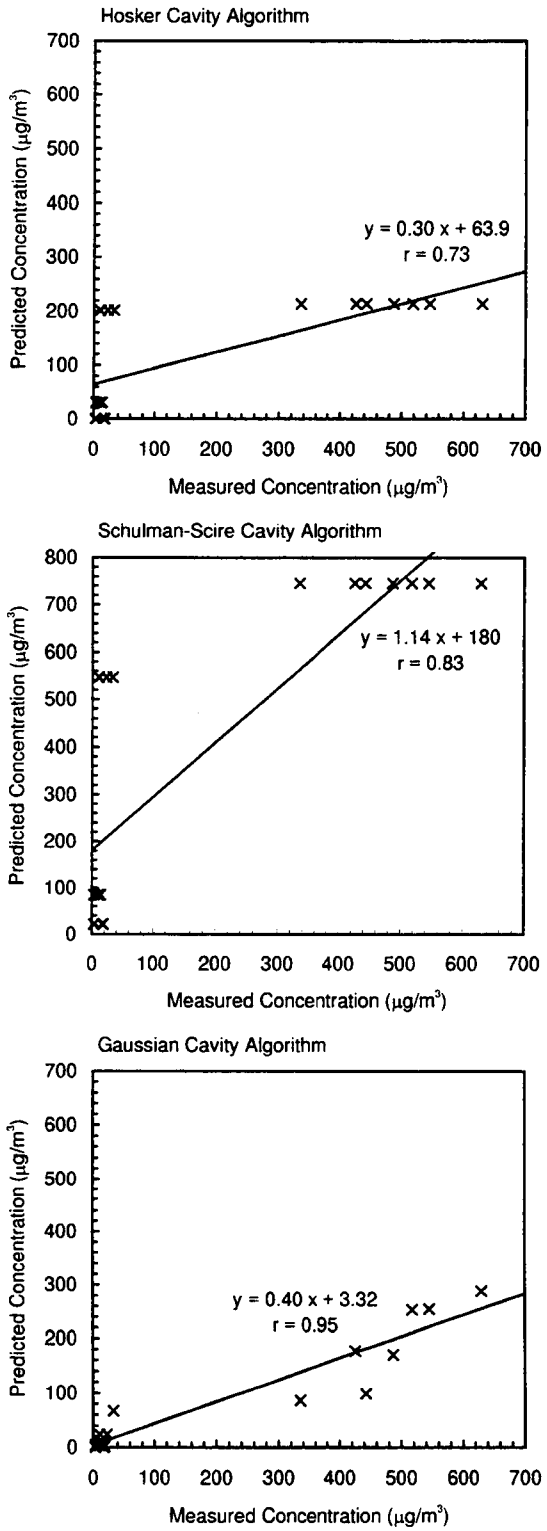


FIGURE 4.51 Scatter Diagrams of Measured Versus Predicted Concentrations Within the Cavity Region of the EOCR Building, 5.0 m/s < u_h

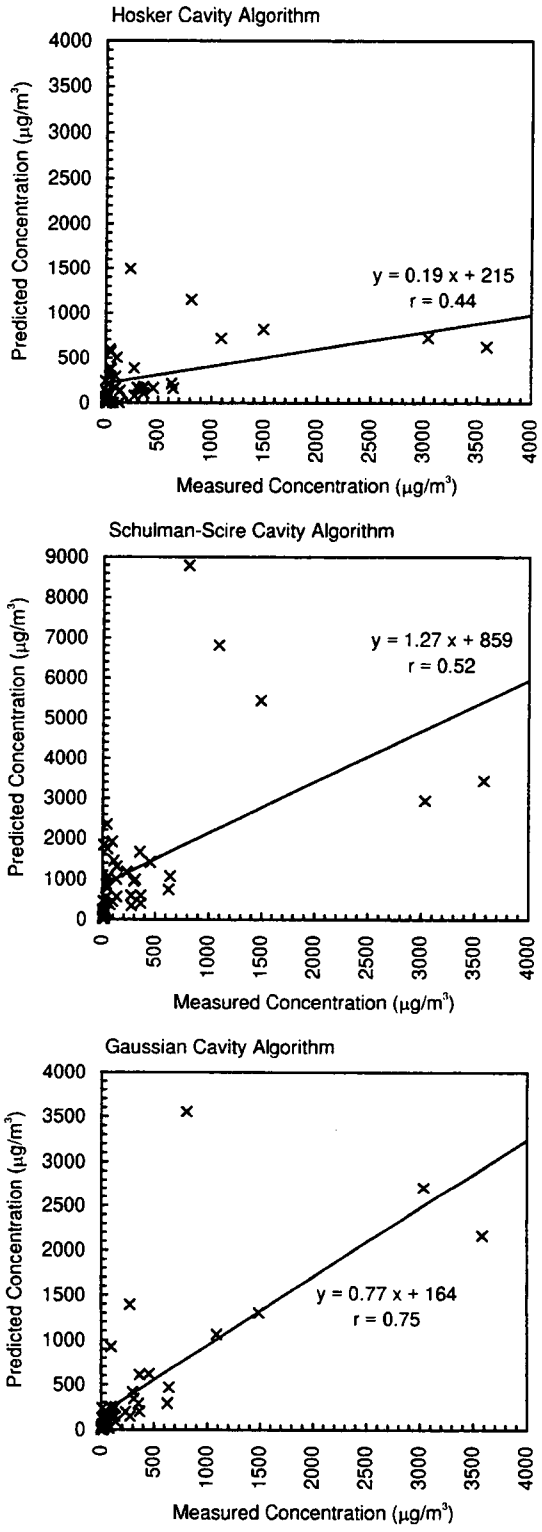


FIGURE 4.52 Scatter Diagrams of Measured Versus Predicted Concentrations Within the Cavity Region of the EOCR Building, Plume Centerline Locations

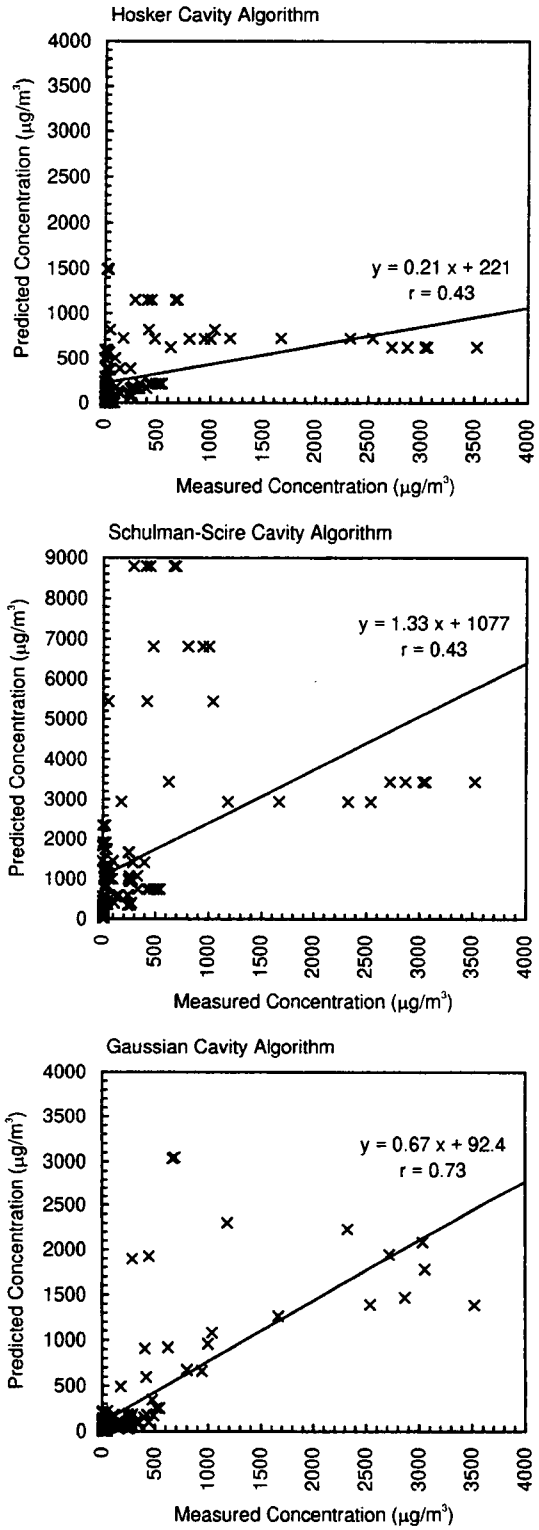


FIGURE 4.53 Scatter Diagrams of Measured Versus Predicted Concentrations Within the Cavity Region of the EOCR Building, Crosswind Locations

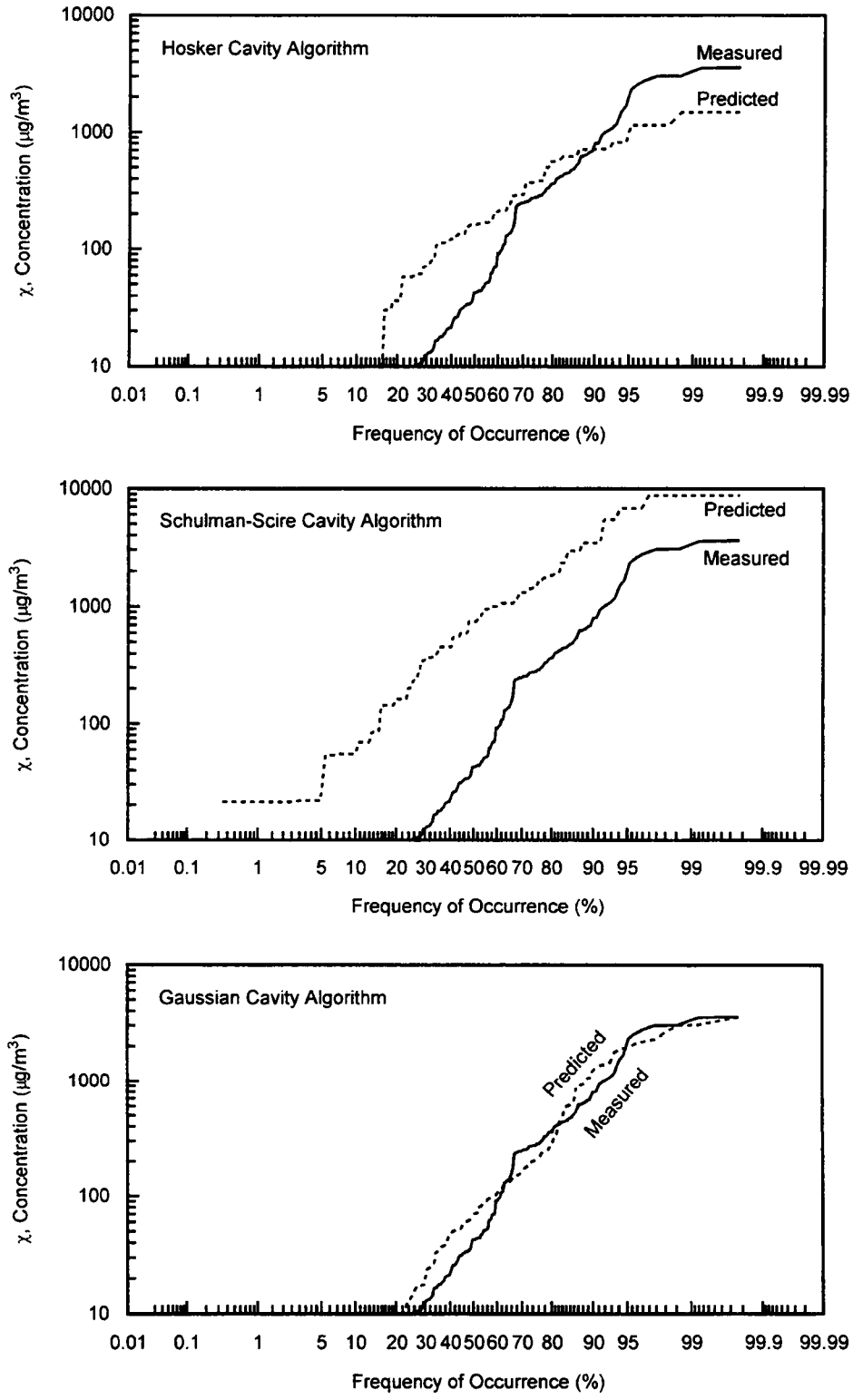


FIGURE 4.54 Cumulative Frequency Distributions of Measured and Predicted Concentrations Within the Cavity, All Data

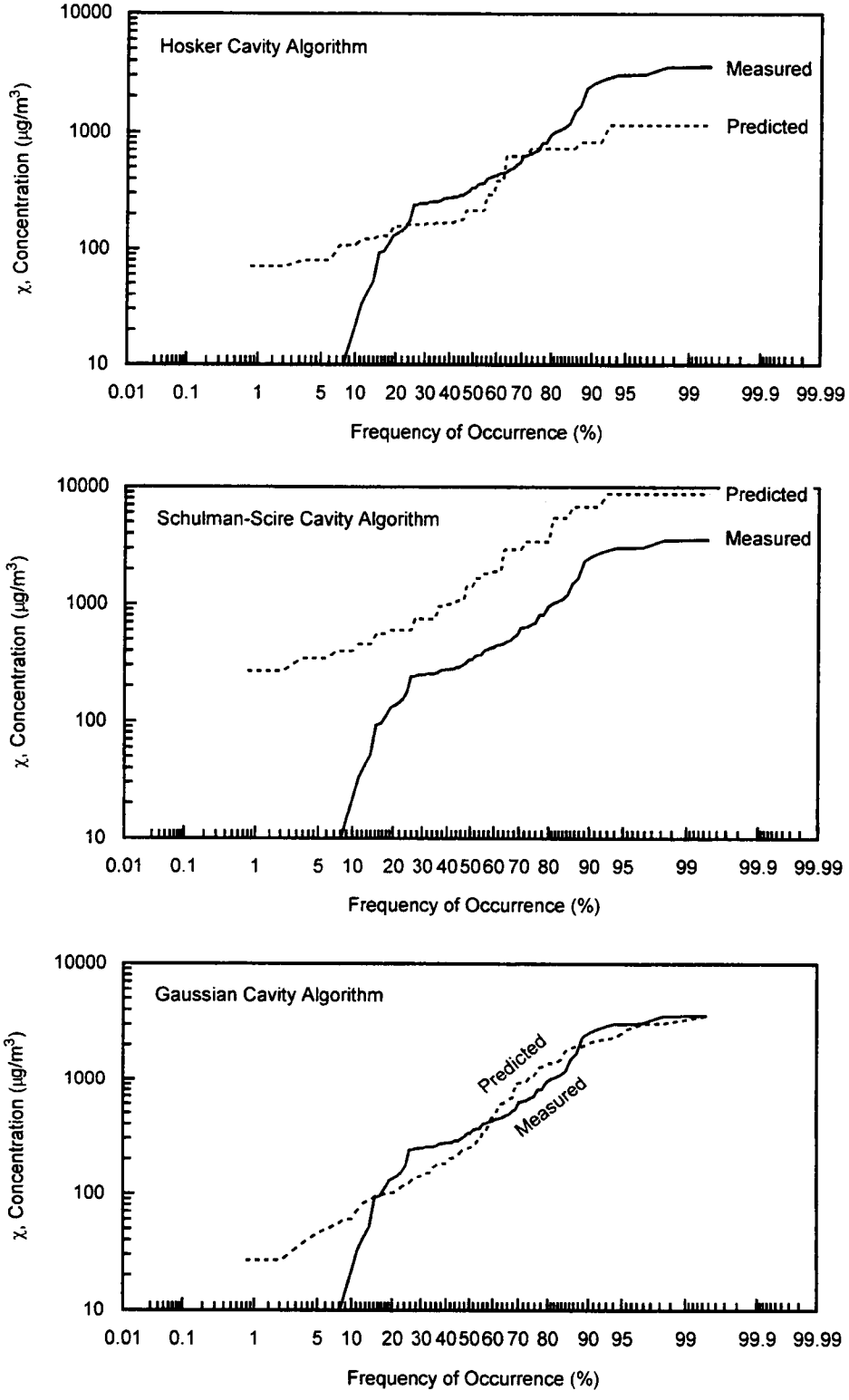


FIGURE 4.55 Cumulative Frequency Distributions of Measured and Predicted Concentrations Within the Cavity, Ground-Level Release

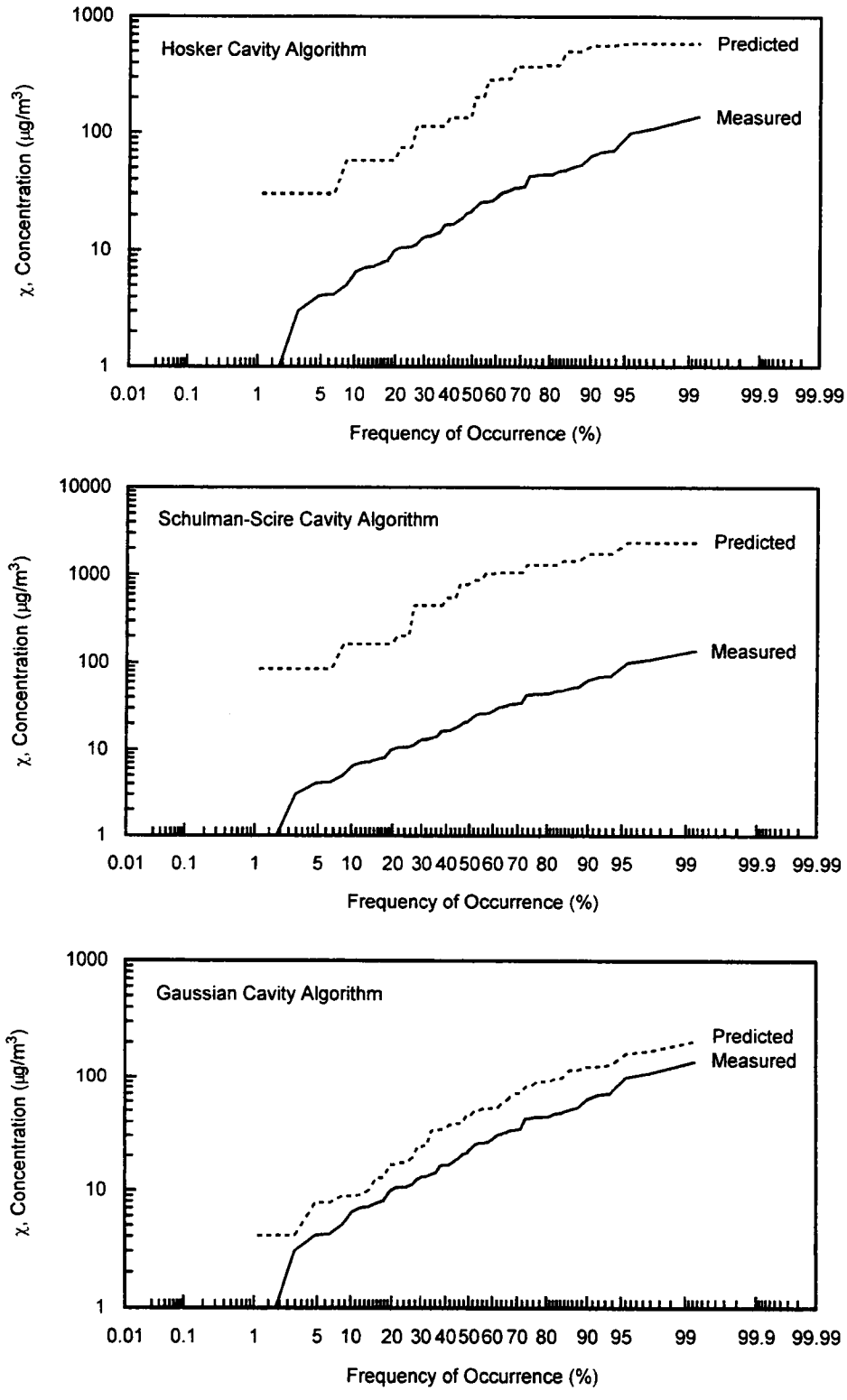


FIGURE 4.56 Cumulative Frequency Distributions of Measured and Predicted Concentrations Within the Cavity, Roof-Level Release

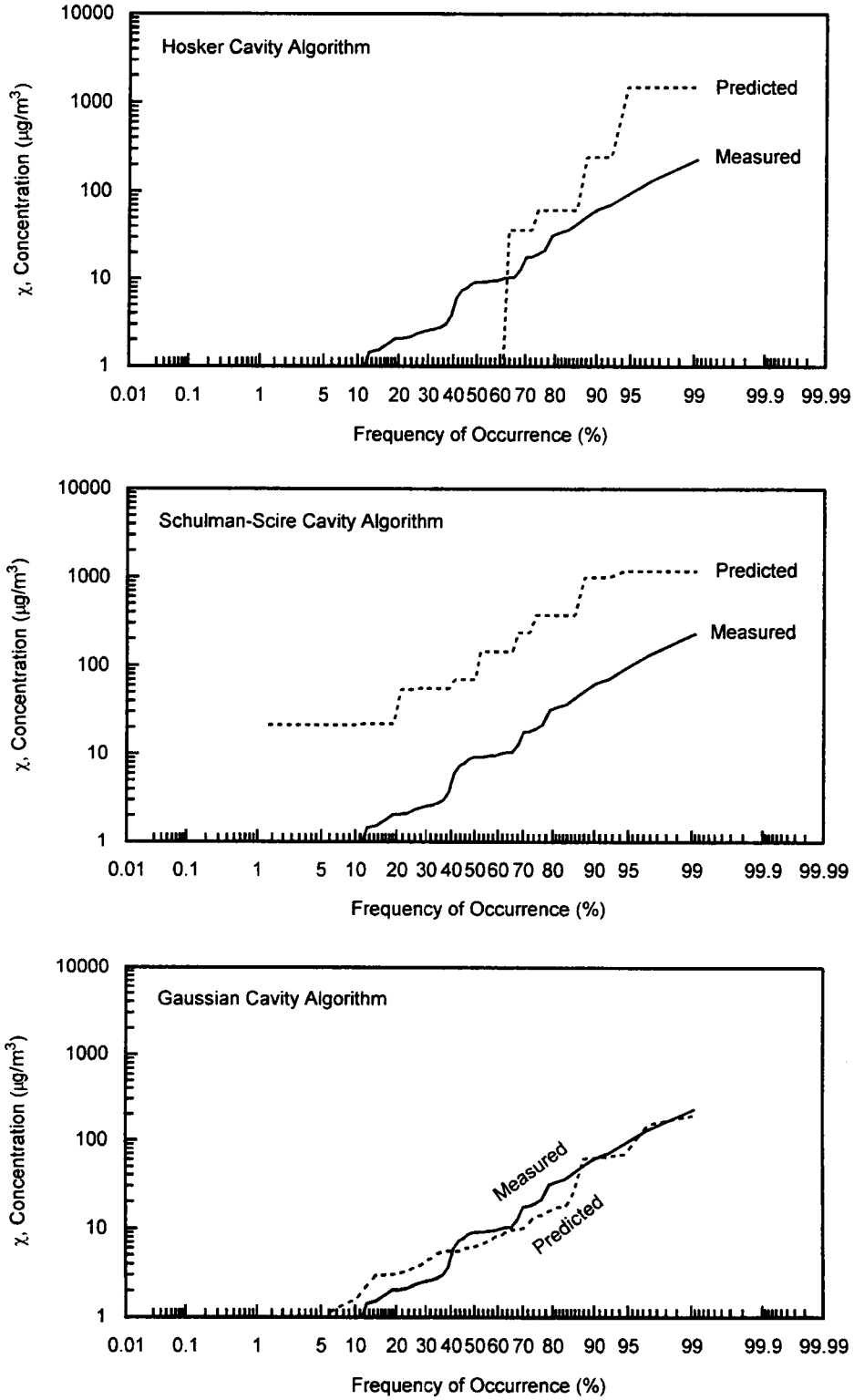


FIGURE 4.57 Cumulative Frequency Distributions of Measured and Predicted Concentrations Within the Cavity, Stack-Level Release

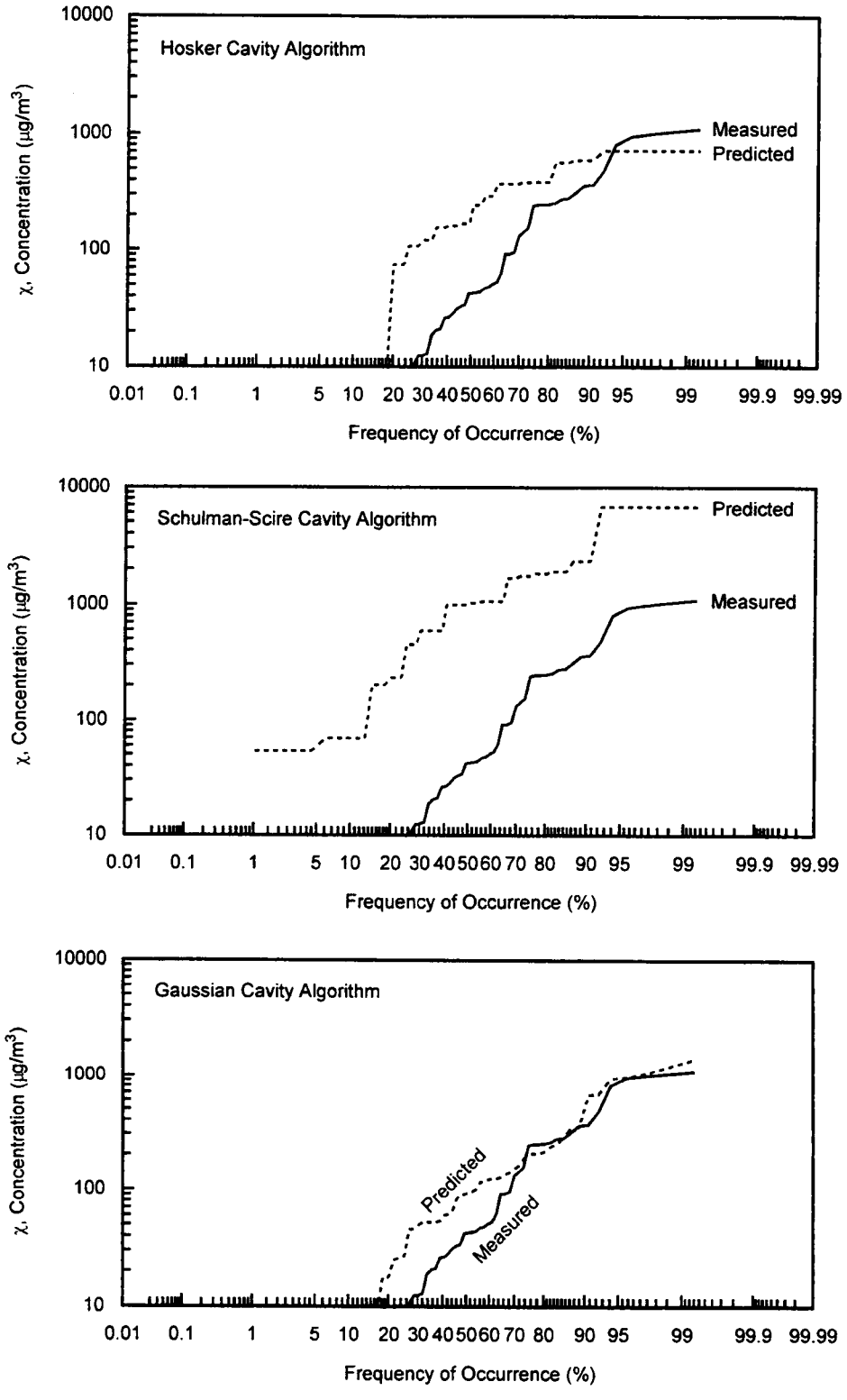


FIGURE 4.58 Cumulative Frequency Distributions of Measured and Predicted Concentrations Within the Cavity, Unstable Atmosphere

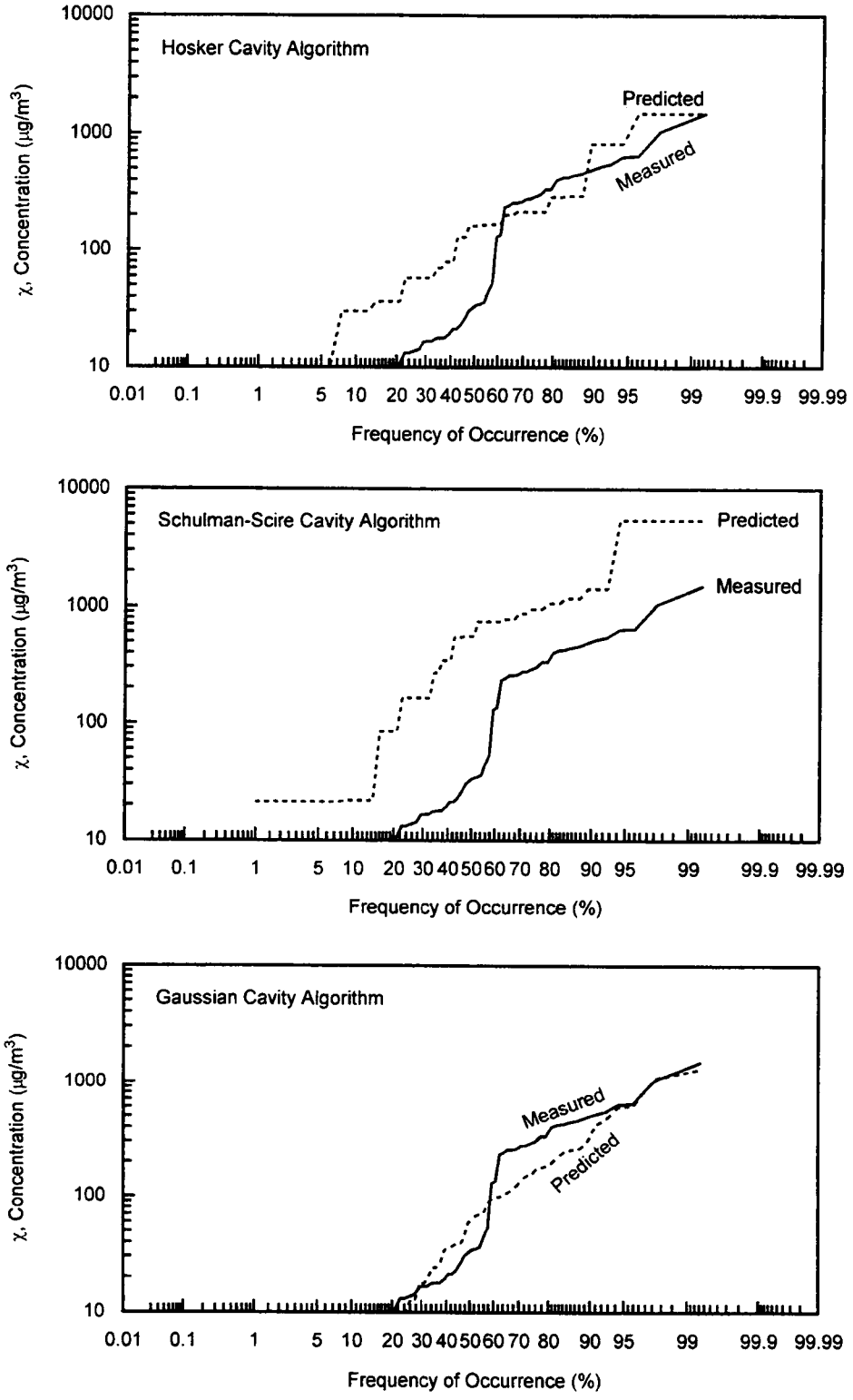


FIGURE 4.59 Cumulative Frequency Distributions of Measured and Predicted Concentrations Within the Cavity, Neutral Atmosphere

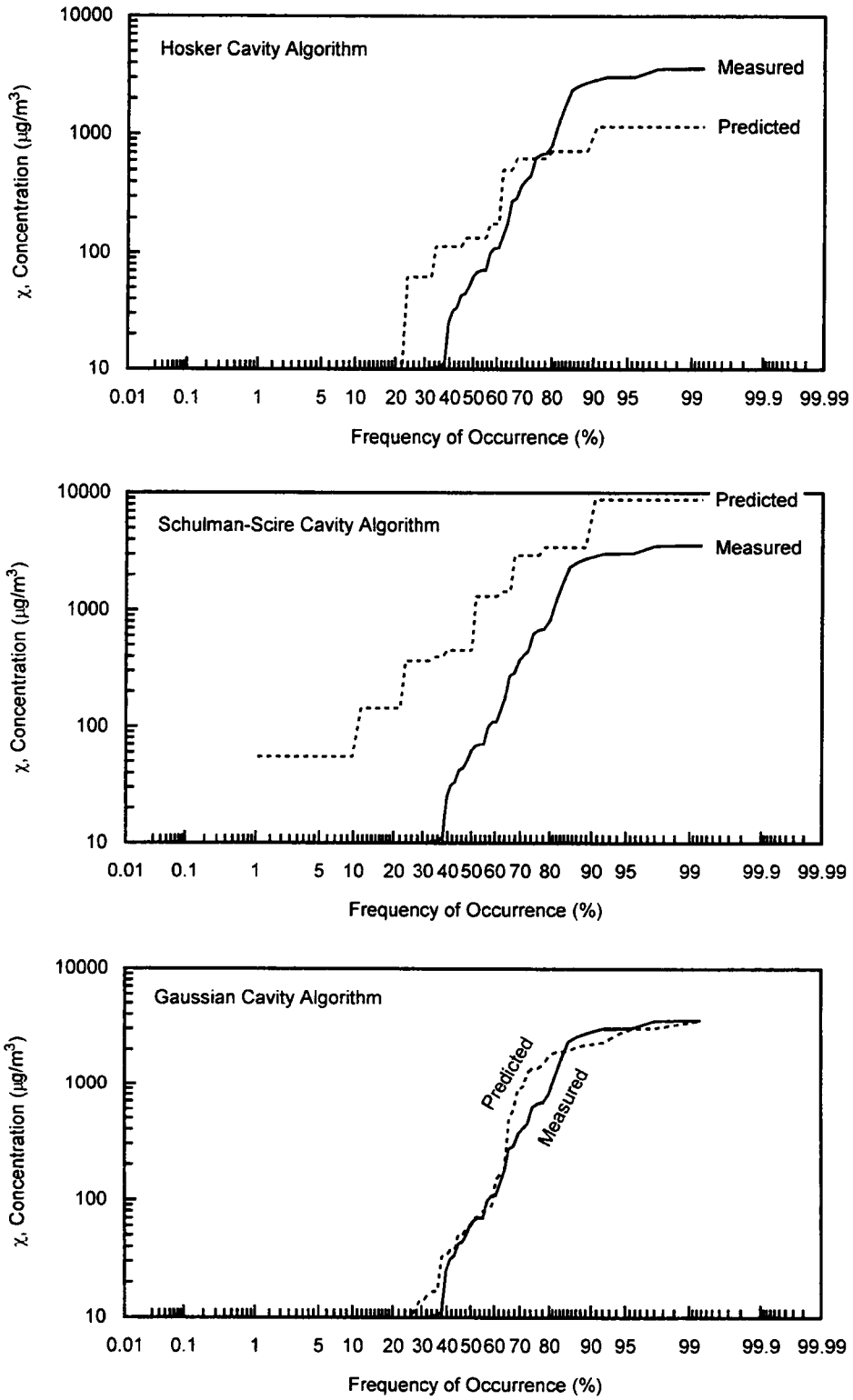


FIGURE 4.60 Cumulative Frequency Distributions of Measured and Predicted Concentrations Within the Cavity, Stable Atmosphere

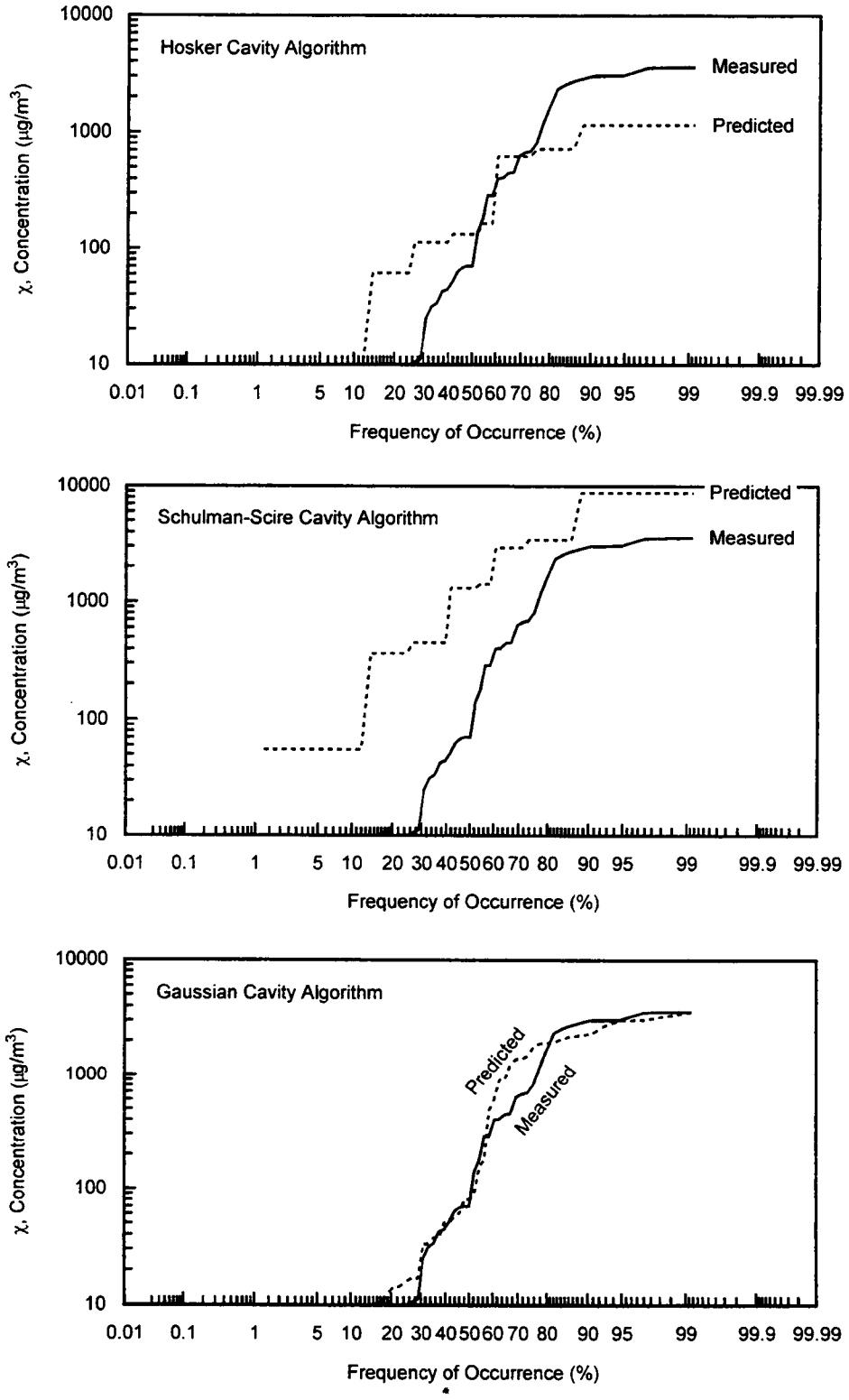


FIGURE 4.61 Cumulative Frequency Distributions of Measured and Predicted Concentrations Within the Cavity, $u_h \leq 1.0$ m/s

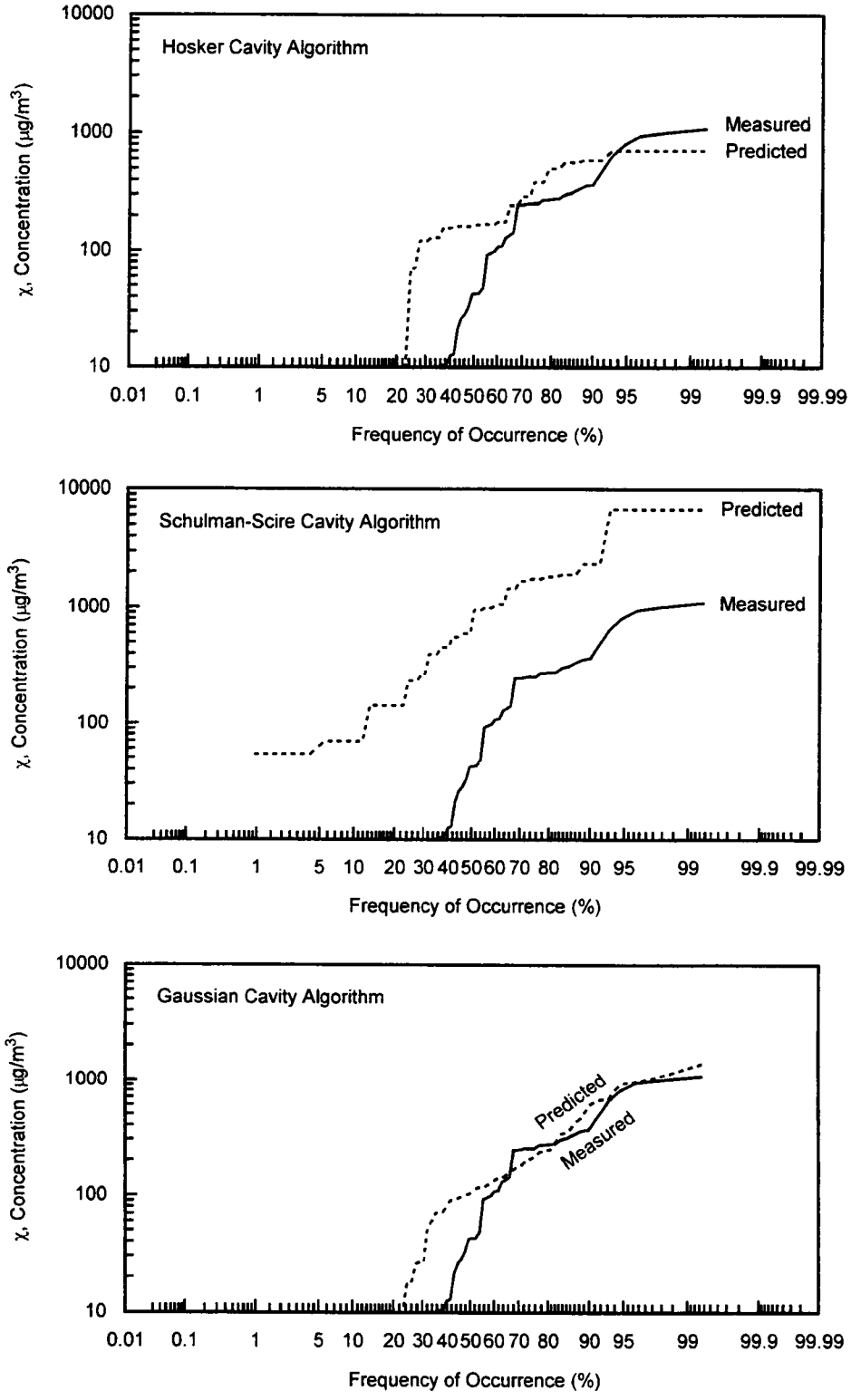


FIGURE 4.62 Cumulative Frequency Distributions of Measured and Predicted Concentrations Within the Cavity, 1.0 m/s < $u_h \leq$ 3.0 m/s

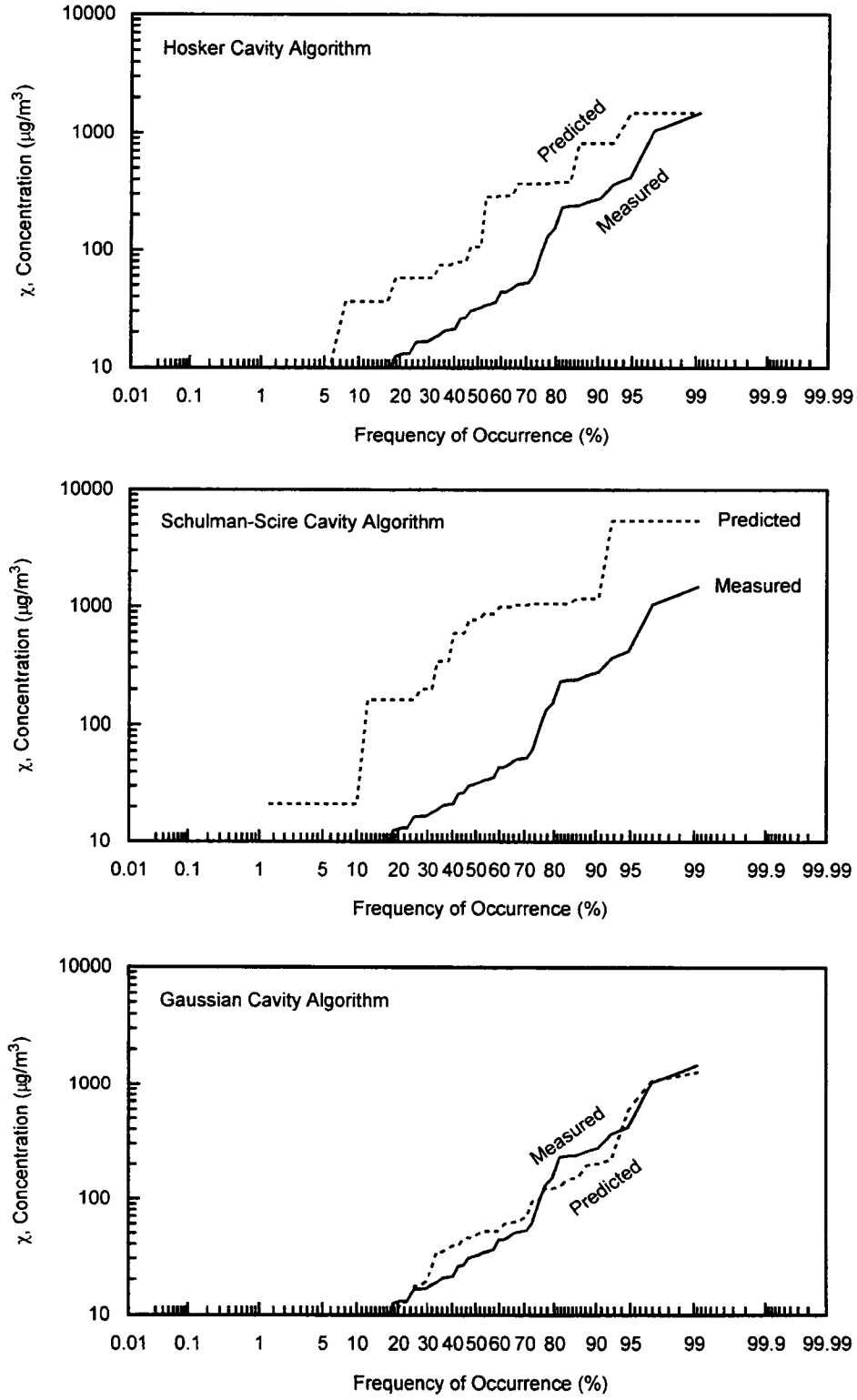


FIGURE 4.63 Cumulative Frequency Distributions of Measured and Predicted Concentrations Within the Cavity, 3.0 m/s < $u_h \leq$ 5.0 m/s

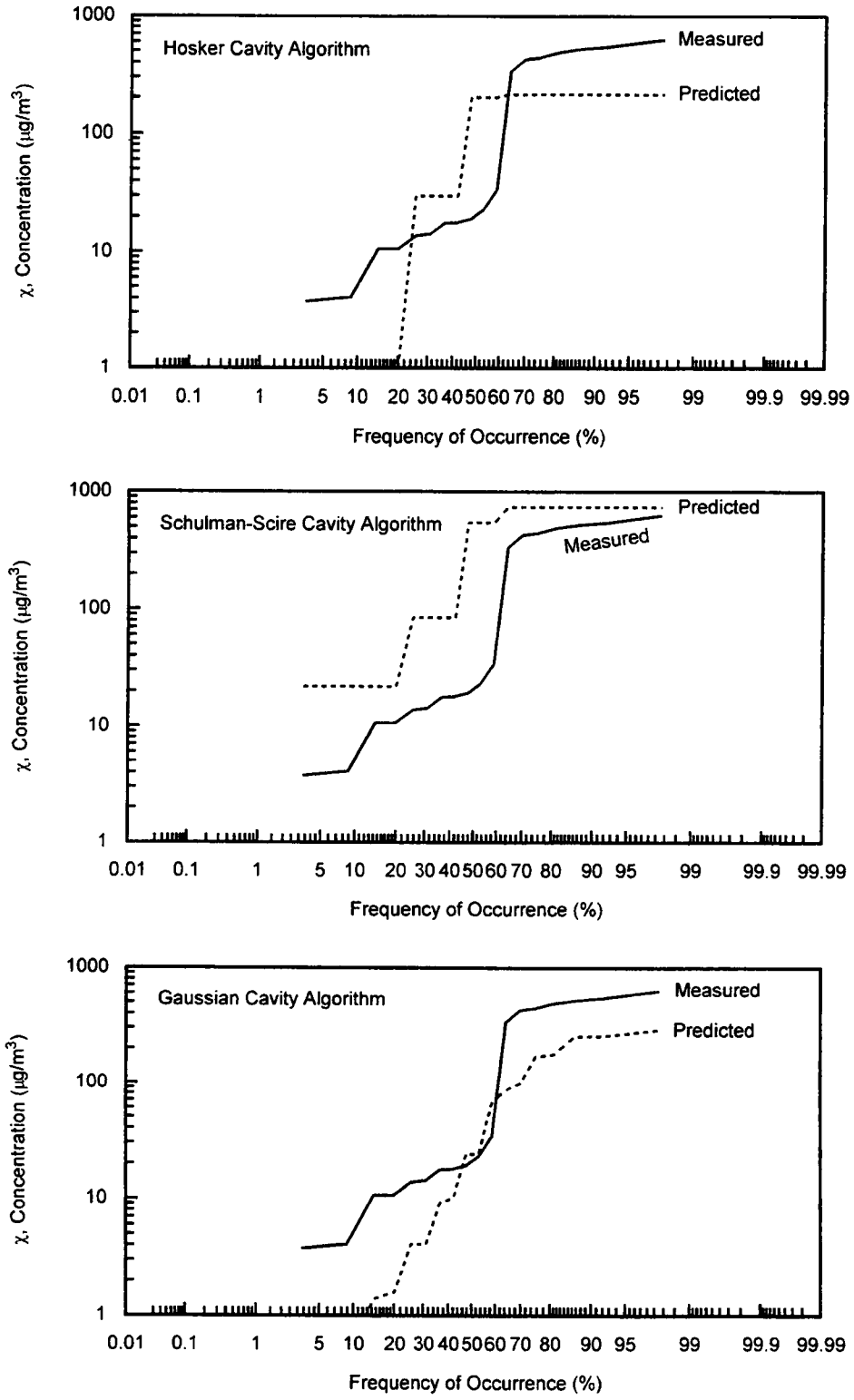


FIGURE 4.64 Cumulative Frequency Distributions of Measured and Predicted Concentrations Within the Cavity, $u_h > 5.0$ m/s

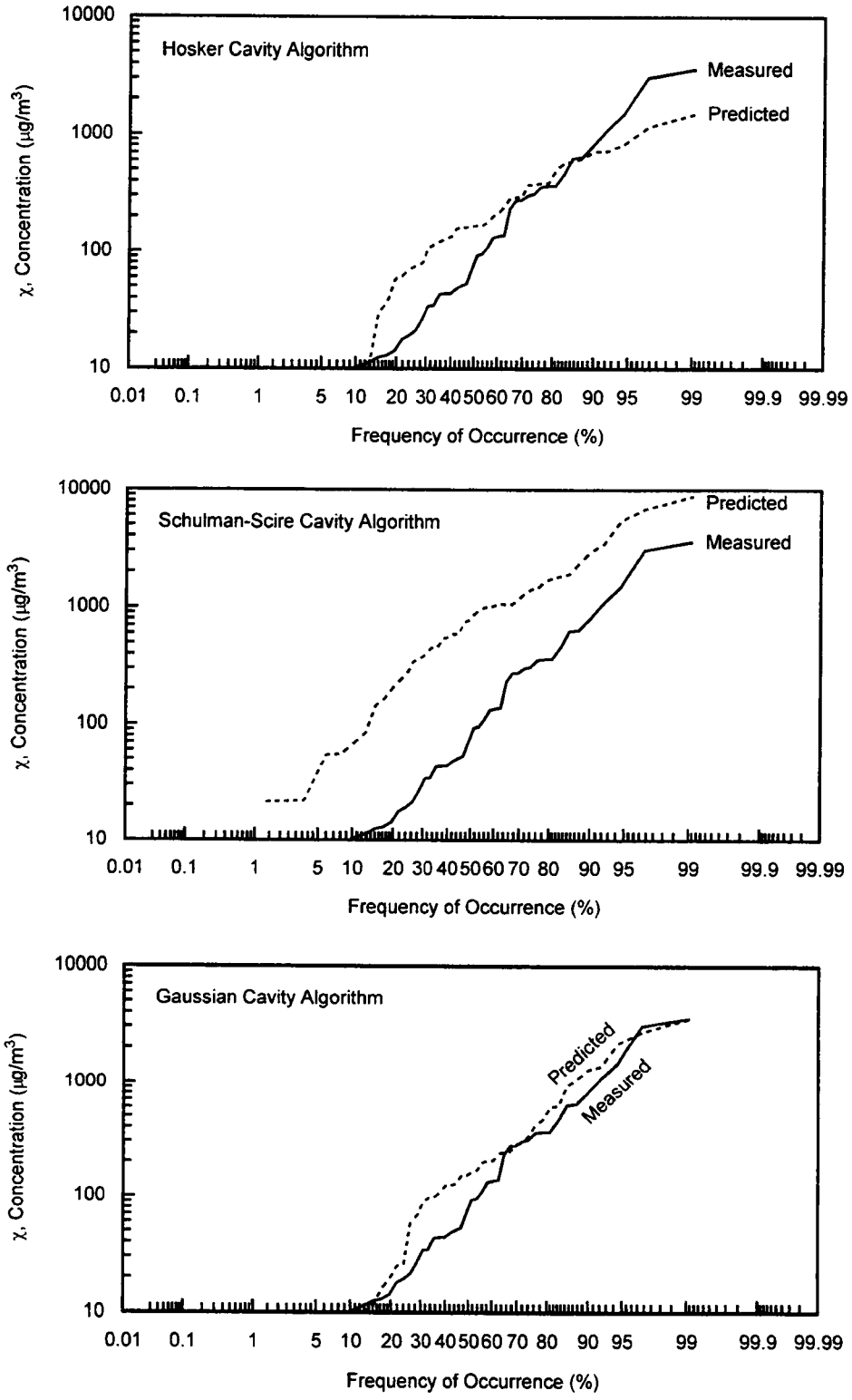


FIGURE 4.65 Cumulative Frequency Distributions of Measured and Predicted Concentrations Within the Cavity, Plume Centerline Locations

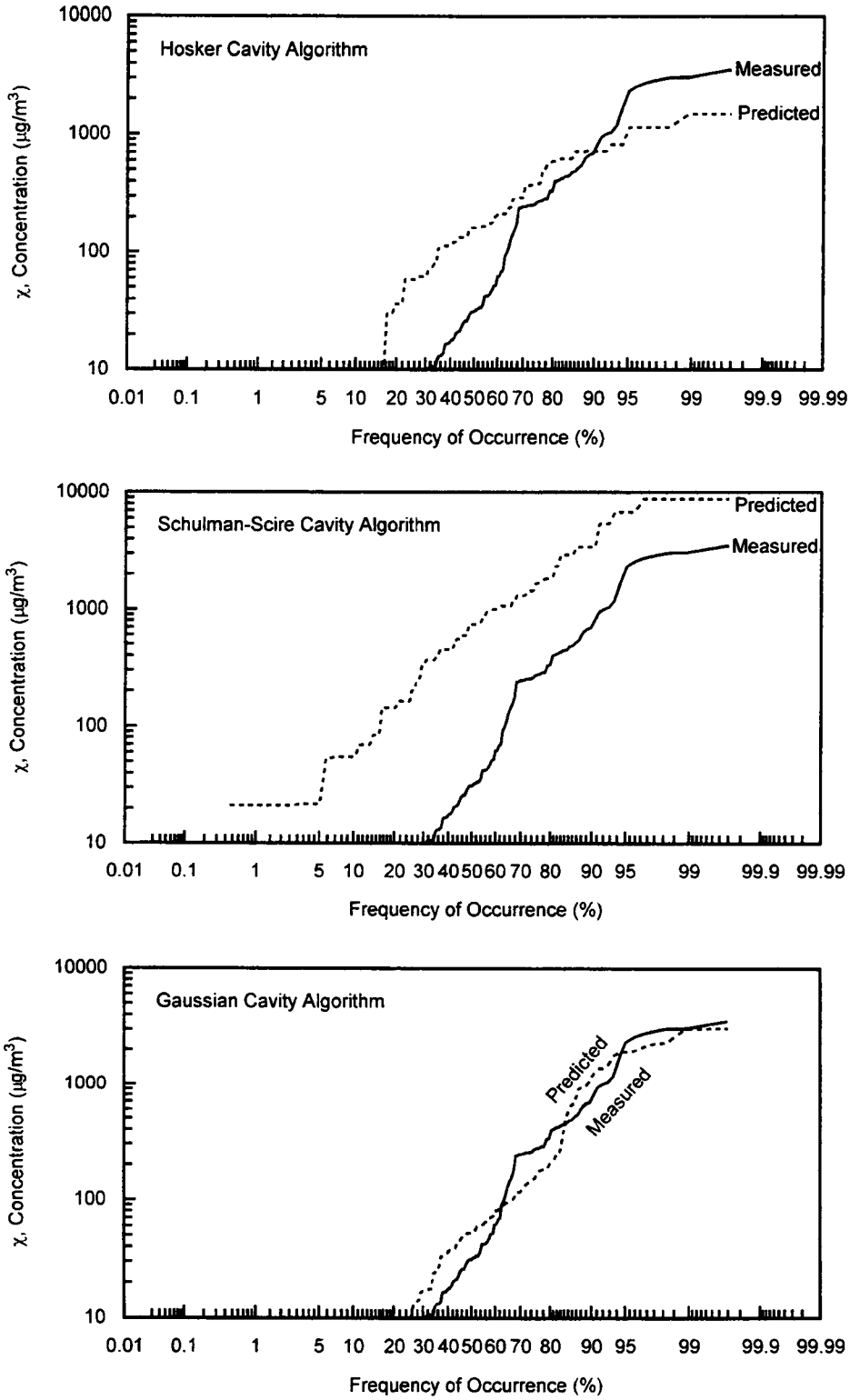


FIGURE 4.66 Cumulative Frequency Distributions of Measured and Predicted Concentrations Within the Cavity, Crosswind Locations

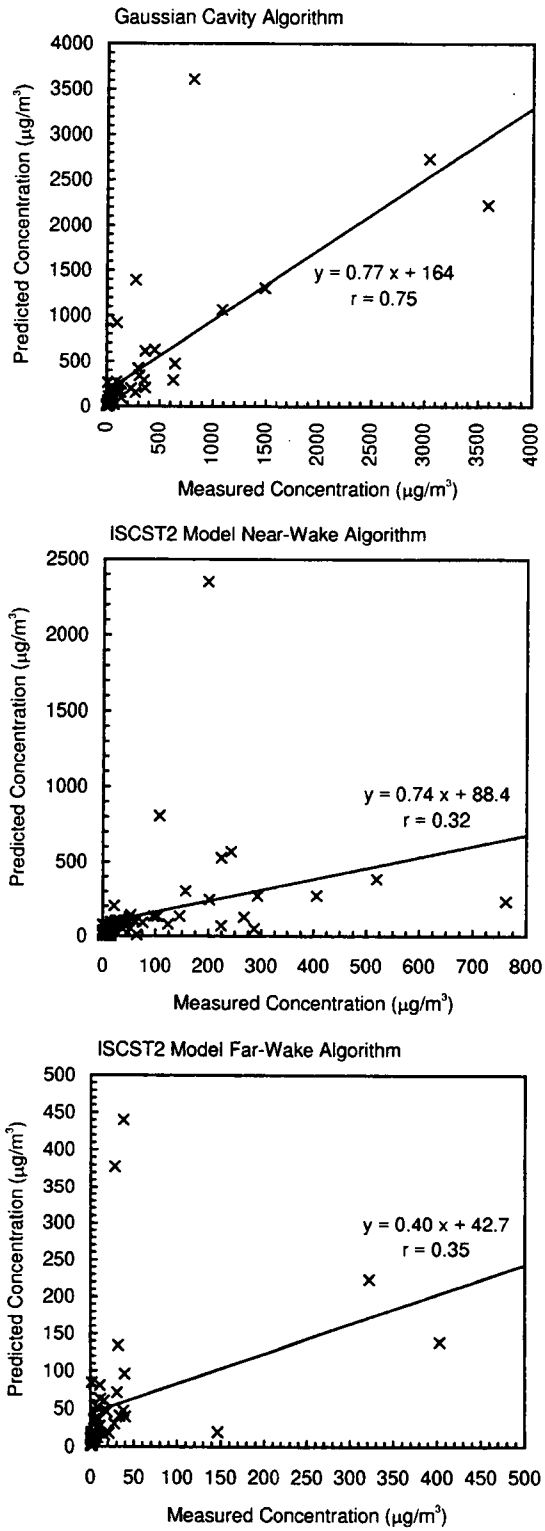


FIGURE 4.67 Scatter Diagrams of Measured Versus Predicted Concentrations at Plume Centerline Locations in the Cavity, Near-Wake, and Far-Wake Regions

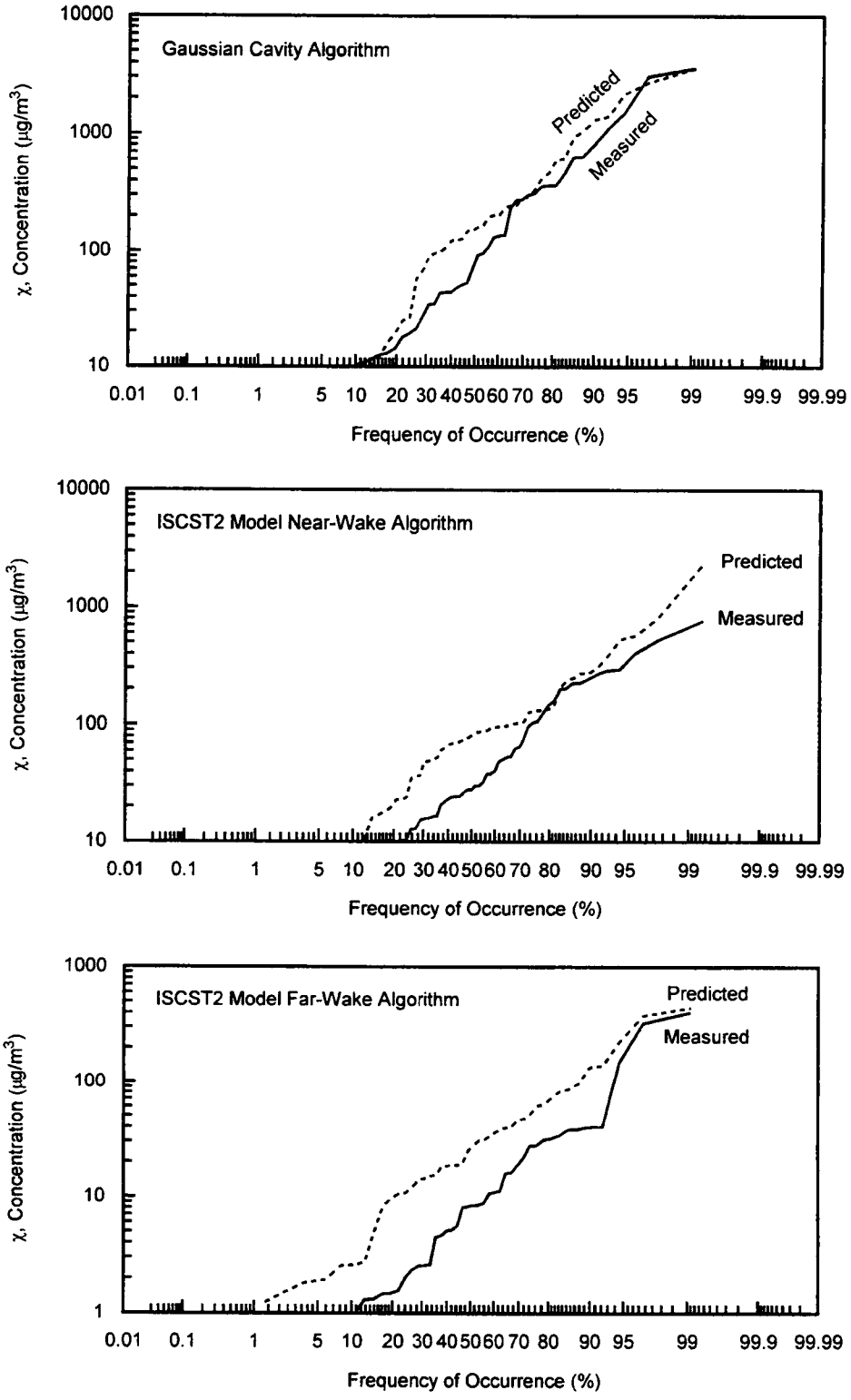


FIGURE 4.68 Cumulative Frequency Distributions of Measured and Predicted Concentrations Along Plume Centerline in the Cavity, Near-Wake, and Far-Wake

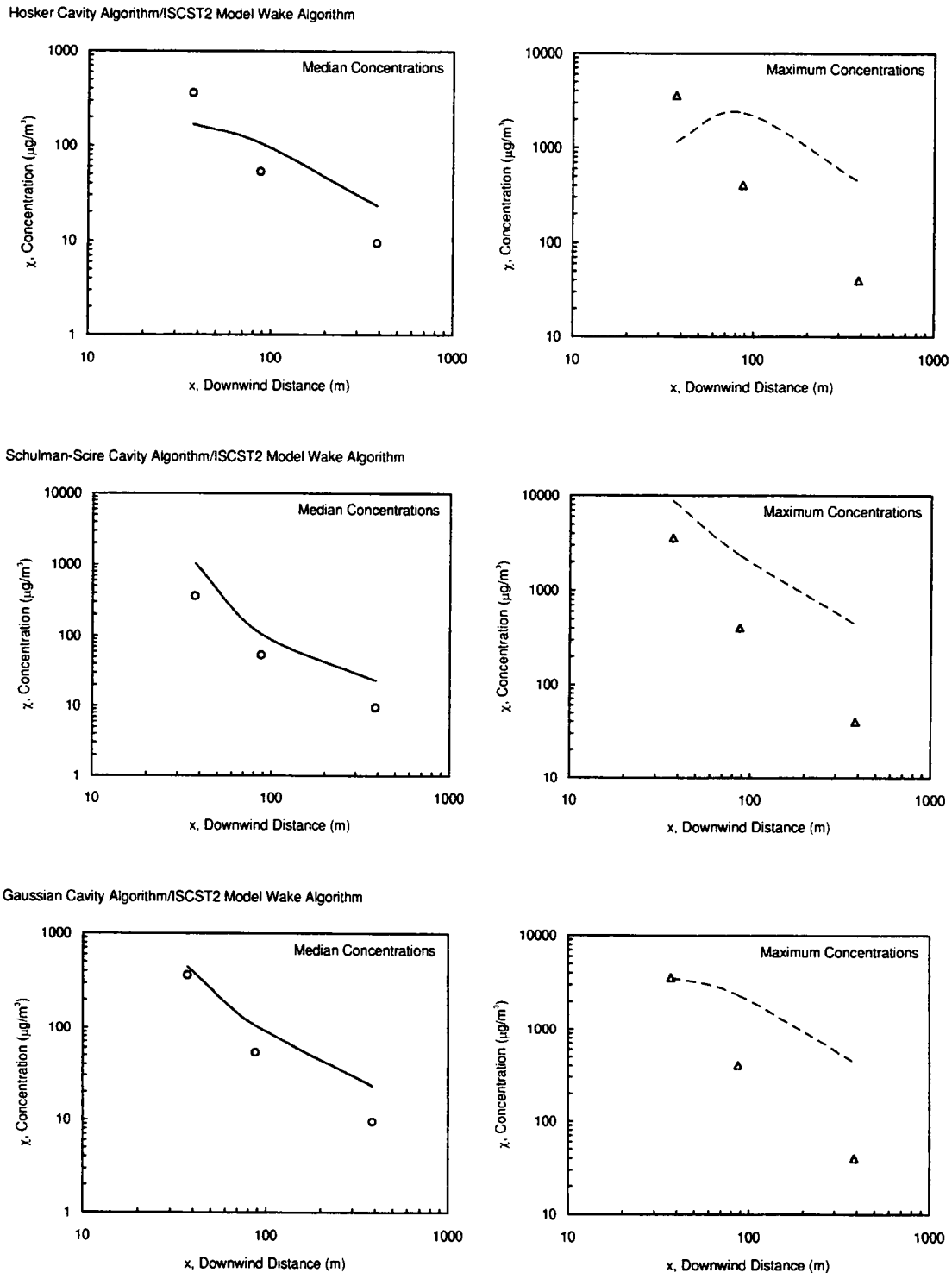


FIGURE 4.69 Concentration Profiles, Ground-Level Release, (Measurements denoted by symbols ° and $^{\Delta}$; Predictions denoted by lines—— and – – ·)

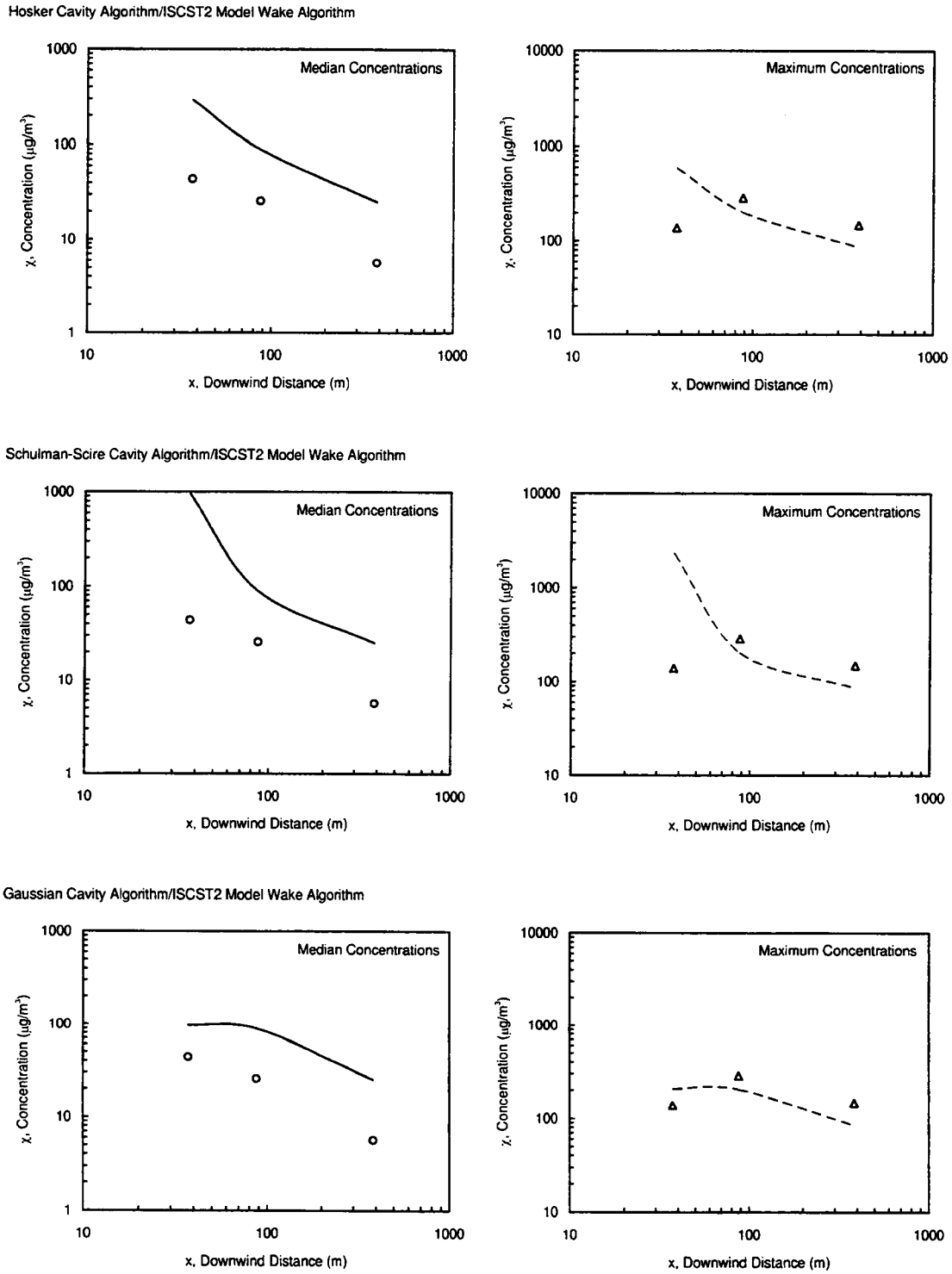


FIGURE 4.70 Concentration Profiles, Roof-Level Release, (Measurements denoted by symbols ° and $^{\Delta}$; Predictions denoted by lines—— and – – ·)

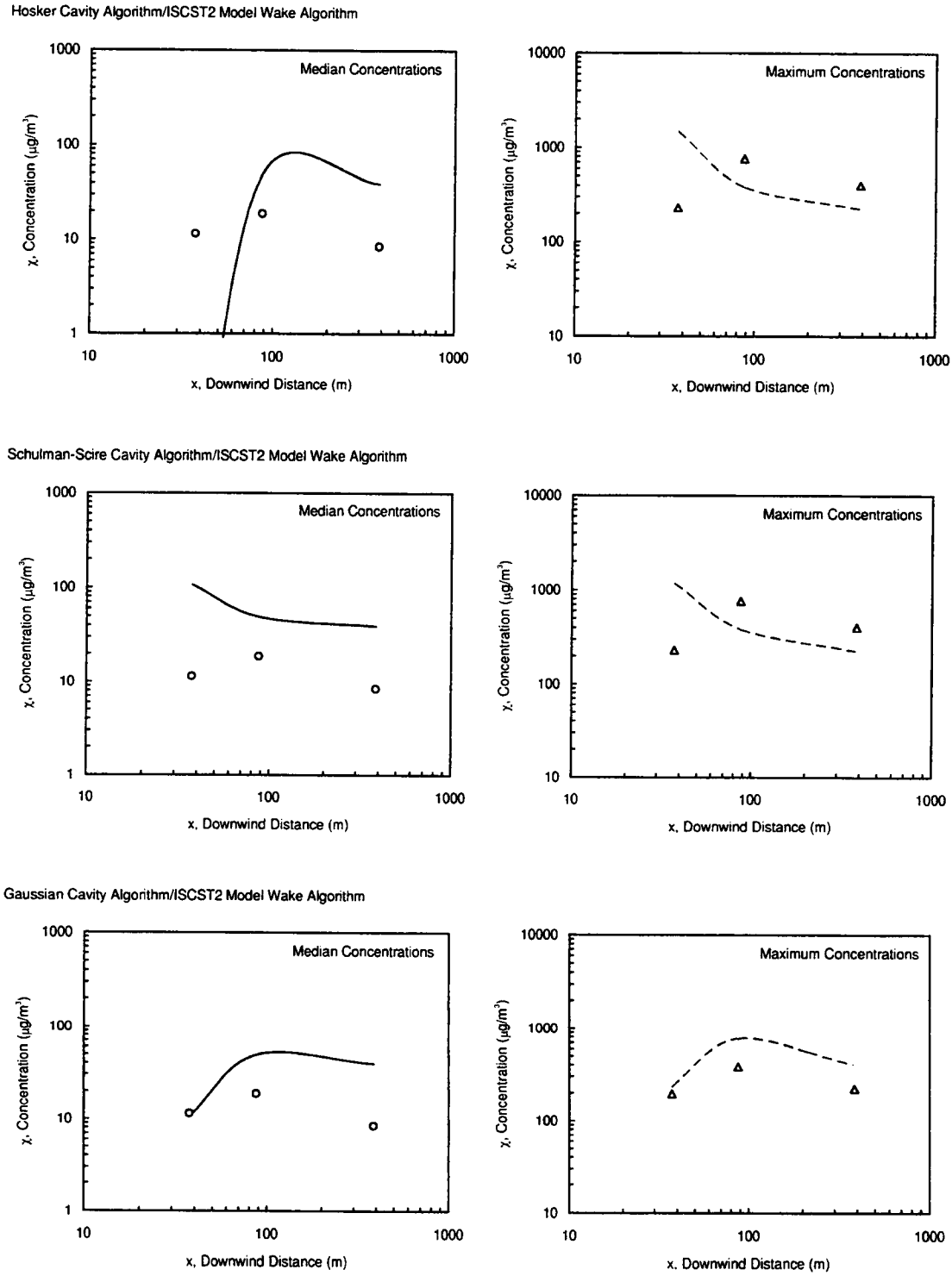


FIGURE 4.71 Concentration Profiles, Stack-Level Release, (Measurements denoted by symbols ° and Δ ; Predictions denoted by lines—— and – – ·)

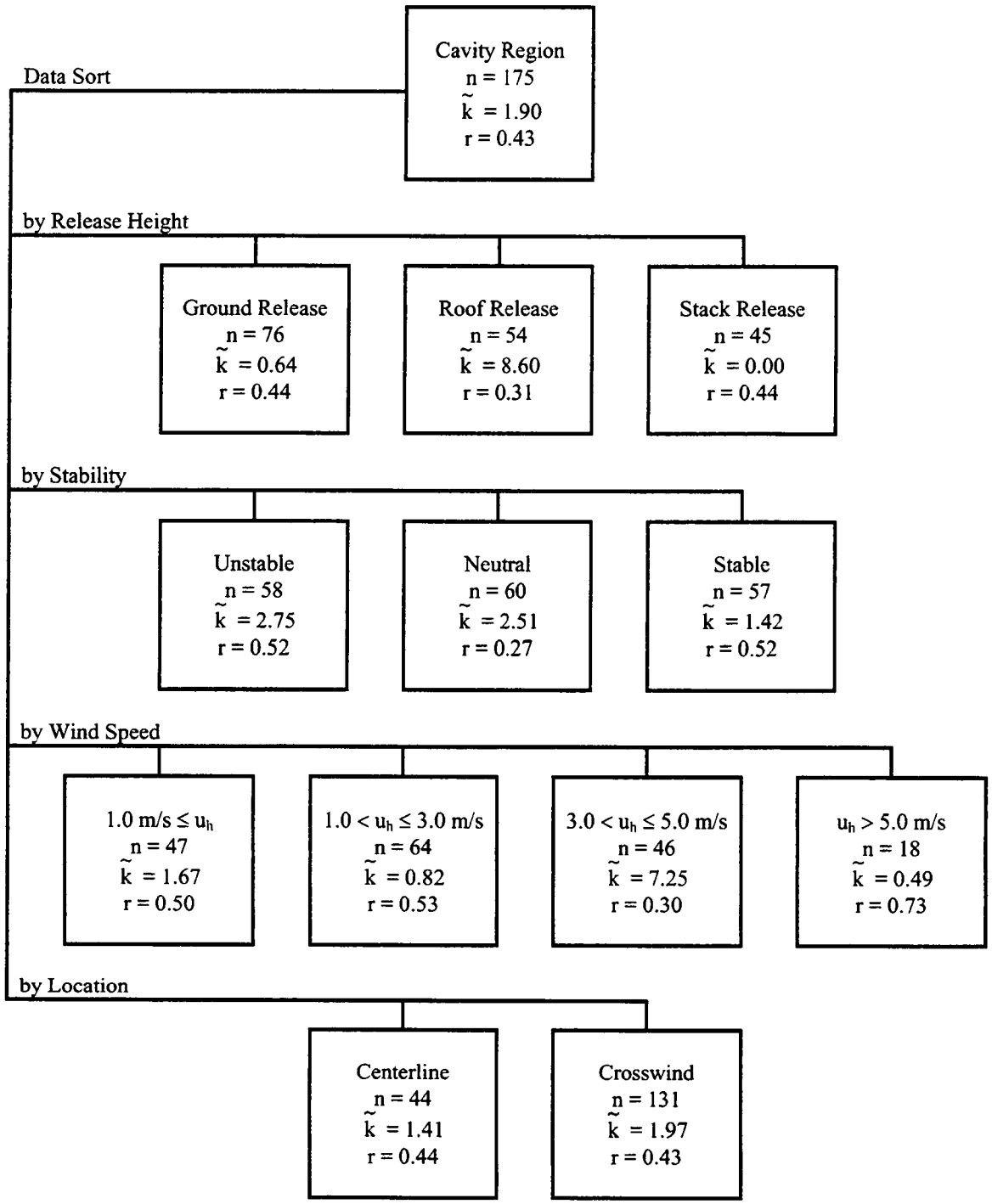


FIGURE 5.1 Statistical Summary Diagram, Hosker Cavity Algorithm

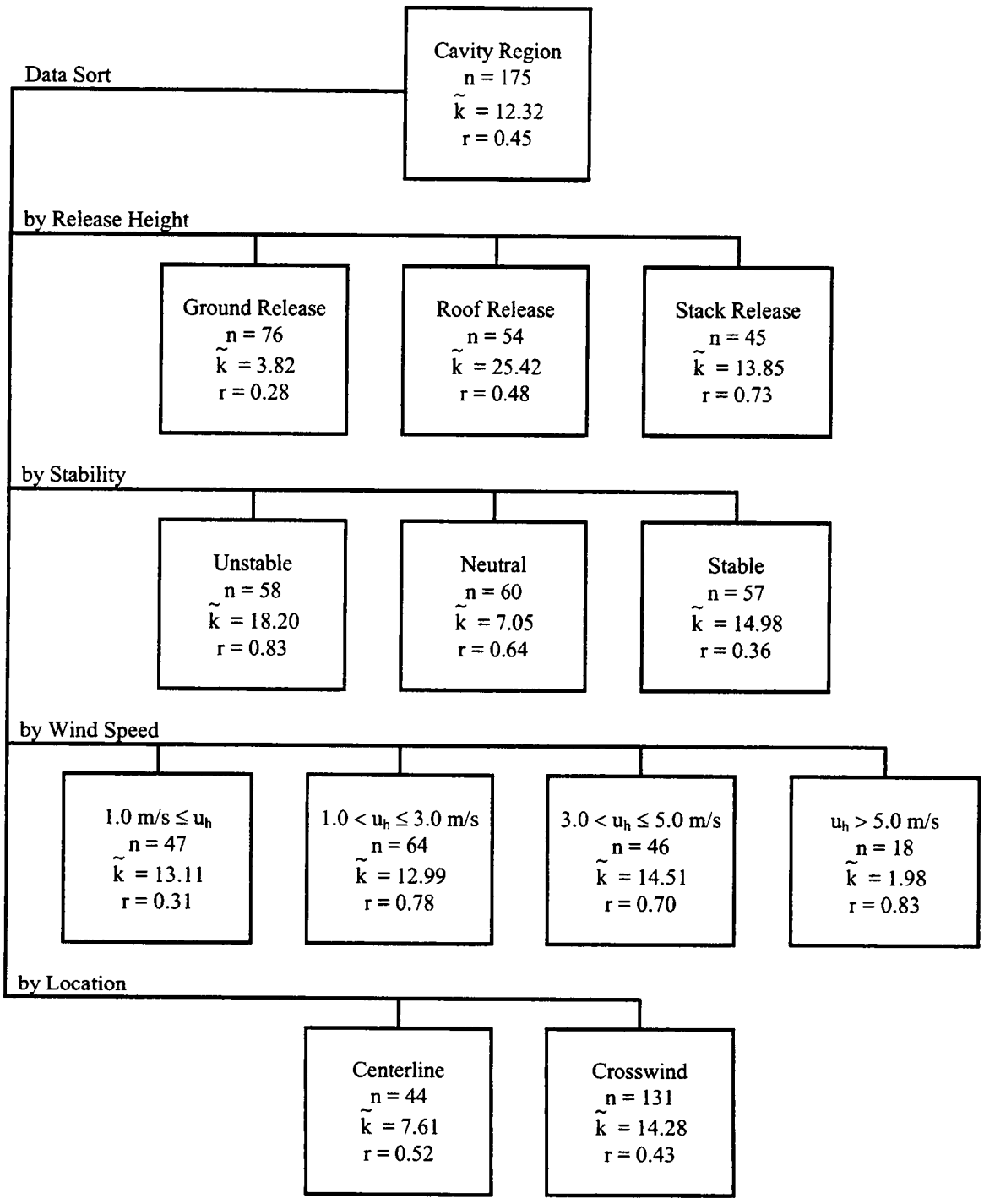


FIGURE 5.2 Statistical Summary Diagram, Schulman-Scire Cavity Algorithm

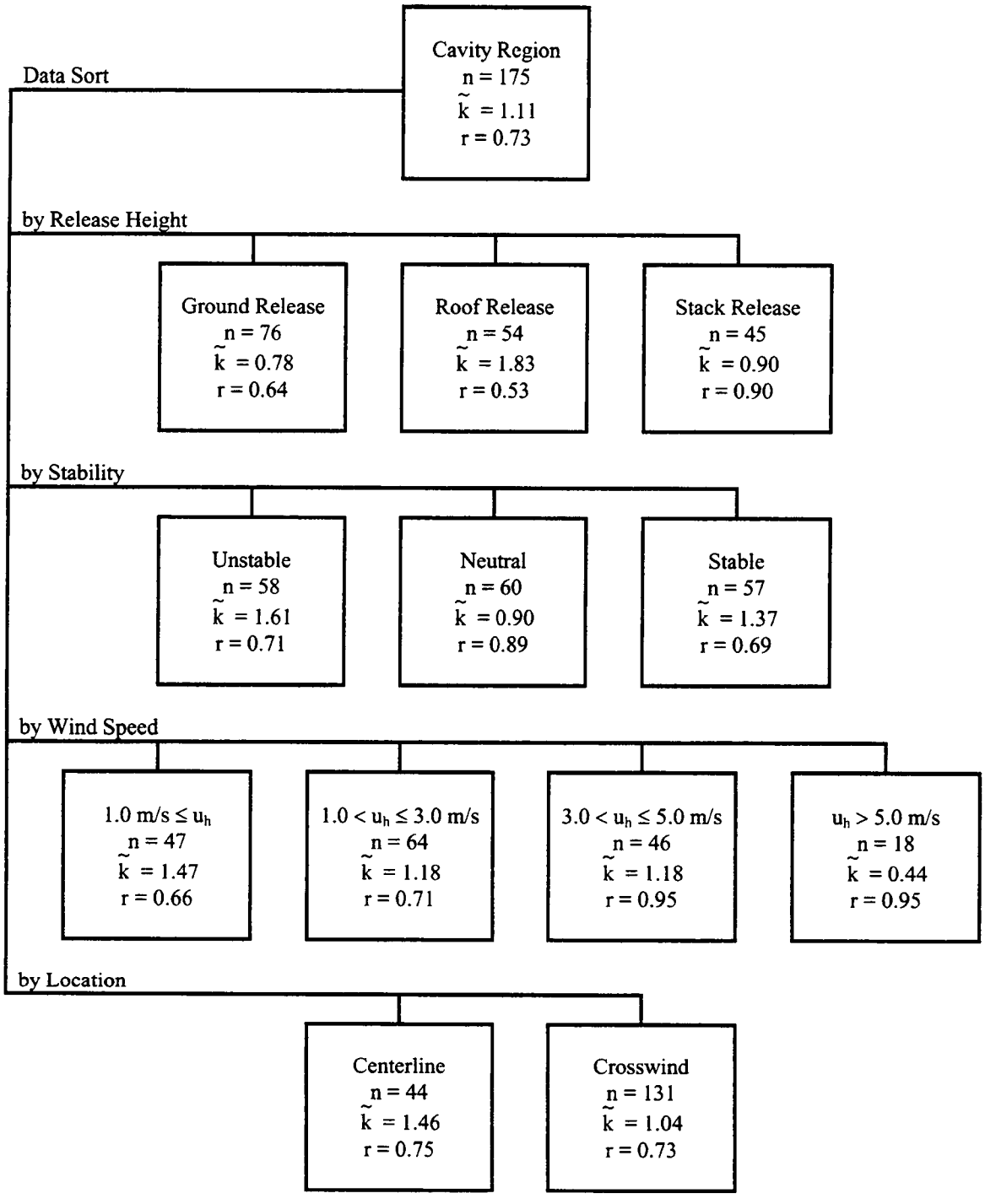


FIGURE 5.3 Statistical Summary Diagram, Gaussian Cavity Algorithm

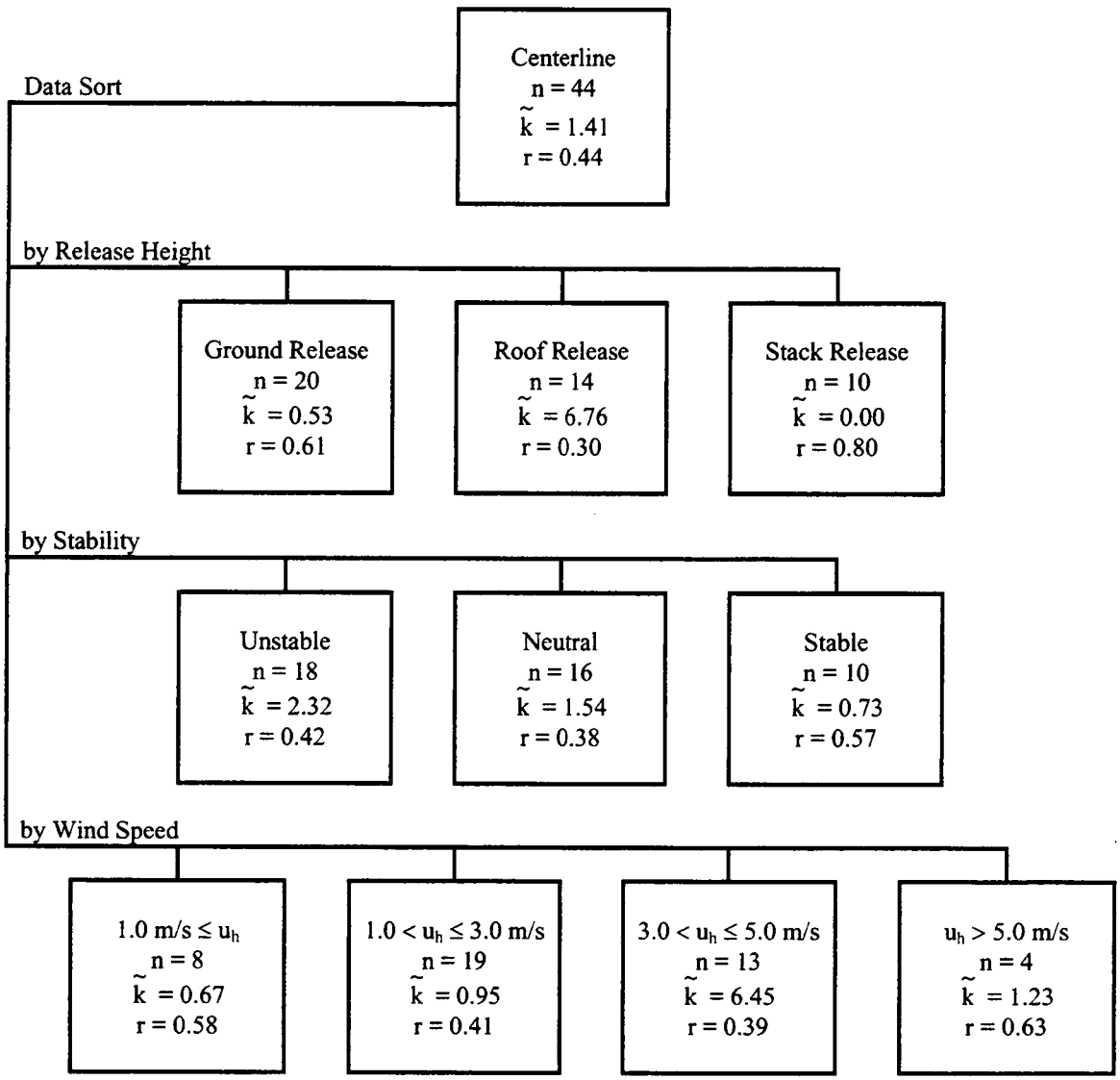


FIGURE 5.4 Statistical Summary Diagram, Hosker Cavity Algorithm, Plume Centerline Locations Within the Cavity

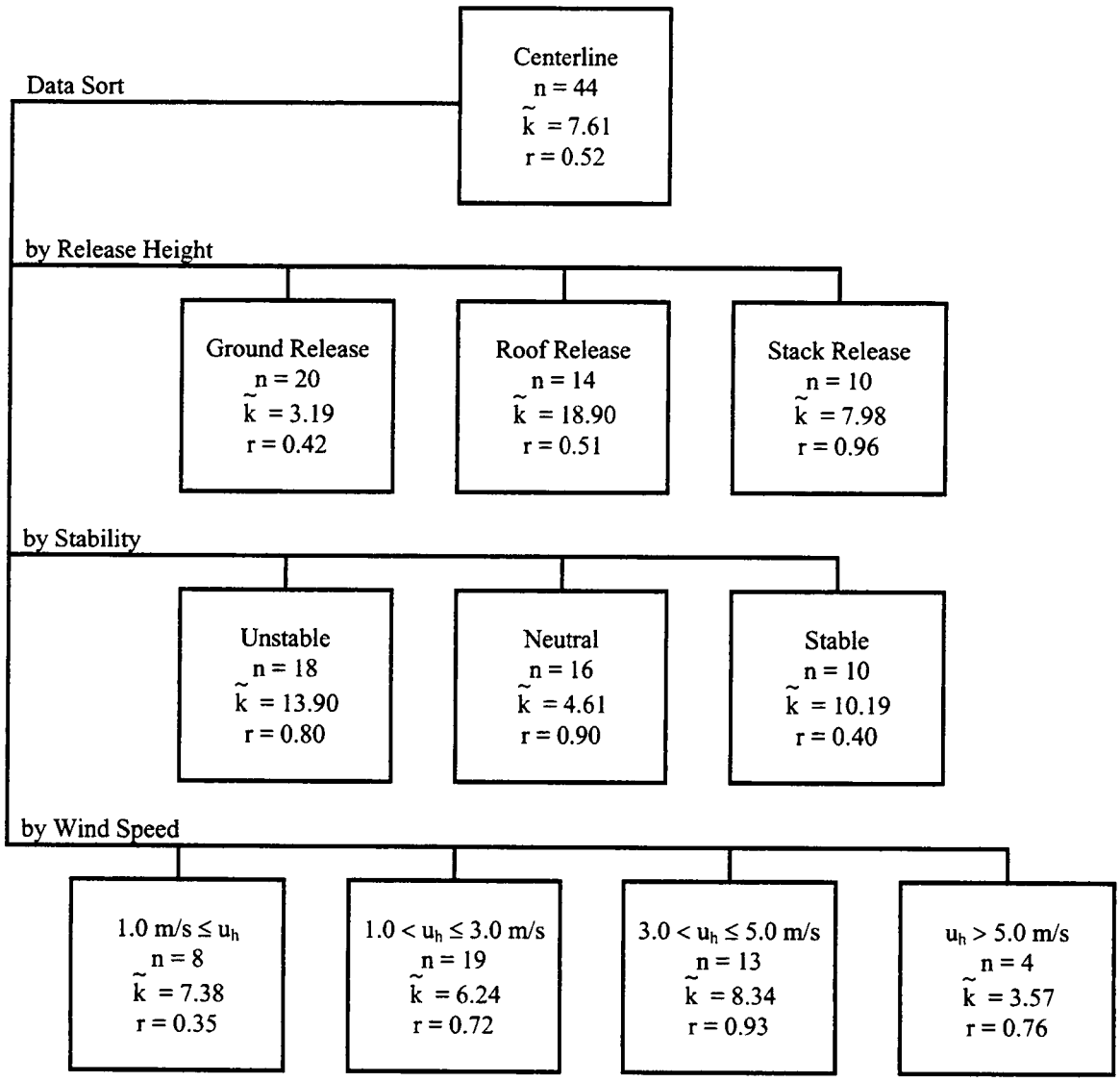


FIGURE 5.5 Statistical Summary Diagram, Schulman-Scire Cavity Algorithm, Plume Centerline Locations Within the Cavity

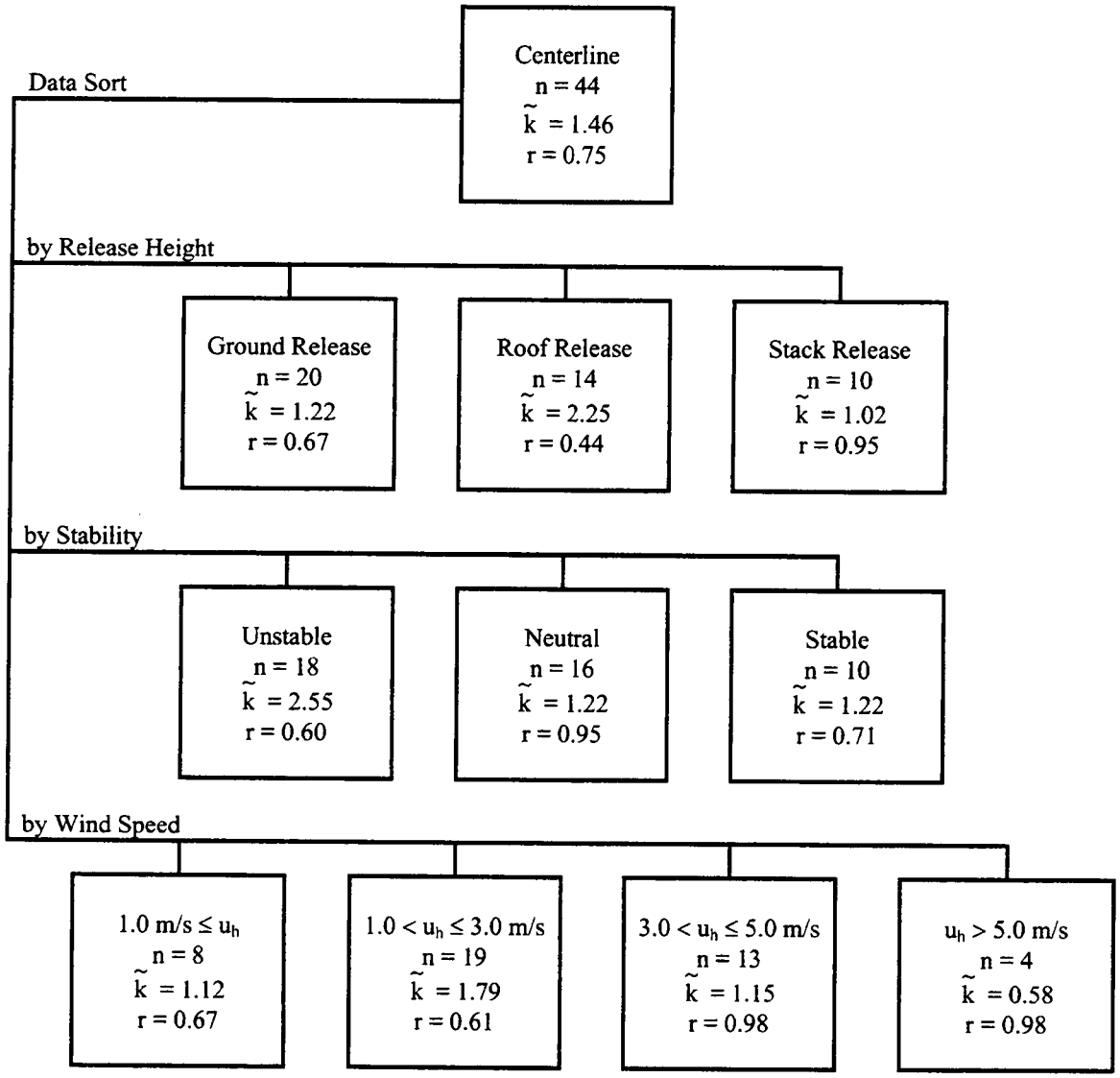


FIGURE 5.6 Statistical Summary Diagram, Gaussian Cavity Algorithm, Plume Centerline Locations Within the Cavity

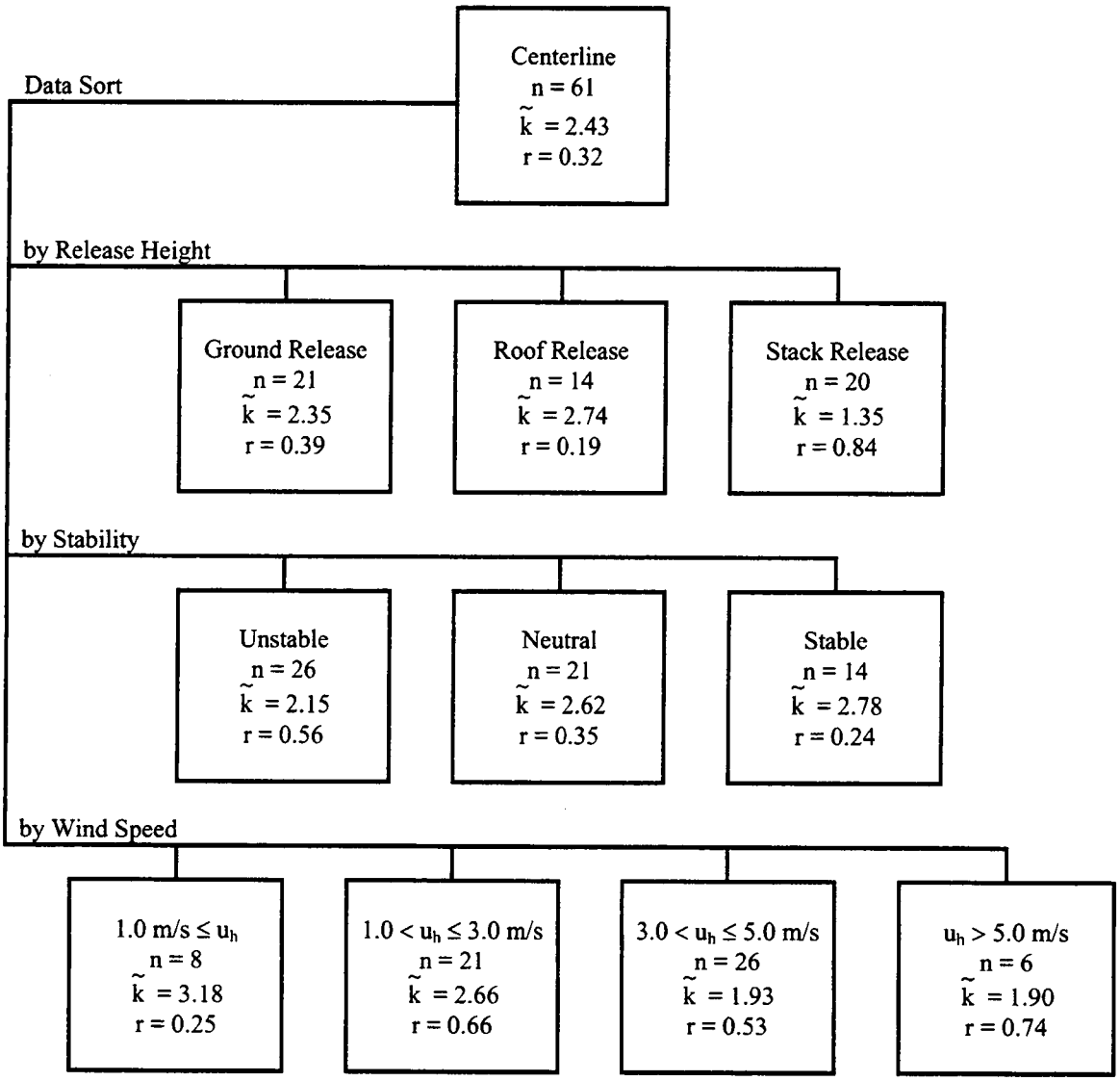


FIGURE 5.7 Statistical Summary Diagram, ISCST2 Wake Algorithm, Plume Centerline Locations Within the Near-Wake

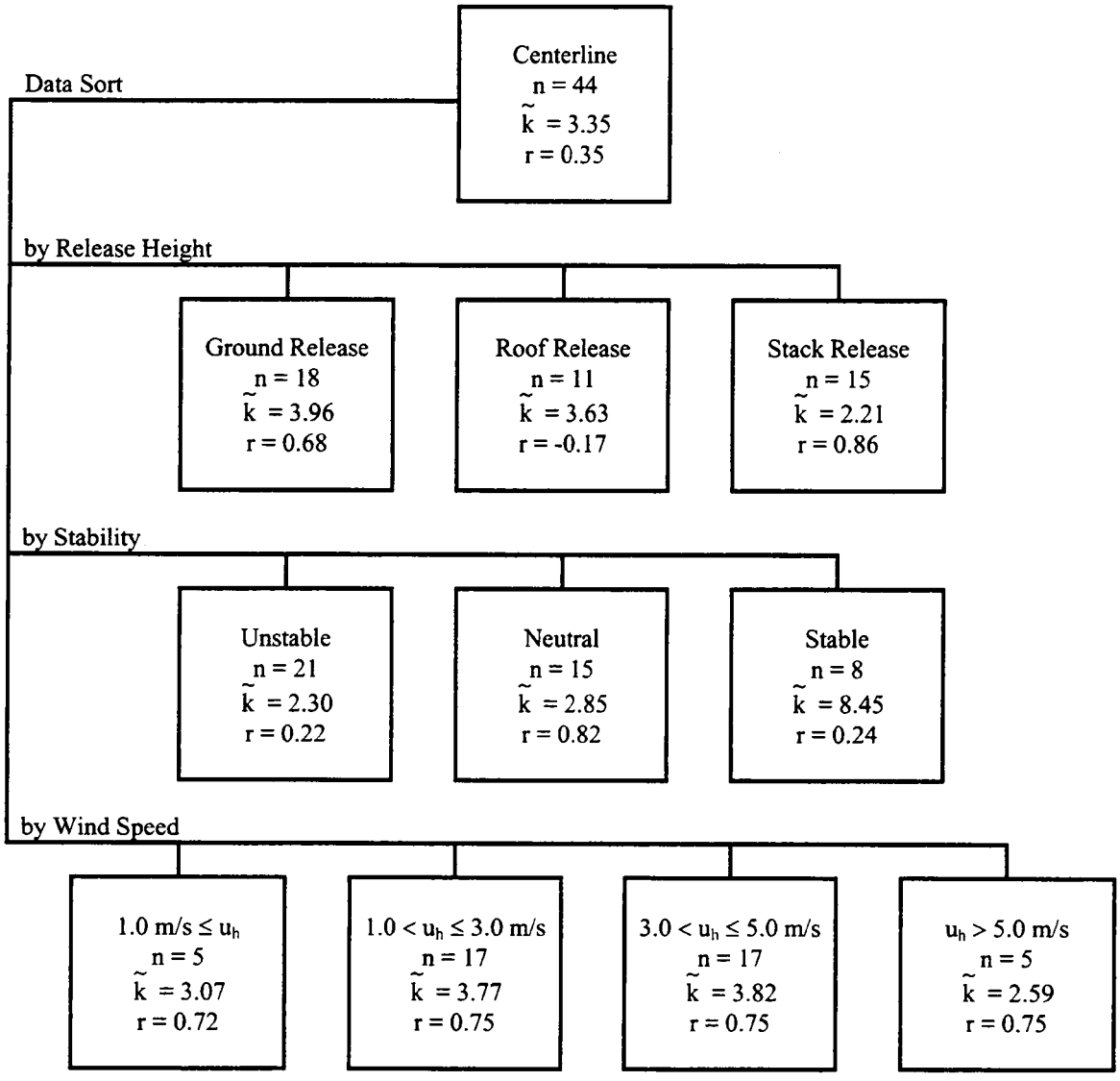


FIGURE 5.8 Statistical Summary Diagram, ISCST2 Wake Algorithm, Plume Centerline Locations Within the Far-Wake

APPENDIX C

QUICK REFERENCE OF PATHWAYS/KEYWORDS/PARAMETERS

DESCRIPTION OF CONTROL PATHWAY KEYWORDS AND PARAMETERS

CO Keywords	Type	Parameters
TITLEONE	M-N	Title1
TITLETWO	O-N	Title2
MODELOPT	M-N	DFAULT CONC RURAL GRDRIS NOSTD NOBID NOCALM MSGPRO or or DEPOS URBAN
MODELSEL[1]	**M-N**	**ISCST2 HOSKER CMPLXI** **or or** **SCHULM SHORTZ** **or** **CAVITY**
AVERTIME	M-N	Time1 Time2 Time3 Time4 MONTH PERIOD
POLLUTID	M-N	Pollut
HALFLIFE	O-N	Haflif
DCAYCOEF	O-N	Decay
TERRHGTS	O-N	FLAT or ELEV **(Taf(i),i=1,6 Hmin)[1]**
ELEVUNIT	O-N	METERS or FEET
FLAGPOLE	O-N	(Flagdf)
RUNORNOT	M-N	RUN or NOT
EVENTFIL	O-N	(Evfile) (Evopt)
SAVEFILE	O-N	(Savfil) (Dayinc) (Savf12)
INITFILE	O-N	(Inifil)
MULTYEAR	O-N	Savfil (Inifil)
ERRORFIL	O-N	(Errfil) (DEBUG)

Type: M - Mandatory N - Non-repeatable
O - Optional R - Repeatable

Note: Parameters noted in parenthesis are optional.

1) Added option in the ISCST2C model. ISCST2C model CO options discussed in Section 3.3.4 of this dissertation.

DESCRIPTION OF SOURCE PATHWAY KEYWORDS AND PARAMETERS

SO Keywords	Type	Parameters
LOCATION	M-R	Srcid Srctyp Xs Ys (Zs) (Srctyp = POINT, VOLUME, or AREA)
SRCPARAM	M-R	Srcid Ptemis Stkhgt Stktmp Stkvel Stkdia (POINT Source) Vlemis Relhgt Syinit Szinit (VOLUME Source) Aremis Relhgt Xinit (AREA Source)
BUILDHGT	O-R	Srcid (or Srcrng) Dsbh(i),i=1,Nsec
BUILDWID	O-R	Srcid (or Srcrng) Dsbw(i),i=1,Nsec
BUILDLNG[1]	**O-R**	**Srcid (or Srcrng) Dsbl(i),i=1,Nsec**
BUILDSTK[1]	**O-R**	**Srcid (or Srcrng) Dwsl(i),i=1,Nsec**
LOWBOUND	O-R	Srcid (or Srcrng) Idswak(i),i=1,Nsec
EMISFACT	O-R	Srcid (or Srcrng) Qflag Qfact(i),i=1,Nqf
EMISUNIT	O-N	Emifac Emilbl Conlbl (or Deplbl)
SETVELOC	O-R	Srcid (or Srcrng) Vsn(i),i=1,Nvs
MASSFRAX	O-R	Srcid (or Srcrng) Phi(i),i=1,Nvs
REFLCOEF	O-R	Srcid (or Srcrng) Gamma(i),i=1,Nvs
SRCGROUP	M-R	Grpid Srcid's Srcrng's

Type: M - Mandatory N - Non-repeatable
O - Optional R - Repeatable

Note: Parameters noted in parenthesis are optional.

1) **Added option in the ISCST2C model. ISCST2C model CO options discussed in Section 3.3.4 of this dissertation.**

DESCRIPTION OF **RE**CEPTOR PATHWAY KEYWORDS AND PARAMETERS

RE Keywords	Type	Parameters
GRIDCART	O-R	Netid STA XYINC Xinit Xnum Xdelta Yinit Ynum Ydelta or XPNTS Gridx1 Gridx2 Gridx3 ... GridxN, and YPNTS Gridy1 Gridy2 Gridy3 ... GridyN ELEV Row Zelev1 Zelev2 Zelev3 ... ZelevN FLAG Row Zflag1 Zflag2 Zflag3 ... ZflagN END
GRIDPOLR	O-R	Netid STA ORIG Xinit Yinit DIST Ring1 Ring2 Ring3 ... RingN DDIR Dir1 Dir2 Dir3 ... DirN or GDIR Dirnum Dirini Dirinc ELEV Rad Zelev1 Zelev2 Zelev3 ... ZelevN FLAG Rad Zflag1 Zflag2 Zflag3 ... ZflagN END
DISCCART	O-R	Xcoord Ycoord (Zelev) (Zflag)
DISCPOLR	O-R	Srcid Range Direct (Zelev) (Zflag)
BOUNDARY	O-R	Srcid Dist(I),I=1,36
BOUNDELV	O-R	Srcid Zelev(I),I=1,36

Type: M - Mandatory N - Non-repeatable
O - Optional R - Repeatable

Notes: Parameters noted in parenthesis are optional.

While all RE keywords are optional, at least one receptor must be defined for each run.

DESCRIPTION OF METEOROLOGY PATHWAY KEYWORDS AND PARAMETERS

ME Keywords	Type	Parameters
INPUTFIL	M-N	Metfil (Format)
ANEMHGHT	M-N	Zref (Zrunit)
SURFDATA	M-N	Stanum Year (Name) (Xcoord Ycoord)
UAIRDATA	M-N	Stanum Year (Name) (Xcoord Ycoord)
STARTEND	O-N	Strtyr Strtmn Strtdy (Strthr) Endyr Endmn Enddy (Endhr)
DAYRANGE	O-R	Range1 Range2 Range3 ... RangeN
WDROTATE	O-N	Rotang
WINDCATS	O-N	Ws1 Ws2 Ws3 Ws4 Ws5
WINDPROF	O-R	Stab Prof1 Prof2 Prof3 Prof4 Prof5 Prof6
DTHETADZ	O-R	Stab Dtdz1 Dtdz2 Dtdz3 Dtdz4 Dtdz5 Dtdz6
SIGMAELV[1]	**O-N**	**SigE1 SigE2 SigE3 SigE4 SigE5 SigE6**
SIGMAAZM[1]	**O-N**	**SigA1 SigA2 SigA3 SigA4 SigA5 SigA6**
ANEMELEV[1]	**O-N**	**ZA (ZAunit)**

Type: M - Mandatory N - Non-repeatable
O - Optional R - Repeatable

Note: Parameters noted in parenthesis are optional.

1) Added option in the ISCST2C model. ISCST2C model CO options discussed in Section 3.3.4 of this dissertation.

DESCRIPTION OF OUTPUT PATHWAY KEYWORDS AND PARAMETERS

OU Keywords	Type	Parameters
RECTABLE	O-R	Aveper FIRST SECOND ... SIXTH or 1ST 2ND ... 6TH
MAXTABLE	O-R	Aveper Maxnum
DAYTABLE	O-N	Avper1 Avper2 Avper3 Avper4
MAXIFILE	O-R	Aveper Grpid Thresh Filnam (Funit)
PLOTFILE	O-R	Aveper Grpid Hivalu Filnam (Funit) Aveper Grpid Filnam (Funit) (period ave)
POSTFILE	O-R	Aveper Grpid Format Filnam (Funit)

Type: M - Mandatory N - Non-repeatable
O - Optional R - Repeatable

Note: Parameters noted in parenthesis are optional.

APPENDIX D

FULL REFERENCE OF PATHWAYS/KEYWORDS/PARAMETERS

DESCRIPTION OF CONTROL PATHWAY KEYWORDS

CO Keywords	Type	Keyword Description
STARTING	M-N	Identifies the start of CONTROL pathway inputs
TITLEONE	M-N	First line of title for output
TITLETWO	O-N	Optional second line of title for output
MODELOPT	M-N	Job control and dispersion options
MODELSEL[1]	**O-N**	**Dispersion algorithm options**
AVERTIME	M-N	Averaging time(s) to process
POLLUTID	M-N	Identifies type of pollutant being modeled
HALFLIFE	O-N[2]	Optional half life used for exponential decay
DCAYCOEF	O-N[2]	Optional decay coefficient
TERRHGTS	O-N	Specifies whether to assume flat terrain (default) or to allow use of receptors on elevated terrain
ELEVUNIT	O-N	Defines input units for receptor elevations (defaults to meters)
FLAGPOLE	O-N	Specifies whether to accept receptor heights above local terrain (m) for use with flagpole receptors, and allows for a default flagpole height to be specified
RUNORNOT	M-N	Identifies whether to run model or process setup information only
EVENTFIL[3]	O-N	Specifies whether to generate an input file for EVENT model
SAVEFILE[4]	O-N	Option to store intermediate results for later restart of the model after user or system interrupt
INITFILE[4]	O-N	Option to initialize model from file of intermediate results generated by SAVEFILE option
MULTYEAR[4]	O-N	Option to process multiple years of meteorological data (one year per run) and accumulate high short term values across years
ERRORFIL	O-N	Option to generate detailed error listing file (error file is mandatory for CO RUNORNOT NOT case)
FINISHED	M-N	Identifies the end of CONTROL pathway inputs

Type: M - Mandatory N - Non-repeatable
O - Optional R - Repeatable

Notes 1), 2), 3), and 4) continued on the next page

DESCRIPTION OF CONTROL PATHWAY KEYWORDS (continued)

Notes:

1) **Added option in the ISCST2C model.**

2) Either HALFLIFE or DCAYCOEF may be specified. If both cards appear a warning message will be issued and the first value entered will be used in calculations. Default assumes a half life of 4 hours for SO_2 modeled in urban mode.

3) The EVENTFIL keyword controls whether or not to generate an input file for the ISCEV2 (EVENT) model. The primary difference between ISCST2C and ISCEV2 processing is in the treatment of source group contributions. The ISCST2C model treats the source groups independently, whereas the ISCEV2 model determines individual source contributions to particular events, such as the design concentrations determined from ISCST2C, or user-specified events. By specifying the EVENTFIL keyword, an input runstream file will be generated that can be used directly with the ISCEV2 model. The events included in the generated ISCEV2 model input file are defined by the RECTABLE and MAXIFILE keywords on the OU pathway, and are placed in the EVent pathway.

4) The SAVEFILE and INITFILE keywords work together to implement the model's re-start capabilities. Since the MULTYEAR option utilizes the re-start features in a special way to accumulate high short term values from year to year, it cannot be used together with the SAVEFILE or INITFILE keyword in the same model run.

DESCRIPTION OF CONTROL PATHWAY KEYWORDS AND PARAMETERS

Keyword	Parameters	
TITLEONE	Title1	
where:	Title1	First line of title for output, character string of up to 68 characters
TITLETWO	Title2	
where:	Title2	Optional second line of title for output, character string of up to 68 characters
MODELOPT	DFAULT CONC or DEPOS RURAL or URBAN GRDRIS NOSTD NOBID NOCALM MSGPRO	
where:	DFAULT	Specifies use of regulatory default options (final rise, stack tip downwash, BID, calms processing, "upper bound" wake calcs, default exponents and DTDZ), overrides presence of GRDRIS, NOSTD, NOBID, NOCALM, and MSGPRO keywords
	CONC	Specifies calculation of concentration values
	DEPOS	Specifies calculation of deposition values
	RURAL	Specifies use of rural dispersion
	URBAN	Specifies use of urban dispersion
	GRDRIS	Option to use gradual plume rise
	NOSTD	Option to use no stack-tip downwash
	NOBID	Option to use no buoyancy-induced dispersion
	NOCALM	Option to bypass calms processing routine
	MSGPRO	Option to use missing data processing routines

DESCRIPTION OF CONTROL PATHWAY KEYWORDS AND PARAMETERS (continued)

Keyword	Parameters	
MODELSEL[1]	ISCST2	HOSKER or SCHULM or CAVITY CMPLXI or SHORTZ
where:	ISCST2	Option to calculate concentrations using the ISCST2 algorithm. If ISCST2 is specified in conjunction with the CMPLXI or SHORTZ parameter, the ISCST2 algorithm is used to predict concentrations at receptors on elevated terrain up to plume height (with terrain elevations higher than stack top "chopped-off" at the stack top elevation) and the COMPLEX I or SHORTZ algorithm is used to predict concentrations at receptors on elevated terrain higher than stack top. For those receptors located on terrain between stack top and plume height (e.g., intermediate terrain), the higher of the ISCST2 and COMPLEX I or SHORTZ predictions is used. This evaluation is made for each source-receptor-hour combination input to the ISCST2C model.
	HOSKER	Option to calculate concentrations using the HOSKER cavity algorithm
	SCHULM	Option to calculate concentrations using the Schulman-Scire cavity algorithm
	CAVITY	Option to calculate concentrations using the Gaussian cavity algorithm
	CMPLXI	Option to calculate concentrations on intermediate and complex terrain in rural areas using the COMPLEX I algorithm. NOTE: The RURAL parameter must also be specified in the MODELOPT keyword for the COMPLEX I algorithm to be involked.
	SHORTZ	Option to calculate concentrations on intermediate and complex terrain using the SHORTZ algorithm. NOTE: The URBAN parameter must also be specified in the MODELOPT keyword for the SHORTZ algorithm to be involked.
AVERTIME	Time1 Time2 Time3 Time4 MONTH PERIOD	
where:	TimeN	Nth optional averaging time (1, 2, 3, 4, 6, 8, 12, 24-hr; number of periods limited by NAVE parameter)
	MONTH	Option to calculate MONTHly averages (counts toward NAVE limit)
	PERIOD	Option to calculate averages for the entire data PERIOD

1) **Added option in the ISCST2C model.**

DESCRIPTION OF CONTROL PATHWAY KEYWORDS AND PARAMETERS (continued)

Keyword	Parameters	
POLLUTID	Pollut	
where:	Pollut	Identifies type of pollutant being modeled. Any name of up to eight characters may be used, e.g., SO2, NOX, CO, PM10, TSP or OTHER. Selection of SO2 with the URBAN DFAULT options forces use of a half life of 4 hours for exponential decay. Use of PM10, PM-10 or OTHER allows for the use of the MULTYEAR option.
HALFLIFE	Haflif	
where:	Haflif	Half life used for exponential decay (s)
DCAYCOEF	Decay	
where:	Decay	Decay coefficient for exponential decay (s^{-1}) = 0.693/HAFLIF
TERRHGTS	FLAT or ELEV (Taf(i),i=1,6 Hmin)[1]	
where:	FLAT	Specifies that flat terrain will be assumed for all calculations (default)
	ELEV	Specifies that receptors may be located on elevated terrain Note that if ELEVated receptors are allowed, then receptor heights must be input on the RE pathway, or they will be assumed to be 0.0.
	Taf[1]	**Optional array of terrain adjustment factors for each of the six stability categories for use in the COMPLEX I algorithm. Default values are 0.5, 0.5, 0.5, 0.5, 0.0, and 0.0 for stability categories A through F, respectively.**
	Hmin[1]	**Optional minimum separation distance (in m) between the plume centerline and the ground surface for use in the COMPLEX I algorithm when Taf = 0. Default value is 10 m.**
ELEVUNIT	METERS or FEET	
where:	METERS	Specifies input units for terrain elevations of meters
	FEET	Specifies input units for terrain elevations of feet Note: This keyword applies to receptor elevations only.
FLAGPOLE	(Flagdf)	
where:	Flagdf	Default value for height of (flagpole) receptors above local ground level, a default value of 0.0 m is used if this optional parameter is omitted

1) Added option in the ISCST2C model. Used in conjunction with the CMPLXI Parameter of the MODELSEL Keyword of the COntrol Pathway.

DESCRIPTION OF CONTROL PATHWAY KEYWORDS AND PARAMETERS (continued)

Keyword	Parameters	
RUNORNOT	RUN or NOT	
where:	RUN NOT	Indicates to run full model calculations Indicates to process setup data and report errors, but to not run full model calculations
EVENTFIL	(Evfile) (Evopt)	
where:	Evfile Evopt	Identifies the filename to be used to generate a file for input to EVENT model (Default=EVENTFIL.INP) Optional parameter to specify the level of output detail selected for the EVENT model: either SOCONT or DETAIL (default is DETAIL if this parameter is omitted)
SAVEFILE	(Savfil) (Dayinc) (Savfl2)	
where:	Savfil Dayinc Savfl2	Specifies name of disk file to be used for storing intermediate results (default = TMP.FIL) file is overwritten after each dump) Number of days between dumps (optional: default is 1) Optional second disk filename to be used on alternate dumps - eliminates risk of system crash during the dump. If blank, file is overwritten each time.
INITFILE	(Inifil)	
where:	Inifil	Specifies name of disk file of intermediate results to be used for initializing run (default = TMP.FIL)
MULTYEAR	Savfil (Inifil)	
where:	Savfil Inifil	Specifies name of disk file to be used for storing results at end of the year Optional name of disk file used for initializing the results arrays from previous year(s). The Inifil parameter is not used for the first year in the multi-year run.
ERRORFIL	(Errfil) (DEBUG)	
where:	Errfil DEBUG	Specifies name of detailed error listing file (default = ERRORS.LST) Option to provide detailed output for debugging purposes, e.g., plume heights, sigmas, etc. Generates Very Large Files -- Use with CAUTION!!!

DESCRIPTION OF SOURCE PATHWAY KEYWORDS

SO Keywords	Type	Keyword Description
STARTING	M-N	Identifies the start of SOURCE pathway inputs
LOCATION	M-R	Identifies coordinates for particular source
SRCPARAM	M-R	Identifies source parameters for a particular source
BUILDHGT	O-R	Building height values for each wind sector
BUILDWID	O-R	Building width values for each wind sector
BUILDLNG[1]	**O-R**	**Building length values for each wind sector**
BUILDSTK[2]	**O-R**	**Distances from the upwind edge of the building to the stack for each wind sector**
LOWBOUND	O-R	Switch to use non-DFAULT option for "lower bound" wake calculations, controlled by sector
EMISFACT	O-R	Optional input for variable emission rate factors
EMISUNIT	O-N	Optional conversion factors for emissions, concentrations, and depositions
SETVELOC	O-R	Input variables for optional settling velocities
MASSFRAX	O-R	Optional input of mass fraction for each settling velocity category
REFLCOEF	O-R	Optional input of surface reflection coefficients for each settling velocity category
SRCGROUP[3]	M-R	Identification of source groups
FINISHED	M-N	Identifies the end of SOURCE pathway inputs

Type: M - Mandatory N - Non-repeatable
O - Optional R - Repeatable

1) **Added option in the ISCST2C model. Used in conjunction with the HOSKER or SCHULM Parameter of the MODELSEL Keyword of the COntrol Pathway.**

2) **Added option in the ISCST2C model. Used in conjunction with the SCHULM Parameter of the MODELSEL Keyword of the COntrol Pathway.**

3) Source groups are treated independently for ISCST2C. The ISCEV2 (EVENT) model provides the contribution from each source to the group total for each specified event.

DESCRIPTION OF SOURCE PATHWAY KEYWORDS AND PARAMETERS

Keyword	Parameters	
LOCATION	Srcid Srctyp Xs Ys (Zs)	
where:	Srcid	Source identification code (alphanumeric string of up to eight characters)
	Srctyp	Source type: POINT, VOLUME, AREA
	Xs	x-coord of source location (m). SW corner for AREA.
	Ys	y-coord of source location (m). SW corner for AREA.
	Zs	Optional z-coord of source location (m). Eelevation above mean sea level, defaults to 0.0 m if omitted.
SRCPARAM	Srcid Ptemis Stkhgt Stktmp Stkvel Stkdia Vlemis Relhgt Syinit Szinit Aremis Relhgt Xinit	
where:	Srcid	Source identification code
	__Emis	Source emission rate: in g/s for Ptemis or Vlemis, $g/s/m^2$ for Aremis for concentration or deposition
	___Hgt	Source physical release height above ground (center of height for VOLUME)
	Stktmp	Stack gas exit temperature (K)
	Stkvel	Stack gas exit velocity (m/s)
	Stkdia	Stack inside diameter (m)
	Syinit	Initial lateral dimension of VOLUME source (m)
	Szinit	Initial vertical dimension of VOLUME source (m)
	Xinit	Length of side of square AREA source (m)
BUILDHGT	Srcid (or Srcrng) Dsbh(i), i=1,36	
where:	Srcid	Source identification code
	Srcrng	Range of sources (inclusive) for which building dimensions apply, entered as two alphanumeric strings separated by a '-'
	Dsbh	Array of direction-specific building heights (m) beginning with 10 degree flow vector and incrementing by 10 degrees clockwise
BUILDWID	Srcid (or Srcrng) Dsbw(i), i=1,36	
where:	Srcid	Source identification code
	Srcrng	Range of sources (inclusive) for which building dimensions apply
	Dsbw	Array of direction-specific building widths (m) beginning with 10 degree flow vector and incrementing by 10 degrees clockwise

DESCRIPTION OF SOURCE PATHWAY KEYWORDS AND PARAMETERS
(continued)

Keyword	Parameters	
BUILDLNG[1]	Srcid (or Srcrng) Dsbl(i), i=1,36	
where:	Srcid	Source identification code
	Srcrng	Range of sources (inclusive) for which building dimensions apply, entered as two alphanumeric strings separated by a '-'
	Dsbl	Array of direction-specific along-wind building lengths (m) beginning with 10 degree flow vector and incrementing by 10 degrees clockwise. If no values of Dsbl are input to the program, the direction-specific building length is set equal to the maximum direction-specific building width for the complement angles to the flow vector, i.e., Dsbl(i) = Max[Dsbw(i+9),Dsbw(i-9)].
BUILDSTK[2]	Srcid (or Srcrng) Dwsl(i), i=1,36	
where:	Srcid	Source identification code
	Srcrng	Range of sources (inclusive) for which building dimensions apply, entered as two alphanumeric strings separated by a '-'
	Dwsl	Array of direction-specific distances (m) from the upwind edge of the building to the stack beginning with 10 degree flow vector and incrementing by 10 degrees clockwise. If no values of Dwsl are input to the program, the stack is assumed to be located on the roof in the center of the building.
LOWBOUND	Srcid (or Srcrng) Idswak(i), i=1,36	
where:	Srcid	Source identification code
	Srcrng	Range of sources (inclusive) for which LOWBOUND option applies
	Idswak	Array of direction-specific wake option switches beginning with 10 degree flow vector and incrementing by 10 degrees clockwise (0=upper bound, 1=lower bound)

1) **Added option in the ISCST2C model. Used in conjunction with the HOSKER or SCHULM Parameter of the MODELSEL Keyword of the COntrol Pathway.**

2) **Added option in the ISCST2C model. Used in conjunction with the SCHULM Parameter of the MODELSEL Keyword of the COntrol Pathway.**

DESCRIPTION OF SOURCE PATHWAY KEYWORDS AND PARAMETERS
(continued)

Keyword	Parameters	
EMISFACT	Srcid (or Srcrng) Qflag Qfact(i), i=1,n	
where:	Srcid	Source identification code
	Srcrng	Range of sources (inclusive) for which emission rate factors apply
	Qflag	Variable emission rate flag: SEASON for seasonal; MONTH for monthly; HROFDY for hour-of-day; STAR for speed-by-stability; SEASHR for season-by-hour
	Qfact	Array of scalar emission rate factors, for: SEASON, n=4; MONTH, n=12; HROFDY, n=24; STAR, n=36; SSTAB, n=24; SSPEED, n=24; SEASHR, n=96; SSTAR, n=144
EMISUNIT	Emifac Emilbl Conlbl or Deplbl	
where:	Emifac	Emission rate factor used to adjust units of output (default value is 1.0 E06 for CONC for grams to micrograms; and 3600. for DEPOS for grams/sec to grams/hour;
	Emilbl	Label to use for emission units (default is
	Conlbl	grams/sec)
	Deblbl	Label to use for concentrations (default is micrograms/m^3)
		Label to use for deposition (default is grams/m^2)
SETVELOC	Srcid (or Srcrng) Vsn(i), i=1,Nvs	
where:	Srcid	Source identification code
	Srcrng	Range of sources (inclusive) for which settling velocities apply
	Vsn	Array of gravitational settling velocities (m/s)
MASSFRAX	Srcid (or Srcrng) Phi(i), i=1,Nvs	
where:	Srcid	Source identification code
	Srcrng	Range of sources (inclusive) for which mass fractions apply
	Phi	Array of mass fractions for each settling velocity category
REFLCOEF	Srcid (or Srcrng) Gamma(i), i=1,Nvs	
where:	Srcid	Source identification code
	Srcrng	Range of sources (inclusive) for which reflection coefficients apply
	Gamma	Array of surface reflection coefficients for each gravitational settling velocity category

DESCRIPTION OF SOURCE PATHWAY KEYWORDS AND PARAMETERS
(continued)

Keyword	Parameters	
SRCGROUP	Grpid Srcid's Srcrng's	
where:	Grpid	Group ID (Grpid = ALL specifies group including all sources), number of source groups limited by NGRP parameter in the computer code
	Srcid's	Discrete source IDs to be included in group
	Srcrng's	Source ID ranges to be included in group
		Note: Card may be repeated with same Grpid if more space is needed to specify sources

DESCRIPTION OF **RE**CEPTOR PATHWAY KEYWORDS

RE Keywords	Type	Keyword Description
STARTING	M-N	Identifies the start of RECEPTOR pathway inputs
GRIDCART	O-R[1]	Defines a Cartesian grid receptor network
GRIDPOLR	O-R[1]	Defines a polar receptor network
DISCCART	O-R[1]	Defines the discretely placed receptor locations referenced to a Cartesian system
DISCPOLR	O-R[1]	Defines the discretely placed receptor locations referenced to a polar system
BOUNDARY	O-R[1]	Defines discrete polar receptor locations corresponding to minimum plant boundary distances for each 10 degree sector
BOUNDELV	O-R	Defines terrain elevations for discrete receptors specified with BOUNDARY keyword
FINISHED	M-N	Identifies the end of RECEPTOR pathway inputs

Type: M - Mandatory N - Non-repeatable
O - Optional R - Repeatable

1) At least one of the following must be present: GRIDCART, GRIDPOLR, DISCCART, DISCPOLR, or BOUNDARY. Multiple receptor networks can be specified in a single run, including both Cartesian and polar, up to an overall maximum controlled by the NREC parameter.

DESCRIPTION OF RECEPTOR PATHWAY KEYWORDS AND PARAMETERS (continued)

Keyword	Parameters	
GRIDCART	Netid STA XYINC Xinit Xnum Xdelta Yinit Ynum Ydelta or XPNTS Gridx1 Gridx2 Gridx3 .... GridxN, and YPNTS Gridy1 Gridy2 Gridy3 .... GridyN ELEV Row Zelev1 Zelev2 Zelev3 ... ZelevN FLAG Row Zflag1 Zflag2 Zflag3 ... ZflagN END	
where:	Netid	Receptor network identification code (up to eight alphanumeric characters)
	STA	Indicates STArt of GRIDCART subpathway, repeat for each new Netid
	XYINC	Keyword identifying grid network generated from x and y increments
	Xinit	Starting x-axis grid location in meters
	Xnum	Number of x-axis receptors
	Xdelta	Spacing in meters between x-axis receptors
	Yinit	Starting y-axis grid location in meters
	Ynum	Number of y-axis receptors
	Ydelta	Spacing in meters between y-axis receptors
	XPNTS	Keyword identifying grid network defined by a series of x and y coordinates
	Gridx1	Value of first x-coordinate for Cartesian grid
	GridxN	Value of 'nth' x-coordinate for Cartesian grid
	YPNTS	Keyword identifying grid network defined by a series of x and y coordinates
	Gridy1	Value of first y-coordinate for Cartesian grid
	GridyN	Value of 'nth' y-coordinate for Cartesian grid
	ELEV	Keyword to specify that receptor elevations follow
	Row	Indicates which row (y-coordinate fixed) is being input
	Zelev	An array of receptor terrain elevations for a particular Row
	FLAG	Keyword to specify that flagpole receptor heights follow
	Row	Indicates which row (y-coordinate fixed) is being input
	Zflag	An array of receptor heights above local terrain elevation for a particular Row (flagpole receptors)
	END	Indicates END of GRIDCART subpathway, repeat for each new Netid

DESCRIPTION OF RECEPTOR PATHWAY KEYWORDS AND PARAMETERS
(continued)

Keyword	Parameters	
GRIDPOLR	Netid STA ORIG Xinit Yinit DIST Ring1 Ring2 Ring3 ... RingN DDIR Dir1 Dir2 Dir3 ... DirN, or GDIR Dirnum Dirini Dirinc ELEV Dir Zelev1 Zelev2 Zelev3 ... ZelevN FLAG Dir Zflag1 Zflag2 Zflag3 ... ZflagN END	
where:	Netid	Receptor network identification code (up to eight alphanumeric characters)
	STA	Indicates STArt of GRIDPOLR subpathway, repeat for each new Netid
	ORIG	Optional keyword to specify the origin of the polar network (assumed to be at x=0, y=0 if omitted)
	Xinit	x-coordinate for origin of polar network
	Yinit	y-coordinate for origin of polar network
	DIST	Keyword to specify distances for the polar network
	Ring1	Distance to the first ring of polar coordinates
	RingN	Distance to the 'nth' ring of polar coordinates
	DDIR	Keyword to specify discrete direction radials for the polar network
	Dir1	First direction radial in degrees (1 to 360)
	DirN	The 'nth' direction radial in degrees (1 to 360)
	GDIR	Keyword to specify generated direction radials for the polar network
	Dirnum	Number of directions used to define the polar system
	Dirini	Starting direction of the polar system
	Dirinc	Increment (in degrees) for defining directions
	ELEV	Keyword to specify that receptor elevations follow
	Dir	Indicates which direction is being input
	Zelev	An array of receptor terrain elevations for a particular direction radial
	FLAG	Keyword to specify that flagpole receptor heights follow
	Dir	Indicates which direction is being input
	Zflag	An array of receptor heights above local terrain elevation for a particular direction (flagpole receptors)
	END	Indicates END of GRIDPOLR subpathway, repeat for each new Netid

DESCRIPTION OF RECEPTOR PATHWAY KEYWORDS AND PARAMETERS
(continued)

Keyword	Parameters	
DISCCART	Xcoord Ycoord (Zelev) (Zflag)	
where:	Xcoord	x-coordinate for discrete receptor location
	Ycoord	y-coordinate for discrete receptor location
	Zelev	Elevation above sea level for discrete receptor location (optional), used only for ELEV terrain
	Zflag	Receptor height (flagpole) above local terrain (optional), used only with FLAGPOLE keyword
DISCPOLR	Srcid Dist Direct (Zelev) (Zflag)	
where:	Srcid	Specifies source identification for which discrete polar receptor locations apply (used to define the origin for the discrete polar receptor)
	Dist	Downwind distance to receptor location
	Direct	Direction to receptor location, in degrees clockwise from North
	Zelev	Elevation above sea level for receptor location (optional), used only for ELEV terrain
	Zflag	Receptor height (flagpole) above local terrain (optional), used only with FLAGPOLE keyword
BOUNDARY	Srcid Dist(i), i=1,36	
where:	Srcid	Specifies source identification for which boundary distances apply
	Dist	Array of 36 values corresponding to minimum plant boundary distances for every 10-degree sector, beginning with the 10 degree flow vector Note: Discrete receptor coordinates are generated with an origin referenced to the location of the source identified with Srcid
BOUNDELV	Srcid Zelev(i), i=1,36	
where:	Srcid	Specifies source identification for which boundary distances apply
	Zelev	Array of 36 values corresponding to terrain elevation for plant boundary distances for 10-degree sectors, beginning with the 10 degree flow vector

DESCRIPTION OF METEOROLOGY PATHWAY KEYWORDS

ME Keywords	Type	Keyword Description
STARTING	M-N	Identifies the start of METEOROLOGY pathway inputs
INPUTFIL	M-N	Describes input meteorological data file
ANEMHGHT	M-N	Input height of anemometer above stack base
SURFDATA	M-N	Describes surface meteorological station
UAIRDATA	M-N	Describes upper air meteorological station
STARTEND	O-N	Specifies start and end dates to be read from input meteorological data file (default is to read entire file).
DAYRANGE	O-R	Specifies days or ranges of days to process (default is to process all data read in).
WDROTATE	O-N	May be used to correct for alignment problems of wind direction measurements, or to convert wind direction from to flow vector
WINDPROF	O-R	Input optional wind profile exponents
DTHETADZ	O-R	Input optional vertical potential temperature gradients
WINDCATS	O-N	Input upper bounds of wind speed categories, five values input - sixth category is assumed to have no upper bound.
SIGMAELV[1]	**O-N**	**Input optional σ_E values as a function of atmospheric stability category**
SIGMAAZM[1]	**O-N**	**Input optional σ_A values as a function of atmospheric stability category**
ANEMELEV[1]	**O-N**	**Input the optional ground elevation above mean sea level of the anemometer measurement location**
FINISHED	M-N	Identifies the end of METEOROLOGY pathway inputs

Type: M - Mandatory N - Non-repeatable
O - Optional R - Repeatable

1) Added option in the ISCST2C model. Used in conjunction with the SHORTZ Parameter of the MODELSEL Keyword of the COntrol Pathway.

DESCRIPTION OF METEOROLOGY PATHWAY KEYWORDS AND PARAMETERS

Keyword	Parameters	
INPUTFIL	Metfil (Format)	
where:	Metfil	Specify filename for meteorological input file
	Format	Specify format for input file: options are to provide FORTRAN read format for ASCII file, (YR,MN,DY,HR,AFV (or WD),WS,TA,KST,ZIRUR,ZIURB); use default ASCII format (4I2,2F9.4,F6.1,I2,2F7.1) if blank; use free format if FREE; use default ASCII format with hourly WINDPROF and DTHETADZ if CARD; or use unformatted RAMMET file if UNFORM
ANEMHGHT	Zref (Zrunit)	
where:	Zref	Reference (anemometer) height above ground for wind speed measurement; also assumed to be height above stack base
	Zrunit	Units of Zref: METERS or FEET (default is METERS)
SURFDATA	Stanum Year (Name) (Xcoord Ycoord)	
where:	Stanum	Station number, e.g. 5-digit WBAN number for NWS surface station
	Year	Year of data being processed (four digits)
	Name	Station name (optional)
	Xcoord	x-coordinate of station location (m) (optional)
	Ycoord	y-coordinate of station location (m) (optional)
UAIRDATA	Stanum Year (Name) (Xcoord Ycoord)	
where:	Stanum	Station number, e.g. 5-digit WBAN number for NWS upper air station
	Year	Year of data being processed (four digits)
	Name	Station name (optional)
	Xcoord	x-coordinate of station location (m) (optional)
	Ycoord	y-coordinate of station location (m) (optional)
STARTEND	Strtyr Strtmn Strtdy (Strthr) Endyr Endmn Enddy (Endhr)	
where:	Strtyr	Year of first record to be read
	Strtmn	Month of first record to be read
	Strtdy	Day of first record to be read
	Strthr	Hour of first record to be read (optional)
	Endyr	Year of last record to be read
	Endmn	Month of last record to be read
	Enddy	Day of last record to be read
	Endhr	Hour of last record to be read (optional)
		Note: File read begins with hour 1 of the start date and ends with hour 24 of the end date if Stahr and Endhr are omitted.

DESCRIPTION OF METEOROLOGY PATHWAY KEYWORDS AND PARAMETERS (continued)

Keyword	Parameters	
DAYRANGE	Range1 Range2 Range3 ... RangeN	
where:	Range1	First range of days to process, either as individual day (XXX) or as range (XXX-YYY); days may be input as Julian dates (XXX) or as month and day (XX/YY)
	RangeN	The 'nth' range of days to process
WDROTATE	Rotang	
where:	Rotang	Specifies angle (in degrees) to rotate wind direction measurements to correct for alignment problems; value of Rotang is subtracted from WD measurements, i.e., rotation is counterclockwise; may also be used to adjust input of wind direction from values to flow vector values by setting Rotang = 180
WINDPROF	Stab Prof1 Prof2 Prof3 Prof4 Prof5 Prof6	
where:	Stab	Specifies stability category (A through F) for the following six values by wind speed class
	Prof1	Wind speed profile exponent for first speed class
	Prof2	Wind speed profile exponent for second speed class
	Prof3	Wind speed profile exponent for third speed class
	Prof4	Wind speed profile exponent for fourth speed class
	Prof5	Wind speed profile exponent for fifth speed class
	Prof6	Wind speed profile exponent for sixth speed class
		Note: Card is repeated for each stability class
DTHETADZ	Stab Dtdz1 Dtdz2 Dtdz3 Dtdz4 Dtdz5 Dtdz6	
where:	Stab	Specifies stability category (A through F) for the following six values by wind speed class
	Dtdz1	Vertical temperature gradient for first speed class
	Dtdz2	Vertical temperature gradient for second speed class
	Dtdz3	Vertical temperature gradient for third speed class
	Dtdz4	Vertical temperature gradient for fourth speed class
	Dtdz5	Vertical temperature gradient for fifth speed class
	Dtdz6	Vertical temperature gradient for sixth speed class
		Note: Card is repeated for each stability class

DESCRIPTION OF METEOROLOGY PATHWAY KEYWORDS AND PARAMETERS (continued)

Keyword	Parameters	
WINDCATS	Ws1 Ws2 Ws3 Ws4 Ws5	
where:	Ws1	Upper bound of first wind speed category (m/s)
	Ws2	Upper bound of second wind speed category (m/s)
	Ws3	Upper bound of third wind speed category (m/s)
	Ws4	Upper bound of fourth wind speed category (m/s)
	Ws5	Upper bound of fifth wind speed category (m/s) (sixth category is assumed to have no upper bound)
SIGMAELV[1]	**SigE1 SigE2 SigE3 SigE4 SigE5 SigE6**	
where:	**SigE1**	**Value of σ_E for stability category A**
	SigE2	**Value of σ_E for stability category B**
	SigE3	**Value of σ_E for stability category C**
	SigE4	**Value of σ_E for stability category D**
	SigE5	**Value of σ_E for stability category E**
	SigE6	**Value of σ_E for stability category F**
		Note: Values of σ_E can be input in radians or degrees. If σ_E < 1.0, then σ_E is assumed to be in radians; if σ_E > 1.0, then σ_E is assumed to be in degrees.
SIGMAAZM[1]	**SigA1 SigA2 SigA3 SigA4 SigA5 SigA6**	
where:	**SigA1**	**Value of σ_A for stability category A**
	SigA2	**Value of σ_A for stability category B**
	SigA3	**Value of σ_A for stability category C**
	SigA4	**Value of σ_A for stability category D**
	SigA5	**Value of σ_A for stability category E**
	SigA6	**Value of σ_A for stability category F**
		Note: Values of σ_A can be input in radians or degrees. If σ_A < 1.0, then σ_A is assumed to be in radians; if σ_A > 1.0, then σ_A is assumed to be in degrees.
ANEMELEV[1]	**ZA (ZAunit)**	
where:	ZA	Ground elevation above mean sea level of the anemometer measurement location.
	ZAunit	Optional units of ZA: METERS or FEET (default is METERS).

1) Added option in the ISCST2C model. Used in conjunction with the SHORTZ Parameter of the MODELSEL Keyword of the COntrol Pathway.

DESCRIPTION OF OUTPUT PATHWAY KEYWORDS

OU Keywords	Type	Keyword Description
STARTING	M-N	Identifies the start of OUTPUT pathway inputs
RECTABLE	O-R	Option to specify value(s) by receptor for output
MAXTABLE	O-R	Option to summarize the overall maximum values
DAYTABLE	O-N	Option to print summaries for each averaging period for each day processed.
MAXIFILE	O-R	Option to list events exceeding a threshold value to file (if CO EVENTFIL option is used, these events are included in the input file generated for the EVENT model).
POSTFILE[1]	O-R	Option to write results to a mass storage file for postprocessing.
PLOTFILE[1]	O-R	Option to write certain results to a storage file suitable for input to plotting routines
FINISHED	M-N	Identifies the end of OUTPUT pathway inputs

Type: M - Mandatory N - Non-repeatable
O - Optional R - Repeatable

1) POSTFILE is used to output concurrent concentration values for particular source groups and averaging times across the receptor network, suitable for postprocessing, such as might be done for implementing the intermediate terrain policy. PLOTFILE is used to output specific design values, such as second high concentrations, across the receptor network, suitable for plotting concentration contours.

DESCRIPTION OF **OU**TPUT PATHWAY KEYWORDS AND PARAMETERS

Keyword	Parameters	
RECTABLE	Aveper FIRST SECOND . . . SIXTH Aveper 1ST 2ND . . . 6TH	
where:	Aveper	Averaging period to summarize with high values (keyword ALLAVE specifies all averaging periods)
	FIRST	Select summaries of FIRST highest values by receptor
	SECOND	Select summaries of SECOND highest values by receptor
	SIXTH	Select summaries of SIXTH highest values by receptor
	1ST	Select summaries of 1ST highest values by receptor
	2ND	Select summaries of 2ND highest values by receptor
	6TH	Select summaries of 6TH highest values by receptor
		Note: If two keywords are input separated by a dash (e.g. FIRST-THIRD), then summaries of all high values in that range are provided. The number of high values allowed is controlled by the NVAL parameter in the computer code (initially set at 3). Also, if the CO EVENTFIL keyword is exercised, then the events generated by the RECTABLE keyword are included in the input file for EVENT model.
MAXTABLE	Aveper Maxnum	
where:	Aveper	Averaging period to summarize with maximum values (keyword ALLAVE specifies all averaging periods)
	Maxnum	Specifies number of overall maximum values to summarize (number of maximum values permitted is limited by the NMAX parameter in the computer code, initially set at 50)

DESCRIPTION OF OUTPUT PATHWAY KEYWORDS AND PARAMETERS (continued)

Keyword	Parameters	
DAYTABLE	Avper1 Avper2 Avper3 . . .	
where:	Avper1	Averaging period to summarize with values by receptor for each day of data processed (keyword ALLAVE for first parameter specifies all averaging periods)
MAXIFILE	Aveper Grpid Thresh Filnam (Funit)	
where:	Aveper	Specifies averaging period for list of values equal to or exceeding a threshold value
	Grpid	Specifies source group to be output to file
	Thresh	Threshold value (e.g. NAAQS) for list of exceedances
	Filnam	Name of disk file to store maximum values
	Funit	Optional parameter to specify the file unit Note: If the CO EVENTFIL keyword is exercised, then the events generated by the MAXIFILE keyword are included in the input file for the EVENT model.
POSTFILE	Aveper Grpid Format Filnam (Funit)	
where:	Aveper	Specifies averaging period to be output to file, e.g., 24 for 24-hr averages, PERIOD for period averages
	Grpid	Specifies source group to be output to file
	Format	Specifies format of file, either UNFORM for unformatted files or PLOT for formatted files for plotting
	Filnam	Specifies filename for output file
	Funit	Optional parameter to specify the file unit
PLOTFILE	Aveper Grpid Hivalu Filnam (Funit)	
where:	Aveper	Specifies averaging period to be output to file, e.g., 24 for 24-hr averages, PERIOD for period averages, WINTER for winter averages, etc.
	Grpid	Specifies source group to be output to file
	Hivalu	Specifies high value summary (e.g. FIRST, SECOND, 1ST, 2ND, etc.) to be output to file
	Filnam	Specifies filename for output file
	Funit	Optional parameter to specify the file unit

VITA

Steven Michael Claggett was born in Morganfield, Kentucky on June 7, 1951. He spent his childhood in Irvington, Kentucky (population 1200) where he attended elementary school, then Breckinridge County High School in Harned, Kentucky. After graduating from high school in 1969, he entered Western Kentucky University (WKU) in Bowling Green. He attended Virginia Polytechnic Institute and State University in Blacksburg for a short time, but returned to WKU where in 1974 he received a Bachelor of Science in Engineering Physics. He was offered several positions with the Kentucky Department of Transportation, and chose to enter the relatively new occupation of environmental assessment in which he performed air dispersion modeling. While attending a training course on highway air quality assessment sponsored by the Federal Highway Administration, he was recruited into the Master of Science program in Environmental Engineering at The University of Tennessee in Knoxville. He received an Environmental Protection Agency Fellowship to help finance his Master's education. After graduating in 1976, he began a career in air quality consulting. In 1977, he joined Enviro-Measure, Inc. and worked with other graduates from the Environmental

Engineering program. The company was successful and was eventually bought by IT Corporation in 1986. In 1989, he returned to The University of Tennessee on a part-time basis to pursue a Doctor of Philosophy in Civil Engineering with an emphasis in Environmental Engineering. In 1994, he left IT Corporation and became an independent consultant. The doctoral degree was received in May 1996.

He plans to continue air quality consulting and to continue his affiliation with the University by teaching a graduate-level course on air dispersion modeling. In a year, he is scheduled to begin teaching the Federal Highway Administration training course on highway air quality assessment.